

e-ISSN : 2320-0847
p-ISSN : 2320-0936



American Journal of Engineering Research (AJER)

Volume 3 Issue 8 – August 2014

www.ajer.org

ajer.research@gmail.com

Editorial Board

American Journal of Engineering Research (AJER)

Dr. Moinuddin Sarker,

Qualification :PhD, MCIC, FICER,
MInstP, MRSC (P), VP of R & D
Affiliation : Head of Science / Technology
Team, Corporate Officer (CO)
Natural State Research, Inc.
37 Brown House Road (2nd Floor)
Stamford, CT-06902, USA.

Dr. June II A. Kiblasan

Qualification : Phd
Specialization: Management, applied
sciences
Country: PHILIPPINES

**Dr. Jonathan Okeke
Chimakonam**

Qualification: PHD
Affiliation: University of Calabar
Specialization: Logic, Philosophy of
Maths and African Science,
Country: Nigeria

Dr. Narendra Kumar Sharma

Qualification: PHD
Affiliation: Defence Institute of Physiology
and Allied Science, DRDO
Specialization: Proteomics, Molecular
biology, hypoxia
Country: India

Dr. ABDUL KAREEM

Qualification: MBBS, DMRD, FCIP, FAGE
Affiliation: UNIVERSITI SAINS Malaysia
Country: Malaysia

Prof. Dr. Shafique Ahmed Arain

Qualification: Postdoc fellow, Phd
Affiliation: Shah Abdul Latif University
Khairpur (Mirs),
Specialization: Polymer science
Country: Pakistan

Dr. Sukhmander Singh

Qualification: Phd
Affiliation: Indian Institute Of
Technology, Delhi
Specialization : PLASMA PHYSICS
Country: India

Dr. Alcides Chaux

Qualification: MD
Affiliation: Norte University, Paraguay,
South America
Specialization: Genitourinary Tumors
Country: Paraguay, South America

Dr. Nwachukwu Eugene Nnamdi

Qualification: Phd
Affiliation: Michael Okpara University of
Agriculture, Umudike, Nigeria
Specialization: Animal Genetics and
Breeding
Country: Nigeria

Dr. Md. Nazrul Islam Mondal

Qualification: Phd
Affiliation: Rajshahi University,
Bangladesh
Specialization: Health and Epidemiology
Country: Bangladesh

CONTENTS

Volume-3 Issue-8

S.No.	Manuscript Title	Page No.
01.	Miscibility Studies of Cashew Gum and Khaya Gum Exudates in Dilute Solution by Viscometry and FTIR Analysis. David E. Arthur, C. E. Gimba, Eddy O. Nnabuk	01-12
02.	Algorithmic Finance Approach in Media Stock Analysis Dr Debasis Patnaik , Mr Saurabh Suman	13-36
03.	Petro-Physical Analysis Of Reservoir Rock Of Fenchuganj Gas Field (Well#03) Using Wireline Log Shamim Ahammod, Md. Abdul Hai, Dr. Md. Rafiqul Islam, S.M Abu Sayeem	37-48
04.	Deformation Patterns of Non-cohesive Soil Bases under Foundations with Different Vertical Cross-sectional Shapes Musa Alhassan	49-54
05.	Strength And Behavior Of Polypropylene Fibre In Impact Characteristics Of Concrete K.Anbuvelan	55-62
06.	Examination of thermal comfort in a naturally ventilated hostel using PMV-PPD model and field survey OLANIPEKUN Emmanuel Abiodun	63-78
07.	Identification and determination of gross thickness of hydrocarbon bearing zone of Habiganj gas field. Md. Abdul Hai, Shamim Ahammod ,Mohammed Omar Faruque, Md. Ashraf Hussain, Jewel Ahmed	79-89
08.	Quantitative and Qualitative Assessment of Drinking Water Sources in Ile-Ife and Environs Olanipekun E.A.	90-100
09.	Dwt-Aes Based Information Security System For Unmanned Vehicles Renjith V Ravi, Dr.R. Mahalakshmi	101-112
10.	Vermittreatment of Pharmaceutical Wastewaters and Nutrient Bioassay of Treated Effluents for Reuse as Irrigation Water Sharda Dhadse, P.R. Chaudhari, Shanta Satyanarayan, S. R. Wate	113-123
11.	Determination of Caffeine In Beverages: A Review Igelige Gerald, David Ebuka Arthur, Adebisi Adedayo	124-137
12.	Creating 3D model for new urbanized area from limited resources and data in developing countries Rebaz Nawzad , Nabaz Gharib Mohammed & Hawar Othman Sharif	138-144

13.	Prediction of Global Solar Radiation Using Angstrom-Page Equation Model for Makurdi Benue State, Nigeria. M. S. Kaltiya, M. S. Abubakar, I.N. Itodo	145-150
14.	THE SIXTH SENSE OF HUMAN?... (A New theory on " Sleepless Human" M.Arulmani, B.E. , V.R.Hema Latha	151-161
15.	Novel Microstrip Patch Antenna (MPA) Design for Bluetooth, IMT, WLAN and WiMAX Applications Amarveer Singh, Ekambir Sidhu	162-170
16.	Impact of Maintenance Strategies on the Performance Of Industrial Facilities In Selected Industrial Estates In Lagos State, Nigeria Oseghale, G.E	171-179
17.	Comparison between the Performance of Basic SEPIC Converter and modified SEPIC Converter with PI Controller Satyendra Kumar Gupta , Shahab Ahmad	180-186
18.	Dual-Band Annular-Ring Microstrip Patch Antenna for Satellite Applications Tvs Divakar, Dr. D.C.Panda	187-190
19.	An Appraisal of the Population Total of Nigeria Using One Unit per Stratum (Based On 2006 Census Result) T.J. Akingbade, O.S. Balogun, O.S. Babatunde	191-201
20.	Performance and Emission Characteristics of Direct Injection Diesel Engine Running On Canola Oil / Diesel Fuel Blend Anbarasu.A, Karthikeyan.A.	202-207
21.	Investigation of the Potential of Jatropha Seed Oil as Austempering Quenchant for Medium Carbon Steel Akor, T., Ashwe, A.	208-211
22.	Denosing Of TDM Signal Using Novel Time Domain and Transform Domain Multirate Adaptive Algorithms C Mohan Rao, Dr. B Stephen Charles, Dr. M N Giri Prasad	212-226
23.	Social safety's women in urban public space (Case study: Mashhad metropolitan) Yasha Taheri Khameneh, Maryam Ebrahimpour	227-233
24.	Using A Battery Storage Wind / PV Hybrid Power Supply System Based Stand-Alone PSO To Determine The Most Appropriate Amam Hossain Bagdadee	234-242
25.	Numerical Solution of Higher Order Linear Fredholm – Integro – Differential Equations. Gegele. O.A , Evans. O.P , Akoh,D	243-247
26.	Insight on the Projective Module Udoeye Adaobi Mmachukwu , Akoh David	248-262
27.	Durability of Laterite/Sand Hollow Blocks in Magnesium Sulphate Environment ATA Olugbenga	263-266

28.	Design and Analysis of Compact UWB Bandpass Filter with Wide Passband Using Defected Ground Structure Yashika Saini, Mithilesh Kumar	267-272
29.	Laboratory and Field Performance of stabilized soft subgrade SATISH SAJJA, V K CHAKRAVARTHI	273-283
30.	Fast and Secure Initial Access Authentication Protocol for Wireless LANs Sandhya K, Nagaraju Rayapati	284-294
31.	THIRI KURAL?... (jphp Fuy;) M.Arulmani,V.R.Hema Latha	295-304
32.	THE WHITE BLOOD ANCESTOR?... (A New theory on "Angel Blood") M.Arulmani,V.R.Hema Latha	305-315
33.	Evaluation of life quality indicators in cities & improving urban environmental (Case Study: Boroujerd city) Fatemeh Olfaty, Mahdi Garavand	316-322
34.	Design and Performance Analysis of MIMO-DSSS System for 2.4 GHz ISM Band Wi-Fi Applications Using Microstrip Antennas Harshal Nigam, Mithilesh Kumar	323-332
35.	Analyzing of spatial-physical structure of urban spaces by using SWOT & GIS techniques (Case study: Borujerd historic bazaar) Fatemeh Olfaty, Mahdi Garavand	333-343
36.	Validation of Predicted California Bearing Ratio Values from Different Correlations K Shiva Prashanth Kumar, P M B Raj Kiran Nanduri, Prof.N Darga Kumar	344-352
37.	Web based authentication scheme using images Viswa Subramanian Sekar	353-361
38.	Soil Improvement By Using Bamboo Reinforcement Md Asaduzzaman , Muhammad Iftiarul islam	362-368
39.	Effects of Particle Size on the Thermal Properties of Sawdust, Corncobs and Prosopis Africana Charcoal Briquettes. Tokan, A., Sambo, A.S., Jatau, J.S., Kyauta, E.E.	369-374

Miscibility Studies of Cashew Gum and Khaya Gum Exudates in Dilute Solution by Viscometry and FTIR Analysis.

David E. Arthur^{1*}, C. E. Gimba¹, Eddy O. Nnabuk¹

¹Department of Chemistry, Ahmadu Bello University Zaria, Nigeria

Abstract: The FTIR and coefficient of viscosity for Cashew/Khaya blends in deionized water were measured, the changes in specific viscosity of the blends with corresponding effect of temperature and ionic salts, i.e. KCl, KBr and AlCl₃ were modeled. The measured parameters were used to estimate other related physical quantities using Huggins, Tanglerpaibul and Rao, Frankel-eyring and Arrhenius-frankel models etc. these quantities includes the intrinsic viscosity (η), conformation parameter (b_{law}), standard Enthalpy and Energy change of blend flow (ΔH and ΔE), Huggins parameter (K), Interaction parameter ($bm1$) were proposed by Higiroy et al., to identify the molecular conformation and the interaction arising in solution of gum blends. The peculiar deviation confirmed the structural changes in the solution of the blends, while the FTIR confirmed the formation of physical blends.

Keywords: Viscosity, polymer blends, Cashew gum (AO), Khaya gum (KS), molecular interaction, FTIR

I. INTRODUCTION

Polymer blending provide a wide range of benefits which are of importance in aiding the engineering of new materials, some of this benefits includes Improved process-ability, product uniformity, scrap reduction, Quick formulation changes, Inherent recyclability of products, etc. (Rhooy et al., 1997; Stephen et al., 2000;). The miscibility of polymer blends depends on the balance of small enthalpic and non-configurational entropic effects and the Sensitivity of this balance to small variation of the macromolecular structure is illustrated in the series of papers on miscibility of model polyolefins Rabeony et al., 1998. The term gum is generally applied to a wide variety of colloidal substances that are similar in appearance and have peculiar characteristics (Columbia Encyclopedia, 2006). Ghani (1988) described gums as a group of non-crystalline polysaccharides which usually contain sugars such as mannose and galactose and their uronic acid derivatives, although in practical terms, gums are defined as molecular structures, tending to high molecular mass, usually with colloidal properties, which in an appropriate solvent produce gels or suspensions of high viscosity or solutions of low matter content that can absorb water at ten times their weight. (Umoren et al., 2006d).

Plant gums are obtained as an exudation from fruit, trunk or branches of the trees spontaneously or after mechanical injury of the plant by incision of the bark, the exudates become hard nodules or ribbons on dehydration to form a protective sheath against microorganism, an example of these gums includes cashew gum (*Anacardium occidentale*) and khaya gum (*Khaya senegalensis*) have been found to show promising properties for both industrial and pharmaceutical applications. *Khaya senegalensis* commonly called African mahogany in English, 'Homra' in Arabic, 'Dalehi' in Fulani, 'Madaci' in Hausa, 'ono' in Igbo and 'ogonowo' in Yoruba, belongs to the Family, *Meliaceae*, it is a tall plant of 15-30 meters in height and about 1 meter in diameter, which is easily recognized by its ever green crown, while its gum occur in long, thin glass-like translucent fragments. The gum which is dark brown, is known to contain highly branched polysaccharides consisting of D galactose, L-rhamnose, D-galacturonic acid and 4-O-methyl-D-glucuronic acid (Aspinall and Bhattacharjee, 1970). Khaya gum has been evaluated as a directly compressible matrix system for controlled release. The findings suggested that the gum could be useful in the formulation of sustained release tablets for up to 5 hrs and may provide a time independent release for longer periods when appropriately combined with HPMC (Oluwatoyin, 2006). Cashew tree (*Anacardium occidentale* L.) resin is synthesized in the epithelial cell lining pockets or canals and then secreted into these internal cavities. The gum is similar to gum arabic and may be used

as to a substitute for liquid glue for paper, in the pharmaceutical/cosmetic industry and as an agglutinant for capsules and pills Bovin (1998), De Paula *et al* (1998) and Amadeo *et al* (2003). The major cations of *A. occidentale* L. are K^+ , Na^+ , Ca^{+2} and Mg^{+2} . The crude *A. occidentale* gum, containing these cations tends to be naturally transformed into Na salt, after purification or dialysis against NaCl 0.15 M [De Paula *et al* (1998), Charlwood *et al* (1998), Carver (1997) and León de Pinto (1994)]. The cost of polymer or gum production is virtually fixed by the material and the compounding method and the economy depends on blend's morphology, tailored for a specific application, hence the objective of this study was to explore the effect of ionic environment on the interaction of the selected plant gums in dilute solution as well as other conditions: temperature, salt, acid etc. A sensitive rheometry technique was employed to capture this interaction. Different intrinsic-viscosity models and the elastic component of the gum blends was used to determine any conformational change or interaction occurring between the gums.

The results in this study aid us in improving on the quality or properties of this gums by carefully modeling their behaviours when salts are added to the gum blends as well its effect on the blends elastic component.

II. MATERIALS:

Crude *Khaya senegalensis* (chewstick tree) gum was obtained as dried exudate from the parent tree grown at Kanya babba village in Bubura local Government Area of Jigawa State, the gum was collected around mid-November during the day time. The plant material had earlier been identified and authenticated and assigned a voucher number 872 in the herbarium Department of Biological Sciences of Ahmadu Bello University Zaria, while the crude *Anacardium occidentale* L gum was obtained as dried exudate from its parent tree grown in Ahmadu Bello university Zaria, close to the postgraduate school.

III. PURIFICATION OF THE GUM:

The procedure adapted for the purification of the gum was that of Femi – Oyewo *et al.*, (2004) but with some modifications. The gums were dried in an oven (BS Size 3, Gallenkamp) at 40°C for 2hrs and their size reduced using a blender (Model. MJ-176 NR, Matsushita Electric Industrial Co., Ltd. Osaka, Japan). It was hydrated in double strength chloroform (Sigma-Aldrich, Germany) water for five days with intermittent stirring to ensure complete dissolution of the gum and then strained through a 75µm sieve to obtain particulate free slurry which was allowed to sediment. Thereafter, the gums were precipitated from the slurry using absolute ethanol (Sigma-Aldrich, Germany), filtered and defatted with dried flakes. The precipitate was dried in the oven at 40 for 48 hours. The dried flakes were then pulverized using a blender and finally stored in an air tight container.

Preparation of Polymeric Blends:

Ternary solutions for the present system were prepared by mixing the calculated quantity of polymer solutions in different weight ratios up to the concentration of 1.0% (w/v). Dilutions to yield four lower concentrations were made by adding appropriate aliquots of solvent. To study the interaction between the gums, the following treatments were considered: *Anacardium occidentale* L (AO) 100%, *Khaya senegalensis* (KS) 100%, KS 80%- AO 20%, KS 60%- AO 40%, KS 50%-AO 50%, KS 40%-AO 60%, KS 20%-AO 80%.

Effects of Temperature, Concentration And Salt Changes on Viscosities of Gums:

The Ostwald viscometer was used as described by Higiro *et al.*, 1 % w/v concentrations of each of the gums were prepared and their viscosities at temperature range (30-70) °C were determined. Another 1 % w/v concentrations of each of the gums were studied with different concentrations of KCl, AlCl₃, KBr i.e. (0.2, 0.4, 0.6, 0.8 and 1.0M). Viscosity values of the blends and the pure gums at different concentrations of the salts as well as temperature were measured.

IV. FTIR ANALYSIS:

FTIR analyses of the gums were carried out using (Scimadzu FTIR-8400S) Fourier transform infrared spectrophotometer. The sample was prepared using KBr and the analysis was done by scanning the sample through a wave number range of 400 to 4000cm⁻¹.

RHEOLOGICAL PROPERTIES:

The elastic and viscous components of each gum solution and of the blends were measured as a function of shear viscosity by using an Ostwald viscometer.

Rheological measurements were carried out at 20°C by using a temperature- controlled circulating water bath (Haake DC5, Gebr. Haake GmbH, Karlsruhe, Germany).

Microsoft Excel 2007 (Microsoft Corporation, Seattle, WA) was used to plot viscosities against

concentrations, as well as to obtain linear regression lines with the corresponding equations and correlation coefficients (R^2), to assess the best model.

V. DETERMINATION OF INTRINSIC VISCOSITY:

The intrinsic viscosity $[\eta]$ is a measure of the hydrodynamic volume occupied by a macromolecule, which is closely related to the size and conformation of the macromolecular chains in a particular solvent (Lai and Chiang, 2002). The intrinsic viscosity $[\eta]$ is determined experimentally from measurements of the viscosity of very low concentration (C) solutions. Denoting solution and solvent viscosity as, respectively, η_{solution} and η_{solvent} ,

$[\eta]$ is defined by the following relationships:

Relative viscosity: $\eta_{rel} = \frac{\eta_{\text{solution}}}{\eta_{\text{solvent}}}$ (1)

Specific viscosity: $\eta_{sp} = \eta_{rel} - 1$ (2)

Intrinsic viscosity: $[\eta] = \lim_{C \rightarrow 0} \frac{\eta_{sp}}{C}$ (3)

The intrinsic viscosity can be obtained by measuring specific viscosities at different concentrations at the same shear-rate, and extrapolating the course of specific viscosity to infinite dilution (Heitmann and Mersmann, 1995). The intrinsic viscosity $[\eta]$ is, therefore, obtained by extrapolating data to zero concentration by using a linear regression, which will be called the graphic double-extrapolation procedure (GDEP) in this study. McMillan (1974) showed that

$\frac{\eta_{sp}}{C}$ also called reduced viscosity, could be written in the form of a Huggins equation (Huggins, 1942)

$$\frac{\eta_{sp}}{C} = [\eta] + K^l [\eta]^2 C \text{ (4)}$$

where k^l is the Huggins constant. The determination of the intrinsic viscosity is, therefore, the extrapolation of reduced viscosity to the value at zero solute concentration. The extrapolations are usually done in very dilute regimes ($C \ll C^*$) with relative viscosity values between 1.2 and 2.0, the corresponding specific viscosities being between 0.2 and 1.0 (Da Silva and Rao, 1992). C^* is defined as the overlap concentration, the transition from the dilute to the semi-dilute region which mark the onset of polymer entanglement (Launay, Cuvelier, and Martinez- Reyes, 1997). In the present work, gum solutions were therefore diluted to be within the described range. In addition, McMillan (1974) reported that the intrinsic viscosity could be obtained from the Kraemer equation (Kraemer, 1938) by extrapolation to zero concentration (C)

$$\frac{\ln \eta_{rel}}{C} = [\eta] + k^{ll} [\eta]^2 C \text{ 5}$$

where k^{ll} is the Kraemer constant. For very dilute solutions, however, Eq. (5) can be shortened by retaining only the first-order term, and $[\eta]$ can be determined from the slope of a plot of C against $\ln \eta_{rel}$ (Sornsrivichai, 1986).

McMillan (1974) showed that methods of determination of the intrinsic viscosity that were based on slopes of plots had higher correlation coefficients and lower standard errors, compared with those based on intercepts of plots.

On the basis of such findings, Tanglertpaibul and Rao (1987) used the following equations to obtain the intrinsic viscosity of tomato serum:

$$\eta_{rel} = 1 + [\eta]C \text{(6)}$$

The intrinsic viscosity $[\eta]$ is the slope obtained by plotting η_{rel} vs. C

$$\eta_{rel} = e^{[\eta]C} \text{(7)}$$

The intrinsic viscosity $[\eta]$ is the slope obtained by plotting $\ln \eta_{rel}$ vs. C

$$\eta_{rel} = \frac{1}{1 - [\eta]C} \text{(8)}$$

The intrinsic viscosity is the slope obtained by plotting $1 - \frac{1}{\eta_{rel}}$ vs. C.

The intrinsic viscosity $[\eta]$ was estimated based on the slope of η_{sp} vs. C for polyelectrolytes, as suggested by Chou and Kokini (1987); this is similar to the method discussed in Eq. (6). Chou and Kokini (1987) reported that when there is essentially no molecular interaction, as in dilute solutions, the second term of the Huggins equation (Eq. (4)) is negligible, and a plot of η_{sp} against concentration is linear. In this study, the intrinsic viscosity in the dilute domain was estimated on the basis of Eqs. (3), (6), (7), and (8), and the four methods were statistically compared for a better fit.

The intrinsic viscosity of the gum samples was determined in distilled water. The gum solutions were

prepared by dispersing 10 mg of each of the gum sample (db, dry basis) separately in 100 ml of the distilled water at room temperature and mixing with magnetic stirring overnight. 2 ml of solution was transferred into an Ostwald viscometer which was immersed in a precision water bath to maintain the temperature at 25.0±0.1 °C and after equilibration for 10 minutes, the flow time was determined between the two etched marks. Serial dilution was performed in situ and three readings were taken for each dilution and averaged. The relative viscosity (η_{rel}) would be calculated using the equation

$$\eta_{rel} = \frac{t - t_0}{t_0}$$

Where t is the flow time of gum solution in seconds, t_0 is the flow time of solvent (water) in seconds.

VI. DETERMINATION OF THE MOLECULAR CONFORMATION AND POLYMER INTERACTION:

The power-law equation

$$\eta_{sp} = aC^b \dots\dots\dots 9$$

Was used to estimate the exponent b from the slope of a double logarithmic plot of η_{sp} against concentration, and provides an indication of the conformation of polysaccharides (Lai, Tung, and Lin, 2000). To determine the gums interaction, the verified theory (Chee, 1990; Sun, Wang, and Feng, 1992), based on the classical Huggins equation expressing the specific viscosity (η_{sp}) of a polymer as a function of polymer concentration C , was used

$$\frac{\eta_{sp}}{C} = [\eta] + bC \dots\dots\dots 10$$

and

$$b = K[\eta]^2 \dots\dots\dots 11$$

Where $[\eta]$ is the intrinsic viscosity, and b and K are Huggins parameters. Chou and Kokini (1987) reported that for dilute solutions, the term bC from Eq. (11) is negligible, and the plot of the specific viscosity against the concentration gives a straight line. The term b was approximated from the small intercept value of the plot of specific viscosity against the concentration (Higiro, Herald, and Alavi, 2006).

According to this theory, the following equation applies to a ternary polymer–polymer–solvent dilute solution, in which there is no aggregation between molecules

$$\alpha = b_m - (\sqrt{b_1}W_1 + \sqrt{b_2}W_2)^2 \dots\dots\dots 12$$

Where b_m , b_1 , and b_2 are the Huggins coefficients for blend, polymer 1, and polymer 2, respectively. W_i is the weight fraction of polymer i in the polymer blend ($i = 1$ or 2). The equation may be used to provide qualitative information on polymer–polymer interaction: two polymers are attractive in solution when $\alpha \geq 0$, whereas they are repulsive when $\alpha < 0$ (Wang, Sun, and Wang, 2001).

Three types of interaction contribute to the value of b_m for a ternary polymer–polymer–solvent interaction (Cragg and Bigelow, 1955)

1. Long-range hydrodynamic interaction of pairs of single molecules:

$$b_{m1} = b_1W_1^2 + b_2W_2^2 + 2\sqrt{b_1b_2}W_1W_2 \\ = (\sqrt{b_1}W_1 + \sqrt{b_2}W_2)^2 \dots\dots\dots 13$$

Where b_i is the Huggins parameter b for component i ($i = 1$ or 2). W_i is the weight fraction of polymer i in the blend.

2. The formation of double molecules. This assumes actual contact:

$$b_{m2} = K^l([\eta]_1 - [\eta]_2) \dots\dots\dots 14$$

Where $[\eta]_1$ and $[\eta]_2$ are intrinsic viscosities of double- and single-molecule species, respectively, and K^l is a constant. In the absence of aggregation between molecules and at sufficiently low concentrations ($C \ll C^*$), this term is neglected.

3. Intermolecular attraction or repulsion:

$$b_{m3} = \alpha \dots\dots\dots 15$$

Where $\alpha \geq 0$ means attraction, whereas $\alpha < 0$ means repulsion.

Therefore,

$$b_m = b_{m1} + b_{m2} + b_{m3} \approx b_{m1} + b_{m3} \dots\dots\dots 16$$

$$b_m = (\sqrt{b_1}W_1 + \sqrt{b_2}W_2)^2 + \alpha \dots\dots\dots 17$$

$$\alpha = b_m - (\sqrt{b_1}W_1 + \sqrt{b_2}W_2)^2 \dots\dots\dots 18$$

By measuring b_m from the Huggins equation for polymer– polymer–solvent solution, a was calculated and the interaction was characterized.

Statistical Analyses

A two-way factorial design was used to generate the best-fitting intrinsic viscosity model. For each gum blend as well as for the effects of these three salts (KCl, KBr and $AlCl_3$) at the concentration ($10g/dm^3$ or $1g/dl$) were compared for the intrinsic viscosity, the elastic component, the molecular conformation coefficient b , the miscibility coefficient a , and the Huggins coefficient K , in a factorial design. In each instance, the analysis of variance and means comparison were conducted by the general linear models procedure (Proc GLM), with Statistical Package for social science (version 16.0). Comparisons among treatments were analyzed by using Duncan and Tukey significant test, with a significance level at $P < 0.05$

VII. RESULTS AND DISCUSSION:

In order to successfully study the trend in the specific viscosity as a result of addition of inorganic salt, a uniform concentration of the gums were maintained at ($1.0 g/dl$) while that of the salts chosen were varied from ($0.20-1.00 g/dl$). The AO-KS blends viscosity decreased when KCl and KBr were added with an exception of 80:20 and 60:40, which increased as the concentration of the salts were added. The blends of AO:KS increased in specific viscosity when $AlCl_3$ was added (fig 3), whereby a pronounced increase was noticed for 40:60 and 50:50 blends when the concentration added increases between $0.4 - 0.6 g/dl$, while a continuous smooth decrease was noticed for 80:20 and 60:40 blends. Due to impracticability in the obtaining a good regression model for the AO:KS blends when these salts are added it would be difficult to generate an intrinsic viscosity at these conditions, Lai *et al.* (2000) reported similar results when determining the intrinsic viscosity of hsian-tsao leaf gum in different salt solutions. Lapasin and Pricl (1995) reported that non-ionic polysaccharides (i.e., LBG) exhibited linear plots of lower slope, whereas ionic polysaccharides (i.e., xanthan) displayed a sharp increase in slope, possibly due to expanded coil dimensions and electrostatic repulsion between chain segments, dependence upon concentration was observed, with the appearance of a maximum, becoming more pronounced and shifting to the left. Without salt addition, the specific viscosity of the gums increased steadily with dilution, and very rapidly at high dilution. Our results showed an increase of specific viscosity/concentration for 95% of all the blends when $AlCl_3$ was added and decreased for the other salts used except AO:KS (80:20 and 60:40) in some salt concentrations.

As shown in fig 1, 2 and 3, the hydrodynamic behavior of *Khaya senegalenses* and *Anacardium occidentale* blends was strongly affected by ion types and ion concentrations. Within each gum blend, trivalent ions from $AlCl_3$ showed a more pronounced effect on the specific viscosity, compared with monovalent ions from KCl and KBr. The increase in ionic strength of the three salts from 0.2 to 1 caused a significant increase in specific viscosity for all gum blends. The specific viscosity increased by more than 30% of the value obtained with the pure gums and their blends when only $1g/dl$ salt was added to the gum blends.

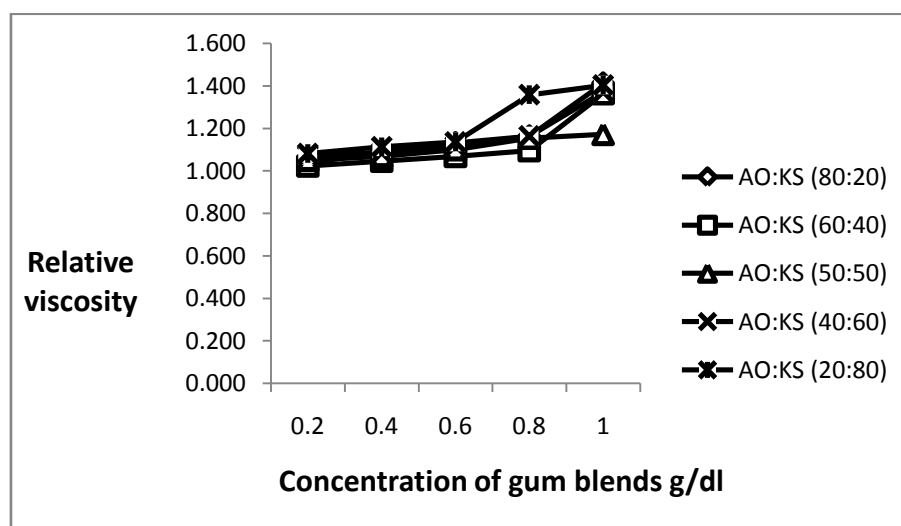


Fig 1: Variation of relative viscosity of the blend AO:KS with concentration of the blends at room temperature

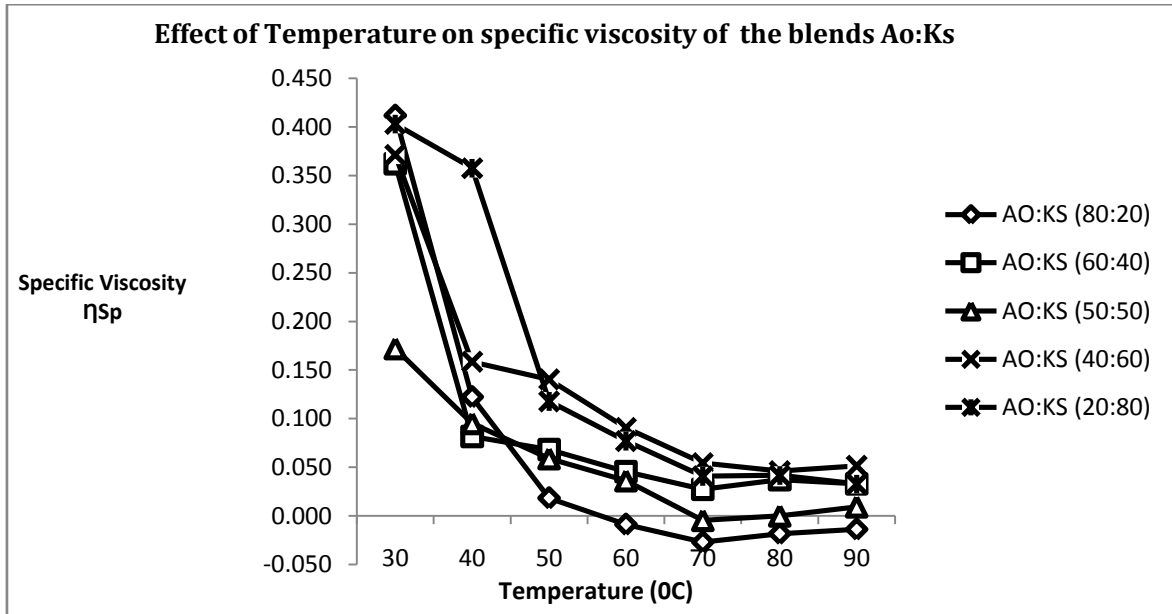


Fig. 2: Variation of specific viscosity of the blend Ao:Ks with temperature

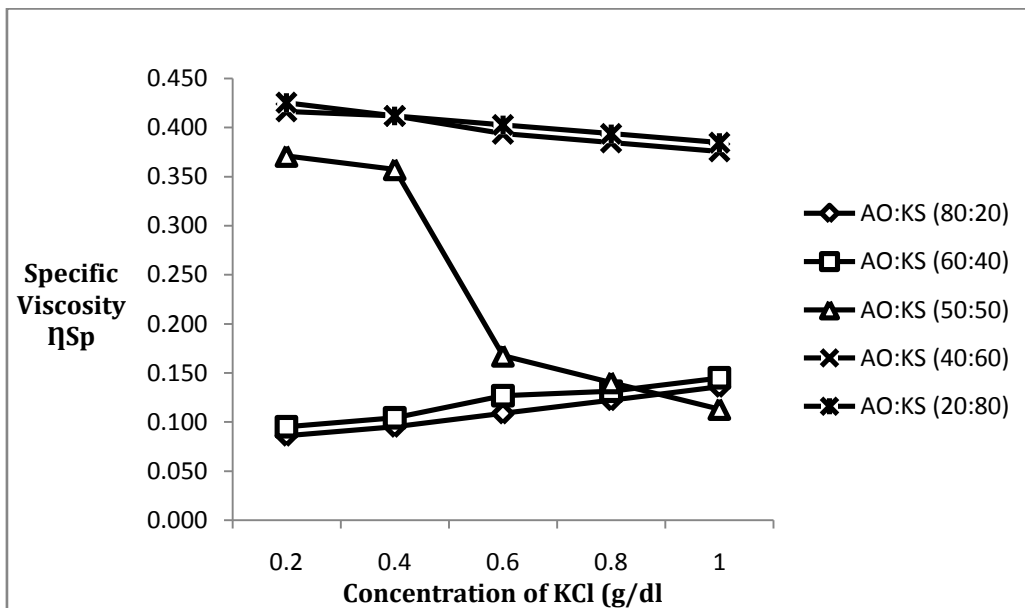


Fig. 3: Variation of specific viscosity of Ao:Ks gum blends with concentration of KCl

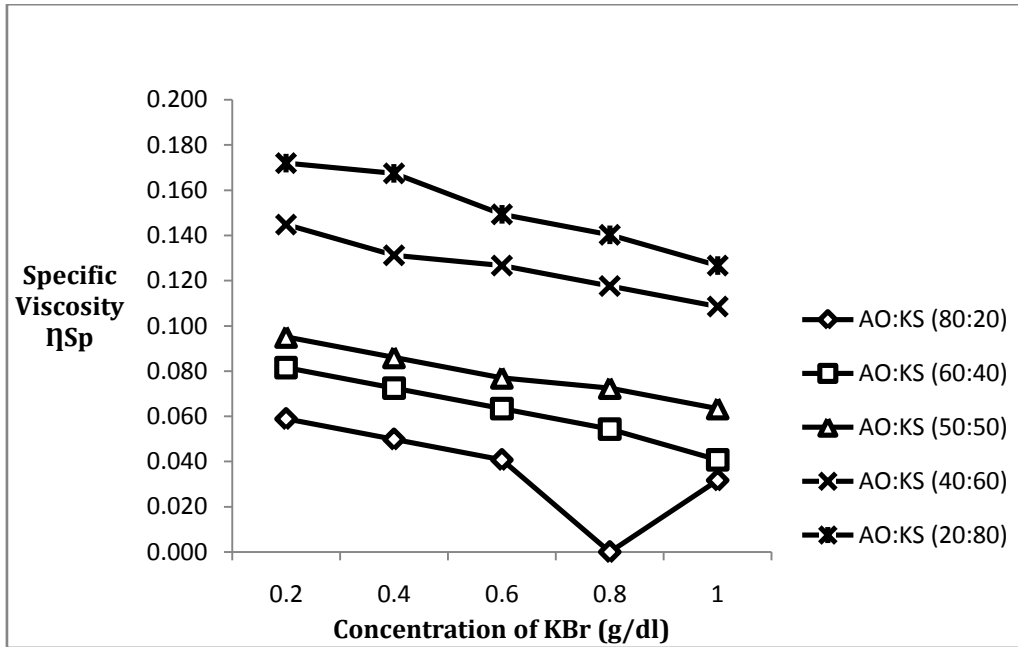


Fig. 4: Variation of specific viscosity of the blend AO:KS with concentration of KBr

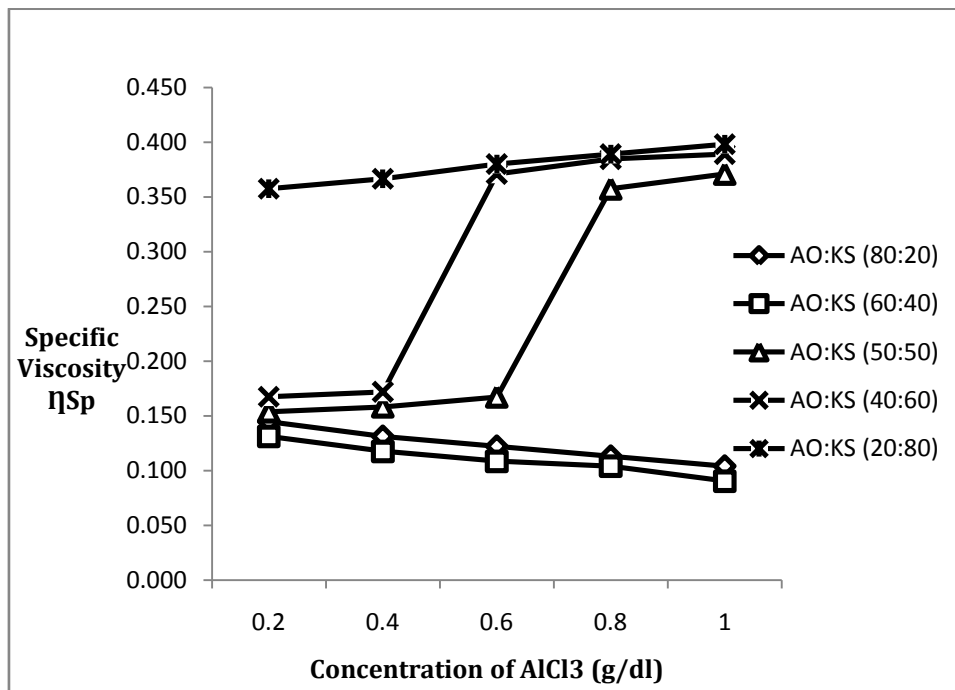
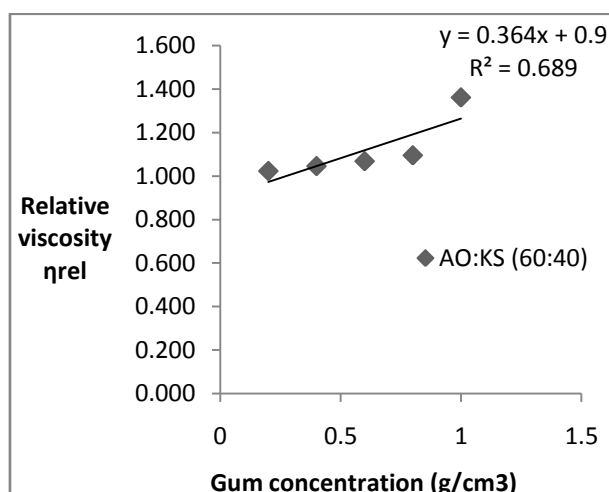
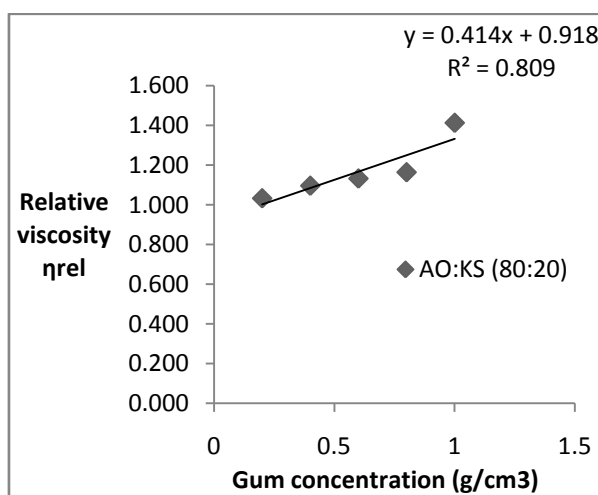


Fig. 5: Variation of specific viscosity of the blend AO:KS with increasing concentration of AlCl₃

VIII. INTRINSIC VISCOSITY:

The intrinsic viscosity determined for all the pure gums and their blends had an increase in relative viscosity which was observed as the concentration increases (Table 1), but a more pronounced increase in relative viscosity was evident for concentrations more than 0.4 g/dl. The GDEP therefore failed to generate the intrinsic viscosity for the pure gums and their blends since the datas generated did not fit with the linear regression model. The Huggins and Kraemer plots did not provided a better fit and, therefore, Tanglertpaibul and Rao plot was used, it was found to have the best fit (Chou and Kokini, 1987; Tanglertpaibul and Rao, 1987), this was done to determine the intrinsic viscosity by plotting η_{rel} vs. C. Straight-line relationships with large linear regression coefficients were obtained for all the gums. McMillan (1974) reported that methods of determination of intrinsic viscosity based on slopes of plots had larger correlation coefficients and smaller standard errors than those based on intercepts of plots. The values of the *intrinsic* viscosities resulting from these models differed, but showed similar trends, the intrinsic viscosity values calculated by using Tanglertpaibul and Rao plot was chosen as the best model for intrinsic viscosity determination because it showed a better linear fit, with higher correlation (R^2) for all blends. The intrinsic viscosity calculated for the blend AO:KS (20:80) had the highest intrinsic viscosity value at 44.31 dl/g, the value was seen to be lower than the intrinsic viscosity of a pure Khaya gum, but significantly higher than that of a pure cashew gum, which was found to be 6.31 dl/g this trend was found to decrease slightly as the composition of cashew gum was added. This shows that at precise blend combinations a synergism is archived which could have been as result of some interaction between the polymeric materials found within both gums.



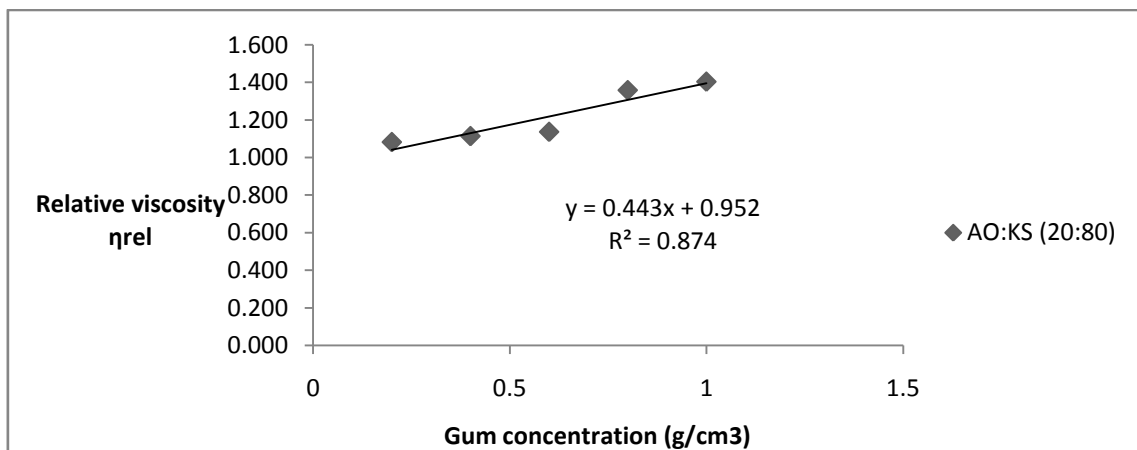
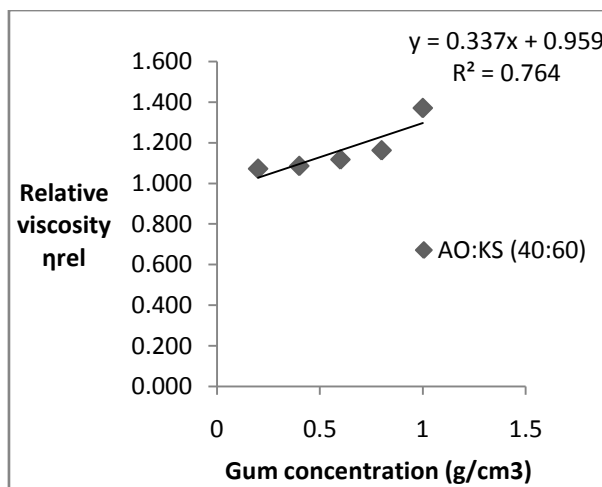
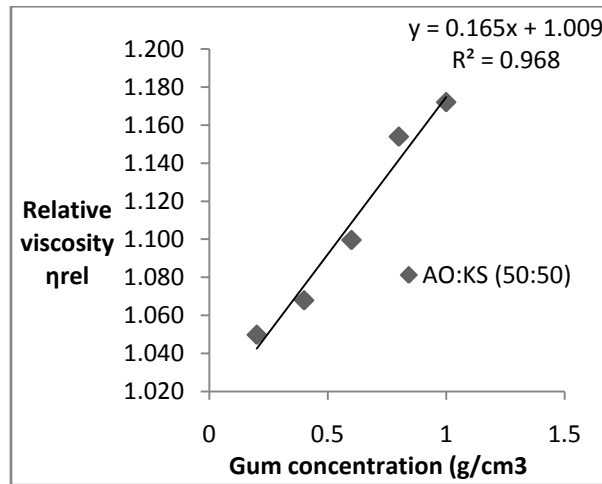


Fig. 6: Tangiertpaibul and Rao plot for the blends of AO:KS with concentration

Table 1: The intrinsic viscosity calculated from the slope of Tangelertpaibul and Rao (1987) plot are given below as

GUM BLENDS	INTRINSIC VISCOSITY (dl/g)	R2
AO	6.31 ± 0.01	0.915
KS	59.02 ± 0.02	0.912
AO:KS (80:20)	41.41 ± 0.01	0.809
AO:KS (60:40)	36.37 ± 0.14	0.689
AO:KS (50:50)	16.52 ± 0.02	0.968
AO:KS (40:60)	33.71 ± 0.01	0.764
AO:KS (20:80)	44.31 ± 0.01	0.874

The Results are expressed as mean ± SD for three replications. The means were found to be significantly different (p < 0.05)

IX. Thermodynamic Parameters And Polymer Conformation:

Temperature has an important influence on the flow behavior of plant gum sample content hydrocolloids. Since different temperatures are usually encountered during processing of hydrocolloids, their rheological properties are studied as a function of temperature. The Arrhenius equation to a great extent explains the relationship between the temperature and viscosity. The viscosity is dependent up on the intermolecular distances. As the temperature is increased, the intermolecular distances increase and therefore the viscosity will decrease for these main reasons. The viscosity is a function of temperature and the equation is given below

$$\ln \eta = \ln A + \frac{E_F}{RT} \dots\dots\dots 19$$

Equation 19 revealed that a plot of $\ln \eta$ versus $1/T$ should be linear with slope and intercept equal to E_F and $\ln A$ respectively. Activation parameters deduced from the plots are presented in Table 2. The results obtained indicated excellent correlation through R^2 values. The calculated values of E_F were 6.28 and 10.05 kJ/mol for AO and KS pure gums respectively. The activation energy for the blend flow was found to be highest in (80:20) with the value of 8.424KJ/mol, this value was found to decrease with increase in composition of khaya gum, but a change in trend was noticed from the 40:60 to 20:80 of the AO:KS blend. It has been found that low activation energy of flow indicates few inter- and intra-interactions between polysaccharide chains in the concentration range investigated and that the higher the value of E_F , the less sensitive is the polymer to temperature change (Shaikh *et al.*, 2011; Nair *et al.*, 2002). Hence the change in trend maybe associated with some other polymeric constituent of the KS gum that promoted interaction within the blend as its composition was increased, this result suggests the use of the blends (40:60 and 20:80) at higher temperature in food or drugs application.

According to Acevedo and Katz (1990), thermodynamic parameters of viscous flow can be calculated using the Frenkel-Eyring equation in the form,

$$\ln \eta = \left(\ln A - \frac{\Delta S_V}{R} \right) + \frac{\Delta H_V}{RT} \dots\dots\dots 20$$

where A is the pre-exponential factor, R is the universal gas constant, T is the absolute temperature, ΔS_V and ΔH_V are the entropy and enthalpy changes of viscous flow. From equation 20, a plot of $\ln \eta$ versus $1/T$ is expected to be linear with slope and intercept equal to $\frac{\Delta H_V}{R}$ and $\left(\ln A - \frac{\Delta S_V}{R} \right)$ respectively. Values of Frenkel-Eyring flow parameters deduced from the plots are also presented in Table 2. Calculated values of ΔH_V were found to be positive. This indicates the attainment of the transition state for viscous flow is accompanied by bond breaking.

The enthalpy change and activation energy of melt flow were accounted for using the Arrhenius-frenkel and frenkel-eyring model respectively (Ravindranatha, 2002)

Table 2: shows the values for ΔH and E_f for the gums and their blends

GUM BLENDS	ΔH (KJ/mol)	E_f (KJ/mol)	Gum Conformation	b_{law}
AO	14.477	6.2872	rod-like	0.730
KS	23.160	10.0581	random coil	1.715
AO:KS (80:20)	19.398	8.4244	random coil	1.414
AO:KS (60:40)	13.657	5.9316	random coil	1.482
AO:KS (50:50)	8.816	3.8293	rod-like	0.809
AO:KS (40:60)	14.156	6.1480	rod-like	0.889
AO:KS (20:80)	19.040	8.2691	random coil	1.028

The power-law equation is used to estimate the exponent b from the slope of double logarithmic plot of against concentration, which provides an indication of the **conformation of polysaccharides** (Lai, tung, and lin, 2000), If $b > 1$, then suggest random coil conformation (lapasin and pricl, 1995) and when $b < 1$ is for rod-like conformation (lai and chiang, 2002). Khaya gum molecule has a random coil conformation, while the pure cashew gum had a rod-like conformation, the conformation of the blends changes from a random coil conformation to rod-like conformation as the composition of Khaya gum was increased. This trend was found to confirm the formation of a blend or an existing interaction within the dilute solution of the blends.

Table 3: Shows the calculated Huggins parameter and hydrodynamic interaction of the gums.

GUM BLENDS	Huggins Parameter K	Interaction Type	$bm1$	A
AO	0.3066	no aggregation		
KS	0.0001	no aggregation		
AO:KS (80:20)	0.0048	no aggregation	8.3452	-0.155
AO:KS (60:40)	0.0075	no aggregation	5.2399	4.760
AO:KS (50:50)	0.0035	no aggregation	3.9570	-3.007
AO:KS (40:60)	0.0035	no aggregation	2.8539	1.176
AO:KS (20:80)	0.0024	no aggregation	1.1872	3.612

when $bm1 \geq 0$, whereas they are repulsive when $bm1 < 0$ (Wang, Sun, and Wang, 2001)

Table 3 summarizes the nature of interaction as well the hydrodynamic behavior of the blends, it shows that for all the blends the calculated value of the Huggins parameter was found to be less than unity, which according to Higuro *et al.*, indicates that no aggregation exists in the blends, but their affinity for water increased as the composition of cashew gum (AO) gum was increased, this was found to be evident in the interaction parameter $bm1$

X. FTIR STUDY OF THE GUMS:

The use of infrared spectroscopy for the characterization of polymer blends is extensive, coleman *et al.*, 1991. The IR spectra fig 7, shows the graphical representation of the frequencies of radiation absorbed and the percentage transmittance. Very strong bands which occur at $2854-3008\text{cm}^{-1}$ in the gums can be mostly attributed to absorption of CH stretch and CH_2 - asymmetric stretch in aliphatic groups closer to those bands. C-O stretch vibration due to carboxylic acid, alcohol and ester was noticed at 1054.13cm^{-1} and the characteristic peak at 1381cm^{-1} was attributed to O- CH_3 deformation, while the peak at 755cm^{-1} was due to the CH_2 rocking mode of vibration. The (C-C) vibrational mode appeared at 1514cm^{-1} , while peak at 1083cm^{-1} was attributed to C-C-C bending vibrational modes. The FTIR spectra of AO:KS blends (80:20, 60:40, 50:50, 40:60 and 20:80 %w/w) composition respectively showed that the blends did not indicate the existence of any chemical interaction between the components, although thorough analysis of the IR spectra for these blends showed a decrease in the transmittance of the carbonyl group, as well as other vibrational modes in the blend when the composition of khaya gum in the blend was increased

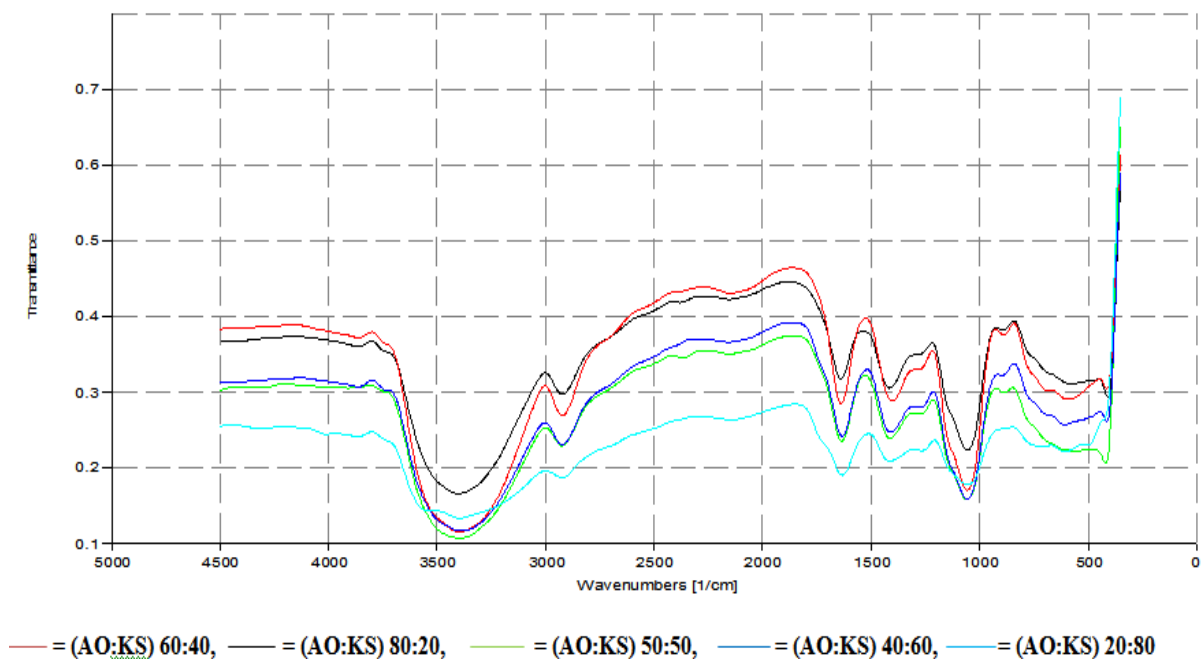


Fig. 7: FTIR spectrum of the gum blends of *Khaya senegalenses* and *Anacardium occidentale* gum

REFERENCES

- [1]. Higiroy, J., Herald, T. J., & Alavi, S. (2006). Rheological study of xanthan and locust bean gum in dilute solution. *Food Research International*, 39(2), 165–175
- [2]. Lai, L. S., & Chiang, H. F. (2002). Rheology of decolorized hsian-tso leaf gum in the dilute domain. *Food Hydrocolloids*, 16, 427–440.
- [3]. Lai, L. S., Tung, J., & Lin, P. S. (2000). Solution of hsian-tso (Mesona procumbens Hemsl) leaf gum. *Food Hydrocolloids*, 14, 287–294.
- [4]. Lapasin, R., & Priel, S. (1995). Rheology of polysaccharide systems. In R. Lapasin & S. Priel (Eds.), *Rheology of industrial polysaccharides: Theory and applications* (pp. 250–494). Glasgow: Blackie Academic and Professional.
- [5]. Launay, B., Cuvelier, G., & Martinez-Reyes, S. (1997). Viscosity of locust bean, guar, and xanthan gum solutions in the Newtonian domain: a critical examination of the master curves. *Carbohydrate Polymers*, 34, 385–395.
- [6]. Launay, B., Doublier, J. R., & Cuvelier, G. (1986). Flow properties of aqueous solutions and dispersions of polysaccharides. In J. R. Mitchell & D. A. Ledward (Eds.), *Functional properties of food macromolecules* (pp. 1–78). London: Elsevier Applied Science
- [7]. Heitmann, D. I. T., & Mersmann, A. (1995). Determination of the intrinsic viscosity of native potato starch. *Starch/Stärke*, 47, 426–429
- [8]. McMillan, D. E. (1974). A comparison of five methods for obtaining the intrinsic viscosity of bovine serum albumin. *Biopolymers*, 13, 1367–1371
- [9]. Huggins, M. L. (1942). The viscosity of dilute solutions of long-chain molecules. IV. Dependence on concentration. *Journal of the American Chemical Society*, 64, 2716–2718.
- [10]. Da Silva, J. La. L., & Rao, M. A. (1992). Viscoelastic properties of food hydrocolloid dispersions. In M. A. Rao & J. F. Steffe (Eds.), *Viscoelastic properties of foods* (pp. 285–315). New York: Elsevier Applied Science
- [11]. Kraemer, E. O. (1938). Molecular weights of celluloses and cellulose derivatives. *Industrial and Engineering Chemistry*, 30, 1200–1203
- [12]. Sornsrivichai, T., 1986. A study on rheological properties of tomato concentrates as affected by concentration methods, processing conditions, and pulp content. Ph.D. thesis, Cornell University, Ithaca, New York
- [13]. Tanglertpaibul, T., & Rao, M. A. (1987). Intrinsic viscosity of tomato serum as affected by methods of determination and methods of processing concentrates. *Journal of Food Science*, 52(6), 1642–1688
- [14]. Chou, T. D., & Kokini, J. L. (1987). Rheological properties and conformation of tomato paste pectins, citrus, and apple pectins. *Journal of Food Science*, 52, 1658–1664
- [15]. Chee, K. K. (1990). Determination of polymer–polymer miscibility by viscometry. *European Polymer Journal*, 26(4), 423–426.
- [16]. Sun, Z., Wang, W., & Feng, Z. (1992). Criterion of polymer–polymer miscibility determined by viscometry. *European Polymer Journal*, 28(10), 1259–1261
- [17]. Wang, F., Sun, Z., & Wang, Y. J. (2001). Study of xanthan gum/waxy corn starch interaction in solution by viscometry. *Food Hydrocolloids*, 15, 575–581
- [18]. Cragg, L. H., & Bigelow, C. C. (1955). The viscosity slope constant k_0 - ternary systems: polymer–polymer–solvent. *Journal of Polymer Science*, 16(82), 177–191.
- [19]. Rochefort, W. E., & Middleman, S. (1987). Rheology of xanthan gum: salt, temperature, and strain effects in oscillatory and steady shear experiments. *Journal of Rheology*, 31, 337–369

Algorithmic Finance Approach in Media Stock Analysis

¹, Dr Debasis Patnaik , ² Mr Saurabh Suman

¹(Asst Prof, University Of Bits Pilani, K. K. Birla Goa Campus, India)

² (Final Year, Deptt Of Economics And Finance, University Of Bits Pilani, K. K. Birla Goa Campus, India)

ABSTRACT: Literature is scanty on how to understand the dynamics of media stock and Factors that affect them. An algorithm with variables accounting for changes is developed. This algorithm will help in generating automatic trade signals and to create superior profits vis a vis individual speculation. Algorithmic trading improves market efficiency with higher liquidity and better price discovery. It improves the informativeness of the quotes. Focus on control or regulatory structure is also addressed on media stocks. The relative superiority of supervised and unsupervised learning is undertaken.

KEY WORDS: Media stocks, algorithmic design, eigen vector, covariance matrix, control theory, hidden markov, trading rules.

I. INTRODUCTION

Media stocks are becoming a key factor in stock market analysis in the context of a burgeoning knowledge economy. While fundamentals will help explain the movement of robust economic and financial factors, stock market analysis and technical analysis will justify results, positive or negative and throw interpretative light on fundamentals. Algorithmic approach is being used frequently to show whether mathematical/ algebraic manipulation can help factor in more relevant variables along with a control structure for regulatory freedom that is available to regulators.

II. LITERATURE REVIEW

Fischer, Thomas (2011), News Reaction in Financial Markets within a Behavioral Finance Model with Heterogeneous Agents Algorithmic Finance 1 (2011) 123–139 IOS Press

The paper introduces the phenomenon of under reaction and overreaction in the market by using heterogeneous agent model^[a] and stability in the prices are assessed using control theory. The basic model in this assumes two agents chartist and fundamentalist whose demand functions are arrived at by using mean variance portfolio optimizations^[c]. Different agents differ in their weights which is derived by multinomial logit model^[see appendix]. The expectation of chartists and fundamentalist are modeled based on knowledge of true fundamental value and moving average rule respectively^[d].

The classical control theory is then applied to the model with several simplification to take care of non-linearity^[e]. When variables are observed in frequency domain, we get for first order fundamentalist system. Under reaction stronger when

- Price adjustment^[b] speed is low
- Low aggressiveness of fundamental agent
- High overall risk aversion

For second order chartist system

- 1) Under reaction
 - Low Price adjustment speed
 - Low aggressiveness of fundamental agent
 - High overall risk aversion

- Low aggressiveness of chartist agent
- 2) Overreaction
 - High Price adjustment speed
 - Low liquidity
- 3) Instability
 - High price adjustment speed
 - High chartist aggression
 - Low overall risk aversion

[a] exhibit bounded rationality and heterogeneous beliefs

[b] Finite price adjustment speed assumed

[c] Zero net supply in market clearing

[d] Degree of rationality in choosing a strategy taken into consideration while framing demand function

[e] Continuous time function assumed for simplifying calculations.

Wieland Cristian, Westerhoff Frank H. (2003) Exchange rate dynamics, central bank interventions and chaos control methods Journal of Economic Behavior & Organization Vol. 58 (2005) 117–132

The paper shows the usefulness of chaos control algorithms in improving the effectiveness central bank intervention in controlling the exchange rates^[a]. It basically goes into 3 different chaos control methods namely OGY (ott-Grebogi-yorke), DFC (delayed feedback control), and CF (constant feedback)^[see appendix]. The two strategies studied here are “leaning against the wind” and “targeting long run fundamentals”.

The performance of central bank is measured through volatility^[see appendix] and distortion.

OGY : Small wisely chosen swift kicks in the form of intervention tends to bring it near the desired unstable periodic orbit^[b]. The level of intervention in the small neighborhood is determined using the intervention level of the central bank. However, leaning against the wind fails to calm down the exchange rates.

DFC : The feedback^[see appendix] perturbation applied is proportional to the deviation of the current state of the system from one period in past so that the control signal^[c] vanishes when stabilization is achieved.

CF : It simply varies the strength of the constant signal fed^[c] in the system in the form of intervention of bank. Choice of the type of signal positive or negative depends on the response of the system to the previously applied signal. Thus it helps a nation in carrying out “beggar thy neighbor” policy^[see appendix].

[a] The exchange rate p for period $t + 1$ is given as $p_{t+1} = p_t + cE[p_t]$,

[b] Periodic orbit which is dynamically unstable.

[c] Intervention from central bank in this case.

Feldman Todd (2011), Behavioral biases and investor performance Algorithmic Finance 1 (2011) 45–55 IOS Press

This paper shows the different behavioral traits that force person to trade excessively and simultaneously underperform in the market. Agent based approach has been used with each agent having different alpha^[a].

Four different groups of investor has been assumed with each having its different risk assumption.

Group 1:

- a) uses mean variance approach
- b) long run averages

Group 2:

- a) heavily weight current return
- b) Recency bias^[see appendix]

Group 3:

- a) more affected by losses
- b) loss averse^[see appendix]

- Group 4:
- hold on loss, sell wins
 - disposition effect^[see appendix]

II. RESULTS:

Group 4 trades most and 1 least. Even Group 2 trades more than Group 1. But Group 1 outperforms other groups in terms of long term return.

Louis K.C. Chan, Josef Lakonishok, and Bhaskaran Swami Nathan (2007), Industry Classifications and Return Comovement Financial Analysts Journal Volume 63 (56-70)

The paper takes a look into industry based classification of the stocks and the co-movement of returns associated. It considers two basic systems GICS^[see appendix] and Fama French system (based on SIC^[see appendix])

[a] ratio of portfolio holding of the agent.

Authors talks about various method of homogeneous stock grouping of which he claims industry affiliation being the most popular one. GICS being the system that takes not only operational characteristics but investors perception also into consideration while classifying the industry.

The methodology adopted here is that coincident movement of stock prices of the group is measured by pairwise correlation^[see appendix] In-group^[a] and that of the Out-group^[b]. Averaging of correlation^[c] is done over the group and then values obtained are used for arriving at the conclusion.

The results thus obtained were that co-movement in returns were stronger for large companies. Even the contaminations due to trading issues are less likely. GICS classification was found to be better due to more diversity of industry classification. This was observed through the contrast in in and out industry correlation.

Rachana Sharma (2012) Algorithmic Trading: A Study The international journal RJSITM: Volume: 01 (23-28)

The paper introduces us with the growth of algorithmic trading in India. It describes certain common algorithms used in the markets such as arrival price, time weighted average price (TWAP)^[see appendix], volume weighted average price (VWAP)^[see appendix], market-on-close (MOC), and implementation shortfall. It also throws some light on basic strategies that are used for developing the algorithm such as pair trading, delta neutral, arbitrage mean reversion and scalping. Author emphasizes on developing state of algorithm as the main challenge however she raises concern over certain aspects like lack of visibility, unfair advantages to the institutional investors, and selection of appropriate algorithm. She then compares Algorithms with human saying that they cannot replicate the gut feel element of human nature wherein they decide on the strategy on whether to be more aggressive or subdued. Also human reaction to an unexpected situation is better than an algorithm.

Domowitz Ian (2005), The Cost of Algorithmic Trading: A First Look at Comparative Performance

Algorithmic Trading: Precision, Control, Execution Institutional Investor, Inc. (1-23)

[a] $\rho_{ij} = \frac{\sum_{j \in I, j \neq i} \rho_{ij}}{N-1}$, pairwise correlations between stock i's return and the return on each of the other members of its industry.

[b] $\phi_{ii} = \frac{\sum_{j \in I} \rho_{ij}}{K-N}$. The average pairwise correlation between stock i's return and the returns of all other stocks not in its industry.

[c] $\bar{\rho}_I = \frac{\sum_{i=1}^K \rho_{ii}}{K}$ $\bar{\phi}_I = \frac{\sum_{i=1}^K \phi_{ii}}{K}$ Average correlation between a stock and other stocks

The author in this paper talks about media, its relation with finance and how it has penetrated into the market affecting the volatility. The importance of media has increased in recent time due to technological advances. The introduction of derivatives trading, multi-channel TV and pressure on the state to provide appropriate condition has fueled its growth. The growth of finance can also be observed by the number of financial publication, reporting of finance in mainstream media, and large scale advertising of financial products.

Media has also been dressing up financial news into entertainment so that more and more views gets attracted. Now the audience are more heterogeneous than before with greater level of literacy. Audiences are now more actively entering into information gathering industry.

Author concludes saying that finance has become more performative rather than a continuous activity of rational entity

W. H. Laverty, M. J. Miket and I. W. Kelly (2002), Simulation of Hidden Markov Models with EXCEL
Journal of the Royal Statistical Society. Series D (The Statistician), Vol. 51, No. 1(2002), pp. 31-40, Wiley

The paper illustrates the simulation of equation that are used for hidden markov model^[Ref] in excel. The functions of excel is slightly limited when compared to other high end software that are designed specifically for carrying out extensive calculation. However through this paper author has not only provided valuable aid for learning but also it has led understanding of basic of excel concept and to probability concepts.

Alvaro Cartey and Sebastian Jaimungal (2011) Modeling Asset Prices for Algorithmic and High Frequency Trading Forthcoming, Applied Mathematical Finance, SSRN (121-149)

In this paper author points out how the intraday dynamics of market has changed. The microstructure of the market is now different each and every second. This has also led to need of developing new algorithmic trading strategies. For this she has used hidden markov model to capture different states in which market can be at any time. These states are also important from the point of view of price change. Author has chosen 7 different stocks to show not only the change in the frequency of trading but also change in the fundamentals. HMM in this respect has advantage over other models as it also captures probabilities of states with zero price revision.

HENRIK HULT AND JONAS KIESSLING (2010) ALGORITHMIC TRADING WITH MARKOV CHAINS Department of Mathematics, KTH, Stockholm, Sweden

Author in this paper uses markov chains to study the evolution of the entire order book to design and understand optimal algorithmic trading strategies. The order book changes rapidly due to high number of and frequent orders being executed. Since these orders can be observed, it gives opportunity to use markov chain process to find out an efficient algorithm out of it. The author finally goes on to find that this method of optimization provides significant improvement in expected price for buying. He follows a method whereby parameters are selected and calibrated using historical data, optimal strategies are developed and then used to make trading decisions. Not only market buy/sell order but cancel order also play an important role.

Jeff Bilmes (2002) What HMMs Can Do UWEE Technical Report Number (UWEETR-2002-0003) January 2002

This paper mainly deals with finding new model that is better than hidden markov model in terms computational requirements as well as noise insensitivity. It starts by praising HMM, and displaying its capabilities but later turns towards reasoning its ability thoroughly. He shows its advantages in artificial speech recognition. He starts off with formal definition of HMM, then he compiles a list of properties that may or may not apply to HMM. Finally he concludes by presenting several alternatives to HMM.

12. Md. Rafiul Hassan and Baikunth Nath, **StockMarket Forecasting Using Hidden Markov Model: A New Approach** Computer Science and Software Engineering, The University of Melbourne, Carlton 3010, Australia

This paper shows the usage of HMM^[appen] for forecasting prices of specific market. Author has used airlines stocks. Further he adds the usage of HMM for predicting needs training of data. HMM interpolates the nearby values to forecast the future values. He further adds to it the advantages of HMM such as

- HMM has strong statistical foundation
- It is able to handle new data robustly

- Computationally efficient to develop and evaluate
- It is able to predict similar patterns efficiently

He concludes by appreciating the statistical foundation of HMM and expects future development in collaboration with artificial intelligence.

Patrik Idvall, Conny Jonsson(2008) Algorithmic Trading Hidden Markov Models on Foreign Exchange

Department of Mathematics, Linköping's University January 2008

Hidden markov model are used as a tool to forecast movements of time series data. Author points that out as one of the field along with other fields of application in the beginning. Further improvements in HMM are depicted like Gaussian mixture Model to enhance its prediction capability where one for each state assign a set of single Gaussians that are weighted together to replicate the density function of the stochastic process. Author has conducted his analysis on foreign exchange data and compared the results with Sharpe ratio.

He goes through derivation of HMM from Bayes theorem. He also thoroughly explains the chain problem. The three fundamental problems of decoding the chain, training and getting the most expected path has also been addressed. Extensions are also suggested here but later on he concluded that these extension are not of much advantage.

Barbara Resch, **Hidden Markov Models** Signal Processing and Speech Communication Laboratory
Inffeldgasse 16c

Author in this paper explains the hidden markov by taking some basic examples of weather change pattern and how to predict the future weather. Additionally he has explained the Viterbi algorithm^[appen] that is used to predict the sequence. The different orders of markovian chain have been dealt in this paper. The various terminology like transition probabilities emission probabilities and prior probabilities have been explained. He has also used trellis diagram to familiarize readers to the concept.

III. METHODOLOGY:

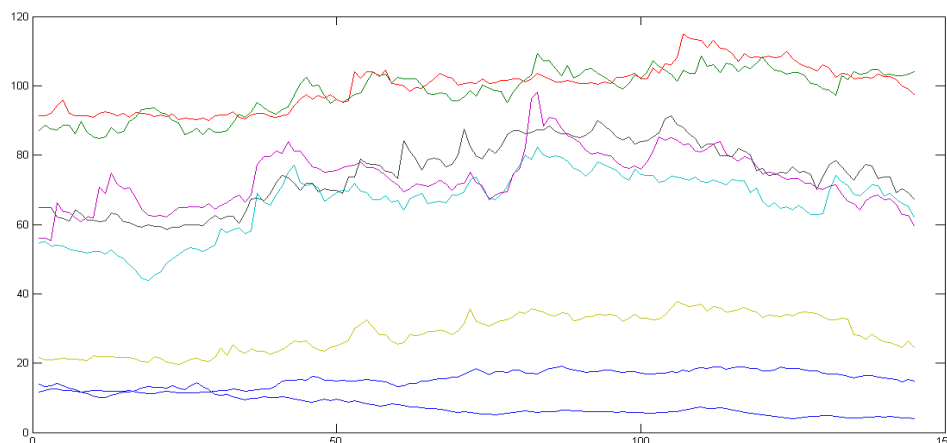
Principal component analysis is used to factor in more relevant variables form data sets. Then a hidden markov is used to generate trading rules.

IV. DATA PROCESSING AND ANALYSIS

Step 1:

Applying principal component analysis:

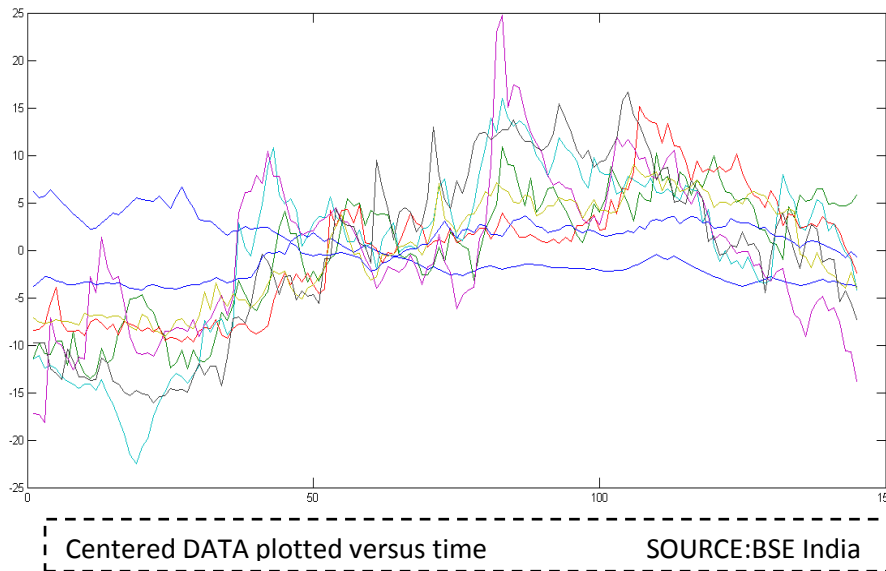
The actual data is distributed as given in the figure. Therefore for applying PCA. The data is centered first which is: the mean of the each data column is subtracted from each variable.



DATA plotted versus time

SOURCE: BSE India

The data so obtained after centering is

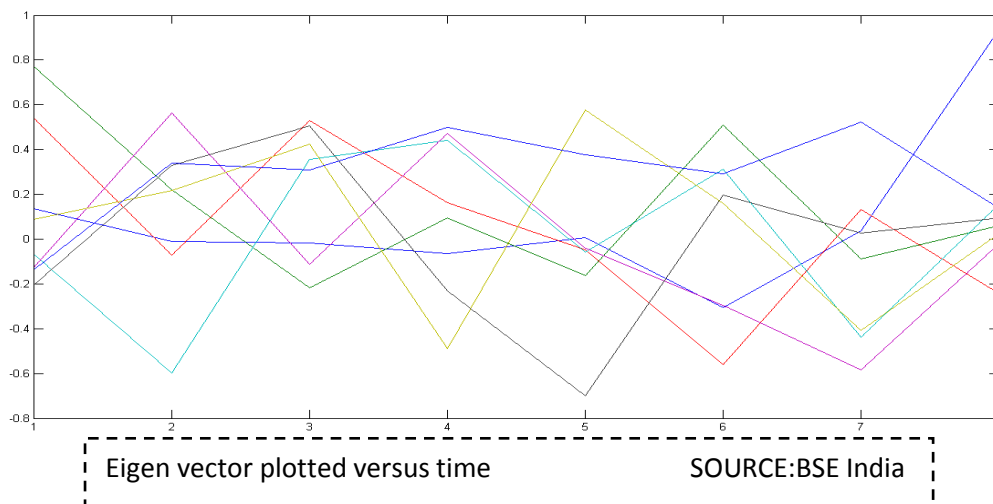


Next we find out the covariance matrix

8.712678	-16.1528	-14.8668	-19.7982	-9.59943	-12.8634	-20.8053	-6.24903
-16.1528	43.70523	35.87588	47.11569	31.55942	29.28417	48.66163	13.95813
-14.8668	35.87588	41.0498	38.42098	25.96126	31.11942	45.19926	13.96647
-19.7982	47.11569	38.42098	82.69685	55.71067	39.25421	75.88563	18.87618
-9.59943	31.55942	25.96126	55.71067	63.47724	29.17569	53.72267	12.77449
-12.8634	29.28417	31.11942	39.25421	29.17569	29.45039	45.12726	12.77348
-20.8053	48.66163	45.19926	75.88563	53.72267	45.12726	88.04748	20.17886
-6.24903	13.95813	13.96647	18.87618	12.77449	12.77348	20.17886	6.249111

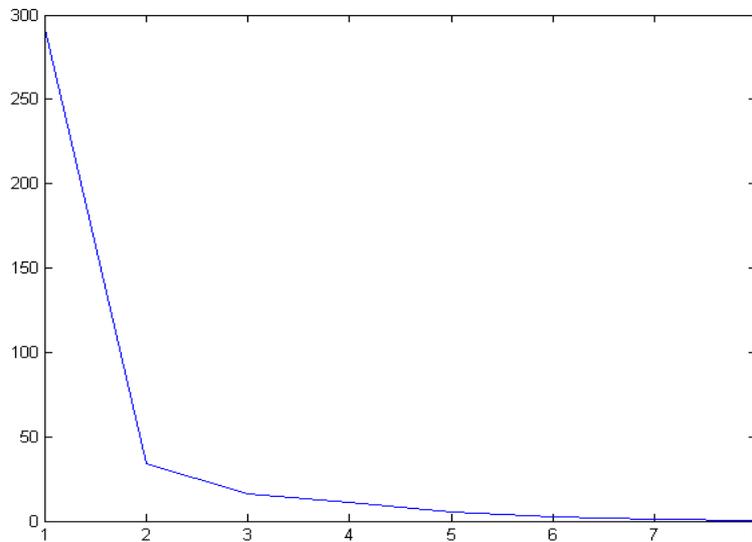
This covariance matrix is used to find out the Eigen vectors and Eigen values ^[see appendix] the plot of Eigen vector is as follows:

The Eigen values gives variance captured by that particular Eigen vector:



To find the number of components to be included we have created a screen plot^[append] and a cumulative percentage of variance captured by each of them.

In scree plot we take vectors till we observe the first shoulder. Since this is observed at 2nd component therefore we take 2 vectors as our feature vector.



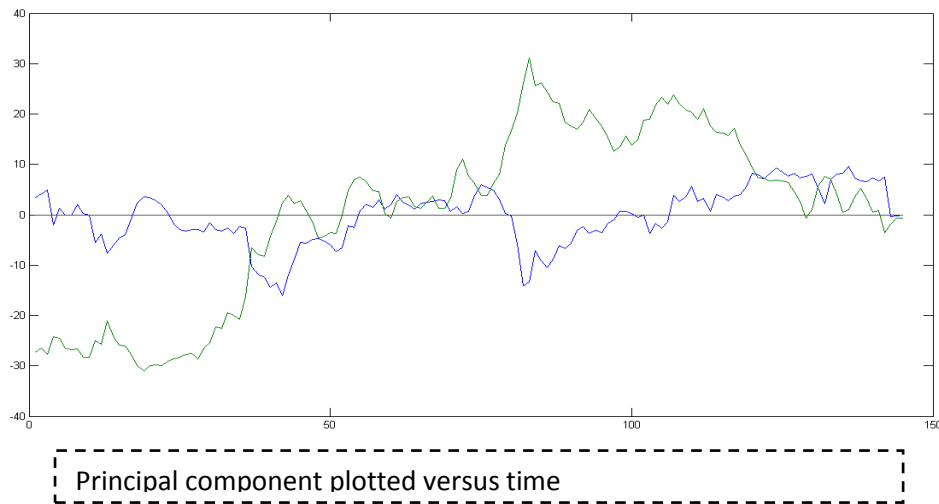
The % of variance captured by it is given by

Cum. Eigen value	Cumulative %
293.1557544	80.67275909
326.8911224	89.95630608
343.0592009	94.40555696
354.2048331	97.47269411
359.4493539	98.91591995
361.7485525	99.54863035
362.9599175	99.8819827
363.3887792	100

Cumulative% plotted vs. No. of components

Hence, we see that the first two component when arranged in decreasing order captures 89.95% variance. These are known as feature vector.

The plot of data on the first two component is:



Step 2:

Using the hidden Markov model, forecasting data so obtained:

This is done using the statistic toolbox of Matlab and functions like

```
[seq,states] = hmmgenerate (len, TRANS, EMIS)
```

```
PSTATES = hmmdecode(seq,TRANS,EMIS)
```

```
[TRANS,EMIS] = hmestimate(seq,states)
```

```
[ESTTR,ESTEMIT] = hmmtrain(seq,TRGUESS,EMITGUESS)
```

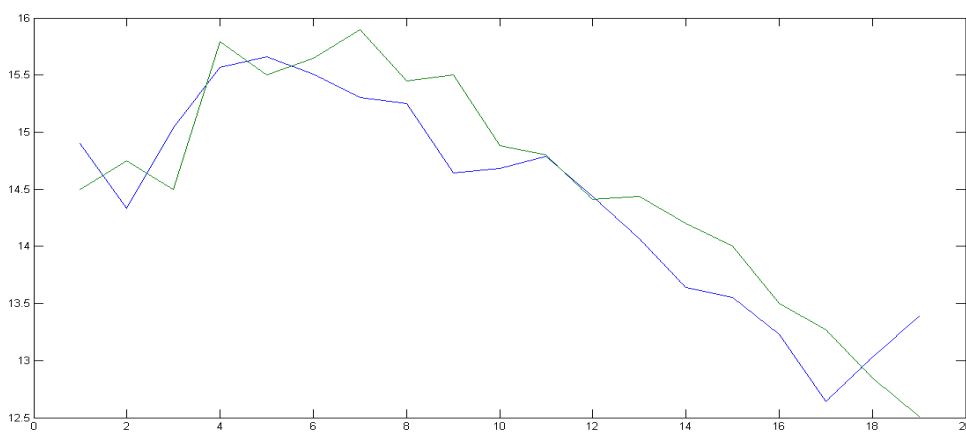
```
STATES = hmmiterbi(seq,TRANS,EMIS)
```

Where trans and emis are transition and emission matrix respectively^[appen.]

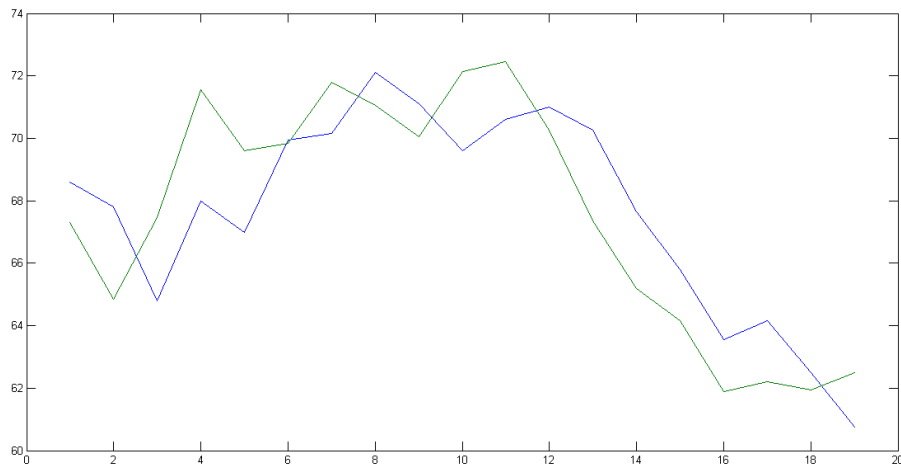
The data from 1 Aug 2012 to 28th Feb is used for training the model in `hmmtrain` function. This is then used in `hmmiterbi` to find out the most probable state. It is then fed in to `hmmgenerate` to generate the future sequence of data. Then `hmestimate` finds out Tran and emis based on the next iteration. This whole process is repeated until we get the complete sequence of forecasted data.

The forecasts for the two principal components that were obtained in PCA is given:

Actual (Green) Vs. Forecast (blue) graph for TV TODAY (March)



Actual (Green) Vs. Forecast (blue) graph for Zee News (March)



Similarly forecasts for all other firms were obtained and returns were calculated accordingly:

Step 3:

For calculating the return certain assumption were made and a simple trading rule was followed:

Assumptions:

- [1] The return is calculated for the month of March.
- [2] Transaction is executed only once in a day.
- [3] Buyer can sell/buy only 1 share at a time. (Even if he sells more than 1 share at a time we only need to multiply our calculation with that fixed value).
- [4] It is assumed that cost of equity for media industry (print/non-print) is fixed at 12.33% per annum.
- [5] Broker charges fixed rate of .55% of the selling/buying value as a transaction cost.
- [6] Buying/selling value is assumed to be the average price of scrip for that month.
- [7] If the price is expected to decrease in future then trader can short-sell thereby earning profit.

Trading rule: A filter of 2% is used for executing the trading signal. That is if the actual value of the next day is 2% more or less than the forecasted value then only trade is executed. It is carried out at the end of each day.

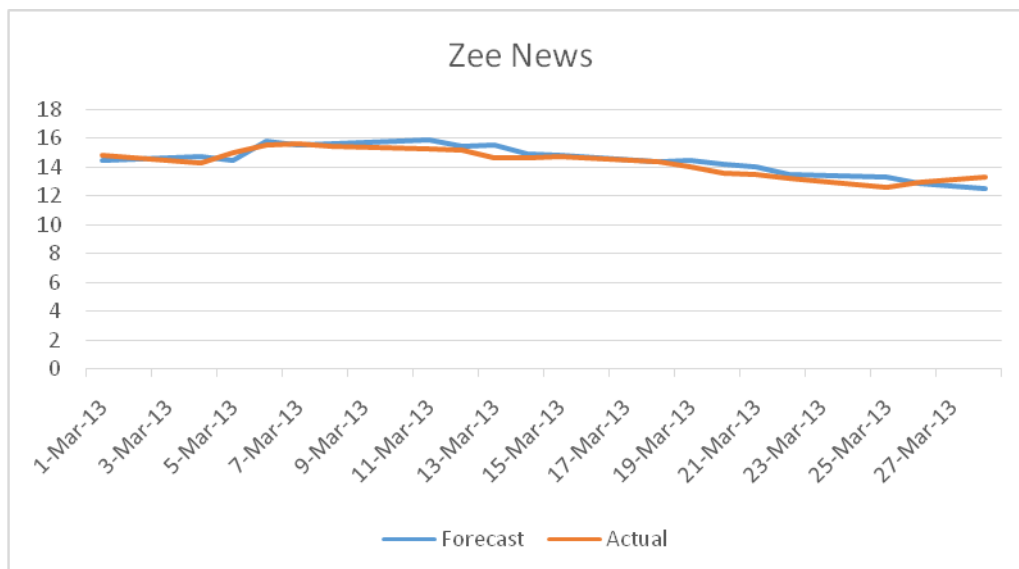
The blue band here denotes that filter rule is followed and individual made a gain from it whereas red band denotes loss due to incorrect forecasting.

Hence we see that if the (expected % change) is of the same sign as the (actual change) then it is profit for the trader whereas they being of opposite sign means loss. As the observation was opposite to that of expectation.

ZEE NEWS:

	Forecast	Actual	expected% change	Actual change
1-Mar-13	14.5	14.9	-1.01	-0.57
4-Mar-13	14.75	14.33	1.19	0.71
5-Mar-13	14.5	15.04	4.99	0.53
6-Mar-13	15.79	15.57	-0.45	0.09
7-Mar-13	15.5	15.66	-0.06	-0.15
8-Mar-13	15.65	15.51	2.51	-0.21
11-Mar-13	15.9	15.3	0.98	-0.05
12-Mar-13	15.45	15.25	1.64	-0.61
13-Mar-13	15.5	14.64	1.64	0.04
14-Mar-13	14.88	14.68	0.82	0.11
15-Mar-13	14.8	14.79	-2.57	-0.35
18-Mar-13	14.41	14.44	0.00	-0.37
19-Mar-13	14.44	14.07	0.92	-0.43
20-Mar-13	14.2	13.64	2.64	-0.09
21-Mar-13	14	13.55	-0.37	-0.32
22-Mar-13	13.5	13.23	0.30	-0.59
25-Mar-13	13.27	12.64	1.66	0.39
26-Mar-13	12.85	13.03	-3.99	0.36
28-Mar-13	12.51	13.39		

Gain	0.88	%gain	15.33%
loss	0.3		
Brokerage	0.396		
total gain	0.396		

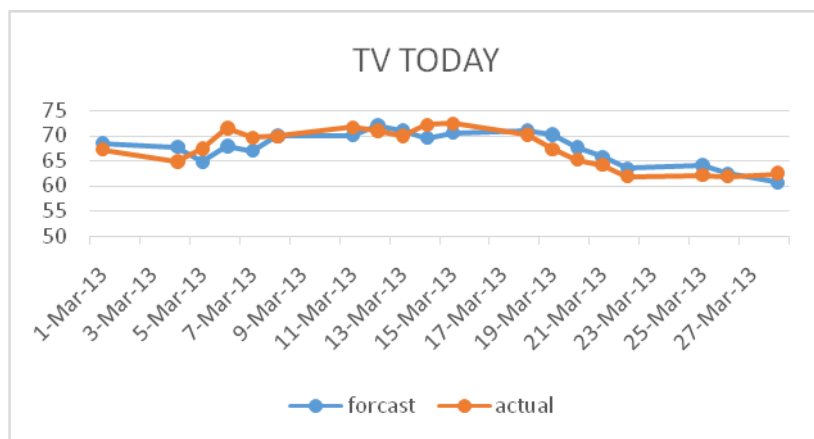


All figures in Rs. SOURCE: BSE India

TV TODAY:

	Forecast	Actual	expected% change	Actual change
1-Mar-13	68.6	67.3	0.74	-2.45
4-Mar-13	67.8	64.85	-0.08	2.6
5-Mar-13	64.8	67.45	0.82	4.1
6-Mar-13	68	71.55	-6.36	-1.95
7-Mar-13	67	69.6	0.50	0.25
8-Mar-13	69.95	69.85	0.43	1.95
11-Mar-13	70.15	71.8	0.42	-0.75
12-Mar-13	72.1	71.05	0.07	-1
13-Mar-13	71.1	70.05	-0.64	2.1
14-Mar-13	69.6	72.15	-2.15	0.3
15-Mar-13	70.6	72.45	-2.00	-2.2
18-Mar-13	71	70.25	0.00	-2.9
19-Mar-13	70.25	67.35	0.45	-2.15
20-Mar-13	67.65	65.2	0.92	-1.05
21-Mar-13	65.8	64.15	-0.94	-2.25
22-Mar-13	63.55	61.9	3.63	0.3
25-Mar-13	64.15	62.2	0.48	-0.25
26-Mar-13	62.5	61.95	-1.94	0.55
28-Mar-13	60.75	62.5		

Gain	4.45	% gain	47.32%
loss	0.03		
Brokerage	1.486		
total gain	2.664		

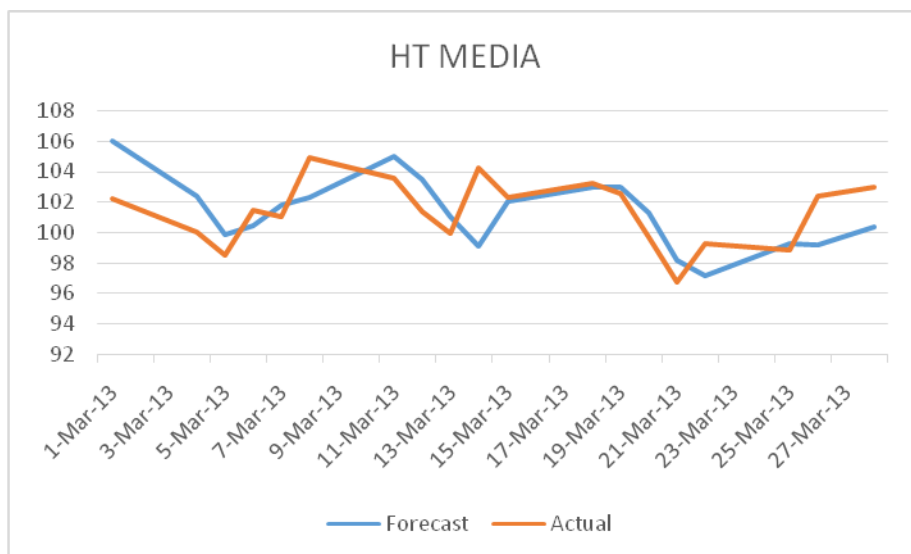


All figures in Rs. SOURCE: BSE India

HT MEDIA:

	Forecast	Actual	expected% change	Actual change
1-Mar-13	106	102.2	0.20	-2.2
4-Mar-13	102.4	100	-0.15	-1.5
5-Mar-13	99.85	98.5	1.93	2.95
6-Mar-13	100.4	101.45	0.34	-0.4
7-Mar-13	101.8	101.05	1.24	3.85
8-Mar-13	102.3	104.9	0.10	-1.35
11-Mar-13	105	103.55	-0.05	-2.2
12-Mar-13	103.5	101.35	-0.35	-1.45
13-Mar-13	101	99.9	-0.80	4.35
14-Mar-13	99.1	104.25	-2.11	-1.95
15-Mar-13	102.05	102.3	0.64	0.9
18-Mar-13	102.95	103.2	-0.19	-0.65
19-Mar-13	103	102.55	-1.27	-2.85
20-Mar-13	101.25	99.7	-1.50	-3
21-Mar-13	98.2	96.7	0.47	2.55
22-Mar-13	97.15	99.25	0.00	-0.45
25-Mar-13	99.25	98.8	0.40	3.55
26-Mar-13	99.2	102.35	-1.95	0.6
28-Mar-13	100.35	102.95	-100.00	-1.64

Gain	1.95	%gain	16.49%
loss	0		
Brokerage	0.557		
total gain	1.393		

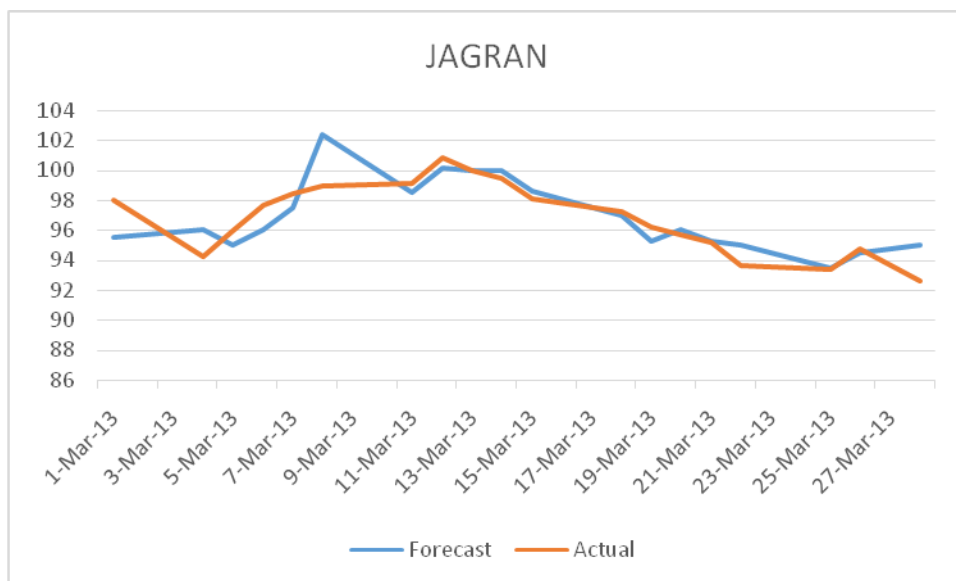


All figures in Rs. SOURCE: BSE India

JAGRAN:

	Forecast	Actual	expected% change	Actual change
1-Mar-13	95.5	98.05	-2.09	-3.75
4-Mar-13	96	94.3	0.74	1.7
5-Mar-13	95	96	0.05	1.7
6-Mar-13	96.05	97.7	-0.20	0.75
7-Mar-13	97.5	98.45	4.01	0.5
8-Mar-13	102.4	98.95	-0.45	0.15
11-Mar-13	98.5	99.1	1.06	1.75
12-Mar-13	100.15	100.85	-0.84	-0.85
13-Mar-13	100	100	0.00	-0.55
14-Mar-13	100	99.45	-0.85	-1.35
15-Mar-13	98.6	98.1	-1.12	-0.8
18-Mar-13	97	97.3	-2.06	-1.05
19-Mar-13	95.3	96.25	-0.21	-0.55
20-Mar-13	96.05	95.7	-0.47	-0.45
21-Mar-13	95.25	95.25	-0.26	-1.55
22-Mar-13	95	93.7	-0.27	-0.3
25-Mar-13	93.45	93.4	1.18	1.4
26-Mar-13	94.5	94.8	0.21	-2.15
28-Mar-13	95	92.65		

Gain	5.3	%gain	45.88%
loss	0		
Brokerage	1.597		
total gain	3.703		

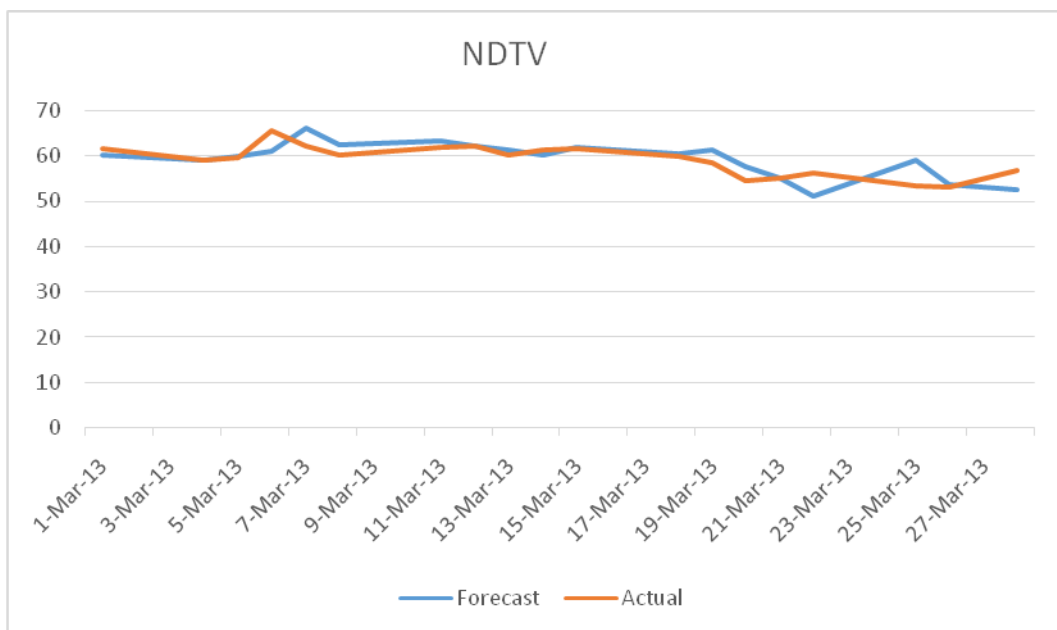


All figures in Rs. SOURCE: BSE India

NDTV:

	Forecast	Actual	expected% change	Actual change
1-Mar-13	60.1	61.6	-4.22	-2.6
4-Mar-13	59	59	1.69	0.7
5-Mar-13	60	59.7	2.18	5.95
6-Mar-13	61	65.65	0.91	-3.45
7-Mar-13	66.25	62.2	0.56	-1.85
8-Mar-13	62.55	60.35	5.05	1.6
11-Mar-13	63.4	61.95	0.32	0.25
12-Mar-13	62.15	62.2	-1.37	-1.9
13-Mar-13	61.35	60.3	0.00	1.1
14-Mar-13	60.3	61.4	0.90	0.3
15-Mar-13	61.95	61.7	-1.78	-1.7
18-Mar-13	60.6	60	2.08	-1.35
19-Mar-13	61.25	58.65	-1.62	-4.1
20-Mar-13	57.7	54.55	0.82	0.6
21-Mar-13	55	55.15	-7.52	1
22-Mar-13	51	56.15	5.08	-2.65
25-Mar-13	59	53.5	0.19	-0.35
26-Mar-13	53.6	53.15	-1.13	3.8
28-Mar-13	52.55	56.95	-100.00	-56.95

Gain	10.15	%gain	64.86%
loss	5		
Brokerage	1.952		
total gain	3.198		

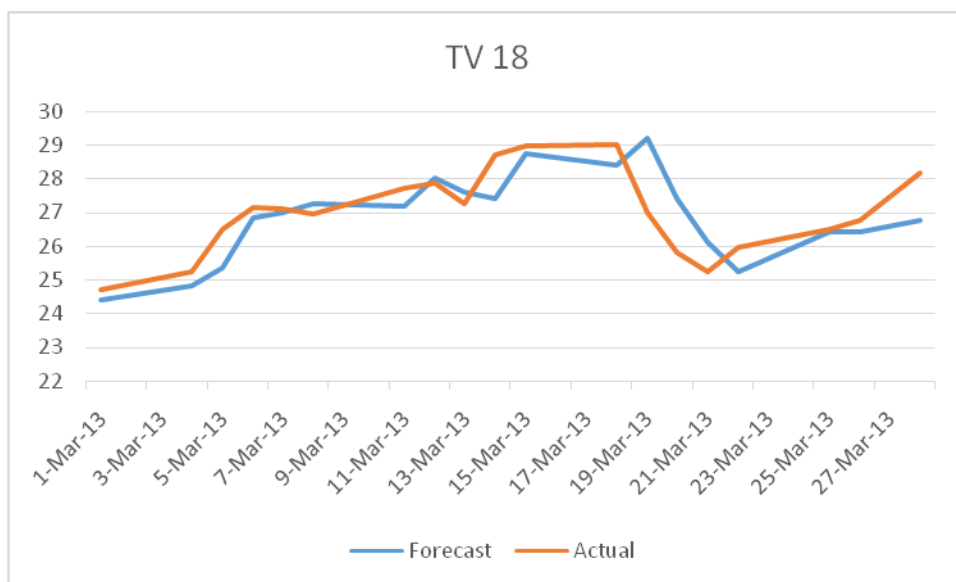


All figures in Rs. SOURCE: BSE India

TV 18:

	Forecast	Actual	expected% change	Actual change
1-Mar-13	24.4	24.7	0.40	0.55
4-Mar-13	24.8	25.25	0.40	1.25
5-Mar-13	25.35	26.5	1.32	0.65
6-Mar-13	26.85	27.15	-0.55	-0.05
7-Mar-13	27	27.1	0.55	-0.15
8-Mar-13	27.25	26.95	0.93	0.75
11-Mar-13	27.2	27.7	1.08	0.15
12-Mar-13	28	27.85	-0.90	-0.6
13-Mar-13	27.6	27.25	0.55	1.45
14-Mar-13	27.4	28.7	0.17	0.25
15-Mar-13	28.75	28.95	-1.90	0.05
18-Mar-13	28.4	29	0.69	-2
19-Mar-13	29.2	27	1.48	-1.2
20-Mar-13	27.4	25.8	1.16	-0.55
21-Mar-13	26.1	25.25	0.00	0.7
22-Mar-13	25.25	25.95	1.73	0.55
25-Mar-13	26.4	26.5	-0.38	0.25
26-Mar-13	26.4	26.75	0.00	1.4
28-Mar-13	26.75	28.15		

No transaction within this period

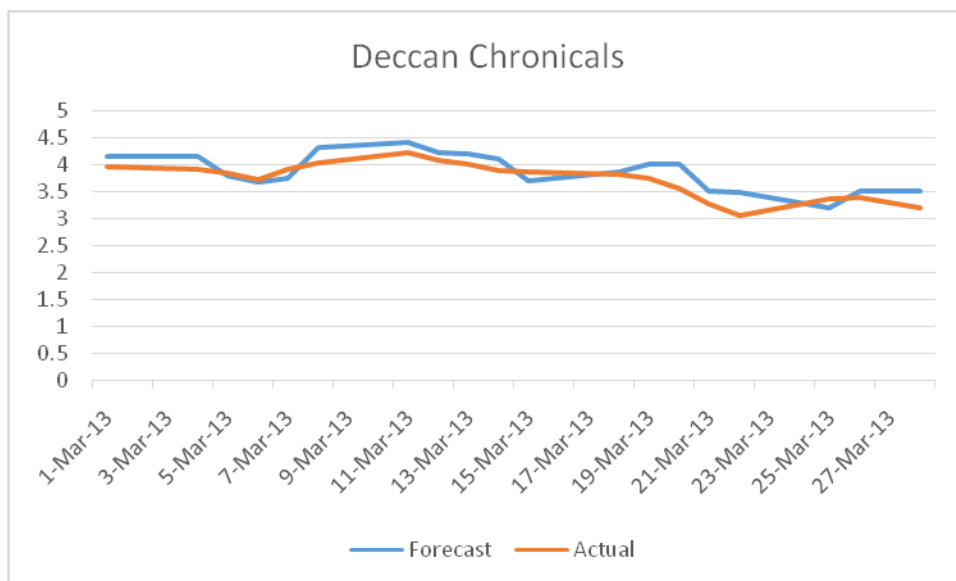


All figures in Rs. SOURCE: BSE India

Deccan Chronicles:

	Forecast	Actual	expected% change	Actual change
1-Mar-13	4.15	3.96	4.80	-0.05
4-Mar-13	4.15	3.91	-2.81	-0.08
5-Mar-13	3.8	3.83	-3.92	-0.11
6-Mar-13	3.68	3.72	0.81	0.19
7-Mar-13	3.75	3.91	9.97	0.12
8-Mar-13	4.3	4.03	9.18	0.18
11-Mar-13	4.4	4.21	0.00	-0.13
12-Mar-13	4.21	4.08	2.94	-0.09
13-Mar-13	4.2	3.99	2.76	-0.12
14-Mar-13	4.1	3.87	-4.39	-0.02
15-Mar-13	3.7	3.85	0.00	-0.04
18-Mar-13	3.85	3.81	4.72	-0.06
19-Mar-13	3.99	3.75	6.40	-0.19
20-Mar-13	3.99	3.56	-1.69	-0.28
21-Mar-13	3.5	3.28	6.40	-0.22
22-Mar-13	3.49	3.06	4.58	0.3
25-Mar-13	3.2	3.36	4.17	0.02
26-Mar-13	3.5	3.38	3.55	-0.19
28-Mar-13	3.5	3.19	-100.00	-3.19

Gain	0.83	%loss	121.00%
loss	0.92		
Brokerage	0.2867		
total gain	-0.3767		

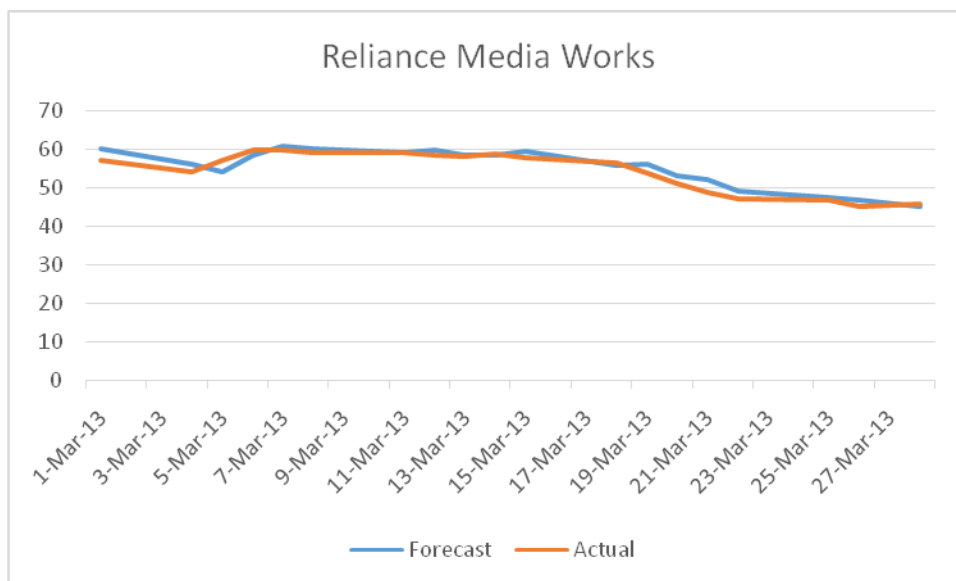


All figures in Rs. SOURCE: BSE India

RELIANCE MEDIA:

	Forecast	Actual	expected% change	Actual change
1-Mar-13	60	56.9	-1.58	-2.8
4-Mar-13	56	54.1	0.00	2.7
5-Mar-13	54.1	56.8	2.82	2.8
6-Mar-13	58.4	59.6	2.01	-0.15
7-Mar-13	60.8	59.45	0.93	-0.55
8-Mar-13	60	58.9	0.17	0.1
11-Mar-13	59	59	1.36	-0.6
12-Mar-13	59.8	58.4	0.17	-0.5
13-Mar-13	58.5	57.9	0.86	0.75
14-Mar-13	58.4	58.65	1.36	-0.95
15-Mar-13	59.45	57.7	-3.64	-1.45
18-Mar-13	55.6	56.25	-0.44	-2.55
19-Mar-13	56	53.7	-1.21	-2.65
20-Mar-13	53.05	51.05	1.86	-2.45
21-Mar-13	52	48.6	0.82	-1.45
22-Mar-13	49	47.15	0.11	-0.4
25-Mar-13	47.2	46.75	0.00	-1.65
26-Mar-13	46.75	45.1	-0.22	0.8
28-Mar-13	45	45.9		

Gain	4.25	%gain	70.79%
loss	0.15		
Brokerage	0.8961		
total gain	3.2		



OBSERVATION:

All figures in Rs. SOURCE:BSE India

Scrip	No. of transaction	% Gain
Deccan Chronicles	14	-121
TV 18	0	0
NDTV	6	64.86
JAGRAN	3	45.88
HT MEDIA	1	16.49
ZEE NEWS	5	15.33
TV TODAY	4	47.32
Reliance Media	3	70.79

CONCLUSION:

- [1] We see that we almost always get positive returns and that too more than the market cost of equity (12.33%)
- [2] In two cases of Deccan chronicles and TV 18 we see that we could not satisfy the investor. The possible explanation for this can be the excessive number of order executed in the case of Deccan chronicles and no orders executed for TV 18.
- [3] These two problems can be dealt with by adjusting the filter value.
- [4] The general trend in the return on equity is around 40%. This is quite overoptimistic mainly because of the low transaction cost of 0.55% per sale value assumed.
- [5] The two principal components of media industry ZEE NEWS and TV TODAY show an average return of 31.25% which sufficient enough for this algorithm comprising of HMM and filter rule to be used in this industry.

APPENDIX

DATA:

All figures in Rs. SOURCE: BSE India

Date	Deccan Chronicals	HT MEDIA	JAGRAN	NDTV	Reliance Media Works	TV 18	Tv Today	Zee News
1-Aug-12	13.95	86.95	91.3	54.75	56.15	21.55	64.8	11.64
2-Aug-12	13.3	88.55	91.4	55.1	56.05	21.05	64.85	12.05
3-Aug-12	13.55	87.4	91.95	53.8	55.25	21	64.85	12.64
6-Aug-12	14.2	87.35	94.2	54.1	66.3	21.1	62.15	12.51
7-Aug-12	13.5	88.7	95.9	53.7	63.7	21.35	61.6	12.2
8-Aug-12	12.85	88.75	92.1	52.85	63.4	21.15	60.95	12.12
9-Aug-12	12.25	86.2	91.25	52.4	62	21.15	64.15	11.83
10-Aug-12	11.65	89.75	91.25	52.1	60.85	20.95	63	11.76
13-Aug-12	11.1	86.55	91.35	51.65	62.1	20.8	61.3	11.85
14-Aug-12	10.55	85.35	90.8	52.1	61.95	22	61.25	12.05
16-Aug-12	10.05	84.8	92.15	52.1	70.65	21.75	60.9	12.05
17-Aug-12	10.15	85.35	92.55	51.4	68.95	21.8	61	11.82
21-Aug-12	10.65	88	92.05	52.55	74.8	21.85	63.25	11.88
22-Aug-12	11.15	86.4	91.45	51.1	71.65	21.55	62.8	12
23-Aug-12	11.7	86.9	92	50.05	70.35	21.7	60.75	11.9
24-Aug-12	11.55	89.85	90.9	48.45	70.6	21.7	60.5	12.01
27-Aug-12	12.1	90.95	92.3	46.85	67.7	21.25	59.65	11.72
28-Aug-12	12.7	93.2	91.95	44.6	64.35	20.6	59.25	11.46
29-Aug-12	13.3	93.3	91.75	43.7	62.65	20.25	59.85	11.31
30-Aug-12	13.1	93.65	91.2	45.45	62.45	21.95	59.45	11.22
31-Aug-12	13	92.35	91.65	46.35	62.65	21.5	59.4	11.74
3-Sep-12	12.9	91.75	91.1	48.7	62.25	20.2	58.55	11.81
4-Sep-12	13.54	90.05	91.75	50.2	63.4	20	59.15	11.61
5-Sep-12	12.87	89.35	90.25	51.25	64.85	19.6	59.3	11.42
6-Sep-12	12.23	85.9	90.6	52.6	64.85	20.2	60	11.44
7-Sep-12	13.45	86.5	90.5	53.25	65.2	21.25	59.85	11.37
8-Sep-12	14.48	87.75	90.15	52.85	65.15	21.45	59.9	11.48
10-Sep-12	13.26	85.85	90.65	52.2	64.9	20.65	59.7	11.73
11-Sep-12	12.25	87.8	90.1	53	66.05	20.45	61.3	11.76
12-Sep-12	11.03	86.65	91.25	53.95	64.35	21.6	62.7	11.82

13-Sep-12	10.84	86.55	91.6	58.75	65.5	24.25	61.45	12.09
14-Sep-12	10.9	87.1	91.55	57.55	66.15	22.4	62.4	12.19
17-Sep-12	10.36	89.3	92.5	58.6	67.55	25.2	62.4	12.52
18-Sep-12	9.85	91.8	90.85	58.95	68.6	23.65	60.35	12.25
20-Sep-12	9.36	90.9	90.5	57.3	66.55	22.75	63.3	11.95
21-Sep-12	9.82	92.5	91.5	58.1	68.5	24.1	67.4	12.14
24-Sep-12	9.85	95.15	92	69.05	77.3	23.45	67.55	12.43
25-Sep-12	10.34	93.65	91.95	66.4	79.5	23.45	66.95	12.48
26-Sep-12	9.98	92.4	91.2	65.55	79.55	22.55	68.8	12.55
27-Sep-12	10.12	91.9	91	68.4	81.25	23.15	72.1	13.39
28-Sep-12	10.22	93.2	91.35	71.05	80.4	23.9	74.15	14.72
1-Oct-12	10.16	93.9	91.8	75.05	83.8	25.1	73.45	15.16
3-Oct-12	9.71	97.2	94.4	77	81.2	26.4	71.9	15.06
4-Oct-12	9.49	100.75	96.1	72.05	81.2	26.15	69.95	15.31
5-Oct-12	9.03	102.4	97.5	71.1	78.8	26.4	71.8	14.96
8-Oct-12	8.73	100.05	96.1	71.65	76.55	24.7	71.95	16.24
9-Oct-12	9.12	100.1	97.25	70.45	76.15	23.95	69.35	15.89
10-Oct-12	9.53	97.25	96.4	66.65	74.95	23.5	70.35	15.08
11-Oct-12	9.15	94.95	97.4	67.7	75.35	24.65	69.75	15.05
12-Oct-12	9.6	96.05	96.15	69.1	75.45	25	69.9	14.82
15-Oct-12	9.13	95.1	95.2	69.75	76.4	25.75	68.95	15.05
16-Oct-12	8.71	96.45	95.65	69.65	76.8	26.7	73.75	14.94
17-Oct-12	9.1	97.4	103.95	71.85	77.2	30	73.7	14.87
18-Oct-12	8.67	98	102.25	69.7	77.9	31.2	78.95	15.07
19-Oct-12	8.34	101.1	104	69.2	76.5	32.4	77.55	15.2
22-Oct-12	7.93	103.7	104.05	67.1	76.35	30.4	77.25	14.96
23-Oct-12	7.54	102.95	102.7	67.1	75.4	28.2	77.1	14.85
25-Oct-12	7.91	103.3	104.5	68.3	74.1	28.3	75.35	14.63
26-Oct-12	8.3	100.95	100.55	66.4	72.55	26.35	75	13.9
29-Oct-12	8.06	102.5	100.4	67	71.45	25.5	73.25	13.25
30-Oct-12	7.78	102	99.9	64.15	69.4	25.9	84.05	13.39
31-Oct-12	7.46	102.1	98.45	67.35	70.25	28.25	81.2	14.05
1-Nov-12	7.29	102	99.5	68.2	71.65	28.05	79	14.22
2-Nov-12	7.2	100.2	99.35	69.05	71.4	28.25	75.7	14.76
5-Nov-12	6.96	97.8	100.6	66	71.05	29	78.6	14.87

6-Nov-12	6.87	97.5	102.1	66.5	71.65	29.15	79.1	15.38
7-Nov-12	6.68	97.95	103.65	66.6	72.85	29.6	78.65	15.55
8-Nov-12	6.42	97.6	102.65	66.3	71.6	29.05	76.55	15.55
9-Nov-12	6.1	95.7	102.25	68.45	69.8	28.15	77.35	16.04
12-Nov-12	5.8	95.7	100.15	68.6	71.65	29.35	80.15	16
13-Nov-12	6.09	96.7	100.65	69.4	71.95	31.3	87.6	16.79
15-Nov-12	5.79	98.6	100.9	72.85	75.05	35.65	82.5	17.62
16-Nov-12	5.51	97	100.55	73.7	72.15	32	79.9	18.5
19-Nov-12	5.24	100.25	102.1	70.4	71.1	31.4	78.95	17.58
20-Nov-12	5.25	99.35	100.55	67.55	67.2	30.6	81.9	16.72
21-Nov-12	5.1	98.7	100.85	67.15	68.6	31.6	80.6	17.54
22-Nov-12	5.35	98.45	101.55	68.8	69.25	32.35	82.6	17.6
23-Nov-12	5.59	95.15	101.45	70.95	69.45	32.45	85.85	17.23
26-Nov-12	5.85	98.05	102.1	74.45	74.7	33.5	86.95	18.07
27-Nov-12	6.09	100.45	102.1	76.95	75.85	34.85	87	17.98
29-Nov-12	6.13	101.85	101	80.15	82.4	34.35	86.25	17.1
30-Nov-12	5.96	103.1	101.95	78.65	96.4	35.75	86.7	17.07
3-Dec-12	5.78	109.2	103.65	82.2	98.15	35.1	87.3	16.9
4-Dec-12	5.95	107.3	102.75	80.15	88.45	34.85	87.3	17.7
5-Dec-12	6.08	107.2	102.05	79.3	90.85	33.75	88.35	18.55
6-Dec-12	6.1	104.85	101.1	79.85	90.55	33.6	86.85	18.7
7-Dec-12	6.34	102.95	101.1	79.4	87.8	34.5	86.05	19.05
10-Dec-12	6.37	105.95	101.45	78.25	85.8	34.3	86.1	18.55
11-Dec-12	6.22	102.3	101.05	76.2	84.7	32.25	85.45	17.9
12-Dec-12	6.21	103.15	100.65	75.4	83.65	32.55	85.1	17.8
13-Dec-12	6.07	104.75	100.6	74	81.3	33.35	85.6	17.25
14-Dec-12	5.92	105	100.95	75.6	80.25	33.3	86.95	17.5
17-Dec-12	5.99	103.6	100.5	78.05	80.65	34.15	90.05	17.55
18-Dec-12	5.96	102.5	101.1	77.05	80	33.85	88.4	18
19-Dec-12	5.9	101.3	100.65	76.45	79.85	34	87.05	18
20-Dec-12	5.88	99.85	102.4	75.55	78.05	33.6	85.15	17.55
21-Dec-12	5.89	99.15	102.4	73.65	76.7	32	84.25	17.25
24-Dec-12	5.76	100.75	102.95	72.75	76.15	33.05	85.15	17.55
26-Dec-12	5.83	103.15	103.5	75.95	76.9	34	83.3	17.45
27-Dec-12	5.71	102.3	101.9	74.45	76.05	32.9	83.9	17.1

28-Dec-12	5.55	103.75	101.95	74.15	78.05	32.85	84.05	16.9
31-Dec-12	5.61	107.15	105.1	74.2	81.25	32.55	85.25	16.95
1-Jan-13	5.68	105.7	103.6	72.1	85.3	32.75	86.4	17.15
2-Jan-13	5.69	104.6	106.35	72.5	84.35	33.95	90.35	17.15
3-Jan-13	5.9	103.25	106.1	74	85.05	35.95	91.25	17.45
4-Jan-13	6.11	101.4	108	73.6	84.25	37.7	88.8	17.25
7-Jan-13	6.38	104.4	114.95	73.25	83	36.95	87.85	17.95
8-Jan-13	6.69	103.6	113.8	72.85	83.15	36.35	86.25	17.6
9-Jan-13	7.02	103.5	113.35	73.75	81.25	36.55	84.9	18.45
10-Jan-13	7.37	108.55	113.15	72.3	80.9	36.95	82	18.7
11-Jan-13	7.01	105.65	111.05	72.15	81.9	34.95	83.15	18.5
14-Jan-13	6.83	106.05	113.1	72.7	83.15	36.25	83.3	18.9
15-Jan-13	7.17	103.9	110.8	72.05	83.95	35.95	79.7	18.95
16-Jan-13	6.82	106.55	110.65	71.4	80.2	34.85	79.85	18.25
17-Jan-13	6.48	106	109.15	73	79.35	35.05	79.5	18.65
18-Jan-13	6.16	104.15	107	72.55	78.3	35.45	81.9	18.95
21-Jan-13	5.86	105.7	109.15	72.5	79.55	36.1	81.1	18.9
22-Jan-13	5.57	105	108	69.15	78.85	35.1	80	18.35
23-Jan-13	5.3	106.55	108.3	70.45	76.95	34.75	75.55	18.4
24-Jan-13	5.04	108.3	108	66.6	74.5	33.15	76.1	17.75
25-Jan-13	4.79	106	108.55	65	75.05	33.75	74.1	17.85
28-Jan-13	4.56	104.5	108	66.15	74.75	33.7	74.3	17.95
29-Jan-13	4.34	104.3	108.35	64.75	73.95	33.4	75.1	18.8
30-Jan-13	4.13	103.35	109.95	65.15	73.1	34	74.9	18.4
31-Jan-13	3.93	103.75	107.9	64.3	73.25	33.55	76.55	18.35
1-Feb-13	4.12	103.75	106.6	65.5	73.3	34.55	75.15	18.35
4-Feb-13	4.32	102.8	105.55	64.1	71.8	34.8	75.3	18.05
5-Feb-13	4.53	100.55	105.2	62.85	71.95	34.55	74.4	17.7
6-Feb-13	4.75	100.45	104.25	62.75	70.6	34.35	70.1	17.85
7-Feb-13	4.98	99.1	106.05	63.05	70.15	33.4	73.9	17.15
8-Feb-13	4.76	98.9	105.15	69.35	71.05	32.5	77.1	16.9
11-Feb-13	4.53	97.3	102.4	74.2	71.5	32.6	78.55	16.85
12-Feb-13	4.31	102.85	103.55	72.3	68.8	33.05	76.6	16.55
13-Feb-13	4.23	101.75	103.4	71.3	66.7	32.8	74.5	16.2
14-Feb-13	4.1	104.15	102.05	68.65	66.1	28.2	72.7	15.7

15-Feb-13	4.12	103.45	102.25	68.35	64.3	27.95	75.4	16.25
18-Feb-13	4.32	103.6	102.55	69.8	66.9	26.85	77.3	16.4
19-Feb-13	4.52	104.75	102.25	71.5	67.95	28.4	76.85	16.35
20-Feb-13	4.7	104.8	103.3	71.1	68.55	27.1	73.35	16
21-Feb-13	4.47	103.15	102.65	68.2	67.05	26.25	73.7	15.75
22-Feb-13	4.55	103.25	102.6	69	67.35	26	73.6	15.45
25-Feb-13	4.33	103	101.7	67.3	65.8	25.25	69.15	15.2
26-Feb-13	4.12	103	100	65.95	62.75	24.65	70.3	14.6
27-Feb-13	4.12	103.25	99	65.25	62.7	26.35	69.1	15.3
28-Feb-13	3.96	104.1	97.4	62.05	59.6	24.65	67.3	14.75

CONVARIANCE MATRIX:

8.712678	-16.1528	-14.8668	-19.7982	-9.59943	-12.8634	-20.8053	-6.24903
-16.1528	43.70523	35.87588	47.11569	31.55942	29.28417	48.66163	13.95813
-14.8668	35.87588	41.0498	38.42098	25.96126	31.11942	45.19926	13.96647
-19.7982	47.11569	38.42098	82.69685	55.71067	39.25421	75.88563	18.87618
-9.59943	31.55942	25.96126	55.71067	63.47724	29.17569	53.72267	12.77449
-12.8634	29.28417	31.11942	39.25421	29.17569	29.45039	45.12726	12.77348
-20.8053	48.66163	45.19926	75.88563	53.72267	45.12726	88.04748	20.17886
-6.24903	13.95813	13.96647	18.87618	12.77449	12.77348	20.17886	6.249111

Eigen Value Matrix:[Error! Not a valid link.](#)

Eigen vectors:

-0.13748604	-0.205821768	0.088058	-0.12919	-0.06564	0.542803	0.772436	0.136705
0.339571377	0.328533177	0.216655	0.565276	-0.59703	-0.0726	0.220082	-0.01116
0.308978617	0.506276332	0.423626	-0.11335	0.356676	0.53049	-0.21671	-0.01764
0.500514006	-0.232230465	-0.48958	0.470383	0.441664	0.161972	0.096567	-0.06306
0.375985206	-0.701145855	0.576667	-0.04127	-0.05686	-0.04805	-0.16488	0.007182
0.293139092	0.19520635	0.158767	-0.29663	0.312518	-0.55917	0.509809	-0.30417
0.523947651	0.025896556	-0.40938	-0.58282	-0.43707	0.131975	-0.0873	0.038242
0.13412781	0.095262675	0.028505	-0.01704	0.158191	-0.24503	0.062496	0.939608

REFERENCES

- [1] Fischer Thomas (2011), *News Reaction in Financial Markets within a Behavioral Finance Model with Heterogeneous Agents* Algorithmic Finance 1 IOS press (123-139)
- [2] Wieland Cristian, Frank H. Westerhoff (2005) *Exchange rate dynamics, central bank interventions and chaos control methods* Journal of Economic Behavior & Organization Vol. 58 117–132
- [3] Feldman ,Todd (2011), *Behavioral biases and investor performance* Algorithmic Finance 1 (2011) IOS Press (45-55)
- [4] Louis K.C. Chan, Josef Lakonishok, and Bhaskaran Swaminathan(2007), *Industry Classifications and Return Comovement* Financial Analysts Journal Volume 63 (56-67)
- [5] Sharma Rachana (2012) *Algorithmic Trading: A Study* The international journal RJSITM: Volume: 01 (23-28)
- [6] Domowitz Ian (2005), *The Cost of Algorithmic Trading: A First Look at Comparative Performance* Algorithmic Trading: Precision, Control, Execution Institutional Investor, Inc. (1-23)

- [7] Clark Gordon L. Clark, Nigel Thrift (2004) *Performing finance: the industry, the media and its image International Political Economy*, May 2004 (289-310)
- [8] W. H. Laverly, M. J. Miket and I. W. Kelly (2002), *Simulation of Hidden Markov Models with EXCEL* Journal of the Royal Statistical Society, Series D (The Statistician), Vol. 51, No. 1(2002), pp. 31-40, Wiley
- [9] Alvaro Cartea and Sebastian Jaimungal (2011) *Modeling Asset Prices for Algorithmic and High Frequency Trading* Forthcoming, Applied Mathematical Finance, SSRN (121-149)
- [10] Henrik Hult And Jonas Kiessling (2010) *Algorithmic Trading With Markov Chains* Department of Mathematics, KTH, Stockholm, Sweden pp.1-35
- [11] Jeff Bilmes (2002) *What HMMs Can Do* UWEE Technical Report Number (UWEETR-2002-0003) January 2002, pp.1-45
- [12] Md. Rafiul Hassan and Baikunth Nath, *Stock Market Forecasting Using Hidden Markov Model: A New Approach* Computer Science and Software Engineering The University of Melbourne, Carlton 3010, Australia ,pp.1-18
- [13] Patrik Idvall, Conny Jonsson(2008) *Algorithmic Trading Hidden Markov Models on Foreign Exchange* Department of Mathematics, Linkoping's University January 2008
- [14] Barbara Resch, *Hidden Markov Models* Signal Processing and Speech Communication Laboratory Inffeldgasse pp.1-32
- [15] Cars Homes, *Heterogeneous Agent Models in Economics and Finance*
- [16] Andre Christoer Andersen, Stian Mikelsen *A Novel Algorithmic Trading Framework Applying Evolution and Machine Learning for Portfolio Optimization*
- [17] von der Fakult'at fuer Wirtschaftswissenschaften des Karlsruher Instituts fuer Technologie ,*Theoretical and Practical Aspects of Algorithmic Trading*
- [18] Willy Hereman ,*The Tanh Method: A Tool to Solve Nonlinear Partial Differential*
- [19] Ying So, Warren F. Kuhfeld, *Multinomial Logit Models*
- [20] Selçuk Emiroğlu et al. ,*Control of a chaotic finance system with passive control*
- [21] Kestutis Pyragas(2006), *Delayed feedback control of chaos*
- [22] S. Parthasarathy and Somdatta Sinha, *Controlling chaos in unidimensional maps using constant feedback*

Petro-Physical Analysis Of Reservoir Rock Of Fenchuganj Gas Field (Well#03) Using Wireline Log

Shamim Ahammod¹, Md. Abdul Hai², *Dr. Md. Rafiqul Islam², S.M Abu Sayeem²

¹Department of Earth and Environmental Science, Wright State University, Dayton, OH 45324, USA

²Department of Petroleum & Mining Engineering, Shahjalal University of Science & Technology, Sylhet, Bangladesh, *BAS-TWAS Gold Medal Scientist-2013

ABSTRACT: The present paper highlights the results of a study conducted to determine and evaluate the petrophysical properties of Fenchuganj Gas Field, well#03 in Sylhet district of Bangladesh with a view to understand their effects on the reservoir hydrocarbon prospects and gas productivity of the field. The evaluated properties include porosity, permeability and fluid saturation which are all inferred from geophysical wireline logs. A suite of wireline logs comprising of gamma ray, spontaneous potential, caliper log, resistivity, neutron log, density log and sonic log for well # 03 from Fenchuganj Gas Field were analyzed for reservoir characterization of the field. The analysis carried out involves lithology identification and determinations of petrophysical parameters. Seven reservoirs zone namely: A, B, C, D, E, F and G were delineated with their tops and bases at depth from 1656 m to 2627 m. Computed petrophysical parameters across the reservoir gave porosity as ranging from 16 to 25%; permeability from 14 to 195 mili Darcy(md) and average hydrocarbon saturation of 86%, 35%, 57%, 52%, 47%, 97%, and 47% for reservoir zone A, B, C, D, E, F and G, respectively. These results suggest high hydrocarbon production potential and a reservoir system which performance is considered satisfactory for hydrocarbon production.

KEYWORDS: porosity, permeability, petrophysical properties, wireline logs.

I. INTRODUCTION

Petrophysics is the study of rock properties and their interactions with fluids (gases, liquid hydrocarbons and aqueous solutions). The amount of hydrocarbon present in a reservoir is a function of its porosity and its hydrocarbon saturation [1]. In addition, the efficiency, reservoir can perform, is function of its permeability. Table 1 provides an effective explanation of porosity and permeability description of reservoirs [2]. These parameters can be measured on core plugs, which are often considered as representing "ground truth." However, core plug measurements are also affected by errors. In addition, coring is very expensive and there is never any guarantee that the target reservoir won't be missed by the core, or that the full cored interval will be recovered. This is why wireline logs have become the primary source of data for petrophysical evaluation of reservoirs and are routinely recorded on every oil and gas well. . In this study the gamma ray (GR), spontaneous potential (SP), caliper log, resistivity log (LLD), and density (PHID) logs have been used to categorize the lithology of the prospective zones, differentiate between hydrocarbon bearing and non-hydrocarbon bearing zones and determine the values of petrophysical properties of the zones of interest (reservoir) in the field such as porosity, permeability, resistivity, water saturation and hydrocarbon saturation. The Fenchuganj Gas Field (FGF) is one of the largest gas fields of Bangladesh which is located in the northern-east part of the country (Figure 1). The major objective of the present study is to evaluate the petro-physical characterization of the reservoir rocks including the porosity, permeability and fluid saturation of the Fenchuganj Gas Field.

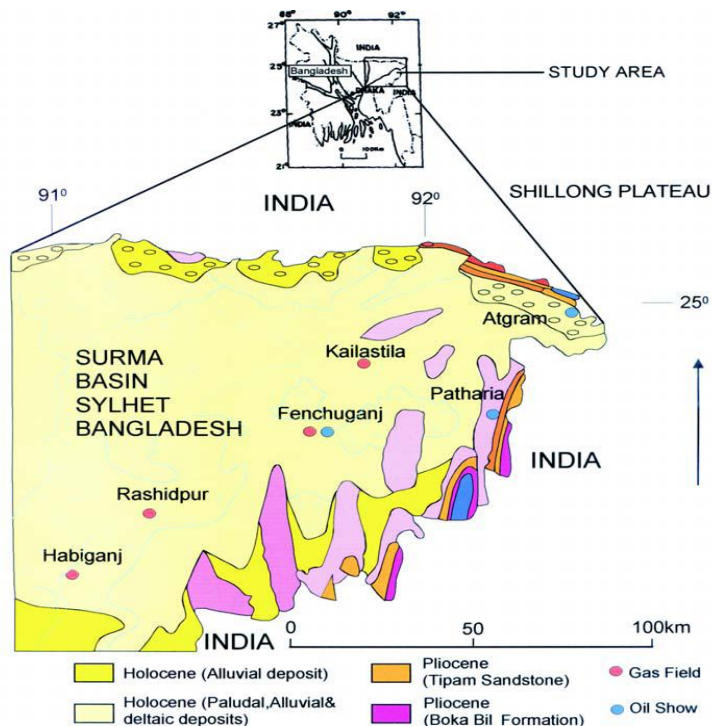


Figure 1: Geological map of Surma Basin, Sylhet, Bangladesh. Showing the location of Fenchuganj Gas Field.(after Alam et al. 1990 [3])

Table I: Porosity and Permeability values for Reservoirs Qualitative Description [2] (Adapted from Rider, 1986)

Qualitative Evaluation of Porosity	
Percentage Porosity (%)	Qualitative Description
0 - 5	Negligible
5 - 10	Poor
15 - 20	Good
20 - 30	Very Good
> 30	Excellent
Qualitative Evaluation of Permeability	
Average K Value (md)	Qualitative Description
< 10.5	Poor to fair
15 - 50	Moderate
50 - 250	Good
250 - 1000	Very Good
> 1000	Excellent

II. METHOD AND MATERIALS

LITHOLOGY IDENTIFICATION & PETROPHYSICAL ANALYSIS OF RESERVOIR ROCK

Reservoir rock :A rock capable of producing oil, gas and water is called a reservoir rock. In general, to be of commercial value, a reservoir rock must have sufficient thickness, areal extent and pore space to contain a large volume of hydrocarbons and must yield the contained fluids at a satisfactory rate when the reservoir is penetrated by a well. Any buried rock, be it sedimentary, igneous or metamorphic, that meets these conditions may be used as a reservoir rock by migrating hydrocarbons. Oil and gas fields are geological features that result from the coincident occurrence of four types of geologic features (Figures 2 and 3) [4]:

- (1) Source Rocks,
- (2) Reservoir Rocks,
- (3) Seals, and (4) Traps

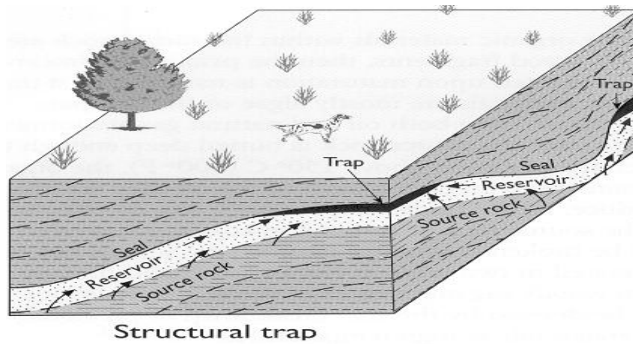


Figure 2: Structural Trap

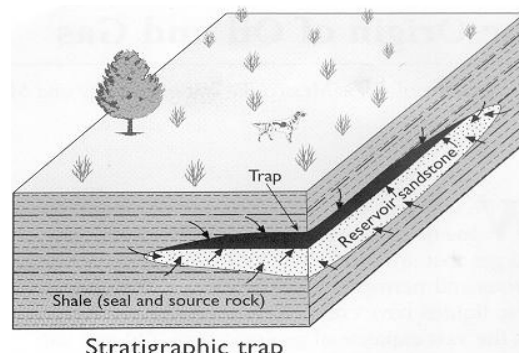


Figure 3: Stratigraphic Trap

However, most reservoir rocks are sedimentary rocks. Sandstones and carbonates (limestone and dolomites) are the most common reservoir rocks. They contain most of the world’s petroleum reserves in about equal proportions even though carbonates make up only about 25% of sedimentary rocks. The reservoir character of a rock may be primary such as the intergranular porosity of a sandstone, or secondary, resulting from chemical or physical changes such as dolomitization, solution and fracturing.

Shales frequently form the impermeable cap rocks for petroleum traps. The distribution of reservoirs and the trend of pore space are the end product of numerous natural processes, some depositional and some post-depositional. Their prediction, and the explanation and prediction of their performance involve the recognition of the genesis of the ancient sediments, the interpretation of which depends upon an understanding of sedimentary and diagenetic processes.

Well Log Analysis : Well log is a continuous record of measurement made in borehole respond to variation in some physical properties of rocks through which the bore hole is drilled. Traditionally Logs are display on girded papers shown in figure. Nowadays the log may be taken as films, images, and in digital format [6].

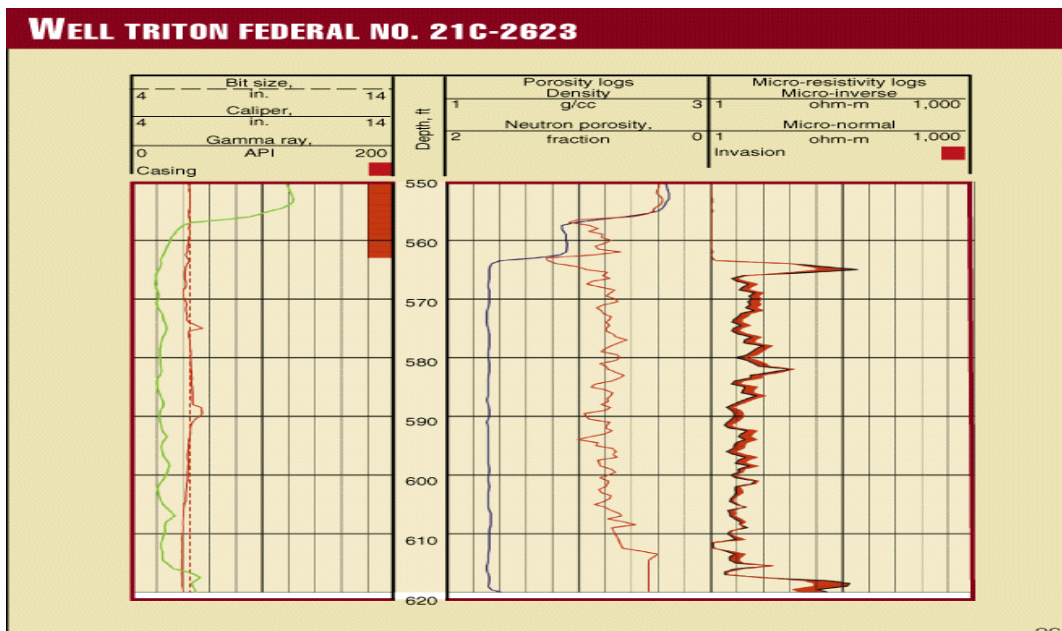


Figure 4: Well log showing different kinds of log presentation.

The analysis of petrophysical logs in this study was aimed at a qualitative and quantitative determination of the properties of delineated reservoirs. The gamma ray (GR) and spontaneous potential (SP) logs were examined for lithologic information. In the reservoir formations vis a vis at shale beds, gamma ray (GR) log which measures natural radioactivity in formations reflects the shale contents while the SP log displays excursion from the shale base line, hence both logs were used for the identification of sand / shale lithology in the study area [5]. The resistivity log in combination with the GR log were used to differentiate between hydrocarbon and non-hydrocarbon bearing zones. In hydrocarbon bearing formation, the resistivity log signatures show high resistivity values than when in water bearing formation. The discrimination of the various fluid types i.e. oil / gas within reservoirs could not be achieved because of the non availability of neutron log among materials used in carrying out the study.

Lithology Identification of Fenchugonj Gas Field (Well # 03) using Gamma Ray (GR) Log

Lithology is often used to describe the solid(matrix) portion of the rock, generally in the context of a description of the primary mineralogy of the rock (e.g., a sandstone as a description of a rock composed primarily of quartz grains , or a limestone composed primarily of calcium carbonate) [5]. The Gamma Ray (GR) log measures the natural radioactivity of the formations in the borehole. The log is therefore, useful for identifying lithologies and for correlation purposes. In sedimentary formations, the GR log normally reflects the shale content of the formations because of the concentration of radioactive materials in the shale\clays. Shale-free sandstones and carbonates have low gamma ray values, unless radioactive contaminants (volcanic ash, granite wash, or potassium rich fluids) are present [6]. Shale exhibit relatively high GR count rates due to presence of potassium ions in the lattice structure of clay mineral .On the other hand, reservoir rock (calcite, dolomite, quartz) exhibit relatively low GR count rates due to absence of potassium ions in the lattice structure of mineral [7].Some of low radioactivity and high radioactivity’s material are shown in table II.

Table II: Distribution of common rocks with respect to their radio activities

Low Radioactivity	High Radioactivity
Halite	Shales Igneous rock
Gypsum	
Anhydrite	
Limestone	
Dolomite	
Sandstone	

Scale of GR: It is plotted as API Gamma Ray Units ranging from a low of zero (0) to as high as two hundred (200) or more. One should always check the scale being used. In common use today is a scale of zero (0) to 200 API Units [8]

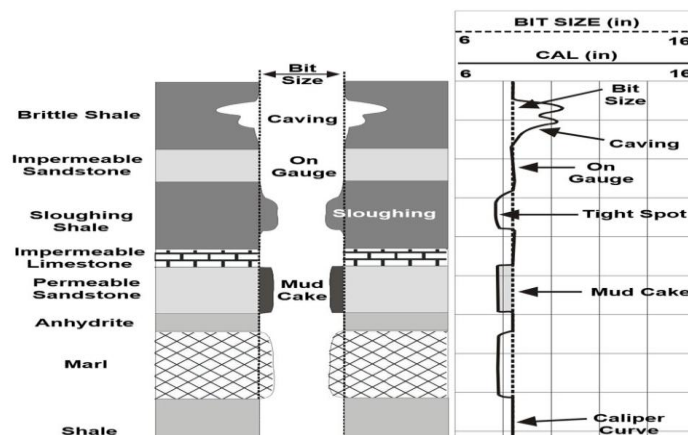


Figure 5: Well Log showing Gamma Ray , Caliper Log , Resistivity Log and Porosity log scale.

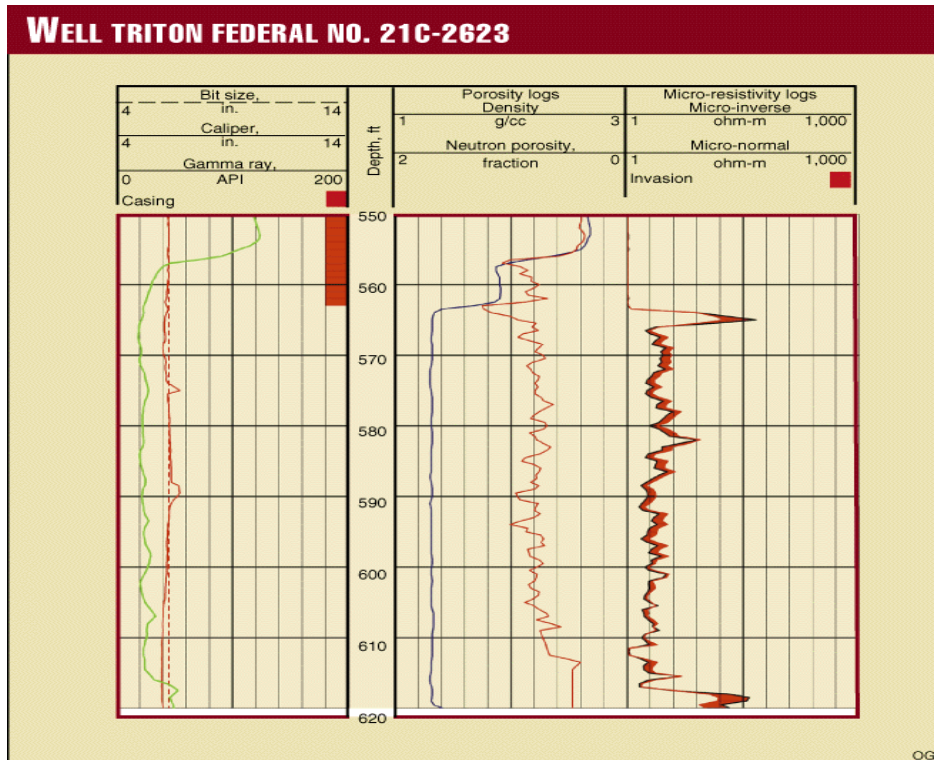


Figure 6: Mud cake formation in porous zone indicating permeability

Lithology Identification of Fenchugonj Gas Field (Well # 03) using Spontaneous Log (SP)

The SP tool is one of the simplest tools and is generally run as standard when logging a hole, along with the gamma ray. SP data can be used to find where the permeable formations are present. Permeable zone has been identified in the SP log. Since Negative maximum deflection from shale base line in SP log indicates the permeable zone [7]. Negative deflection at reservoir zone A, B, C, D, E, F and G which are indicating that these zone are porous formation at FGF (well#03).

Permeable formation determination based on Caliper log

Hole diameter is smaller than bit size due to development of mud cake for porous and permeable formation which are indicating the permeability [5,13]. According to Gamma Ray Log, SP Log and Caliper log, reservoir formation i.e. sandstone has been identified in FGF (well#03) and shown in table III.

Table III: Lithology Identification of Fenchugonj Gas Field (well # 3) using GR Log, SP Log and Caliper Log

Depth (meter)	Lithology	Remark
1500-1656	Shale	
1656-1680	Sand	Zone A
1680-1992	Shale	
1992-2017	Sand	Zone B
2017-2030	Shale	
2030-2086	Sand	Zone C
2086-2148	Shale	
2148-2154	Sand	Zone D
2154-2206	Shale	
2206-2260	Sand	Zone E
2260-2511	Shale	
2511-2526	Sand	Zone F
2526-2612	Shale	
2612-2627	Sand	Zone G
2627-2700	Shale	

DETERMINATION POROSITY USING DENSITY LOG, NEUTRON LOG AND SONIC LOG

Definition of Porosity : Porosity gives an indication of the rock's ability to store fluids. It is defined as the ratio of the pore volume to the bulk volume of the porous medium as shown in the following equation [5]:

$$\text{Porosity, } \Phi = \frac{V_p}{V_b} = \frac{V_b - V_s}{V_b} \quad (1)$$

where Φ = Porosity, %, V_p = Pure volume, V_b = Bulk volume and V_s = Solid volume

Principle of Density log:

The density logging tool has a relatively shallow depth of investigation, and as a result, is held against the side of the borehole during logging to maximize its response to the formation. The tool is comprised of a medium-energy gamma ray source (cobalt 60, cesium 137). Two gamma ray detectors provide some measure of compensation for borehole condition. When the emitted gamma rays collide with electrons in the formation, the collisions result in a loss of energy from the gamma ray particle. The scattered gamma rays that return to the detectors in the tool are measured in two energy ranges [5]. This type of interaction is known as Compton scattering. The scattered gamma rays reaching the detector, at a fixed distance from the source, are counted as an indication of the formation density.

Hence, the expression for bulk density is [7]

$$\rho_b = \rho_{ma} (1 - \phi) + \rho_f \phi \quad (2)$$

Where, ϕ , ρ_{ma} , ρ_b and ρ_f are porosity from density log, density of formation matrix, g/cm^3 (for Sand 2.65), bulk density from log measurement, g/cm^3 and density of fluid in rock pores, g/cm^3 (formation water, 1.1) respectively.

$$\text{Porosity from density log, } \Phi_D = (\rho_{ma} - \rho_b) / (\rho_{ma} - \rho_f) \quad (3)$$

Where ρ_{ma} = matrix of sand (2.65), ρ_b = Bulk density (from log data)

ρ_f = Fluid density (from chart, formation water, 1.1)

Principle of Neutron Log

Neutron logs are basically a measure of the amount of hydrogen contained in the formation [9]. High neutron count rate indicates low porosity, while low neutron count rate indicates high porosity. While there is very little difference between oil and water, the neutron tool will distinguish between gas and oil saturations. When gas is measured, the porosity will appear very low because there is a lower concentration of hydrogen in gas than in oil or water. A decrease in neutron porosity by the presence of gas is called gas effect [5].

Porosity from Density and Neutron log

The combination of the neutron and density measurements is probably most widely used porosity log combination. The response of the combination is such that for reconnaissance evaluation one can forego the crossplot and rely on recognition of the curve patterns to quickly determine the most likely predominant lithology and formation porosity [5].

$$\Phi_{D-N} = \sqrt{(\Phi_D)^2 + (\Phi_N)^2} / 2 \quad (4)$$

Where Φ_D = from equation (3)

Φ_N = Neutron Log provides Φ_N directly

Principle of Sonic Log (Acoustic Log)

The Sonic log is a porosity log that measures interval transit time (Δt) of a compressional sound wave travelling through the formation along the axis of the borehole. The sonic log device consists of one or more ultrasonic transmitters and two or more receivers [5]. Known as the interval transit time, Δt is the reciprocal of the velocity of the compressional sound wave. To avoid fractions, the interval transit time is scaled by 106 and reported in micro-seconds per ft ($\mu\text{sec}/\text{ft}$). Thus, $\Delta t = 106/v$, where Δt is the interval transit time in $\mu\text{sec}/\text{ft}$ and V is the compressional wave velocity in ft/s

Wyllie time-average porosity equations (Wyllie et al., 1958):

$$\Phi_s = (T_{\text{log}} - T_{\text{matrix}}) / (T_f - T_{\text{mat}}) \quad (5)$$

T_{log} = from sonic log

T_{matrix} = 55-51 micro second, for sand

T_{fluid} = 185 micro second, for salt base water and 189 for fresh water.

Determining porosity from different log using above mentioned equation has been shown in **table V**.

III. RESULTS AND DISCUSSION

3.1 Qualitative Interpretation

According to GR log, SP log and Caliper Log, seven sand bodies marked reservoir zone A, B, C, D, E, F and G were found across the FGF at Well # 03. From the analysis, particularly the resistivity logs, all the seven delineated reservoirs were identified as hydrocarbon bearing reservoir across the FGF at well # 03.

3.2 Quantitative Interpretation

Quantitatively, the petrophysical parameters are estimated using empirical formulae as follows. The methodology as earlier reported was chosen for the quantitative interpretation of the delineated reservoirs in each reservoir zone. Table IV represents the results of some computed petrophysical parameters for well #03 in reservoir zone A.

Table IV: Picking value from FGF (well #03) log at zone A (depth 1656-1680 meter)

Depth	GR	SP	LL3	ILM	ILD	Density log	Neutron log	Sonic transit time
Meter	API		Ohm-m	Ohm-m	Ohm-m	Bulk density(ρ) gm/cc	Porosity(Φ), %	T_{Log} $\mu\text{sec}/\text{ft}$
1656-1658	150	50	3.5	6.5	7	2.25	0.36	120
1658-1660	130	54	3	5.5	9	2.225	0.36	148
1660-1662	115	53	3.2	5	9.5	2.225	0.195	148
1662-1664	130	53	2.5	5	8	2.35	0.195	120
1664-1666	130	52	2.8	5	6	2.3	0.195	100
1666-1668	130	52	3.5	5	5.5	2.35	0.195	95
1668-1670	130	52	3.5	5	6	2.35	0.195	100
1670-1672	130	52	3.5	5	6	2.32	0.195	98
1672-1674	130	52	5	5	6	2.28	0.195	100
1674-1676	130	55	5	5.5	8	2.3	0.195	100
1676-1678	130	52	5	5.5	5.5	2.32	0.195	100
1678-1680	150	50	3.5	5	6.5	2.33	0.195	90

Table V: Porosity calculation for reservoir zone A at FGF (well#03) using above mentioned equation

Reservoir Zone A/ Depth	Bulk density from Density log, eq ²	Porosity from Density log, eq ³	Porosity from Neutron log	Porosity from Density- Neutron log, eq ⁴	Transit time from Sonic log,	Porosity from Sonic log Eq ⁵
(meter)	ρ_b (gm/cc)	Φ_D (100%)	Φ_N (100%)	Φ_{D-N} (100%)	T Log(μ sec/ft)	Φ_s (100%)
1656-1658	2.25	0.258	0.36	0.31318	120	0.507576
1658-1660	2.25	0.27412	0.36	0.319957	148	0.719697
1660-1662	2.22	0.27412	0.195	0.237876	148	0.719697
1662-1664	2.35	0.1935	0.195	0.194251	120	0.507576
1664-1666	2.3	0.2257	0.195	0.211	100	0.356
1666-1668	2.35	0.1935	0.195	0.194251	95	0.318182
1668-1670	2.35	0.1935	0.195	0.194251	100	0.356061
1670-1672	2.32	0.21285	0.195	0.20412	98	0.340909
1672-1674	2.28	0.23865	0.195	0.217921	100	0.356061
1674-1676	2.3	0.22575	0.195	0.210936	100	0.356061
1676-1678	2.32	0.21285	0.195	0.20412	100	0.356061
1678-1680	2.33	0.2064	0.195	0.200781	90	0.280303
Average		0.22575	0.2225	0.225215		43.119%

4.2.7: Porosity determination from neutron Log, density log, density-neutron log and sonic log

After calculating porosity for Zone A, we can similarly estimate the porosities for Zone B, Zone C, Zone D, Zone E, Zone F and Zone G revealed in table VI.

Table VI: Average porosity for reservoir Zone A, B, C, D, E, F and G at FGF Well # 03

Zone /Depth	Average Density porosity %	Average Neutron porosity%	Average Density-Neutron porosity%	Average Sonic porosity %
A(1656m-1680)	22.575	22.25	22.5215	43.1187
B (1992-2018)	18.66	21.24	20.08	52.38
C(2030- 2086)	26.81	19.01	23.38	54.89
D(2148-2154)	29.50	20.67	25.72	46.04
E (2206-2260)	20.54	23.67	22.27	34.01
F (2511-2526)	21.45	24.75	16.39	18.51
G(2612-2628)	17.01	23.13	20.52	22.92

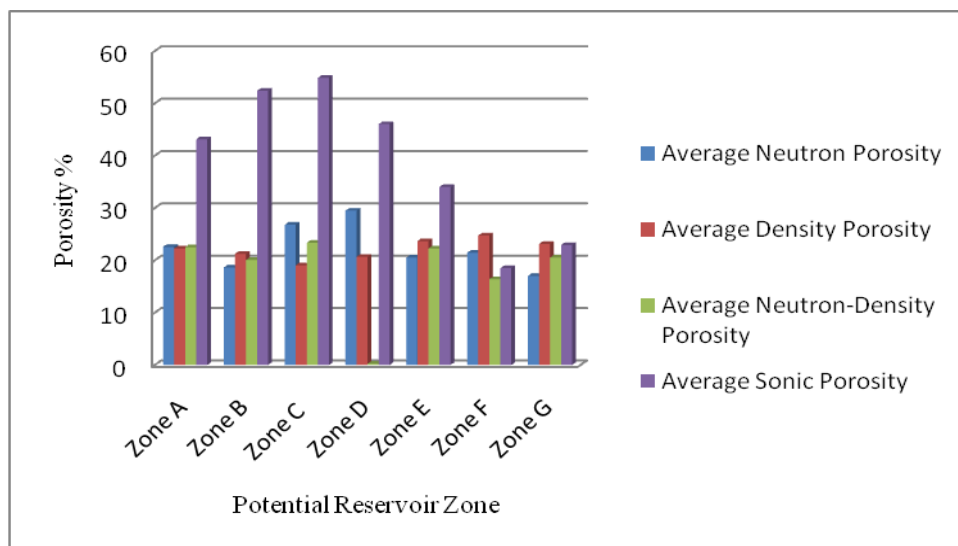


Figure 7: Comparison of porosities of neutron log, density log, density-neutron log and sonic log

HYDROCARBON ZONE DETECTION BASED ON RESISTIVITY LOG

The resistivity log is a measure of a formation's resistivity. In log interpretation, the hydrocarbons, the rock, and the fresh water of the formation are all assumed to act as insulators and are, therefore, nonconductive (or at least very highly resistive) to electric current flow. Salt water, however, is a conductor and has a low resistivity. Resistivity is a basic measurement of a reservoir's fluid saturation and is a function of porosity, type of fluid (i.e. hydrocarbon, salt water, or fresh water), amount of fluid, and type of rock. Because both the rock and hydrocarbons act as insulators but salt water is conductive, resistivity measurements made by logging tools can be used to detect hydrocarbons and estimate the porosity of a reservoir [5]. In this research, deep resistivity and shallow resistivity were studied. Deep resistivity is the resistivity recorded farther away from the inversion core created by the drilling mud. Shallow resistivity log is the resistivity recorded close to the oil well bore. A deep resistivity and shallow resistivity with low gamma ray log is indicative of hydrocarbon (HC) presence. Shales show low resistivity values with high gamma ray values.

CALCULATION OF WATER SATURATION

To calculate water saturation, S_w of uninvaded zone, the method used requires a water resistivity R_w value at formation temperature calculated from the porosity and resistivity logs within clean water zone, using the R_o method given by the following equation:

$$R_w = \frac{\Phi^m \cdot R_o}{a} \quad (6)$$

R_w is the water resistivity at formation temperature, Φ and R_o are the total porosity and deep resistivity values in the water zone respectively. Tortuosity factor is represented as "a" and m is the cementation exponent, usually 2 for sands [10]. In the water zone, saturation should be equal to 1, as water resistivity R_w at formation temperature is equal to $R_w a$, Water saturation, S_w can then be calculated using Archie's method, given by:

$$S_w = \sqrt[n]{(R_w / R_w a)} \quad (7)$$

where n is the saturation exponent and $R_w a$ is water resistivity in the zone of interest, calculated in the same manner as R_w at formation temperature [11].

Formation water equivalent Resistivity

$$R_{we} = \Phi_{D-N}^2 \cdot R \quad (8)$$

R_o = Formation water resistivity = R_{LL3} (from log data), for 100% water

Lowest value of $R_{we} = R_w$

$$R_t / R_{LL3} = ? \text{ (using } R_{LL3} / R_{ILD} \text{ versus } R_{LL3} / R_{ILM} \text{ at tornado curve)} \quad (9)$$

$$R_t = (R_t / R_{LL3}) \cdot R_{LL3} \quad (10)$$

$$F = 0.81 / \Phi_{D-N}^2, \text{ if } \Phi_{D-N} \text{ value less than 16\%} \quad (11)$$

$$F = 0.62 / \Phi_{D-N}^{2.15}, \text{ if } \Phi_{D-N} \text{ value greater than 16\%} \quad (12)$$

$$S_w = \sqrt{(R_o / R_t)} = \sqrt{(F R_w / R_t)} \quad (13)$$

Determination of Hydrocarbon Saturation

Hydrocarbon Saturation, S_{HC} is the percentage of pore volume in a formation occupied by hydrocarbon. It can be determined by subtracting the value obtained for water saturation from 100%

$$\text{i.e. } S_{HC} = 1 - S_w \quad (14)$$

Determination of Permeability

Permeability, K is the property of a rock to transmit fluids. For each identified reservoir permeability, K is calculated using equation [10].

$$K = \sqrt{\frac{250 \cdot \Phi^2}{S_{wi}}} \quad (15)$$

where S_{wir} is the irreducible water saturation [12]

Table VII: Picking value from Well Log of FGF(well #03) and determine formation factor, hydrocarbon saturation

Depth (meter)	Φ_{DN} %	R_{LL3}	R_{we} Eq^3 (Ω - m)	R_{ILM} Ω - m	R_{ILD} Ω - m	R_{LL3}/R_{ILM}	R_{LL3}/R_{ILD}	R_t/R_{LL3} Eq^9	R_t Eq^{10} Ω -m	F $Eq^{11/12}$	S_w Eq^{13} %	Shc Eq^{14} %	Permeability Eq^{15} md
1656-1658	0.3	3.5	0.23	6.5	7	0.54	0.5	1.9	6.65	7.52	0.06	0.93	194
1658-1660	0.3	3	0.22	5.5	9	0.55	0.33	1.9	5.7	7.18	0.07	0.93	179
1660-1662	0.2	3.2	0.24	5	9.5	0.64	0.34	1.9	6.1	13.6	0.13	0.87	88
1662-1664	0.2	2.5	0.09	5	8	0.5	0.31	1.9	4.8	21.0	0.25	0.75	63
1664-1666	0.1	2.8	0.14	5	6	0.56	0.47	1.9	5.3	17.6	0.19	0.81	36
1666-1668	0.2	3.5	0.13	5	5.5	0.7	0.64	1.9	6.6	21.0	0.18	0.82	75
1668-1670	0.2	3.5	0.13	5	6	0.7	0.58	1.9	6.6	21.0	0.18	0.81	75
1670-1672	0.2	3.5	0.16	5	6	0.7	0.58	1.9	6.6	18.9	0.16	0.84	79
1672-1674	0.2	5	0.28	5	6	1	0.83	1.9	9.5	16.4	0.11	0.90	95
1674-1676	0.2	5	0.25	5.5	8	0.91	0.63	1.9	9.5	17.6	0.11	0.89	95
1676-1678	0.2	5	0.23	5.5	5.5	0.91	0.91	1.9	9.5	18.9	0.11	0.88	95
1678-1680	0.2	3.5	0.15	5	6.5	0.7	0.54	1.9	6.6	19.6	0.17	0.83	77
Average									6.9	0.14			95

Table VIII: Summary of the Average Petrophysical Parameters for Reservoirs zone A, B, C, D, E, F and G at well #03 of FGF

Reservoir Zone	Average Porosity	Average Water Saturation (%)	Average Hydrocarbon Saturation (%)	Average Permeability md
A (1656-1680)	22.5215	14.25	85.68	95
B (1992-2017)	20.0726	64.8	35.2	85
C (2030-2086)	23.375	42.99	57.01	91
D (2148-2154)	25.72	47.24	52.76	105
E (2206-2260)	22.27125	53.14	46.86	48
F (2511-2526)	16.3945	2.80	97.20	14
G (2612-2627)	20.52	52.85	47.145	32

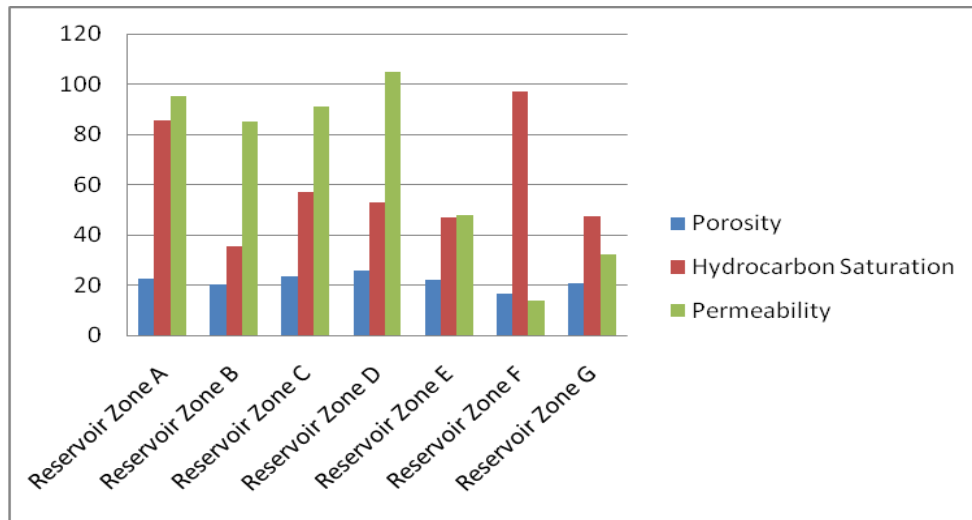


Figure 8: Relationship between percentage average effective porosity, water saturation, hydrocarbon saturation and permeability of reservoir zone A – G.

IV. CONCLUSION

An engineer or geologist or geophysicist can interpret the log readings to reach certain conclusions about the formation. For example, negative maximum deflection from shale base line in SP log indicates the permeable zone and an increase in a porosity log might indicate that the formation has porosity and is permeable [7]. Besides, resistivity logs determine what types of fluids are present in the reservoir rocks by measuring how effective these rocks are at conducting electricity. Because fresh water, oil and gas are poor conductors of electricity. They have high resistivity [5]. By contrast, most formation waters are salty enough that they conduct electricity with ease. Thus, formation waters generally have low resistivity. Hydrocarbon saturation and formation porosity are the two key parameters determined from wire line logs that are used in the evaluation of a subsurface reservoir as a potential hydrocarbon producer. They are the measures of reservoir content but not reservoir performance and by themselves do not provide an actual indication of the hydrocarbon productivity of a reservoir.

The petrophysical properties evaluation of 'FGF' (Well# 03) field for its reservoirs characterization was made possible by careful analysis and interpretation of its well logs. The results show the field's delineated reservoir units having porosity ranging from 0.16 to 0.25 indicating a suitable reservoir quality, permeability values from 14 md to 105 md attributed to the well sorted nature of the sands and hydrocarbon saturation range from 35.2% to 97.20% implying high hydrocarbon production. These results suggest high hydrocarbon potential and a reservoir system which performance is considered satisfactory for hydrocarbon production. The endeavor of this paper is to show the petrophysical properties of reservoir rock of FGF (well#03) using wire line logging technique. This work has introduced the practical application of wireline log and interpreted porosity, water saturation, hydrocarbon saturation and permeability. All calculation in this work was done without consideration of mud composition, mud temperature plus other sophisticated parameter.

REFERENCES

- [1] E. Abdolla, "Evaluation of Petrophysical Properties of an Oil Field and their effects on production after gas Injection," 1st International Applied Geological Congress, Department of Geology, Islamic Azad University– Mashad Branch, Iran, pp. 26-28, 2010.
- [2] M. Rider, "The Geological Interpretation of Well Logs," Blackie, Glasgow, pp. 151-165, 1986.
- [3] Alam MK, Hasan AKM, Khan MR & Whitney JW (1990) Geological map of Bangladesh. Published by Ministry of Energy and Mineral Resources, Geological Survey of Bangladesh with cooperation of U S Geological Survey.
- [4] Badrul Imam (2005), Energy Resources of Bangladesh, UGC publication no. 89, page: 19–32.
- [5] G. Asquith & D. Krygowski, "Basic well Log Analysis" pp.2, 4, 5, 31, 37, 37, 41-42, 19, 2004.
- [6] Schlumberger, "Principle and application of log interpretation," Schlumberger Education services, Houston, 1989.
- [7] R.H. Merkel, "Well Log Formation Evaluation" pp. 7, 17, 20, 1979.
- [8] Wahl, J.S.: "Gamma Ray Logging," Geophysics (1983) 48 No. 11
- [9] Mr D G Bowen-Core Laboratories - Formation Evaluation and Petrophysics
- [10] G. Asquith and D. Krygowski, "Basic Well Log Analysis," AAPG Methods in Exploration Series, No 16, 2004

- [11] G.E. Archie, "*The Electrical Resistivity as an Aid in Determining Some Reservoir Characteristics,*" *Journal of Petroleum Technology*, vol. 5, pp. 54-62, 1942
- [12] M.P. Tixier, "*Evaluation of Permeability from Electric Log Resistivity Gradients,*" *Oil and Gas Journal*, vol. 8, pp. 75-90, 1949.
- [13] W. S. keys, "*Techniques of Water-Resources Investigations of the United States Geological Survey*" pp. 112, 1990.

Deformation Pattern of Non-cohesive Soil Bases under Foundations with Different Vertical Cross-sectional Shapes

Musa Alhassan

Department of Geotechnics and Environmental Engineering, Belarusian National Technical University, Minsk, Belarus.

ABSTRACT: Pattern of vertical deformations of soil bases, under shallow foundation model of different vertical cross-sectional shapes were experimentally studied on three different modeled non-cohesive subsoil conditions. Foundations models with rectangular, wedge and T shape vertical cross-sections were studied. Result of the study showed that, under the action of vertical load, bulk of the vertical deformation of subsoil bases at the instance of foundations with rectangular vertical cross-sectional shapes, is mostly associated with the soil beneath the foundation, while at the instances of those with wedge and T vertical cross-sectional shapes, deformation of the soil occurs both under the foundations' bases and along their vertical stems. This indicates that, although less loads were generally resisted by the wedge and T shape foundations, using them can help in mobilizing substantial mass of soil above the foundation bases, to function not only as surcharge to the soil below the base, but also in resisting structural loads.

KEYWORDS: Deformation pattern; Foundation shape; Non-cohesive soil; Soil base; Vertical load.

I. INTRODUCTION

The earth provides the ultimate support for most civil engineering structures including, bridges, earth fills, earth and concrete damsetc., as such the behavior of the supporting ground, under these structures, directly affects their stability. Soil (since sound rocky stratum is often rare to come by) is usually the supporting ground. Since soil is weaker than most other construction materials like wood, concrete, steel or masonry, hence, compared to structural members made out of these materials, a larger area or mass of soil will necessarily be required to carry the same load. Foundations are the structural elements that transmit the structural loads to the ground in a way that the supporting soil is not overstressed and do not undergo deformation that would cause excessive settlement of the structure [1]. This is achieved through choice of foundation type and its geometry (shape). Foundations are generally classified into shallow foundations and deep foundations. Shallow foundations are considered those types that transmit structural loads to the soil strata at a relatively small depth. Terzaghi [2] defines shallow foundation as that which is laid at a depth D_f not exceeding the width B of the foundation, that is $D_f/B \leq 1$. However, subsequent studies have shown that, for shallow foundations, D_f/B can be as large as 3 to 4 [3-5].

Various types (shapes) of shallow foundations are known, with strip, square, rectangular and circular being the most widely used. These types of shallow foundations have different shapes which only vary from each other plan-wise or by horizontal cross-section. Depending on the design thicknesses, the shapes of their vertical cross-sections are basically the same. This makes the mode of their interaction with the soil base trunk-wise (vertically) basically the same. Their interaction with the soil bases is such that the soil above their bases contributes to the resistance of the structural loads mostly by surcharging the soil below the base of the foundation. Therefore the study of other shapes of shallow foundations that can both partly distribute structural loads vertically along their trunks and bases is presented. V and T shape foundation were considered along with the conventional rectangular shaped foundation. The study presents pattern of vertical deformation (settlement) of non-cohesive soil bases under foundations of these shapes. This study was based on the fact that, in the design of shallow foundations, it is commonly believed that settlement (deformation) criterion is more critical than that of the bearing capacity [6]. Settlement of 25 mm is usually taken as the allowable in the design of shallow foundations such as pad or strip [7].

II. EXPERIMENTAL METHODOLOGY

Four wooden models of shallow foundations were used for the study. The first model (labeled as rectangular shape-1) was a rectangular shape block with dimension of $30 \times 60 \times 60$ mm for width, length and height respectively, the second model (labeled as rectangular shape-2) was a rectangular shape block with dimension of $50 \times 60 \times 60$ mm for width, length and height respectively, the third was a wedge shape block of 60 mm height with width and length for top and lower sides as 60×60 mm and 30×60 mm respectively, while the fourth was a T-shape block of 60 mm height with width and length for top and lower parts as 60×60 mm and 30×60 mm respectively (fig. 1). The dimensions of the models were chosen so as to be within $D_f/B \leq 2$ (D_f and B are depth of foundation embedment and width respectively). Three subsoil conditions of non-cohesive soil were modeled in the geotechnical laboratory of the Department of Geotechnics and Environmental Engineering of Belarusian National Technical University, Minsk, Belarus. The experimental stand used for the study was a rectangular container with dimension $1100 \times 600 \times 250$ mm for length, height and width respectively, with a transparent front side (fig. 2).

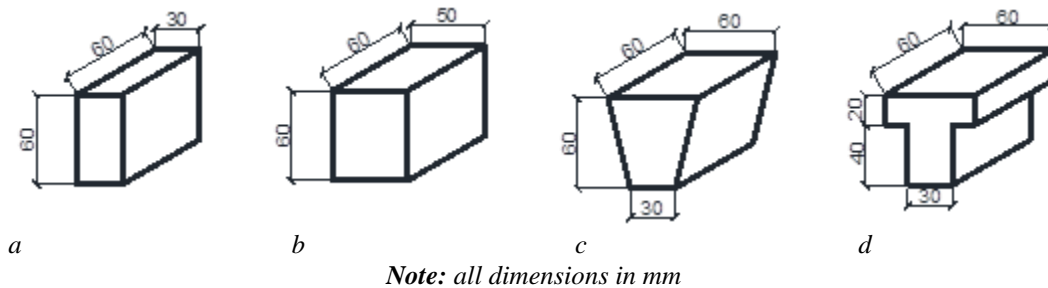


Fig. 1: Foundation prototypes: a- rectangular shape, b- wedge-shape, c- T-shape.



Fig. 2: Experimental stand

Two types of non-cohesive (sandy) soils were used in modeling the subsoil bases. The first soil was classified according to Russian standard [8] as coarse grain sand, while the second soil was classified as medium grain sand. The subsoil bases were modeled by compaction of the soils at various moisture contents and densities. Figs. 3-5 show the modeled subsoil conditions. The experimental stand was filled with the soils in layers of 50 and 25 mm, with each layer compacted to the respective unit weight (density) and at respective moisture contents. The top of each layer was marked from the inside side of the transparent side of the box with thin layer of powdered chalk, while thin marker was used to trace the marks on the outside surface. With these, and using gauges, the vertical deformations (displacements) of the soil layers at the instance of each of the foundation models were measured. The markings also make visual observations of the deformation process possible. The foundation models were placed during placement and compaction of the last two upper layers as shown in figs. 3-5. Using 1:10 loading lever, loads were statically, vertically, centrally and uniaxially applied to the foundation models.

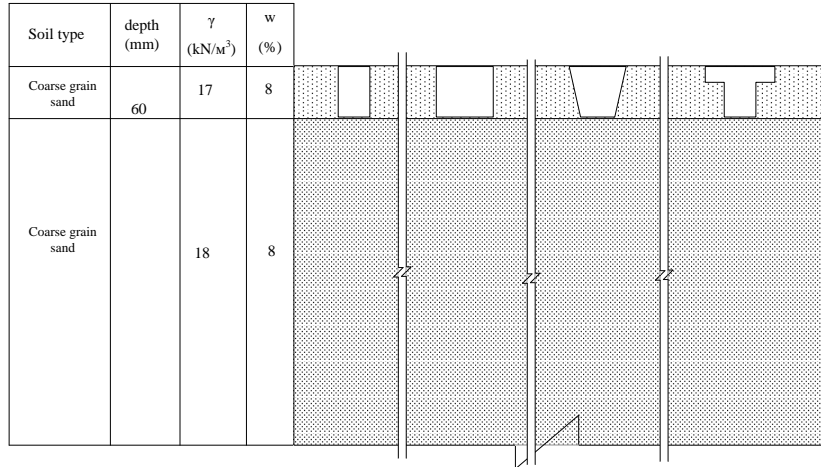


Fig. 3: First modeled subsoil condition

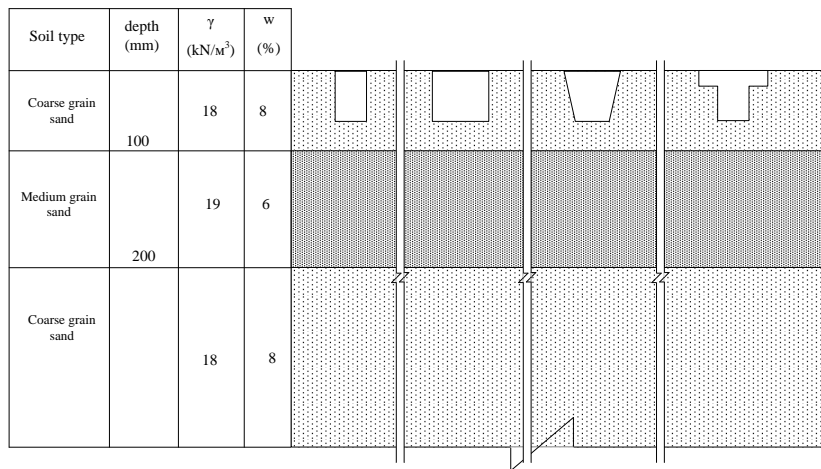


Fig. 4: Second modeled subsoil condition

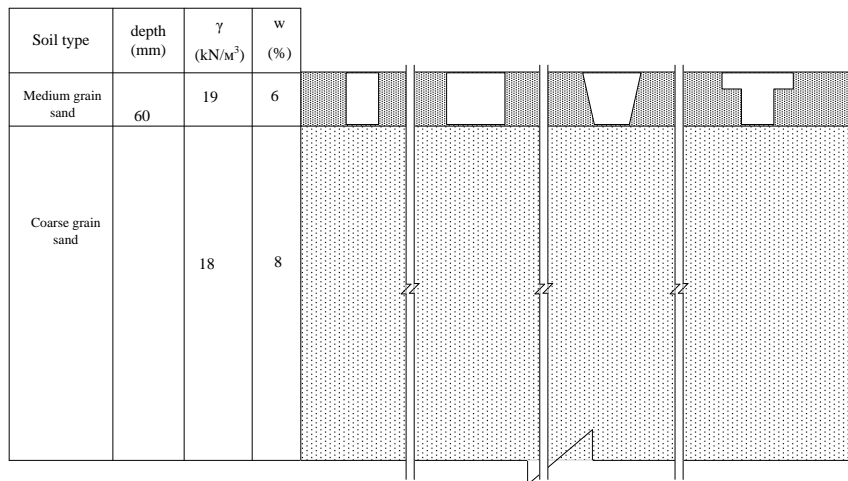


Fig. 5: Third modeled subsoil condition

On the first modeled subsoil condition, maximum loads of 339, 267, 228 and 285kPa were applied to rectangular-1, rectangular-2, wedge and T shape foundation models respectively. Maximum loads of 394, 400, 228 and 285kPa respectively, were applied to rectangular-1, rectangular-2, wedge and T shape foundation models, on the second subsoil condition. On the third modeled condition, 450, 400, 285 and 285kPa loads were applied respectively to rectangular-1, rectangular-2, wedge and T shape foundation models respectively. At these respective loads, the patterns of vertical deformation of the subsoil bases at the instance of these models foundations were studied.

III. RESULTS AND DISCUSSION

Investigation on the first modeled subsoil condition showed that on loading the rectangular shape foundation models, heaving and bulging of the ground surface to $0,1b$ and $0,04b$ (b – width of the foundation models) respectively for rectangular-1 and 2, occurred. Soil under their bases to a depth of b deformed, the maximum deformation occurs in the soil directly below the foundation, and decrease with depth. This observation is similar to those reported by ALChamaa *et al* [9]. On loading wedge shape foundation models, two deformation zones were observed – along its vertical trunk and below the base. Minimum deformation of the soil base was observed at the ground surface and increases to the maximum at the base of the foundation model. Heaving and bulging of the ground surface was not observed in this case. On loading the T-shape foundation model, two deformation zones in the subsoil were also observed. The first deformation zone occurs from the ground surface of the soil along the vertical sides of the foundation to the depth h . Maximum deformation in this zone occurs at depth h . The second deformation zone occurs under the foundation to a depth of b' (b' – width of the stem part of the foundation model), with the maximum observed with the soil directly beneath the base of the foundation, and decreases with depth. Heaving and bulging of the soil surface was not observed.

Fig. 6 shows the vertical deformation of the soil bases under the respective maximum loads for the foundation models on the first modeled subsoil condition.

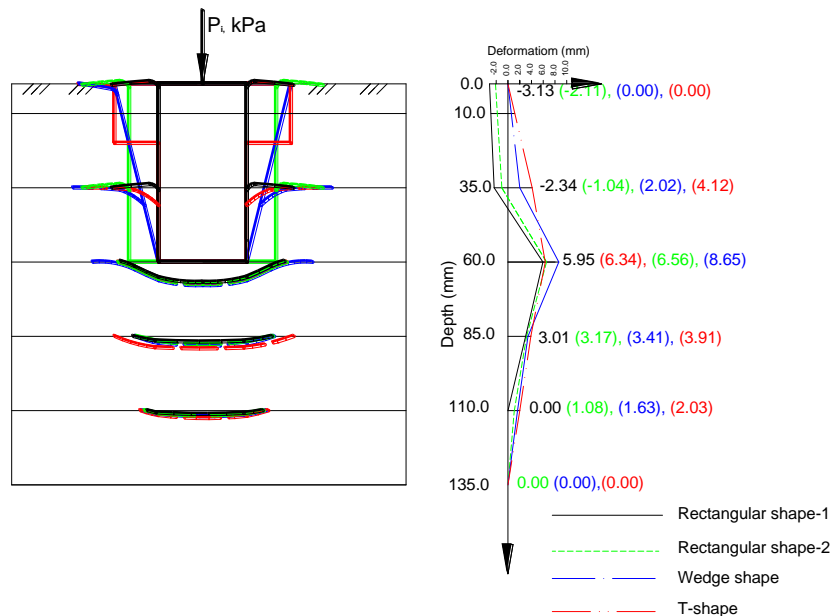


Fig. 6: Deformation of soil under foundation models on the first modeled subsoil condition

Study of the deformation patterns of the soil on the second modeled subsoil condition showed two types of deformation on loading rectangular and wedge shape foundation models. First type of deformation is heaving of the soil along the vertical trunks of the foundation, from $0,6h$ (h – thickness of the foundation) to the ground surface, while the second type of deformation was settlement of the soil from $0,6h$ to the depth of $1b$ below the foundation bases. Maximum deformation (settlement) occurred at depth $1h$ and decreases to $1b$ below the foundation bases. Heaving and bulging of the soil surface was not observed with rectangular-1 and wedge shape models, but in the case of rectangular-2 heaving and bulging of the soil surface to $0,06b$ height was observed. On loading the T-shape foundation model on the second modeled subsoil condition, both soil along the vertical trunk and beneath the foundation base settles (deformed). Minimum deformation was observed at the ground surface and increases to its maximum value at the base of the foundation i.e. at the depth $1h$. Heaving and bulging of the soil surface was not observed with in this case. Fig. 7 shows the vertical deformation of the soil bases under the respective maximum loads for the foundation models on the second modeled subsoil condition.

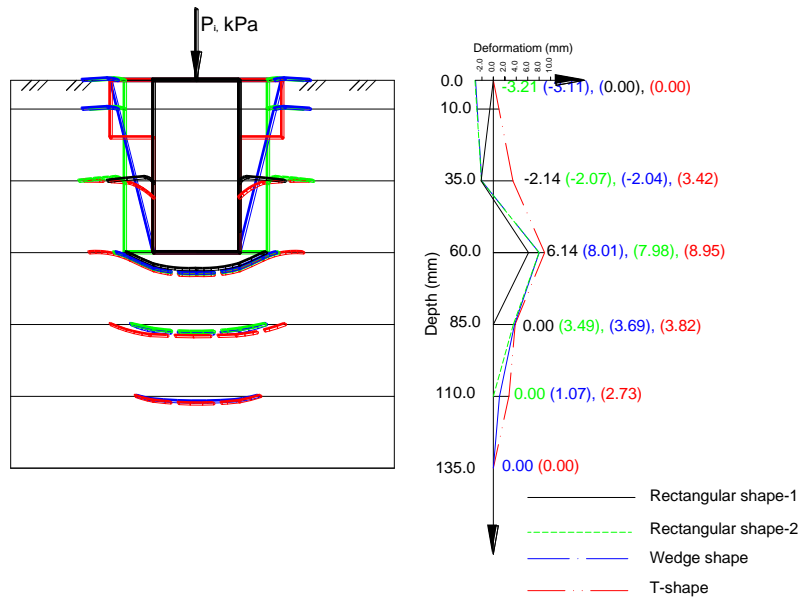


Fig. 7: Deformation of soil under foundation models on the second modeled subsoil condition

Study of the deformation patterns on the third subsoil conditions showed two zones of deformation on loading rectangular shape foundation models. The first zone of deformation was heaving of the soil along the vertical trunk of the foundation to $0,6h$ depth, while the second zone was settlement of the soil, which occurs from $0,6h$ depth to $1b$ below the base of the foundations. Maximum deformation occurs with the soil directly at the foundation bases, and decreases with depth. Heaving and bulging of ground surface was observed. Heaving of the soil occurred from $0,6h$ depth to the ground surface. The ground surface rose to a height of $0,07b$ and $0,05b$ respectively for rectangular shapes 1 and 2. On loading wedge and T shape foundation models on third subsoil condition, two deformation zones were also observed. The first zone of deformation (heaving of the soil) occurs from the ground surface along their trunks to a depth of $0,25h$, while the second zone of deformation (settlement) occurs from $0,25h$ depth to the bases of the foundations. Heaving of the soil occurred from $0,25h$ to the ground surface. The ground surface heaved to a height of $0,04b$ and $0,04b$ for wedge and T shape models respectively, bulging was observed at the surface. In all the models, maximum deformation of soil base occurred with the soil directly under the base of the foundations, and decreases with increasing depth. Fig. 8 shows the vertical deformation of the soil bases under the respective maximum loads for the foundation models on the second modeled subsoil condition.

It was observed that more soil mass is involved in the deformation process around wedge and T shape foundation models than around the rectangular shapes. The result of the study of the deformation patterns of the soil bases at the instances of foundations with these shapes can be summarized as shown in fig. 9.

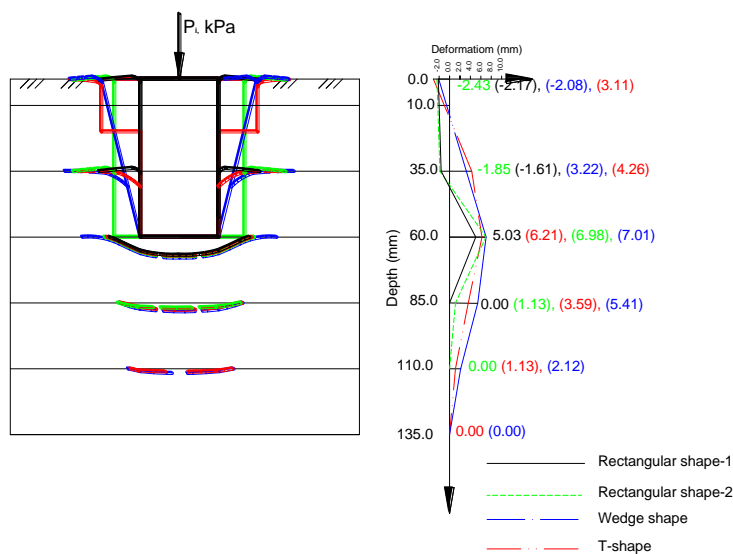


Fig. 8: Deformation of soil under foundation models on the second modeled subsoil condition

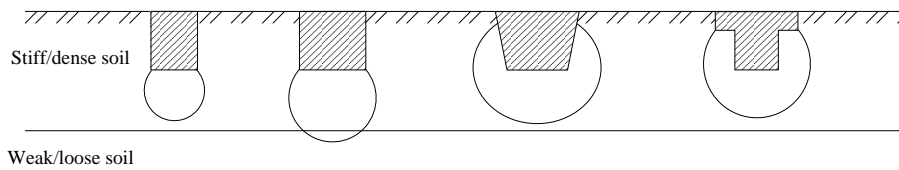


Fig. 9: Summarized patterns of deformation of the soil bases under the studied foundations shapes

IV. CONCLUSION

Deformation patterns of foundation models with different vertical cross-sectional shapes on non-cohesive subsoil bases under vertically applied load were studied. The results generally showed that bulk of the vertical deformation of the soil bases under shallow foundations with rectangular vertical cross-sectional shapes is mostly associated with the soil below the base of the foundations, while those with wedge and T vertical cross-sectional shapes, both soil along the trunks and below their bases, vertically deformed. This shows that although, less loads were resisted by these (wedge and T) shapes, using them can help in mobilizing substantial mass of soil above the foundation bases, to function not only as surcharge to the soil below the bases, but also in resisting structural loads. This potential can especially be used when stronger soil layers are underlain by weaker ones.

REFERENCES

- [1] G. Ranjan, and A. S. R. Rao, Basic and applied soil mechanics (2nd edition, New Age International (P) Limited, New Delhi), 2000, p. 474.
- [2] K. Terzaghi, Theoretical soil mechanics (John Wiley & Sons, New York), 1943.
- [3] B. M. Das, Shallow foundations - Bearing capacity and settlement (CRC Press LLC, USA), 1999, pp. 2.
- [4] B.M. Das, Principles of foundation engineering (7th edition. CL Engineering), 2010.
- [5] S. Shakiba rad, A. A. Heshmati and H.Salehzadeh, Application of Adaptive Neuro-Fuzzy Inference System (ANFIS) to Predict the Ultimate Bearing Capacity of Shallow Foundation on Cohesionless Soil. *Electronic Journal of Geotechnical Engineering (EJGE)*, Vol. 16, Bund. 5, 2011, pp. 1459-1469.
- [6] B. M. Das and N. Sivakugan, Settlements of Shallow Foundations on Granular Soil - an overview. *International Journal of Geotechnical Engineering, J. Ross Publishing, Inc. 1(1)*, 2007, pp. 19–29.
- [7] K. Terzaghi, R. B. Peck, and G. Mesri, Soil mechanics in engineering practice. (3rd Edition, John Wiley & Sons, New York), 1996.
- [8] GOCT 25100, Soil Classification (Interstate Scientific-Engineering Council on Standardization, Engineering Norms and Certification in Civil Engineering), 2011.
- [9] R. ALChamaa, M.Yabu and M.Yoshimine, Deformation and Bearing Capacity of Foundation with Various Shapes under Static Loading. 60th Annual Scientific Conference of the Japan Society of Civil Engineers. 2005. [Online] Available: <http://geot.civil.ues.tmu.ac.jp/~my/publications/jsce05d.pdf> (October 20, 2012).

Strength And Behavior Of Polypropylene Fibre In Impact Characteristics Of Concrete

K.Anbuvelan

Associate Professor, Department of Civil Engineering, Jerusalem College of Engineering,
Chennai – 600100, India. E-mail: ksanbuvelan@gmail.com

ABSTRACT: Concrete structures are often subjected to short duration (static or dynamic) due to relatively low tensile strength and fracture energy, the impact resistance of concrete is poor. There are several situations in which concrete structural elements are subjected to impact loading. The behavior of concrete under impact loads is far from adequate and there is significant variability in the published literature. In this work, an attempt is made to study the impact resistance of fibrous concrete using ACI drop weight Impact tester. Three grades of concrete's namely M1, M2, and M3 are considered in this investigation with 0.1%, 0.2%, 0.3% dosage of Polypropylene fiber. The experimental test results of fiber concrete's are compared with plain concrete and conclusions are arrived.

KEYWORDS: ACI drop weight Impact testing, Fibrous Concrete, Impact Strength, Polypropylene Fiber, Ultimate load

I. INTRODUCTION

Research work carried out so far towards the development of concrete that exhibits improved impact resistance than conventional concrete. There are several situations in which concrete structural elements are subjected to impact loading. The behaviour of concrete under impact loads is far from adequate and there is significant variability in the published literature. The primary reason for this is the lack of a standardized technique of testing concrete under impact. The primary reason for this is the lack of a standardized technique of testing concrete under impact.

II. REVIEW OF LITERATURE

Benter .etal (1989) has investigated the effects of low volumes of fibrillated fiber reinforcement on the properties of concrete, in particular on impact resistance. Low content of polypropylene fiber reinforcement (0.1 to 0.5%) had only a small positive influence on the impact resistance of both normal and high strength concretes. Chauvel el at (1989) have investigated impact resistance of slab are increased by fiber addition together, with the ultimate deformation energy for impact load subjecting the specimen to flexure shear and torsion. Chu el at (1989) has investigated Polypropylene fibers in impact test on small concrete beams. The impact resistance is increased by 29% for the beam in presence of Polypropylene fibers. Sivaraj.etal (1989) have presented the results of an investigation carried out to determine the flexural, endurance limit and impact strength of steel fiber reinforced refractory concrete at 0.5%, 1.0% and 1.5% by volume of fiber. These properties are compared to the same refractory concrete mix without steel fiber. The fatigue strength of increased 61%, 159% and 199% to 0.5%, 1.0% and 1.5% by volume of steel fiber respectively. The endurance limit expressed as a percentage of plain concrete modulus of rupture, increased 60%, 160% and 200%. When reinforced with 0.50%, 1.0% and 1.5% of steel fiber by volume, respectively. The addition of steel fiber also substantially increased the strength of refractory concrete. Bischoff.etal (1990) has studied polystyrene aggregate to minimize potential impact damage to structure—low crushing strength and a high degree of deformability energy absorbing material properties demonstrate through experiments on impact testing. Soroushian el at (1992) has studied the effects of Collated Fibrillated Polypropylene fiber on the impact resistance, chloride permeability and abrasion resistance materials, and incorporating different types of pozzolanic materials. Plain pozzolan concrete has 40% less ultimate impact resistance than conventional

concrete, and percentage increase in ultimate resistance of conventional and pozzolan concrete with addition of polypropylene fibers were 50% and 100% respectively. Souatchof .etal (1993) has found that energy absorption capability of GRC plates can be realistically estimated by the energy loss of the hammer during impact. It was found that the absorbed energy was linearly related to the plate's thickness. No significant changes in the energy absorption of GRC plates were found due to change to change boundary conditions. Gorst el at (1992) has studied special types of specimens to create failure due to flexure, shear and torsion. Steel and Polypropylene fiber reinforced concrete is studied

Lifshitz .etal (1995) have investigated low velocity impact of carbon fiber reinforced epoxy and it was conducted in 48 and 40 layered beams of different combination of 0°, 90°, 45° and -45° stacking sequences. The test setup included an instrumented drop weight and data acquisition system. Beams of two lengths were tested. Long (199mm) and "short" (55mm), under impact and quasi-static loading conditions. They acceleration pulse was analyzed in the frequency domain to determine the source of high frequency vibrations and a simple two degree of freedom model was used to distinguish between the force on the Sticker and the force applied to the beam. It is shown that the elastic response of the beams is the same under the two loading regimes. Zhou el at (1995) have investigated thick glass, polyester woven roving laminated plates subjected to low velocity impact using a guided drop weight testing and found that the impact resistance is increased by 36% for thin plates and by 22% for the thick plates. Wang el at (1996) has used polypropylene and steel fiber in impact tests on small on small concrete beams. Polypropylene fiber less than 0.5% gave a modest increase in fracture energy. Steel fibers could bring about much greater increase in fracture energy. Fiber breaking was the primary failure mechanism for steel fibers less than 0.5%. Fiber pull out was the primary mechanism for failure with fibers more than 0.75%.

III. EXPERIMENT

All the samples were prepared using designed mix. Mix design for the M1 grade concrete was done based on I.S. code method. M2 and M3 grade concrete was done based on ACI method and Trial method respectively. The optimum mix obtained for M1, M2, and M3 grade concrete is shown in Table -1. Table 2 & 3 shows the test result of controlled concrete & details of the specimen. Table – 4 describes the impact strength test results.

ACI Drop weight impact test

The experimental set up is as shown in Figure – 1 .The test specimens is to move horizontally, 2.8mm off the center between the four positioning lugs. The steel ball is free to move vertically with the sleeve 45 N drop hammers through a height of 457 mm to cause the first visible crack and ultimate failure.

Testing Procedure

Thickness of the specimens is recorded to the nearest millimeter at its center and at the end of a diameter prior to the test. The specimens were placed on the base plate with finished face up and positioned within four lugs of the impact testing equipment. The bracket with the cylindrical sleeve ball is placed on the top of the specimens within bracket. The drop hammer was then placed with base upon the steel ball and held vertically. The hammer was dropped repeatedly, and the number of blows required for the first visible crack to form at the top surface of the specimen and for ultimate failure was recorded.

The first crack was based on visual observation. White washing the surface of the test, specimens facilitated the identification of this crack. Ultimate failure is defined in terms of the numbers of required to open the crack in the specimens sufficiently to enable the fractured Pieces to touch three of the four positioning lugs on the base plate. The stage of ultimate failure is clearly recognized by the fractured specimens butting against lugs on the base plate. With fiber reinforced concrete specimens the pieces were not often broken clearly, whereas in plain concrete specimens were clearly broken. Figure - 2 and 3 shows the failure pattern of Plain Concrete and Fibre Concrete. Figure – 4 shows the overview of the tested specimens.

IV. FIGURES AND TABLES



Figure 1: Experimental setup



Figure 2: Plain Concrete Specimen



Figure 3: Polypropylene fibre Concrete Specimen



Figure 4: Overview of tested specimen

Table 1: Mix Proportions

Sl. No	Concrete	M1	M2	M3
	ITEM	Quantity (kg/m ³)	Quantity (kg/m ³)	Quantity (kg/m ³)
1.	Cement (OPC)	479	683	950
2.	Fine aggregate	530	784	552
3.	Coarse aggregate	1140	768	761
4.	Water	191	205	205
5.	Mix proportion adopted	1:1.10:2.4 w/c: 0.40	1:1.14:1.12 w/c 0.38	1:0.58:0.80 w/c 0.36
6	Super plasticizer 1% by the weight of cement	----	6.8 liters	9.5 liters

Table 2: Test results of control specimens

Sl. No	Grade of concrete	Mix proportion	Average compressive Strength in 7 days N/mm ²
1.	M1	1:1.10:2.40/0.38	21.37
2.	M2	1:1.14:1.12/0.36	32.50
3.	M3	1:0.58:0.80/0.36	48.30

Table 3: Details of specimens

Sl. No	Grade of concrete	Dosage of Polypropylene fibres in Plain Concrete, %	No. of Specimens
1.	M1	0.0, 0.1, 0.2, 0.3	4 X 5 = 20
2.	M2	0.0, 0.1, 0.2, 0.3	4 X 5 = 20
3.	M3	0.0, 0.1, 0.2, 0.3	4 X 5 = 20

Total No. of Specimens = 60

Table 4: Impact strength test results

Grade of concrete	Dosage of fiber In concrete %	No. of blows for first crack (Average of 5 Specimens)	No. of blows for ultimate strength (Average of 5 Specimens)
M 1	0.0	348	368
	0.1	400	425
	0.2	437	482
	0.3	493	537
M 2	0.0	448	510
	0.1	493	552
	0.2	558	622
	0.3	490	551
M 3	0.0	624	691
	0.1	705	796
	0.2	945	1015
	0.3	1059	1204

Table 5 Characteristic Impact strength of concrete

(a) For First Crack

Grade of Concrete	N _{CK} Value for first crack in no. of blows			
	0.0%	0.1%	0.2%	0.3%
M1	338	390	427	493
M2	437	482	547	479
M3	613	621	863	1208

(b) For Ultimate Strength

Grade of Concrete	Improvement in no. of blows of Polypropylene fibre concrete over plain concrete for first crack		
	0.1%	0.2%	0.3%
M1	15.38	26.33	45.85
M2	10.29	25.17	9.61
M3	1.30	40.78	97.06

Table 6: Improvement in no. of blows of Polypropylene fibre concrete over Plain concrete

(a) For First Crack

Grade of Concrete	N _{CK} Value for first crack in no. of blows			
	0.0%	0.1%	0.2%	0.3%
M1	361	415	472	527
M2	499	541	611	540
M3	686	17	934	1398

(b) For Ultimate Strength

Grade of Concrete	Improvement in no. of blows of Polypropylene fibre concrete over plain concrete for first crack		
	0.1%	0.2%	0.3%
M1	14.95	30.74	45.98
M2	8.41	22.44	8.21
M3	4.51	36.15	103.79

Table 7: Comparison of % Improvement in no. of blows of Polypropylene fibre concrete over Plain concrete

(a) For First Crack

Grade of Concrete	0.1 % ~ 0.2 %	0.1 % ~ 0.3 %
M1	71.19%	198.11%
M2	144.60%	-6.60%
M3	3036.92%	7366.15%

(b) For Ultimate Strength

Grade of Concrete	0.1 % ~ 0.2 %	0.1 % ~ 0.3 %
M1	105.61%	207.55%
M2	166.82%	-2.37%
M3	701.55%	2201.33%

* -ve sign represents, the % of improvement in no. of blows decreases

Table 8: Comparison of test results of M1 grade concrete with M2 &M3 grade concrete

(a) For First crack

Grade of Concrete	N _{CK} Value for first crack in no. of blows			
	0.0%	0.1%	0.2%	0.3%
M1 ~ M2	29.28	23.58	28.10	-2.83
M1 ~ M3	81.36	59.23	102.10	145.03

(b) For Ultimate Strength

Grade of Concrete	N _{CK} Value for ultimate strength in no. of blows			
	0.0%	0.1%	0.2%	0.3%
M1 ~ M2	38.22	30.36	29.44	2.46
M1 ~ M3	90.02	72.77	97.88	65.27

* -ve sign represents, the % of improvement in no. of blows decreases

Table 9: Cost comparisons of different fibres

S1 .No	Name of the fiber	Dosage in kg/m ³	Cost Per m ³ in Rs.
1.	Steel (0.5%)	40.0	2000.00
2.	Polypropylene (0.1%)	0.910	745.00
3.	Reengineered Plastic Shreds (0.5%)	4.0	600.00

V.

RESULTS DISCUSSION

The results of impact strength measured as no. of blows for first cracking and failure show a wide variation. Using means of measures of deviation, the characteristic value number of blows for first and ultimate cracking are obtained as,

$$NCK = N - 1.64 \times S$$

Where,

NCK=Characteristics no of blows

N = Average no of blows

S =Sample deviation

From Table - 5 & 6 shows the performance improvement in no. of blows for first and ultimate strength. From the Table - 5 addition of 0.1%, 0.2%, 0.3% of fibres in plain concrete shows the improvement in no. of blows for first crack to an extent of 15.38%,26.33%,45.85% for M1, 10.29%, 25.17%, 9.16% for M2 and 1.30%, 40.78%, 97.06% respectively.

From the Table - 6 addition of 0.1%, 0.2%, 0.3% of fibres in plain concrete shows the improvement in no. of blows for Ultimate strength to an extent of 14.92%,30.74%,45.98% for M1, 8.41%, 22.49%, 45.98% for M2 and 4.51%, 36.15%, 103.79% respectively.

From Table – 7 shows comparison of percentage of improvement in no. of blows between different dosages of fiber content in plain concrete. Addition of 0.2% & 0.3% of Polypropylene fibre in plain concrete shows improvement in no. of blows over 0.1% incorporation of fibre in plain concrete are 71.19%, 198.11% and 105.61%, 207.55% for M1 grade of concrete, 144.60% -6.60% and 166.82%, -2.37% for M2 grade of concrete and 3036.92%, 7366.15% and 705.55%, 2201.33% for M3 grade of concrete for first crack and ultimate strength respectively.

From Table – 8 shows comparison of test results of M1 grade concrete with M2 & M3 grade concrete. The percentage of Improvement in no. of blows increases to an extent of 29.28% - 81.36%, 23.58 – 59.23%, 28.10 – 102.10%, 145.03 – 2.83% for first crack, 38.22% - 90.92%, 30.36% - 72.77%, 29.44 – 97.88%, 2.46 – 165.27% for ultimate strength of M2 and M3 over M1 grade of concrete with 0.0%, 0.1%, 0.2% and 0.3% incorporation of fibres in Plain concrete respectively.

Table – 9 Shows the cost comparison of Polypropylene fibres with other available artificial fibres.

VI. CONCLUSIONS

The following conclusions are presented based on experimental results from investigations,

For M1 Grade of Concrete

Addition of 0.0%, 0.1%, 0.2% and 0.3% dosage of Polypropylene fibres in plain concrete improves the characteristic no. of blows to a maximum extent of 15.38% - 45.85% for first crack and 14.95% - 45.98% for ultimate strength. Addition of 0.2% and 0.3% dosage of Polypropylene fibres in plain concrete shows improvement in no. of blows by 71.19% , 198.11% and 105.61% , 207.55% for first crack & ultimate strength of M2 and M3 grade of concrete compared to M1 grade of concrete.

For M2 Grade of Concrete

Addition of 0.0%, 0.1%, 0.2% and 0.3% dosage of Polypropylene fibres in plain concrete improves the characteristic no. of blows to a maximum extent of 9.61% - 25.17% for first crack and 8.21% - 22.44% for ultimate strength. Addition of 0.2% and 0.3% dosage of Polypropylene fibres in plain concrete shows improvement in no. of blows by 144.60% and 166.82% for first crack & ultimate strength of M2 and M3 grade of concrete compared to M1 grade of concrete.

For M3 Grade of Concrete

Addition of 0.0%, 0.1%, 0.2% and 0.3% dosage of Polypropylene fibres in plain concrete improves the characteristic no. of blows to a maximum extent of 1.30% - 97.06% for first crack and 4.51% - 103.79% for ultimate strength. Addition of 0.2% and 0.3% dosage of Polypropylene fibres in plain concrete shows improvement in no. of blows by 3036.92% - 7366.15% for first crack & ultimate strength of M2 and M3 grade of concrete compared to M1 grade of concrete.

REFERENCES

- [1]. Bentur, A., Mindess S., and Skalny, J.,1989, 'Reinforcement of normal and high strength concrete with fibrillated polypropylene', fiber reinforced cements and concretes recent developments edited by R.N.Swamy, ISBN 1-18166-415-7,pp.229-239.
- [2]. Bischoff, H., Yamura, Perry, 'Polystyrene aggregate concrete subjected hard impact'. Structural Engineering Group Part 2, 1990, 89 June 225-239.
- [3]. Chauvel, D.Razani, M., 'Impacts on Fibre Reinforced Concrete slabs', fiber reinforced cements and concretes recent developments edited by R.N.Swamy, 1989, ISBN 1-85166-415-7, pp.274-283
- [4]. Chu, G.S., Bentur, T., 'impact loads on fiber reinforced concrete', international journal of impact engineering, Vol.27, No.8,pp.622-631,1997.
- [5]. Gorst.N.J.S., and Wood.J.G.M.,1992, A torsional test for the assessment of the deterioration of the concrete , Fracture Mechanics of Concrete Structures, edited by Z.P. Basant , Elsevier, London,pp.582-587.
- [6]. IS 383-1970, specification for coarse and fine aggregates from natural sources for concrete
- [7]. IS 10262-1982, Code of Practice for Concrete Mix Design Indian Standard.
- [8]. IS 456:2000, Code of Practice for Plain and Reinforced Concrete Indian Standard.
- [9]. Lifshitz, J.M., Gov f., and Gandelsman, M., 'Instrumented low-velocity impact of CFRP beams', international journal of impact engineering Vol.16, No.2, pp.201-215, 1995.
- [10]. P. Soukatchoff , M.A. Glinicki, A. Vautrin, , J. François-Brazier, 1993, Plate impact testing method for GRC materials, Cement and Concrete Composites, Volume 16, Issue 4, Pages 241-251.
- [11]. Shivaraj .K, George.Y., and Sokke, 1989, Flexural fatigue strength, endurance, limit and impact strength of the fibre reinforced refractory concretes, Fibre reinforced cements and concretes recent developments edited by R.N.Swamy , ISBN, 1-85166-415-7,pp.261-273.
- [12]. Soroushian P., and Mirza, F., 'Permeability and resistance to Impact and abrasion of polypropylene fiber reinforced concrete', fiber reinforced cement and concretes recent developments. Edited by R.N.Swamy, 1982 published by E & FN spon, 2-6 boundary row, London SE1 SHN, ISBN 0419 18130, pp.218-233.
- [13]. Wang.N, SidneyMindness and Keith Ko, 1996, Fibre Reinforced concrete beams under impact loading, Cement and concrete research, Vol.26,No.3,pp.363-376.
- [14]. Zhou G., and Davies, G.RO., 'Impact response of thick glass fiber reinforced polyester lamintes', international journal impact engineering. Vol.16, No.3, pp.357-374.1995.

Examination of thermal comfort in a naturally ventilated hostel using PMV-PPD model and field survey

OLANIPEKUN Emmanuel Abiodun

¹Department of Building Obafemi Awolowo University, Ile-Ife, Nigeria

ABSTRACT : The application of Predicted Mean Vote (PMV) and Predicted Percentage Dissatisfied (PPD) indices for thermal comfort quality assessment in naturally ventilated (NV) buildings in warm-humid climate has been observed to lead to overestimation of occupants' comfort and dissatisfaction levels. The thermal comfort quality in a naturally ventilated hostel located in Obafemi Awolowo University, Ile-Ife was determined using PMV and PPD indices. The measured indoor air temperature and relative humidity were 28.1-34°C and 30.8%-75.5%. The subjective assessments showed that more than 80% of the respondents were comfortable (PD < 20%) while the PPD index predicted that 58% of the occupants were not comfortable. The calculated PMV index on the average was +1.63. There was no correspondence between the thermal conditions predicted by PMV-PPD index and actual comfort vote. Fanger's PMV-PPD model cannot be used to predict indoor climate in the study area as it overestimated occupants' comfort and dissatisfaction levels.

KEY WORDS: PMV-PPD model, thermal comfort, NV hostel, field survey.

I. INTRODUCTION

Based on the relevant statistics, people spend 80% of their lifetime indoors [Wei et al., 2011]. Indoor environment, therefore, should be made safe, healthy and comfortable as much as possible. It has been shown that the productivity will be increased by 15% when occupants are satisfied with their thermal environments [Kim and Kim, 2007]. In students housing it has been found that thermal comfort affects the academic performance, intellectual capability and development of students [Dhaka et al., 2013; Appah-Dankyi and Koranteng, 2012]. Fanger [1972] also believed that human intellect performance and perception in general will reach its maximum potential if human being is in a comfortable thermal condition. Zhang et al. [2009] observed that thermal comfort also played a very important role in the provision of quality sleeping environment for occupants of hostel buildings. A quality night sleep has been observed to play a significant role in allowing adequate daytime functioning: concentration, attention and comprehension as well as learning level [Sekhar and Goh, 2011; Lin and Deng, 2006]. Sleep has been shown also to be an important factor that affects students' health [Teli et al. 2012].

Naturally ventilated buildings (NV) used the freely available resources of wind and solar energy and with proper design, they could represent an alternative technique for reducing the energy consumption in buildings and for creating sustainable thermal comfort and healthy indoor conditions [Stavrakakis et al., 2012]. According to Stavridou and Prinos [2013] natural ventilation promotes not only protection and restoration of indoor air, but also sustainability and energy saving. Despite these acclaimed benefits, the results of recent studies conducted on NVBs often deviated from the actual scenario [Cândido et al., 2010; Haase and Amato, 2009]. Respondents demanding for cooler environment and more air movement were more numerous than those demanding for warmer and less air movement and that they did not provide a significant cooling potential during hot season in warm-humid tropical climate. Besides this, the issues that often arose and complained about by residents of NV hostel buildings were that; less comfortable indoor environment in their inhabited buildings because of high temperatures in the building and that air movement was less effective and these problems were mainly noticed in the afternoon. Recent trends showed a heavy usage of mechanical ventilation devices for effective distribution of air in securing thermal comfort. This led to tremendous amount of energy required for improving indoor thermal environment.

It is well known that poor thermal comfort forced the users to look for high energy alternatives to achieve thermal comfort [Indraganti, 2010]. With the ever growing awareness for a need to reduce building energy use and the roles naturally ventilation can play in achieving this goal, it is therefore important to study the adequacy of natural wind in providing thermal comfort in buildings. Examination of thermal comfort may help in recognizing the agents of thermal problems in buildings and important variables responsible for this trend in higher energy usage. In Nigeria, several researchers have investigated indoor thermal environment and occupants' thermal comfort in climate responsive design buildings using field surveys and theoretical analyses [Olanipekun, 2012; Adunola and Ajibola, 2012; Adebamowo and Olusanya, 2012; Adunola, 2011; Adebamowo and Akande, 2010]. However, many of these studies were biased towards family residential buildings, although few studies were noted in office and hospital buildings. Besides, many of these researchers characterised the thermal comfort of buildings they studied from a microclimatic perspective, only a very few papers employed the PMV and PPD indices in the analysis of the indoor climate. Currently, there has been no discussion on the examination of the suitability of PMV and PPD indices in naturally ventilated hostel buildings. There is another matter that seems to be not investigated at all in the past studies; calculating the percentage of dissatisfied on the basis of the judgement of those people who voted ± 2 and ± 3 is consistent with the subjective judgement of those people who rated the environment as acceptable. Therefore, it is the intention of this study to fill this gap, by providing information on the applicability of PMV and PPD indices to evaluate the thermal comfort in this type of dwellings where the use of non-air conditioning was employed, focusing on a naturally ventilated hostel building in Obafemi Awolowo University, Ile-Ife. The first objective assessed the indoor thermal conditions of the selected hostel through measurement of microclimatic parameters. The second objective characterised the indoor thermal conditions of the selected hostel using PPM-PPD model and Percentage Dissatisfied (PD) index based on questionnaire. The third objective investigated the actual thermal sensation of the students to their environment. The fourth objective examined the compatibility of the PMV-PPD model with the actual thermal sensation of the students. Finally, the applicability of PMV-PPD index in the selected NV hostel was investigated.

II. RESEARCH METHODOLOGY

The selected method in this research is field survey. Field studies allowed for analyses of many of the contextual factors and other factors than those that can be simulated in climate chamber, as the subjects provided responses in their everyday habitats, wearing their everyday clothing and behaviour without any additional restrictions. In the field survey people are able to act as 'meters' of their environment [Adebamowo and Olusanya, 2012]. The field study was conducted in hot season from January to March, 2013. Meteorological data showed that hot season in Ile-Ife is characterised by high humidity and temperature with low air movement.

Climate and characteristics of the selected hostel building

In this study, a prototype for the examination of thermal comfort in hostel buildings was presented using PMV-PPD model in addition to field measurement of thermal comfort parameters and thermal sensation vote (TSV) of occupants. The field survey was carried out in a naturally ventilated hostel building located on the campus of Obafemi Awolowo University, Ile-Ife. The city of Ile-Ife is located on latitude $4^{\circ}35'N$ and longitude $7^{\circ}30'E$. Ile-Ife, situated in the well-known "Southwest" part of Nigeria, is about 250 km away from Lagos (former capital city of Nigeria). Within a warm-humid tropical area, the town has its unique climatic characteristics of evident rain and dry seasons that correspond to the months of April to October and November to March respectively [NIMET, 2009].

The hostel building is a low-rise reinforced concrete structure of three floors and oriented at 15 degrees to the true north [as shown in Fig.1]. The walls were made of sandcrete hollow blocks. The thickness of the external and the internal wall (north, south, west, and east walls) is 300 mm. The building is rectangular in shape, being 65m long, 12 m wide and 10 m high. Its window is 1.5 m wide by 1.8 m high and consisted of wooden/aluminum frame and single (4mm) common plain glass. The window to wall ratio (WWR = 0.35). The hostel building with its north-south facing windows, is in the midst of other hostel buildings of similar height and construction. Purposive sampling was adopted for the selection of the hostel due to insufficient measuring equipment and was specifically selected for thermal comfort performance analysis as regards to its implementation of bioclimatic design strategies. Specifically, passive design strategies related to the use of natural ventilation for cooling, important thermal mass, orientation and morphology of the building were optimised, overhangs are dimensioned to ensure reduced solar gain and avoidance of direct solar heat gain during the year, similar construction map and layout, same material and walls as other hostel buildings, besides the availability and will of the occupants to take part in the investigation.

(a)



(b)



Fig. 1: General view of the case study building (a) roof overhang (b) screen wall

Data collection method

Thermal comfort logging, questionnaire survey and observation were utilized for data collection in this short-term field study investigation. Using a combination of research methods is common in field studies and helps to balance the strength and weakness inherent in individual data collection strategies.

Objective measurement of the outdoor and indoor environment

The six physical parameters needed for the evaluation of PMV and PPD indices are air temperature, relative humidity, air movement, mean radiant temperature, metabolic rate and clothing insulation. Typically, thermal comfort field studies measured the first three parameters with instruments and calculated the later three factors from measurements, questionnaire data and observation. In this study, the first three parameters were measured by thermal comfort meter (Kestrel model 4500 pocket and handheld weather tracker. The other three parameters were determined using information derived from measurements, questionnaire data and observation. The measurements of thermal comfort parameters were carried out at three points in each room and at each sampling point each parameter was measured three times to ensure accurate data collection. The average value of each measured variable was used for subsequent analysis. The instrument setup was placed closed to the subjects when recording the environmental conditions, while the respondents filled in the comfort questionnaire. To maximize the reliability of the calculation of the PMV index and minimize the effect of the measurement accuracy on the assessment of the thermal environment, the measurement protocols and the instruments used for the assessment of physical variables were compliance with ISO 7726 [2003]. In order to compare the thermal comfort on the inside of the hostel building with outside thermal conditions, the meteorological data were obtained from the Department of Physics, Obafemi Awolowo University, Ile-Ife.

Subjective measurement

In the next stage of data collection, questionnaire survey was employed to evaluate the thermal sensation of the respondents regarding the thermal comfort parameters. The questionnaire was divided into four sections: the first section centred on the demographic data of the respondents. The second section of the

questionnaire was used to collect data on the clothing and the activities of the respondents. The third second section asked the respondents to evaluate their thermal environment at the moment of measurement. The last section was a checklist on the use of different thermal environmental controls. However, this was not discussed in this paper. The influence of thermal environment on occupants was assessed using the subjective scales according to the ISO 10551 Standards [2003]. The questionnaire was distributed directly by the researcher in company of research assistants. The survey was done in the rooms of the selected hostel systematically stratified. The number of respondents who answered the questionnaire was 96.

Thermal sensation model

PMV is an index that predicts the mean value of the votes of a large group of persons on a seven-point thermal sensation scale (see Table 3). To calculate PMV and PPD indices equations derived by Fanger [1970] were used for the evaluation of PMV and PPD indices. The mathematical expression of Fanger's PMV-PPD model are as given by Eqs. (1) and (2)

$$PMV = (0.303e^{-0.036M} + 0.028) \{ (M - W) - 3.05 \times 10^{-3} (5733 - 6.99 (M - W - Pa) - 0.42 (M - W) - 58.15) - 1.7 \times 10^{-5} M (5867 - Pa) - 0.0014M (34 - T_{mrt}) - 3.96 \times 10^{-8} f_{cl} (T_{cl} + 273)^4 - (T_{mrt} + 273)^4 - f_{cl} h_c (T_{cl} - T_{mrt}) \} \quad (1)$$

$$PPD = 100 - 95 \exp(-0.03353 PMV^4 + 0.2179 PMV^2) \quad (2)$$

where M is the metabolic rate (W/m^2), W (W/m^2) is the external work (equal to zero for most activity), Pa (kPa) is the partial water vapour pressure, T_i ($^{\circ}C$) is the indoor mean temperature, f_{cl} (-) is the ratio of body's surface area when fully clothed to body's surface area when nude, T_{cl} ($^{\circ}C$) is the surface temperature of clothing, T_{mrt} ($^{\circ}C$) is the mean radiant temperature, h_c (W/m^2C) is convective heat transfer coefficient between the occupant and the environment.

$$T_{cl} = 35.7 - 0.028(M - W) - I_{cl} \{ 3.96 \times 10^{-8} f_{cl} [(T_{cl} + 273)^4 - (T_{mrt} + 273)^4] + f_{cl} h_c (T_{cl} - T_i) \} \quad (3)$$

$$h_c = \max [2.38(T_{cl} - T_i)^{0.25}; \sqrt{12.1 v_{ar}}] \quad (4)$$

$$v_{ar} = v_a + 0.005(M/A_{DU} - 58.15) \quad (5)$$

$$f_{cl} = \begin{cases} 1.00 + 1.290 I_{cl} & \text{for } I_{cl} < 0.078 \\ 1.05 + 0.645 I_{cl} & \text{for } I_{cl} > 0.078 \end{cases} \quad (6)$$

where v_a (m/s) is the air velocity, v_{ar} (m/s) is the relative air velocity to the human body, and I_{cl} ($m^2/^{\circ}CW$) is the thermal resistance of clothing.

$$Ps_1 = -\log^{-1} [30.59051 - 8.2 \log (T_i + 273.16) + 0.0024804 (T_i + 273.16) - \frac{3142.31}{T_i + 273.16}] \quad (7a)$$

$$Ps_2 = 0.1333 \exp [18.6686 - \frac{4030.31}{T_{mrt} + 235}] \quad (7b)$$

To decrease the calculation error, the partial water vapour pressure was obtained using

$$Pa = \frac{Ps_1 + Ps_2}{2} RH \quad (8)$$

where RH (%) is the relative humidity of the indoor air.

$$A_{DU} = 0.202 W_b^{0.425} + H_b^{0.725} \quad (9)$$

It can be observed from Eqns (1) – (9) that the calculation of PMV is an iterative process.

With a computer program developed in Microsoft Excel software based on the algorithms proposed in the ISO 7730 standard [2005], the values of PMV index were estimated using all the four environmental parameters (air temperature, MRT, air velocity and relative humidity) and the two personal variables (activity and clothing of respondents) collected during the monitoring period as input parameters. The MRT was determined using the regression model proposed by Nagano [2004]. Clothing thermal insulation and metabolic rates values were determined from the individual clothing articles indicated in the survey responses and observation made during the survey. Based on this information and observation and using the standard lists, the clothing insulation (clo) was estimated using the summation formula [ANSI/ASHRAE Standard 55-2004] $I_{cltot} = \sum I_{clu,i}$ where, I_{cltot} was the insulation of the entire ensemble and $I_{clu,i}$ was the insulation of the individual piece of garments. On the average the values of the clothing ensemble insulation and the metabolic rates of the respondents were calculated as 0.42 clo and 1.06 met respectively. Based on the calculated PMV, the thermal comfort of the space was determined from Table 1. For comparison purpose, the appropriate range for thermal comfort were $-0.5 < PMV < 0.5$ and $-1.0 < PMV < 1.0$ in which 90% and 80% of people have comfort sense.

Table 1

The qualitative and quantitative statements of thermal sense

PMV	-3	-2	-1	0	+1	+2	+3
Thermal sensation	Cold	Cool	Slightly cool	Neutral	Slightly warm	Warm	Hot

Percentage Dissatisfied (PD) index based on questionnaire was also computed. To determine PD index, the number of respondents who expressed discomfort on 7-point ASHRAE thermal comfort sensation scale were determined. The expression of discomfort is known if the respondent answers between (-2, -3) and (+2, +3) to any of the thermal sensation questions, this question was labelled as a discomfort one. Following Pourshaghaghly and Omidvari [2012] methodology the PD index based on the questionnaires in any section of the hostel building was then computed using the following expression

$$PPD = \frac{\text{The number of questionnaire having discomfort label}}{\text{Total number of questionnaire in any section}} \times 100 \quad (10)$$

III. RESULTS AND DISCUSSION

Environmental conditions during the monitoring period

During the period of the field measurement, the weather conditions vary with time on different days of months. An extremely hot day of every month was chosen as the representative day for the field survey in the present paper. Statistical summaries of measured physical thermal comfort parameters of indoor and outdoor climatic data are provided in Table 2. For the month of January, outdoor air temperature (t_a) ranged between 22.5°C and 32.6°C (mean = 29.3°C, STD = 3.21). In February from 25.1°C to 32.9°C (mean = 30, STD = 2.36) and in March from 26°C to 31.8°C (mean = 29.5°C, STD = 1.97) representing temperature swing of 10.1°C, 7.8°C, and 9.6°C, respectively. In January, outdoor relative humidity showed low values in January and fell within 20.36% and 49.34% (mean = 28.86%, STD = 8.70). In February, the relative humidity (RH) fell within 42.88% and 85.82% (mean = 59.01%, STD = 13.99). In March, relative humidity showed high mean value (66.34%) as against January (28.86%) and February (59.015%).

In January, the indoor air temperature varied from 28.4°C and 33.7°C (mean = 30.9°, STD = 1.71), in February from 28.1°C to 33.9°C (mean = 31.2°C, STD = 1.87), and in March from 28.5°C to 34°C (mean = 31.3°C, STD = 1.96) representing temperature swing of 5.3°C, 5.8°C, and 5.5°C, respectively. In January, RH fell within 31.8% and 71% (mean = 46.16%, STD = 12.45). In February, the RH ranged from 30.8% and 75.5% (mean = 45.72%, STD = 14.03) about 4% higher than January record. RH decreased in March with a range of 32.8-66% (mean = 44.48%, STD = 11.89).

Table 2:

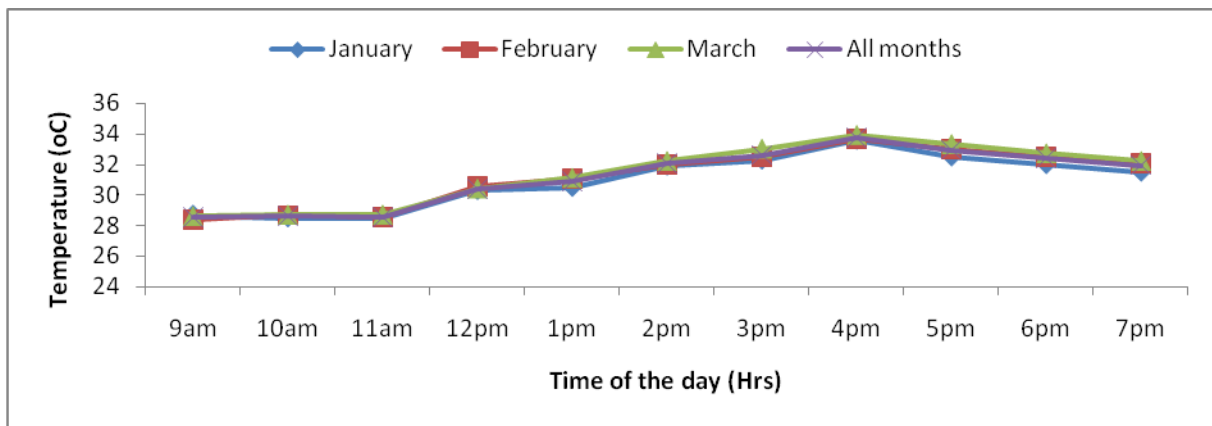
Statistical summaries of measured physical thermal comfort parameters of indoor and outdoor climatic data

Month	Descriptive statistic	T_o (°C)	RH _o (%)	T_a (°C)	RH (%)	PMV	PPD
Jan	Mean	29.3	28.86	30.9	46.16	1.6	56.65
	Max	32.6	49.34	33.5	71	2.28	87.65
	Min	22.5	20.36	28.4	31.8	0.87	20.83
	STD	3.21	8.70	1.71	12.45	0.49	24.39
Feb	Mean	30	59.01	31.2	45.72	1.61	56.75
	Max	32.9	85.82	33.7	75.5	2.31	88.6
	Min	25.1	42.88	28.1	30.8	0.86	20.81
	STD	2.36	13.99	1.86	14.03	0.53	25.90
Mar	Mean	29.5	66.34	31.3	44.48	1.65	58.32
	Max	31.8	84.02	34	66.3	2.39	90.82
	Min	26	51.19	28.5	32.8	0.88	21.51
	STD	1.98	10.89	1.96	11.89	0.57	27.67
All months	Mean	29.6	51.40	31.1	45.45	1.63	57.81
	Max	32.9	85.82	34.0	75.5	2.24	86.21
	Min	22.5	20.36	28.1	30.8	0.87	21.09

	STD	2.50	19.83	1.81	12.64	0.51	25.29
--	-----	------	-------	------	-------	------	-------

Fig. 2(a) and (b) show the profiles of measured indoor air temperature and relative humidity data respectively. The maximum proportion (63.6%) of indoor air temperature fell within 30°C and 33°C while 36.4% ranged between 28°C and 30°C. The lowest temperature was recorded at 9 am in the morning, while the highest temperature occurred at 4 pm in the afternoon. There was minimum deviation of the measured air temperature across the three months (mean $T_a = 30.9^\circ\text{C}$, 31.1°C , 31.3°C). The low change in various temperature intervals was because for these months the difference between mean radiant temperature and dry bulb temperature is less than 1°C and wind speed is less than 0.1 m/s . Similar higher indoor air temperature was also experienced across the three months. According **Djamila et al. [2013]**, the higher temperature variations observed are common with concrete structure in this climatic zone. In comparison with standards, none of the measured temperature data fell within 23°C and 26°C , which is the summer thermal comfort zone limits defined by the ASHRAE Standard 55-2004. For all months about 58% of measured RH data was in the range of 30%-70%. 21% of the data fell below 30% while the same percentage (21%) also fell above 70%. The percentage of relative humidity on the higher floor was better than that on the ground floor. The diurnal variation in relative humidity in these three months was moderate (20-42%).

(a)



(b)

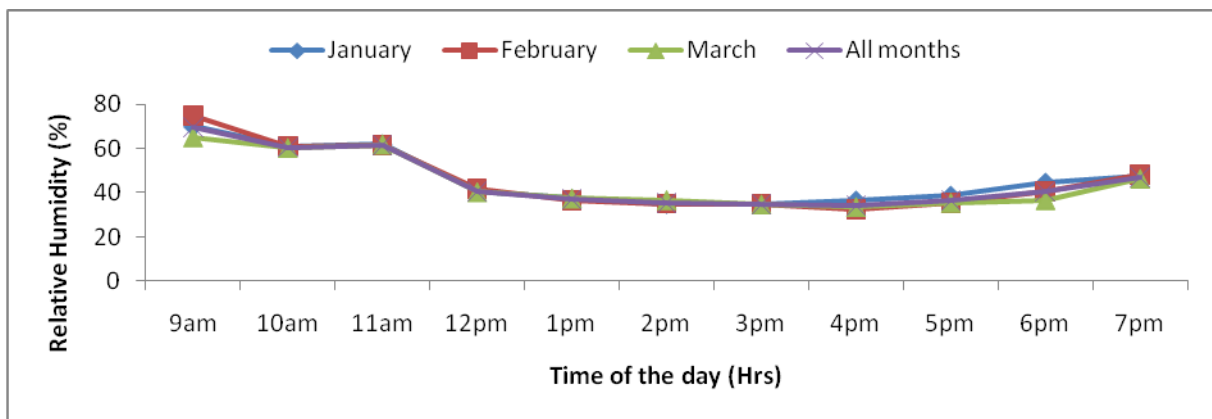


Fig. 2: Profiles of measured indoor environmental variables (a) Air temperature data (b) RH

Relationship between indoor and outdoor climatic data

Fig. 3 shows the relationship between the indoor and outdoor environmental variables recorded during this survey. The indoor environments followed the outdoor conditions closely. There was a close match of indoor air temperature with outdoor temperature climate, which is a key feature of NV buildings that is greatly different with a constant indoor temperature in AC (Fig. 3 (a)). The change in the indoor temperature was similar to the change of the outdoor temperature, but the difference between the indoor and outdoor temperatures was

small. In most cases, the indoor temperature was always higher in comparison to outdoor temperature. So, it can be concluded that, this thermal behavior may lead to discomfort. The relative humidity of the indoor condition during this study was lower than the outdoor relative humidity except in January when low values of relative humidity were recorded may be due to prolonged harmattan with dry spell (Fig. 3 (b)). The indoor temperature correlated strongly with outdoor temperature ($r = 0.7742, 0.8011, 0.918, N = 96, p < 0.01$), outdoor RH but their relativities were negative ($r = -0.5598, -0.8684, -0.7306, N = 96, p < 0.01$) and robustly with indoor RH as well ($r = -0.8393, -0.8905, -0.9058, N = 96, p < 0.01$). Indoor RH showed a significant relationship with outdoor RH ($r = 0.9406, 0.9178, 0.9651, N = 96, p < 0.01$). This makes humidity an important variable for thermal comfort in this area. The same tendency between indoor and outdoor temperature correlation was noted in Indraganti et al. [2013] and Hwang et al. [2009] studies.

The temperature profiles also provided important information regarding temperature swing and time lag between maximum temperatures of both indoors and outdoors of the hostel. The indoor and outdoor temperature swing in these three months was very small. Outdoor temperature swings were 10.1°C , 7.8°C , and 5.8°C for the months of January, February and March respectively. The corresponding indoor temperature swings were 5.1°C , 5.5°C and 5.6°C for the above months, respectively. Maximum temperature swing inside the hostel was 5.6°C , which is quite acceptable for naturally ventilated buildings [Singh et al., 2010]. The difference between the maximum outdoor and indoor temperature was 1.1°C . The highest outdoor temperature was 32.9°C and occurred at 03:00 pm while the highest indoor temperature noted for all sample hostels was 34°C , occurred at 4 pm. This gave a temperature difference of 1.1°C and time lag of 1 h. This time lag also provides critical information regarding the insulation level of the hostel.

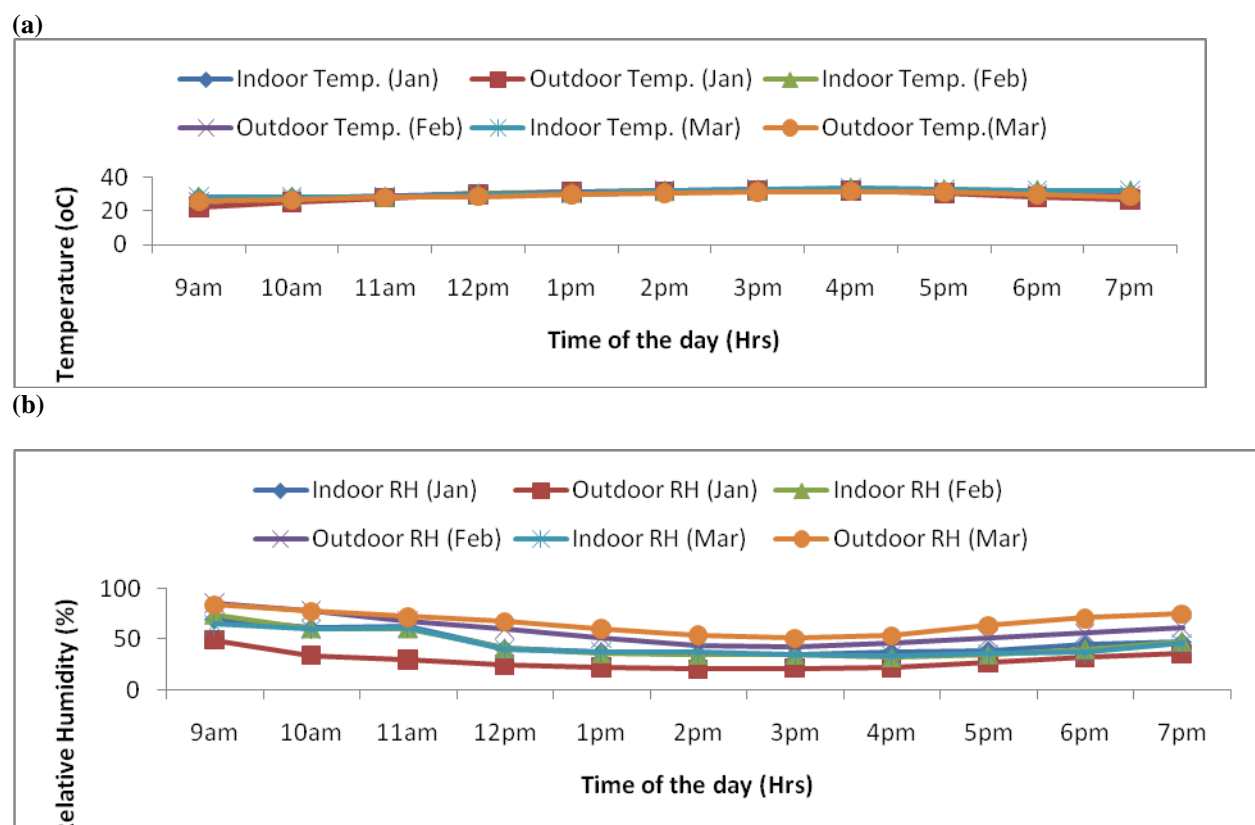


Fig. 3: Relationship between the indoor and outdoor environmental variables (a) Relationship between the indoor and outdoor air temperature (b) Relationship between the indoor and outdoor RH

Results of PMV and PPD indices

The results of the calculated values of PMV and PPD indices across different months and floors are shown in Tables 3 and 4. For the sample months, the calculated PMV index on the average was +1.63 while the calculated value of PPD index was 57.8% and these indicated that the hostel was observed to be in between

“slightly warm” and “warm” category and that approximately 58% of respondents were predicted to express dissatisfaction with the environment. Table 4 showed that in January when the PMV was +1.60, the PPD was 56.65%. In February, when the PMV was +1.63 PPD value was 56.75% while in March when the PMV was +1.65, PPD was 58.32%. In terms of floor performance (Fig. 6), the PMV values on the ground were lower as its values showed (PMV values = +1.37, +1.54 and +1.57) as against second floor with (PMV = +1.65, 1.67, 1.71]. Based on Table 5, the worst thermal conditions occurred on the second floor across the different months. The t-test on data presented in Tables 5 and 6 revealed that there was no noticeable difference between the PMV values across all floors and different months. This was due to the fact that in these months there was no much difference in the measured indoor environmental variable. The PMV-PPD model was also verified with a set of observations obtained in some previous field studies in NV buildings. It was found through comparison that the values of PMV and PPD indices of the present study were very similar with those obtained by Dhaka et al. [2013], Wafi et al. [2011] and Mohazabieh et al. [2010] in their studies on NV buildings.

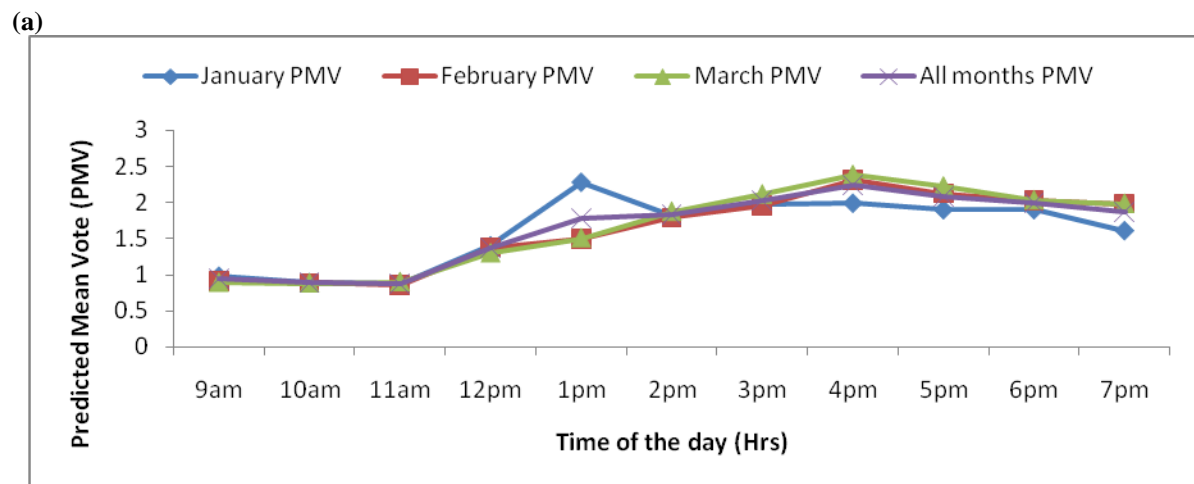
Table 3
Summary of PMV and PPD indices across different months

	January	February	March	All months
PMV	1.60	1.63	1.65	1.63
PPD	56.65	56.75	58.32	57.81

Table 4
Summary of PMV an PPD indices by floors across different months

	January			February			March		
	Grd	Sec	All	Grd	Sec	All	Grd	Sec	All
PMV	1.37	1.65	1.53	1.54	1.67	1.64	1.57	1.71	1.64
PPD	44.41	58.41	53.22	53.27	59.5	58.04	54.48	61.25	57.81

Fig. 4 shows the profile of the PMV values versus time of the day. For the sample months, the range of calculated values of PMV index fluctuated from -0.87 to +2.39 and the majority of them were between +1.37 and +2.24 regardless of the month. It was also observed that for the day and at different time, the PMV values fluctuated rapidly with time because of the drastic fluctuation of solar radiation. Although, the hostel building is protected from direct solar radiation, it was found that there was an increasing trend for the PMV values-directly influenced by the outdoor conditions with time from morning (+0.82-+1.08) to afternoon (1.25-2.39). This showed that outdoor conditions play a role in influencing indoor thermal environment (i.e. PMV values). While the main climatic elements affecting building thermal comfort level (PMV) are solar radiation, air temperature, humidity, wind and rainfall [Mohazabieh et al., 2010; Markus and Morris], solar radiation is the most important element among all, as it influenced the amount of heat transfer to buildings and residents. Besides, the thermo-physical properties, structure, size and orientation are of significant effects on the indoor thermal environment. It is essential for designers to pay more attention to these factors in the early stage of hostel building design.



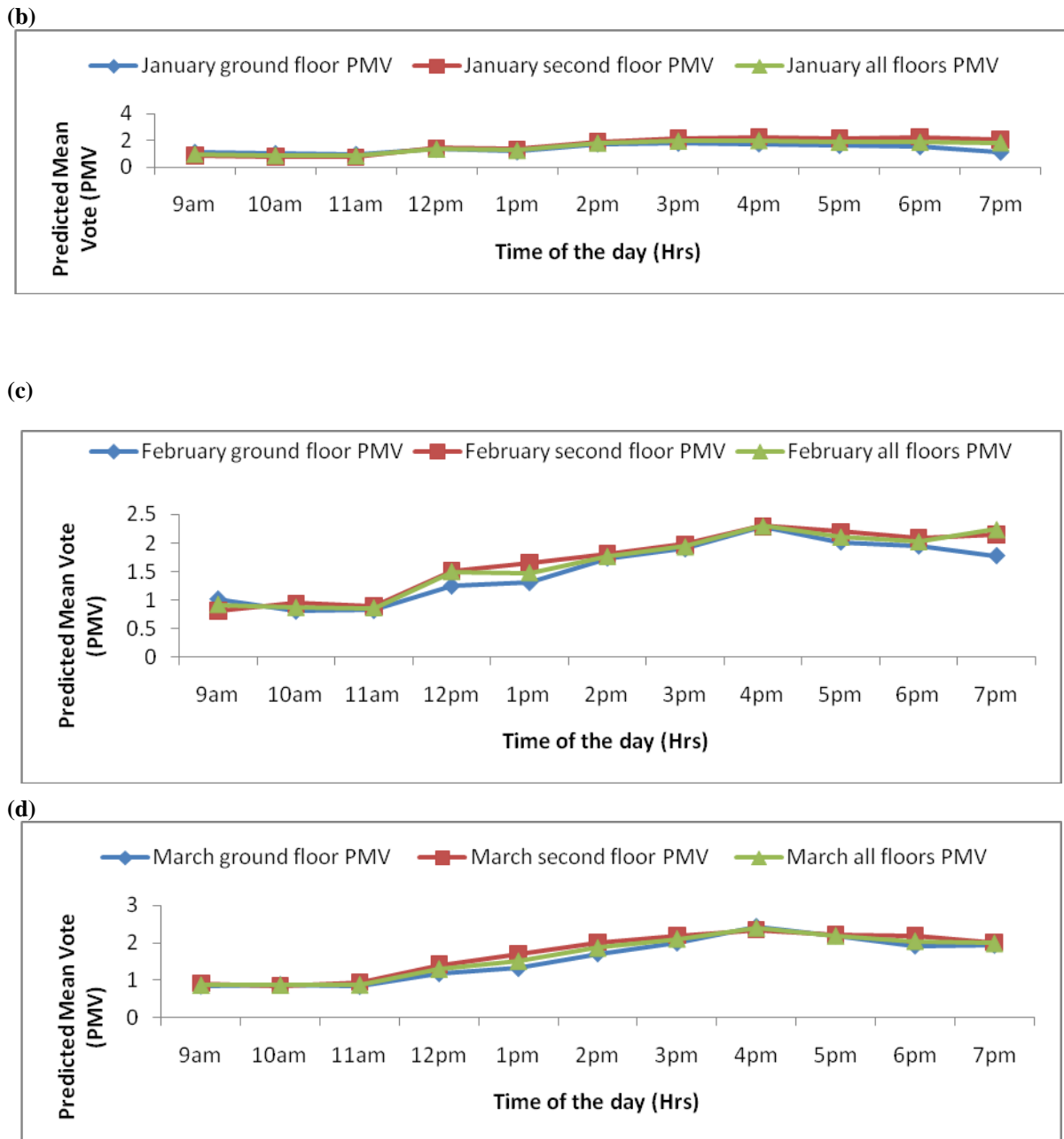


Fig. 4: Time series of PMV values versus time (a) monthly distribution (b) distribution by floor in January (c) distribution by floor in February (d) distribution by floor in March

Fig. 5 illustrated the profile of PPD values plotted against local time for the typical hottest days for the monitoring months. For the three months PPD values approximately fluctuated from 21.09% to 86.21% and great majority of them were between 50% and 70%. From Fig.56, one could observed that there was an increasing trend with time in the PPD values from morning to afternoon directly influenced by the outdoor conditions.

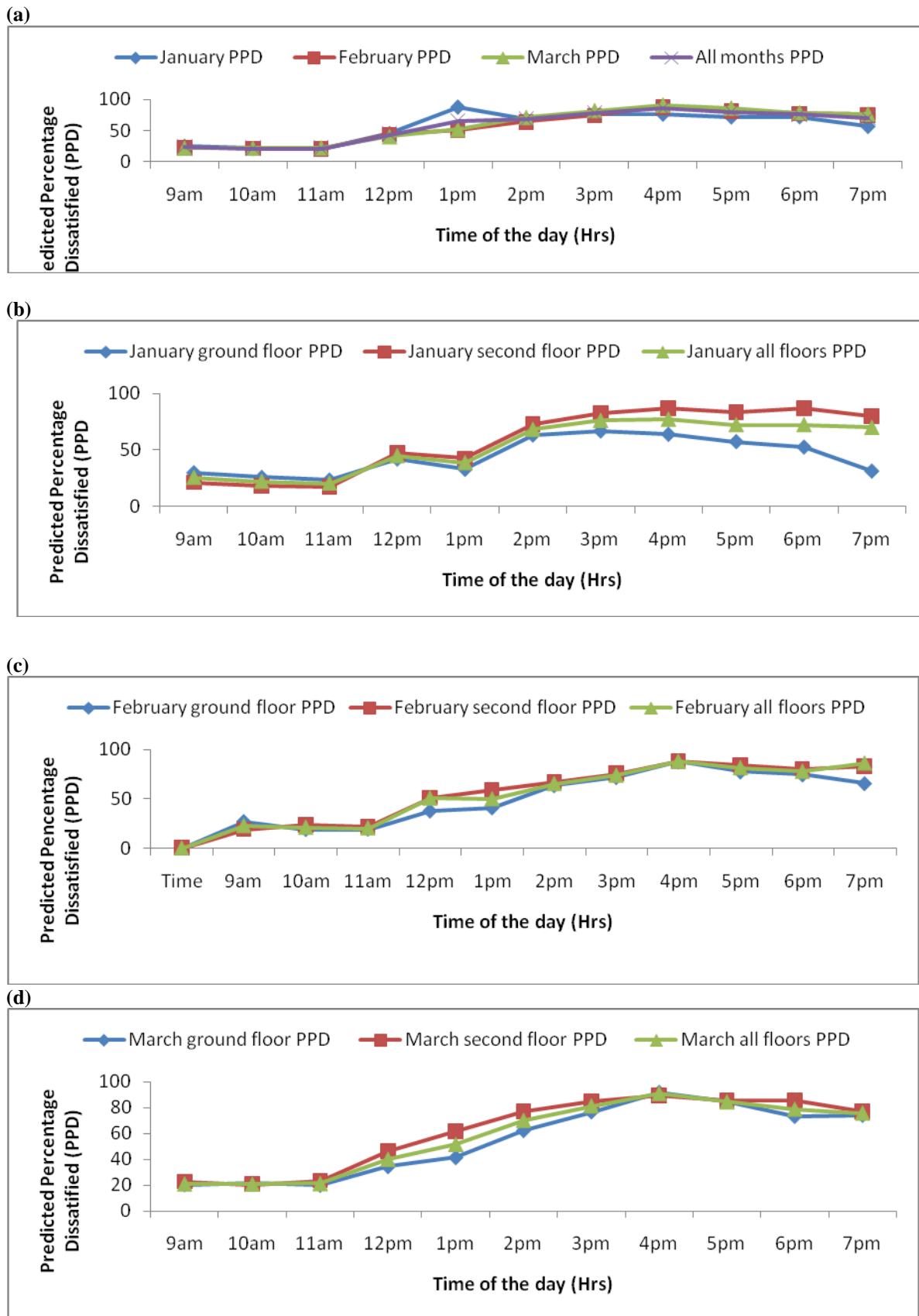


Fig. 5: Time series of PPD values versus time (a) monthly distribution (b) distribution by floor in January (c)

distribution by floor in February (d) distribution by floor in March

The effects of different times of the day on thermal comfort (PMV index) were also analysed. The average indoor PMVs were calculated in three sections of the day and the results are depicted in Fig. 6. The PMV values were not within the acceptable range [-0.5, +0.5] and [-1, +1]. It was observed from this figure that the thermal conditions in the morning were better than those of the noon and the evening hours. The poorest thermal conditions occurred in noon hours between 12.00 and 16.00 pm. However, there was no significant difference between the values recorded.

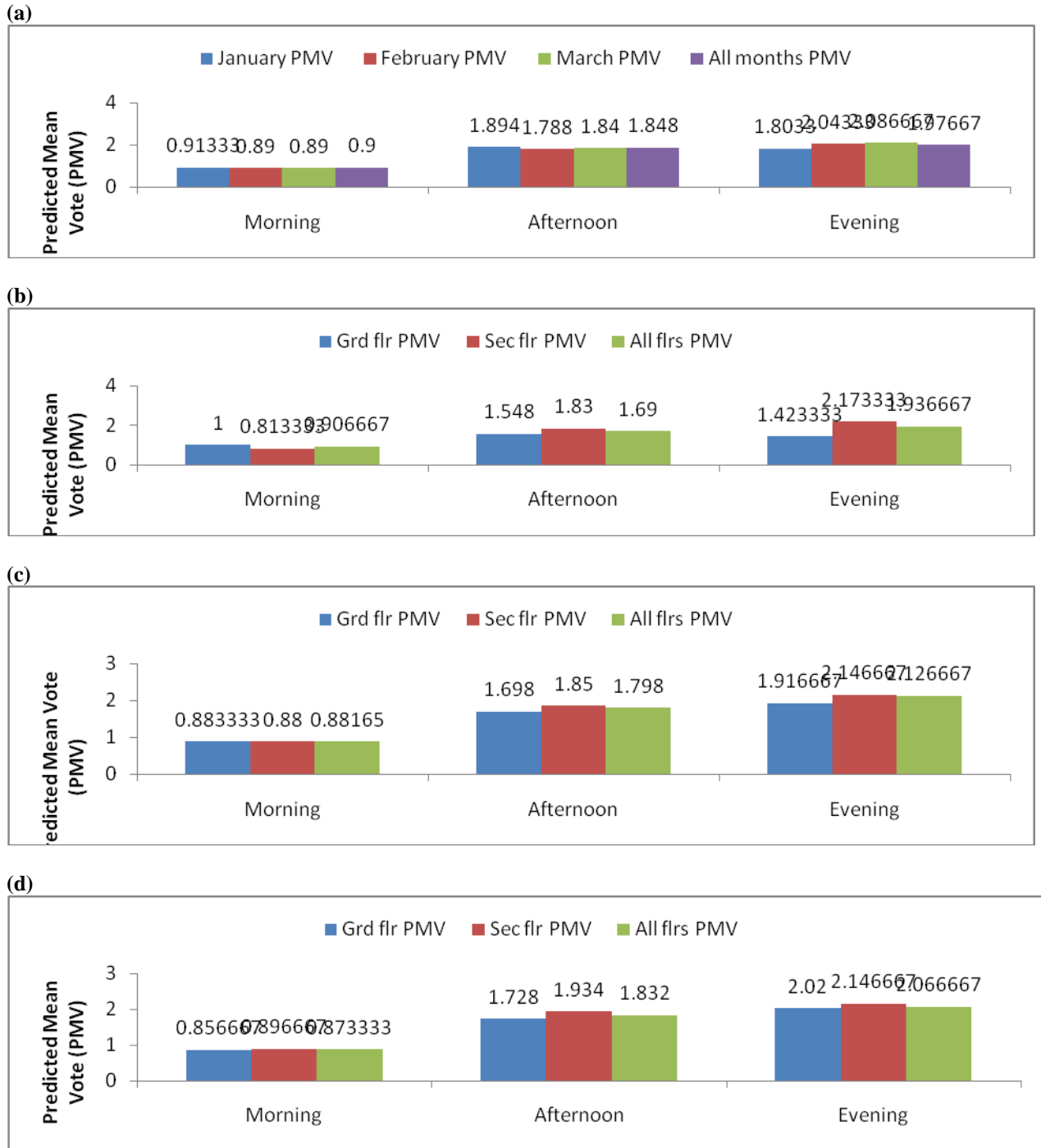


Fig. 6: PMV values by various times of the day (a) distribution by month (b) distribution by floor January (c)

distribution by floor February (d) distribution by floor March

The Percentage Dissatisfied (PD) from the questionnaire survey is presented in Table 5. In all the sections of the buildings and across the different months, the PD values obtained from questionnaire survey were less than 20%. This indicated that the percentage of respondents who were dissatisfied from thermal conditions was less than 20%. Table 5 also compared between the calculated values of PPD index and the Percentage Dissatisfied (PD) obtained from the questionnaire survey. ASHRAE Standard 55 [2004] was designed to provide 80% acceptability of the environment based on 10% dissatisfaction for general (whole body) thermal comfort and an addition of 10% dissatisfaction resulting from local discomfort. By comparing the PPD index and actual dissatisfaction (PD), it was found that there were large differences between the actual dissatisfaction rates and the calculated PPD across the different months. While the calculated values from PPD index showed that as much as 58% of respondents in the hostel building were predicted to have stated a thermal dissatisfaction with their environment, on the other hand, in all the sections of the buildings and across the different months, the PD values obtained from questionnaire survey were less than 20%. This showed that the values of PPD index were not within the acceptable range of 20% in all sections and across the different months as recommended by standard. On the contrary, the PD values were within the acceptable range of 20%. Generally, the value of PPD index based on Eqn. (2) was on the average 38% higher than that which was obtained from actual sensation vote of the respondents (Eqn. 10). Statistical Z-test showed again that there was significant difference between the respondents' opinions (questionnaire survey results) and the computed PPDs ($p < 0.005$). This indicated that the standard PPD of the ISO 7730 and ASHRAE Standard 55 overestimated the level of dissatisfaction in the selected hostel during the hot season. This is a validation of the results of previous studies and also confirmed no agreement between the real sense of thermal comfort in people and the PPD index.

TABLE 5
Comparison of PD from questionnaire with Fanger's PPD index

Indices	January	February	March	All months
Calculated PPD index	56.65	56.75	58.32	57.81
PD (questionnaire survey)	9	14.1	18	13.9

Thermal comfort on the questionnaire

Respondent demographic characteristics

Subjects of this field research were young female students of same age group average 24 years. The sample size varied each month, however, a maximum of 96 subjects voluntarily participated in the short-term survey. They were Nigerian national from different ethnic group (Yoruba, Hausa, Igbo and Edos) living in the surveyed hostel building for at least six months. Table 8 depicted the demographic characteristics of the subjects.

Table 6
Demographic characteristics of the subjects

N=96	Height (m)	Weight (kg)	Age (yrs)	Body surface area	Clothing insulation (clo)
Mean	1.68	58	24	1.65	0.58
Maximum	1.92	75	34	2.14	0.73
Minimum	1.25	47	17	1.41	0.42
STD	8.85	9.6	1.6	0.15	0.14

Respondents' real vote

Thermal sensation is the most important human responses to thermal environments and their relationships to a large extent determine the definition of optimal conditions and acceptable ranges. The real vote was based on the respondents vote regarding the thermal comfort of the hostel building. Based on the questionnaire answers of respondents, the characteristics of respondents' real vote value are described in Table 6. The ASHRAE standard 55 [2004] specified that the thermal acceptability should be defined as the condition where 80% of occupants vote for the central three categories (-1, 0, +1). The thermal sensation votes were not the same in all the months. However, there was minimum deviation of the thermal sensation votes across the different months. Comparison among the thermal sensation votes in these months showed that in January 91% of comfort votes recorded by respondents ranged from slightly cool (-1) to slightly warm (+1). The warm and

hot sides of the scale accounted for 9%. The mean thermal sensation vote (MTSV) was +0.45. In February, 85.9% of votes also ranged from slightly cool (-1) to slightly warm cool (+1). The cool side of the scale accounted for 2% and the warm side 12.1% of the votes. The MTSV was +0.56. In March, 82% of respondents perceived thermal sensation as comfortable, votes ranged from slightly cool (-1) to slightly warm (+1). The warm and hot sides of the scale accounted for 18% of the votes cast. The MTSV of respondents were around slightly warm (+0.73). It was observed that, in these three months, there was a biased towards the slightly warm category on the 7-point scale. This is to be expected since the survey was conducted in the hot season.

Table 7
Relative percentage frequency of ASHRAE thermal sensation votes

Thermal perception vote	January	February	March
Cold (-3)	0	1	0
Cool (-2)	0	1	0
Slightly cool (-1)	13.6	10.5	8.7
Neutral (0)	41	37	34.3
Slightly warm (+1)	36.4	38.4	39
Warm (+2)	4.5	8.6	11.3
Hot (+3)	4.5	3.5	6.7
Mean vote	+0.45	+0.56	+0.73

IV. SUITABILITY OF PMV-PPD MODEL FOR PREDICTING QUALITY OF INDOOR CLIMATE IN NV HOSTEL

Comparison of PMV-PPD model and standard

The PMV-PPD model employed in ISO 7730 Standard is the most accepted and widely applied thermal comfort model. However, its applicability in NV buildings has been doubted for its basis in climate chamber experiments and ignorance of thermal adaptation that usually occurred in real buildings [Zhang et al., 2010]. To ascertain its applicability in predicting the quality of indoor climate in the present building, a comparative analysis was carried out between the calculated values of PMV index and the recommendations of the standard. According to ISO 7730 [2005] an indoor environment is considered very comfortable when the values of PMV index varied between [-0.5, +0.5] and it is comfortable between [-1, +1]. These values lead to a PPD of 20% and 10% respectively. In other words, the values of PMV index between the limits of [-1, +1] and [-0.5, +0.5] correspond to the point where 80% and 90% of the respondents feel satisfied. When PMV is zero that is to say for the perfect case, the PMV is 5%. The comparison of the PMV values across the different months showed that PMV values deviated more from the acceptable range [-0.5, +0.5] and [-1, +1]. It was also observed that all sections did not have suitable thermal comfort in these months as majority of the values of PMV index were not placed within the range [-0.5, +0.5] and [-1, +1]. The comparison of the values of PMV index across the different sections of the day showed that the hostel building experienced poor thermal conditions in this season as their PMV values also deviated more further from the acceptable range [-0.5, +0.5] and [-1, +1]. The thermal conditions fell below 80% and 90% acceptability ranges. More than 80% of PMV results were mainly located in the warmer region (+1, +2) than recommended by the standard. This indicated that the microclimatic conditions observed in the hostel were typical of non-thermal neutrality $PMV > 0$. Using statistic Z-test, it was found that there was a significant difference between calculated values of indoor PMV index and the ISO 7730 recommended values ($p < 0.05$). Similarly, the obtained values of PPD index showed similar distribution with a much overestimation of the percentage dissatisfied under neutrality conditions. The calculated values of dissatisfaction (PPD) index were found to be higher (21-86%) than what the standard required. This difference in calculated values of indoor PMV and PPD indices and the ISO 7730 recommended values has also been mentioned by some researchers [d' Ambrosio Alfano et al., 2013; Azizpour et al., 2013; Giuli et al., 2013; Zhong et al., 2012].

Relationship between PMV and TSV

To further ascertain the applicability of PMV index in the selected hostel and for the purpose of discovering whether PMV and TSV were compatible, the statistical distributions of the percentage of acceptability by employing the PMV index and TSV were also verified (Table 7). The results showed no correspondence between the two different approaches. The PMV was found to be always more than the actual thermal sensation measured. The calculation of PMV using Fanger's equation showed that the values of PMV index predicted on the average between slightly warm and warm sensation category (+1.60, +1.63, +1.65) as regards different months and (+1.37, +1.57, +1.65) in relation to floor levels, which were much higher than the

direct comfort votes (MTSV = +0.45, +0.56, +0.73). Based on the above analysis, the Fanger's PMV equation predicted warmer than what respondent actually felt. This showed that the values of PMV index significantly overestimated the actual mean sensation votes of the respondents. The results in terms of voting patterns showed also that the PMV scale of thermal comfort and the thermal sensation of the hostel residents did not have enough compatibility. The values of PMV index showed that less than 80% of respondents were comfortable according to 80% acceptability of ISO 7730, 2005). On the other hand, more 80% of respondents voted for comfortable and satisfaction in their thermal environment. From the above discussion it can be inferred that the PMV vote distributions in this study have reflected that PMV predicted more pessimistically towards uncomfortable warmer prediction. Similarly, the Standard PPD model greatly overestimated the percentages of dissatisfied respondents.

It was apparent from this study that the standard model which addressed only the physical factors in the evaluation of PMV, overestimated the actual thermal sensation, which is probably affected by additional factors such as the actual or perceived level of available control over the environmental conditions, the actual ambient climate outdoor and culturally conditioned expectations. The lack of correspondence between PMV and TSV on the one hand, the disagreement between the actual levels of dissatisfaction and the Standard PPD line on the other hand, and the observed discrepancies compared with standard raised serious doubts as to the applicability, under local conditions, of the standard model in its current formulation. There were many reasons for this thermal comfort behaviour. The PMV model being a heat balance model, did not take all the adaptation of occupants into consideration although it account for clothing, metabolic rate and air velocity modification to a limited extent. Another reason was that the base temperature and clothing insulation ranges of PMV model differed from what we had come across during our survey. The PMV model considered clothing as a passive insulation around the body, but as evidenced in the present study clothing was used in more dynamic ways to alter the micro-climate around the skin. The clothing ensembles encountered in the hostel have tremendous potential for thermal adaptation and the respondents fully exploited this opportunity. This was not included in the PMV model. As Nicol and Humphreys [2004] noted PMV is a model that represents thermal equilibrium as a heat balance 'at a point in time' that cannot fully explained the temporal conditions that occupants experience in reality. In nutshell, PMV completely ignored many behavioural changes of people in Nigerian hostel building. The cumulative effect of these minor sources of error led to the gross deviation of the PMV from the actual sensation. Thus, PMV being a static heat balance model could not explicate this. Humphreys and Nicol [2002] demonstrated with convincing evidence that the errors in PMV are not just confined to NV buildings alone, but are masked by the narrow range of temperatures experienced in AC buildings as well. Our present data adds to this evidence.

Table 8
Comparison of PMV and MTSV

Index	January	February	March
PMV	+1.60	+1.61	+1.65
MTSV	+0.45	+0.56	+0.73

V. CONCLUSION AND RECOMMENDATION

The applicability of PMV-PPD model in predicting the quality of indoor climate in a NV hostel building in warm-humid area of Ile-Ife was investigated in the present study. In addition, the study examined the existing indoor thermal environmental conditions as well as occupant perception. The key findings from this study were as follows:

- Empirical measurements showed that the physical condition of air temperature, RH and velocity in the hostel were not within the limits set out by the ASHRAE Standard 55 and ISO 7730 Standard. However, occupants found their thermal environment comfortable, satisfying and acceptable.
- The measured indoor air temperature in the hostel ranged between 28.1-34°C. Relative humidity ranged from 30.8% and 75.5%.
- The thermal environment in the hostel was unacceptable to the occupants judging by the values of PMV and PPD indices
- There was no correspondence between PMV model and MTSV. While the calculated PMV index predicted the hostel indoor climate to be between slight warm and warm the MTSV showed it to be between neutral and slightly warm.
- The subjective assessments showed that the occupants were comfortable while the PPD index predicted that 58% of the occupants were not comfortable.

In conclusion, the results of this study confirmed the suggestion by previous researchers about the limitation

of the PMV-PPD model for predicting thermal comfort in NV buildings.

REFERENCES

- [1] Adebamowo, M.A. and Akande, O.K. (2010): Indoor Thermal Comfort for Residential Buildings in Hot-Dry Climate of Nigeria, 2010. <http://www.nceub.org.uk>. (Accessed: September 10, 2012).
- [2] Adebamowo, M.A. and Olusanya, O. Energy savings in housing through enlightened occupants behaviour and by breaking barriers to comfort: a case study of a hostel design in Nigeria. Proceedings of 7th Windsor Conference: The changing context of comfort in an unpredictable world Cumberland Lodge, Windsor, UK, 12-14 April 2012. London: Network for Comfort and Energy Use in Buildings, <http://nceub.org.uk>
- [3] Adunola, O. A. and Ajibola, K.O. Thermal considerations and space use within residential buildings in Ibadan. Proceedings of 7th Windsor Conference: The changing context of comfort in an unpredictable world Cumberland Lodge, Windsor, UK, 12-14 April 2012. London: Network for Comfort and Energy Use in Buildings, <http://nceub.org.uk>
- [4] Adunola, O.A. Adaptive comfort and energy-saving sustainable considerations for residential buildings in Ibadan, Nigeria. In Afon, A.O. and Aina, O.O. eds, Issues in the Built Environment in Nigeria, 2011, Chapter 17; 308-326.
- [5] ASHRAE Handbook: Fundamentals. American Society of Heating Refrigerating and Air Conditioning Engineers: specification of the conditions for thermal comfort', International Standards Organization, Atlanta, GA USA: 2009.
- [6] ANSI/ASHRAE 55: Thermal Environmental Conditions for Human Occupancy, American Society of Heating Refrigerating and Air-conditioning Engineers Inc., Atlanta, USA, 2004.
- [7] Appah-Dankyi, J. and Koranteng, C. An Assessment of Thermal Comfort in a Warm and Humid School Building at Accra, Ghana. *Advances in Applied Science Research* 2012; 3 (1):535-547
- [8] ASHRAE Standard 55: Thermal Environmental Conditions for Human Occupancy, American Society of Heating, Refrigerating and Air-Conditioning Engineering, Atlanta, GA, 2004.
- [9] Azizpour, F.S., Moghimi E., Salleh S., Mat C.H., Lim K. Sopian (2013): Thermal Comfort Assessment of Large-Scale Hospitals in Tropical Climates A Case Study of University Kebangsaan Malaysia Medical Centre (UKMMC).. *Building and Environment* 2013 (In print, Access June 8, 2013).
- [10] Becker R, Paciuk M. Thermal comfort in residential buildings e failure to predict by Standard model. *Build Environ* 2009; 44 (5):948-60.
- [11] Brager, G.S. and de Dear, R.J. (1998): Thermal Adaptation in the Built Environment: A Literature Review. *Energy and Buildings* 1998;27 (1):83-96.
- [12] Cândido, C., de Dear, R.J., Lambert, R. and Bittencourt, R.L. Air movement acceptability Limits and Thermal Comfort in Brazil's Hot Humid Climate Zone. *Building and Environment* 2010;45:222–229
- [13] d'Ambrosio-Alfano F.R., Ianniello E. and Palella B.I. PMV – PPD and acceptability in naturally ventilated schools. *Building and Environment* (2013), doi: 10.1016/j.buildenv.2013.05.013.
- [14] de Giuli, V., Zecchin, R., Salmaso, L., Corain, L. Michele and De Carli, M. (2013): Measured and Perceived Indoor Environmental Quality: Padua Hospital Case Study. *Building and Environment*, (59), pp. 211-226
- [15] Dhaka, S., Mathura, J., Wagner, A., Das Agarwal, G. and Garg, V. (2013): Evaluation of Thermal Environmental Conditions and Thermal Perception at Naturally Ventilated Hostels of Undergraduate Students in Composite Climate. *Building and Environment*, 66:42-53
- [16] Fanger, P.O. Thermal comfort, analysis and applications in environmental engineering. New York: McGraw-Hill; 1972.
- [17] Feriadi, H. and Wong, N. H. Thermal comfort for naturally ventilated houses in Indonesia. *Energy and Buildings* 2004;36:614–626
- [18] Haase, M and Amato, A. An investigation of the potential for natural ventilation and building orientation to achieve thermal comfort in warm and humid climates. *Solar Energy* 83 (2009) 389–399.
- [19] Humphreys MA, Nicol JF. The validity of ISO-PMV for predicting comfort votes in everyday thermal environments. *Energy and Buildings* 2002; 34: 667-684.
- [20] Hwang, R., Cheng, M., Lin, T., Chien H.J. and Ho, M. Thermal Perceptions, General Adaptation Methods and Occupant's Idea about the Trade-off between Thermal Comfort and Energy Saving in Hot-humid Regions. *Building and Environment* 2009;44:1128–1134.
- [21] Indraganti M, Ooka R, Rijal HB. Thermal comfort in offices in summer: findings from a field study under the 'Setuden' conditions in Tokyo, Japan. *Building and Environment* 2013; 61: 114-132.
- [22] Indraganti M. Thermal comfort in naturally ventilated apartments in summer: findings from a field study in Hyderabad, India. *Applied Energy* 2010; 87(3):866-83.
- [23] Indraganti, M., Ooka, R. and Rijal, H.B. (2013): Field Investigation of Comfort Temperature in Indian Office Buildings: A case of Chennai and Hyderabad. *Building and Environment* 2013; 65: 195-214.
- [24] International Standard Organisation (EN ISO 7726): Ergonomics of the Thermal Environment-Instruments for Measuring Physical Quantities, International Standardisation Organisation, Brussels, 2003.
- [25] ISO International Standard 7730. Moderate thermal environment: determination of the PMV and PPD indices and specifications of the conditions for thermal comfort, International Organisation for Standardisation, 2005, Geneva.
- [26] ISO 10551. Ergonomics of the thermal environment -- Assessment of the influence of the thermal environment using subjective judgement scales. Geneva: International Standardization Organization, 1995.
- [27] Kim K, Kim BS, Park S. Analysis of design approaches to improve the comfort level of a small glazed-envelope building during summer. *Solar Energy* 2007; 81(1):39-51.
- [28] Lin, Z. and Deng, S. (2006): A questionnaire Survey on Sleeping Thermal Environment and Bedroom Air Conditioning in High-rise Residences in Hong Kong. *Energy and Buildings*, 38:1302-1307.
- [29] Moujalled B, Cantin R, Guarracino G. Comparison of thermal comfort algorithms in naturally ventilated office buildings. *Energy and Buildings* 2008; 40 (12):2215-23.
- [30] Nicol, J.F. and Humphreys, M.A. (2002): Adaptive Thermal Comfort and Sustainable Thermal Standards for Buildings. *Energy and Buildings*, 34 (6):563-572.
- [31] Nicol, J.F. and Humphreys, M.A. (2004): A stochastic approach to thermal comfort-occupant behaviour and energy use in buildings, *ASHARE Transactions* 110 [2]:554-568.
- [32] Olanipekun, E.A. Post occupancy performance characteristics of office buildings in selected universities in Southwest, Nigeria. A PhD Thesis submitted to the Department of Building Obafemi Awolowo University, Ile-Ife 2012.

- [33] Pourshaghagh, A and Omidvari M. Examination of thermal comfort in a hospital using PMV-PPD model. *Applied Ergonomics* 2012;43:1089-1095
- [34] Sekhar, S.C. and Goh, S.E. Thermal comfort and IAQ characteristics of naturally/mechanically ventilated and air-conditioned bedrooms in a hot and humid climate *Building and Environment* 2011; 46:1905-1916
- [35] Singh, M.K., Mahapatra, S. and Atreya, S.K. Adaptive thermal comfort model for different climatic zones of North-East India. *Applied Energy* 2011; 88:2420-2428.
- [36] Stavrakakis, G.W., Zervasa, P.L., Sarimveis, K. and Markatos, N.C. Optimization of window-openings design for thermal comfort in naturally ventilated buildings. *Applied Mathematical Modelling* 2012;36:193–211
- [37] Stavridou, A.D. and Prinos, P.E. Natural ventilation of buildings due to buoyancy assisted by wind: Investigating cross ventilation with computational and laboratory simulation *Building and Environment* 2013;66: 104-119
- [38] Teli, D., Jentsch, M.F. and James, P.A.B. Naturally ventilated classrooms: An assessment of existing comfort models for predicting the thermal sensation and preference of primary school children. *Energy and Buildings* 53 (2012) 166–182.
- [39] Wafi, S.R.S., Ismail, M.R. and Ahmed, E.M. (2011) A Case Study of the Climate Factor on Thermal Comfort for Hostel Occupants in Universiti Sains Malaysia (USM), Penang, Malaysia *Journal of Sustainable Development* 2011; 4(5); 50-61
- [40] Wei, S., Li, M., Lin, W. and Sun, Y. Parametric studies and evaluations of indoor thermal environment in wet season using a field survey and PMV–PPD method. *Energy and Buildings* 42 (2010) 799–806
- [41] Zhang, L., Yuan, Q., Wu, Q., Kwauk, S., Liao, X. and Wang, C. Sleep quality and sleep disturbing factors of inpatients in a Chinese General Hospital. *Journal of Clinical Nursing* 2009; 18: 2521-2529.
- [42] Zhang, Y., Wang, J., Chen, H., Zhang, J. and Meng, Q. Thermal Comfort in naturally ventilated buildings in hot-humid area of China. *Building and Environment* 2010; 45:2562-2570.
- [43] Zhong, K., Fu, H., Kang, Y. and Peng, X. (2012): Indoor Thermal Conditions and the Potential of Energy Conservation of Naturally Ventilated Rooms in Summer, China. *Energy and Buildings*, 55:183–188.

Identification and determination of gross thickness of hydrocarbon bearing zone of Habiganj gas field.

Md. Abdul Hai¹, Shamim Ahammod², Mohammed Omar Faruque¹,

Md. Ashraf Hussain¹, Jewel Ahmed¹

¹(Department of Petroleum & Mining Engineering, Shahjalal University of Science & Technology, Sylhet, Bangladesh)

²(Department of Earth and Environmental Science, Wright State University, Dayton, OH 45324, USA)

ABSTRACT : Formation evaluation is a very important stage in prospecting for reservoir characterization and hydrocarbon bearing zone identification. The study has been carried out by qualitative and quantitative analysis. The logging data studied comprises of gamma ray, dual induction micro spherical focused log, borehole compensated sonic log, spectral density dual spaced neutron log. The gamma ray log is used to determine lithology, reservoir and non reservoir rocks, facies and depositional environment. Dual induction micro spherical focused log calculates the resistivity of the flushed zone as well as medium and deep resistivity of the invaded and uninvaded zone. Borehole compensated sonic log measures travel time through the formation and thus porosity. It analyzes fluid rock type such as hydrocarbon or formation water. Porosity is calculated by both density and neutron log. Neutron log is used to identify hydrocarbon bearing zone as well as fluid type. In well#10, Habiganj Gas Field, the hydrocarbon bearing zone is found between the depth ranging 1311m to 1505m and gross thickness is 194m. In well#11, two gas zones upper gas sand (UGS) & lower gas sand (LGS), have been detected and they are prevailed in the depth ranging from 1373m to 1485m and 3076 m to 3081m .

KEYWORDS: Formation Evaluation, porosity, resistivity, fluid type, gross thickness.

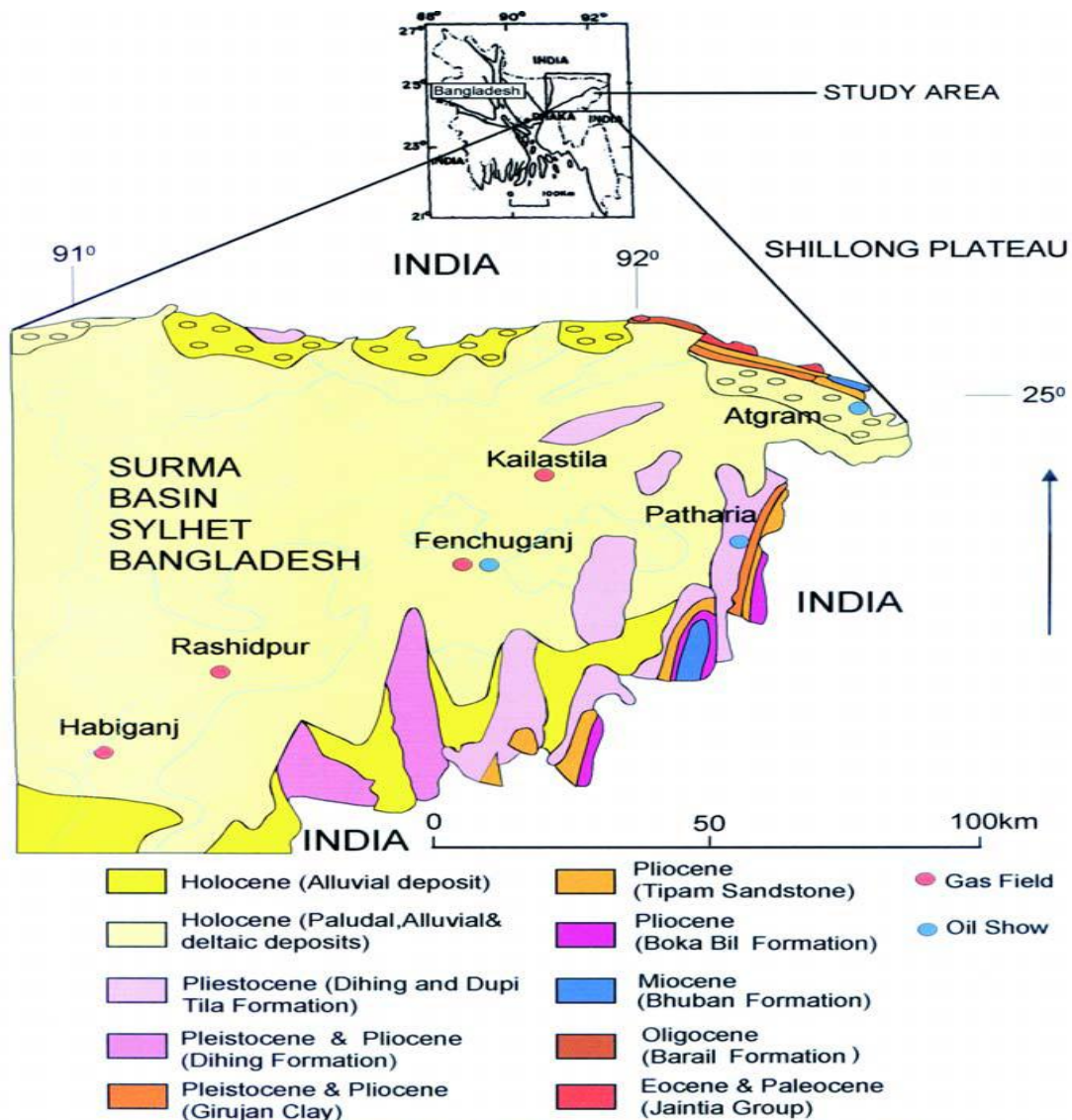
I. INTRODUCTION

Formation evaluation, a sub discipline of petroleum engineering, specializes in the gathering of data and the quantification of parameters needed for the practice of the other three major sub disciplines: drilling, production and reservoir engineering. Formation evaluation methods include rock-and fluid-sample analysis, well logging, and pressure and production testing. A combination of these methods usually is required for a complete and thorough evaluation. [1]

Well-logging technology embraces three distinct areas. The first area consists of the definition of mathematical and empirical models that relate a formation property of interest to the property measured with the logging tool. The second area consists of the log measurement itself and encompasses tool design and calibration. The third area is analysis and interpretation. [2]

Different types of methods were applied to acquire data to evaluate the hydrocarbon bearing zone of Habiganj Gas Field. The data that were obtained from the well no. 10 & 11 of Habiganj Gas Field were provided by Bangladesh Gas Field Company Limited (BGFCL). Resistivity log, Neutron log, Density log and sonic log were used to detect hydrocarbon zone.[3]

Figure 1: Location map of the study area (Surma Basin, Sylhet, Bangladesh). (After alam MK et al. 1990)[7]



Porosity logs (density, neutron, and sonic) have relatively shallow radii of investigation. Gas saturation near the wellbore in all types of formations causes an increase in density log porosity and a decrease in neutron log porosity. The presence of gas results in an appreciable increase in sonic log porosity only in poorly compacted sands, which is the case of most shallow sands and some abnormally pressured formations. Using density or sonic log porosity values uncorrected for gas effect usually results in a low apparent value of the formation factor, F . This, in turn, results in a low apparent R_0 value. Consequently, clean gas formations will be identified easily as hydrocarbon zones by use of an interpretation technique, such as the apparent water resistivity, R_{wa} , and porosity resistivity cross plots. The hydrocarbon saturation estimated under these conditions usually will be exaggerated. Use of uncorrected neutron log porosity produces the opposite effect. A low apparent porosity results in a high F , which, in turn, results in a high estimated R_0 value. Subsequently, a gas zone can pass undetected. [4,5]

Several interpretation techniques have been used to detect hydrocarbon-bearing zones and to estimate their porosities and fluid saturations. The optimum interpretation technique for analyzing a formation of interest depends on the quantity and the quality of the data available to the log analyst.

Log analysts are faced with four main questions.

- Does a specific formation or zone contain hydrocarbons?
- Which hydrocarbon is present, oil, gas or both?
- Is the hydrocarbon saturation high enough to indicate sufficient effective permeability to hydrocarbons?
- Is the hydrocarbon accumulation large enough to warrant the completion of the well?

If the log analyst can answer all four questions conclusively and positively, the well is completed in the zone of interest. If the answers are conclusively negative, the formation is abandoned. More frequently, especially in exploration, the role of well log is limited by the complexity of the problem to identify the relatively high potential zones. These zones will undergo additional testing, before the final decision to complete or abandon the well is made. Under certain circumstances, however, the additional tests cannot be performed or are inconclusive. In such cases, the decision is based on well-log interpretation. [2, 6]

II. METHODS AND MATERIALS

Determination of R_w :

Water Resistivity (R_w) can be obtained from water bearing formation. [12, 13]

$$R_w = \frac{R_{mf} * R_t}{R_{xo}} \text{ ----- (1)}$$

Where,

- R_w = water Resistivity in uninvasion zone
- R_{mf} = Resistivity of mud filtrate (1.5 ohm-m @ 124F BHT)
- R_t = True Resistivity (Deep Induction)
- R_{xo} = water Resistivity in flushed zone (MSFL)

Using the above equation, R_w is calculated and all the findings are tabulated in Appendix.

Bulk Porosity (By Neutron Log & Density Log)

Bulk porosity includes both primary porosity (intergranular void space) and secondary porosity (vugs and fractures). It can be measured by both Neutron log and Density log. [14-17]

Neutron log shows comparatively higher porosity in the formation. But in the gas zone Density log reads greater value than Neutron log. Finally the bulk porosity is calculated as root-mean-square (rms) porosity and given by $\Phi = \sqrt{[(\text{Neutron } \Phi)^2 + (\text{Density } \Phi)^2] / 2}$ (2)

Using Eqⁿ (2) the bulk porosity is calculated for every 5 meter interval ranging 1180m to 1540m depth.(Appendix)

Calculating Porosity Using Litho density

Bulk density is a function of the amount of matrix and the amount of fluid in the formation, as well as their respective densities. [18-20]

$$\Phi = \frac{\rho_{matrix} - \rho_{bulk}}{\rho_{matrix} - \rho_{fluid}} \text{ ----- (3)}$$

The density log reads the bulk density fairly well. Errors in calculated porosity appear, however, because the grain density and fluid density are often not measured and erroneous values of their magnitude are assumed. Using the equation stated above, the bulk porosity of well #11 is calculated for every 5 meter interval ranging 1200m to 1900m dept and 1920m to 3190m. Matrix porosity and fluid porosity are assumed to be 2.65 g/cc(sandstone) and .2g/cc(gas).(Appendix)

Analysis Based on Resistivity Log

There are two general types of resistivity tools. Electrode forces a current through the rock and measures resistivity. Electrode logs need a conductor in the well bore so they don't work with fresh water and oil based mud, or air. Electrode tools over the past 40 years are able to focus the current to control the depth of measurement in the borehole environment. The flushed zone resistivity is normally measured with an electrode log (MSFL). Induction uses a fluctuating electro-magnetic field to induce electrical currents in the rock; it measures conductivity which is converted to resistivity. Induction tools do not need a conductor in the bore hole and can be used with fresh water and oil based mud and air. They are designed to read intermediate and deep resistivities and are labeled ILM and ILd respectively.

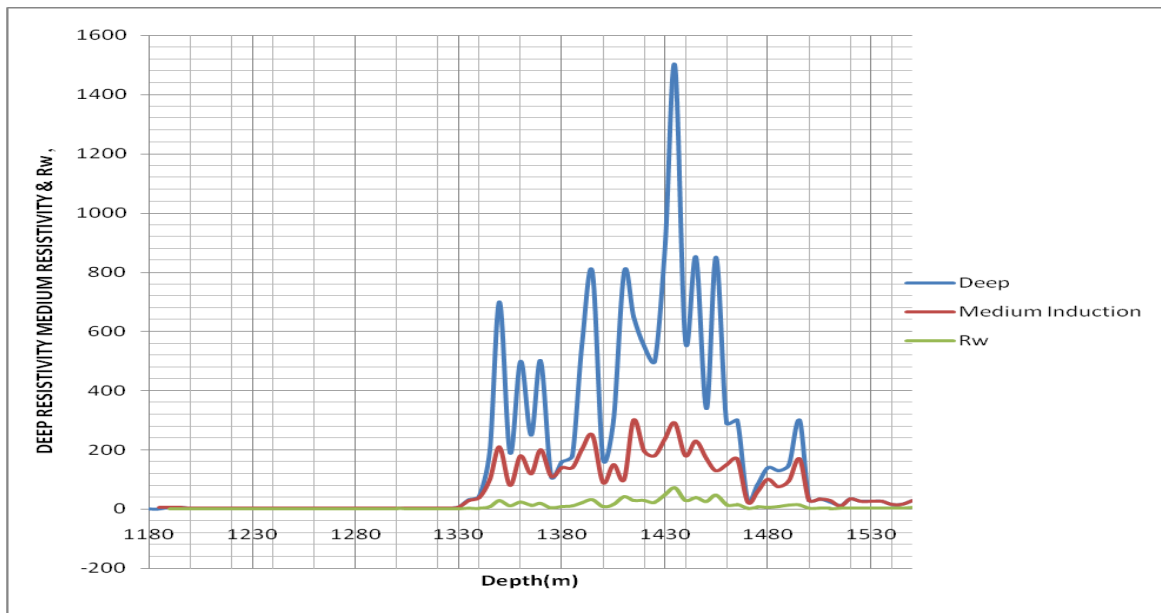


Figure 2: Depth Vs Deep Resistivity Medium Resistivity & Rw of Well#10 (Step 1)

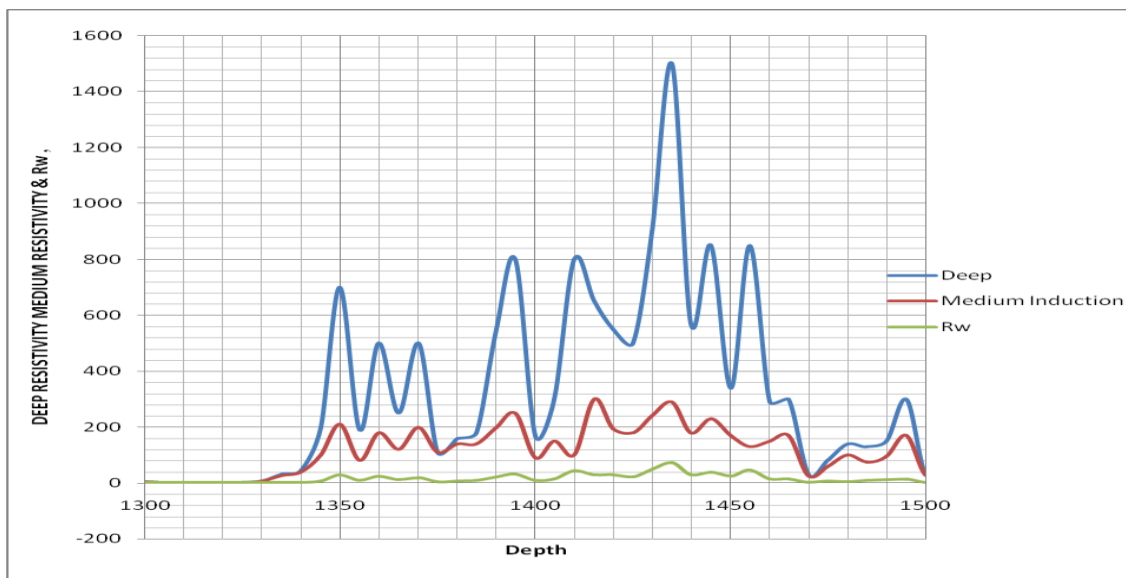


Figure 3: Depth Vs Deep Resistivity Medium Resistivity & Rw of Well# 10 (Step 2)

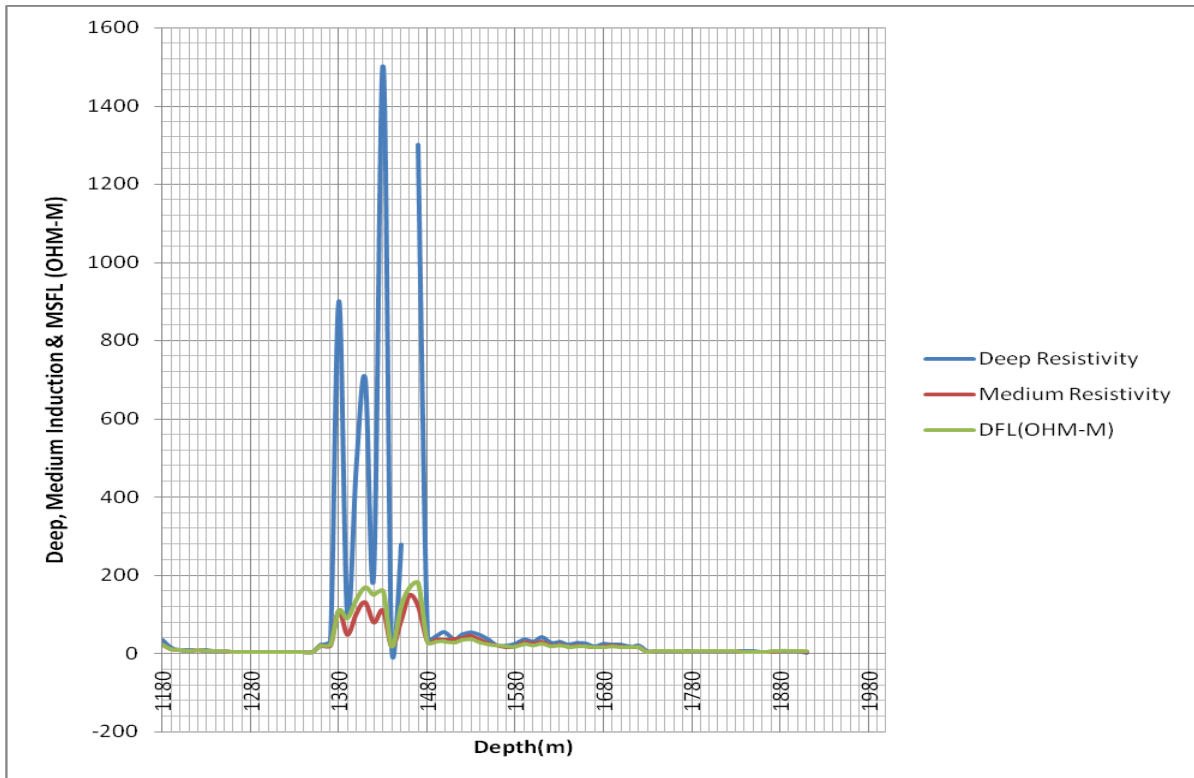


Figure 4: Depth VS Deep Resistivity Medium Resistivity & DFL of well#11(UGS)

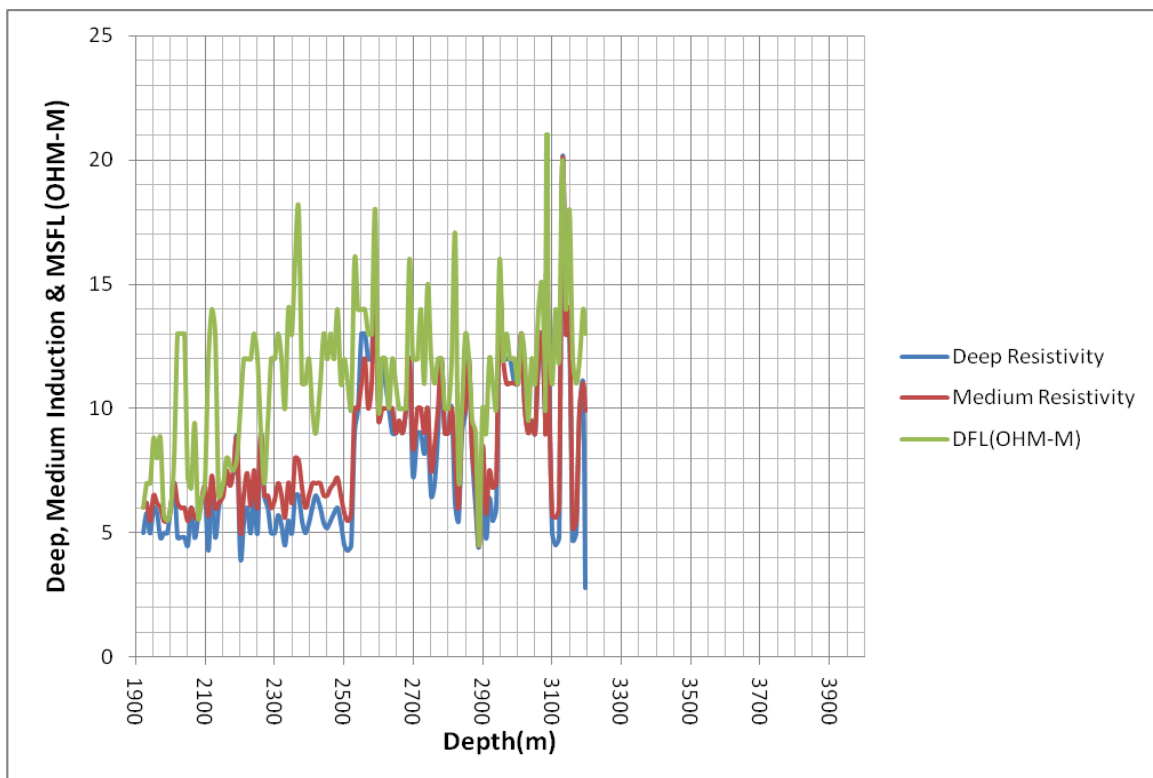


Figure 5: Depth VS Deep Resistivity Medium Resistivity & DFL of well# 11(LGS)

Induction tools do not work well in formations with low conductivity (high resistivity) because only weak currents will be induced in the rock and are hard to measure. High resistivity indicates the potentiality of hydrocarbons (absence of free electron) that is the true resistivity (R_t) of the formation is greater than that of the resistivity (R_w) of the formation water. Such occurrence is prevailed in the figure 2, 3 & 4 except figure 5. The results are tabulated below.

Table 1: resistivity log result

Well No.	Year	TD (mSS)	Type	UGS (mSS)	UGS GWC (mSS)	LGS (mSS)	LGS GWC (mSS)
well#10	1999	1531	Vertical	1345-1495	1500		
well#11	2008	3200	Vertical	1370-1480	1490		

Sonic Log Analysis

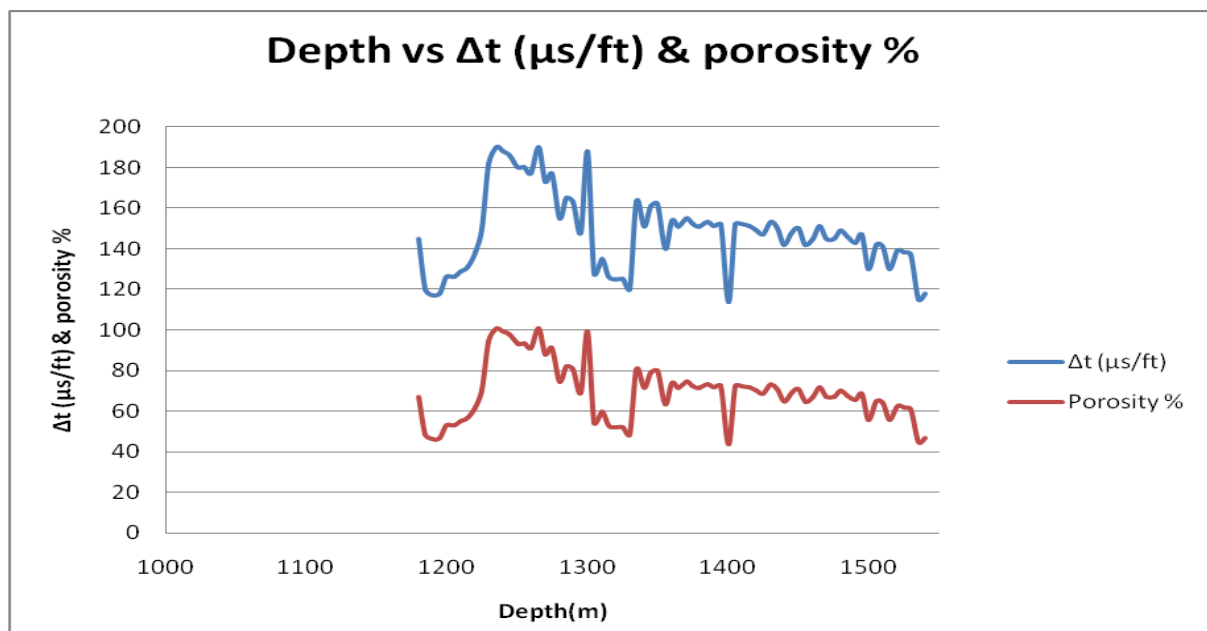


Figure 6: Depth VS Δt ($\mu s/ft$) & Porosity % well#10

In figure 6, due to dampening of first arrival at far receiver of the sonic log sonic curve shows spiking or abrupt changes towards a higher travel time. Greater travel time in porous media filled with gas(as acoustic wave takes less time in solid medium than that of lighter zone). There are unconsolidated formations (particularly gas bearing) or fractured formations.

Table 2: result from sonic log

Well No.	Year	TD (mSS)	Type	UGS (mSS)	LGS (mSS)
well# 10	1999	1531	Vertical	1255-1520	

Neutron Log Analysis

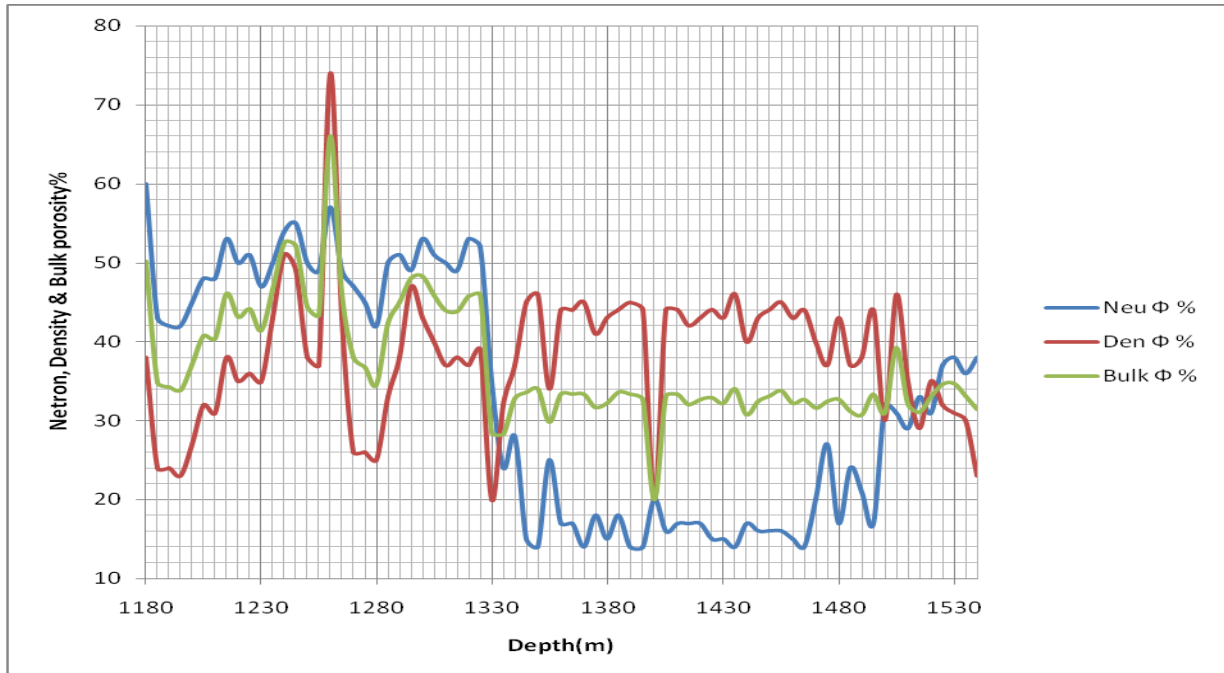


Figure 7: Depth VS Neutron, Density & Bulk Porosity % of well#10(step1)

The Neutron Log is primarily used to evaluate formation porosity, but the fact that it is really just a hydrogen detector should always be kept in mind. Most oils have a hydrogen index close to one, except light oils and gas; they have lower values due to lower hydrogen content. Consequently, the log estimates too low of porosity in zones containing gas or light oil. Gas zones are more easily picked when the neutron and density porosities are plotted on the same scale

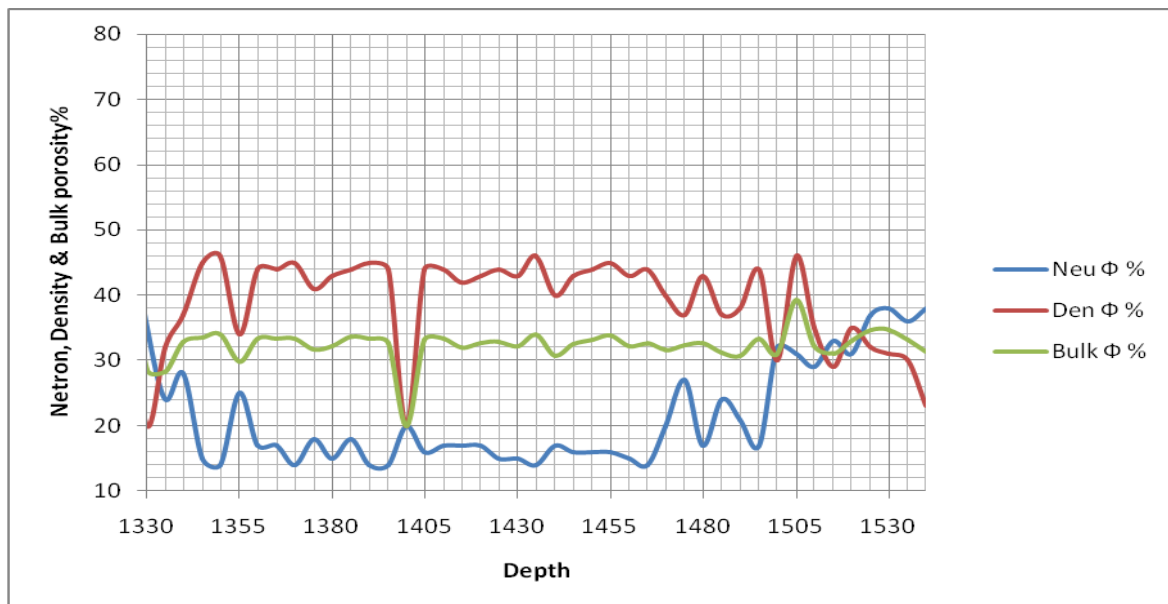


Figure 8: Depth VS Neutron, Density & Bulk Porosity % of well#10(step2)

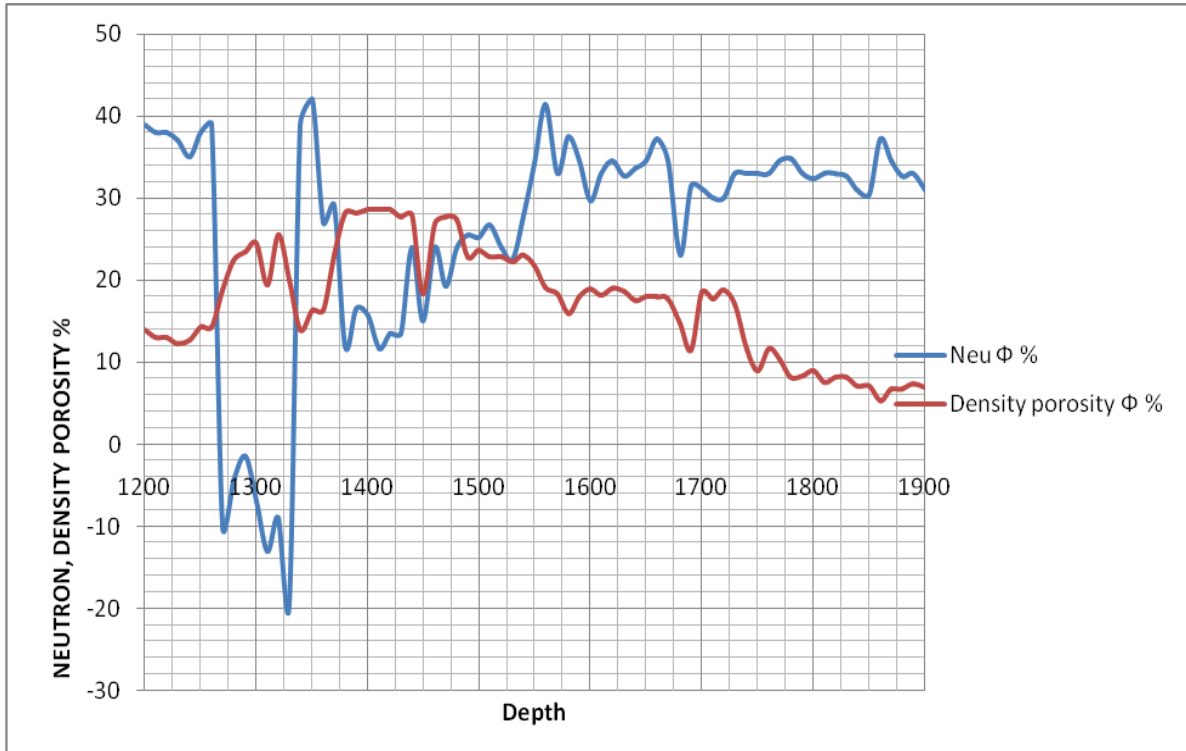


Figure 9: Depth VS Neutron, Density Porosity % of well#11(UGS)(step1)

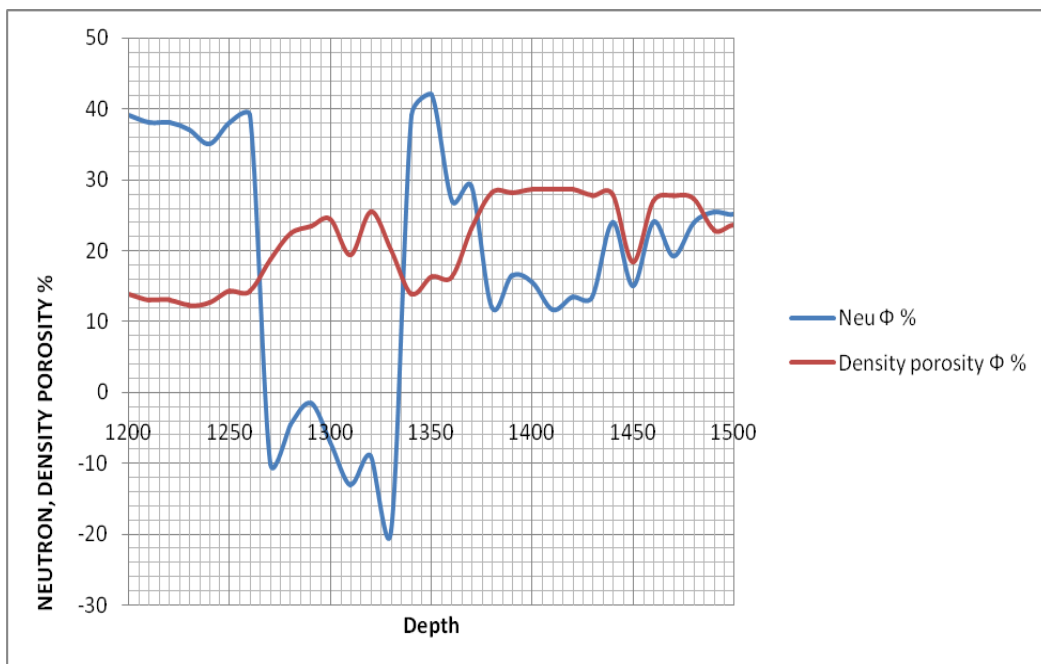


Figure 10: Depth VS Neutron, Density Porosity % of well#11(UGS)(step2)

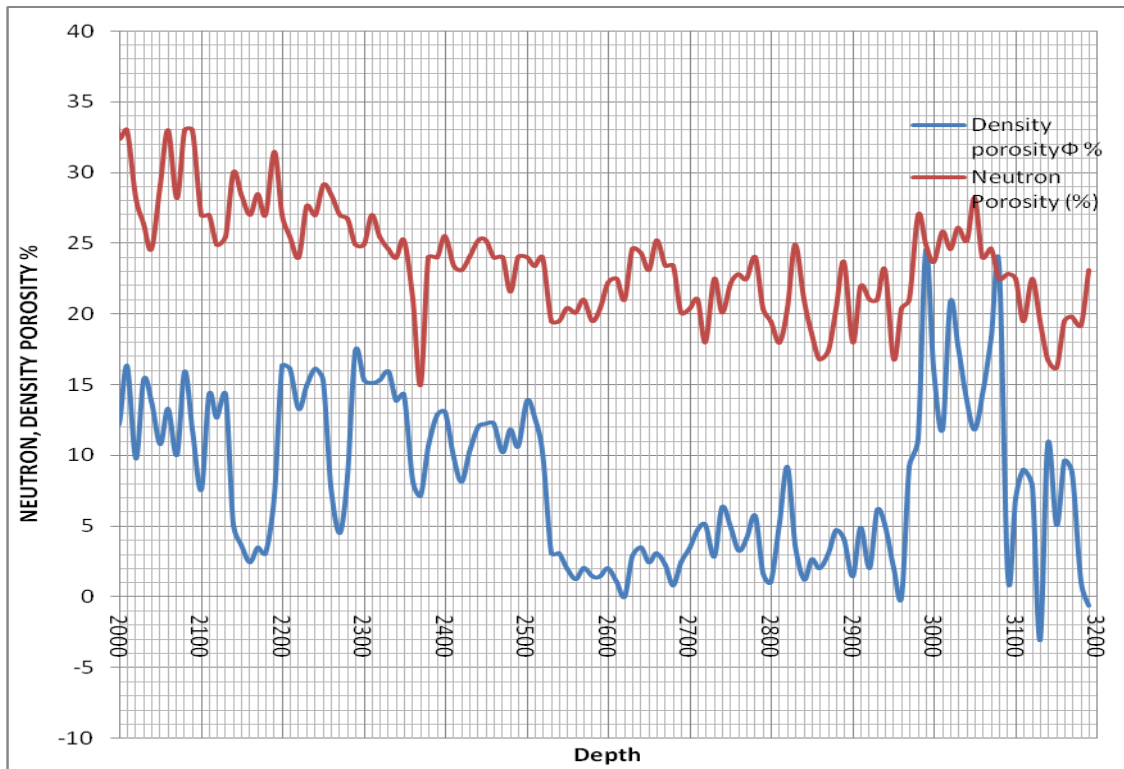


Figure 11: Depth VS Neutron, Density Porosity % of well#11(LGS) (Step1)

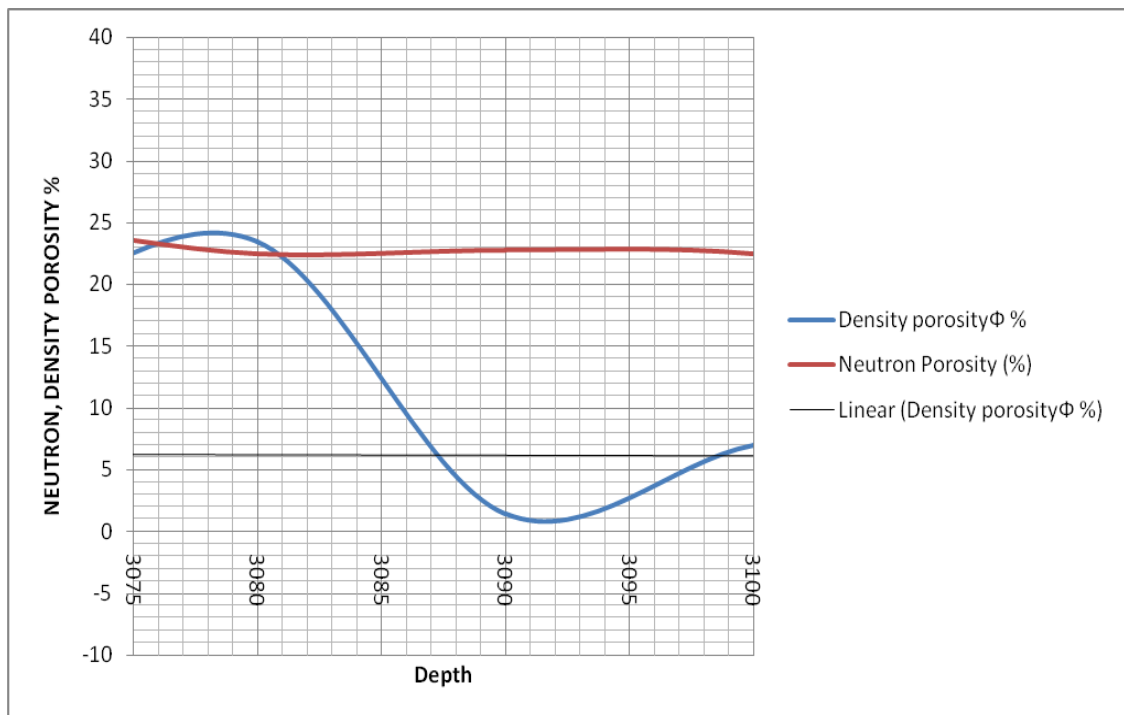


Figure 12: Depth VS Neutron, Density Porosity % of well#11(LGS)(Step2)

The computed density porosity will read high in gas zones (a fluid density assumption that is too high would be used) and the neutron log will read low, therefore, a cross-over will occur. The density porosity will track to the left and the neutron porosity will shift to the right. Based on the principal stated above, we have concluded the result tabulated below.

Table 3: result from neutron log

Well No.	Year	TD (mSS)	Type	UGS (mSS)	UGS GWC (mSS)	LGS (mSS)	LGS GWC (mSS)
well#10	1999	1531	Vertical	1335-1500	1515		
well#11	2008	3200	Vertical	1375-1490	1500	3076-3081	

III. RESULT AND DISCUSSION

In this study, I have strived to find out hydrocarbon bearing zone, the gross thickness of the pay zone and the fluid type of well#10 and well#11. Finally I have come out with the results varying for different logging tools. Actually the geological structure is the great factor to trap hydrocarbon in the underground. On the other hand, the results are not measured rather than estimated. So in well#10, Habiganj Gas Field, the hydrocarbon bearing zone is found between the depth ranging 1311m to 1505m and gross thickness is 194m. In well#11, two gas zones UGS & LGS, have been detected and they are prevailed in the depth ranging from 1373m to 1485m and 3076 m to 3081m. From the previous study it has been found that the hydrocarbon zone of well#10 is exists in the depth between 1297m-1464m using all Log data and all stratigraphic data. The total thickness of the gas zone is 167m. In well#11, the upper gas zone prevails in the depth between 1357m – 1474m and the lower gas zone is in the range of 3084m-3087m and 3144m-3147m. For detecting hydrocarbon zone, the accuracy of log data is too much important. If the collected log data is authentic, the result also is reliable. For collecting authentic data, we must use the sophisticated method and tools. There are a lot of methods for well logging but we used some selective method. So the result is not completely right. Even there is a continuous debate about the reserve of the gas field of Bangladesh due to method selection for reserve estimation. So I think, there are a lot of drawbacks in my method selection. If I used all of the logging data, then my result would be more reliable. But logging is very expensive. Sometimes it requires millions of money for one type of logging. For a good result of a study, tools and instruments used in the field should be well designed and sophisticated. Since the logging tools are also very expensive, may be the tools used in the logging was obsolete. The result can also vary due to the obsolescence of the tools and instruments.

IV. CONCLUSION

Determination of clay or shale volume, porosity, resistivity and water saturation is very important in the formation evaluation. Sonic curve shows spiking or an abrupt change towards a higher porosity. The porosity values are strongly affected by clay volume but less influenced by hydrocarbon fluids content. The increasing of clay volume will result in decreasing porosity. The resistivity log is strongly affected by the water saturation. Increasing of resistivity will result in decreasing water saturation. The result of this study and the actual result have not matched. That is, there are some limitations in this study. I have come across the study that the accuracy of log data is too much important. If the collected log data is authentic, the result is reliable. For collecting authentic data, we must use the sophisticated method and tools. There are a lot of methods for well logging but we have used some selective method. Besides, sufficient data were not available. Lab facilities were not worth mentioning. Some values for several parameters have been assumed. On the other hand, the result from log interpretation is estimated rather than measured. That is why, drawbacks may have occurred.

From the study it is clear that, the Habiganj gas field is very prospective area in Bangladesh. It is especially clear from the result of well # 11. Total two hydrocarbon bearing zones were found though the thicknesses of lower gas zone were small. But this zone is the indicator of the presence of huge amount of gas in Surma Basin.

REFERENCES

- [1] Zaki Bassiouni, Theory, Measurement and Interpretation of Well Logs (1994), v. 4, page: 1-13 & 329-339.
- [2] Log interpretation charts. Schumberger Well Surveying Corp.,Huston(1979)
- [3] <http://www.greatgeophysics.com/index.htm>
- [4] Risnes, R. - Petroleum Related Rock Mechanics
- [5] Silva, P.L, and Bassiouni,Z. "A New Approach to the Determination of Formation Water Resistivity from the SP Log," (1981)
- [6] Silva, P.L, and Bassiouni,Z. "Application of New SP Interpretation Charts to Gulf Cast Louisiana Fields,"(1983)
- [7] Graham *et al.* 1975, Salt *et al.* 1986, Kuchl *et al.* 1989
- [8] Alam M (1972) Tectonic classification of Bengal Basin. Geol Soc Am Bull 83: 519–522.
- [9] Mr D G Bowen-Core Laboratories - Formation Evaluation and Petrophysics
- [10] Ahmed M, Khan SI & Sattar MA (1991) geochemical characterization of oils and condensates in the Bengal Foredeep. Bang Jour SE Asian Earth Sciences 5: 391–399.
- [11] http://en.wikipedia.org/wiki/Well_logging
- [12] Archie, G.E. "Electrical Resistivity Log as an Aid in Determining Some Reservoir Characteristics," (1942)
- [13] Well Log Interpretation Resistivity Logs. Earth & Environmental Science University of Texas at Arlington
- [14] Wahl, J.S.: "Gamma Ray Logging," Geophysics (1983) 48 No. 11
- [15] Russell, W.L.: "The Total Gamma Ray Activity of Sedimentary Rocks as Indicated by Geiger Counter Determinations," Geophysics (April 1944) IX, No.2,180-216
- [16] "Neutron Logging," Welex,1979
- [17] Tittman, J. et al.: "The Sidewall Epithermal Neutron Porosity Logging," JPT(Oct.1966) 1351-62.
- [18] Abdul Mannan, Stratigraphic Evolution and Geochemistry of the Neogene Surma group, Surma basin, Sylhet, Bangladesh University of Oulu, 2002
- [19] Log interpretation Principles, Schumberger, Huston(1972)
- [20] Newton, G.R et al.: " Subsurface Formation Density Logging," Geophysics (1954) 19 No. 3, 636
- [21] Thermal Decay Time Log, Schlumberger, Huston(1968)
- [22] Alam MK, Hasan AKM, Khan MR & Whitney JW (1990) Geological map of Bangladesh. Published by Ministry of Energy and Mineral Resources, Geol Surv of Bangladesh with cooperation of U S Geol Surv.
- [23] Worthington, P.F.: "The Evaluation of Shaly-Sand Concepts in Reservoir Evaluation," The Log Analyst(1985)
- [24] Altschuler ZS, Dwornik EJ & Kramer H (1963) Transformation of montmorillonite to kaolinite during weathering. Science 141: 148–152.
- [25] Ashraf AR, Utescher T & Mosbrugger (1997) Proceeding 4th EPPC: Palaentological-meteorological palaeoclimate reconstructions Neogene Lower Rhine Embayment: 263–269.
- [26] Badrul Imam (2005), Energy Resources of Bangladesh, UGC publication no. 89, page: 19–32.
- [27] http://www.banglapedia.org/httpdocs/HT/G_0078.HTM
- [28] <http://www.propertiesofgeologicmaterials.com/porosity.html>
- [29] http://www.ldeo.columbia.edu/~martins/sen_sem/thesis_org.html#Structure
- [30] http://www.bgfcl.org.bd/habiganj_map.html

Quantitative and Qualitative Assessment of Drinking Water Sources in Ile-Ife and Environs

Olanipekun E.A.¹

¹Department of Building Obafemi Awolowo University Ile-Ife

ABSTRACT: Most water supply programmes in Nigeria have focused on providing access to quantitative drinking water to the populace, an approach, which has led to an increasing reliance on ground water supply through sinking of boreholes and wells. However, there has been very few data collected on the quality of the underground source for drinking water purpose in the area. Quality assessment of ground water supply in Ile-Ife and its environs was carried out because much of the population in the area relies on groundwater supplies as a sustainable drinking water source. Laboratory analysis was conducted on water samples collected from 14 public boreholes and wells located at various sections of the study area. Sampling occurred for 12 months from January-December, 2013. The samples were analyzed for bacteriological, physical and chemical qualities. The results show that total coliform and heterotrophic bacteria were present in 50% and 20% of samples analyzed. Heterotrophic bacteria of concern include *Trichodema* sp, *Cladosporium herbarium*, *microsporium andouini*; *Rhizopus stolonifer* and *pulluria pullularis*. The physical and chemical properties of the various sources of water compared favourably with the World Health Organisation Standards (WHO). The study showed that there are several parameters of health concern as biological analysis exceeded the minimum standards set by WHO.

KEY WORDS: drinking water, assessment, health, water quality, Ile-Ife.

I. INTRODUCTION

Water is essential to life. The provision of water of adequate quantity for human use and consumption is not only a pre-requisite for development but also a major contribution towards the improvement of health, hygiene and welfare of people [Howard and Bartram, 2003]. They added that access to safe water reduces water-borne and water-washed diseases. More importantly the provision of regulated in-house piped water would lead to massive overall health gains [Hutton and Haller, 2004]. A review of the existing literature revealed that the supply of portable piped-borne water helps to decrease the mortality and morbidity rate particularly among infants and children as well as making life easier for women. Significant health gains accrue by ensuring access to an improved water source within 1 kilometer of the user's house [Esrey et al., 1985; Howard and Bartram, 2003]. Beyond reducing water-borne and water-related diseases, providing better access to improved water and sanitation confers many other diverse benefits ranging from cost offsets, time saved to convenience and well-being. Cost offsets are costs avoided due to less illness, cost savings to health sector mainly due to the reduced number of treatments of diarrhea and patients avoided costs incurred in seeking treatment (expenditures on care, drugs and transport as well as the opportunity costs of time spent on seeking care). Another set of benefits related to less illness are the avoided days lost with respect to formal or informal employment, other productive activities in the household, or school attendance, gained related to lower morbidity and less death. Time savings occur due to the relocation of a well or boreholes to a site closer to use communities and the installation of piped water supply in house. In contrast, poor access to safe and adequate sanitation continues to be a threat to human health. Where the basic access level has not been achieved, hygiene cannot be assured and consumption requirements may be at risk. The adverse impacts on public health from poor water supply take the form of outbreaks and contribution to background rates of disease [Esrey et al., 1991; Ford, 1999; Payment and Hunter, 2001]. Water-borne and water related diseases like cholera, typhoid fever, hepatitis A, schistosomiasis and dysentery can break out in any community that does not have access to safe water supply of adequate quantity.

The most important and immediate risks to human health from using contaminated water drinking water is diarrhea disease especially among children in poor countries [World Health Organisation, 2007]. Data from epidemiological and zero prevalence studies indicate that endemic transmission of disease associated with diarrhea and other gastro intestinal disease estimated at 2.2 million deaths and over 72 millions disability adjusted life years were attributable to unsafe water and sanitation, including lack of hygiene, [Pruss et al., 2002; WHO, 2002; Priss-Uston et al., 2004; Hutton and Haller, 2004; Howard and Bartram, 2005; Bartram, 2007]. The available evidence suggests that, improving access to safe water supply and sanitation services is a preventive intervention and proven contributors to controlling this disease burden, whose main outcome is a reduction in the number of episodes of diarrhea and accordingly a proportionate reduction in the number of death [WHO 2002; Hutton and Haller, 2004; Bartram, 2007]. Given the link between vulnerability to disease and poverty [Payment and Hunter, 2002] the assessment of adequacy and quality of water supplies for human consumption is imperative. For informed rational decision- making it is crucial to carry out a sound quality evaluation of the sources of water supply in different settings. Such information can be acquired through water monitoring and examination, which is the continuous and vigilant public health assessment and oversight of the safety and acceptability of water supplies [WHO, 1976, 1993, 2004]. The regular examination of drinking water samples requires by law in most countries is for the sole purpose of ensuring the supply is safe for consumption. The practice will help to curb the spread of waterborne diseases which can lead to epidemics as well. The examination of water samples will provide information on water quality level. It will also show whether the water is in physically, chemically and bacteriologically accepted conditions, and if it is not, it may indicate why and where the deterioration of quality has occurred and how the quality may be restored.

II. WATER SUPPLY ARRANGEMENT IN NIGERIA

Water supply access in Nigeria is complex. In the pre-colonial Nigeria, the sources of water supply to a community for drinking and households purposes were mainly from rain, dug wells, flowing streams and rivers. Due to urbanization and industrialization, there were organised public water supply systems, where treated and quality water was transmitted from water works, distributed and supplied to households via pipeline networks. Almost all sections of the society especially in urban centres and growing towns have access to safe water piped to their homes. In the last two decades, due to the collapse of public water supply system many of the inhabitants in the study area use unreliable water supplies of poor quality, which are costly and are distant from their home. Poor access to safe water and adequate sanitation continues to be a threat to human health. Factors such as poor reliability (continuity of supply), costs (affordability) and distance between a water source and the home leads the inhabitant to depend on less safe sources, to reduce the volume of water used for hygiene purposes.

The Millennium Declaration Goal (MDG 7) launched in 2000 brought about huge interventions of home governments of most developing countries in the provision of portable water to growing cities rural communities. In Nigeria, the provision of basic amenities to the urban centres and developing cities has been a priority of the Federal, States and Local Governments. Huge sum of money have therefore gone and are still going into mini-water scheme projects such as sinking of boreholes and wells around the vicinity of the neighbourhood as means of sustainable water supply (the study area inclusive). Esrey et al. [1985], Howard and Bartram [2003] and Howard and Bartram [2005] noted that significant health gains accrue by securing access to an improved water source within 1 kilometer of the user's house. Further significant health gains are accrued once water supply is delivered `on-plot` through at least one tap [Howard and Bartram, 2003]. However, the water needs to be of good quality that represents a tolerable level of risk [Howard and Bartram, 2003]. Information about the quality and health risks faced by the inhabitants in the study area through this intervention remains scarce. The providers hardly performed routine monitoring of water supplies to the growing population. Drinking water from groundwater supply is believed to be sufficiently safe, excellent quality, purer, attractive and palatable to be used without treatment since impurities would not be expected in it because of the filtering action of the aquifer [Throne et al., 2002]. A lot of reasons call for constant examination of quality of drinking water got from groundwater supply. Groundwater sources may be liable to be contaminated by sewage from septic tank and pit latrines if they are not properly constructed, protected and the mandatory minimum distance of 30 m from septic tanks/pit latrines recommended by World Health Organisation is not observed [Ayanlaja et al., 2005; Adejuwon, 2009]. A review of literature also showed that most important source of serious illness and death especially among young children, in both rural and poor urban settlements in developing countries are traceable to the use of untreated water from groundwater sources [Nasinyama et al., 2000; Pokhrel and Viaragham, 2004; World Health Organisation, WHO, 2007]. Furthermore, it may almost be impossible to find a source of natural water that will meet basic requirements for public water supply without requiring some forms of treatments. This is because water is a universal solvent; as such most natural as well as man-made substances are soluble in it.

Underground water supply sources may contain much matter dissolved from strata through which it passes. Groundwater absorbs gases of decomposition and degradable oxygen organic matter (such as H_2S , methane) within the pores of soil mantle through which it percolates. In strata which are rich in organic matter, oxygen is removed from percolating water and CO_2 is added. Groundwater has low Ph values. Consequently, water in nature contains dissolved substances and impurities. Therefore, it may be necessary to remove colour, odour and taste imparted to the stored water by the decomposition of organic matter or growth of algae. Infact monitoring of the quality of water got from these interventions become very important because preliminary site investigation showed that septic tank and pit latrines are often dug within few metres from these wells and boreholes. This according to Adejuwon [2009] and Ayanlaja et al. [2005] is dangerous because it may results into massive groundwater contamination. In the past, there have been many cases of recurring epidemic of enteric fevers traceable to drinking water from groundwater supplies. Besides, previous studies [Akinbode, 1986; Ako et al., 1990] in the area showed that a larger percentage of wells in Ile-Ife have high turbidity level and water from them was not fit for human consumption without treatment since the quality was below the appropriate standard recommended by the World Health Organisation. The need was therefore identified for a systematic investigation into the quality of water supplies from this min-water scheme projects as an input to prevent health problems.

The purpose of this study is to critically review the adequacy and quality of water supply through these interventions. The quality of the water supplies was pursued through the analysis of physical, chemical and bacteriological characteristics of water supplies. This information is relevant to public health professionals in helping to set priorities for water supply improvements.

III. METHODOLOGY

Field work: This involved collection of relevant data from local water corporation office, oral interview with residents in various section of the town and collection of water samples from identified sources of water supply.

Zoning of the study area



Fig.1: Map of Ile-Ife showing sources and location of sample collected.

Fig.1 is the map of Ile-Ife showing sources and location of sample collected. Ile-Ife and its environs were divided into five zones using the major road network. This was done to enable a representative of the zone to be sampled and analyzed. Zone 1 consisted of Ajebamidele, Ibadan road, Ede road and Faola layout. Zone 2 made up of Fashina, Ife Central Local Government Secretariat area, Asherifa-Ola Estate, Moremi Estate, Omole

Estate and Oba layout. Zone 3 comprises Mayfair and Parakin Scheme. Zone 4 consists of Eleyele, Moore, Ojoyin, Enuwa, Otutu and Oni's palace while zone 5 comprises Fajuyi, Igboya, Ikoyi quarters, Aladanla and General Hospital area.

Interview and site observation assessment: The five zones into which the study area was divided into was visited for on-spot assessment of water supply technologies and oral interview was conducted with the inhabitants to ascertain the various sources of water supply available to them, frequency of supply, ease and access as well as the quality of water supply. The questions asked during the oral interviews were the same in all the five zones to enable uniformity in data collection.

Sample collection: The water samples analysed for this study were collected from January-December 2013. A structured inspection and sampling programme was created to include a total of 14 samples. The samples were selected purposively based on relative occurrence and importance, ensuring that at least one from each zone was included. This method was employed because it is a difficult task identifying all the households in the study area. A sample was also taken for on-site determination of appearance. All the samples were collected in sterilized containers labeled as indicated in Table 1. The collection of water samples, the sampling equipment, procedures and technique were done according to standards procedures laid down. This was to ensure that changes in the constituents to be analysed did not occur between the time the samples were collected and the time they are analysed. The water samples and were taken to the laboratory for analyses.

Table 1: Sources and location of the samples collected

Source	Sample code	Location	Coordinate	
			Easting (m)	Northing (m)
Deep Well	A	Asherifa-Ola Estate	667824	828358
Private Borehole	B	Women Hostel Ede Road	669058	828202
Deep Well	C	Faola Layout Ibadan Road	665659	828934
Private Borehole	D	Hilton Hotel Mayfair	669149	827886
Timber Market Federal Government Borehole	E	Eleyele	670822	828751
State Government Borehole	F	General Hospital	672789	830075
State Government Borehole	G	Enuwa Otutu	672283	827649
Deep Well	H	Fajuyi	672471	828751
Deep Well	I	Omole Estate	668782	827933
Federal Government Borehole	J	Oluorogbo Road 7	670672	829335
Federal Government Borehole	K	Mbabimbayo	670705	829525
Public Pipe Borne Water	L	Ibadan Road	665306	828615
Public Pipe Borne Water	M	Ojoyin	670781	827625
Public Pipe Borne Water	N	Omole Estate	669149	827806

Laboratory analysis: In the laboratory, the samples were tested for physical characteristics (total solid, total dissolved solids, total suspended solids, apparent colour, turbidity and conductivity), chemical characteristics (pH, alkalinity and acidity) and bacteriological characteristics (total coliform). The following presumptive, confirmatory, completed, isolation and identification, morphological characteristics of the isolates by gram staining technique, triple sugar iron medium, sulphide-iodide-motility, catalase, citrate utilization, methyl red and Voges-Proskauer, nitrate reduction, oxidation and sugar fermentation tests were also carried out in order to isolate and narrow down E-Coli bacteria. For determination of dissolved gases field analysis was also carried out. All analyses were carried out according to the standard laboratory procedures. Special precaution was also observed during determination of bacteriological characteristics.

IV. RESULTS AND DISCUSSION

Sources and adequacy of water supply : The various sources of drinking supply water in Ile-Ife are presented in Table 2. Table 2 shows that out of five zones only zones 1 and 2 have access to public pipe borne water supply as their primary source of drinking water. The other three zones depend majorly on underground water

supply system for their source of drinking water. Even in zone 1 and 2, majority of the people still depend majorly on underground supply system. Further analysis shows that only 10% of the quantity of drinking water required by the inhabitants is met through public pipe borne water supply. Consequent, the inhabitants relies on alternative sources of supply such as individual small point water supplies (dug wells) (Appendix D). This means that the supply of pipe borne water to Ile-Ife and environ is highly inadequate.

Table 2: Sources of Drinking Water

Zone	Location	Primary Source	Secondary Source	Remarks
One	Ajebamidele	Public tap water	Well	Constant public water supply
	Faola Layout	Well	Borehole	Intermittent public water supply
	Ede Road (from Ede)	Public water	Well	Constant public water supply
	Ede Road (to Mayfair)	Well and borehole	Public tap water	Intermittent public water supply
	Ibadan Road	Public tap water	Well	Constant public water supply
	Asherifa-Ola estate	Well	Borehole	Intermittent public water supply
Two	Oloke	Public tap water	Well	Constant public water supply
	Alawode Estate	Well	Borehole	Intermittent public water supply
	Moremi Estate	Public tap water	Well	Constant public water supply
	Omole Estate	Public tap water	Well	Intermittent public water supply
	Mayfair	Well	Borehole	Constant public water supply
	Parakin	Well	Borehole	Intermittent public water supply
	Road 7	Borehole	Well	Constant public water supply
	Sabo	Borehole	Well	Intermittent public water supply
	Eleyele	Borehole	Well	Constant public water supply
	Ilesa road	Well		Intermittent public water supply
	Iremo road	Well		Constant public water supply
	Koyiwo Layout	Well	Public tap water	Intermittent public water supply
Three	Moore	Well	Borehole	Constant public water supply
	Enuwa	Borehole	Well	Intermittent public water supply
	Ojoyin	Well	Public tap water	Constant public water supply
	Fajuyi	Well		Intermittent public water supply
	General	Well	Boreholes	Constant public water supply
	Ikoyi	Well		Intermittent public water supply
Four	Igboya	Well		Constant public water supply
Five	Aladanla	Well		Intermittent public water supply

Physical Analysis : Table 3 shows the results of total solid, (TS), total dissolved solid (TDS), total suspended solid (TSS), apparent colour, turbidity and conductivity tests carried out on the samples collected, The results indicated that the total solid (TS), total dissolved solid (TDS), total suspended solid (TSS), conductivity and turbidity contents of the water samples collected ranging from 200mg/l-900 mg/l, 120 mg/l-650 mg/l, 20mg/l-380mg/l, 59us 10l0us and 1.53 TNU-4.56 TNU respectively. Figures 2, 3, 4 and table 4 compared the total solid (TS), total dissolved solid (TDS) turbidity and conductivity results with the World Health Organization approved standards. The results also revealed that sample G (Enuwa Otutu Bore hole drinking water source) had a very high content of total solid. The quantity of total solid in the water supplied on Ibadan

road is less than the water supplied in Omole Estate and this in turn is less than water supplied in Ojoyin (samples, L, N and M). This means that as the distance along the pipeline increases so also the total solid increases.

Table 3: Results of Physical Analysis

Sample code	TS (mg/i)	TDS (mg/i)	TSS (mg/i)	Turbidity (TNU)	Conductivity (ii)	Apparent colour
A	400	120	280	1.53	87	Light brown
B	200	180	20	1.53	298	Colourless
C	200	150	50	4.56	59	Colourless
D	200	150	250	4.56	162	Colourless
E	500	260	240	4.56	160	Colourless
F	300	200	100	4.56	281	Colourless
G	900	650	250	4.56	1010	Colourless
H	300	160	140	4.56	312	Colourless
I	500	300	200	4.56	300	Colourless
J	300	130	170	4.56	168	Colourless
K	500	150	350	4.56	165	Colourless
L	200	120	80	1.53	160	Colourless
M	600	220	380	1.53	158	Colourless
N	400	300	100	1.53	155	Colourless

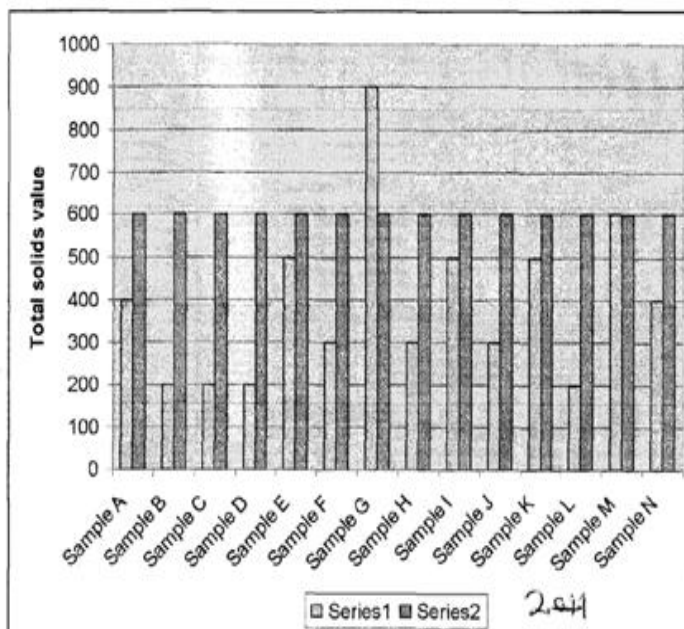


Fig 2: Result of Total Solid (TS) Compared with W.H.O Approved Standards

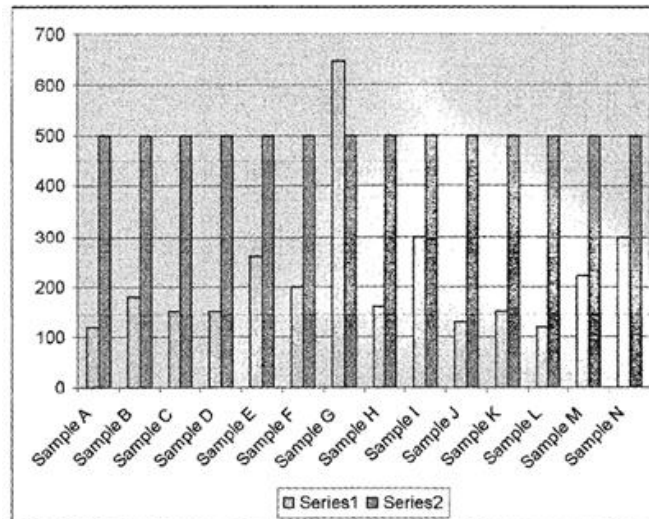


Fig 3: Result Total Dissolved Solid (TDS) Compared with the W.H.O Approved Standards

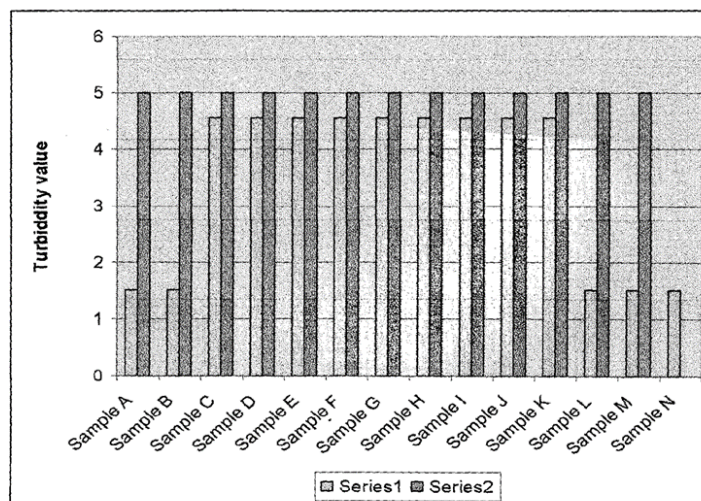


Fig 4: Result of Turbidity (TNU) Compared with the W.H.O. Approved Standards

Table 4: Result of Conductivity analysis compared with the W.H.O Standards

Sample Code	Conductivity	WHO Approved Standards
A	87.0	
B	298.0	
C	59.0	
D	162.0	
-E	160.0	
F	281.0	
G	101.0	
H	312.0	
I	300.0	
J	168.0	
K	165.0	
L	160.0	
M	158.0	
N	155.0	

Chemical Analysis : Table 5 shows the results of PH, Acidity, Alkalinity, hardness and chloride contents of the drinking water sources, while Figures 5, 6, 7 and 8 compared the results of chemical analysis with the World Health Organization approved standards. The comparison demonstrated that the chemical contents of the water samples compared favourably with the World Health Organization approved standards. Furthermore, the alkalinity and acidity values of the water samples were found to be lesser than the hardness values revealing the presence of salts of calcium and magnesium which were more likely to be sulphates instead of carbonates.

Table 5: Results of Chemical Analysis

Sample code	PH	Acidity Mg/1 CaCO3	Alkalinity CaCO3	Mg/I	Hardness (mg/L)	Chloride (mg/L)
A	6.50	56	28		270.2	20.0
B	6.45	58	26		162.0	10.0
C	6.25	54	24		252.0	10.0
D	6.48	44	84		189.0	20.0
E	6.8	40	110		135.0	10.0
F	7.4	40	166		140.0	20.0
G	7.0	48	188		248.0	10.0
H	6.44	62	24		142.0	10.0
I	6.40	58	24		135.0	20.0
J	6.7	42	112		142.0	10.0
K	6.8	43	110		162.0	10.0
L	7.0	30	26		248.0	20.0
M	7.0	30	26		270.0	10.0
N	7.0	35	25		135.0	10.0

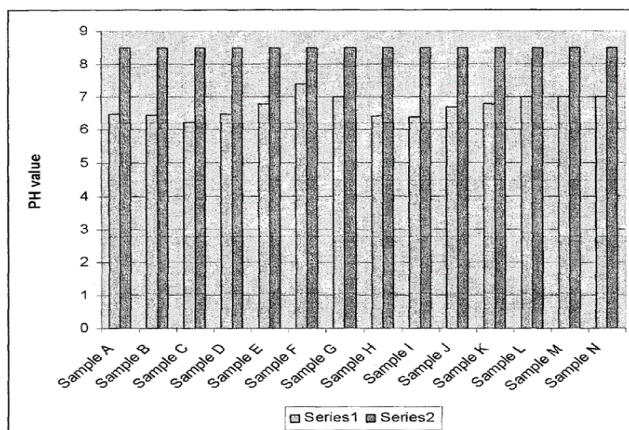


Fig 5: Result of PH Value Compared with the W.H.O Approved Standards

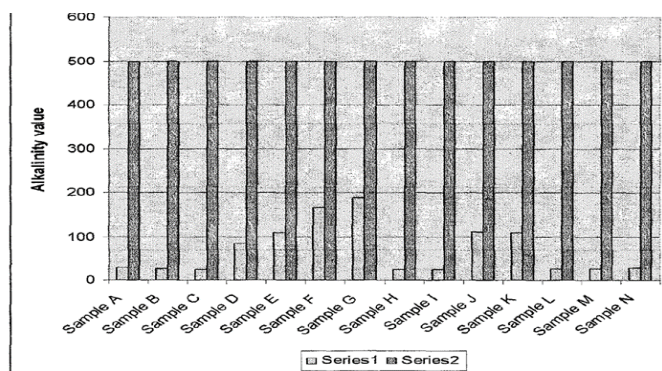


Fig. 6: Result of Alkalinity compared with the W.H.O Approved Stand

Bacteriological Analysis : Table 6 shows the results of the various microbiological tests carried out on the water samples. The results reveal the absence of coli form in the water samples collected from sample D (private borehole), sample E (Timber market Federal Government borehole), sample G (state borehole), sample J (Federal Government borehole), sample L (Public Taps), sample M (Pipe borne water) and sample N (Pipe borne water). The other water samples (A, B, C, F, H, I and K) have coli form, counts ranged between 200 and 1100, the highest value however was recorded in the water samples collected from Deep well at Asherifa Estate, Deep well at Faola layout Ibadan Road and Deep well at Fajuyi. Figure 9 compared the bacteriological analysis results with the World Health Organization approved standards and it revealed that the coli form counts in Samples A, B, C, F, H, I and K were above the recommended standards. Further tests show the presence of Trichodema sp, Cladosporium herbarium, Microsporium audouinii in sample A, Rhizopus stolonifer, Absidia sp, Cladosporium herbarium in sample C, Mucor mucedo, Rhizopus orzae, pullularis pullularis, Rhizopus Japoricus, Cladosporium herbarium in sample H. However, no form of E. coli was detected in all the samples.

Table 6: Result of Bacteriological Analysis

Sample code	Coliform count/100ml	E. coli
A	1100	Negative
B	240	Negative

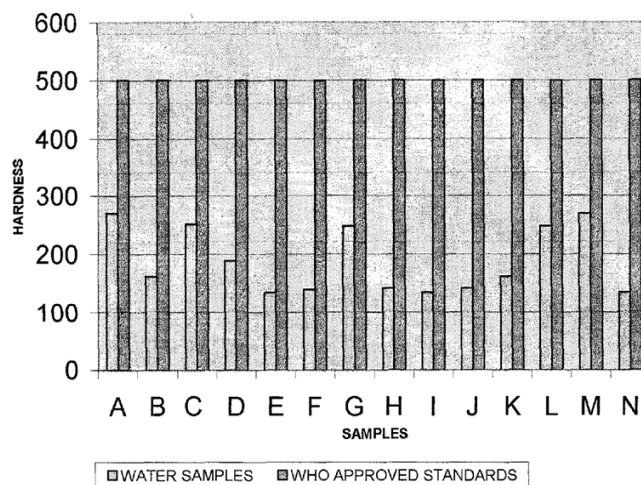


FIG. 7 RESULTS OF HARDNESS COMPARED WITH THE WHO APPROVED STANDARDS

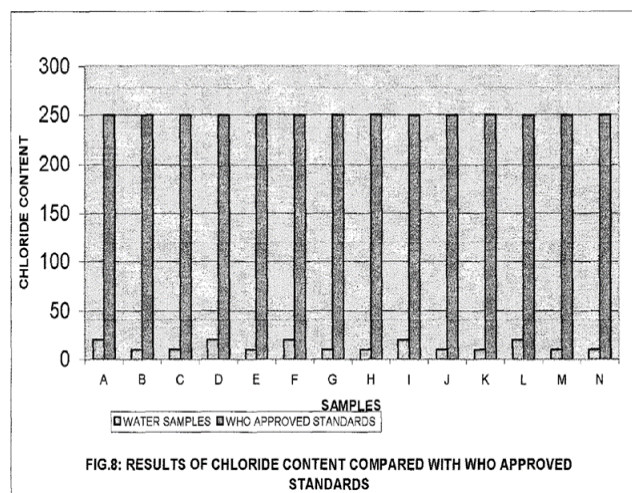


FIG.8: RESULTS OF CHLORIDE CONTENT COMPARED WITH WHO APPROVED STANDARDS

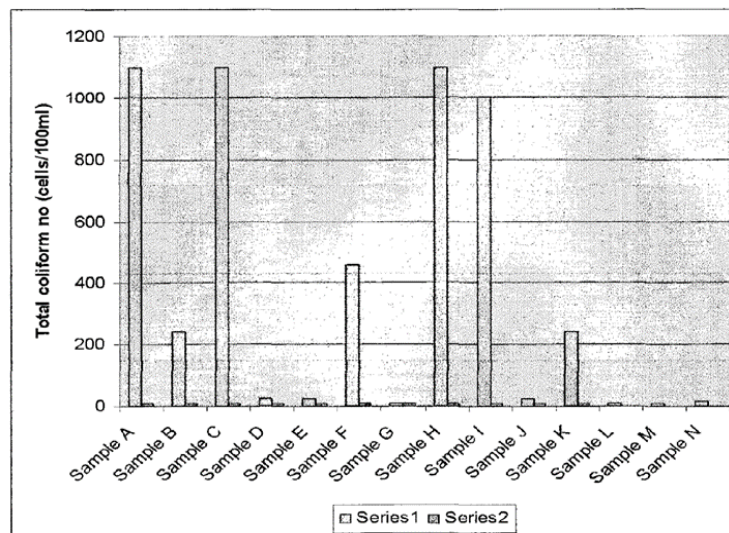


Fig 9: Result of Bacteriological Analysis with the W.H.O Approved Standards.

V. CONCLUSION

This paper probed into the quantitative and qualitative assessment of drinking water supply in Ile-Ile Town. The following conclusions were drawn from the findings. The sources of drinking water supply are public pipe borne water and underground supply system through sinking of boreholes and dug wells. However, underground supply system (boreholes and wells) accounted for the highest source of drinking water supply. Only 10% of the population had access to constant supply of public pipe borne water. The bacteriological tests results of the various sources of drinking water supply exceeded the World Health Organisation approved standards. The total solid content of all the untreated water sources are high. As a temporary solution, the use of alum for coagulation, boiling and filtration of water for drinking purpose should be encouraged. Bacteriological examination and analysis of the various sources of drinking water supply especially the untreated sources should be undertaken at reasonable intervals.

REFERENCES

- [1] J.O. Adejuwon, Assessment of fecal bacteria in shallow wells in urban slum of Abeokuta, Nigeria. *Journal of Environmental Design and Management* 2009; 2 (2); 12-16, June edition.
- [2] O. Akinbode, An appraisal of water supply to Ile-Ife. An unpolished B.Sc.(Building) final year project, Department of Building, Obafemi Awolowo University, Ile-Ife, 1986.
- [3] B.D. Ako, F.I. Adeniyi and J.F. Adepoju, Statistical tests and chemical quality of shallow groundwater from a metamorphic terrain, Ile-Ife/Modakeke. *Journal of African Earth Science* 1990; 10 (4); 603-613.
- [4] S.A. Ayanlaja, O.O. Kehinde-Philips, F. Ogunkolo, B. Dada and B. Senjobi, Quality of water from hand dug wells, boreholes and streams in 2 localities in south western Nigeria. In Implication of the 4th International Ground Water Quality Conference, Waterloo, Canadian IAHS publication 2005; 47; 97-108.
- [5] J. Bartram, Managing water in the home: accelerated health gains from improved water supply. World Health Organisation 2007
- [6] S.A. Esrey, J.B. Potash, L. Roberts and C. Schiff, Effects of improved water supply and water, sanitation on ascariasis, diarrhea, dracunculiasis, hookworm infection, schistosomiasis and trachoma Bull. World Health Organisation 1991; 65 (5); 609-621.
- [7] G.M. Fair, J.C. Geyer, D.A. Okun and J.K. Sherwani, Elements of water supply and water disposal 2nd. John Wiley and Sons, Inc.
- [8] T.E. Ford, Microbiological safety of drinking water: United States and global perspectives. *Environmental Health Perspectives* 2002/1999; 107(SI); 191-206.
- [9] G. Howard and J. Bartram, Domestic water quantity, service level and health. World Health Organisation 2003, WHO/SDE/WSH/03.02 Ex. Sum. English only.
- [10] G. Howard and J. Bartram, Effective water supply surveillance in urban areas of developing countries. *Journal of Water and Health* 2005; 03 (1); 31-43.
- [11] G. Hutton and L. Haller, Costs and benefits of water and sanitation improvements at the global level: Evaluation of the costs and benefits of water and sanitation improvement at the global level. WHO 2004
- [12] G.W. Nasinyama, S.A. Ewen, J.B. Wilson, D. Waltner-Tower, C.L. Gyles and J. Opuda-Asibo, Risk factors for acute diarrhea among inhabitant of Kampala District, Uganda. *South Africa Medical Journal* 2000; 90 (90); 891-898.
- [13] S. Padley and G. Howard, The public health implication of Microbiological contamination of groundwater. *Quarterly Journal of Geology* 1997; 30; 179-188.
- [14] P. Payment and P.R. Hunter, Endemic and epidemic infectious intestinal diseases and its relationship to drinking water. In: *Water Quality: Guidelines, Standards and Health* (Fewtrell, L. & Bartram, J. eds). International Water Association Publishing, London, pp. 61-88.
- [15] D. Pokhrel and T. Viargharan, Diarrhea disease in Nepal vis-a-viz water supply and sanitation status. *Journal of water and Health* 2004; 2(2); 71-81.

- A. Priss-Uston, D. Kay, L. Fewtrel, and J. Bartrain, Unsafe water, sanitation and hygiene in comparative quantities of health risks. In Egzat, M., Lopez, A., Rogers, D. and Murray, C.T.C (eds), Global and Regional Burden of disease attributed to selected major risk factors, World Health Organisation 2004; 2; 1321-1352.
- [16] Pruss, D. Kay, L. Fewtrel and J. Bartram, Estimating the burden of disease from Water, sanitation and hygiene at a global level. Environmental Health Perspective 2002; 110(5); 537
- [17] J.B. Weisman, G.F. Graun, D.N. Lawrence, R.A. Pullard, M.S. Suslar and E.J. Gangarosa, An epidemic of gastroenteritis trend to a contaminated public water supply. American Journal of Epidemiology 1976; 103; 319-398.
- [18] World Health Organisation (WHO). Surveillance of drinking water Quality: World Health Organization, Geneva, 1976.
- [19] World Health Organisation (WHO). Reducing Risks, promoting healthy life, World Health Report 2002, World Health Organisation, Geneva.
- [20] World Health Organisation (WHO). Guidelines for drinking water quality, 1985; 3; 28...
- [21] World Health Organisation (WHO). The International Network to Promote Households Water Treatment and Safe Storage 2007.

Appendix A: Determination of adequacy of public pipe-borne water supply

Step 1: calculation of population figure

The population census conducted in 1991 put population of Ile-Ife to be 147, 938 people. Using annual growth rate of 3.2% as given by National Population Commission, the population for the year 2013 was calculated from

$$P = X (1+r)^n$$

where, P = Population for 2013

X = Population for 1991

r = growth rate

n = number of year after the last population count

$$P = 147, 934 \times (1 + 0.032)^{22}$$

$$P = 295, 815 \text{ people}$$

Step 2: determination of litres of water demanded by the populace

The average daily water consumption per capital as prescribed by W.H.O. is 85 litres per day/person. The quantity of pipe borne water required based on the per capital per person and population figure of 2013 is now expressed mathematically as given below

Total water required, TD = P x per capita

$$TD = 295, 815 \times 85 \text{ Litres/day}$$

$$TD = 25, 144, 275 \text{ Litres/day}$$

However, the Local Water Corporation pumps 1, 250, 000; 00 litres of water per day.

Step3: Percentage of water requirement met by pipe-borne water supply in the study area

$$= \frac{1,250,000}{25,144,275} \times 100\%$$

$$= 5\% \text{ of total Required.}$$

DWT-AES BASED INFORMATION SECURITY SYSTEM FOR UNMANNED VEHICLES

Renjith V Ravi¹ Dr.R. Mahalakshmi²,

¹(Ph.D Research Scholar, Karpagam University, Coimbatore, India)

renjith_v_ravi@yahoo.co.in

¹(Professor and HOD, Dept. of EEE, Sree Krishna College of Technology, Coimbatore, India)

ABSTRACT: Security of data is crucial in present day telecommunication framework, AES algorithm is one of the prominent methods for information Encipherment. For secure image communication needed for unmanned robotics, Discrete Wavelet Transform (DWT) is embraced for image decomposition, quantization and determination of appropriate sub bands is needed to precede encryption and to decrease execution time. In this paper, a modified algorithm for secure image encoding is proposed, demonstrated and is examined for its execution. Different images are considered as experiments for encoding, with parallel operation of AES algorithm the aggregate time in encoding the image is decreased to 2 seconds (evaluated focused around programming reference model). PSNR for different images acquired exhibit the exhibitions of the proposed model for image encoding. Image size of 1024x1024 is considered for encryption and unscrambling. The results got exhibit the exhibitions of AES algorithm.

KEY WORDS : DWT, AES cryptography, software model of AES, image encryption

I. INTRODUCTION

One among the most mainstream momentum research territory in civil and defense is unmanned robotics. Adjustments of self-sufficient vehicles are developing particularly in provisions, for example, producing, perilous materials taking care of, observation, remote sensing, and protection part and country security. The fundamental errand in any such requisition is the view of the surroundings through one or more sensors overwhelmingly by utilizing image sensors. Unmanned robotics is eagerly being produced for both non military person and military utilization to perform dull, grimy, and unsafe exercises. These unmanned vehicles (UVs) are remote-worked and the vehicles are controlled by a human administrator through a communications join. Control movements are dictated by the administrator based upon either coordinate visual perception or remote review through a Polaroid. Since computerized feature or images taken from UVs transmission framework generally incorporates a packing module that intends to decrease the transmitted bit rate. Throughout transmission over an open communication join encryption of compacted information is extremely critical and consequently the cryptography strategies must be precisely outlined. In this work, encryption of the image is completed utilizing specific key while getting the first image the same key is utilized. Information exchange through open system is constantly unsecured, in this way security is one of the significant difficulties that need to be tended to guarantee the dependable information exchange. The security issue in this manner turns into an imperative issue in today's wired or remote Internet provisions. A standout amongst the most helpful systems to secure information is utilizing a cryptographic framework, as the outline of figure algorithms is focused around a propelled numerical hypothesis. It generally blends distinctive sorts of cryptosystems in a safe convention to give a safe channel to information transmission. As a rule, asymmetric-key crypto frameworks, and RSA stands for Rivest, Shamir and Adleman who first freely depicted it in 1978. Symmetric-key crypto frameworks, for example, Data Encryption Standard (DES) or Advanced Encryption Standard (AES), are utilized to encrypt mass data in the transmission stage. Because of restricted figuring assets in compact requisitions, the framework normally off-burdens the security methodology to devoted unique hardware. As of late, there have been numerous chips away at outlining savvy encryption hardware utilized as a part of versatile provisions [1]–[10].

A few works [1]–[5] concentrate on territory diminishment of AES, while others [6]–[10] propose to lessen hardware cost for both ECC and RSA crypto frameworks. Image processing is discovering essentialness in different provisions as after most recent 10 years. Interactive media requisitions are ruled by image processing. It is obligatory to secure or ensure sight and sound substance from unapproved access. Securing the image or video content in a sight and sound data is of essential imperativeness as image passes on more data than whatever available wellspring of data. Images are huge in size and oblige expansive capacity unit, consequently encryption of image substance is additionally drawn out [14]. Conventional encryption algorithm set aside a few minutes expending for huge size of image data, henceforth encryption algorithms ought to be altered for bigger image sizes and need to be quicker. [13,14,15] reports that symmetric key algorithm have computational time short of what asymmetric key algorithms. Symmetric key algorithms, for example, AES, DES have been effectively utilized for encryption of data, hardware algorithms for AES have made them quick and consequently expend less time, however for images with extensive data size AES is still prolonged. Image processing is discovering vitality in different provisions as following the time when most recent 10 years. Multimedia requisitions are commanded by image processing. It is required to secure or ensure multimedia content from unapproved access. Ensuring the image or video content in a multimedia data is of essential significance as image passes on more data than any viable wellspring of data. Images are expansive in size and oblige huge storage unit, consequently encryption of image substance is likewise time intensive [12]. Conventional encryption algorithm set aside a few minutes devouring for extensive size of image data, consequently encryption algorithms ought to be modified for bigger image sizes and need to be speedier. [11, 12, 13] reports that symmetric key algorithm have computational time short of what asymmetric key algorithms. Symmetric key algorithms, for example, AES, DES have been effectively utilized for encryption of data, hardware algorithms for AES have made them quick and consequently spend extremely less time, however for images with huge data size AES is still lengthy. In [14, 15, 16] fast symmetric architectures for hardware execution of AES algorithm is accounted for. These algorithms have not been approved for image encoding. A focal attention for any cryptographic framework is its vulnerability to conceivable strike against the encryption algorithm, for example, measurable ambush, differential assault, and different animal assaults. Lapses in channel likewise degenerate the encrypted data and thus there is a requirement for suitable strategy that could be utilized to distinguish and right the mistakes. In this paper, we investigate the exhibitions of AES algorithm for different inputs, keys and commotion in channel. Execution investigation completed aides in distinguishing a suitable mistake redressing algorithm for AES.

II. RELATED WORK

Secured image encoding is one of the novel methodologies that have been embraced in UVs for data transmission to the base station. The input image caught by the UVs is transformed utilizing Discrete Wavelet Transform (DWT) to get different sub bands, the sub bands are quantized and the quantized sub bands are encrypted. The encoding strategy, for example, Huffman encodes the encrypted data and compresses the data caught, and is transmitted to the base station. Figure 1 shows the block diagram of secured image coding [17]. DWT has been generally utilized as a part of numerous diverse fields of audio and video signal processing. DWT is constantly progressively utilized as compelling answers for the issue of image compression. Quantizer is the procedure of approximating the continuous set of values in the image data with a finite set of values. The outline of the quantizer has a critical effect on the measure of compression got and loss caused in a compression plan. AES is a block cipher with variable key length (128-bit, 192-bit, and 256-bit separately) and block size of 128-bit. AES require low memory to make it extremely appropriate for confined space situations, in which it additionally shows great execution. Huffman coding is a manifestation of encoding that makes the most productive set of prefix codes for a given content. The standard is to utilize a lower number of bits to encode the data that happens all the more as often as possible. The controller is a module required for improving provisions security prerequisites based on a variable framework assets.

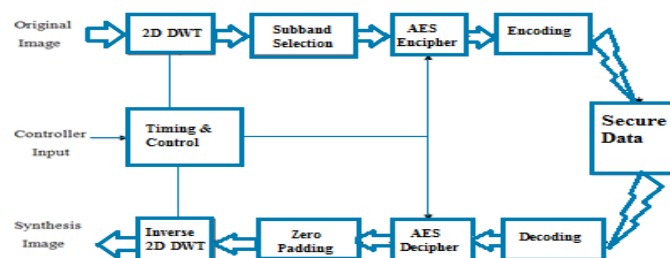


Figure 1 Secure Image Codec[17]

Clients can characterize their security necessities for a specific security benefit by indicating a security range. G. Liu, T. Ikenaga, S. Goto and T. Baba in their paper have proposed another video security scheme , which incorporates two encryption methods. The conspicuous feature of this system is a shuffling of AC occasions produced after DCT transformation and quantization stages [18]. DCT presents blocking ancient rarities and thus, DWT is received. M. Zeghid, M. Machhout, L. Khriji, A. Baganne and R. Tourki [19], in their paper, they dissected the Advanced Encryption Standard (AES), and they include a key stream generator (A5/1, W7) to AES to guarantee enhancing the encryption execution; mostly for images portrayed by diminished entropy. Equipment implementation of DWT with encryption forces significant difficulties and have been examined in [20][21][22],[23]. In this paper we investigate the execution of secure image coding utilizing software reference model.

A. Two Dimensional Discrete Wavelet Transform for Image Compression

The two dimensional DWT is turning into one of the standard apparatuses for image fusion in image and signal processing field. The DWT methodology is done by progressive low pass and high pass filtering of the digital image or images. This methodology is known as the Mallat algorithm or Mallat-tree decomposition. Figure 2 shows an implementation structure of the 2-D DWT-IDWT. The primary level of transformation is performed along the rows and the second level of transformation happens along the column. The four sub band segments (LL, LH, HL and HH) catch the low frequency parts (DC part), high frequency segments (edges along vertical, horizontal and diagonal axis). On the reverse process, the original image is reconstructed based on inverse transformation methodology utilizing IDWT.

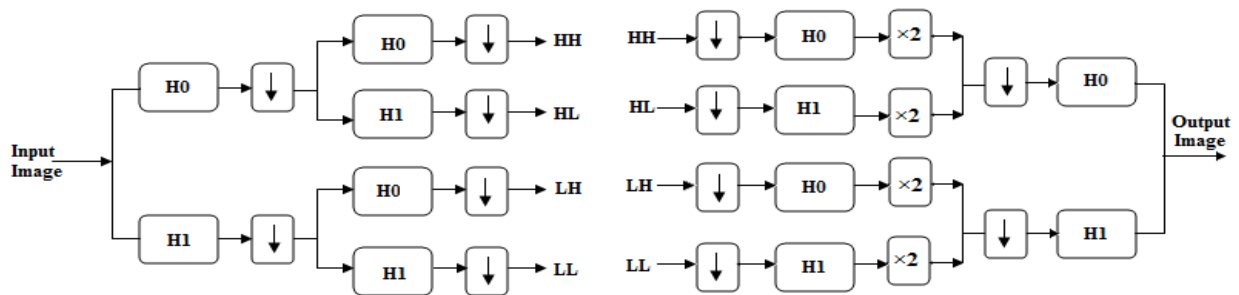


Figure 2 Analysis and synthesis filter bank structure of DWT

For perfect reconstruction, the coefficients for the high pass and low pass filters needed to satisfy the following two properties shown in Eq. 1 and Eq. 2 respectively .

$$\frac{1}{2} \left[H_0(z^{1/2})X(z^{1/2}) + H_0(-z^{1/2})X(-z^{1/2}) \right] \dots \text{Eq. (1)}$$

$$\frac{1}{2} \left[H_1(z^{1/2})X(z^{1/2}) + H_1(-z^{1/2})X(-z^{1/2}) \right] \dots \text{Eq. (2)}$$

The discrete wavelet transform used in this work is Daubche’s db4 wavelet. Figure 4(a) and 4(b) shows its scaling and wavelet functions respectively.and Figure 5; (a),(b),(c) and (d) shows the coefficients of its decomposition and reconstruction lowpass and high pass filters respectively.

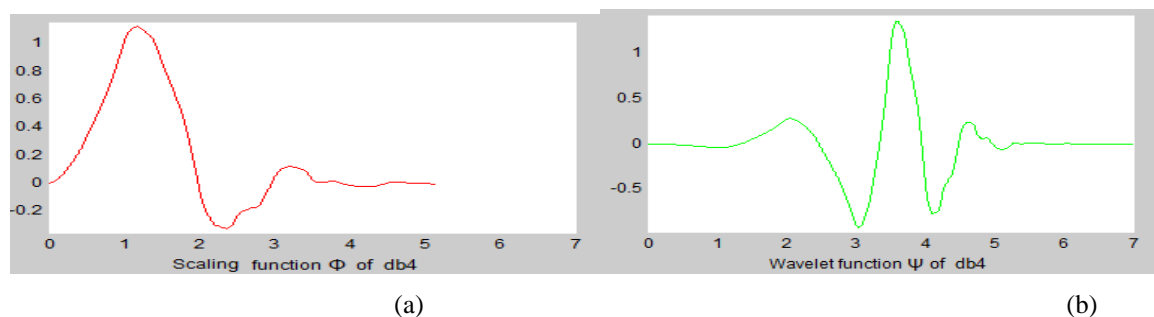


Figure 4 Scaling and wavelet functions of db4 ; (a) Scaling function of db4 , (b)Wavelet Function of db4

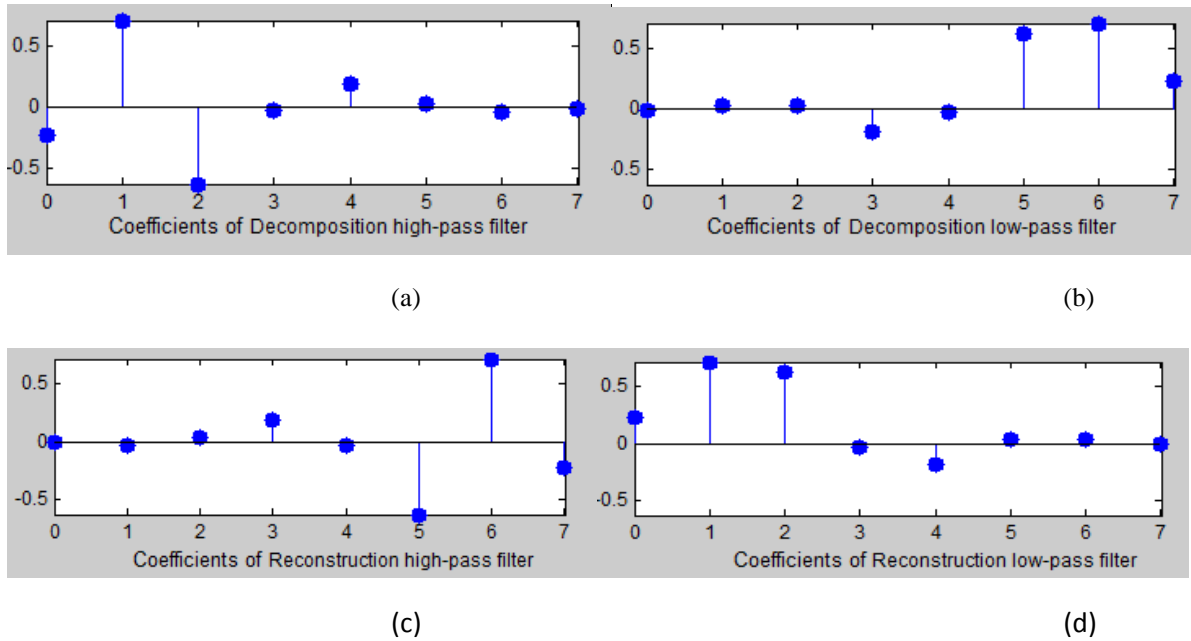


Figure 5 Decomposition; (a) high pass filter, (b) Low pass filter; Reconstruction filters; (c) high pass filter, (d) Low pass filter

Figure 3(a) shows the general concept for image decomposition using dwt . In the first level, input image is disintegrated into four sub bands (LL,LH,HL, HH), the LL sub band part is further decayed into four more sub band segment in the second level. figure 4 shows the pyramidal decomposition of input image utilizing DWT.In Figure 4(a) shows the input image, Figure 4(b) shows the aftereffects of first level decomposition, Figure 4(c) shows the second level decomposition stage and Figure 4(d) shows the synthesized image. The information is really display in the LL sub band the other three sub bands give information on edges of a given protest in the original image.

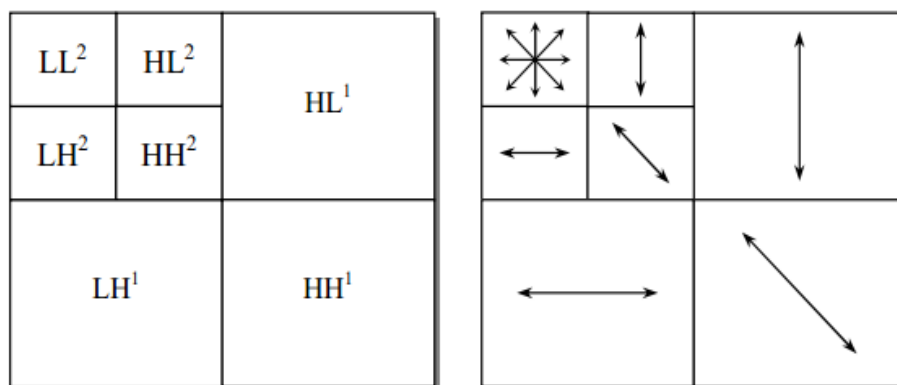


Figure 6 shows the general concept for image decomposition using dwt.

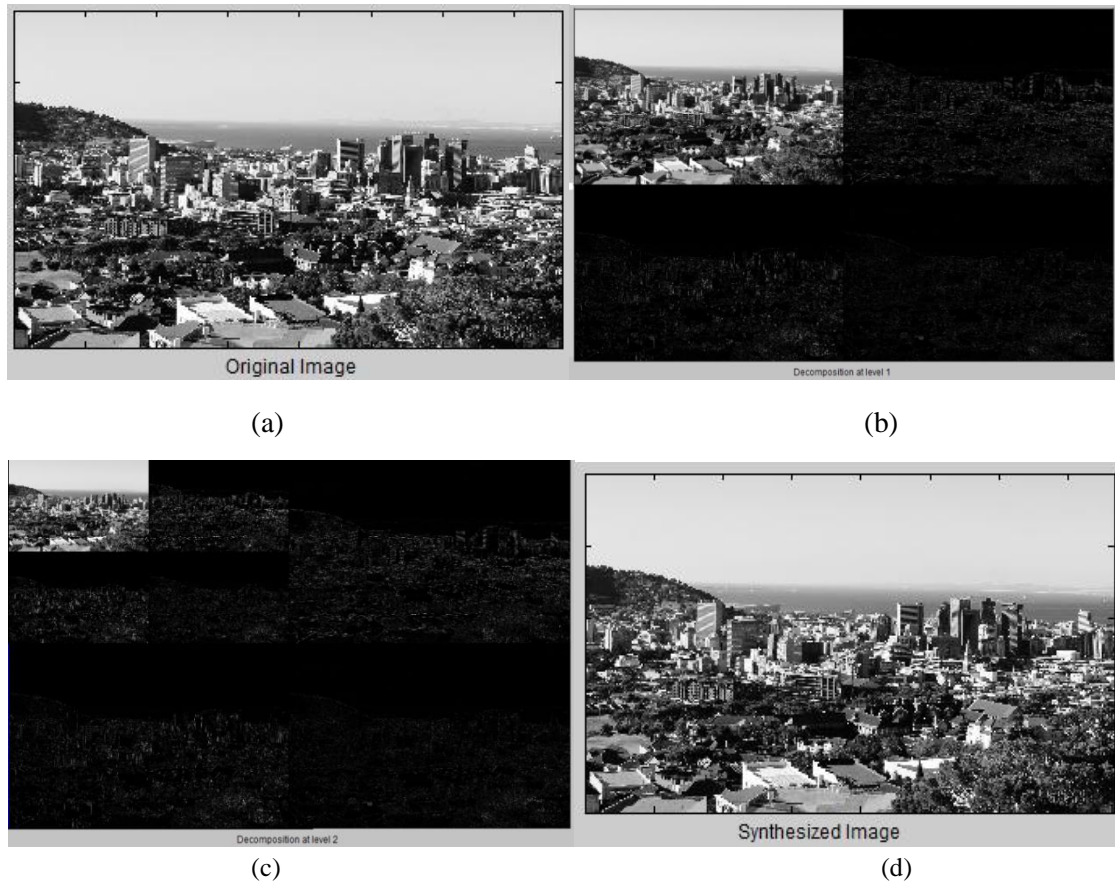


Figure 7 Image decomposition reconstruction of DWT; (a) Original Image (b) 1st level decomposition (c) Second level decomposition (d) synthesized Image

Figure 5 shows the histograms of original and synthesized image. These two histograms are almost same. Figure 6 shows the histograms of approximation components at level 1 and level 2, those are having slight difference. Figure 7, 8, and 9 are the histograms of horizontal, vertical and diagonal components at level 1 and level 2 respectively, these are significantly different from each other.

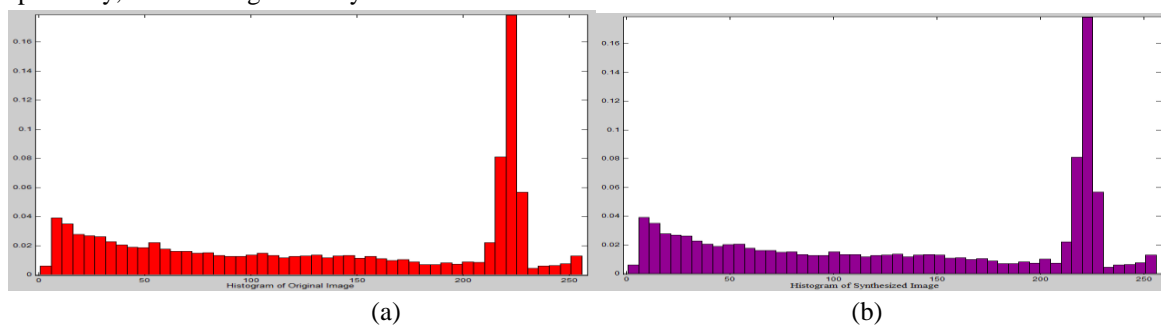


Figure 8 Histograms of original image and synthesized image; (a) Histogram of original image, (b) Histogram of Synthesized Image

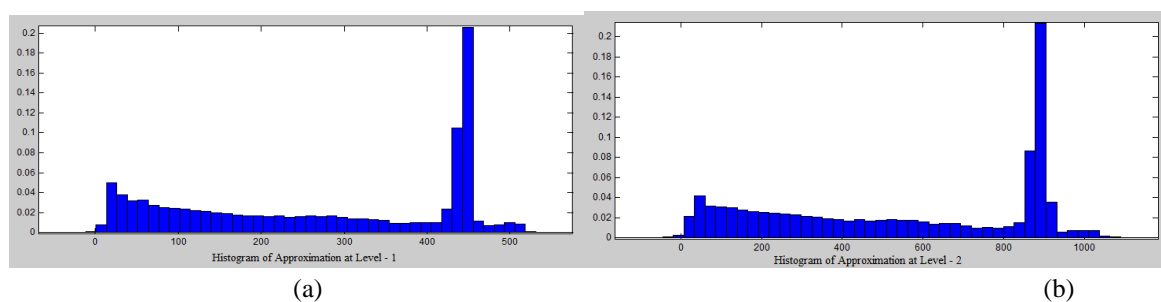


Figure 9 Histograms of Approximation components; (a) at level 1, (b) at level 2

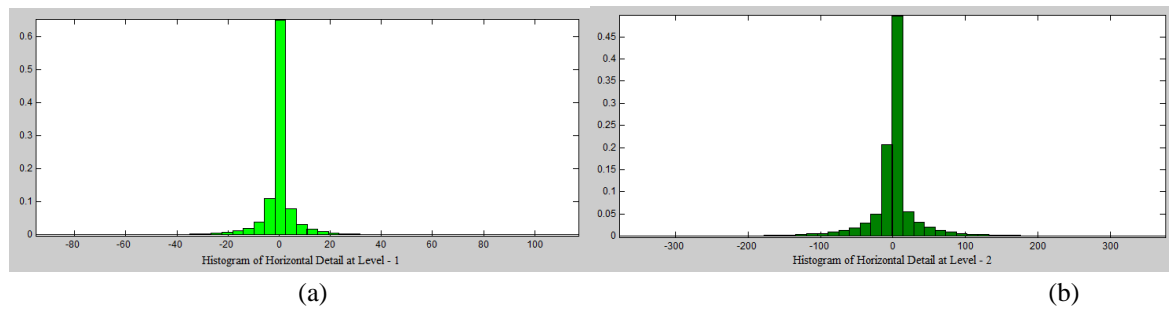


Figure 10 Histograms of Horizontal components; (a) at level 1, (b) at level 2

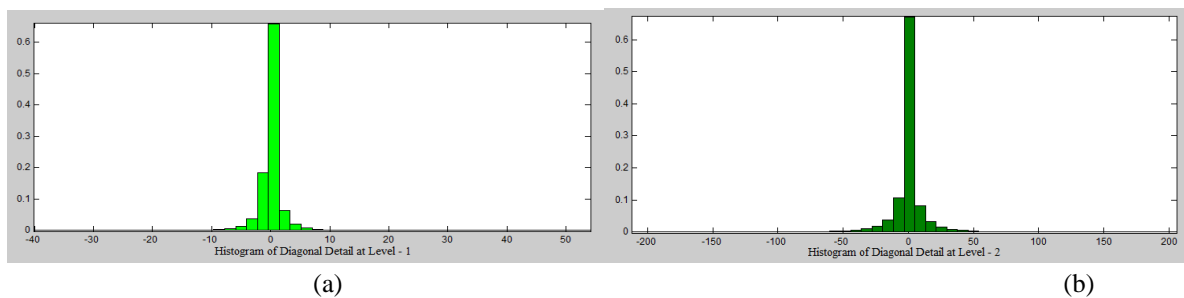


Figure 11 Histograms of Diagonal components; (a) at level 1, (b) at level 2

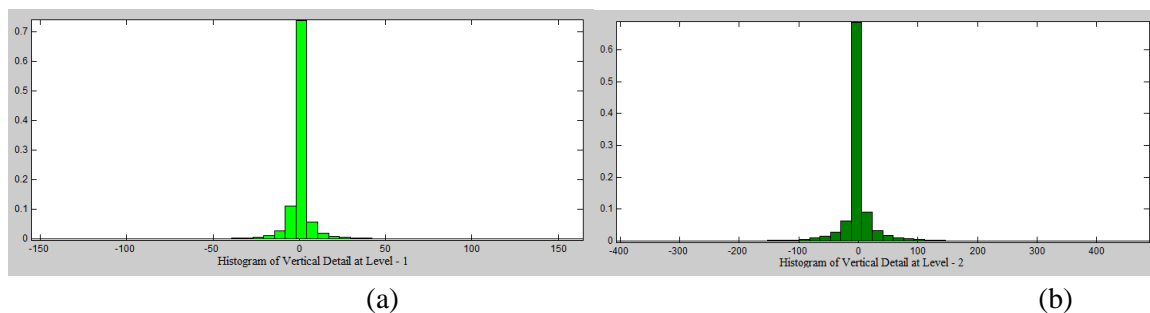


Figure 12 Histograms of Vertical components; (a) at level 1, (b) at level 2

Image compression is accomplished by quantizing the higher sub bands that are not exceptionally noteworthy and transmitting the LL sub band without quantization. An input image of size $N \times N$ after two level decomposition will offer ascent to 7 sub bands (three more elevated amount sub bands of size $N/2 \times N/2$ at the first level, three $N/4 \times N/4$ at the second level and one low frequency sub band of $N/4 \times N/4$). Image compression is accomplished by picking just the noteworthy sub bands that give information and quantizing all other sub bands.

B. Advanced Encryption Standard

Advanced Encryption Standard (AES) is a symmetric block cipher that methodologies data blocks of 128 bits utilizing the cipher key of length 128, 192, or 256 bits. The AES algorithm [2] composes the data block in a four row and row-significant requested matrix. The first AES encryption/ decryption system is demonstrated in Figure 5. In both encryption and decryption, the AES algorithm utilizes a round function, which comprises of four distinctive byte situated transformations:

- [1] Sub Bytes substitutes each one State of the data block with a substitution table (S-box) estimation of that byte.
- [2] Shift Rows shifts the each one row of the state cluster by distinctive counterbalances cyclically, and the counterbalance relies on upon row-list.

- [3] Mix Columns transforms every section of the matrix by multiplying it with a consistent GF polynomial.
- [4] Add Round Key adds a Round Key to the State by a straightforward bit wise XOR operation.

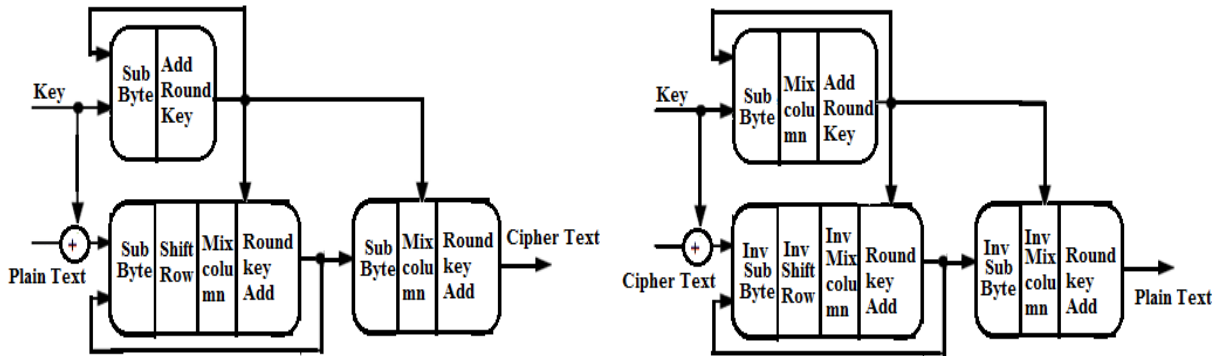


Figure 13 AES Encryption and Decryption

In AES algorithm, every 128-bit data is masterminded as a 4 x 4 state, worked by four primitive transformations. Throughout the encryption/decryption transform, the four primitive transformations are executed iteratively in Nr rounds, where the estimation of Nr will be 10, 12, or 14, contingent upon which key size is chosen. In the encryption technique, the approaching data will first be bit wise XORed with an introductory key, and afterward, four transformations are executed in the accompanying request: Sub-Bytes, Shiftrows, Mix columns, and Add Round key. Recognize that the Mix Columns transformation is not performed in the last round. The execution grouping is turned around in the decryption process, where their converse transformations are Inv Sub bytes, Inv Shift Rows, Inv mix columns, and Add Round key, individually. Since each one round needs a round key, a beginning key is utilized to create all round keys before encryption/decryption. In the AES algorithm, the Sub bytes transformation is a nonlinear byte substitution made out of two operations: 1) Modular inversion over GF(28), modulo an irreducible polynomial $p(x) = x^8 + x^4 + x^3 + x + 1$ and 2) affine transformation characterized as $y = mx + v$, where M is a 8 x 8 b matrix, v is a 8-b constant, and x/y indicates 8-b data/yield. In the Mixcolumns transformation, the 128-b data organized as a 4 x 4 state are worked column by column. The four components of every column structure a four-term polynomial that is multiplied by a constant polynomial $C(x) = \{03\}x^3 + \{01\}x^2 + \{01\}x + \{02\}$ modulo $x^4 + 1$. The Shift Rows transformation is a basic operation in which each one line of the state is cyclically shifted right by different offsets. The Add Roundkey transformation is a bitwise XOR operation of each one round key and current state.

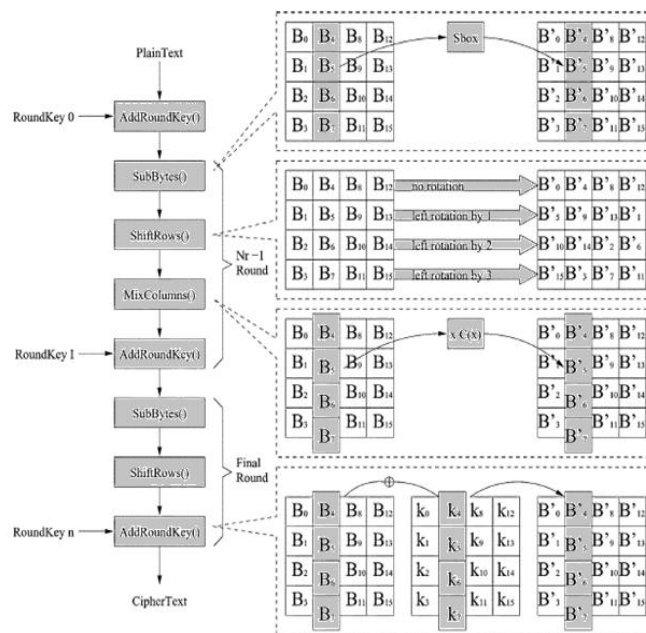


Figure 14 AES algorithm

The creation of s-box functioned in two steps, first finding the multiplicative inverse of the element over Galois Field $GF(2^8)$ modulo and the irreducible polynomial given in Eq. 1

$$x^8 + x^4 + x^3 + x + 1 \text{ ----- Eq.1}$$

Second, apply affine transformation of the structure $y = Mx + C$ to the inverse, where $M = 8 \times 8$ bit matrix, $C = 8$ -bit constant and $x/y = 8$ -bit input/output. Shift rows implies cyclic shift of each one column to the left by a predefined offset as demonstrated in Figure 14. Mix column works on every column exclusively. Every byte is mapped into another value which is a function of each of the 4 bytes in that column. In Add Round Key, the 128 bits of state are bit wise XORed with 128 bits of the round key. Each one round key generated in the key expansion and scheduling process. 10 rounds of the entire AES process are reshaped for a key length of 128 bit. The round keys are generated by a key expansion process. The expanded key is 176 bytes in length. Software modeling of AES encryption algorithm utilizing Matlab has been completed and different transformations utilized as a part of the algorithm in changing over plain text to cipher text were examined. The software modeling has been completed such that the main program calls the initialization function and the encryption function which thus calls other sub functions to fulfill the undertaking of encryption. Next segment talks about the software model for AES algorithm.

III. PROPOSED METHOD FOR SECURE IMAGE CODING

The real limits saw in image encoding are the aggregate computation time in AES algorithm when connected to image data (16,384 frames). So as to lessen the computation time, input image is transformed to sub bands utilizing DWT and each one sub band is quantized and encoded utilizing AES. The computation time is reduced and likewise is more suitable for real time provisions. The modified block diagram for secure image encoding is demonstrated in Figure 15. In the modified algorithm the input image is decomposed into 7 sub bands of high and low frequency components. The LL2 sub band is encoded utilizing AES algorithm. The other sub bands are LH2, HL2 and HH1 are picked and quantized. Consequently the picked sub bands are scrambled utilizing AES algorithm independently. The aggregate number of bits that are encoded after 2D DWT and quantization are demonstrated in Table 1.

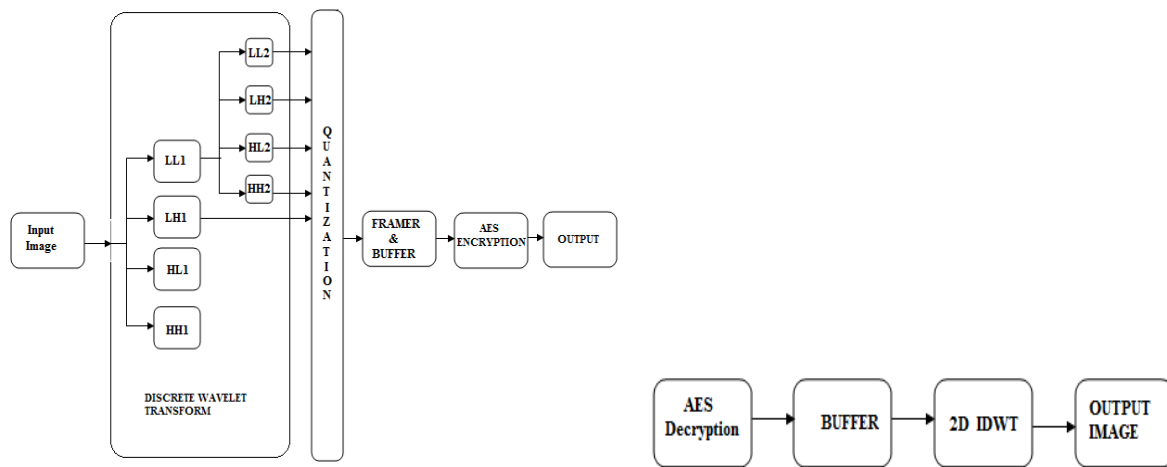


Figure 15 Modified Secure Image Encoding Transmitter and Receiver; (a) Transmitter (b) Receiver

In the modified encoding scheme LH2, HL2 and HH1 are picked as they hold the high frequency components of the input image along the vertical, horizontal and diagonal directions. The vertical component and horizontal component information is caught from the second level decomposed sub band, the diagonal component is caught structure the first level sub band component. Further, the L12 component might be decomposed to four more sub bands in the third level and suitable sub band components could be quantized and encoded utilizing AES algorithm freely.

TABLE 1 NUMBER OF BITS AND FRAMES IN PROPOSED METHOD

Input Image Size	Bits per frame	LL2/LH2/HL2 /HH2 size (in No. of bits)	LH1/HL1/HH1 size (in No. of bits)	No. of bits to be encoded using AES after selection
64 x 64	32768 (256)	2034	9126	15228 (119)
128 x 128	131072 (1024)	9126	36864	64242 (502)
256 x 256	524288(4096)	36864	147456	258048 (2016)
512 x 512	2097152(16384)	147456	589824	1032192(8064)

The table 1 shown above presents the number of bits encrypted using AES algorithm for different image sizes. In the image encoding scheme without DWT, the number of frames to be encoded (each of 128 bits), are shown in brackets in column 2. After decomposition using 2d-DWT using two level, the number of frames to be encoded is shown in brackets in column 5. After DWT, the pixels are spoken to using 9 bits. The aggregate number of frames to be encrypted after DWT is diminished by half accordingly the computation time for AES algorithm is lessened to short of what 8 seconds (16 seconds is the time without DWT). As the AES algorithm is encoding the sub bands independently, the aggregate time for encoding is short of what 2 seconds in the altered algorithm.

IV. RESULTS AND DISCUSSION

The modified algorithm proposed is demonstrated utilizing Matlab and is confirmed for its usefulness utilizing different test images. Figure 8 shows the test images considered for encryption and decryption. The info image is decomposed into sub bands and the sub bands are encrypted utilizing AES algorithm, the encrypted information is decrypted and inverse DWT is connected to acquire the first image. Top Signal to Noise Ratio (PSNR) is registered to gauge the exhibitions of the encryption plan.





Figure 16 Test images for secure encoding

The software reference model created in Matlab, performs DWT of each one image and the decomposed sub bands are taken and focused around the information accessible in the sub bands. The picked sub bands are quantized and encrypted. The quantization process in this work contrasts the sub band coefficients and a threshold, the coefficients beneath threshold are made zero, and coefficients over the set threshold are held. In this work, for the LL2 the threshold is situated to ± 61 , for the LH2 and HL2 the threshold is situated to ± 136 , and for the HH1 the threshold is situated to ± 212 . The thresholds have been recognized focused around trial and error, so that the information in the decomposed image is not lost. After quantization the information is lost in the decomposed image, however the image size is diminished and along these lines reduces postpone in AES processing. Table 2 shows the PSNR consequences of AES with DWT and without DWT. Quantization process presents losses in the image, without quantization the PSNR is very nearly closer to the PSNR acquired without DWT.

TABLE 2 RESULTS OF PROPOSED METHOD

Test Image	Without DWT		With DWT and Without Quantization		With DWT and With Quantization	
	MSE	PSNR in dB	MSE	PSNR in dB	MSE	PSNR in dB
Dam	2.307	44.50	3.014	43.34	3.557	42.62
Old street	2.711	43.80	3.909	42.21	4.765	41.35
Office	3.007	43.35	4.286	41.81	5.201	40.97
Flower	1.466	46.47	2.173	44.76	2.723	43.78
Houseboat	1.816	45.54	2.489	44.17	2.898	43.51
Coconut trees	2.455	44.23	3.282	42.97	3.855	42.27
Church	1.941	45.25	2.736	43.76	3.358	42.87
Hill	1.582	46.14	2.005	45.11	2.383	44.36
Valley	2.033	45.05	2.774	43.70	3.428	42.78
Fruits	2.980	43.36	4.286	41.81	5.141	41.02
Cityscapes	2.323	44.47	3.343	42.89	3.954	42.16
Townatnight	1.779	45.63	2.530	44.10	2.979	43.39
Street	1.205	47.32	1.783	45.62	2.114	44.88
Sunset	1.439	46.55	1.968	45.19	2.329	44.46
Shore	2.806	43.65	3.742	42.40	4.53	41.57
Keralasunset	1.225	47.25	1.722	45.77	2.124	44.86
Wind	1.055	47.90	1.626	46.02	1.919	45.30

Boy	2.905	43.50	3.954	42.16	4.689	41.42
Braches	1.200	47.34	1.300	46.99	1.507	46.35
Forest	1.928	45.28	2.972	43.40	3.532	42.65
Fox	2.979	43.39	4.54	41.56	5.371	40.83
Rail	2.345	44.43	2.952	43.43	3.508	42.68
Warehouse	1.775	45.64	2.484	44.18	2.885	43.53
Lake	1.047	47.93	1.497	46.38	1.775	45.64
Cat	0.853	48.82	1.286	47.04	1.556	46.21
Staircase	1.127	47.61	1.479	46.43	1.795	45.59
Vegetables	1.808	45.56	2.637	43.92	3.274	42.98
Grapes	0.893	48.62	1.371	46.76	1.679	45.88

PSNR results got without and with quantization are demonstrated in column 3 and 4 respectively and are contrasted and the consequences of image coding with AES encoding in column 2. The greatest deviation as far as PSNR for the picked images is 4 db and 9 db without quantization and with quantization. To enhance the PSNR and lessen computation time, the input image might be decomposed into various progressive sub bands and quantization threshold could be set fittingly to acquire the first image without misfortune. DWT is performed to decrease computation time in AES encoding on the input image straightforwardly. Further, exhibitions of different DWT filters can likewise be evaluated on the reconstruction process. In this work, Db4 wavelets have been utilized for deterioration and reconstruction. From the results got we exhibit that the decision of DWT channel, choice of sub bands, quantization threshold and parallelism of AES calculation assumes an indispensable part in secure image encoding for Unmanned Vehicles.

VI. CONCLUSION

In this work we have developed a secure image coding scheme with multi level of security based on DWT and AES algorithm and utilized the AES algorithm for the encryption of consistent image information and two dimensional DWT for image decomposition. We have developed a software reference model of DWT, with AES algorithm for security and have proposed a fractional encryption procedure based on AES. Exploiting the DWT in our work, one may decide to encrypt LL band with security level goes from low to high. Expanded protection is exchanged off against more encryption time. The percentage of information subjected to encryption while keeping up medium confidentiality is fundamentally diminished as contrasted with full encryption .The encryption of just LL2 sub band information as of now conveys a fulfilling secure result. The proposed procedure might be utilized as a part of telecommunication between an unmanned vehicle and its base station. Test results exhibit that the proposed secure image encoding scheme is quick and is appropriate to give high security provisions.

REFERENCES

- [1] A. E. Rohiem, F. M. Ahmed and A. M. Mustafa "FPGA Implementation of Reconfigurable Parameters AES Algorithm", *13th International Conference on Aerospace Sciences and Aviation Technology, ASAT- 13*, May 26 – 28, 2009.
- [2] A. Hodjat, I. Verbauwhede, "A 21.54 Gbits/s Fully Pipelined AES Processor on FPGA". *Proceedings of the 12th Annual IEEE Symposium on Field-Programmable Custom Computing Machines (FCCM'04)*.
- [3] A. Mansouri, A. Ahaitouf, and F. Abdi, "An Efficient VLSI Architecture and FPGA implementation of High-Speed and Low Power 2-D DWT for (9, 7) wavelet Filter", *IJCSNS International Journal of Computer Science and Network Security*, VOL.9 No.3, March 2009.
- [4] A. Satoh and K. Takano, *A scalable dual-field elliptic curve cryptographic Processor*, IEEE Transactions on Computer Science, Vol. 52, No.4, pp.449–460, 2003
- [5] Ashwini M. Deshpande, Mangesh S. Deshpande and Devendra N. Kayatanavar, "FPGA implementation of AES Encryption and Decryption", *International Conference on Control , Automation, Communication and Energy Conservation -2009*, 4th-6th June 2009.
- [6] Bruce Schneir, *Applied Cryptography*, 2nd Edition, John Wiley and Sons Publishers, 1996

- [7] Chen-Hsing Wang, Chieh-Lin Chuang, and Cheng-Wen Wu, *An Efficient Multimode Multiplier Supporting AES and Fundamental Operations of Public-Key Cryptosystems*, IEEE Transactions on Very Large Scale Integration Systems (VLSI), Vol.18, No.4, pp.553-563, 2010
- [8] D. Dia, M. Zeghid, M. Atri, B. Bouallegue, M. Machhout and R. Tourki, "DWT-AES Processor for a Reconfigurable Secure Image Coding", International Journal of Computer Science and Engineering, vol.1, no.2, June 2009.
- [9] D. Dia, M. Zeghid, M. Atri, B. Bouallegue, M. Machhout and R. Tourki, "DWT-AES Processor for a Reconfigurable Secure Image Coding", International Journal of Computer Science and Engineering, vol.1, no.2, June 2009.
- [10] Deepthi, H.S., Manure, S.S.; Prasanna Raj, C.; Bhusare, S.S.; Naik, U.L., "Design and FPGA implementation of improved lifting scheme based DWT for OFDM systems" 3rd International Conference on Advances in Recent Technologies in Communication and Computing (ARTCom 2011),
- [11] Dominik Engel Thomas stutz, Andreas Uhl, "A survey on JPEF2000 encryption", Multimedia systems [online] SpringerLink Verlag pp.1 -29, 2008.
- [12] Flayh, N.A.; Dep. of Comput. Sc., JMI, New Delhi, India; Parveen, R.; Ahson, S.I., "Wavelet based partial image encryption", IEEE International Conference on Multimedia, Signal Processing and Communication Technologies, 2009. IMPACT '09.
- [13] G.Liu, T.Ikenaga, S.Goto and T.Baba, "A Selective Video Encryption Scheme for MPEG Compression Standard", in IEICE Transactions on Fundamentals of Electronics, Communications and Computer Sciences, 89 (2006), pp. 194-202.
- [14] Harris D., Krishnamurthy R., Anders M., Mathew S., and Hsu S., *An improved unified scalable radix-2 Montgomery multiplier*, Proceedings of 17th IEEE Symposium on Computer Arithmetic, pp. 172-178, 2005
- [15] Herstein I. N., *Abstract Algebra*, Macmillan Publishing Company, 1990
- [16] K. Gaj, P. Chodowicz, "Fast implementation and fair comparison of the final candidates for advanced encryption standard using field programmable gate arrays", CT-RSA 2001, pp.84-99
- [17] K. Janvinen, M. Tominisko, J. Skytta, "A fully pipelined memoryless 17, 8 Gbps AES-128 encryptor", in International symposium of Field programmable Gate arrays, 2003, pp.207-215.
- [18] M. McLone, J.V. McCanny, "Rijndael FPGA implementations utilizing look-up tables", J.VLSI signal process, syst. 34(3)(2003)261-275.
- [19] M. Zeghid, M. Machhout, L. Khriji, A. Baganne and R. Tourki, "A Modified AES Based Algorithm for Image Encryption", International Journal of Computer Science and Engineering, 1(2007), pp.70-75.
- [20] Manure, S.S.; M. Tech (VLSI Design & Embedded Syst.), KLECEL, Belgaum, India; Raj, C.P.P.; Naik, U.L., "Design and performance analysis of DWT/FFT based OFDM systems", 3rd International Conference on Advances in Recent Technologies in Communication and Computing (ARTCom 2011)
- [21] Qibin Hou; Inst. of Autom., Chinese Acad. of Sci., Beijing, China; Yangsheng Wang, "Security traffic image transmission based on EZW and AES", IEEE Intelligent Transportation Systems (Volume:1), 2003. Proceedings. 2003
- [22] Ramanaiah, K.V.; Narayana Eng. Coll., Gudur, India; Raj, C.P., "VLSI Architecture for Neural Network Based Image Compression", 3rd International Conference on Emerging Trends in Engineering and Technology (ICETET), 2010
- [23] Safari, A.; Dept. of Electron., Macquarie Univ., Sydney, NSW, Australia; Yinan Kong, "Performance comparison of orthogonal and biorthogonal wavelets using technology libraries", 13th International Symposium on Communications and Information Technologies (ISCIT), 2013.
- [24] Satoh A., Morioka S., Takano K., and Munetoh S., *Unified hardware architecture for 128-bit block ciphers AES and Camellia*, Proceedings of cryptographic Hardware and Embedded Systems, pp. 304-318, 2003
- [25] Shiguo Lian, "Quasi-commutative watermarking and encryption for secure media content distribution", [online], Multimedia Tools and Applications Volume 43, Number 1 / May, 2009
- [26] Shtewi, A.M. "An Efficient Modified Advanced Encryption Standard (MAES) adapted for image cryptosystems" IJCSNS International Journal of Computer Science and Network Security, VOL.10 No.2, pp 226-232 February 2010
- [27] Sugreev Kaur and Rajesh Mehra, "High Speed and Area Efficient 2D DWT Processor Based Image Compression", Signal & Image Processing: An International Journal (SIPIJ) Vol.1, No.2, December 2010.
- [28] Tenca A. F. and Koç C. K., "A scalable architecture for modular multiplication based on Montgomery's algorithm", IEEE Transactions on Computer Science, Vol. 52, No. 9, pp. 1215-1221, 2003
- [29] Wang J., Zeng X., and Chen J., "A VLSI implementation of ECC combined with AES", Proceedings of International Conference on Solid State and Integrated Circuit Technology, pp. 1899-1904, 2006
- [30] William Stallings, *Cryptography and Network Security Principles and Practices*, 4th edition, Prentice Hall, 2007

Vermiretreatment of Pharmaceutical Wastewaters and Nutrient Bioassay of Treated Effluents for Reuse as Irrigation Water

Sharda Dhadse¹, P.R. Chaudhari², Shanta Satyanarayan³ and S. R. Wate⁴

¹ National Environmental Engineering Research Institute, Nagpur 440020, India

² Ex-Deputy Director, National Environmental Engineering Research Institute, Nagpur 440020 (India)

³ Ex-Deputy Director, National Environmental Engineering Research Institute, Nagpur 440020 (India)

⁴ Director, National Environmental Engineering Research Institute, Nagpur 440020 (India)

ABSTRACT: Present investigation was undertaken to study the low cost efficient treatment system for the treatment of high organically polluted industrial wastewater. The herbal and bulk drug pharmaceutical industry wastewaters were characterized and treated by vermifilter units and the treated effluents were assessed for its toxicity or nutrient enrichment by algal assay procedure to explore the feasibility of use of treated effluents for the agriculture. Both the raw wastewaters were observed to be high strength organic wastewaters with very high COD and BOD₅ with dark yellow color. Results of study established vermifiltration as the low cost efficient method for the treatment of herbal and bulk drug pharmaceutical wastewaters. Significant observations were recorded with respect to reduction of color, heavy metals and pollutants, and stabilization of organic waste. The algal growth potential studies were carried out by using *Scenedesmus bijugatus*. The significant enhancement of algal growth in algal growth potential test indicated the value addition to the effluents during vermifiltration process in terms of nutrients and growth promoting factors. The effluents from low organic loading (0.8 kg COD/m³.d) unit complied with the Indian standard for irrigation water while the effluents from higher organic loading (3.2 kg COD/m³.d) required further treatment for polishing. Vermifilter system was, thus, proved to be suitable for the treatment of organically polluted industrial effluents, for their value addition and making them suitable for further recycling and reuse in agriculture as aerial spray or a liquid manure to increase the productivity of crop.

KEYWORDS: Pharmaceutical Wastewater, Vermifiltration, *Eudrilus eugeniae*, Algal Bioassay

I. INTRODUCTION

Pharmaceutical wastewater is high strength organically polluted industrial wastewater. The conventional treatment of pharmaceutical wastewater is highly technological and costly. Attempt has been made to use coagulants and synthetic polyelectrolytes for the treatment of herbal pharmaceutical wastewater [1, 2]. There is need to explore low cost method for the wastewater treatment, amenable to producing nutrient-rich effluent suitable for recycle and reuse for agricultural irrigation. Vermifilter is known to be simple and low-cost method for the stabilisation of waste organic residues producing high quality nutrient-rich vermifiltrate containing plant growth promoting factors. No one has used vermifilter for the treatment of pharmaceutical wastewater. Therefore, vermifilters were selected for the treatment of pharmaceutical wastewater.

Algal bioassay is the main tool in water pollution monitoring because algae are more sensitive for contamination than fish or invertebrates as test organisms. The nature of the effluents can be assayed by algae since the responses can be measured in terms of biomass production or through the metabolic response generated [3, 4, 5]. Toxicity of raw wastewaters treated by advanced oxidation processes namely Fenton and Photo-fenton reactions was evaluated by algal bioassay [6, 7, 8]. Present investigation envisages studying the treatment efficiency of vermifilters for treatment of herbal and bulk drug pharmaceutical wastewaters and their nutrient assay by algal growth potential (AGP) test.

II. MATERIALS AND METHODS

2.1 Vermi-treatment of Wastewaters

The laboratory scale model of vermifilters was fabricated using glass columns having 10 cm diameter and 45 cm length with an outlet at the bottom to collect effluents. The filters were operated on down-flow mode, using flow meters and Watson Marlow pump. The reactors were packed with 1:1:1 ratio of sand, soil and vermicast, leaving 6 cm of upper column empty for the distribution of wastewater. The particle size of the packing material ranged from 0.4 to 0.6 mm that provided surface area of 600 to 650 m²/gm with voidage of 55%. The filters were operated at downflow mode which prevents flooding of the reactor. Earthworm species *Eudrilus eugeniae* was used in the experiment. A total of five reactors for each wastewater were used. The working volume of the filters was maintained at 850 ml. In every vermifilter a total of 15 healthy earthworms were introduced. Schematic of the experimental setup is shown in Fig. 1.

For both the wastewaters viz. bulk drug pharmaceutical wastewater (BDP) and herbal pharmaceutical wastewater (HPW), two day hydraulic retention time at 0.8 kg COD/m³.d and 3.2 kg COD/m³.d organic loadings rate was found to be the optimum. Therefore, the vermitreated effluents collected at these loadings, as described below, were selected for the algal bioassay to study its efficiency for the agricultural purpose.

BDL : Vermitreated bulk drug pharmaceutical effluent at low organic loading rate of 0.8 kg COD/m³.d

BDH: Vermitreated bulk drug pharmaceutical effluent at high organic loading rate of 3.2 kg COD/m³.d

HPL: Vermitreated herbal pharmaceutical effluent at low organic loading rate of 0.8 kg COD/m³.d

HPH: Vermitreated herbal pharmaceutical effluent at high organic loading rate of 3.2 kg COD/m³.d

The raw wastewater samples and effluent samples were analysed for their physico-chemical characteristics [9].

2.2 Algal Growth Potential Test

Algal growth potential (AGP) test was carried out using fresh water green alga *Scenedesmus bijugatus* (Fig. 2) as test organism, which was grown and maintained in basal medium (Table 1). Nutrient concentration in basal medium was treated as 100% nutrients for the alga. pH of basal medium was adjusted to 7.8 by 1% NaOH solution. *Scenedesmus* culture was isolated from clean lake water and grown in the basal medium. The stock culture was maintained in 2 litre flasks under 1500 lux light intensity. Every care was taken to keep them in sterile conditions.

2.3 Algal Inoculum

Required aliquots of exponentially growing stock of algal culture were centrifuged. The centrifuged biomass was washed with distilled water and again centrifuged. To this, required amount of distilled water was added so that 1 ml of this inoculum gave an optical density of 0.03 in test culture.

2.4 Procedure for Algal Bioassay

Clean, sterilized test tubes were used for AGP test. Three sets were prepared, first with serial dilutions of treated effluents with distilled water viz. 10% effluent, 20% effluent, 40% effluent, 60% effluent, 80% effluent and 100% effluent, second and third sets with same dilutions fortified with 30% and 100% basal medium nutrients respectively. Required amount of algal inoculum was added to each of the test tube in equal amount to give initial optical density of 0.03. Then the inoculated test tubes were kept in racks illuminated with cool white fluorescent tubes giving light intensity of 300 lux units. Algal growth was monitored in all the dilutions for 7 days period starting on 0 day. The growth of *Scenedesmus* was studied by "in-situ" measuring the optical density (OD) of the cultures by the spectrophotometer at the wavelength of 560 nm.

2.5 Estimation of Specific Growth Rate and Doubling Time

Specific growth rate of alga (1) and doubling time (2) were calculated as per the following method.

$$\text{Specific growth rate } (\mu): \frac{\text{Final } (\log_2 \text{OD} + 10) - \text{Initial } (\log_2 \text{OD} + 10)}{\text{No. of days (Exponential growth period)}} \text{----- (1)}$$

$$\text{Doubling Time} = 1 / (\mu) \text{----- (2)}$$

III. RESULTS AND DISCUSSION

3.1 Pharmaceutical Wastewaters

Physicochemical characteristics of HPW and BDP raw wastewaters are given in Table 2. Both the wastewaters were dark yellow in colour. HPW was acidic (pH 3.9-4.0) and BDP was near neutral (pH 7.5). Both the wastewaters were highly organic with very high COD and BOD₅ values and high concentration of total nutrients. The wastewaters also showed the presence of heavy metals. The BOD₅:COD ratio in these bulk drug and herbal pharmaceutical wastewaters ranged from 0.38 to 0.52 (Table 3). This range is near to 0.5 recorded

for domestic wastewater. It is generally assumed that when this ratio is below 0.2, the wastewater/effluent is toxic. Thus these effluents are not toxic and may be used for irrigation. At the same time, the COD:BOD₅ ratio of these effluents varied from 1.92 to 2.65, which is near to ratio 2.5 for domestic wastewater and thus may be suitable for recycling as irrigation water in agriculture. It was observed that the physicochemical characteristics of bulk drug and herbal pharmaceutical effluent from low organic loading (0.8 kg COD/m³.d) treatment unit comply with Indian standard for irrigation water (IS:2490 - 1982) (Table 4) and can be used for agricultural irrigation. The effluent from higher organic loading (3.2 kg COD/m³.d) treatment units will require further treatment to refine the effluent quality with respect to dissolved solids, BOD₅ and Iron content.

3.2 Treatment Efficiency

The physicochemical characteristics of the treated effluents and the percentage reduction in the pollution indicator parameters are shown in Table 5. In both the effluents, pH has been improved to alkaline side, turbidity significantly reduced along with concomitant reduction in TSS by 91.6% to 93.6% in low organic loading and 83.1% to 89% in high organic loading. TDS was reduced by 64.2% to 75.92%. COD and BOD₅ reduction ranged from 83.34% to 96.26%. Similarly significant reductions were observed in chlorides, sulphides, sulphates, total phosphorus, total nitrogen, sodium, potassium, Pb, Cd, Ni, Co, Fe, Mn, Cr, and Cu. Though the overall reduction is satisfactory, it is observed that percent reductions in different parameters (except TDS) are more in low organic loading rate (0.8 kg COD/m³.d) in both the effluents. Thus, the low organic loading to vermifilters gives better quality of effluent.

3.3 AGP Test with Different Dilutions of BDL and BDH with Distilled Water

The results of the AGP experiments with serial dilutions of BDL and BDH are shown in Tables 6 and 7. It has been observed that in both the effluents, the lag phase, exponential growth period are similar. In BDL, maximum exponential growth rate and standing crop enhancement on 7th day were in 40% dilution, while the same was maximum in 60% dilution of BDH effluent. However the 100% effluent also had better results with respect to exponential growth rate and doubling time and enhancement of standing crop on 7th day. These results indicate that both the effluents were having rich quantity of available nutrients and had stimulating effect significantly over the control and the BDL had maximum growth stimulatory effect than BDH. This indicates that the vermifilter effluents contain sufficient nutrients and can be used for application on crops or on soil.

3.4 AGP Test with BDL Effluent Diluted with Basal Medium

The results of experiments carried out with BDL dilutions fortified with 30% and 100% basal medium nutrients are shown in Tables 8 and 9. The control and 10% and 20% dilutions of BDL with 30% basal medium nutrients showed 48 hours lag phase, while there was no lag phase in other test cultures in both the effluents. This may be due to rich availability of nutrients in the test cultures. Exponential growth period was the same in all test cultures. In BDL dilutions with 30% basal medium nutrients, exponential growth rate was increasing upto 80% dilution; doubling time was minimum in 40% effluent, and maximum enhancement of standing crop on 7th day was in 40% dilution. This indicate that 30% nutrient fortification was favourable for enhancing the algal growth till 40% dilution of effluent, but in 60% to 100% effluent dilution, nutrient fortification might have resulted in excess nutrients and showed reduction in growth potential. In other words, BDL effluent had enough nutrient content and do not require nutrient fortification, except for dilutions from 10% to 40%. Fortification of BDL dilutions with 100% basal medium nutrients (Tables 9) showed that enhancement of standing crop was very less with relatively lower exponential growth rate and relatively higher doubling time. This indicates excess enrichment of test cultures due to fortification of nutrients. These observations show that the fortification of nutrients to the BDL effluent did not enhance the algal growth significantly.

3.5 AGP Test with BDH Effluent Diluted with Basal Medium

Similar observations were recorded in case of BDH effluent. In case of 30% nutrient fortification, standing crop showed enhancement in 10% to 60% dilution, concomitant with gradual reduction in doubling time and increase in exponential growth rate (Table 10). In case of fortification of 100% nutrients, exponential growth period was reduced to 6 days, Standing crop showed reduction upto 40% dilution and then slight enhancement; reduction in exponential growth rate upto 40% dilution then slight increase; and increase in doubling time upto 40% dilution and then slight decrease (Table 11). This indicates that BDH is rich in nutrients at optimum level and do not require nutrient fortification except at 40% dilution and that is upto 30% nutrients only.

3.6 AGP Test with HPL and HPH Effluent Serially Diluted with Distilled Water

The results of the AGP test carried out with different dilutions of HPL and HPH effluents with distilled water are given in Tables 12 and 13. It has been observed that there was no lag phase in any of the test cultures. In both the effluents, the growth potential of alga showed significant improvement in exponential growth rate, decrease in doubling time and enhancement of standing crop over control with the increase in concentration of effluent in dilutions. Exponential growth period showed reduction with increase in concentration of effluent in dilution. This was due to faster nutrient utilization in shorter period in batch cultures. The 80% and 100% HPH effluent showed maximum enhancement of algal growth.

The above discussions lead to following salient observations.

- ◆ Vermittreated effluent of herbal pharmaceutical wastewater contains nutrients and growth promoting factors which significantly enhances the algal growth.
- ◆ The growth potential was better in HPL effluent as compared to that in HPH effluent. This may be due to better stabilization of waste organic matter under low organic loading resulting in slightly higher concentration of available nutrients in HPL effluent.

3.7 AGP Test with HPL Effluent Diluted with 30% and 100% Basal Medium Nutrients

The results of the AGP test with serial dilutions of HPL effluent fortified with 30% and 100% basal medium nutrients are shown in Tables 14 and 15. In both sets, the standing crop showed enhancement upto 60% dilution with concomitant increase in exponential growth rate and reduction in doubling time. However, there is reduction in standing crop and exponential growth rate, and increase in doubling time at 80% to 100% dilution. On the contrary, 100% nutrient fortification significantly increased the standing crop upto 80% dilution concomitant with increase in exponential growth rate and reduction in doubling time and then showed slight reduction, however better than control,. These observations show that HPL effluent might have sub-optimum concentration of available nutrients and growth promoting factors, thus showed improvement in algal growth potential significantly at 30% nutrient fortification and still more at 100% nutrient fortification.

3.8 AGP Test with HPH Effluent Diluted with 30% and 100% Basal Medium Nutrients

The results of the AGP test with serial dilutions of HPL effluent fortified with 30% and 100% basal medium nutrients are shown in Tables 16 and 17. Exponential growth period was of 7 days in 30% nutrient fortification and 6 days in 100% nutrient fortification. This was due to faster algal growth in a short time in the later. Algal growth potentials were tremendously increased in both the fortifications, higher in 100% fortification. However, highest algal growth potential was in case of 40% dilution in 30% nutrient fortification and in case of 60% dilution in 100% nutrient fortification. Comparison of algal growth potentials in HPL and HPH showed that HPL is more enriched with available nutrients and growth factors and thus showed less enhancement in standing crop after nutrient fortification over the control, while HPH being less enriched, showed significant enhancement in standing crop after nutrient fortification over the control.

IV. CONCLUSION

Bulk drug and herbal pharmaceutical wastewater were observed to be highly organically polluted wastewater having high suspended solids, total dissolved solids, COD and BOD₅ and dark yellow colour. Vermifilters were observed to be technically simple, low cost, efficient method for the treatment of high organically polluted wastewaters of pharmaceutical industry. The BOD₅:COD ratio of the vermittreated effluents ranging from 0.38 to 0.52 and COD:BOD₅ ratio ranging from 1.92 to 2.65 indicate that the effluents were not toxic in nature. Effluents from low organic loading (0.8 kg COD/m³.d) treatment units were found to comply with Indian irrigation water standard (IS:2490-1982), while effluents from high organic loading (3.2 kg COD/m³.d) treatment units may require further treatment to reduce their dissolved solids content, BOD₅ and iron content.

The biological characteristics of effluents were studied through AGP test. No residual toxicity was observed. AGP test showed that the vermittreated bulk drug and herbal pharmaceutical effluents were enriched with nutrients and growth promoting factors due to their treatment by the earthworm species *Eudrilus eugeniae*. Low organic loading (0.8 kg COD/m³.d) treatment units produced effluent with better amount of available nutrients, while at higher organic loading (3.2 kg COD/m³.d) units, the effluents might contain some amount of partially stabilised organic matter and thus may require dilution for favourable effect on plant growth. Vermittreated bulk drug effluents contained more than optimum level of nutrients and 40% to 60% dilutions gave maximum beneficial impact on plant growth. HPL and HPH required fortification of nutrients for increasing its growth stimulatory effects. It is recommended that field trials on the crops may be carried out by using these vermittreated effluents from low organic loading treatment units either in spray form or as liquid

manure or as irrigation water.

V. ACKNOWLEDGEMENT

The authors are grateful to the Council of Scientific and Industrial Research (CSIR), New Delhi for providing financial support and to the Director, NEERI, Nagpur for providing required facilities for carrying out the above mentioned research work.

REFERENCES

- [1]. A.P. Vanerkar, S. Satyanarayan, and D.M. Dharmadhikari, Herbal pharmaceutical wastewater treatment by conventional coagulants and synthetic polyelectrolytes. *Pollution Research*, 24(2), 2005, 341-346.
- [2]. A.P. Vanerkar, S. Satyanarayan, and D.M. Dharmadhikari, Enhancement of organic removals in high strength herbal pharmaceutical wastewater. *Environmental Technology*, 26, 2005, 389-395.
- [3]. Ekholm Petri, Jouttijärvi Timo, Priha Maarit, Rita Hannu, and Nurmesniemi Hannu, Determining algal available phosphorus in pulp and paper mill effluents: Algal assays vs routine phosphorus analyses. *Environmental Pollution*, 145(3), 2007, 715-722.
- [4]. M. Hala, Migid Abdel, A. Yehia, Azab, M. Waeel, Ibrahim, Use of plant genotoxicity bioassay for the evaluation of efficiency of algal biofilters in bioremediation of toxic industrial effluent, *Ecotoxicology and Environmental Safety*, 66(1), 2007, 57-64.
- [5]. L. Augulyte, D. Kliugaite, V. Racys, D. Jankunaite, and A. Zaliauskiene, Chemical and ecotoxicological assessment of selected biologically activated sorbents for treating wastewater polluted with petroleum products with special emphasis on polycyclic aromatic hydrocarbons, *Water, Air, & Soil Pollution*, 195(1-4), 2008, 243-256.
- [6]. A.M. Abdel-Aty, M.A. EL-Dib, M.I. Bdaway, Toxicity of pesticide industry wastewater to the green alga *Scenedesmus obliquus*. *Pakistan Journal of Biological Sciences*, 9(3), 2006, 563-567
- [7]. T.S. Melek and A.B. Isil, A case study on algal response to raw and treated effluents from an aluminium plating plant and a pharmaceutical plant, *Journal of Ecotoxicology and Environmental Safety*, 64(2), 2006, 234-243.
- [8]. C. Ram, P.K. Pandey, and A. Srivastava, Comparative toxicological evaluation of untreated and treated tannery effluent with *Nostoc muscorum* L., in *Algal assay and Microtox Bioassay*, (ITRC, Lucknow, 2003).
- [9]. D. Eaton Andrew, Mary Ann H. Franson (eds), *Standard Methods for the Examination of Water and Wastewater*. 21st edition (American Public Health Association, American Water Works Association, Water Environment Federation, 2005)

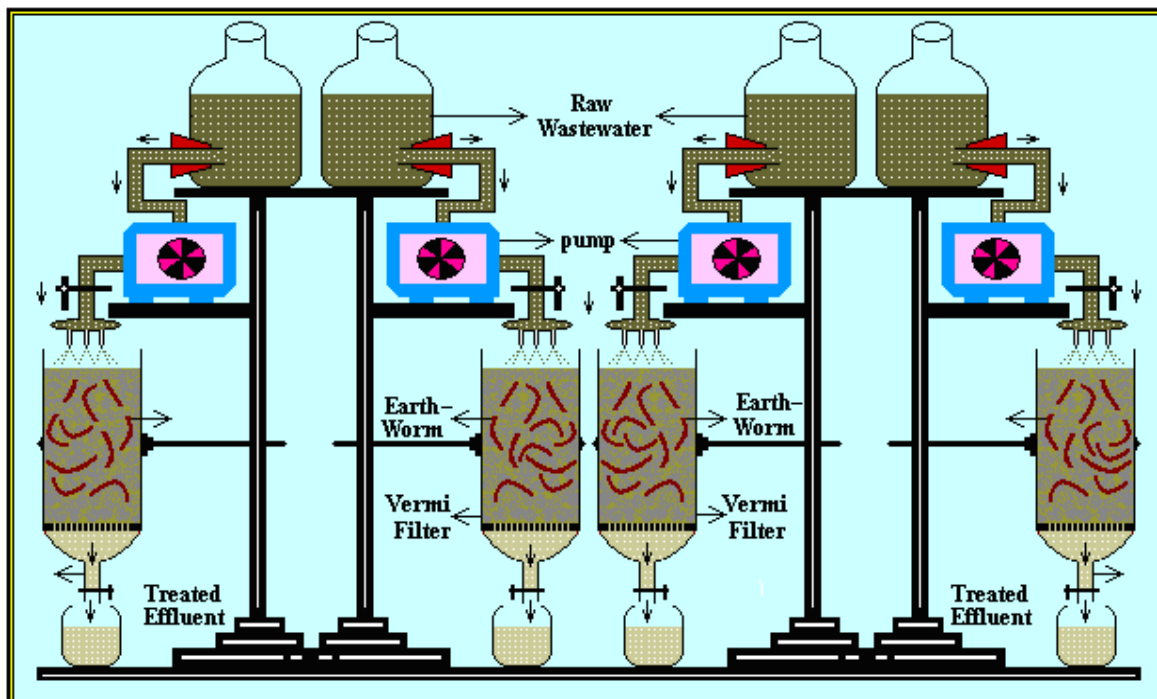


Figure 1: Experimental setup (Flow adjustment unit)

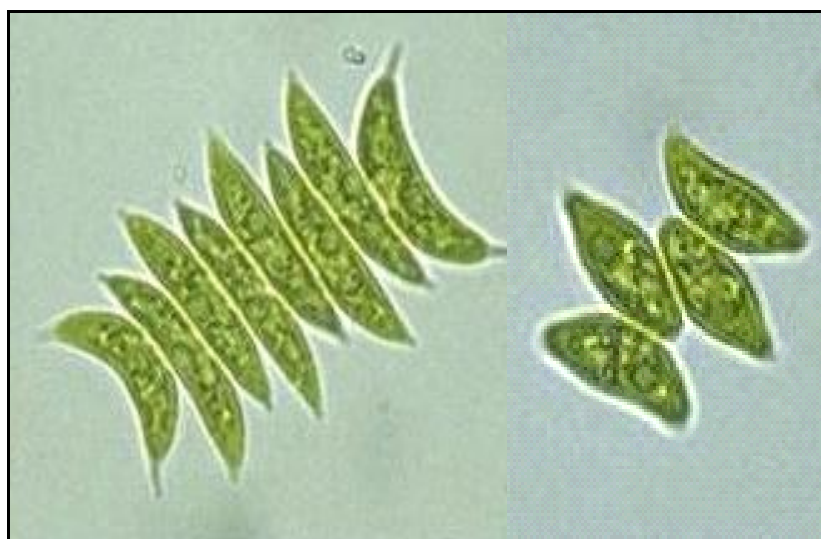


Figure 2: *Scenedesmus bijugatus* species

Table 1: The Nutrient Composition of Basal Medium for Culturing Alga *S. Bijugatus*

S.N.	Nutrient Salts	Concentration
1.	Urea	60 mg/l
2.	N_2CO_3	25 mg/l
3.	Na_3PO_4	25 mg/l
4.	NaCl	25 mg/l
5.	$(NH_4)_2SO_4$	20 mg/l
6.	$MgSO_4$	10 mg/l
7.	$FeSO_4$	2 mg/l

Table 2: Physico-Chemical Characteristics of Combined Herbal and Bulk Drug Pharmaceutical Wastewaters

Sr. No.	Parameters	HPW wastewater	BDP wastewater
1	pH	3.9 – 4.0	7.5
2	Colour (Visual)	Dark yellow	Dark yellow
3	Total acidity/ alkalinity as CaCO ₃	3000	6200
4	Turbidity	64.4	58.8
5	Suspended solids (SS)	5460 – 7370	6100
6	Total dissolved solids (TDS)	2564 – 3660	25.934
7	Total solids	8024 – 11030	
8	Chemical oxygen demand (COD)	21960 – 26000	34800
9	Biochemical oxygen demand (BOD ₅)	11200 – 15660	16000
10	Chloride	660-638	4193.69
11	Sulfide as S ⁻	42 – 54	330
12	Sulphates as SO ₄	82 – 88	325
13	Total phosphates as PO ₄	260 – 280	7.144
14	Total nitrogen as NH ₃ -N	389 – 498	370
15	Oil and grease	140 – 182	-
16	Sodium as Na	155 – 266	7197
17	Potassium as K	128 – 140	1120
18	Heavy metals		
	- Zn	0.314	0.00
	- Pb	0.434	0.525
	- Cd	0.185	0.298
	- Ni	0.156	0.178
	- Co	0.16	0.048
	- Mn	4.54	3.256
	- Fe	33.8	9.189
	- Cr	0.253	0.187
	- Cu	0.042	0.01
	- As	0.0062	-

All values are expressed in mg/l except pH and colour

HPW: Herbal Pharmaceutical Wastewater; BDP: Bulk drug Pharmaceutical Wastewater

Table 3: Effluent Characteristics with Respect to Ratios of BOD₅ and COD

Effluent parameters	HPL	HPH	BDL	BDH
COD	69	703	126	1097
BOD ₅	26	367	60	563
BOD ₅ :COD	0.38	0.52	0.48	0.51
COD:BOD ₅	2.65	1.92	2.1	1.95

Table 4: Compliance of Pharmaceutical Effluents to Indian Irrigation Water Standard

Parameters	Indian irrigation water standard (IS:2490 – 1982)	Pharmaceutical effluent from low organic loading (0.8 kg COD/m ³ .d)	Excess parameters of pharmaceutical effluent from high organic loading (3.2 kg COD/m ³ .d)
Suspended solids, mg/l	200	19 - 177	--
Dissolved solids (inorganic), mg/l, max.	2100	190 - 827	3706 (BDH)
pH	5.5 – 9.0	7.8 – 8.2	--
BOD ₅ , mg/l, max.	100	26 - 60	367 - 563
Chlorides (as Cl), mg/l, max.	600	39 - 226	--
Sulphate (as SO ₄), mg/l, max	1000	25-110	--
Manganese (as Mn), mg/l	2	0.022 – 0.136	--
Iron (as Fe), mg/l	3	2.1 – 3.21	6.55 (BDH)
Nitrate nitrogen, mg/l	20	Total nitrogen: 1.36 – 1.82	--

Table 5: Physico-Chemical Characteristics of Effluents of Herbal and Bulk Drug Pharmaceutical Wastewater at 2 Days HRT

Sr. No.	Parameter	Organic loading rate (kg COD/m ³ d)			
		0.8 (HPL)	3.2 (HPH)	0.8 (BDL)	3.2 (BDH)
1	pH	8.2	7.8	8.2	7.8
2	Alkalinity as CaCO ₃	373	466	284	340
3	Turbidity (NTU)	0.88	1.82	4.6	9.0
4	Total suspended solids (TSS)	22.0	177.0	19	127
5	%TSS reduction	91.6	83.1	93.6	89.0
6	Total dissolve solids (TDS)	190	809	827	3706
7	%TDS reduction	35.8	26.6	32.2	24.08
8	Chemical oxygen demand (COD)	69	703	126	1097
9	%COD reduction	94.48	85.44	92.34	83.34
10	Biochemical oxygen demand (BOD ₅)	26	367	60	563
11	%BOD ₅ reduction	96.26	89.77	93.92	85.73
12	Chloride as Cl	39	86	224	256
13	Sulphide as S ⁻	ND	ND	ND	ND
14	Sulphate as SO ₄	25	34	94	110
15	Total phosphate as PO ₄ (%)	0.26	0.82	0.25	0.40
16	Total nitrogen as NH ₃ -N (%)	1.40	1.82	1.36	1.60
17	Sodium as Na	85.5	168	146	284
18	Potassium as K	0.29	0.49	0.29	0.69
19	Sodium adsorption ratio (SAR)	3.95	4.76	4.16	5.03
20	Heavy Metals				
	- Zn	0.126	0.156	0.086	0.097
	- Pb	0.098	0.142	0.26	0.392
	- Cd	0.016	0.31	0.192	0.232
	- Ni	0.033	0.049	0.106	0.143
	- Co	0.015	0.041	0.028	0.042
	- Mn	0.712	0.091	1.02	1.32
	- Fe	2.1	3.21	2.35	6.55
	- Cr	0.022	0.036	0.112	0.136
	- Cu	ND	0.016	0.004	0.009

*Above readings are averages of ten sets

**All the parameters are expressed in mg/l except, pH, turbidity, conductivity and percentage reduction (r).

Table 6: Growth of *S. Bijugatus* at Different Dilutions of BDL Effluent

Treated effluent dilutions	Lag phase (days)	Exponential growth period day	Exponential growth rate (μ)	Doubling time in hours	Enhancement of standing crop on 7 th Day (%)
Control (Basal medium)	Nil	0 – 7	0.2486	96.54	-
10%	Nil	0 – 7	0.3186	75.32	40
20%	Nil	0 – 7	0.3386	70.88	55
40%	Nil	0 – 7	0.3557	43.09	68
60%	Nil	0 – 7	0.2957	81.16	26
80%	Nil	0 – 7	0.2857	84.00	20
100%	Nil	0 – 7	0.2771	86.61	15

Table 7: Growth of *S. Bijugatus* in Different Dilutions of BDH Effluent

Treated effluent dilutions	Lag phase (days)	Exponential growth period days	Exponential growth rate (μ)	Doubling time in hours	Enhancement of standing crop on 7 th day (%)
Control (Basal medium)	Nil	0 – 7	0.2057	116.7	-
10%	Nil	0 – 7	0.2529	94.9	26.3
20%	Nil	0 – 7	0.2814	85.3	45.3
40%	Nil	0 – 7	0.3271	73.4	81.1
60%	Nil	0 – 7	0.3314	72.4	84.2
80%	Nil	0 – 7	0.2971	80.8	55.8
100%	Nil	0 – 7	0.2914	82.4	51.6

Table 8: Growth of *S. Bijugatus* in Different Dilutions of BDL Effluent Fortified with 30% Basal Medium Nutrients

Treated effluent dilutions	Lag phase (hrs)	Exponential growth period	Exponential growth rate (μ)	Doubling time in hours	Enhancement of standing crop as on 7 th Day (%)
Control (Basal Medium)	48 hrs.	0 – 7	0.3643	65.9	-
10%	48 hrs.	0 – 7	0.3586	66.9	- 3.13
20%	48 hrs.	0 – 7	0.4071	59.0	23.2
40%	Nil	0 – 7	0.4429	54.2	46.4
60%	Nil	0 – 7	0.3871	62.0	11.6
80%	Nil	0 – 7	0.4257	56.4	34.8
100%	Nil	0 – 7	0.3529	68.0	-5.36

Table 9: Growth of *S. Bijugatus* in Different Dilutions of BDL Effluent Fortified with 100% Basal Medium Nutrients

Treated effluent dilutions	Lag phase (days)	Exponential growth period days	Exponential growth rate (μ)	Doubling time in hours	Enhancement of standing crop as on 7 th day (%)
Control (Basal medium)	Nil	0-7	0.3557	67.5	-
10%	Nil	0-7	0.3586	66.9	0.27%
20%	Nil	0-7	0.3743	64.1	1.70%
40%	Nil	0-7	0.38	63.2	2.30%
60%	Nil	0-7	0.42	57.1	6%
80%	Nil	0-7	0.4586	52.32	9.70%
100%	Nil	0-7	0.4714	50.9	10.90%

Table 10: Growth of *S. Bijugatus* in Different Dilutions of BDH Effluent Fortified with 30% Basal Medium Nutrients

Treated effluent dilutions	Lag phase (days)	Exponential growth period days	Exponential growth rate (μ)	Doubling time in hours	Enhancement of standing crop as on 7 th day (%)
Control (Basal medium)	Nil	0-7	0.3429	70	-
10%	Nil	0-7	0.42	57.1	45.50%
20%	Nil	0-7	0.4357	55.1	63.80%
40%	Nil	0-7	0.4514	53.2	69.40%
60%	Nil	0-7	0.49	49	105%
80%	Nil	0-7	0.4629	51.9	80.20%
100%	Nil	0-7	0.4443	54	64.50%

Table 11: Growth of *S. Bijugatus* in Different Dilutions of BDH Effluent Fortified with 100% Basal Medium Nutrients

Treated effluent dilutions	Lag phase	Exponential growth period days	Exponential growth rate (μ)	Doubling time in hours	Enhancement of Standing crops as on 7 th day (%)
Control (Basal medium)	Nil	0-6	0.3657	65.63	-
10%	Nil	0-6	0.3414	70.3	-2.27%
20%	Nil	0-6	0.3586	66.93	-0.67%
40%	Nil	0-6	0.3558	67.45	-0.93%
60%	Nil	0-6	0.39	61.54	2%
80%	Nil	0-6	0.4543	52.83	8.27%
100%	Nil	0-6	0.4614	52.02	8.93%

Table 12: Growth Potential of *S. Bijugatus* in Different Dilutions of HPL Effluent

Treated effluent dilutions	Lag phase (days)	Exponential growth period days	Exponential growth rate (μ)	Doubling time in hours	Enhancement of standing crop over control as on 7 th day (%)
Control (Basal medium)	Nil	0-7	0.3357	71.5	-
10%	Nil	0-7	0.3429	69.9	3.9
20%	Nil	0-7	0.38	63.2	24.5
40%	Nil	0-5	0.56	42.9	43.1
60%	Nil	0-5	0.57	42.1	52.9
80%	Nil	0-5	0.614	39.1	82.4
100%	Nil	0-5	0.604	39.7	61.8

Table 13: Growth Potential of *S. Bijugatus* in Different Dilutions of HPH Effluent

Treated effluent dilutions	Lag phase (days)	Exponential growth period days	Exponential growth rate (μ)	Doubling time in hours	Enhancement of standing crops as on 7 th day (%)
Control	Nil	0-7	0.2629	91.3	-
10%	Nil	0-4	0.47	51.1	0.9
20%	Nil	0-4	0.455	52.7	9.3
40%	Nil	0-5	0.42	57.1	23.4
60%	Nil	0-5	0.44	54.5	36.4
80%	Nil	0-5	0.502	47.8	62.6
100%	Nil	0-5	0.52	46.2	69.2

Table 14: Growth of *S. Bijugatus* in Different Dilutions of HPL Effluent Fortified with 30% Basal Medium Nutrients

Treated effluent dilutions	Lag phase (days)	Exponential growth period days	Exponential growth rate (μ)	Doubling time in hours	Enhancement of standing crops as on 7 th day (%)
Control (Basal medium)	Nil	0-7	0.4457	53.8	-
10%	Nil	0-7	0.4514	53.2	7.8
20%	Nil	0-7	0.4829	49.7	19.3
40%	Nil	0-7	0.7214	33.3	29.8
60%	Nil	0-7	0.75	30.1	35.8
80%	Nil	0-7	0.4429	54.2	- 1.4
100%	Nil	0-7	0.3443	69.7	- 39.0

Table 15: Growth of *S. Bijugatus* in Different Dilutions of HPL Effluent Fortified with 100% Basal Medium Nutrients

Treated effluent dilutions	Lag phase (days)	Exponential growth period days	Exponential growth rate (μ)	Doubling time in hours	Enhancement of standing crop as on 7 th day (%)
Control (Basal medium)	Nil	0 – 6	0.27	88.89	-
10%	Nil	0 – 6	0.3017	79.55	13.82
20%	Nil	0 – 6	0.4067	59.01	76.42
40%	Nil	0 – 6	0.465	51.61	125.20
60%	Nil	0 – 6	0.5333	45.00	200
80%	Nil	0 – 6	0.5283	45.43	192.68
100%	Nil	0 – 6	0.4417	54.34	104.07

Table 16: Growth of *S. Bijugatus* in Different Dilutions of HPH Effluent Fortified with 30% Basal Medium Nutrients

Treated effluent dilutions	Lag phase (days)	Exponential growth period days	Exponential growth rate (μ)	Doubling time in hours	Enhancement of standing crop as on 7 th day (%)
Control (basal medium)	Nil	0-7	0.3671	65.38	-
10%	Nil	0-7	0.5042	47.52	94.01
20%	Nil	0-7	0.5071	47.33	97.60
40%	Nil	0-7	0.52	46.15	109.58
60%	Nil	0-7	0.4743	50.60	68.26
80%	Nil	0-7	0.4657	51.54	61.68
100%	Nil	0-7	0.3857	62.22	9.58

Table 17: Growth of *S. Bijugatus* in Different Dilutions of HPH Effluent Fortified with 100% Basal Medium Nutrients

Treated effluent dilutions	Lag phase	Exponential growth period days	Exponential growth rate (μ)	Doubling time in hours	Enhancement of standing crop as on 7 th day (%)
Control (basal medium)	Nil	0 – 6	0.1617	148.4	-
10%	Nil	0 – 6	0.385	62.3	138.3
20%	Nil	0 – 6	0.4717	5.1	240.4
40%	Nil	0 – 6	0.5083	47.2	296.8
60%	Nil	0 – 6	0.5433	44.1	358.5
80%	Nil	0 – 6	0.4967	48.3	277.7
100%	Nil	0 – 6	0.3517	68.2	106.4

Determination of Caffeine In Beverages: A Review

Igelige Gerald¹, David Ebuka Arthur¹, Adebisi Adedayo².

¹Department of Chemistry, Ahmadu Bello University Zaria.

²Sheda Sci. and Tech. complex FCT, PMB 186 Garki Abuja

ABSTRACT :Caffeine is a well-known stimulant which is added as an ingredient to various carbonated soft drinks. Caffeine has drawn more attention due to its physiological effects beyond that of its stimulatory effect. Consumers are interested in knowing the exact amounts of caffeine existing in beverages. However, limited data exist, especially for store brand beverages. Therefore, it is pertinent to review the various methods that will effectively determine the caffeine contents in different carbonated drinks. HPLC, UV-Visible Spectrometry and Gas Chromatography are among the popular used methods.

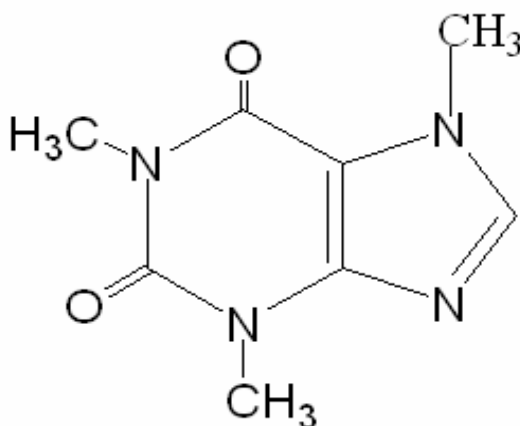
KEYWORDS;Carbonated-drinks, Analysis, Extraction, Additive, Determination, Caffeine.

I. INTRODUCTION

Caffeine is a naturally occurring alkaloid which is found in the leaves, seeds and fruits of over 63 plants species worldwide (Abdul Muminet *al.*, 2006; NourVioletaet *al.*,2008; Wanyikaet *al.*, 2010; VioletaNouret *al.*, 2010) It is an alkaloid of methylxanthine family (Wanyikaet *al.*,2010; Marcia *et al.*, 2002). The methylxanthines caffeine (1,3,7-trimethylxanthine), theobromine (3,7- dimethylxanthine), and theophylline (1,3-dimethylxanthine) can be normally found in cola nuts, coffee beans, cocoa beans, tea leaves, mate leaves and other kinds of plants (Paradkar and Irudayaraj, 2002). While coffee and tea beverages naturally contain caffeine and other methylxanthines, caffeine serves as an ingredient in many carbonated soft drinks including colas, pepper-type beverages, and citrus beverages. Pure caffeine occurs as odorless, white, fleecy masses, glistening needles of powder. Its molecular weight is 194.19g, melting point is 236°C, point at which caffeine sublimates is 178°C at atmospheric pressure, pH is 6.9 (1% solution), specific gravity is 1.2, volatility is 0.5%, vapor pressure is 760mmHg at 178°C, solubility in water is 2.17%, vapor density 6.7 (Komeset *al.*, 2009; NourVioletaet *al.*, 2008; Hiroshi Ashiharaet *al.*, 1996; Abdul Muminet *al.*, 2006).Caffeine has drawn more attention in the past decades due to its physiological effects beyond that of its stimulatory effect. The Food and Drug Administration (FDA) defines caffeine as a generally recognized as safe (GRAS) substance. However, FDA specifies that the maximum amount in carbonated beverages is limited to 0.02% (FDA 2006). Therefore, the highest legal amount of caffeine allowed in a 355 mL (12oz) can of soft drink is about 71mg. Caffeine has attracted the interest of consumers and health professionals alike due to its wide consumption in the diet by a large percentage of the population and its pharmacological effects in humans (Mandel 2002). The human's saliva caffeine level, which demonstrates the extent of absorption, peaks around 40 minutes after caffeine consumption (Liguori *et al* 1997). Its physiological effects on many body systems have been reported by researchers, including the central nervous, cardiovascular, gastrointestinal, respiratory, and renal systems (Nehlig *et al* 1992). The International Olympic Committee (IOC) defined caffeine as a drug and abuse is indicated when athletes have urine caffeine concentrations higher than 12µg/mL (de Aragaoet *al* 2005).

II. CAFFEINE CHEMISTRY AND GENERAL INFORMATION

Caffeine (1,3,7-trimethylxanthine), theophylline (3,7- dimethylxanthine), and theobromine (1,3-dimethylxanthine) are in the family of alkaloid methylxanthines.



Caffeine (1, 3, 7-trimethylxanthine)

Caffeine is an odorless, white solid that has the form of needles or powder. Caffeine has a bitter taste. The molar mass of caffeine is 194.19 g/mol. Caffeine is slightly soluble in water due to its moderate polarity. Caffeine is a natural central nervous system stimulant, having the effects of reducing drowsiness and recovering alertness. Since it is widely consumed by humans, caffeine is considered the most frequently used psychoactive substance in the world (Ligouriet *al* 1997).

Physiological effects of caffeine to human

Caffeine has numerous physiological effects on major organ systems, including the nervous system, cardiovascular system, digestive system, and respiratory system. Renal function and skeletal muscles are also affected by caffeine. Numerous studies have proven caffeine to be a stimulant to human's central nervous system (Spiller, 1998). It also increases heart rate, dilates blood vessels and elevates levels of free fatty acids and glucose in plasma. 1 g of caffeine leads to insomnia, nervousness, nausea, ear ringing, flashing of light derillum and tremulousness. In cases of overdosing and in combination with alcohol, narcotics and some other drugs, these compounds produce a toxic effect, sometimes with lethal outcome (Mamina and Pershin, 2002; Ben Yuhas, 2002; Wanyikaet *al.*, 2010; James *et al.*, 1990; Tavallali and Sheikhaei, 2009). Caffeine facilitates the conduction velocity in the heart and directly affects the contractility of the heart and blood vessels. Nevertheless, caffeine may significantly reduce cerebral blood flow by constricting of cerebral blood vessels. Caffeine provides a diuretic effect due to elevating the blood flow and glomerular filtration rate of the kidneys. Heartburn is an issue for some subjects' gastrointestinal system after consuming caffeine. The effects of caffeine to skeletal muscles are mainly the increasing occurrence of tremors (James 1991; Spiller 1998).

Relevant Literatures

Many methods exist for determining the methylxanthine contents of food and beverages. Some of these methods include UV-Visible spectrophotometry, potentiometry, high performance liquid chromatography (HPLC), ion chromatography, high performance thin layer chromatography (HPTLC), capillary electrophoresis, micellar capillary electrophoresis, gas chromatography, and solid-phase microextraction gas chromatography (Armenta *et al.*, 2005). Of the above methods, HPLC has become one of the most commonly used analytical methods. One study demonstrated using an HPLC method with an octadecylsilyl (ODS) column and a water-acetonitrile-phosphoric acid mobile phase to analyze eight catechins and caffeine. Within 20 min, the catechins (epicatechin, epigallocatechin, epicatechingallate, epigallocatechingallate, catechin, catechingallate, galocatechin and galocatechingallate) and caffeine were separated by an acetonitrile gradient. Two different types of Japanese green teas, Matcha and Sencha, both high and low grades for each tea, had their catechins and caffeine contents determined. The researchers found the caffeine contents were higher in Matcha tea than in Sencha tea (Gotoet *al.*, 1996). Wang *et al.*, (2000) applied an isocratic elution system to determine the contents of catechins, caffeine, and gallic acid in green and black tea. The separation system included a C18 reverse-phase column, a mobile phase of methanol/water/orthophosphoric acid (20/79.9/0.1), and an UV detector. The flow rate was set at 1.0 mL/min. The wavelength of detection was 210 nm. The validation of this method was confirmed by all analytes exhibiting good linearity within the range tested and correlation coefficients ranging from 0.988 to 1.000. The amounts of caffeine in Gunpower, roasted green tea (RGT), Sencha, Keemun, and Sri Lanka were found to be 23.9, 30.3, 28.9, 38.2, and 22.9 mg/100 mL, respectively (Wang *et al.*, 2000).

Mashkouriet *al.*, (2003) quantitated the caffeine existing in black tea leaves by Fourier transform infrared (FTIR) spectrometry. The caffeine of tea samples was extracted using CHCl_3 after wetting with an aqueous NH_3 solution. The spectrometric data were collected over the wave number range of $1800\text{-}1300\text{ cm}^{-1}$. This method had a detection limit of $35\mu\text{g/mL}$, a sampling frequency of 6 h^{-1} , and a coefficient of variation of 0.8%. A black tea sample contained 3.68% w/w caffeine. The authors obtained similar results for the caffeine content from FTIR ($3.68 \pm 0.03\%$ w/w) and a reference HPLC technique ($3.60 \pm 0.07\%$ w/w). The advantages of the FTIR method for determining caffeine in tea leaves includes its quickness, precision, and accuracy, enabling it to be a possible alternative to the HPLC method (Mashkouriet *al.*, 2003). However, one potential shortcoming of this method is the fairly high detection limit.

Nishitani and Sagesaka (2004) developed an improved HPLC analytical method for simultaneously determining caffeine and the eight catechins as well as other phenolic compounds in tea. The proposed method provided additional ability to analyze phenolic compounds when compared with former HPLC methods. This procedure was based on an improved reverse-phase ODS column operated at 4°C , a binary gradient elution system of water-methanol-ethylacetate-phosphoric acid, and a photodiode array detector. The quantitative measurement of eight catechins and caffeine confirmed the validity of this proposed method. The detection limits of these analytes ranged from 1.4-3.5 ng per injection volume. The recovery rates of the analyses were in the range of 96-103%. The caffeine contents of Sencha, Matcha, Gunpowder, Tie Kuan yin, and Darjeeling determined in this study were 2.94 ± 0.007 , 3.62 ± 0.005 , 2.61 ± 0.059 , 2.51 ± 0.019 , and $3.24\pm 0.016\%$ (dry weight), respectively (Nishitani and Sagesaka 2004). Caudle *et al.*, (2001) tried to improve the Association of Official Analytical Chemists (AOAC) official analytical method for analyzing methylxanthines in cocoa-based food products. Theobromine and caffeine contents could be obtained by 12 reverse-phase HPLC. The AOAC method's degree of accuracy and precision was not reliable, especially for caffeine. In this study, the AOAC analytical method only showed recoveries of theobromine and caffeine to be 89.3 and 74.5%, respectively. The authors successfully changed from an organic extraction to an aqueous extraction and analyzed the samples via reverse-phase HPLC to improve the recoveries of theobromine samples via reverse-phase HPLC to improve the recoveries of theobromine and caffeine to 99.6 and 103.4%, respectively (Caudle *et al.*, 2001).

Zuoet *al.*, (2002) analyzed various substances in several green, Oolong, black and pu-erh teas by HPLC. They used a methanol-acetate-water buffer gradient elution system and a C-18 column; detection utilized a photodiode array detector. After multiple extractions with aqueous methanol and acidic methanol solutions, four major catechins, gallic acid and caffeine could be simultaneously determined within 20 min. This improved the previous studies' problem of catechins and caffeine remaining in tea residues after a single extraction. The results demonstrated that green teas contain higher amounts of catechins than Oolong, pu-erh, and black teas due to their fermentation processes reducing the levels of catechins significantly. An interesting finding was a lower caffeine content in Oolong teas, especially in Fujian Oolong tea (Zuoet *al.*, 2002).

Horieet *al.*, (1997) adapted capillary zone electrophoresis (CZE) in order to simultaneously determine the major compounds in green tea. Separation occurred in a fused-silica capillary column. The borax buffer was set at pH 8.0, and UV detection was at 200 nm. The major compounds in green tea were epicatechin, epigallocatechin, epicatechingallate, epigallocatechingallate, catechin, caffeine, theanine, and ascorbic acid. The authors found the concentration of each compound was significantly different among each tea sample. One interesting finding was relatively lower caffeine contents in canned tea drinks. The authors concluded CZE is more appropriate for analyzing the properties and contents of green tea than HPLC due to its shorter analysis time and ability to separate more compounds (Horieet *al.*, 1997). Schulz *et al.*, (1999) investigated the accuracy of rapidly predicting the amounts of polyphenol and alkaloid compounds in the leaves of green tea by a near-infrared reflectance spectroscopic (NIRS) method. The pretreatment of the NIR spectra with weighted multiple scatter correction effectively eliminated interferences of scatter and improved the final calibration results. The results were compared with those from analysis by HPLC. The potential of this NIRS method is demonstrated by the high correlation between its prediction and HPLC values for caffeine and major catechins. The authors claimed that the NIRS method may be an alternative technique to HPLC due to its high degree of accuracy for prediction and analysis time of less than 1 min per measurement (Schulz *et al.*, 1999). Farah *et al.*, (2006) investigated the relationship between the Arabica coffee cup quality and the contents of sucrose, caffeine, trigonelline, and chlorogenic acids. The researchers applied reverse-phase HPLC analysis to determine each compound. Sucrose was analyzed by using 80% acetonitrile and 20% water as the mobile phase and a refractive index detector. For analyzing caffeine, the UV detector was set at 272 nm. The mobile phase was composed of

60% water and 40% methanol. The results demonstrated that the caffeine content was the highest in the highest quality sample and the lowest content was found in the poorest quality sample. However, trigonelline and 3,4-dicaffeoylquinic acid gave a better indication of high quality coffee (Farah *et al.*, 2006). Huck *et al.*, (2005) compared the contents of caffeine, theobromine, and theophylline in 83 liquid coffee extracts determined by a NIRS method and HPLC coupled to mass spectrometry method. In the NIRS method, the spectra were recorded over a wave number range of 4008 to 9996 cm^{-1} with a resolution of 12 cm^{-1} in the reflectance mode. The authors obtained high robustness and reproducibility of the NIRS model for quantification of caffeine and theobromine. The lower limit of detection made it difficult for theophylline to fit the NIRS model and correctly be determined. Nevertheless, NIRS provides the coffee industry with an alternative method to quickly determine caffeine and theobromine (Huck *et al.*, 2005).

Chen and Wang (2001) analyzed the level of artificial sweeteners (sodium saccharin, aspartame, acesulfame-K), preservatives (benzoic acid, sorbic acid), caffeine, theobromine, and theophylline in carbonated cola drinks, fruit juice drink, fermented milk drink, preserved fruit, and one pharmaceutical preparation by an ion exchange chromatography method. Analytes were separated using an anion-exchange analytical column maintained at 40°C and detected by wavelength-switching ultraviolet absorption. The detection limits ranged from 4-30 ng/mL for all analytes. The average recoveries for samples ranged from 85 to 104%. In addition, the data obtained from this method were in good agreement with those determined by reference HPLC procedures. Two carbonated cola drinks were found to contain around 36 mg caffeine/12 oz (Chen and Wang 2001). Chen *et al.* (2006) investigated the feasibility of using near infrared (NIR) spectroscopy as a fast method which is non-destructive and less time consuming than other frequently used analytical methods for estimating the content of caffeine and total polyphenols in green tea. The calibration was performed by a partial least squares (PLS) algorithm. The result indicated that correlation coefficients of the prediction models were approximately 0.97 for the caffeine and 0.93 for total polyphenols. This method's potential to rapidly determine the caffeine and polyphenols of tea to control industrial processes has been proven by this study (Chen *et al.*, 2006).

Yao *et al.* (2006) examined 20 leaf tea and 36 teabag samples obtained from Australian supermarkets. Each sample was prepared as a diluted tea solution, which was treated with lead acetate and hydrochloric acid solutions. After filtering and treating with a sulfuric acid solution, the measurement of caffeine was completed by using a UV/Visible spectrophotometer at 570 nm. The results showed that caffeine contents of black leaf tea and teabags were 3.89 and 3.87%, respectively. Similar results were found in the green leaf tea and teabags, 3.71 and 3.83%, respectively. These contents are generally higher than that claimed by the manufacturers (i.e., < 3%). This study revealed a need to establish quality control for both imported and Australian-made teas (Yao *et al.*, 2006). Brunetto *et al.* (2007) developed a reversed-phase HPLC method with an on-line sample cleanup to determine theobromine, theophylline, and caffeine in cocoa samples. The cocoa samples were prepared by an on-line solid-phase extraction of analytes and loaded into a home-made dry-packed precolumn with ODS-C18 in a column-switching system. The mobile phase consisted of 20% of methanol in water, under isocratic conditions, at a flow-rate of 1.4 mL/min. Chromatographic separation was performed on a NOVA-PAK C18 column (150 mm x 3.9 mm, 4 μm). The procedure demonstrated a recovery of over 95% with coefficients of variation less than 3.2%. The precolumn proved its long average life span by showing no signs of deterioration after approximately 1000 injections of sample cocoa extracts (Brunetto *et al.*, 2007).

Pura (2001) modified a HPLC method for determining caffeine and theobromine contents in aqueous cocoa extracts. Instead of directly injecting the extracts on the column, the improved method can successfully remove the interfering cocoa pigments by passing them through a Sep-pak C18 cartridge which was also used to separate the theobromine and caffeine. This method enhanced the efficiency of the column and prolonged its life. After this treatment, the recoveries of caffeine and theobromine were 98.0-100.1 and 97.8-100%, respectively. The modified method displayed good resolution and sharp peaks on chromatograms that favored correct determination of theobromine and caffeine (Pura, 2001). Thomas *et al.* (2004) measured the contents of caffeine, theobromine, and theophylline in a food-matrix standard reference material (SRM) 2384, Baking Chocolate by a reverse-phase HPLC method. The stationary phase was composed of an inactive silica support to which C-18 was bonded. The mobile phase consisted of 10% acetonitrile/90% water (pH acidified to 2.5 with acetic acid). The flow rate was at 1.5 mL/min and UV detection was at 274 nm. The results of each sample could be obtained within 15 min. The results showed the reproducibility for caffeine, theobromine, and theophylline determinations was 5.1, 2.3, and 1.9%, respectively. This method had a limit of determination for all analytes at levels less than 100 ng/mL or 0.1 $\mu\text{g/mL}$. The measurements of caffeine, theobromine, and theophylline of SRM 2384

Baking Chocolate were comparable with those from National Institute of Standard and Technology (Thomas *et al.*, 2004). Abourashed and Mossa (2004) applied HPTLC densitometric analysis to determine the level of caffeine in several herbal products and energy drinks. The HPTLC plates were made of pre-coated silica gel. The solvent system contained 85% ethyl acetate and 15% methanol. The wavelength for detecting caffeine was set at 275 nm. The proposed method had a mean recovery of $98.9 \pm 3.5\%$ with a coefficient of variation less than 5%. The caffeine ranges of herbal products and energy drinks in this study were found at 4.76-13.29% (w/w) and 0.011-0.032% (w/w), respectively. The HPTLC method demonstrated effective determination of caffeine for stimulant herbal products and carbonated energy drinks (Abourashed and Mossa 2004). Armenta *et al.* (2005) applied a solid-phase Fourier transform-Raman (SP-FT-Raman) spectrometry-based method to determine caffeine contents in commercial energy drinks. The caffeine content of each sample was obtained from setting Raman intensity between 573 and 542 cm^{-1} with a two points corrected baseline between 580 and 540 cm^{-1} . The limit of detection of SP-FT-Raman method was 18 $\mu\text{g/mL}$. The combination of FT-Raman and solid-phase increased the sensitivity of detecting caffeine by a factor of 31 times when compared with using direct Raman measurement alone. The results of caffeine contents obtained from SP-FT-Raman method and liquid chromatography (LC) found no significant differences between the two methods. The SP-FT-Raman method displayed higher sampling frequency than the LC method. However, the LC method had a lower detection limit (0.05 $\mu\text{g/mL}$). The reduced reagent consumption and waste generation are also benefits of this method as compared to the LC method (Armenta *et al.*, 2005).

Lucena *et al.* (2005) manipulated a continuous flow auto analyzer for sequential determination of total sugars, class IV caramel and caffeine contents in 20 different soft drink samples. This apparatus consisted of on-line coupling of a continuous solid-phase extraction unit and two detectors which were UV-visible and evaporative light scattering (ELSD) detectors. The caffeine has the property of being retained on the sorbent column and other compounds can be preferentially determined due to their low affinity to the sorbent column. The caffeine can be detected later by the ELSD after it has been eluted with acetonitrile and the signal registered in the ELSD. In order to evaluate the performance of this analyzer, the authors carried out a recovery test. The results ranged from 90 to 102%. Unspecified colas were found to contain caffeine ranging from 14.9 mg/12 oz to 49.7 mg/12 oz (Lucena *et al.*, 2005). Walker *et al.* (1997) utilized capillary electrophoresis (CE) to simultaneously analyze the aspartame, benzoic acid, and caffeine contents of carbonated beverages in 2 min with 20 mM glycine buffer at pH 9.0 and detection at 215 nm. Good reproducibility for both peak area and migration times were observed (2.0-3.8% and 0.13-0.37%, respectively). The spiked recovery of the analytes ranged from 98 to 114%. The results of soft drinks samples in this study were comparable with those data evaluated by HPLC, but slightly higher in some cases using CE. The main advantages of CE over HPLC are relatively simpler operation, lower cost, no organic mobile solvents, and a shorter analysis time (Walker *et al.*, 1997).

Types of drinks : Non-alcoholic soft drink beverage can be divided into fruit drinks and soft drinks. Soft drinks can be divided into carbonated and non-carbonated drinks. Examples of carbonated drinks are Cola, lemon and oranges and non-carbonated drinks include mango drinks. Soft drinks can also be divided into cola products and non-cola products. Cola products like Pepsi, Coca-Cola, Thumps Up, and Diet Coke, Diet Pepsi etc. account for nearly 61-62% of the total soft drinks market. Non-Cola products constitute 36%, and based on the types of flavors available can be divided into Orange, Cloudy Lime, Clear Lime and Mango (India Infoline Sector Report, 2002). Below are highlight of some work which employed the various methods in analyzing the level of caffeine from different beverages. In this review, I will attempt to go in details into some of the experiments carried out in determining caffeine content and also publishing of some of their results as shown below;

The quantitative determination of caffeine in beverages and soft drinks using UV wavelength spectroscopy

JENWAY, producers of instrumentations for Chemistry related practical, sampled five beverages and soft drink. Samples were chosen they include instant coffee (Nescafe), brewed tea (PG Pyramid Tea Bags), Coca Cola, Pepsi Cola and Red Bull. The analysis is performed on a Jenway 7305 spectrophotometer controlled using the free-of charge PC software, supplied with each model in the 73 series. The software allows the user to emulate all measurement tasks normally performed on the instrument with the additional benefit of allowing data to be seamlessly transferred to external Microsoft office applications. The Reagents used are Caffeine, Dichloromethane and Purified water

Standard Preparation: A 1000 ppm stock standard of caffeine was prepared by dissolving 198.2mg of caffeine in 200.0ml purified water. Working standards were prepared by pipetting 25, 12.5, 10, 7.5, 5 and 2.5ml aliquots of the stock standard solution into separate 50.0ml volumetric flasks and diluting to volume with purified water.

Sample Preparation: 200ml aliquots of boiling purified water was added to each of two 250ml beakers containing 2g of instant coffee and a single PG pyramid tea bag (3.2g of dried tea leaves) respectively. The coffee and tea preparations were stirred for 30 seconds using a magnetic stirrer (500rpm) and allowed to cool to room temperature.

Caffeine Extraction Procedure: A 50ml aliquot was taken from each working standard or sample solution. This aliquot was placed into a separating funnel and 25ml of dichloromethane was added. The caffeine was extracted by inverting the funnel at least three times, venting the funnel after each inversion. The dichloromethane layer was removed to a clean flask and the extraction procedure was repeated twice more and the solvent layers combined.

Sample Measurement: Aliquots of the extracted standards were placed into quartz cuvettes (part code 035 028) and analysed using a 7305 spectrophotometer. The Photometrics mode was accessed by selecting the Photometrics icon from the main menu screen in the PC software and measurements were performed according to the procedure described in the instrument and PC software operating manuals. Microsoft Excel was used to tabulate the measurement data and perform a linear regression analysis. This allowed a concentration factor to be calculated which was then input into the settings in the Concentration mode of the 7305 PC software. The concentration mode was then used to quantify the caffeine concentration of the sample solutions with measurements performed against a dichloromethane blank.

III. RESULT

The absorbance values of the six working standard solutions were measured; A linear regression of absorbance versus standard concentration, forced through the origin, gave equation 1.
 $y = 0.0181x \dots \dots \dots [1]$

A linear regression of concentration vs absorbance allowed the factor of 55.358, included in equation 2, to be determined.

Equation 2 was then used to calculate the concentration of caffeine in the extracted sample solution, from the solutions measured absorbance value.

$\text{Conc (ppm)} = 55.358 \times \text{Abs} \dots \dots \dots [2]$

The final caffeine content of the beverage under test is then calculated from the extracted sample solution's concentration using equation 3. Dividing this value by the volume of the drink gives the caffeine content per ml.

$$\text{Caffeine content mg} = \text{Conc (ppm)} \times \frac{(\text{Total Sample Vol [ml]})^2}{(\text{Measured Sample Vol [ml]})} \times 1000 \dots \dots \dots [3]$$

Of the five samples tested the sample of Red Bull had the highest total volume per ml content of caffeine. When ranking the drinks in terms of caffeine content per serving the order was Red Bull \Rightarrow Pepsi Cola \Rightarrow Instant Coffee \Rightarrow Coca Cola \Rightarrow PG Tea. Instant coffee and PG Tea rise from third and fifth places to second and third respectively when the drinks are ranked in order of the caffeine content per ml.

IV. CONCLUSIONS

When the results obtained in this application note are compared to data published in previous reports, or by the drinks manufacturer, it can be seen that the results obtained using the 7305 spectrophotometer are broadly in line with expectations with the exception of the two cola drink samples. The higher than expected values obtained for the cola drink samples may be the result of additional compounds, that absorb light at the wavelength used in this application note, being extracted into the dichloromethane sample solution. The resulting solution would give a higher than expected absorbance reading and calculated caffeine content. Alternative extraction procedures could be investigated to see if the interfering compounds could be excluded from the extraction solution. Also using UV spectrophotometric procedures Ahmad H, *et al* 2005 determined the content levels of some food additives in 29 different beverage samples commercially available in Riyadh local markets. These analytical measurements were undertaken primarily to assess the compliance of content levels of the investigated food additives and their daily intake doses with the permissible levels. They observed that the results obtained from this study indicated that the average quantity level of caffeine in the analyzed beverages is 18.99 ppm.

In addition, the concentrations of these food additives have been converted into the daily intake doses based on beverages consumption. It was estimated that the mean daily intakes of aspartame, caffeine and

sodium benzoate by the adult population of Riyadh city through the consumption of the analyzed beverages were 92.5 mg, 6.3 mg and 6.46 mg, respectively. None of the analyzed beverage samples was found to violate the current legal limits practiced in the Saudi food regulations. In order to establish the spectrophotometric determination of caffeine, they studied the wavelength within the interval 220–320 nm using a 3.88 ppm caffeine standard solution. The obtained results gave an absorption spectrum, which was characterized by a single intensive absorption band located in the UV range at $\lambda_{\text{max}} = 276\text{nm}$.

It was observed that as the concentration of caffeine was varied over the range from 2.5×10^{-6} to $3.6 \times 10^{-4} \text{mol l}^{-1}$ (0.5-70 ppm), it was accompanied by a proportional enhancement in the monitored absorption intensity over such wide concentration range.

The calibration equation was calculated by least-squares method from nine measurements and it has the form:

$$A = -0.032 + 1.01 \times 10^4 C \text{ (mol l}^{-1}\text{)} \quad r = 0.999, n = 9$$

In addition, the analytical utility of the employed quantitative method was also investigated in similar manner to that previously discussed for the spectrometric analysis of aspartame artificial sweetener. The recovery of the used procedure, which reflects the accuracy of the analytical method, was evaluated by analyzing caffeine-free drink sample spiked with 9.7 ppm caffeine. The mean recovery of five measurements obtained by standard addition approach was found to be 97.66% with standard deviation of $\pm 0.3\%$. The mean of the obtained results was found to be not significantly different from the value of added caffeine concentration, since the calculated t-test value (2.6) was less than the tabulated t-test value (4.6) at 99% confidence level. The analytical precision of the spectrophotometric method was assessed from the reproducibility of 10 determinations of 10 ppm caffeine solution and a relative standard deviation of 0.1 RSD% was calculated.

Practical determination of the studied food additive in commercial drink samples : Different kinds of beverages brands, including regular and diet cola, carbonated refreshment drinks, beverages with added fruit juices, energy drinks and preservatives free canned fruit juices were purchased from different local supermarkets and 29 samples were analyzed in quintuplicate ($n = 5$) using the indicated spectrophotometric method. Once sample bottles were open, the drinks were degassed, homogenized and filtered. In all cases, five aliquots of each drink sample were placed in the spectrophotometric cell after adequate dilution. In order to reduce the interference effect particularly that expected with fruit juices, all analytical determinations were carried out by the standard addition approach.

They discovered that the concentrations of caffeine food additive (flavor enhancer) in what so called energy drinks collected from local supermarkets are noticeably higher than their counterpart concentration levels in the refreshment soft drinks. The calculated analytical results in Table 3 and Table 4 demonstrate the caffeine content levels in energy drinks and carbonated soft drinks, respectively. The caffeine contents in energy drink samples ranged from 22.64 ppm to 34.96 ppm. The minimum caffeine content level was observed in Drink 4 sample, while Drink 2 sample showed the highest caffeine content. The mean of caffeine quantity in the analyzed energy drinks was found to be in the level of 28.23 ppm. However, the analyzed carbonated soft drink samples contained much lower caffeine contents since its mean concentration level of 9.76 ppm is virtually one third the average caffeine content observed in energy drinks. The analyzed samples in the carbonated soft drink group showed caffeine content in the range of 2.8 - 12.76 ppm.

Table 1. Caffeine content levels in the carbonated soft drink

Soft drinks	Caffeine content (ppm)	Daily intakes (mg)
Regular Cola	18.58 ± 0.04	3.25
Regular Cola 2	11.89 ± 0.07	4.5
Regular Cola 3	8.84 ± 0.02	3.38
Regular Cola 4	2.84 ± 0.02	1.07
Diet Cola 1	12.76 ± 0.03	4.79
Diet Cola 2	11.77 ± 0.08	4.41
Lemon Cola 11	62 ± 0.07	4.38

All over the world, the caffeine contents in soft drinks varies according to the type of the brand, yet its average content in soft drinks is approximately 18 mg per six ounce (i.e. 100 ppm) (Barone and Roberts, 1984.). In fact, the US Food and Drug administration (FDA) limits the maximum caffeine amount in carbonated beverages to 6 mg/oz (72 mg/355 ml). Therefore, caffeine content level allowed in soft drinks is up to 200 ppm.

Clearly, the caffeine mean content level in the analyzed beverage samples manufactured and marketed in Riyadh city, is well below the above food industry guidelines.

Quantitative Determination of Caffeine and Alcohol in Energy Drinks and the Potential to Produce Positive Transdermal Alcohol Concentrations in Human Subjects

According to the Journal of Analytical Toxicology, Vol. 33, January/February 2009 Quantitative analysis of caffeine was performed by gas chromatography–mass spectrometry (GC–MS) using an Agilent 5975 MSD based upon a previously published procedure by “S. Kerrigan and T. Lindsey. Fatal caffeine overdose: two case reports. *Forensic Sci. Int.* **153(1)**: 67–69 (2005)”. Briefly, energy drinks were diluted 1:100 with 100mM pH 6.0 phosphate buffer prior to analysis. Energy drinks, calibrators and controls (1 mL) were fortified with 50 μ L 0.1 mg/mL caffeine-d10 in methanol. Because of the large dilution of energy drinks (1:100), calibrators and controls were prepared directly in phosphate buffer. A methanolic working standard was used to prepare caffeine calibrators in the range 1–10 mg/L (0.001–0.010 mg/mL). Samples were transferred to SPE columns and drawn through the column under vacuum. Columns were then successively rinsed using 1 mL deionized water, 1 mL acetic acid (1 M) and dried under full vacuum for 5 min. Ethyl acetate (1 mL) was added to the column and the eluate collected. Columns were rinsed once again using methanol (1 mL). A second eluent consisting of ethyl acetate with 2% concentrated ammonium hydroxide (1 mL) was added and the eluate collected. The two fractions were combined, evaporated to dryness under nitrogen at room temperature, and reconstituted in 25 μ L of ethyl acetate.

Samples were analyzed by GC–MS using an Agilent 6890 GC with a 5975 MSD. The injector and interface were set at 250 and 280°C, respectively. Separation of components in each 2- μ L injection was achieved using a 30-m DB-5 capillary column. Injections were made in split mode with a 10:1 split ratio. Following an initial oven temperature of 160°C and hold time of 0.5 min, the temperature was increased at 30°C/min to 290°C. The final hold time was 7.17 min, and the total run time was 12 min. Helium was used as the carrier gas at a flow rate of 1.3 mL/min. Caffeine (*m/z* **204**, 115, 70) was used as the internal standard for the quantitative determination of caffeine (*m/z* **194**, 109, 67). Acquisition was in selected ion monitoring mode, and quantitation ions are shown in bold. The limit of quantitation (LOQ), defined as the concentration of caffeine that produced a signal-to-noise ratio of at least 10:1 with a calculated concentration within 20% of the expected value, was < 1 mg/L. The linear range of the assay was 1–25 mg/L, accuracy was 102%, and intra-assay CV was < 3% (*n* = 2) at 1 mg/L.

Linear regression analysis of calibrators in the range 0–10 mg/L yielded an *R*² value of 1.000 and the control sample fortified with 1.0 mg/L caffeine produced a calculated concentration of 1.02 mg/L (102%). Quantitative caffeine determinations in diluted samples yielded concentrations ranging from 2.74 to 5.31 mg/L. These correspond with caffeine doses of 65–126 mg per 8-oz serving. In another study where caffeine content of energy drinks was quantitatively determined, doses of 33–77 mg were reported per 8-oz serving (16). Although caffeine content in the beverages tested in this study were considerably higher (65–126 mg) for equivalent serving sizes, results for the one energy drink (Red Bull) that was included in both studies were in excellent agreement: 67 mg and 69 mg, respectively. Caffeine (1,3,7-trimethylxanthine, guaranine) is a plant-derived alkaloid and psycho stimulant that is present in tea leaves, coffee, cocoa beans, and kola nuts. Individuals may be exposed to caffeine via beverages, food, over-the-counter drugs, prescription drugs, dietary supplements, and cosmetic treatments. An average cup of coffee is reported to contain 100 mg caffeine, although much higher doses have been reported, particularly among specialty coffees (17). Caffeine is also available in numerous dietary supplements, over-the-counter drugs, and in prescription drug mixtures at doses ranging from 32 to 200 mg (18). A dose of 50–200 mg is generally consistent with mild stimulation.

Ken-Hong, (2005) analyzed the caffeine content of 56 types of national and 75 types of store brand carbonated beverages. The caffeine determination was accomplished by utilizing high performance liquid chromatography (HPLC) equipped with a UV/Visible detector. The mobile phase consisted of 20%:80% (v/v) acetonitrile and deionized water. The chromatographic separation occurred on two C-18 columns. Each beverage sample was diluted 3-fold with deionized water. Duplicate analyses of multiple lots were performed on all beverage samples.

Chemicals and reagents

Anhydrous caffeine used for preparation of the standard solutions was purchased from Sigma (St. Louis, MO, USA). The acetonitrile for the mobile phase was HPLC grade (Fisher Scientific, Pittsburgh, PA,

USA). Deionized water was obtained from a water purification system. Sodium phosphate monobasic and HPLC- grade 85% phosphoric acid was obtained from Fisher Scientific (Pittsburgh, PA, USA).

Preparation of standard solution

Caffeine (about 25 mg) was weighed with an electric balance and transferred into a 250 mL volumetric flask. Deionized water was added to get a 250 mL bulk standard solution. Sonication was applied to completely dissolve the caffeine. One vial was filled and labeled with the bulk standard. The 2nd, 3rd, and 4th vials were obtained through consecutive 2-fold dilution with deionized water by pipetting (Precision Pipette, Atlanta, GA, USA). A second bulk solution was prepared using about 15 mg caffeine/250 mL water. The second bulk was diluted in the same manner as described above. The eight standard solutions were stored at 4°C in the refrigerator. These eight standard solutions were analyzed during each day's analysis to prepare the appropriate standard curve.

Preparation of mobile phase

Volumetric flasks were used to measure 250 mL of acetonitrile and 1000 mL of deionized water to achieve 20 % acetonitrile concentration (v/v). Sodium phosphate monobasic (1 g) was dissolved into the solution. The purpose of adding sodium phosphate monobasic was to increase the mobile phase's resistance to pH change. Phosphoric acid was added to acidify the solution to pH 3. The solution was vacuum filtered through a 0.45µm nylon filter. The solution was poured into a storage bottle and degassed by sonication.

Samples and sample preparation

The national-brand prepackaged (e.g., cans, bottles) carbonated beverages were collected across the southeastern United States. The samples were stored at room temperature until analysis. The store-brand beverages were acquired from Bruno's, Food Lion, Dollar General, IGA, Winn-Dixie, Kroger, Ingle's, Piggy Wiggly, Publix, Save-a-lot, 7-Eleven, Rite-Aid, Walgreens, Supervalu, and Wal-Mart. The cola, citrus, and pepper-type carbonated beverages as well as their diet varieties were analyzed in the present study. Average caffeine contents of each carbonated beverage were determined from a minimum of two different lots. The beverages analyzed in this study were purchased from June 2005 to July 2006. Each beverage (50 mL) was poured into an Erlenmeyer flask and degassed in a sonicator. Each sample was diluted 3-fold with deionized water (1 mL sample + 2 mL water). Duplicate dilutions were performed on all samples. An aliquot of these diluted samples was injected into the HPLC system to quantitate the caffeine concentration.

Apparatus

The caffeine content was determined by isocratic reverse-phase high performance liquid chromatography (HPLC) equipped with a UV/Visible detector adapted from that used by Grand and Bell (1997). The injector with a 20 µL loop introduced a known sample volume into the system. The chromatographic separation occurred on a Prodigy 150-mm x 4.6-mm C-18 column (Phenomenex, Torrance, CA, USA) in series with a Novapak C-18 150-mm x 3.9-mm C-18 column (Water, Eatontown, NJ, USA). The mobile phase consisted of 20%:80% (v/v) acetonitrile and deionized water, acidified to pH 3 with phosphoric acid. The combination of these two analytical columns was designed to eliminate the interference of caffeine separation caused by other components in some samples, such as colors, artificial sweeteners, flavors, and preservatives. The wavelength of detection was set at 254 nm and flow rate was set at 1 mL/min. Caffeine eluted around 4.1 min. Data were recorded by a Hewlett Packard HP3395 integrator (Palo Alto, CA, USA). Sample chromatograms for Diet Coke and Dr. Pepper are shown in Figure 3.1 and 3.2, respectively.

Test for HPLC recovery and variability

Specific amounts (12.6 mg and 43.1 mg) of caffeine were measured and put into different 250 mL volumetric flasks. Degassed caffeine-free diet coke (250 mL) was added to each volumetric flask to obtain two spiked samples. A 1 mL aliquot of the first spiked sample was transferred to 5 vials and diluted 3-fold with deionized water. The same method was used to treat the second spiked sample to obtain another 5 diluted solutions. Samples were analyzed using the HPLC method described previously; using the standard

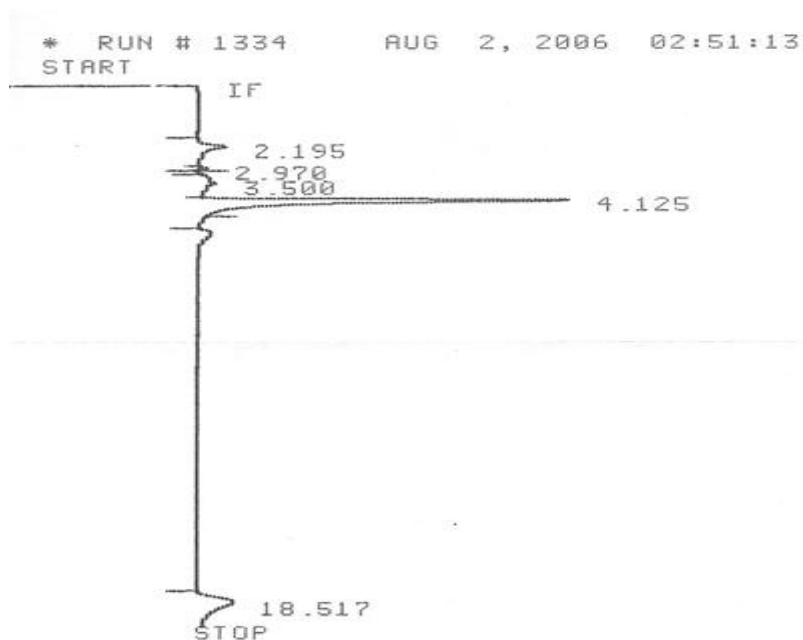


Figure showing Chromatogram of Diet Coke HPLC analysis by two C-18 columns using 20%/80% (v/v) acetonitrile and deionized water as mobile phase.

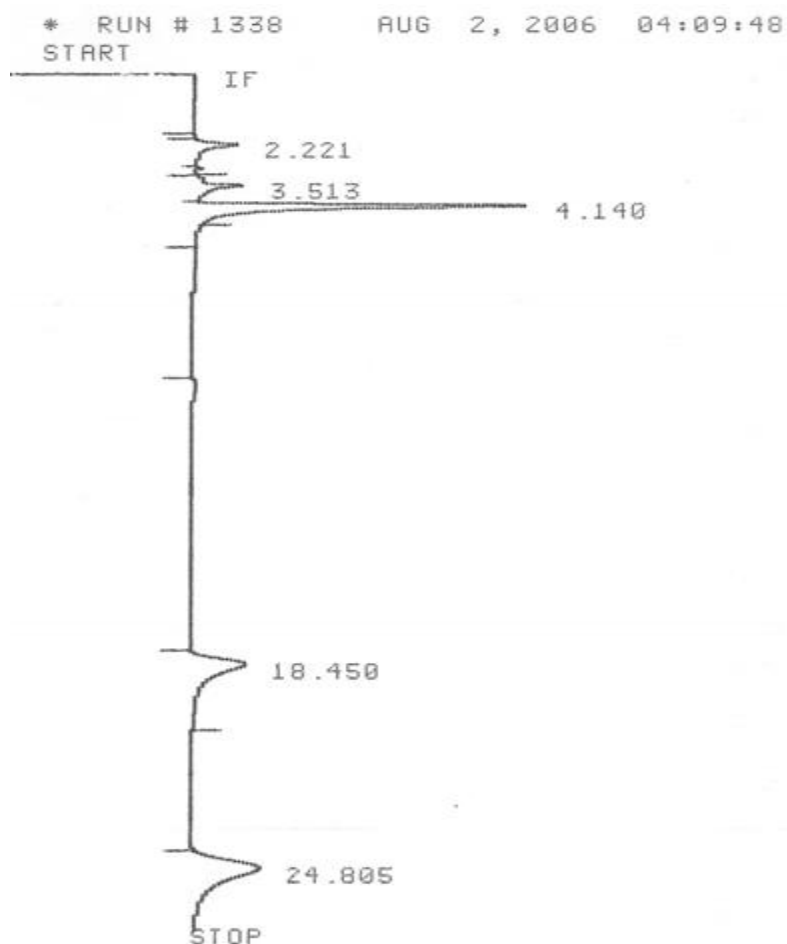


Figure showing Chromatogram of Dr. Pepper HPLC analysis by two C-18 columns using 20%/80% (v/v) acetonitrile and deionized water as mobile phase

calibration curve, the concentration of each sample was calculated. The coefficients of variation were determined from the standard deviation of the measurements divided by the sample's average. The percent recovery was calculated by the average of the measurements divided by the original concentration. The percent recovery and coefficients of variation were 96.7 to 100.8 % and 0.6%, respectively for this analytical method. These values are similar to that found by Grand and Bell (1997).

V. DATA ANALYSIS

The caffeine contents of the samples were calculated using the peak areas reported by the integrator and the standard curve. The caffeine content per 12 oz can was calculated. Every type of beverage had duplicate measurements per lot, which were averaged to give the mean caffeine content for the lot. Data from these duplicate dilutions were typically found to vary by less than two percent. The caffeine contents for the various lots were then averaged to give the mean caffeine content for the beverages. Within the national brand beverage category, the lowest caffeine content was determined to be in Ritz Cola, which contained 10 mg caffeine per 12 oz. The highest caffeine values of the national brand beverages were observed among Vault Citrus, Vault Zero, and Diet SunDrop at 70-74 mg caffeine per 12 oz. There is approximately a 6-fold difference between the highest and lowest caffeine values within national brand beverages. Most colas and pepper-type products contained around 40 mg caffeine per 12 oz. A more robust extent of quality control appeared to exist in the national brand carbonated beverages as demonstrated by less lot to lot variability. Within the store brand beverage category, the IGA Cola contained the lowest caffeine value (5 mg per 12 oz). The highest caffeine contents (around 60 mg per 12 oz) were found in Big Fizz Cola and Dr. IGA. The caffeine contents within beverage types were quite disperse for the store brand beverages. In addition, variability between lots was greater than for the national brand beverages. The caffeine data of the current study may be used as a more extensive database to replace that removed from the American Beverage Association website and improve the vague classification of beverages by the USDA. The caffeine data determined in the present study suggests that consumers concerned about limiting daily caffeine ingestion from carbonated beverages may select the lower caffeine-containing store brand beverages. Consumers desiring caffeine may likewise select from the higher caffeine products. However, broad generalizations about the caffeine contents of carbonated beverages are difficult to make. The varied contents should be either accounted for in databases or caffeine values placed on food labels so consumers can be better informed.

Mei Musa *et al.*, (2012) in his study of determining caffeine in some Sudanese beverages by high performance liquid chromatography validate simple reversed-phase HPLC.

VI. MATERIALS AND METHODS

Experimental: All reagents used in this study were of analytical or HPLC grade and all solutions were prepared by using distilled water.

Standard solution preparation: Caffeine stock standard solution of 1000 ppm was prepared by dissolving 0.1000 gram of caffeine standard (Sigma- Aldrich) in 80 mL distilled water and sonicated for 10 min. Then solution was transferred to 100 mL volumetric flask and the volume was completed to mark by distilled water. The stock solution was stored in dark places at +4°C. Working standard solutions were prepared by suitable dilution for stock solution and they were prepared freshly.

Sample preparation: Different kinds of beverages brands including regular and diet cola, energy drinks, tea and coffee were purchased from different local supermarkets and 15 samples were analyzed using the HPLC method. All measurements were performed in triplicate were opened, the drinks were degassed by sonication, homogenized and filtered. Then each sample was filtered through a 0.45 μm syringe filter with a 5 mL syringe. Filtered drink sample of 2 mL were 5 times diluted in distilled water. 20 μL of each diluted sample was injected into the HPLC column. The relative peak areas were determined for three replicates of each dilute sample. Then the concentration of each dilute sample and finally the concentration of caffeine in soft drinks samples were calculated from calibration curve. One sample of Pepsi cola, Coca cola, energy drink (Red Bull) was spiked with 20 ppm caffeine standard for recovery determination.

Tea and coffee samples preparation: 2.00 g of tea and coffee samples were weighed and put into 250 mL beakers. 100 mL of boiling distilled water was added and let to stand for five minutes with stirring, the solution was cooled and filtered into conical flasks. 5 mL of the filtrate were pipetted into clean 50 mL volumetric flasks

and made to the mark with the distilled water. The samples were filtered through 0.45 μm syringe filter and run in the HPLC system according to experimental conditions.

Tea and coffee samples were spiked with 20 ppm caffeine standard for recovery determination.

Instrumentation: The HPLC system used in this study was isocratic Waters HPLC, which consisted of a model 1515 isocratic pump, vacuum degasser and 2996 PDA detector (USA). The injector was a model 7725i Rheodyne injector with injection loop 20 μL . The analytical column used was Shim-pack VP-ODS with internal diameter 4.6 mm and length 250 mm (Shimadzu Corporation, Kyoto, Japan). All chromatographic results were acquired and processed by Empower software (Waters Corporation).

VII. METHOD VALIDATION

Precision: The analytical precision of the method was assessed from the reproducibility of 6 determinations of 40 ppm caffeine solution and a relative standard deviation of 1.25% was calculated for peak area.

The retention time of caffeine was 7.347 min, with a relative standard deviation RSD = 0.5% therefore, in standard solutions, the HPLC method provides stable retention times.

Detection and quantification limits: Table 2 summarizes the method detection limit (MDL) and Method Quantification Limit (MQL). MDL was estimated as Standard Deviation (SD) of the peak area of seven injections multiplied by 3.14 (at $n = 7$). MQL was calculated by multiplying SD by 10 (Dionex, 2007).

Linearity: The calibration graph was generated using 20 μL injection loop. Six different concentrations of caffeine from 10 ppm to 100 ppm were analyzed according to experimental conditions. Then the calibration curve was established according to the obtained response (peak area) and the concentrations of caffeine in standard solutions. The results show a good linear relationship.

Rachel *et al.* while studying the caffeine content of specialty of coffees using samples of Starbucks Breakfast Blend purchased over the course of six consecutive days from Starbucks shop in Gainesville, FL, used a method that can also be used in determining caffeine content in carbonated drinks. The caffeine was extracted from coffee using a liquid-liquid extraction procedure. To 0.1 mL of coffee, 10 μL of mepivacaine and 10 μL of 10M of NaOH was added. All samples were vortex mixed for 5s, and 4.0 mL of chloroform (Fischer, certified ACS) was added. All samples were placed on a rotator for 15 min and then centrifuged for 10 min 3000 rpm. The organic layer was then transferred to auto sampler vials, and analysed by gas chromatography (GC).

1.0 mg/mL caffeine (Alltech-Applied science labs) stock standard solution was prepared in methanol (Fischer Scientific, certified ACS). Caffeine stock control solution were prepared in methanol from two separate sources (Alltech-Applied Science Labs and Sigma-Aldrich Company), both at concentrations of 1.0 mg/mL. A 1.0 mg/mL solution of mepivacaine was prepared in methanol for use as an internal standard. Quantization of caffeine was based on a calibration curve prepared in a concentration range of 50-500 mg/L with mepivacaine as the internal standard. Control samples, prepared at concentrations of 75 and 250 mg/L (three each), were included in each batch. An Agilent 6890 series GC system with nitrogen-phosphorus detector was utilized. The GC was fitted with a cross-linked methyl siloxane capillary column (HP-5, 30 m x 0.32 mm i.d., 0.25 mm film thickness) with ultra-high-purity helium as the carrier gas (constant flow rate, 1.0 mL/min). Injections (0.5 mL) were made in the splitless mode. The GC temperature settings were as follows: injection port, 250 °C; detector, 300 °C; initial column temperature, 90 °C; hold time, 0.50 min. The total run time was 11.70 min.

VIII. CONCLUSION

The validated HPLC method for the quantification of caffeine in beverages was found to be simple, precise, sensitive and accurate and allowed the obtaining of good results. In spite of the number of drink samples analyzed is small, the data presented in this study gave a preliminary outline about the content levels in tea, coffee, soft and energy beverages frequently. Shim-pack VP-ODS column was used with methanol: water (30:70)% (v/v) eluent. The detector wavelength was set at 270 nm. Linearity of the method was checked from 10-100 ppm and the correlation coefficient was 0.9999. The method detection limit was 0.023 ppm and the precision was 1.25% at 40 ppm caffeine concentration. The spiked recoveries for caffeine were 99%, 105%, 99.2%, 102% and 102% in Pepsi Cola, Coca Cola, Red Bull, Gazaltain black tea and Coffee samples respectively. The caffeine contents in tea samples ranged from 440 ppm to 473 ppm with average concentration of 458.6 ppm. The caffeine concentrations in energy drinks samples ranged from 170.6 ppm to 324 ppm with average concentration of 255.6 ppm. The coffee sample contains 252.4 ppm. The carbonated soft drinks showed caffeine content in the range of 32.4 ppm to 133.3 ppm with average concentration of 96 ppm. In addition, the concentrations of caffeine have been converted into the daily intake doses based on beverage consumption. The mean values of caffeine daily intakes were 183 mg, 101 mg, 64 mg and 38 mg through the ingestion of tea, coffee, energy drinks and soft drinks, respectively.

REFERENCES

- [1] Abourashed EA and Mossa JS. (2004). HPTLC determination of caffeine in stimulant herbal products and power drinks. *Journal of Pharmaceutical and Biomedical Analysis* 36:617-20.
- [2] Ahmad A.H., Alghamdi F.A. and Alwarthan, A.A. (2005). Determination of content levels of some food additives in beverages consumed in Riyadh City. *J. King Saud Univ.* 18: 99-109.
- [3] Armenta S, Garrigues S, de la Guardia M. (2005). Solid-phase FT-Raman determination of caffeine in energy drinks. *Analytica Chimica Acta* 547: 197-203.
- [4] Barone, J.J. and Roberts, H. (1990). Human Consumption of Caffeine. In: Dews, P.B. (Ed.), *Caffeine*. New York: Springer-Verlag.
- [5] Brunetto M.R., Gutierrez L, Delgado Y, Gallignani M, Zambrano A, Gomez A, Ramos G, Romero C. (2007). Determination of theobromine, theophylline and caffeine in cocoa samples by a high-performance liquid chromatographic method with on-line sample cleanup in a switching-column system. *Food Chemistry* 100:459-67.
- [6] Caudle A.G, Gu Y and Bell LN. (2001). Improved analysis of theobromine and caffeine in chocolate food products formulated with cocoa powder. *Food Research International* 34:599-603.
- [7] Chen Q-C and Wang J. (2001). Simultaneous determination of artificial sweeteners, preservatives, caffeine, theobromine and theophylline in food and pharmaceutical preparations by ion chromatography. *Journal of Chromatography A* 937:57-64.
- [8] Chen Q, Zhao J, Huang X, Zhang H and Liu M. (2006). Simultaneous determination of total polyphenols and caffeine contents of green tea by near-infrared reflectance spectroscopy. *Microchemical Journal* 83:42-7.
- [9] de Aragao, N.M, Veloso, M.C.C., Bispo, M.S., Ferreira, S.L.C., de Andrade, J.B. (2005). Multivariate optimisation of the experimental conditions for determination of three methylxanthines by reversed-phase high-performance liquid chromatography. *Talanta* 67: 1007-1013.
- [10] Farah A, Monteiro M.C, Calado V, Franca A.S and Trugo LC. (2006). Correlation between cup quality and chemical attributes of Brazilian coffee. *Food Chemistry* 98:373-80.
- [11] Goto T, Yoshida Y, Kiso M, Nagashima H. (1996). Simultaneous analysis of individual catechins and caffeine in green tea. *Journal of Chromatography A* 749:295-9.
- [12] Grand, A.N. and Bell, L.N. (1997). Caffeine Content of Fountain and Private-Label Store Brand Carbonated Beverages. *Journal of the American Dietetic Association* 97:179-182.
- [13] Hiroshi, A., Monteiro, A.M., Gillies, M.F. and Crozier, A. (1996). Biosynthesis of caffeine in leaves of coffee. *Plant Physiol.* 111: 747 - 753.
- [14] Horie H, Mukai T and Kohata K. (1997). Simultaneous determination of qualitatively important components in green tea infusions using capillary electrophoresis. *Journal of Chromatography A* 758:332-5.
- [15] Huck CW, Guggenbichler W, Bonn GK. 2005. Analysis of caffeine, theobromine and theophylline in coffee by near infrared spectroscopy (NIRS) compared to high-performance liquid chromatography (HPLC) coupled to mass spectrometry. *Analytica Chimica Acta* 538:195-203.
- [16] James J. (1991). *Caffeine and Health*. Academic Press Inc., San Diego, pp. 26-32.
- [17] *Journal of Analytical Toxicology*, Vol. 33, January/February 2009
- [18] Kerrigan, S. and Lindsey. T. (2005). Fatal caffeine overdose: two case reports. *Forensic Sci. Int. Journal of Analytical Toxicology*, 153(1): 67-69
- [19] Komes, D., Horzic, D., Belscak, A., Kova K.C., Ganic, C. and A. Baljak, K. (2009). Determination of caffeine content in tea and maté tea by using different methods. *Czech. J. Food Sci.* 27: 213-216.
- [20] Liguori, A., Hughes, J.R., Grass, J.A. (1997). Absorption and Subjective Effects of Caffeine from Coffee, Cola and Capsules. *Pharmacology Biochemistry and Behavior* 58: 721-726.
- [21] Mandel H.G. (2002). Update on caffeine consumption, disposition and action. *Food and Chemical Toxicology* 40: 1231-1234.
- [22] Marcia, B.S.C., Marcia, C.V.C., Heloísa, L.P., Rodolfo De Oliveira, F.S., Reis, N.J.O. and Jailson De Andrade, B. (2002). Simultaneous determination of caffeine, theobromine and theophylline by high-performance liquid chromatography. *J. Chromatographic Sci.*, 40: 45-48.
- [23] McCusker, R.R., Goldberger, B.A. and Cone, E.J. (2006). Caffeine content of energy drinks, carbonated sodas, and other beverages. *J. Anal. Toxicol.* 30(2): 112-114
- [24] Nehlig, A., Dava, J.L., and Debry, G. (1992). Caffeine and the central nervous system: mechanisms of action, biochemical, metabolic and psychostimulant effects. *Brain Research Reviews* 17: 139-170.
- [25] Nishitani E and Sagesaka YM. (2004). Simultaneous determination of catechins, caffeine and other phenolic compounds in tea using new HPLC method. *Journal of Food Composition and Analysis* 17:675-85.
- [26] Nour V. Trandafir, I. and Ionica, M.E. (2010). Chromatographic determination of caffeine contents in soft and energy drinks available on the Romanian market. *St. Cerc. St. CICBIA*, 11: 351-358.
- [27] Pura N.J. (2001). Improved high-performance liquid chromatography method to determine theobromine and caffeine in cocoa and cocoa products. *J Agric Food Chem* 49:3579-83.
- [28] Mashkouri N.N, Hamid AS, Afshin RK. (2003). Determination of caffeine in black tea leaves by Fourier transform infrared spectrometry using multiple linear regression. *Microchemical Journal* 75:151-8.
- [29] Mei, M.A., Mawahib, E., Mohammed, I.T., Badawi, A.Z., and Abdalla A.E. (2012). Determination of Caffeine in Some Sudanese Beverages by High Performance Liquid Chromatography. *Pakistan Journal of Nutrition* 11 (4): 336-342.
- [30] Paradkar, M.M. and Irudayaraj, J. (2002). Rapid determination of caffeine content in soft drinks using FTIR-ATR spectroscopy. *Food Chemistry* 78: 261-266.
- [31] Rogers, P.J., Deroncourt, C. (1998). Regular caffeine consumption: a balance of adverse and beneficial effects for mood and psychomotor performance. *Pharmacol Biochem Behav.* 59(4): 1039-45.
- [32] Schulz H, Engelhardt U.H, Wegent A, Drews H and Lapczynski S. (1999). Application of near-infrared reflectance spectroscopy to the simultaneous prediction of alkaloids and phenolic substances in green tea leaves. *J Agric Food Chem* 47:5064-7.
- [33] Smith, A.P. (2005). Caffeine at Work. *Hum Psychopharmacol.* 20(6): 441.
- [34] Spiller G. (1998). *Caffeine*. CRC Press, New York, pp. 225-230.
- [35] Thomas J.B, Yen J.H, Schantz M.M, Porter B.J and Sharpless KE. (2004). Determination of caffeine, theobromine, and theophylline in standard reference material 2384, baking chocolate, using reversed-phase liquid chromatography. *J Agric Food Chem* 52:3259-63.
- [36] U.S. Food and Drug Administration, Department of Health and Human Services, FDA and You, Issue 14, Fall 2007
- [37] Violeta, N., Trandafir, I. and Elena, I. M. (2008). Quantitative determination of caffeine in

- [37] carbonated beverages by an HPLC method. *J. Agroalimentary Processes Technol.* 14: 123-127.
- [38] Wang H, Helliwell K, You X. (2000). Isocratic elution system for the determination of catechins, caffeine and gallic acid in green tea using HPLC. *Food Chemistry* 68:115-21.
- [39] Wanyika, H.N., Gatebe, E.G., Gitu, L.M., Ngumba, E.K. and Maritim, C.W. (2010). Determination of caffeine content of tea and instant coffee brands found in the Kenyan market. *Afr. J. Food Sci.*, 4: 353-358.
- [40] Zuo Y, Chen H and Deng Y. (2002). Simultaneous determination of catechins, caffeine and gallic acids in green, Oolong, black and pu-erh teas using HPLC with a photodiode array detector. *Talanta* 57:307-16.
- [41]

Creating 3D model for new urbanized area from limited resources and data in developing countries

Rebaz Nawzad , Nabaz Gharib Mohammed & Hawar Othman Sharif

Abstract: Technology developments ratify web based Geographical Information System (GIS) for further developments especially in the developing countries. However, the progress of technology made the consumers to expect the corresponding progression in the field of GIS too. Perhaps GIS recently developed further and allows visual tours over 3D models in numerous places, while these models are barely available in the developing countries, due to the lack of data, techniques and professionals.

One of the popular applications for GIS data demonstration is World Wide Web (www), which presenting spatial and Geo-data for period of time statically and dynamically. However, this study aims to increase the numbers of three dimensional models on the web for more GIS virtual tours in the developing countries where they suffer from lack and inadequacy of data quality. Nevertheless, this can be done by intriguing simple and poor quality data through different process of enhancement by applies different methods, techniques and tools to enhance and enrich the data to the level that can be uses in GIS application and 3D model production, therefore this study provide the stage of data improvements and 3D model production from a poor quality data.

3D data means the data with three dimensions that facilitates 3D model production using the third dimension. Although 3D model can built with three dimensional data, but building 3D model for GIS especially for the web virtual tour requires other attributes such as location reference, as it require the model to be build on the correct location. Consequently, the aim of this paper is to deliberate the opportunities for rising 3D model from limited data and resources, also this study over comes all the issues with the adequate data for this purpose.

Keywords:- Spatial Data, 3D Model, Web based GIS, SketchUp, Geo-referencing, AutoCAD, ArcGIS, Google SketchUp and GIS, Limited GIS data and 3D modeling.

I. INTRODUCTION

The term GIS frequently applied to geographically oriented computer technology [1]. The benefits of GIS and its progresses increasing significantly in numerous fields to improve and develop public and private sectors [2] such as: urbanization, regional planning, cartography, tourism sector, environmental conservation and utilities [3]. However, GIS benefits come from integration of hardware, software and data for capturing, managing, analyzing, displaying, understanding, interpreting, and visualizing of information [4]. Although there are, many applications using GIS technology, but the users of GIS are also increasing significantly, since its growths and improvements touched a considerable level in approving GIS futures and it influence in many countries [5]. One of the GIS futures is 3D presentation, that is attracting many users since it has established, as it is presenting data in a ways, which have virtual depth, height, and width, similar to x, y and z-axes [6], this development can scale according to user's preference and desires. 3D data also have capability to rotate, zoom and represent multiple uninterrupted views, regardless of their attributes, beside they have ability to show and manipulate spatial relationships and support users to envisage an object in the way that is close to its real looking in reality [7]. Despite the fact GIS is a powerful tool, however the growth of Internet also created superior infrastructure to widespread distribution and dissemination [8], alongside to software developments which also helped GIS development further, these developments made it easy to integrate and create 3D model on the web application too. However, the image below showing the competences of 3D features in GIS that is combining different file formats [9] to achieve a particular work and make a use of different futures accurately.

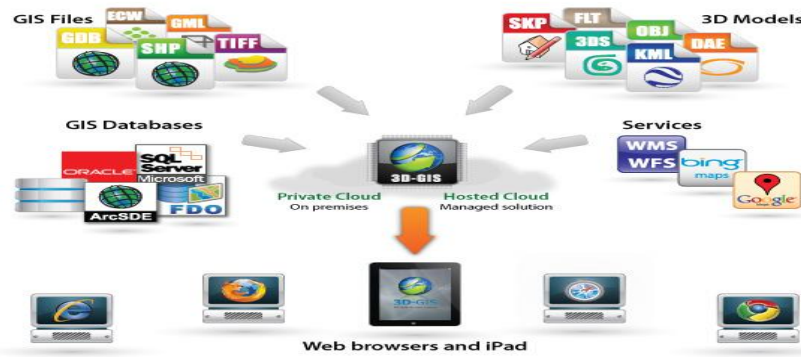


Image No.1: 3D-GIS in the Cloud supported data sources and clients [12]

GIS technology relies significantly on data from different kinds to create 3D models, analysis and other form of location-based techniques. However, spatial data is one of the vital kinds of data to GIS, as they are easier to deployments and require less process for conversion, whereas the study area suffers from the lack of quality data and limitation of skills in developing GIS and it futures in the region that is also the case in many other developing countries. Therefore poor quality data affects the decision-making, developing, enhance of technology and often expensive to fix. The way 3D using GIS, also depending a great emphasis on data quality, as quality is paramount when using GIS especially 3D [10].

Developing countries suffers from lack, limitation and shortage of GIS data, it is important to mention the key answers to many problems in the developing countries often inhibited by lack of access and availability to relevant data, or to the data quality [11]. Consequently, this study looks into data enhancements, through combination of data, different procedures and tools to promote the best ways to enhance limited and poor data.

II. CHALLENGES

In the field of GIS, the system to handles 3D map or model within web environment is scarcely available, since it requires advance browser and applications for that purpose. Hence this study intends to build a 3D model that is compatible and ready to demonstrate on web interface or web map from a limited and poor quality data. This is only achieved if developer manages to improve and enhance the data quality by enrich the data thorough adding more attributes. Consequently the challenge covers: conversion, methods, techniques and tool for the enhancement of insufficient data, and eventually converts the limited and the inadequate data to reach facilitation of 3D model production for GIS and web map.

III. STUDY AREA

Department of Computer Science in University of Sulaimani/New Campus. It is located in the city of Sulaimani which is one of the Kurdistan Region of Iraq cities. This city situated in the northeastern tip of the country, and the city is known as a cultural capital of Kurdistan Region [13]. This campus initiated in 2006 that built on 1,000,000sqm land, located on the coordination of 35.575053 Latitude, and 45.362978 Longitude [14].

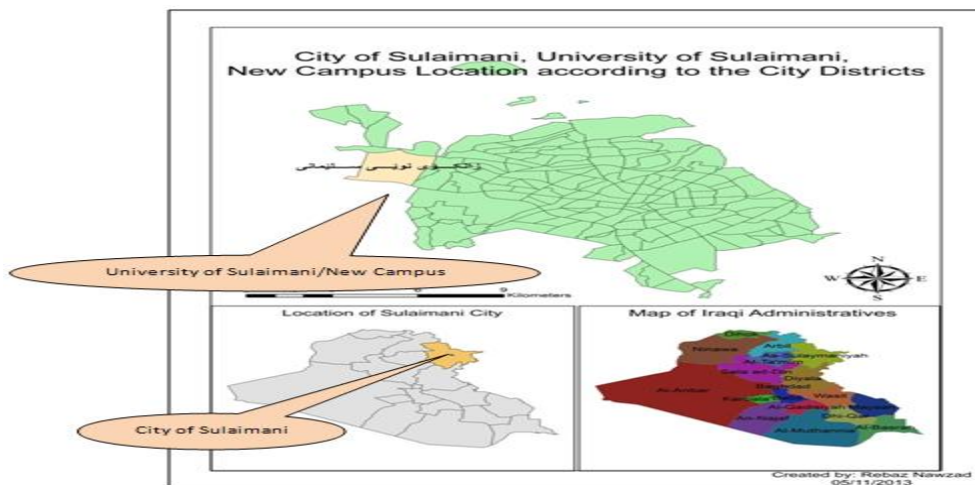


Image No.3: Research Area: Location of University of Sulaimani, New Campus according to the city Districts,



Image No.2: University of Sulaimani, New Campus Location [15]

IV. MATERIALS

The materials for this study came from different sources and quality:

1. Buildings floor plans for the entire university are AutoCAD files (.dwg) formats, created by Construction Company. This file contains the entire campus drawing in 2D. with no elevation and referencing.
2. City master plan and city satellite images are another source of materials, they contains city districts, roads, administrative areas. These data provided by the city Principality, these data are includes reference and coordination, which can be used for geo-referencing purpose.
3. Building actual photo, to complete the 3D model, someone requires taking the actual photographs of the building, from different points to assist the 3D model creation.
4. Height measurements of the building must be taken manually, if the wall drawing is not available, or it must come from other sources.
5. 3D model production software, which is Google Sketch Up.

Methodology and Design: [Data Enhancements, Design and 3D Model creation]:

Combination of tools and techniques used throughout this study to produce the demanding work. The key information are the AutoCAD and the Shape file data, however there are other source of data and information used during this study, such as JPEG Image, building height data and satellite images. This study tries to integrate different platform together (Mash-up) in order to improve data quality and produce better results.

Usually in the developing country data can be in any quality and formats or unorganized, Hence, it is important to know that different types of data require different techniques and tools for enhancements and developments, and this study focus on integration of multi-platform for 3D production, referencing and data enhancements due to the variety of data.

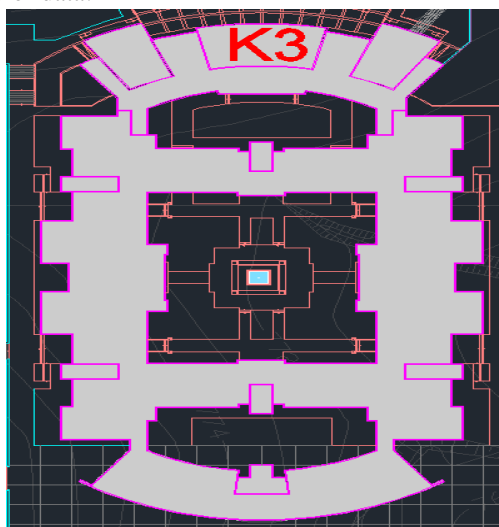


Image No 4: AutoCAD Drawing for the study area

One of the main issues with the AutoCAD data in this study is lack of reference. Perhaps it is one of the drawbacks of the existing AutoCAD data, therefore this will be the first challenge that the study should overcome thru different technique and tools to solve this issue, and add reference to the AutoCAD data. Otherwise, the model will not stand up on the exact real world location.

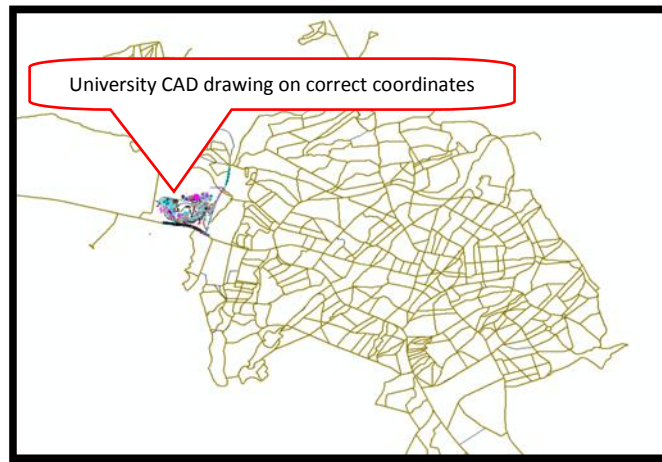


Image No.5: Geo-referenced University AutoCAD site plan using ArcMap software.

In order to add reference, there are different ways and techniques, perhaps the most popular way called Geo-referencing techniques which is achieved in different ways on different software and applications.

1. Applying the technique through AutoCAD: This procedure prepared by moving AutoCAD drawing on the AutoCAD software to its correct location, this achieved by using a specific plugin called *UHGEOREF*, which is used for Geo-referencing of raster maps to raster files. However, inside this plugin, World files are often included, this is a text files with six transformation parameters (affine) for the correct positioning of the raster map in a global coordinate system [16].
2. Applying the technique through ArcMap: this software have the ability to geo-referencing any drawing to its real location from different formats such as JPEG, PDF, AutoCAD, and even hand drawing. It work by scan the maps or drawing and then import it to the software, as it is shown on the image No.5 [17].
3. Applying the technique through Google SketchUp: The innovative geometry of any ground plan may create as an aerial photograph, which is then used as an underlay for a pencil sketch of a proposed re-working of streets and open spaces. However, the 3D model can also build and at the final stage, the model can be highlight and then move to its original location [18].

Figure No.2 concludes the three different techniques mentioned above in a simple diagram. Nevertheless, geo-referencing improves the data quality a step further, and it gets prepared to build the model on the correct coordinates. The experts plays an important role in enhance data, because it require a correct techniques and tools to be applied on the data. This procedure twitches by identify the data layers to be reference to a location, then it fit and scales to the area of interest. As soon as the first control point taken in one location, then the next control points on opposite ends of the image need to be taken, beside it is important to assess accuracy by measuring the disparity between the data layers at multiple points throughout the study area and then the desired geo-referenced location.

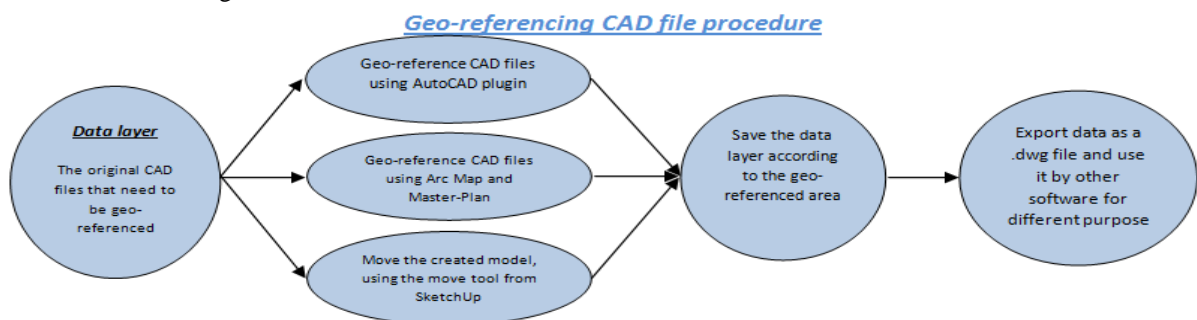


Figure No.1: Geo-referencing procedure and methods

It is important to consider geo-referencing in the field of GIS, although it is a complicated, on the other hand, it improve data quality to a high level. Google SketchUp nowadays has ability to add real location to the interface and user can built their model using the location for reference as it shown in image No.6, also because the AutoCAD data has been geo-referenced at the earlier stage, it can be seen on the correct location in image No.7.

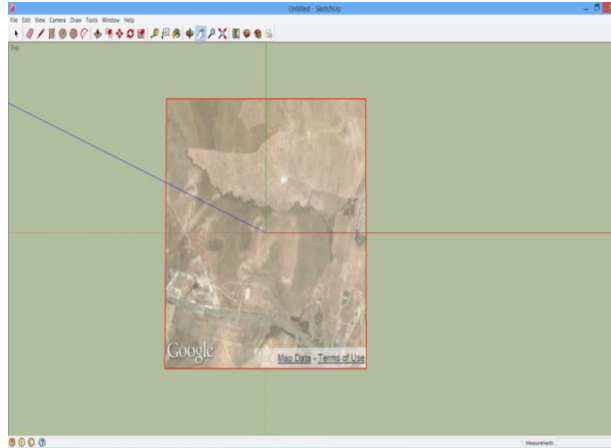


Image No.6: SketchUp adds real world location

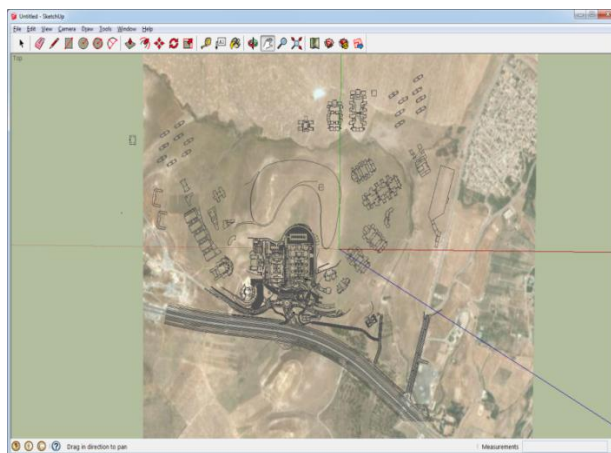


Image No.7: University Campus footprints on SketchUp

Finally, the procedure of 3D model construction can initiate, but the building height data is not available, hence one or more methods require in order to add third dimension to the building. Nevertheless, there are different methods to collect height information depending on the size of the working area.

1. Measuring the height of the building in person, this will require a lot of field work, but it provides accurate records.
2. Stereo image pairs used to perform third dimension data acquisition. Stereo photogrammetry or photogrammetry based on a block of overlapped images is the primary approach for 3D mapping and object reconstruction using 2D images.
3. Close-range photogrammetry, this is another technique that work out the distance between the camera and the building to calculates the building height.
4. Using 3D scanner can collects millions of points for the building or any objects, these points includes height distance and depth too.

Image No.8 showing a wall pushed up, but this is require the height measurements, because the data collected for this purpose, and then the height of building will standup correctly, image No.9 authorize the certainty.

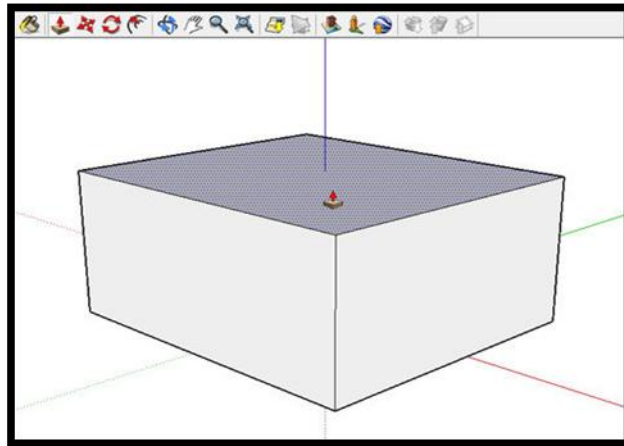


Image No. 8: step one for building first wall



Image No. 9: several wall building completed

Once the building structure completed and then details can be added such as doors, windows texture and colors, which is shown in image No. 10. Eventually as soon as the 3D model finalized, according to image No.11, and then it can be export as .kmz file. This is the file that is accepted by Google Earth for uploading the model into to local Google Earth as a trail, lastly the model can also be submitted to Google Earth forums for approval, once the file is validated and accepted, formerly the model get displayed globally. However, Google Earth and Google Map API (Application Programming Interface) are using JavaScript to allow users to modify applications and add maps to own website.



Image No.10:

Details added to the

Model



Image No. 11: the complete building from the top, Side (east) and front view

VI. INTERFACE

After the 3D models for the dedicated building completed, and then the model need to upload into an interface. This is to make the models accessible and to provide mechanisms to manage it content. However, the interface for the produced 3D model is Google Earth, as it has a "3D Buildings" layer that allows anyone to view 3D models of any objects and edit the database side of the model. This interface enables users to add data after the completion to enrich the model with more information [19]. Google Earth offers opportunity to explore and visualize its stored data on the system, through uses of the visualization and navigation functionality.

VII. CONCLUSION

Although 3D model is become common in the GIS applications, but it wouldn't be available to built without availability of advanced superior data, on the other hand, 3D model doesn't prevail to be part of GIS as a management tools (decision makers) and real world demonstration. Hence, this paper describes initial works to form a 3D model from scratch or limited data. Beside there are various aspects of 3D required to be addressed and investigated, also this research challenged and investigated those aspects. The study also describe approaches that can be used for further 3D model creation using combination of software, data and techniques. This is not only to build 3D model, but also to enhance and enrich simple and non spatial data into an advanced geo-reference and spatial data that make GIS life and 3D creation much easier. Eventually the model building not the only issue, but the details and demonstration is also very important to develop the topic in the future further and open the road for the much more model creation and movements towards a digital 3D model city.

ACKNOWLEDGEMENT

We would like to thank the University of Sulaimani, departments of Computer Science, for their support, and we like to thanks the engineer: Shadan Madhat, for providing the AutoCAD data of the campus from her Directorate Office of new campus building vigilant. In addition, I like to thank any and everyone who provide knowledge and information to reach our particular goal.

Future work

The same principals can be applying to convert the entire University of Sulaimani from 2D drawing into 3D models. This study was an initiation of the entire university 1,000,000 sq. meters to be built in 3D in the future, although in the mean while this study focused on department of Computer Science, but it has produced enough guidance and techniques to for orientation. Conversely, the same method that applied to the single department can be apply to other buildings, as the available data for the university is the same for all the departments.

The same or similar techniques can be applied on other locations and objects even if the data are inadequate, since most of the available information in the developing countries are limited and unorganized.

REFERENCES

- [1]. David J Maguire, M Goodchild, D Rhind. (1991). an Overview and Definition of GIS. Geographical information systems: Principles and applications. 1 (1), 9-20.
- [2]. Idris Kahraman, Ismail Rakip Karas, and Alias Abdul Rahman. (2011). DEVELOPING WEB-BASED 3D CAMPUS INFORMATION SYSTEM. ISG & ISPRS. 1 (1), p1-2.
- [3]. esri. (2013). what is GIS, Available: <http://www.esri.com/what-is-gis/who-uses-gis>. Last accessed 06 Oct 2013.
- [4]. esri. (2012). what is GIS?, Available: http://www.esri.com/what-is-gis/overview#overview_panel. Last accessed 28 Sep 2013
- [5]. N Baby, P Lennox. (2012). Decision support for the naive GIS users. Geospatial Communication Network. 5 (2), 10.
- [6]. Esri, 2013, A New Dimension, 3D GIS Brings the Virtual World to Life, viewed 04 February 2014, <<http://www.esri.com/library/ebooks/a-new-dimension.pdf> >.
- [7]. Scott Glick, Dale Porter and Caroline Clevenger. (2009) System Component Visualization: The Role of 3D Models in Construction Management Education. Unpublished research. Colorado State University
- [8]. Anselmo Cardoso de Paiva, Cláudio de Souza Baptista. (2009). Web-Based GIS. Environmental Informatics. 4 (4053), 4053-4055.
- [9]. Sivan Design. (2013). 3D GIS in the Cloud, Available: <http://www.sivandesign.com/products/3dgis>. Last accessed 06 Oct 2013.
- [10]. Esri White Paper. (2011). GIS Data Quality Best Practices for Water, Wastewater, and Stormwater Utilities. Available: <http://www.esri.com/library/whitepapers/pdfs/gis-data-quality-best-practices.pdf> Last accessed 20 Jan 2014.
- [11]. Ian D. Bishop, Mike Barry, Elsworth McPherson, Joiana Nascarella, Karen Urquhart and Francisco Escobar. (2002). MEETING THE NEED FOR GIS SKILLS IN DEVELOPING COUNTRIES: THE CASE OF INFORMAL SETTLEMENTS. Wiley Online Library. 6, issue 3 (3), 311-326.
- [12]. Sivan Design. (2013). 3D GIS in the Cloud. [Image online]. Available: <http://www.sivandesign.com/products/3dgis>. Last accessed 06 Oct 2013.
- [13]. Dargham al-Rubaie. (2010). Sulaimani City. Available: http://www.iraqhope.com/index.php?option=com_content&view=article&id=274&Itemid=60. Last accessed 29 July 2013
- [14]. Kurdistan Engineers Union journal. (2013). Sulaimani University New Campus. Kurdistan Engineers Union journal. 45 (5), p26-28.
- [15]. Microsoft Corporation (2013) University of Sulaimani. Bing Maps [online].[Accessed 26 October 2013]. Available at: <http://www.bing.com/maps/>.
- [16]. CAD-Huebner.de. (2010). Georeferenzieren von Pixelbildern. Available: <http://www.cad-huebner.de/lisp.htm#Inhalt>. Last accessed 21 April 2014.
- [17]. Paul Cote. (2012). Spatial Data Handling. Available: <http://www.gsd.harvard.edu/gis/manual/georeferencing/>. Last accessed 22 April 2014.
- [18]. Paul Cote. (2012). 3D Site Modeling ni Context. Available: <http://www.gsd.harvard.edu/gis/manual/georeferencing/>. Last accessed 21 April 2014.
- [19]. Google Earth news. (2014). 3D Buildings. Available: <http://www.google.com/earth/explore/showcase/3dbuildings.html>. Last accessed 25 May 2014.

Prediction of Global Solar Radiation Using Angstrom-Page Equation Model for Makurdi Benue State, Nigeria

M. S. Kaltiya¹, M. S. Abubakar¹ and I.N. Itodo²

¹Department of Agricultural and Bio-Environmental Engineering Technology, Federal Polytechnic, P.M.B 35 Mubi

²Department of Agricultural and Environmental Engineering, University of Agriculture, Makurdi

ABSTRACT: The Angstrom-Page model was used to predict the Global solar radiation for Makurdi. This was done by measuring, solar radiation, relative humidity, dry and wet bulb temperatures, hours of cloudiness and bright sun-shine at the interval of one hour from 0600hr to 1800hrs daily for a period of six months (February to July, 2011) and the measurements were carried-out within Makurdi metropolis. Sun meter model DS-05 was used to measure the solar radiation, a digital thermo-hygrometer model IT-202 was used to measure relative humidity, wet and dry bulb temperatures. The hours of cloudiness and brightness were determined from the measured solar radiation. Solar radiation intensity $<20\text{w/m}^2$ was considered as hours of cloudiness and values $\geq 120\text{w/m}^2$ was taken as hours of brightness. The result obtained showed that the mean solar radiation, relative humidity, dry and wet bulb temperatures, hours of cloudiness and bright sun-shine for the location were; 191.64w/m^2 , 60.10%, 30.24°C , 28.25°C , 7.72Hrs and 5.28Hrs respectively. The regression constants 'a' and 'b' in Angstrom-page equation were found to be 0.24 and 0.57 respectively. The performance of the variance between measured and calculated radiation were analysed statistically where Mean Bias Error (MBE) and Root Mean Square Error (RMSE) were 0.16 and 5.06% respectively. Similarly, there is a strong correlation between calculated and actual global solar radiation. Finally, this model can be used to predict average global solar radiation for Makurdi location.

KEYWORDS: Solar Radiation, clearness index, sunshine hours, regression constants and insolation intensity

I. INTRODUCTION

Solar energy is the most important energy resource to man and indeed it is essential factor for human life. Although the use of passive solar energy in drying process is not new and it date back from ancient time when agricultural product were sundried using solar energy. It is evident that our increasing dependent on conventional energy has rendered these energy sources such as fossil fuel, wood, nuclear, electricity etc more expensive. Most disturbing is the fact that these energy sources are fast depleting and they increases the present environmental pollution problems ^[1]. Solar energy is incident on the earth at a rate of $2.0 \times 10^{15} \text{kWh/day}$ and is estimated to last for 704 billion years. In principle, solar energy could supply all the present and future commercial energy needs of the world on continuous basis. This makes solar energy one of the most promising of the entire unconventional energy source ^[2]. Although the supply of solar energy received by the earth is substantial, it has three (3) peculiar characteristics that cause problem in its collection and practical application as an economic substitute for conventional energy source ^[3]. One, the total amount of solar radiation is large, it is spread out over, a very large area and thus it intensity is low. Therefore large collection fields are required to obtain useful amount of energy, which raises the cost of buying and installing solar energy equipment. Two, it varies, that is the intensity of incoming radiation changes drastically during the day and from season to season, making it necessary either to store large quantity of heat or to provide backup system that runs on conventional fuel, which both add cost and complexity of a solar system. Three, it is intermittent that is the incoming energy is subject to unpredicted interruption of passing cloud which obstruct the sunshine.

Now that there is global campaign on how to reduce the pollution problems cause by some conventional energy source to our environment, therefore, there is a need for exploration of solar energy for domestic and industrial uses. It is becomes inevitable to know how to evaluate insolation levels for any location so that the introduction and sustainability of solar energy will be assured^[4]. Energy is the backbone of sustainable technological development of any nation and Nigeria is blessed with abundant supply of solar radiation. According to^{[5]; [6]; and [4]} that Nigeria lied in the high solar radiation belt of the world and it was estimated in the far North of the country the solar energy of 3.5–7.0 kw/m²/day is received annually. Similarly,^[7] estimated that the average bright sunshine of 11.6hr/day is received annually. Since Nigeria has adequate solar energy potential to support it energy need, it is therefore becomes imperative to harness the resources insidiously in order to solve the problems of its energy, shortage that is dwindling the sustainability of it industries and environmental pollution.

In general, it is believed that solar energy available depend on the large extent of the latitude, hour of the day, day of the year, the height above sea level (altitude) and some climatic variables such as temperature, humidity, rainfall, harmatan, sunshine and vegetation affect solar radiation^{[8]; and [9]}. In addition to the foregoing variation in solar radiation received at a particular location, there is obvious variation due to atmospheric absorption by carbon dioxide (CO₂), Ozone layer and scattering cloud. Therefore, to evaluate the solar radiation incident on a particular location the above factors ought to be determined in developing models for prediction of global solar radiation of a location. Several authors have developed regional or location based models to predict the quantity of global solar radiation or energy available in specific locations^[10]. However, with current trend in climatic change due to global warning has shown that most of climate-dependent constants developed by researchers need to be verified from time to time to check their validity. For example^[11] developed that Angstrom-page model equation for Markudi by measuring solar radiation, relative humidity, sunshine hours, dry and wet bulb temperature of the location between August 2008 and December 2009. The Angstrom-page equation was of the form $H/H_o = 0.19 + 0.62(n_s/N)$. Similarly, in this research the parameter measured were solar radiation, sunshine hours, relative humidity, dry and wet bull temperature of Markudi for a period of six months between February and July, 2011 from 0600Hr to 1800Hr daily.

II. MATERIALS AND METHODS

2.1 Study Area

The research was carried out at the Agricultural and Environmental Engineering Department of the University of Agriculture, Markudi, Benue state Nigeria. The study location lies on latitude 7° 7'N and longitude 8° 6'E. It is 1500m above sea level. The area is an agrarian environment marked by dry season between November and April and wet season between May and October. The mean annual rainfall usually ranges from 750mm to 1100mm. The temperature in this climatic region is high throughout the year because of high radiation income which is evenly distributed throughout the year. The maximum temperature can reach up to 40°C particularly in April, while the minimum temperature can be as low as 25°C between December and January. There is a seasonal variation of relative humidity in the area with extremely low (20-30%) between January and March, and reaches the peak (70-80%) between July and September. The ten (10) year mean clearness index for Markudi in the rainy season is 0.49 and 0.69 during the dry season (NASA).

2.2 Global Solar Radiation Model

According to^[12] Angstrom-page model was found applicable to predict global solar radiation to great extent in so many locations. Therefore, the model was used to predict the global solar radiation of Markudi as used by^{[13] and [11]}. The equation can be expressed as follows:

$$H = H_o [a + b(n_s/N)] = H_o k_t \quad (1)$$

where;

H = monthly average daily global radiation on the horizontal surface

H_o = monthly average daily extra-terrestrial radiation

n_s = monthly average daily number of hours of bright sunshine

N = monthly average daily number of hours of possible sunshine (day light between sunrise and sunset)

'a' and 'b' = regression constants.

The extra-terrestrial solar radiation incident on a horizontal surface H_o in equation (1) is computed in equation (2) [14]

$$H_o = \frac{24}{\pi} I_{sc} \left[1 + 0.33 \cos \left(\frac{360n}{365} \right) \right] \left[\cos \varphi \cos \delta \sin \omega_s + \frac{\pi \omega}{180} \sin \varphi \sin \delta \right] \quad (2)$$

where;

I_{sc} = Solar Constant, has the value of 1367 w/m^2 [15]; [16]; [17] and [18]

ω_s = hour angle of sunset or sunrise for the typical day n of each month (degree)

φ = latitude angle of the month (degree)

n = day of the year

δ = declination angle of the month (degree), which varies from +23.450 to -23.450 in the course of the year.

The declination angle is considered positive when sun is in the Northern latitude and negative when in the Southern latitude.

The declinations δ and hours ω_s angles in equation (2) are computed from expressions (3) and (4) respectively as used by [19]; [15]; [20] and [14]

$$\delta = 23.45 \sin \left[\frac{N-80}{370} \times 360 \right] \quad (3)$$

$$\omega_s = \cos^{-1}(-\tan \varphi \tan \delta) \quad (4)$$

The month average daily number of hours of possible sunshine N in equation (1) is determined from equation (5)

$$N = \left(\frac{2}{15} \right)^{\cos^{-1}(-\tan \varphi \tan \delta)} = \frac{2\omega_s}{15} \quad (5)$$

Data Measurements

Solar Radiation Measurement: The solar radiation measurement was carried out in an open field free from obstructions such as trees and buildings. A sun-meter model DS-05 calibrated in Watt/Square meters (w/m^2) was used to measure the solar insolation between 0600Hr to 1800Hr on the daily basis for a period of six months. The device was placed 1.5m above the ground in a horizontal position with the sensor pointing in the direction of the sun, east from morning to midday and west from midday to sunset. The device was set 'ON' to measure the solar radiation intensity (insolation) and the values were read off from the screen at one hour intervals. The mean values of radiation intensity were computed and recorded.

Temperature Measurement: The ambient temperature of the study area was measured using thermo-hygrometer model IT-202 in degree Celsius ($^{\circ}\text{C}$) with temperature range of -5 to $+5^{\circ}\text{C}$ and precision of 0.1°C . The thermo-hydrometer was placed where there was free flow of air and away from obstructions and direct sun rays. The values were read off from the screen at one hour intervals. The mean values were computed and recorded.

Relative Humidity Measurement: The relative humidity of the study area was obtained concurrently with the temperature from the thermo-hydrometer model IT-202. The device can measure the relative humidity value within the range of 30 and 90%.

Sun-Shine Hours Measurement: The sunshine hours were obtained from sun-meter model DS-05 and the time lapse or duration for insolation (radiation was recorded using a stop watch. In this research work the insolation value $\geq 120 \text{ w/m}^2$ is considered as hour of brightness and values $< 120 \text{ w/m}^2$ was regarded as cloudiness hour [21].

Determination of Angstrom–Page Regression Constants: The extra-terrestrial radiation H_o , the hour angle ω_s , and the hour of bright sunshine N were computed from equation 2, 3 and 5 to obtain the regression constants.

The regression constants 'a' and 'b' in the Angstrom-page equation were determined by plotting the clearness index H/H_o on the y-axis and fractional possible sunshine hours n_s/N on the x-axis to obtain the best line of fit.

Statistical Analysis: The performance of the regression constants 'a' and 'b' was computed using Mean Bias Error (MBE) and Root Means Square Error (RMSE) as expressed in equation 6 and 7.

$$MBE = \frac{\sum(Y_c - Y_o)/n}{\sum Y_o/n} \quad (6)$$

Where;

$Y_c = H_{\text{calc}}$.

$Y_o = H_{\text{meas}}$.

n = no. of data i.e no. of months.

$$RME = \frac{[\sum(x_i - y_i)^2]^{1/2}}{[\frac{\sum(y_i)}{n}]} \quad (7)$$

III. RESULT AND DISCUSSION

The mean solar radiation, relative humidity, dry and wet ambient temperatures, hours (Hrs) of cloudiness and bright sunshine for the location were found to be; 191.64W/m², 60.10%, 30.24°C and 28.25°C, 7.72Hrs and 5.28Hrs respectively as shown in Table1. This compares favourably with the findings of [22] for same period. However, it was observed that highest ambient temperature of 32.56°C was recorded in March which are in consonant with the findings of [22] but differ in solar radiation value, this variation could possibly be attributed to the harmattan dust experienced in the month February and March [23].

Table 1: Summary of Measured Monthly Average Daily Total Solar Radiation Parameters from February to July, 2011.

Month	I (w/m ²)	R.H (%)	T _{db} (°c)	T _{wb} (°c)	cloudiness(hr)	Brightness(hr)
February	191.38	53.87	31.38	28.82	7.07	5.93
March	191.37	50.00	32.56	29.92	6.68	6.32
April	202.63	52.32	31.04	28.21	6.63	6.37
May	216.07	66.12	29.75	27.52	7.52	5.48
June	177.22	69.46	28.56	27.76	9.03	3.97
July	171.19	68.80	28.15	27.29	9.42	3.58
Mean	191.64	60.10	30.24	28.25	7.72	5.28

Similarly, the highest radiation of 216.07W/m² was recorded in the month of May which may probably be as a result of on-set of rain in that month when the particles in the atmosphere were negligible after rains and the sun intensities were high. This agrees with the assertion made by [24] and [25], that atmospheric particle (cloud, harmattan and dust) reflect some incoming radiation back to space, thereby reducing the amount of radiation, which reaches the earth surface. Furthermore, the mean sunshine hour (n_s) was found to be 5.28Hrs as against the 7Hrs obtained by [22] in the same study location. However, the mean cloudiness hour was found to be 7.72 hours which contrasted the 6Hrs recorded by [22] for the same period of study. This conforms to the finding of [26] which states that solar radiation is directly proportional to duration of sunshine (Table 1). Furthermore, the result showed that the calculated average extra-terrestrial solar radiation, bright sunshine hour, clearness index (H/H_o), fractional sun-shine duration (n_s/N)

Table 2: Summary of Calculated Monthly Average Solar Parameter from February to July, 2011

Month	H(w/m ²)	H _o (w/m ²)	n _s (hrs)	N(hrs)	H/H _o	n _s /N	H _{cal} (w/m ²)
February	191.38	425.39	5.93	11.34	0.45	0.48	208.55
March	191.37	431.60	6.68	11.96	0.44	0.53	191.99
April	202.63	438.00	6.37	12.17	0.48	0.51	192.76
May	216.07	403.36	5.48	12.35	0.42	0.45	204.96
June	177.22	386.17	3.97	12.44	0.46	0.35	174.29
July	171.19	388.59	3.58	12.40	0.44	0.29	176.27
Total	1149.86	2473.11	32.01	72.66	2.69	2.61	1148.82
Mean	191.64	412.19	5.34	12.11	0.45	0.44	191.47

and predicted solar radiation are; 412.19W/m², 5.34hrs, 12.17hrs, 0.45, 0.44 and 191.47W/m² respectively as against 422.87W/m², 6.76hrs, 12.17hrs, 0.56, 0.54 and 237.59W/m² reported by [22] for same period of study (Table 2).

The summary of the determined Angstrom-Page equation and correlation coefficient for each month was given in Table 3. The regression constants 'a' and 'b' were found to be 0.24 and 0.57 respectively which are in concur with the model developed by [22] for same period of study (February to July, 2009).

Table 3: Summary of the Determined Monthly Angstrom–Page Equation and Correlation Coefficients

Month	H/H ₀	n _s /N	a'	'b'	Equation	R ²	R
February	0.45	0.48	0.29	0.39	$\frac{H}{H_0} = 0.29 + 0.39 \left(\frac{n_s}{N}\right)$	0.73	0.85
March	0.44	0.53	0.33	0.22	" = 0.33 + 0.22 $\left(\frac{n_s}{N}\right)$	0.26	0.51
April	0.48	0.51	0.21	0.53	" = 0.26 + 0.53 $\left(\frac{n_s}{N}\right)$	0.74	0.86
May	0.52	0.45	0.26	0.59	" = 0.18 + 0.59 $\left(\frac{n_s}{N}\right)$	0.68	0.82
June	0.46	0.35	0.18	0.77	" = 0.18 + 0.77 $\left(\frac{n_s}{N}\right)$	0.70	0.84
July	0.44	0.29	0.18	0.91	" = 0.18 + 0.91 $\left(\frac{n_s}{N}\right)$	0.95	0.9
Mean	0.45	0.44	0.24	0.57	$\frac{H}{H_0} = 0.24 + 0.57 \left(\frac{n_s}{N}\right)$	0.68	0.81

This tallies with the plotted Angstrom-Page equation linear graph for same period (February to July, 2009) where the intercept value on the *y*-axis was 0.24 and the slope was 0.56 as shown in Fig.1 and this is slightly above the accepted range of 10% to 20% of the total scattered radiation for regression constants 'a'^[15]. However, for the constant 'b' which is the fraction of the extra-terrestrial global radiation component of the location fall within the accepted range. The mean correlation coefficient for the Angstrom–Page equation used in this study was found to be 0.81 as against 0.76 reported by^[22] for same period of study (Table 1).

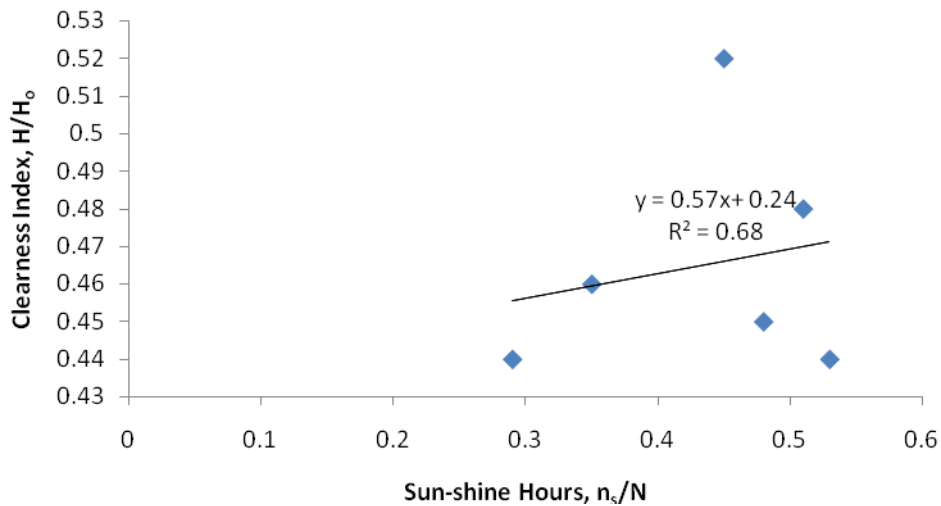


Fig.1:Plot of Angstrom–Page equation for Makurdi location based on monthly means of H/H₀ and n_s/N

This implies that 81% of the variations in the measured solar parameter were explained by the verified model leaving 19% to be explained by other factors^[27] that changes with time and location. The Mean Bias Error (MBE) and the Root Mean Square Error (RMSE) were used to determine the performance of the model. The values obtained were 0.16% and 5.06% respectively as against 0.51% and 1.12% for same period of study reported by^[22]. This variation may likely be as a result of change in weather condition recorded in February and March, 2011.

IV. CONCLUSION AND RECOMMENDATION

Conclusion

This empirical model is developed to predict the solar radiation in Makurdi, located on latitude 7°7'N and 8°53'E using the Angstrom-Page linear equation. The mean correlation coefficient for the Angstrom–Page equation used in this study was found to be 0.81. The Mean Bias Error (MBE) and the Root Mean Square Error (RMSE) were used to determine the performance of the model. The values obtained were 0.16% and 5.06% respectively. The result obtained showed that there is strong relationship between the actual and calculated global solar radiation

Recommendations

The model developed from this study can be used to predict the global solar radiation for Makurdi. Also, further work should be carried out for the months that are not covered by this work to authenticate the model for the year round.

ACKNOWLEDGEMENT

The authors would like to acknowledge the un-quantifiable contributions made by Dr T.K. Philip, of the Department of Agricultural and Environmental Engineering, University of Agriculture Makurdi, Nigeria.

REFERENCES

[1] Awachie, I.R.N. (1985). Use of Solar Energy in the Drying of Fish in Nigerian Environment. *Nigerian Journal of Solar Energy*. Vol. 14: 123-138.

[2] Sukhatme, S.P. (1984): Principle of Thermal Collection and Storage. Tata McGraw Hill Publishing Co.Ltd.

[3] Reikard, G (2009). Predicting Solar Radiation at High Resolution; A Comparison of Time Series Forecasts; *Solar Energy* Vol.83 (3); 342-349.

[4] Umar I.H., Iloje, O.C. and Bala, E.J. (2000). Review of Renewable Energy Technologies in Nigeria. *Nigerian Journal of Renewable Energy*. Vol. 8 (1&2); 99-109.

[5] Iloje, O.C (1997). Renewable Energy Application in Nigeria; Energy Commission of Nigeria, GILS Parco Ltd. Lagos-Nigeria.

[6] Iwe, G.O. (1998). Energy Option in the Industrialization and Development Process of the Nation, What Role for Coal; Bulletin Publication of the Central Bank. Vol. 22(4): 30-38.

[7] Ojoso, J.O (2005). Solar Radiation Map for Nigeria. *Nigerian Journal of Solar Energy*. Vol. 8:370-381.

[8] Awache, I.R.N. and Okeke, C.E. (1985). The Effect of Climatological Factors on Total Solar Radiation in Some Towns in Nigeria. *Nigerian Journal of Solar Energy*, Vol. 4:53-58.

[9] Al-Ajlan S.A., H. Al Faris, H. Khonkar. 2003. "A Simulation Modeling for Optimization of Flat Plate Collector Design in Riyadh, Saudi Arabia" *Renewable Energy* 28(No.): 1325-1339.

[10] Alfayo R. and C. B. S. Uiso. 2002. "Global Solar Radiation Distribution and Available Solar Energy Potential in Tanzania"; *Physical Scripta*. T97, 91-98.

[11] Kuje, J.Y., Itodo, I.N. and Victor I.U. (2011): A Model for Determining the Global Solar Radiation for Makurdi, Nigeria; *International Journal for Renewable Energy*; Elsevier. Vol. 36(7):0960-1481.

[12] Burari, F.N. and Sambo, B.S. (2003). Analysis of Monthly Average Daily Global Solar Radiation for Bauchi, Nigeria. *Nigerian Journal of Tropical Engineering* Vol.4:26-31.

[13] Ejeh, A.C. (2009). A model for determining solar radiation for Makurdi, Unpublished M.Eg Thesis Department of Mechanical Engineering University of Agriculture, Makurdi.

[14] Kituu, G.M., D. Shitanda, C.L. Kanali, J.T. Mailutha, C.K. Njoroge, J.K. Wainaina and J.S. Bongyereire, (2010). A Simulation Model for Solar Energy Harnessing By the Tunnel Section of a Solar Tunnel Dryer. *Agricultural Engineering International: The CIGR Ejournal*. Manuscript 1553. Vol. XII. January, 2010

[15] Stine, W.B and Harrigan, R.W. (1985). *Solar Energy Fundamentals and Design with Computer Applications*. John Wiley and Sons, New York.

[16] Page, J.K. (1986). Prediction of Solar Radiation on inclined Surface. D. Reidel Publication Co. Dordrecht

[17] Nwokoye, A.O.C. (2006). *Solar Energy Technology; Other Alternative Energy Resources and Environmental Issues*; Rex Charles and Patrick Ltd, Nimo, Anambra State, Nigeria Pp1-404.

[18] Montero, G., Escolar, J.M., Rodriguez, E and Montenegro, R. (2009). Solar Radiation and Shadow Modelling with Adaptive Triangular Meshes; *Solar Energy*. Vol.83 (7): 998-1012.

[19] Lunde, P.J. (1980). *Solar Thermal Engineering*; John Wiley and Sons, New York.

[20] Kreidder, J.F. and Kreith .F. (1981). *Solar Energy Handbook*. McGraw- Hill, New York.

[21] Coulson, V.L. (1975). *Solar and Terrestrial Radiation*. Academic Press, New York.

[22] Pidwirny, M. (1999/2006). *Fundamentals of Physical Geography*; University of British Columbia- Okanagan.

[23] Suri, M and Hofierka, J. (2002). The Solar Radiation Model for Open Source GIS: Implementation and Applications. In Benciolin, B, Goui, M, Zatlip(eds) proceedings of the open Source GIS users conferences, Trento Italy; Pp1-15.

[24] Onwualu, A.P; Akubuo, C.O and Ahaneku, I.E. (2006). *Fundamentals of Engineering for Agriculture*; Immaculate Publication Ltd Enugu-Nigeria Pp313.

[25] Kuje, Y.J. (2010). An Empirical Mathematical Model for Estimating the Monthly Average Daily Global Solar Radiation for Makurdi, Benue State, Nigeria. Unpublished Phd. Thesis department of Agriculture and Environmental Engineering. University of Agriculture Makurdi.

[26] Zarzalejo, L.F., Polo, J., Ramirez, L and Espinar, B. (2009). A New Statistical Approach for Deriving Global Solar Radiation from Satellite Images. *Solar Energy* Vol.83 (4); 480-484.

[27] Muneer, T (1997). *Solar Radiation and Daylight Model for the Energy Efficient Design of Building*; Reed Educational and Professional Publishing Ltd. New Delhi, Singapore.

THE SIXTH SENSE OF HUMAN?...

(A New theory on “Sleepless Human”)

¹M.Arulmani, B.E. , ²V.R.Hema Latha,

¹(Engineer)

²M.A., M.Sc., M.Phil. (Biologist)

ABSTRACT: Animals and lower animals do not have **sixth Sense?...** **NO...NO....NO...** All living organism as well as non-living organism considered also have 6th sense in gradient order.

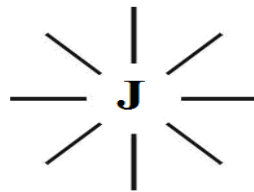
- i. Which University **mosquito** studied to gain Techniques and cleverness to bite on the back beyond the reach of human hands?...
- ii. How the birds and Animals could predict the signals well in advance and move safely to other elevated places during “**TSUNAMI 2004**” Which human could not predict?...
- iii. How the pet dog could steel the chicken waste silently in the kitchen when owner under sleep?...
- iv. How honey bee, spider construct well defined knitted structure house?...

This Scientific research article focus that not only human, all lower animals including Bacteria, Virus have “**Intuition Sense**” (Wisdom).

However human shall be considered as having “**highest level**” of sensory perception and 6th sense compared to other lower animals on origin.

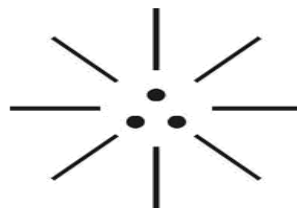
It is further focused that the 6th sense level of human and Animals shall be considered like a “**Communication link**” to the “**Master control unit**” of the white hole region of Universe in a systematic Networking pattern called as “**J-GATE**” (or) “**e-logics**”. The region of J-Gate shall also be called as **6th sense domain**.

(i)



(Universal Control Unit)

(ii)



(Three Domain Logic)

- i. Right dot represents “**Functional region**”
- ii. Left dot represents “**Structural region**”
- iii. Centre dot represents “**6th Sense**” **Sequential logic region**.

“Prayer, Meditation are like “wireless communication link” to master control unit of Universe. Sometime signal may fail. But let us dial continually to resort to the sixth sense link. Death shall be considered as the state of deep subconscious mind.”

- Author

KEY WORDS:

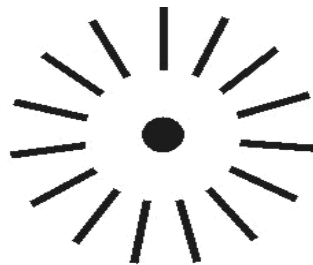
- a) Philosophy of **Brain**?...
- b) Philosophy of **Sleepless human**?...
- c) Philosophy of **Gamma mind human**?...
- d) Philosophy of **Beta mind human**?...
- e) Philosophy of **Alpha mind human**?...
- f) Philosophy of **Death**?...
- g) Etymology of word **6th Sense**?...
- h) Philosophy of **Spirit and Soul**?...

I. INTRODUCTION

It is focused that there are currently so many theories about 6th sense, Common sense, Intelligence, Intuition, Conscious mind, Subconscious mind, Coma mind...

What really “**MIND**” means?...

- i. Mind is source of Brain?..
- ii. Mind is matter (or) Energy?...
- iii. Mind is controller (or) Processor?...



(Mind Logo)

“Mind is like “Fuel”; Brain is like “Energy” derived from fuel. Mind is like “Spirit”, Brain is like “Soul” derived from spirit”,

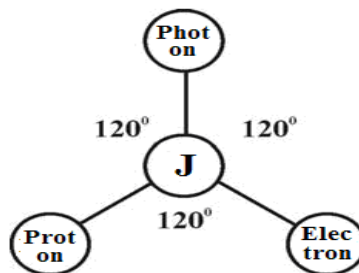
- Author

II. HYPOTHESIS

a) What “**Brain**” is made up of?...

“**Big Bang theory**” focus that the Universe is believed to have been formed **13.7 Billion Years** ago from “**cloud of star dust**”. If so “**Brain**” is the source of “**Stardust**”?...

It is hypothesized that “**BRAIN**” shall be considered as White plasma matter derived from “**J-RADIATION**” composed of fundamental “**ions**” of Photon, Electron, Proton having “**Zero mass**”. The smallest unit of white plasma (plasma mind) shall be called as “**BRAIN CELL**”.



(Brain Cell)

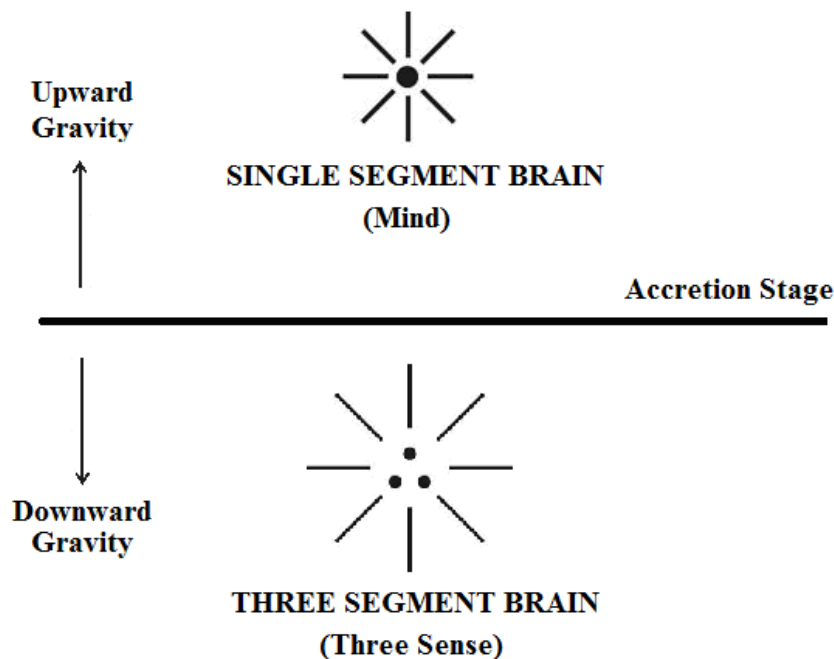
- i. Proton ion is like “DNA”
- ii. Electron ion is like “HORMONE”
- iii. Photon ion is like “RNA”
- iv. “J-RADIATION” is like “MIND”

MIND is like “Central Core” of brain. The philosophy of mind shall be defined within the following scope.

- i. Mind shall also mean “Sixth Sense” (Master Control unit)
- ii. Mind is the source of “All Senses”
- iii. Mind is like “White Element” free from Hydrogen, Carbon, Nitrogen, ozone.

b) Mind differs from Brain?...

It is hypothesized that “MIND” shall be considered as source of “BRAIN”. The Brain cell shall be considered as composed of Particles of **Photon, Electron, Proton** having little **higher mass** compared to ions of mind. The philosophy of MIND, BRAIN shall be described as below. Mind shall mean “SINGLE SEGMENT BRAIN” (only wisdom)



It is hypothesized that the fundamental three-in-one segmental region of Brain shall be considered as master control unit comprise of three most fundamental “SENSES” (i.e) “OPTIC SENSOR“, “ELECTRIC SENSOR”, “MAGNETIC SENSOR”.

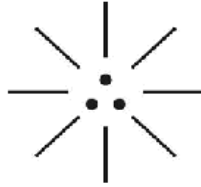
- i. Right dot is like “MAGNETIC” (Right Nostril)
- ii. Left dot is like “ELECTRIC” (Left Nostril)
- iii. Centre dot is like “OPTIC” (Sixth Sense Logic)

“In proto Indo Europe language the MIND, BRAIN shall be called as “MATHI-e”, “MUTHI-e”

- Author

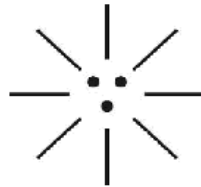
c) Philosophy of conscious mind, Subconscious mind?...

It is hypothesized that “Subconscious mind” shall be considered as the Transformed stare of “Conscious mind” having distinguished varied characteristics as described below.



(CONSCIOUS STATE)

Transformation &
Plasma barrier



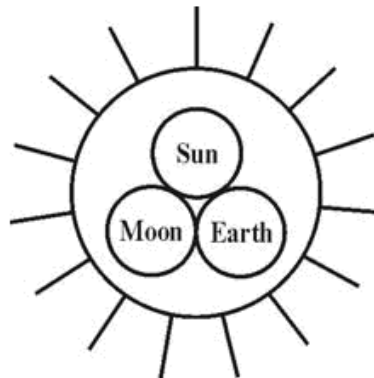
(SUBCONSCIOUS STATE)

- i. Right dot – Common sense domain
- ii. Left dot – Intelligence domain
- iii. Centre dot – Intuition domain

d) Philosophy of Universal “SERVER” (CPU)?...

It is focused that “MIND” is considered as the “MASTER CONTROL UNIT” of universal Brain system. If so what about **Server Unit (CPU)?**... The whole cosmo Universe shall be considered like a **nuclear bomb** comprise of three in one nuclei **Sun, Earth, Moon**.

It is hypothesized that Universal server shall be considered as responsible for **automatic change over** among the “**three domain**” of control unit based on **predefined programmer** called as “**e-Logics**”. The philosophy of “**Universal Server**” shall be described as below.



(Universal Server CPU)

- i) Sun is like **Dark Spirit**
- ii) Moon like **Dark Soul**
- iii) Earth is like **Dark Energy**

It is focused that the relative position of **SUN, EARTH, MOON** shall consider play Vital role for evolution of three distinguished families of MIND, BRAIN system of Human, Animals in “**Three Nuclear Ages**”.

i)	Conscious mind human (white mind)	Human Origin state (Mars Planet)
ii)	Subconscious mind human (Black Mind)	Transformation state to earth
iii)	Gamma mind human (Blue Mind)	1 st generation
iv)	Beta mind human (Green Mind)	2 nd generation
v)	Alpha mind human (Red Mind)	3 rd generation

e) Etymology of word “Sixth sense”?...

Case study shows that ‘Sixth sense’ is considered as the ability to perceive the subtle dimension (or) the unseen world of **Angels, ghosts, heaven** beyond the normal five senses (ie) **smell, taste, sight, touch, and sound**. Extra sensory perception (ESP), clairvoyance, premonition, intuition are synonymous with sixth sense (or) subtle perception ability.

It is hypothesized that in the expanding universe “**J-RADIATION**” shall be considered as the “**SOUL**” of all radiations. The J-Radiation shall be considered as the highest of “**Energy level**” called as “**CHISU**” (OR) “**CHULE**” in proto Indo Europe language. The other five radiations shall be considered as evolved in different phases in the expanding universe having different energy level exist in Tier formation of different Layers. In other words “**J-RADIATION**” shall be considered as the “6th level” (highest energy level) Radiation. The “**J-RADIATION**” shall be considered as primitive stage to “**PLASMA MATTER**” called as “**ALASMA MATTER**”.

f) Prehistoric human had only single type Blood?...

It is hypothesized that the prehistoric human (**Angel population**) had only single type Blood “**AB**” (Universal acceptor) called in Proto Indo Europe language as “**OTHIRAM**”. Othiram shall mean natural Alasma matter composed of ions of **photon, Electron, proton** and free from Hydrogen, Carbon, Nitrogen ozone. The othiram shall be considered responsible for inducing “**Super consciousness**”. It is speculated that after the birth of **first sunlight** on the Earth planet other types of blood might be evolved in three nuclear ages under different environment condition and categorized as below:

i)	Angel family (white mind)	AB type only (ions behavior)
ii)	Gamma mind human (Blue mind)	AB type only (particles behavior)
iii)	Beta mind human (Green mind)	AB, A, B type only (Molecules behavior)
iv)	Alpha mind human (Red mind)	AB, A, B, O type (Complex matter)

It is further hypothesized that Birth of “**Oxygen Breath**” shall be considered as responsible for increase in Intelligence level and reduction in Wisdom level. Further emotional feelings such as fear, worry, stress shall be due to oxygen breath.

“The blood type of ADAM, EVE (Angel family) shall be considered as single blood type AB”

- Author

g) Philosophy of White clay?...

The Author of this article when doing 9th standard (Rural school) one day was scolded by class teacher and saying that Do you have **BRAIN** (or) “**CLAY**”. If so, **BRAIN** is associated with **CLAY**?.... It is hypothesized that in proto Indo Europe language “**BRAIN**” shall be called as “**KALI MANNU**”. “**KALIMANNU**” shall mean “**white clay**” composed of ions of **Photon, Electron, Proton** and free from Hydrogen, Carbon, Nitrogen, ozone.

It is hypothesized that **ADAM, EVE** might have had “**white clay**” before consuming forbidden fruit and under the state of highly conscious. After consuming forbidden fruit white clay might have become “**brain**” by brain cell acquiring higher mass which led to deep “**subconscious state**”.

h) What does mean “Death”?...

It is hypothesized that “**Death**” shall be considered as the state of deactivation of “**SOUL**” from “**J-RADIATION**” and exist under **deep subconscious state**. It shall be **reactivated** if required at later just like “**SIM NUMBER**” in the mobile communication system.

i) Philosophy of sleepless human Ancestor?...

It is hypothesized that “**Human Ancestor**” stated living in “**MARS PLANET**” and descended to **EARTH PLANET** even before origin of **first sun light emission**. The Human Ancestor in the early Universe could breath only “**WIND**” composed of only ions of Photon, Electron, Proton and free from Hydrogen, Carbon, Nitrogen, Ozone. The Hydrogen, carbon, Nitrogen, ozone considered originated only **after origin of Sun light emission**.

Further in the early Universe the “**WIND Breath**” ancestor (**Angel family**) (single segment Brain) shall be considered as having distinguished from **modern human**. The wind Breath ancestor shall also be called as “**Sleepless**” and “**Highly conscious**” state of human. It is hypothesized that modern human could start sleep subsequently gradually due to different Breath in different Nuclear age as described below.

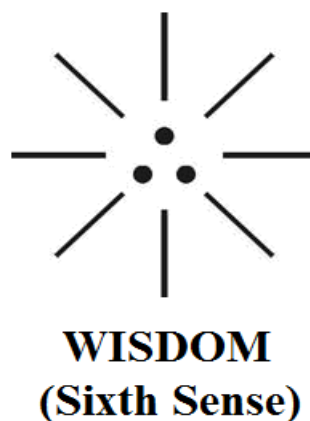
i)	Wind Breath (MARS Planet)	Sleep less state human
ii)	Transformation State to Earth	Subconscious State human (Deep sleep)
iii)	Ozone Breath	Semi awakening state human
iv)	Oxygen Breath	Wakening state human

It is hypothesized that different level of subconscious state may be due to variation in Oxygen level as described below.

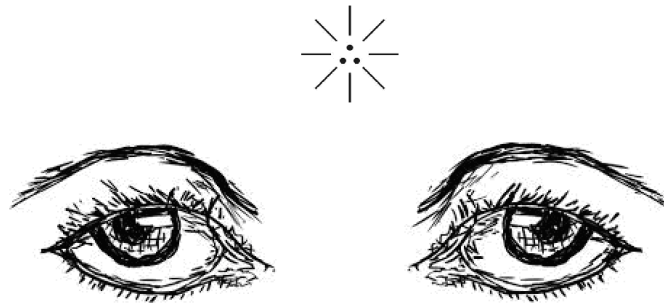
- i. Active waken state - **High level Oxygen Breath.**
- ii. Sleep state - **Decreased Oxygen level Breath**
- iii. Semiconscious state - **low level Oxygen breath**
- iv. Subconscious state - **Ozone level Breath**
- v. High conscious state - **Wind Breath**
- vi. Death state - **Absence of “J-RADIATION”**

The model “**Sleepless Ancestor**” shall be narrated as below.

(i)



(ii)

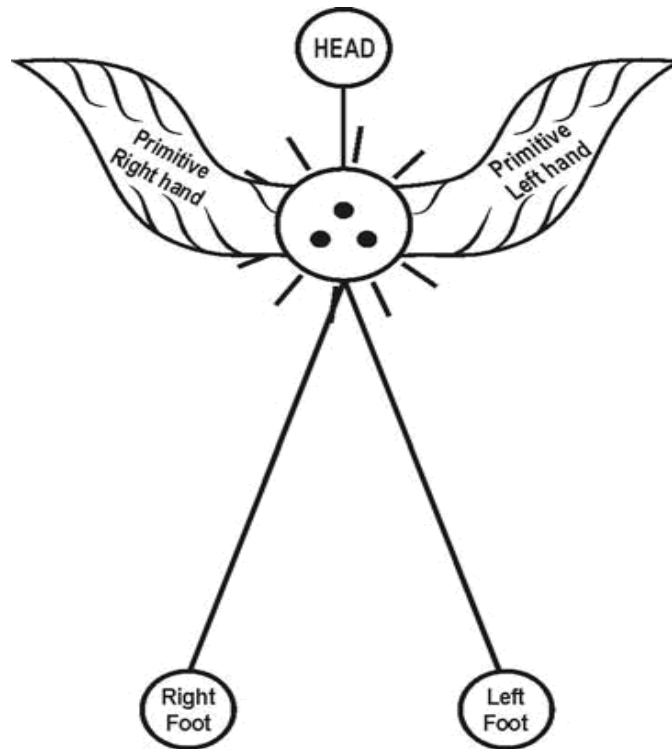


THAI-e (Universal CPU)

In the early universe the “**Sleepless Ancestor**” (100% wisdom) shall be considered as highly Wise, Psychic, Energetic, could not speak through sensory means but could understand on mere **VISION**.

j) Case study on Bible

It is hypothesized that **ADAM, EVE** before consuming **forbidden fruit** could breath **wind** in the early universe and **Sleepless** and could obey the command of **CREATOR** always. After consuming the “**forbidden fruit**” they might have transformed into **deep sleep state** and could be under **Highly Subconscious state** somewhere on the Earth and hence the creator started searching for him and called “**ADAM WHERE ARE YOU**”?...

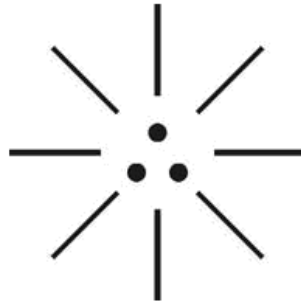


MODEL ADAM (Angel Family)

III. CONCLUSION:

It is focused that “**Absolute wisdom**” state of Brain shall be considered as the Absolute level of “**6th sense**” (100% wisdom) of human. The state of Wisdom could be gradually decreased due to consistent increase in “**BRAIN CELL MASS**” in three Nuclear ages. The wisdom state level of modern human shall be considered around only **10%** but “**Intelligence**”, **Common sense**” resorted to **70%**, **20%** respectively.

It is further focused that **RESPIRATORY SENSE** shall be considered as the most fundamental sense and shall be considered as responsible for “**SIXTH SENSE OF HUMAN**”.



(NOSTRIL)

- i. Right dot - Magnetic Sense (Source of commonsense)
- ii. Left dot - Electric Sense (Source of Intelligence)
- iii. Center dot - Optic Sense (Source of Intuition)

“Common sense is the collection of prejudices acquired by age 18”

- Albert Einstein

IV. PREVIOUS PUBLICATION:

The philosophy of origin of first life and human, the philosophy of model Cosmo Universe, the philosophy of fundamental neutrino particles have already been published in various international journals mentioned below. Hence this article shall be considered as **extended version** of the previous articles already published by the same author.

- [1] Cosmo Super Star – IJSRP, April issue, 2013
- [2] Super Scientist of Climate control – IJSER, May issue, 2013
- [3] AKKIE MARS CODE – IJSER, June issue, 2013
- [4] KARITHIRI (Dark flame) The Centromere of Cosmo Universe – IJIRD, May issue, 2013
- [5] MA-AYYAN of MARS – IJIRD, June issue, 2013
- [6] MARS TRIBE – IJSER, June issue, 2013
- [7] MARS MATHEMATICS – IJERD, June issue, 2013
- [8] MARS (EZHEM) The mother of All Planets – IJSER, June issue, 2013
- [9] The Mystery of Crop Circle – IJOART, May issue, 2013
- [10] Origin of First Language – IJIRD, June issue, 2013
- [11] MARS TRISOMY HUMAN – IJOART, June issue, 2013
- [12] MARS ANGEL – IJSTR, June issue, 2013
- [13] Three principles of Akkie Management (AJIBM, August issue, 2013)
- [14] Prehistoric Triphthong Alphabet (IJIRD, July issue, 2013)
- [15] Prehistoric Akkie Music (IJST, July issue, 2013)

- [16] Barack Obama is Tamil Based Indian? (IJSER, August issue, 2013)
- [17] Philosophy of MARS Radiation (IJSER, August 2013)
- [18] Etymology of word “J” (IJSER, September 2013)
- [19] NOAH is Dravidian? (IJOART, August 2013)
- [20] Philosophy of Dark Cell (Soul)? (IJSER, September 2013)
- [21] Darwin Sir is Wrong?! (IJSER, October issue, 2013)
- [22] Prehistoric Pyramids are RF Antenna?!... (IJSER, October issue, 2013)
- [23] HUMAN IS A ROAM FREE CELL PHONE?!... (IJRD, September issue, 2013)
- [24] NEUTRINOS EXIST IN EARTH ATMOSPHERE?!... (IJERD, October issue, 2013)
- [25] EARLY UNIVERSE WAS HIGHLY FROZEN?!... (IJOART, October issue, 2013)
- [26] UNIVERSE IS LIKE SPACE SHIP?!... (AJER, October issue, 2013)
- [27] ANCIENT EGYPT IS DRAVIDA NAD?!... (IJSER, November issue, 2013)
- [28] ROSETTA STONE IS PREHISTORIC “THAMEE STONE” ?!... (IJSER, November issue, 2013)
- [29] The Supernatural “CNO” HUMAN?... (IJOART, December issue, 2013)
- [30] 3G HUMAN ANCESTOR?... (AJER, December issue, 2013)
- [31] 3G Evolution?... (IJRD, December issue, 2013)
- [32] God Created Human?... (IJERD, December issue, 2013)
- [33] Prehistoric “J” – Element?... (IJSER, January issue, 2014)
- [34] 3G Mobile phone Induces Cancer?... (IJERD, December issue, 2013)
- [35] “J” Shall Mean “JOULE”?... (IRJES, December issue, 2013)
- [36] “J”- HOUSE IS A HEAVEN?... (IJIRD, January issue, 2014)
- [37] The Supersonic JET FLIGHT-2014?... (IJSER, January issue, 2014)
- [38] “J”-RADIATION IS MOTHER OF HYDROGEN?... (AJER, January issue, 2014)
- [39] PEACE BEGINS WITH “J”?... (IJERD, January issue, 2014)
- [40] THE VIRGIN LIGHT?... (IJCRAR, January issue 2014)
- [41] THE VEILED MOTHER?... (IJERD, January issue 2014)
- [42] GOD HAS NO LUNGS?... (IJERD, February issue 2014)
- [43] Matters are made of Light or Atom?!... (IJERD, February issue 2014)
- [44] THE NUCLEAR “MUKKULAM”?... (IJSER, February issue 2014)
- [45] WHITE REVOLUTION 2014-15?... (IJERD, February issue 2014)
- [46] STAR TWINKLES!?... (IJERD, March issue 2014)
- [47] “E-LANKA” THE TAMIL CONTINENT?... (IJERD, March issue 2014)
- [48] HELLO NAMESTE?... (IJSER, March issue 2014)
- [49] MOTHERHOOD MEANS DELIVERING CHILD?... (AJER, March issue 2014)
- [50] E-ACHI, IAS?... (AJER, March issue 2014)
- [51] THE ALTERNATIVE MEDICINE?... (AJER, April issue 2014)
- [52] GANJA IS ILLEGAL PLANT?... (IJERD, April issue 2014)
- [53] THE ENDOS?... (IJERD, April issue 2014)
- [54] THE “TRI-TRONIC” UNIVERSE?... (AJER, May issue 2014)

- [55] Varied Plasma Level have impact on “GENETIC VALUE”?... (AJER, May issue 2014)
- [56] JALLIKATTU IS DRAVIDIAN VETERAN SPORT?... (AJER, May issue 2014)
- [57] Human Equivalent of Cosmo?... (IJSER, May issue 2014)
- [58] THAI-e ETHIA!... (AJER, May issue 2014)
- [59] THE PHILOSOPHY OF “DALIT”?... (AJER, June issue 2014)
- [60] THE IMPACT OF HIGHER QUALIFICATION?... (AJER, June issue 2014)
- [61] THE CRYSTAL UNIVERSE?... (AJER July 2014 issue)
- [62] THE GLOBAL POLITICS?... (AJER July 2014 issue)
- [63] THE KACHCHA THEEVU?... (AJER July 2014 issue)
- [64] THE RADIANT MANAGER?... (AJER July 2014 issue)
- [65] THE UNIVERSAL LAMP?... (AJER July 2014 issue)
- [66] THE MUSIC RAIN?... (IJERD July 2014 issue)
- [67] THIRI KURAL?... (IJIRD August 2014 issue)

REFERENCE

- [1] Intensive Internet “e-book” study through, Google search and wikipedia
- [2] M.Arulmani, “3G Akkanna Man”, Annai Publications, Cholapuram, 2011
- [3] M. Arulmani; V.R. Hemalatha, “Tamil the Law of Universe”, Annai Publications, Cholapuram, 2012
- [4] Harold Koontz, Heinz Weihriah, “Essentials of management”, Tata McGraw-Hill publications, 2005
- [5] M. Arulmani; V.R. Hemalatha, “First Music and First Music Alphabet”, Annai Publications, Cholapuram, 2012
- [6] King James Version, “Holy Bible”
- [7] S.A. Perumal, “Human Evolution History”
- [8] “English Dictionary”, Oxford Publications
- [9] Sho. Devaneyapavanar, “Tamil first mother language”, Chennai, 2009
- [10] Tamilannal, “Tholkoppiar”, Chennai, 2007
- [11] “Tamil to English Dictionary”, Suravin Publication, 2009
- [12] “Text Material for E5 to E6 upgradaton”, BSNL Publication, 2012
- [13] A. Nakkiran, “Dravidian mother”, Chennai, 2007
- [14] Dr. M. Karunanidhi, “Thirukkural Translation”, 2010
- [15] “Manorama Tell me why periodicals”, M.M. Publication Ltd., Kottayam, 2009
- [16] V.R. Hemalatha, “A Global level peace tourism to Veilankanni”, Annai Publications, Cholapuram, 2007
- [17] Prof. Ganapathi Pillai, “Sri Lankan Tamil History”, 2004
- [18] Dr. K.K. Pillai, “South Indian History”, 2006
- [19] M. Varadharajan, “Language History”, Chennai, 2009
- [20] Fr. Y.S. Yagoo, “Western Sun”, 2008
- [21] Gopal Chettiar, “Adi Dravidian Origin History”, 2004
- [22] M. Arulmani; V.R. Hemalatha, “Ezhem Nadu My Dream” - (2 Parts), Annai Publications, Cholapuram, 2010
- [23] M. Arulmani; V.R. Hemalatha, “The Super Scientist of Climate Control”, Annai Publications, Cholapuram, 2013, pp 1-3



M.Arulmani, B.E



V.R.Hema Latha

Novel Microstrip Patch Antenna (MPA) Design for Bluetooth, IMT, WLAN and WiMAX Applications

Amarveer Singh¹, Ekambir Sidhu²

¹Student of Department of Electronics & Communication Engineering, Punjabi University, Patiala, Punjab, India

²Professor of Department of Electronics & Communication Engineering, Punjabi University, Patiala, Punjab, India

ABSTRACT: In this paper, a multi resonant MPA capable of operating satisfactorily in the frequency range of 2.39 GHz to 5.79 GHz have been proposed. The antenna has been designed using substrate of FR4 material having dielectric constant of 4.4 with a conducting radiating patch on the substrate and a conducting ground plane on the bottom side of substrate. The ground plane has been partially reduced to improve the antenna bandwidth. The antenna performance has been analyzed in terms of various antenna parameters such as return loss (dB), impedance bandwidth (GHz), gain (dB), directivity (dBi), Half power Beam width (Degree), current density and VSWR. The antenna has been designed and simulated using CST Microwave Studio (2010). The designed MPA is suitable to be used for Bluetooth, IMT, WLAN and WiMAX applications. The antenna has bandwidth of 3.40 GHz and VSWR of less than 2. The antenna has been successfully fabricated and tested. It has been observed that the practical results obtained by testing the fabricated antenna using Network analyzer E5071C closely matches with the theoretical results obtained by simulating the antenna design in CST MWS 2010.

KEYWORDS: Directivity, Gain, Half Power Beam width (HPBW), Reduced ground plane, Return loss (S_{11}), VSWR

I. INTRODUCTION

The microstrip patch antenna also termed as patch antenna, is usually fabricated on a dielectric substrate which acts as an intermediate between a ground plane at the bottom side of substrate and a radiating patch on the top of substrate [1]. The patch is made up of perfect electric conductor (PEC) material. The patch can be designed in many shapes like rectangular, circular, triangular, elliptical, ring, square and many more but the rectangular shape is widely used [1] because of the simplicity associated with the design. The selection of substrate is the most important parameter while designing an antenna. The substrate consists of a dielectric material which perturbs the transmission line and electrical performance of antenna. The size of an antenna is dependent on the dielectric constant of a substrate. The size of antenna is inversely proportional to dielectric constant i.e. higher is the dielectric constant, lower is the size of antenna [2]. There are variety of substrates available with different dielectric constants but in the antenna design, Fire Resistance 4 (FR4) material with dielectric constant of 4.4 has been used. The antenna can be fed by various methods like coaxial feed, proximity coupled microstrip feed and aperture coupled microstrip feed [3]. The feeding can be defined as a means to transfer the power from the feed line to the patch, which itself acts as a radiator. The microstrip feed line is commonly used in MPA design because it is relatively simple to fabricate [3]. The microstrip antenna has been commonly used for wireless applications because of small antenna size, low cost, light weight, better efficiency, ease of installation, ease of mobility, and is relatively inexpensive to manufacture on printed circuit board (PCB) of specific characteristics and dimensions. However, apart from its advantages, there are some drawbacks of MPA. It handles less power and has limited bandwidth [4].

The bandwidth of MPA can be improved by either using a slotted patch [5][6] or by using reduce ground plane [7]. The slot on the patch can be of any shape like H-slot, E-slot, circular, rectangular, etc. These techniques can also be used to improve the return loss along with the bandwidth enhancement. Different shapes of slots have different effect on antenna parameters. Slotting tends to improve the antenna performance in terms of return loss, bandwidth and VSWR.

II. ANTENNA GEOMETRY

Fig. 1 represents the top view of designed MPA. As shown in the Fig. 1, the shape of patch is rectangular with two rectangular slots (marked - dijk and lmno) cut on the patch, a rectangular notch (marked - abdc) added to the patch top and a step (efgh) between radiating patch and feed line. The patch has been fed by a feed line of certain specified width so as to properly match the antenna impedance with the port impedance for transfer of maximum power from port to the antenna. In Fig. 2, the bottom view of slotted MPA is shown. The ground plane has been designed at the bottom of substrate as shown in Fig. 2. The antenna is fabricated using FR4 substrate having dielectric constant of 4.4 and substrate thickness of 1.57 mm. The feed line width has been adjusted to make sure that the impedance of antenna is nearly 50 ohms so as to perfectly match with the connector impedance for maximum power transfer to antenna with minimal back reflections. The bottom of the substrate consists of ground plane which is partially reduced to improve antenna bandwidth. The dimensions of substrate, patch, feed, slots cut on patch, square notch on the patch and step are listed in Table 1.

TABLE 1: Antenna Parameters

Antenna Parameters	Specifications
Substrate Dimensions (Ls x Ws)	70 x 60 mm
Patch Dimensions (Lp x Wp)	14.4 x 26 mm
Slot 1 (L3 x W3)	5 x 2 mm
Slot 2 (L4 x W5)	8.5 x 5.2 mm
Notch ((L2-L3) x W3)	1 x 1 mm
Step ((L5-L6) x W9)	1.6 x 6 mm
Feed line Dimensions (Wf x Lf)	22 x 5.6 mm
Ground Dimensions (Lg1 x Wg)	23 x 60 mm
Ground Slot (Lg3 x (Wg - (Wg1 + Wg2)))	0.5 x 0.9 mm

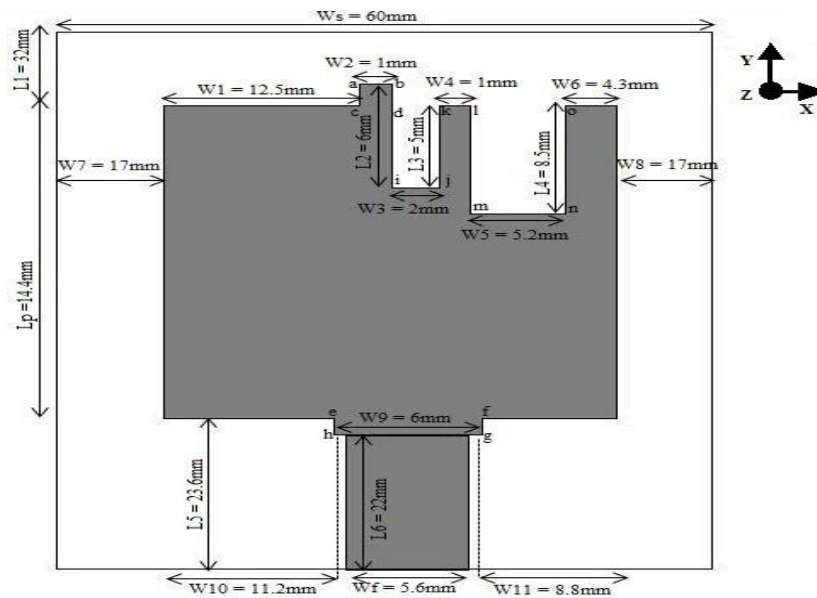


Fig.1 Top view of slotted MPA

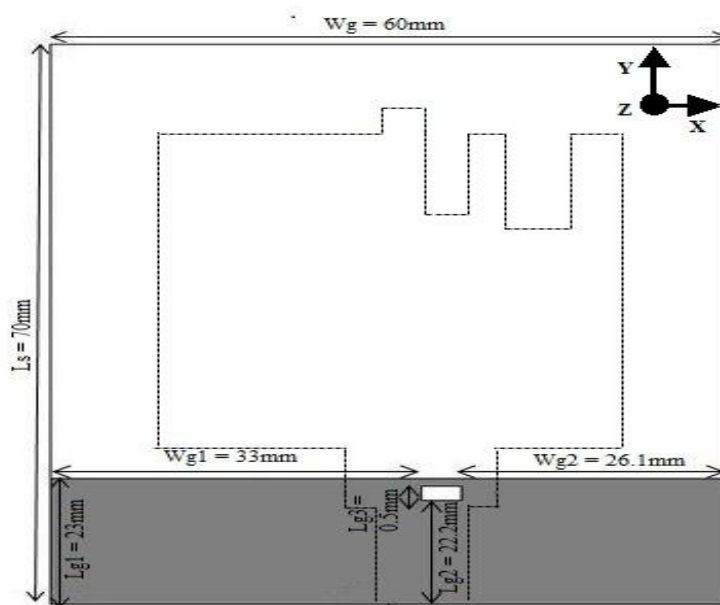


Fig.2 Bottom view of slotted MPA

Note: The dotted portion represented in Fig.2 indicates the projection of patch and feed line on ground.

III. ANTENNA GEOMETRY

The designed slotted antenna have been simulated using CST Microwave Studio 2010 and the performance of the antenna has been analyzed in terms of return loss, VSWR, radiation pattern, directivity, impedance, HPBW(Half Power Beam width) and gain. The experimental results have been also obtained using E5071C ENA series network analyzer and concluded that the practical results closely matches with the simulated theoretical results.

Return Loss : Fig. 3 represents the simulated results of return loss (s_{11}) for designed antenna. Practically, the return loss should be less form minimal back reflections. The return loss has been measured at the resonant frequencies. It has been observed that the return loss is -37.16 dB at 2.62 GHz, -25.26 dB at 3.8 GHz and -30.87 dB at 4.61GHz. The simulated bandwidth of proposed antenna is 3.40 GHz.

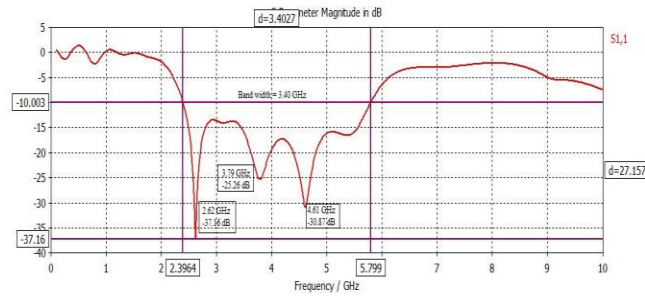


Fig. 3 Return loss plot of Slotted MPA

Directivity : The directivity at resonant frequencies has been obtained and analyzed. Fig. 4(a), Fig. 4(b) and Fig. 4(c) shows the 3D plot of directivity of slotted MPA at resonant frequencies of 2.62 GHz, 3.8 GHz and 4.61 GHz, respectively. The directivity is 2.61 dBi at 2.62 GHz, 3.66 dBi at 3.8 GHz and 3.5 dBi at 4.61 GHz.

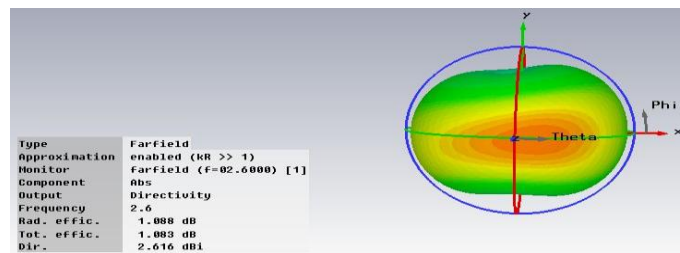


Fig. 4(a) 3D plot of Directivity of MPA at 2.6 GHz

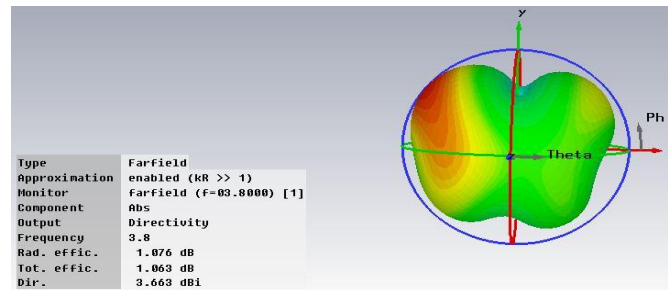


Fig. 4(b) 3D plot of Directivity of MPA at 3.8 GHz

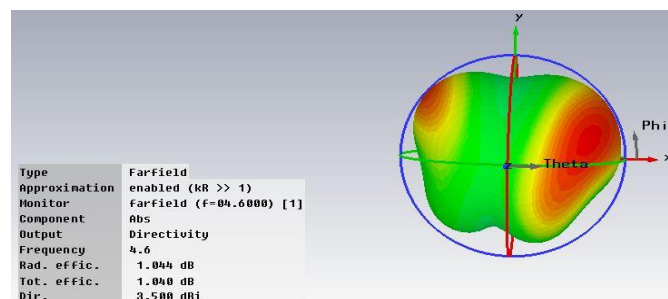


Fig.4(c) 3D plot of Directivity of MPA at 4.6 GHz

Gain

Fig. 5(a), Fig. 5(b) and Fig. 5(c) illustrates the 3D plot of gain for slotted MPA at resonant frequencies 2.62 GHz, 3.8 GHz and 4.61 GHz. The 3D plot shows that the gain is 3.7 dB at 2.62 GHz, 4.73 dB at 3.8 GHz and 4.54 dB at 4.61 GHz, respectively.

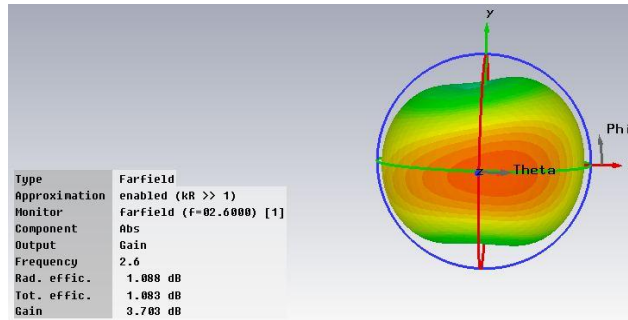


Fig. 5(a) 3D plot of Gain of slotted MPA at 2.6 GHz

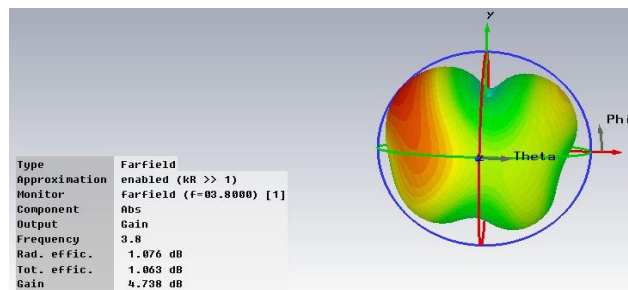


Fig. 5(b) 3D plot of Gain of slotted MPA at 3.8 GHz

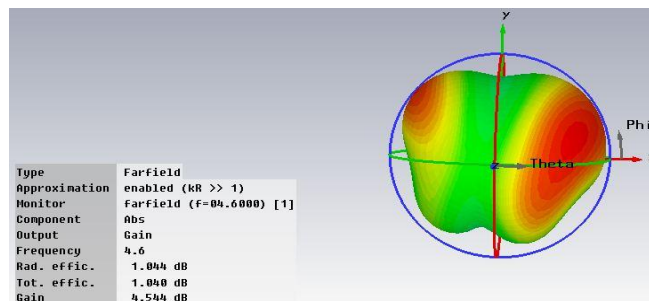


Fig. 5(c) 3D plot of Gain of slotted MPA at 3.8 GHz

Half Power Beam Width (HPBW)

Fig. 6(a), Fig. 6(b) and Fig. 6(c) indicates the half power beam width (HPBW) at resonant frequencies 2.62 GHz, 3.8 GHz and 4.61 GHz, respectively. The half power band width plot indicates the angular width (in degrees) in which maximum power is radiated by antenna. The Fig. 6(a), Fig. 6(b) and Fig.6(c) show that the angular width (3dB) at resonant frequency of 2.62 GHz is 83.3 degree, at 3.8 GHz is 77.0 degree and at 4.61 GHz is 90.1 degree, respectively.

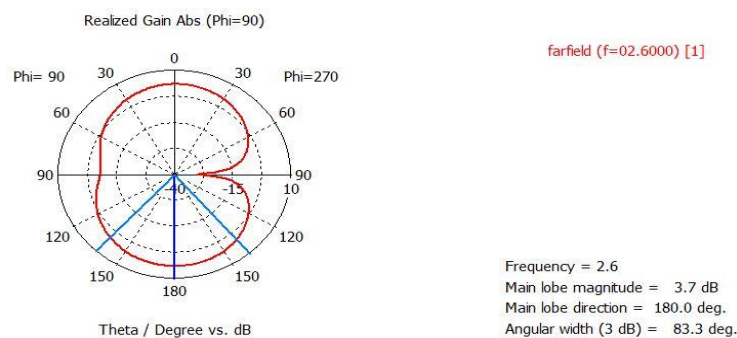


Fig. 6(a) HPBW plot of slotted MPA at 2.62 GHz

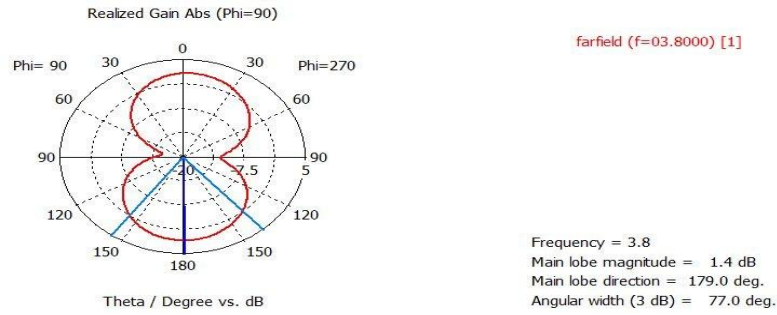


Fig. 6(b) HPBW plot of slotted MPA at 3.8 GHz

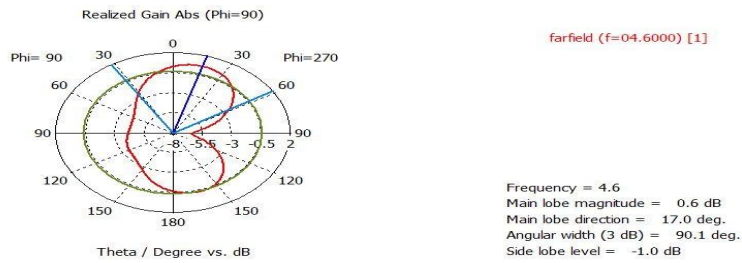


Fig. 6(c) HPBW plot of slotted MPA at 4.61 GHz

VSWR

Fig. 7 depicts the simulated VSWR plot for designed MPA. Practically, the required value of VSWR should be less than 2. Fig. 7 show that value of VSWR for designed MPA is less than 2 in the operating frequency range of 2.39 GHz to 5.79 GHz.

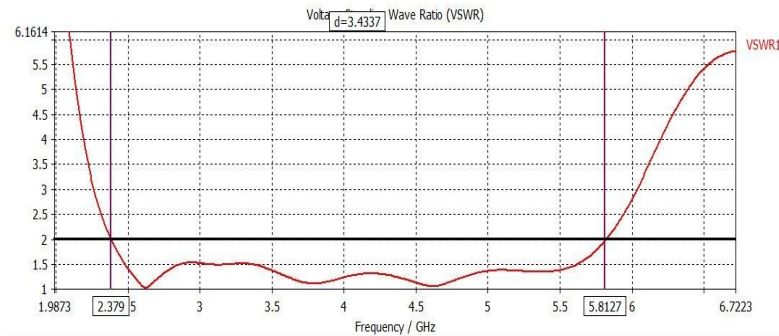


Fig. 7. VSWR plot of designed MPA

Smith Chart : Fig. 8 indicates Smith chart plot for designed MPA. The Smith Chart plot indicates that the variation of impedance of antenna with frequency. The value of impedance should lie near 50 ohms in order to perfectly match the port impedance with the antenna impedance for maximum transfer of power to antenna. The antenna impedance for designed MPA antenna is 49.85 Ω.

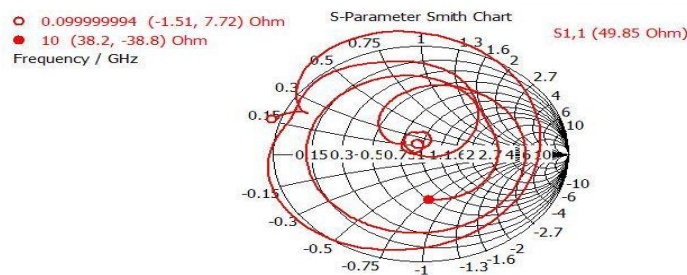


Fig. 8. Smith Chart plot of designed MPA

Current Density

The surface current (H-field) plot indicates the current distribution on the patch surface of antenna. The arrows indicate the direction of power flow back and forth per cycle from the feed to the patch. The arrows in forward direction indicate that the power is radiated in forward direction and the arrow in reverse direction indicates the power reflected back from antenna. The surface current plot at resonant frequencies of 2.6 GHz, 3.8 GHz, 4.61GHz is shown in the Fig. 9(a), Fig. 9(b) and Fig. 9(c), respectively.

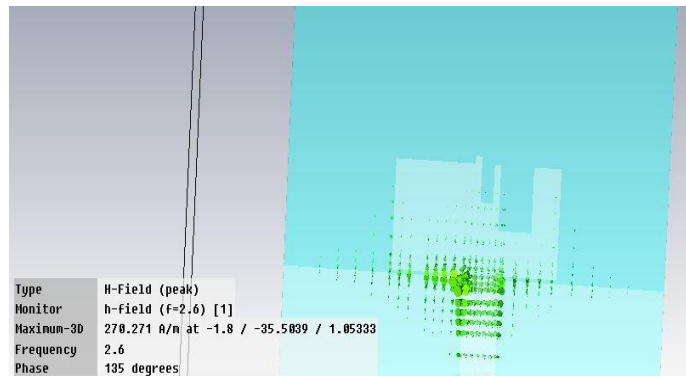


Fig. 9(a) Surface current plot of MPA at 2.62 GHz

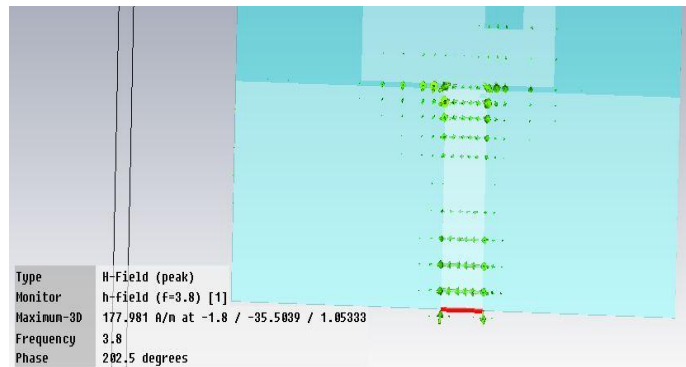


Fig. 9(b) Surface current plot of MPA at 3.8 GHz

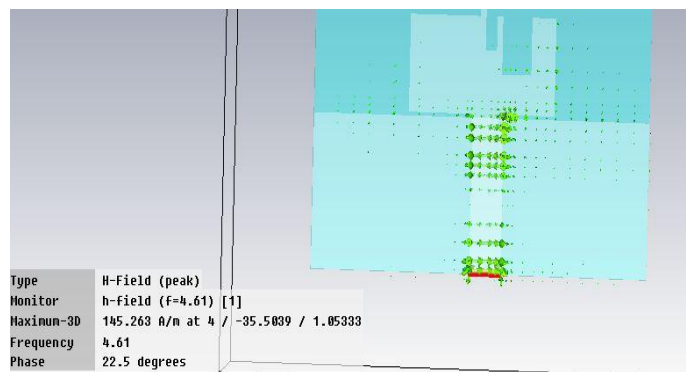


Fig. 9(c) Surface current plot of MPA at 4.61 GHz

IV. EXPERIMENTAL VERIFICATION

The proposed antenna has been physically designed as shown in Fig. 10 and tested using E5071C ENA series Network Analyzer. The Experimental practical results of designed slotted antenna are shown in Fig. 11. It has been observed that return loss at resonant frequencies of 2.62 GHz, 3.8 GHz, and 4.61 GHz is -24.89 dB, -20.925 dB, -28.991 dB, respectively. The bandwidth calculated from practical results of designed MPA is 3.23 GHz.



Fig. 10 Fabricated Microstrip Antenna

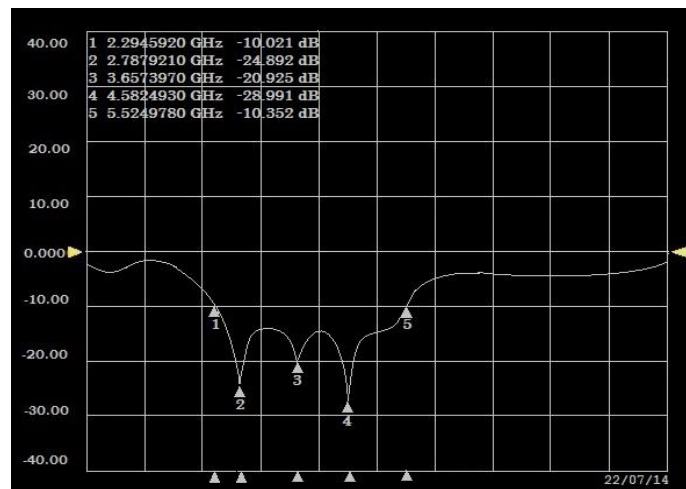


Fig. 11 Experimental Results for fabricated MPA

V. CONCLUSION

From the above discussion, it has been concluded that the slotted microstrip patch antenna has bandwidth of 3.40 GHz with operating frequency range from 2.39 GHz to 5.79 GHz and corresponding resonant frequencies are 2.62 GHz, 3.8 GHz and 4.61 GHz. The directivity corresponding to resonant frequencies of 2.62 GHz, 3.8 GHz and 4.61 GHz are 2.61 dBi, 3.66 dBi and 3.5 dBi, respectively. The gain at 2.62 GHz, 3.8 GHz and 4.61 GHz is 3.7 dB, 4.73 dB and 4.54 dB, respectively. The return loss is -37.16 dB at 2.62 GHz, -25.26 dB at 3.8 GHz and -30.87 dB at 4.61 GHz, respectively. The VSWR for slotted microstrip patch antenna is less than 2. The simulated results of the designed slotted antenna closely match with practical results. It has been observed that the practical results of designed MPA have return loss of -24.89 dB, -24.89 dB, -20.925 dB, -28.991 dB at 2.62 GHz, 3.8 GHz and 4.61 GHz, respectively. The bandwidth obtained from practical results of designed MPA has been 3.23 GHz having frequency range from 2.29 GHz to 5.52 GHz. The designed antenna is suitable to be used for Bluetooth (2.4 GHz to 2.5 GHz [8]), IMT (2.3 GHz to 2.4 GHz, 2.7 GHz to 2.9 GHz, 3.4 GHz to 4.2 GHz, 4.4 GHz to 4.9 GHz [8]), WLAN standard (2.4 GHz to 2.484 GHz, 5.15 GHz to 5.35 GHz, 5.725 GHz to 5.825 [8]) and WiMAX (2.5 GHz to 2.69 GHz, 3.4 GHz to 3.69 GHz, 5.25 GHz to 5.85 GHz [8]) applications [8].

REFERENCES

- [1] Ritu Goyal, Y.K. Jain, Compact Bow Shape Microstrip Patch Antenna with Different Substrates: Proceedings of 2013 IEEE Conference on Information and Communication Technologies (ICT), 2013.
- [2] C.A. Balanis, Antenna Theory Analysis and Design 2nd Edition (John Wiley & Sons, New York, 1996).
- [3] Neha Parmar, Manish Saxena, Krishnkant Nayak, Review of Microstrip Patch Antenna for WLAN and WiMAX Application, International Journal of Engineering Research And Applications, Vol. 4, Issue 1 (Version 1), January 2014, pp.168-171.
- [4] Sunil Kumar Rajgopal and Satish Kumar Sharma, Investigations on Ultrawideband Pentagon Shape Microstrip Slot Antenna for Wireless Communications, IEEE Transaction on Antennas and Propagation, Vol. 57, No. 5, May 2009.
- [5] Govardhani Immadi, K. Swetha, M.Venkata Narayana, M.Sowmya4, R.Ranjana, Design of microstrip patch antenna for WLAN applications using Back to Back connection of Two E-Shapes, International Journal of Engineering Research and Applications ,Vol. 2, Issue 3, May-Jun 2012, pp. 319-323.
- [6] Isha Puri, Bandwidth and Gain increment of microstrip patch Antenna with Shifted elliptical Slot, International Journal of Engineering Science and Technology (IJEST), Vol.3No.7, July, 2011.
- [7] M.K. Mohamed Amin, M.T. Ali, S.Saripuden, A.A Ab Aziz, Design of Dual Rectangular Ring Antenna with DGS Technique for Wireless Application: IEEE Symposium on Wireless Technology and Applications (ISWTA), September 23-26, 2012, Bandung, Indonesia.
- [8] <http://dSPACE.thapar.edu:8080/dSPACE/bitstream/10266/1783/1/thesis.pdf>

Impact of Maintenance Strategies on the Performance Of Industrial Facilities In Selected Industrial Estates In Lagos State, Nigeria

Oseghale, G.E

Department Of Building, Obafemi Awolowo University, Ile-Ife,
Osun State, Nigeria.

ABSTRACT : *The study appraised the facilities and the maintenance management strategies employed in selected industrial estates in Lagos State by identifying and examining facilities maintenance strategies, and determining their impact on the physical condition of the facilities. This was with a view to establishing the optimal strategies. Data were sourced using structured questionnaire administered on the staff of maintenance department of the industrial firms located in the estates, only building materials and plastic manufacturing industries were purposively selected. The Spearman correlation between reactive maintenance and the physical condition of the walls, roofs, floors, windows and doors, electrical fittings, plumbing, manufacturing plant, and generators had R values of 0.113, 0.24, 0.14, 0.26, 0.28, 0.23, 0.32, 0.41 respectively. The result showed a weak positive correlation (statistic) between reactive maintenance and the physical condition of the facilities. The result of analysis of variance (ANOVA) computed between types of maintenance strategies and the respondents' level of satisfaction on the physical condition of their facilities revealed that the different F values were all greater than 0.05 ($P > 0.05$). In other words there was no significant relationship between the types of maintenance strategies and the respondents' level of satisfaction with the physical condition of their facilities, thus the types of maintenance strategy currently used in the maintenance of industrial facilities had no influence on the physical condition of industrial facilities.*

KEY WORDS: *Maintenance, Strategies, Performance, Industrial facilities, Industrial estates.*

I. INTRODUCTION

Maintenance with respect to facilities and their services is a continued process of the construction industry. Maintenance has ceased to be considered a tactical subject with relevant repercussion regarding company cost, but not profits, and started to be viewed as having a strategic dimension, due to its implication in quality, availability, safety and cost, making it just another requirement for doing business [1, 2, 3]. As a result maintenance performance has direct influence on the fulfilling of the objectives established by an organisation, Consequently, the maintenance function is an important element of modern business and must be managed effectively [4]. Therefore, the need for adequate maintenance of the nations assets cannot be over emphasized, especially the industrial sector, which is generally believed to be the life wire of the nation's economy. The author in [5] noted that an effective maintenance management system might be characterized as the product of prudence, of the sentiment that "a stitch in time saves nine" The author in [6] maintained that good maintenance management systems are essential for economically viable and operationally safe facilities. Also, the author in [7] noted that recent research has identified a growing recognition by business managers that the standard of property and facilities management affects the organization as a whole in terms of cost efficiency, service delivery and performance, as well as protecting this substantial property asset. It is generally believed that Industrial sectors are not getting much subsidies and support from the government in real term as expected, and there is thus a greater need for proactive, rather than preventive maintenance management of these facilities [8]. Having an effective maintenance management system in place is critical for maintenance managers of industrial facilities to ensure that maintenance expenditure are kept to a minimum.

Many authorities have studied various aspects of plant maintenance in isolation neglecting such critical issues as the state and conditions of industrial facilities, the effects of maintenance strategies and the impact they have on operational performance of the industrial facilities. This study sought to bring the various aspects of industrial facilities maintenance together to provide a holistic view of the problem and to show how they collectively impact on maintenance of industrial facilities. Through this approach it is believed that maintenance managers of industrial facilities will have a better understanding of the problems and be able to formulate policies to guide their operations from strategy to operational performance. This study appraises facilities maintenance strategies with a view to determining their impact on the performance of industrial facilities. The research work covered only industrial facilities located within the selected industrial estates namely the buildings and facilities within, services, manufacturing plants, driven equipments and the overall cleanings of the surroundings. Only building materials and plastic manufacturing companies listed in the Nigeria business directory and located within the industrial estates were sampled for this research.

II. MAINTENANCE STRATEGIES

The author in [9] identified three strategies, namely: the reactive (day to day) repair preventive (including cyclic and condition-based) maintenance and upgrading. However they fail to include such other maintenance objectives such as satisfy specific and personal changes in taste and to fulfil statutory requirements. According to [10] maintenance manager can decide to carry out periodic maintenance at fixed intervals or carry out regular inspections or simply respond to user request after failure has occurred. The author in [11] believe that all maintenance actions are performed either in anticipation of an element's failure or to logically correct an existing defect. Other authors refer to proactive maintenance and reactive maintenance as planned and unplanned maintenance respectively [12, 13 cited in 14]. The author in [15] noted that maintenance strategy in general includes corrective, preventive or condition-based maintenance

Corrective Maintenance : It has been described as unplanned maintenance [16, 10, and 14]. But the word unplanned is not appropriate in that maintenance action is planned but the logistics of execution allows work to be done only after failure has occurred. The underlying concept is that ALL engineered items are known to fail or deteriorate with time and showing failure is expected or anticipated in facilities. Maintenance may then be FIXED-time OR UNFIXED-TIME based. In the case of reactive maintenance strategy, maintenance action is planned and executed in reaction to a failure occurrence (post failure planning). In this strategic sense, maintenance is in the form of repair work or replacement, and is only performed when facility has failed. Reactive maintenance is merely expressed as a maintenance strategy in which deed of maintenance is actually a reaction to a failure occurrence [17, 9, 18 and 19]. An effective maintenance unit is expected to draw up work programme stating standard procedure to follow upon failure of any component.

There is a strong correlation between safety incidents, injuries, and reactive maintenance. In a reactive situation, maintenance personnel may not take the time they should to plan and think before taking action. The urgent "must be fixed" situation also encourages maintenance crafts people to adopt so called "heroic" measures and take risks they should not take. A reactive, "run till it breakdown", maintenance strategy is often taken for low cost items such as light bulb replacement or for equipment with unpredictable lifespan that are so crucial to operations. The result of reactive maintenance is a steady degradation of equipment performance or a sudden breakdown of equipment. There are some industries that still survive by using a reactive approach, such as certain sectors of the food processing industry. Citing a few large bakeries, for instance they might have three lines running concurrently; if one fails the other two will take up the slack.

Planned Preventive Maintenance (PPM)

Planned maintenance is also known as forward maintenance and involves the forecasting of maintenance needs [20]. In planned preventive maintenance, works are scheduled to be carried out at predetermined times. PPM applies where the incidence of failure can be predicted with some accuracy or where the periods are fixed by statute or contract e.g. the terms in a lease requiring painting to be undertaken at fixed intervals [21]. According to the author in [22] planned maintenance is introduced to overcome the disadvantages of corrective maintenance with the primary objective of minimizing the total cost of inspection and repair and equipment downtime. It is maintenance which can be carried out while an item is in service. It is a concept which is probably more applicable to plant and equipment which is subject to mechanical wear but there are certain building elements which justify this treatment [21]. The author in [23 cited in 21] suggests that planned preventive maintenance is worthwhile if: is cost effective, intended to meet statutory or other legal requirements, meets a client need from an operating point of view, reduce the incidence of maintenance necessitating requisitions for work from user, there is a predominant incidence of work for the craftsman rather than pure inspection. In planned preventive maintenance,

planning and execution of maintenance work is carried out in anticipation of failure of facility (pro-active). Preventive maintenance, unlike corrective maintenance, is the practice of replacing components or subsystems before they fail in order to promote continuous system operation. The schedule for preventive maintenance is based on observation of past system behavior, component wear-out mechanisms and knowledge of which components are vital to continued system operation. Cost is always a factor in the scheduling of preventive maintenance. Reliability can also be a factor but cost is a more general term because reliability and risk can be expressed in terms of cost. In many circumstances, it is financially more judicious to replace parts or components that have not failed at predetermined intervals rather than wait for a system failure that may result in a costly disruption in operations.

Condition Based Maintenance (CBM) : This system is also called “Condition controlled maintenance and it presupposes that there will be inspection at appropriate intervals in order to determine by visual means or measure whether or not the condition of the elements or their performance has deteriorated below that laid down [21]. The author in [24] defined condition-based maintenance as “maintenance carried out in response to a significant deterioration in a unit as indicated by a change in a monitored parameter of the unit’s condition or performance while the author in [14] observed that under the CBM concept, a change in condition of the facility is the primary reason for carrying out maintenance on an item. Thus, the optimal time to execute maintenance work is determined from a condition survey, which shows the actual state of each constituent item in a facility. In the case of buildings, this entails physical close inspection of the structure and its external cladding, all internal surfaces and fittings [9].

The author in [25] researched on condition monitoring in the 21st century. He carried out a strategic review of CBM market place in order to identify and assess the changes occurring within the industry and opportunities and threats that the change represented to the organizations. The study outlined some of the key business opportunities and issues which are driving changes in the industry, some resulting trends were drawn and some condition regarding the implication of the trends for CBM equipment manufacturers suppliers and contractors. The author in [26] research investigated whether it is possible to retrospectively improve the quality of facilities failure histories stored in CMM systems. Finding revealed that it is possible to use the reliability centred maintenance and computerize maintenance management systems (RCM and CMMS) data in an ongoing manner and improved its usefulness over time as well as improve historical work orders. Research was carried out using engine data from HMAS Anzac on plant maintenance. The author in [25] study reviewed RCM and outlined some of the results that have been achieved, and how they have been achieved on different case study of maintaining mobile equipment. The study showed that the traditional approach to maintenance of mobile equipment based on fixed interval component replacement and overhaul is rapidly dying and in its place is a new framework for maintaining this equipment using condition based maintenance approaches, which focuses strongly on the consequences of failure. This work focuses mainly on plant neglecting other facilities that are also very important to the organization. The author in [27] conducted a CBM survey designed to determine present applications of CBM systems with industry. The study revealed that CBM is a globally accepted maintenance practice. CBM is most widely used within the manufacturing petroleum refining, chemical and associated products business sector. No study has examined the impact of maintenance strategies on the performance of industrial facilities in Nigeria, this study will attempt to fill this gap.

III. RESEARCH METHODOLOGY

The research procedure and methods employed in this research cut across the study population and data requirement, sample frame, sampling techniques, sample size, choice of data collection instruments, questionnaire design and techniques of data analysis and presentation. The study population was primarily the maintenance staff of building and plastics manufacturing industries registered with the manufacturers association of Nigeria and located within the selected industrial estates in Lagos state. Maintenance staff comprises technical and administrative staff of maintenance department, maintenance supervisors, and facilities maintenance managers. Data collected for this study were primary data quantitative and qualitative in nature. The primary data collected was through questionnaires administered on the staff of maintenance departments of building materials and plastic manufacturing companies in the selected industrial estates. The sample frame covers all the industrial estates in Lagos. Twenty Two (22) Industrial estates were identified in Lagos State based on information on directory of manufacturing companies prepare by Lagos State Ministry of Commerce, Industry and Tourism. Table 1 shows the list of Industrial Estates located in Lagos State. A total of twenty two (22) industrial estates were identified based on information from the directory of manufacturing companies. The statistically required sample size was calculated from the formula given by the author in [29] as follows:

$$n = n_1 / [1 + n_1 / N]$$

Where;

n = sample size

$n_1 = S_1/V_2$

N = total estimated population

V = standard error of the sampling distribution = 0.05

S_1 = Maximum standard deviation in population. Total error = 0.1 at a confidence level of 95% and $S_2 = (p)(1-P) = (0.5) \times (0.5) = (0.25)$ where p is a proportion of population elements that belong to a defined class. From this formula the sample size for the industrial estates obtained was $n = 18$

A total of three hundred and twenty two (322) companies are located within the industrial estates in Lagos state. For homogeneity of data only building materials and plastic manufacturing industries were purposively selected. There are 54 of such Companies on the register, using the same Sediary equation 35 firms was calculated as the sample size which were selected randomly A total number of thirty five (35) companies was used for this sample, for uniformity and convenience ten questionnaires were administered to the maintenance staff in each of the 35 industrial Firms selected giving a total of 350 questionnaires. In order to determine the relationship and the degree of impact the various maintenance strategies have on the performance of building elements/components correlation analysis were computed for the variables and also a chi- square tests was carried out in order to test the level of significant between the variables. In order to determine the influence on type of maintenance strategy on the respondents' level of satisfaction with the physical condition of industrial facilities analysis of variance was computed between the variables.

IV. DATA ANALYSIS AND DISCUSION OF RESULTS

Table 2 shows the correlation analysis between reactive maintenance strategy and the performance of building elements and facilities. Spearman correlation value for wall = 0.113. This shows that there is a weak positive correlation between reactive/corrective maintenance strategy the physical condition of the wall elements it also shows that only 11% of the wall elements is affected as a result of reactive maintenance strategy. The chi square tests calculated is 0.061 which is greater than 0.05 and therefore shows that there is no significant relationship between reactive/corrective maintenance and the physical condition of the wall. Specimen's correlation has R. value of Roof = 0.240, this means that there is a positive correlation between reactive maintenance strategy and the physical condition of the roof, but the relationship is weak. It also shows that only 24% of the performance of roof element was as a result of corrective/reactive maintenance strategy. The chi-square calculated is equal to 0.006 which is less than 0.05 and therefore means that there is a significant relationship between reactive maintenance strategy and the roof performance.

Spearman correlation has R value of floors = 0.142. This shows that there is a weak positive correlation between reactive maintenance and the physical condition of the floor. it also shows that only 14% of the performance of floor elements were as a result of reactive maintenance strategy. The Pearson chi-square values is 0.83, which is greater than 0.05 ($0.83 > 0.05$) and shows that there is no significant relationship between reactive maintenance strategy and the physical condition of the floors. Windows/doors spearman correlation R value = 0.257 which means that there is a weak positive correlation between reactive maintenance strategy and the physical condition of the windows/doors. It also means that only 26% of the performances of windows /doors elements were as a result of reactive /corrective maintenance strategy. The chi-square value is = 0.001 which is less than 0.05 ($0.001 < 0.05$) which is shows that there is a significant relationship between reactive maintenance strategy and the physical conditions of the windows and doors.

Spearman correlation R value of electrical fittings = 0.276 which means that there is a weak positive correlation between reactive maintenance and the physical conditions of electrical fittings. it also means that 28% of the performance of electrical fitting is as a result of the maintenance strategy used. The chi-square value equal 0.000 which is less than 0.05 ($0.00 < 0.05$) means there is a significant relationship between reactive maintenance strategy and the physical condition of the electrical fittings. The spearman correlation R value of plumbing fittings and appliance = 0.227 which show a weak positive correlation between corrective maintenance and the performance of the plumbing service. It equally means that only 23% of the performance of plumbing services were as result of reactive maintenance strategy. The chi-square value equal 0.003, which is less than 0.005 ($0.003 < 0.005$) mean that there is a significant relationship between reactive maintenance strategy and the performance of the plumbing services in the buildings. The correlation R values of the Air-Conditioning Units = 0.359, which means a weak positive correlation between reactive maintenance and the performance of the air conditioning units/. It equally shows that only 36% of the performance of the air-conditioning units was as a result of reactive maintenance strategy. The Pearson chi-square values 0.000 at 95% which less than 0.005.

This means that there is a significant relationship between the reactive maintenances and the performance of the air conditioning of units. The spearman correlation R value of the driven equipment = 0.32, this means that there is a weak positive correlation between reactive maintenance strategy and the performance of the driven equipment. it also shows that only 32% of the performance of the driven equipment is a result of reactive maintenance. The chi-square value is 0.000 which is less than 0.005; it means that there is a significant relationship between reactive maintenance and the performance of the driven equipment. The spearman correlation R value of generators = 0.40 which means that there is a weak positive correlation between reactive maintenance and the performance of the standby generators. it equal means that 40% of the performance of the standby generators were as a result of reactive maintenance strategy. The chi-square value is 0.00 which is less than 0.05. It shows that there is a significant relationship between reactive maintenance strategy and the performance of the stand-by generators.

The spearman correlation R value of sewage disposal systems = 0.30 which means that there is a weak positive correlation between reactive maintenance strategy and the performance of the sewage disposal systems. It equally shows that only 30% of the performance of the sewage disposal system is as a result of the maintenance strategy used. The chi-square values is 0.00 which is less than 0.05 this means that, there is a significant relationship between reactive maintenance and the physical condition of the sewage disposal systems. The spearman's correlation R value of the drinking fountains = 0.354 which means a weak positive correlation between reactive maintenance and the performance of the drinking fountains. It also shows that only 35% of the performance of the drinking fountains was as a result of the reactive maintenance strategy. The chi-square value = 0.000 which at 95% confidence. Limit, which is less than 0.05 It means that there is a significant relationship of the performance drinking fountains and reactive maintenance strategy. Table 3 shows the correlation coefficient R values and chi-square values for planned preventive maintenance and the physical conditions of the building elements /components. The R values of the physical condition of wall = .135, ROOF = -0.34, floor = .116, electrical fittings = -0.37, plumbing = -0.92 Air condition units = -.028, Driven equipment = <.011. This means that there is a weak negative correlation between planned preventive maintenance and the physical conditions of the above mentioned building elements /components. The R values of the physical condition of the remaining Building elements /components of window/door = .010, fire safety = .084, motor = .088, generator = .041, sewage disposal system = .048, drinking fountains = .064. This means that there is a weak positive correlation between the planned preventive maintenance strategy and the physical conditions of the building elements/components mentioned above. The result reveals that in all the elements /components, not up to 15% of their physical condition was as a result of planned preventive maintenance strategy. Only the chi square values calculated for motors, and air-conditioning units were significant for this maintenance strategy. The implication is that most of the industrial Firms sampled rate of adoption and usage planned preventive maintenance as low and as a result could not have much impact in the physical conditions of their facilities.

Table 4 shows the R values of the spearman correlation between the condition-based maintenance strategy and the physical condition of the building element/components the R values obtained show that there is virtually no correlation between the variables and not up to 8% of the building element /component were as a result of condition based maintenance strategy. This is so because the percentage of industrial firms using condition based maintenance strategy were found to be low and as such could not have impact on the performance of the facilities.

Analysis of Variance (ANOVA) of type of maintenance strategy and the respondents level of satisfaction with the physical condition of industrial facilities.

Table 6 shows the result of analysis of variance (ANOVA) computed between types of maintenance strategies and the respondents' level of satisfaction on the performance of their facilities .The result shows that there is no significant relationship between the types of maintenance strategies and the respondents' level of satisfaction with the physical condition of their facilities. This means that the types of maintenance strategy currently used in the maintenance of industrial facilities in the study area had no significant influence on the performance of the facilities.

V. DISCUSSION OF FINDINGS

In order test for the relationship and the degree of impact between the type of maintenance strategy adopted in an organization and the physical condition of industrial facilities, spearman's correlation coefficient was calculated between the variables. The finding reveals that in all the case of reactive maintenance strategy, that there is a weak positive correlation between reactive maintenance and the performance of the industrial facilities.

The R values for reactive maintenance and the physical condition of the structural elements of the building (foundation, walls beam and column) = 0.113; which mean a weak positive correlation, but the chi-square value = 0.061 >0.05 at 95% confidence limit this means that although there exist a weak relationship between reactive maintenance strategy and the structural elements of the building, that the relationship is not significant.. The spearman's correlation (R value) for reactive maintenance strategy and the physical condition of the roof is 0.240, meaning that there is a weak positive correlation between reactive maintenance and the roof condition. The result also shows that only 24% of the physical condition of the roof was as result of reactive maintenance strategy. The Chi-square value for drinking fountain = 0.00 < 0.05. The chi square values computed between reactive maintenance strategy and the physical condition of the walls = 0.061, and floors = 0.83, both values were greater than 0.05 which mean that there is no significant relationship between reactive maintenance strategy and the physical conditions of the walls and floor. But in all other cases the chi square values were less than 0.05 <0.05 which shows that a significant relationship was established between reactive maintenance strategy and the physical condition of industrial facilities. The finding also revealed that reactive /corrective maintenance strategy was the most widely used maintenance strategy in all the industrial firms sampled.

The finding reveals that in all the facilities not up to 15% of their performance were as a result of planned preventive maintenance (PPM) strategy and only the chi square values calculated for manufacturing plant and air-conditioning units were significant for the PPM strategy. The PPM strategy could not have much impact on the performance of the industrial facilities probably because the adaptation and usage of the PPM strategy were rated low among the industrial firms sampled. The finding reveals that there was no correlation between condition-based maintenance strategy and the physical condition of industrial facilities. This could be explained to be due to the very low adoption and usage of the condition based maintenance in the industrial firms sampled.

VI. CONCLUSION

The study was focused on appraising the state and maintenance of industrial facilities, maintenance strategies adopted, and the impact of the strategies on the performance of the facilities. The most widely maintenance strategy used by maintenance department of building manufacturing and plastic industries in Lagos state was reactive maintenance. A weak positive correlation was established between maintenance strategy adopted and the performance of industrial facilities. The contribution of the study for the literature of industrial facilities maintenance is both methodological and theoretical. The methodological contributions involve efforts at establishing a relationship between maintenance strategy and the physical conductions and performance of industrial facilities. The research is also providing reliable data on the state of industrial facilities and the impact of maintenance strategies on the physical condition of the facilities. While the theoretical contribution lies in establishment of link between of maintenance staff and their attitude toward maintenance of facilities, and preference in the choice of a particular maintenance strategy. Some of the findings of the study provide possible directions for further research. The study only examined facilities maintenance management strategy in the building and plastic manufacturing firms. Further research should be carried out in the following areas:

- [1] It is worthwhile to look into maintenance management strategy in other industries such as food process, breweries etc. This is to establish if there are differences in the performance and therefore compare the opinions of the maintenance staff on the state of physical conditions of the facilities and maintenance strategies adopted.
- [2] Further research work can be carried out on facilities maintenance management practice of industrial plant and machinery. This was not considered as part of the research work due to engineering professionalism involved.

REFERENCES

- [1] A.H.C. Tsang. (1998) "A strategic approach to managing maintenance performance": *Journal of Quality in Maintenance Engineering*, 4 (2), 87-94.
- [2] A. Andgani and S. Duffacia. (2002): "criel evaluation of simulation studies in maintenance systems". *Production Planning and control*, 13, (4), 336-341
- [3] E.A. Autin. (1998): "Selection and design of Computerized Maintenance Management System". *ILE Solution*, 32-35 August.
- [4] D.N.P. Murtjhy., A. Atcen., and J.A. Eccleston. (2002): "Strategic maintenance management". *Journal of quality in Maintenance Engineering*, 8, (4) 287-305.
- [5] R.O.A. Iyagba., O.A. Adenuga., H.N. Onukwube, and A.A. Soyngbe. (2007): "A Comparative Study of Maintenance Management Practice in Public Health Buildings in Nigeria and South Africa". The Professional Builder, *Journal of the Nigerian Institute of Building*.
- [6] K. Rapp and B. George. (1998): "Maintenance Management Concepts in Construction Equipment Curricula" *Journal of Construction Education*, 2(2), 155-169.
- [7] J. Housley. (1996): "A study of the Management of the Estate in Higher Education Establishments", *Proceedings of Cobra 1996 Research Conference*, RICS, London.
- [8] Buys and Nkado (2006): "Bench Marking Model for Maintenance Management Systems in South Africa Tertiary Educational Institutions". The construction and Building Research Conference of the Royal Institution of Chartered Surveyors, University College London. 7-8 September, 2006.

[9] R.M.W. Horner., M.A. El-Haram., and A.K. Munns. (1997): "Building Maintenance Strategy; A New Management Approach", *Journal of Quality in Maintenance Engineering* 3(4), 273-280.

[10] M.A. El-Haram., and M.W. Horner. (2002a): "Factors Affecting Housing Maintenance Cost". *Journal of Quality in Maintenance Engineering* 8 (2), 115-123.

[11] I.F. Colen. and J. Debrito. (2002): "Building Façade Maintenance Support System in Ural", O., Abrantes, V &Tadeu, A (eds) *ibid*, 3, 1899-1907.

[12] T.J. Pitt. (1987): *Using Models to Evaluate Property Maintenance Strategy in Building, P.S (ed): Building Cost Modelling and Computers* E& FN Span, London, 535-544.

[13] S. Duffuaa., M. Ben-Daya., K. Al-sultan. and A. Andijani. (2000): "A Simulation Model for Maintenance Systems in Saudi Arabia". Final Report, KACST Project No AR-16-85.

[14] D.A. Oladapo. (2004): An Evaluation of the Maintenance Management of the Staff Housing Estates of Selected First Generation Universities in South Western Nigeria. Unpublished Ph.D thesis, Department of Building, O. A. U, Ile-Ife.

[15] H.H.Y. Lee. and D. Scott. (2009): "Overview of Maintenance Strategy, acceptable maintenance standard and resources from a building maintenance operation perspective". *Journal of Building Appraisal* Vol. 4, No. 4, PP.269-278

[16] G. Vijverberg. (2000): "Basing Maintenance Needs and Accommodation Policy". *Building Research & Information*. 28(1), 18-30.

[17] A.H.C. Tsang. (1995): "Condition Based Maintenance: Tool and Decision Making". *Journal of Quality in Maintenance Engineering*. 1(3), 3-17.

[18] M. Organ., T. Whitehead. and M. Evans. (1997): "Availability Based Maintenance within an Asset Management Programme". *Journal of Quality in Maintenance Engineering*. 3 (4), 221-232

[19] A.H.C. Tsang. (1999): "Measuring Maintenance Performance. A Holistic Approach." *International Journal of Operations and Production Management*.. 19 (7), 691-715

[20] T.J. Pitt. (1997): "Data Requirement for the Prioritization of Predictive Building Maintenance." *Facilities* 15 (314), 97-104

[21] R. Lee. and P. Wordsworth. (2001): *Lee's Building Maintenance Management* London. Blackwell Publishing.

[22] A. Mann., L. Saxena. and G. Knapo. (1995): "Statistically Based or Condition Based Preventive Maintenance." *Journal of Quality in Maintenance Engineering* 1. (4), 46-59. National Bureau of statistics; Federal Republic of Nigeria retrieved December 14th 2007 retired at 14:n.

[23] R.J. Bushell. (1980): Preventing the Problem. A New Look at Building Planned Preventive Maintenance. Institute of Building Information Service.II.

[24] A. Kelly. and M. Harries. (1978): *Management of Industrial Maintenance*. Butter Worths, London.

[25] S. Dunn. (1997): "Best Practice Maintenance Strategies for Mobile Equipment." A *Conference Paper* Presented to the Maintenance in Mining Conference – Ball, Indonesia.

[26] J. Sikorska., L. Hammond. and D. Kelly. (2008). "Identifying Failure Modes Retrospectively Using RCM Data." www.plant-maintenance.com/articles/identifying failure modes.

[27] P.A. Higgs., R. Parkin. and M. Jackson. (2004): "A Survey of Condition Monitoring Systems in Industry." *Proceedings of ESDA, 7th Biennial ASME Conference on Engineering Systems Design and Analysis*. July 19-22. Manchester, UK

[28] Directory of Manufacturing Companies (1998): Lagos State Ministry of Commerce and Tourism. Lagos State Nigeria.

[29] S.T. Sediary. (1994): "Management of conflict; public sector construction in Saudi Arabia". *International Journal of project management*, 12 (3), 143-151.

Table 1. Industrial estates in Lagos state

S/N	Location	Year of Establishment	Size in Hectares
1	Apapa	1957	100
2	Matori	1958	120
3	Ikeja	1959	180
4	Ilupeju	1962	110
3	Ijora	1965	160
6	Iganmu	1965	80
7	Oshodi/Isolo	1968	120
8	Amuwo-odofin	1969	200
9	Ogba	1969	150
10	Oregun	1981	100
11	Agidingba (CBD)	1969	97
12	Gbagada	1958	50
13	Ikorodu	1976	1,582.27
14	Surulere	1981	20
15	Badiya	1958	15
16	Oyadiran/Yaba	1970	20
17	Ilasamaja	1971	60
18	Lagos South-West	1972	317.04
19	Kirikiri	1981	30
20	Abesan/Ipaja	1981	100
21	Akowonjo	1976	50
22	Oko-afO/Ilogbo	1981	-

Source: [28]

Table 2. Correlation coefficient and the chi square of Corrective Maintenance values and the building elements/facilities sampled.

Physical condition of element/components	R values	Chi-square values
Walls	0.113	0.610
Roof	0.240	0.006
Floors	0.142	0.830
Windows/doors	0.257	0.001
Electrical fittings	0.276	0.000
Plumbing	0.227	0.003
Fire safety equipment	0.115	0.620
Motor	0.356	0.001
Air condition unit	0.359	0.000
Driven equipment	0.320	0.000
Generators	0.400	0.000
Sewage disposal systems	0.300	0.000
Drinking fountain	0.354	0.000

Table 3. Correlation coefficient and the chi square of PPM values and the building elements/components sampled.

Physical condition of element/components	R values	Chi-square values
Walls	-.135	.098
Roof	-0.34	.934
Floors	-.116	.030
Windows/doors	.010	.297
Electrical fittings	-.037	.523
Plumbing	-.092	.180
Fire safety equipment	.084	.582
Motor	.088	.002
Air condition unit	-.028	.001
Driven equipment	-.011	.017
Generators	.048	.011
Sewage disposal systems	.149	.040
Drinking fountain	064	.009

Table 4. Spearman correlation coefficient and chi-square values of condition based maintenance (CBM) and the physical conditions of the Building elements /components.

Physical condition of element/components	R values	Chi-square values
Walls	.036	.263
Roof	.060	.324
Floors	-.051	.077
Windows/doors	-.020	.027
Electrical fittings	-.092	.017
Plumbing	-.125	.005
Fire safety equipment	.032	.413
Motors	-.060	.475
Air condition unit	-.170	.016
Driven equipment	-.164	.001
Generators	-.120	.050
Sewage disposal systems	-.068	.003
Drinking fountain	-.099	.000
Foundation	-.038	.392

Table 5. Spearman correlation coefficient and chi square values of time based maintenance strategy and the physical condition of the building elements /components.

Physical condition of element/components	R values	Chi-square values
Walls	-.064	0.015
Roof	.029	0.282
Floors	-.039	0.113
Windows/doors	-.010	0.000
Electrical fittings	.063	0.003
Plumbing	.021	0.254
Fire safety equipment	-.074	0.063
Motors	-.033	0.306
Air condition unit	-.073	0.278
Driven equipment	-.017	0.000
Generators	-.023	0.001
Sewage disposal systems	.105	0.109
Drinking fountain	.060	0.104
Foundation	-.054	0.269

Table 6. Analysis of variance values (ANOVA) of type of maintenance strategy and the performance of industrial facilities as perceived by maintenance staff

Description	F	Significance
exterior wall condition	1.057	.393
interior wall condition	.670	.698
exterior wall finish condition	1.909	.070
roof condition	1.367	.221
window condition	1.125	.221
door condition	1.800	.089
structural condition	1.804	.088
electrical condition	.759	.622
fire safety	1.295	.254
rest infestation	1.466	.181
plumbing condition	1.792	.090
overall cleanliness	1.674	.117
Motors	1.846	.080.
driven equipment	1.875	.075
Generators	1.718	106

Comparison between the Performance of Basic SEPIC Converter and modified SEPIC Converter with PI Controller

¹Satyendra Kumar Gupta , ²Shahab Ahmad

¹Asst. Professor Electrical Engg Deptt Shri Ram Swaroop Memorial College of Engineering & Managment Lucknow, India

² Asst. Professor Electrical Engg Deptt Pratap institute of Technology & Science Siker, Rajasthan, India

ABSTRACT: There are multiple solutions in which line current is sinusoidal. In addition, in the recent years, a great number of circuits have been proposed with non sinusoidal line current. In this paper, a review of the most interesting solutions for single phase and low power applications is carried out. They are classified attending to the line current waveform, energy processing, number of switches, control loops, etc. The major advantages and disadvantages are highlighted and the field of application is found. The paper presents performance analysis of modified SEPIC dc-dc converter with low input voltage and wide output voltage range. The operational analysis and the design is done for the 380W power output of the modified converter. The simulation results of modified SEPIC converter are obtained with PI controller for the output voltage. The results obtained with the modified converter are compared with the basic SEPIC converter topology for the rise time, peak time, settling time and steady state error of the output response for open loop. Voltage tracking curve is also shown for wide output voltage range.

KEYWORDS: Dc-dc Power Conversion, SEPIC Converter.

I. INTRODUCTION

POWER supplies connected to ac mains introduce harmonic currents in the utility. It is very well known that these harmonic currents cause several problems such as voltage distortion, heating, noise and reduce the capability of the line to provide energy. This fact and the need to comply with “standards” or “recommendations” have forced to use power factor correction in power supplies. Unity power factor and tight output voltage regulation are achieved with the very well known two stage approach, shown in Fig. 1. Since the power stage is composed by two converters, size, cost and efficiency are penalized, mainly in low power applications. However, this is probably the best option for ac-dc converters due to the following reasons.

- [1] Sinusoidal line current guarantees the compliance of any Regulation.
- [2] It gives good performance under universal line voltage.
- [3] It offers many possibilities to implement both the isolation between line and load, and the hold-up time.
- [4] The penalty on the efficiency due to the double energy processing is partially compensated by the fact that the voltage on the storage capacitor is controlled. The fact of having a constant input voltage allows a good design of the second stage.

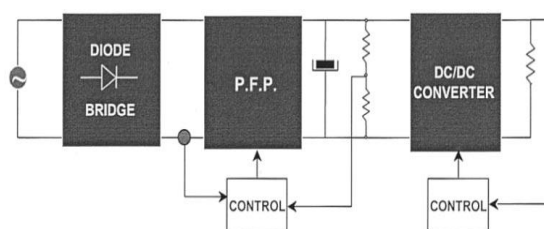


Fig. 1. Two stage ac-dc PFC converter.

Dc-dc converters are widely used in regulated switched mode dc power supplies and in dc motor drive applications. The input to these converters is often an unregulated dc voltage, which is obtained by rectifying the line voltage and it will therefore fluctuate due to variations of the line voltages. Switched mode dc-dc converters are used to convert this unregulated dc input into a controlled dc output at a desired voltage level. The recent growth of battery powered applications and low voltage storage elements are increasing the demand of efficient step-up dc-dc converters. Typical applications are in adjustable speed drives, switch-mode

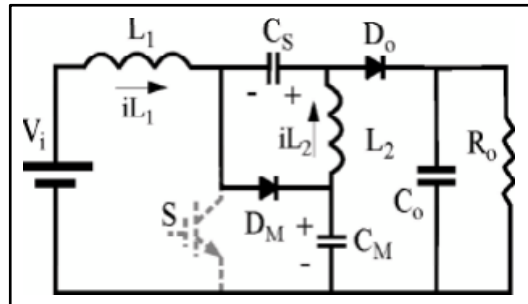


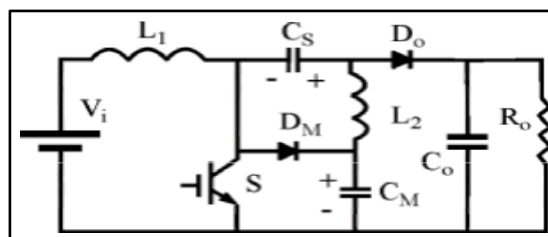
Fig. 2: Circuit of the Modified SEPIC

power supplies, uninterrupted power supplies, and utility interface with nonconventional energy sources, battery energy storage systems, battery charging for electric vehicles, and power supplies for telecommunication systems etc.. These applications demand high step-up static gain, high efficiency and reduced weight, volume and cost. The step-up stage normally is the critical point for the design of high efficiency converters due to the operation with high input current and high output voltage [1]. The boost converter topology is highly effective in these applications but at low line voltage in boost converter, the switching losses are high because the input current has the maximum value and the highest step-up conversion is required. The inductor has to be oversized for the large current at low line input. As a result, a boost converter designed for universal-input applications is heavily oversized compared to a converter designed for a narrow range of input ac line voltage [2]. However, recently new non-isolated dc-dc converter topologies with basic boost are proposed, showing that it is possible to obtain high static gain, low voltage stress and low losses, improving the performance with respect to the classical topologies. Some single stage high power factor rectifiers are presented in [3-6]. A new alternative for the implementation of high step-up structures is proposed in this paper with the use of the voltage multiplier cells integrated with basic non-isolated dc-dc converters. The uses of the voltage multiplier in the basic dc-dc converters add new operation characteristics, becoming the resultant structure well suited to implement high-static gain step-up converters [7]. The use of high static gain and low-switch voltage topologies can improve the efficiency operating with low input voltage, as presented in [8-10].

II. OVERVIEW OF CIRCUIT AND ITS WORKING

The voltage multiplier technique is used to increase the static gain of single-phase boost dc-dc converters. The modified SEPIC converter is accomplished by including of the diode D_M and the capacitor C_M in basic SEPIC converter. An adaptation of the voltage multiplier technique with the SEPIC converter is presented in fig.1. Many operational characteristics of the basic SEPIC converter are changed with the proposed modification. The capacitor C_M is charged with the output voltage of the basic boost converter. Therefore, the voltage applied to the inductor L_2 during the conduction of the power switch S is higher than that in the basic sepic converter, thereby increasing the static gain.

The principle of operation of the modified SEPIC converter presents the following two operation stages. First stage (switch is off) Second stage (switch is on)



The principle of operation of first stage is shown in the fig. 3.

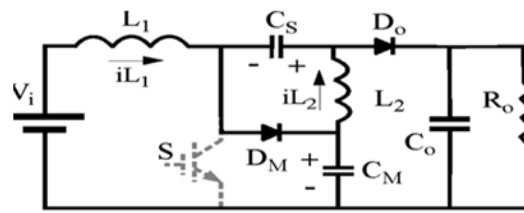


Fig. 3: First Stage (Switch is Off)

The first stage of operation varies from time t_0 to t_1 . At the instant t_0 , the switch S is turned-off and the energy stored in the input inductor L_1 is transferred to the output through the capacitor C_s and output diode D_o , and also to the capacitor C_M through the diode D_M . Therefore, the switch voltage is equal to the capacitor C_M voltage. The energy stored in the inductor L_2 is transferred to the output through the diode D_o . The principle of operation of second stage is shown in the fig. 4.

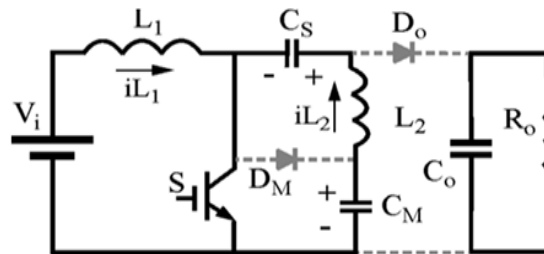


Fig. 4: Second Stage (Switch is ON)

The second stage operation varies from time t_1 to t_2 . At the instant t_1 , the switch S is turned-on and the diodes D_M and D_o are blocked, and the inductors L_1 and L_2 store energy. The input voltage is applied to the input inductor L_1 and the voltage $V_{CS} - V_{CM}$ is applied to the inductor L_2 . The voltage V_{CM} is higher than the voltage V_{CS} . The operating waveforms of modified SEPIC converter are presented in fig. 5. The voltage in all diodes and the power switch is equal to the capacitor C_M voltage. The output voltage is equal to the sum of the voltages across capacitors C_s and C_M respectively. The average L_1 inductor current is equal to the input current and the average L_2 inductor current is equal to the output current [11].

At the instant t_2 , the switch S is turned-off and the diodes D_M and D_o are blocked, and the inductors L_1 and L_2 store energy. The input voltage is applied to the input inductor L_1 and the voltage $V_{CS} - V_{CM}$ is applied to the inductor L_2 . The voltage V_{CM} is higher than the voltage V_{CS} . The operating waveforms of modified SEPIC converter are presented in fig. 5. The voltage in all diodes and the power switch is equal to the capacitor C_M voltage. The output voltage is equal to the sum of the voltages across capacitors C_s and C_M respectively. The average L_1 inductor current is equal to the input current and the average L_2 inductor current is equal to the output current [11].

III. MODIFIED SEPIC

Static gain is a measure of the ability of a circuit to increase the power from the input to the output. It is usually defined as the ratio of the output to the input of a system. At the steady state for the inductor L_1 , the relation presented in (1) occurs:

$$V_i(t_{on} + t_{off}) = V_{CM} t_{off} \dots \dots \dots (1)$$

$$V_i D = (V_{CM} - V_i)(1 - D) \dots \dots \dots (2)$$

Therefore, the CM capacitor voltage is defined by (3), which is the same equation of the classical boost static gain given by

$$\frac{V_{CM}}{V_i} = \frac{1}{1-D} \dots \dots \dots (3)$$

During the period where the power switch is turned-off (t_{off}), the diodes D_M and D_o are in conduction state, and the following relation can be defined:

$$V_o = V_{CS} + V_{CM} \dots \dots \dots (4)$$

$$V_{CS} = V_o - V_{CM} \dots \dots \dots (5)$$

The L_2 average voltage is zero at the steady state, and the following relations can be considered
 As the basic sepic, boost, and the modified sepic converters present the same input stage, the equation for the determination of the input current ripple is the same for all converters. The input current ripple (Δi_{L1}) during the conduction of the power switch is defined by the following equation.

$$\Delta i_{L1} = \frac{V_i D}{f L_1} \dots \dots \dots (6)$$

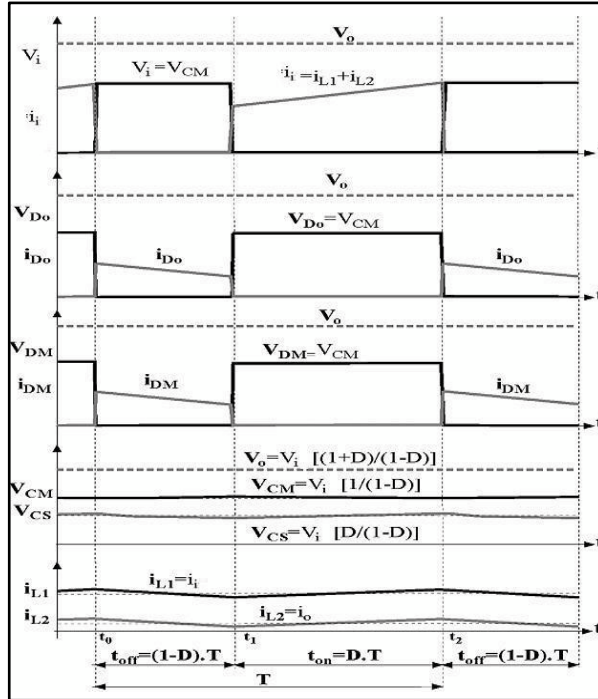


Fig. 5: Steady-State Operation Waveforms

A. Input Current Ripple and L1–L2Inductances

Where, f is the switching frequency.
 The input current ripple Δi_{L1} considered is 18% of the peak input current (i_{inpk}). Therefore, the input current ripple is calculated as follows:

$$\Delta i_{L1} = i_{inpk} \times 0.18 = 6.5 \times 0.18 = 1.17A.$$

The input inductance is calculated for the low input voltage. The input voltage V_i is 115 V, the converter duty cycle is equal to $D = 0.5$, with supply frequency 50Hz and switching frequency 48kHz. The input inductance calculated is equal to

$$L_1 = \frac{V_i D}{f \Delta i_{L1}} \dots \dots \dots (7)$$

The input inductance value utilized in the simulation is equal to $L_1 = 1mH$. As the average input current is higher than the average output current for a step-up converter, the L_2 inductor volume is lower than the L_1 inductor volume. The L_2 inductance utilized in the simulation is half of the L_1 inductance. The L_2 inductance value utilized in the simulation is half of the L_1 inductance i.e. $L_2 = 500\mu H$.

B. Series Capacitor C_s and Multiplier Capacitor C_m

During the power switch turn-on period, the current in the C_s and C_m capacitances is equal to the L_2 inductor current. The capacitor charge variation ΔQ is calculated as

$$\Delta Q = i_{L2} DT \dots \dots \dots (8)$$

The high-frequency capacitor voltage ripple ΔV_C can be defined by equation , as a function of the capacitor charge variation. Therefore, the C_s and C_m capacitances can be defined as follows.

$$C = \frac{i_{L2} D}{f \Delta V_C} \dots \dots \dots (9)$$

Where f is the switching frequency and $C = C_s = C_m$

For an input voltage equal to $V_i = 115V$ and a maximum capacitor voltage ripple equal to 7% of the output voltage ($\Delta V_c = 24.15 V$), and the maximum inductor current L_2 is assumed to 1.5A. The capacitors C_S and C_M can be determined from equation

$$C = 647nF$$

The capacitors utilized in the analysis of the proposed converter are,

$$C = C_S = C_M = 660 nF.$$

C. Output Capacitor C_o

The output filter capacitance is defined by a function of the output power P_o , the supply i.e. grid frequency f_G , and the low frequency output voltage ripple ΔV_o . The output voltage ripple is considered equal to 1% of the output voltage in calculation. The output capacitance is calculated as given below:

$$C_o = \frac{P_o}{2\pi f_G * 2V_o \Delta V_o}$$

The output voltage is calculated from equation. Considering an output voltage ripple equal to 1% of the output voltage for the output power 380W, the output capacitor value is calculated from equation.

$$C_o = 500 \mu F$$

IV. RESULT

The designed parameters of the modified SEPIC system is given in Table 1. The closed loop Simulink model for the modified SEPIC converter is shown in fig. 6. The single phase 115V, 50 Hz ac voltage is the input of the SEPIC. The input voltage waveform is shown in fig. 7. The input ac current is in phase with the input voltage waveform having almost unity power factor as shown in fig. 8. The low order harmonics are also absent in the input current, i.e., less current harmonics are injected into the utility. Fig. 9 and fig. 10, are the rectified input voltage and current waveforms respectively. Open loop output voltage waveforms of Basic SEPIC and Modified SEPIC are shown in fig. 11 and fig. 12, respectively. Different open loop parameters of the Basic and Modified SEPIC

are given Table 2. Fig. 13, shows the output voltage stabilization at 345V, 500V and 600V step voltage references at time $t=0$, $t=0.55$ and $t=0.8s$ respectively.

Table 1: Parameters of the Modified SEPIC.

MODEL PARAMETERS	VALUES
INPUT VOLTAGE, V_i	115V
OUTPUT VOLTAGE, V_o	345V
INDUCTOR, L_1	1mH
INDUCTOR, L_2	500 μ H
SERIES CAPACITOR, C_s	660nF
MULTIPLIER CAPACITOR, C_M	660nF
OUTPUT CAPACITOR, C_o	500 μ F
SWITCHING FREQUENCY, f_s	48kHz
GRID FREQUENCY, f_G	50Hz

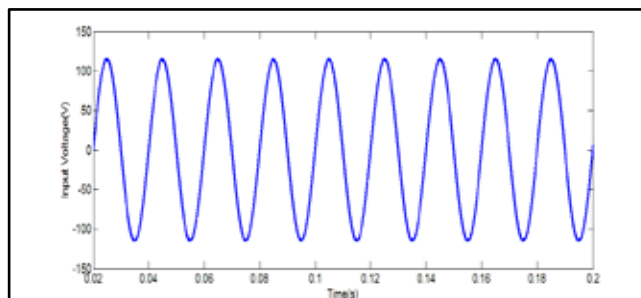


Fig. 6: Input Voltage (115V) Waveform

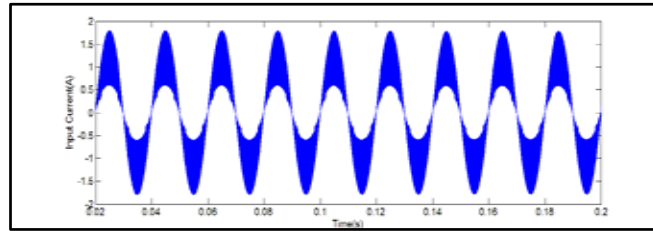


Fig. 7: Input Current Waveform

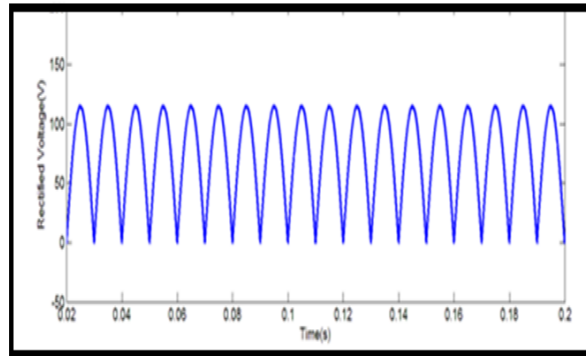


Fig. 8: Rectified Input Voltage Waveform

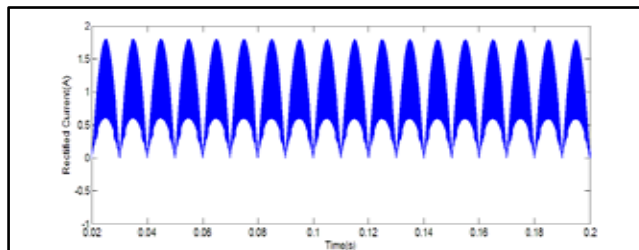


Fig. 9: Rectified Input Current Waveform

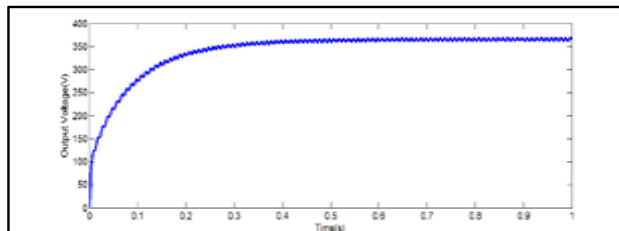


Fig. 10: Output Voltage Waveform of the Basic SEPIC

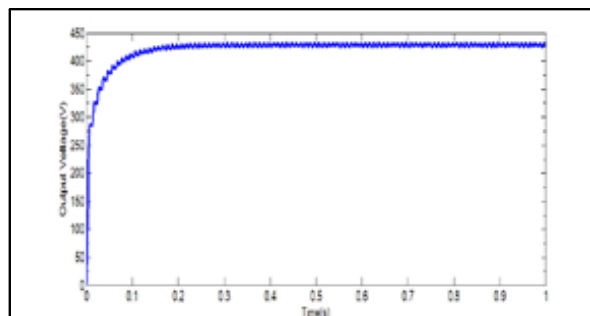


Fig. 11: Output Voltage Waveform of the Modified SEPIC

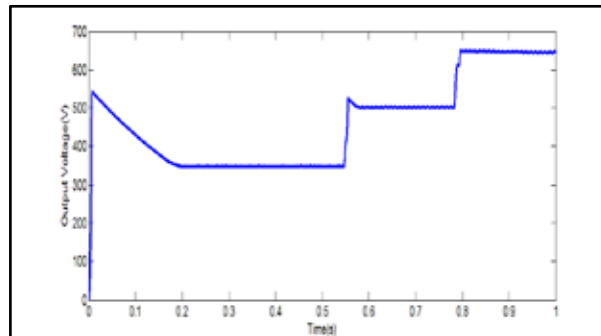


Fig. 12: Output Voltage Variation

V. CONCLUSION

Many proposed solutions for ac-dc power factor correction have been analyzed. They have been classified according to the line current waveform and their performance. If the purpose is to obtain a sinusoidal line current, the classical two-stage approach is the best option, mainly if universal line voltage operation is required. It is desirable to include ZVS if it is feasible to implement it in any or both PFP and dc-dc converter. In general terms, the solutions based on a better energy management (either processing less energy or process it with higher efficiency) do not offer great advantages, unless the efficiency were the unique parameter to consider. Passive solutions are adequate in the low power range for simplicity. A modified SEPIC converter is analyzed and designed. The converter model is simulated on Simulink for open loop as well as closed loop. The PI controller is used to control the output voltage of the modified SEPIC which gives the controlled variation of output voltage from 250V to 650V with input voltage 115V. Although the proposed structure presents a higher circuit complexity than the basic converter but we obtain the higher static gain for the operation with the low input voltage, low switch voltage operation and controlled output voltage variation between 250V and 650V with input voltage 115V with duty ratio 50% with 25kHz switching frequency.

VI. FUTURE SCOPE

The open loop and closed loop models of the modified SEPIC converter may be implemented further for hardware design. There is a classical problem of the reduction of the efficiency due to the additional losses caused by the reverse recovery current of the diodes. This problem is an important source of losses in high power factor rectifiers. This modified SEPIC converter can also be used to reduce the losses associated with the diode reverse recovery current with a regenerative snubbed circuit which can be further implemented.

REFERENCES

- [1] B. Singh, B. N. Singh, A. Chandra, K. Al-Haddad, A. Pandey, D. P. Kothari, "A review of single-phase improved power quality AC-DC converters", IEEE Trans. Ind. Electron., Vol. 50, No. 5, pp. 962-981, 2003. 2nd ed. Norwell, MA: Kluwer, 2001.
- [2] J. Chen, D. Maksimovic, R. W. Erickson, "Analysis and design of a low-stress buck-boost converter in universal input PFC applications", IEEE Trans. Power Electron., Vol. 21, No. 2, pp. 320-329, 2006.
- [3] J. Qian, F. C. Lee, "A high efficient single stage single switch high power factor ac/dc converter with universal input", IEEE Trans. Power Electron., Vol. 13, No. 4, pp. 699-705, 1998.
- [4] C. Qiao, K. M. Smedley, "A topology survey of single-stage power factor corrector with a boost type input current-shaper", IEEE Trans. Power Electron., Vol. 16, No. 3, pp. 360-368, 2001.
- [5] M. H. L. Chow, Y. S. Lee, C. K. Tse, "Single-stage single switch isolated PFC regulator with unity power factor, fast transient response, and low-voltage stress", IEEE Trans. Power Electron., Vol. 15, No. 1, pp. 156-163, 2000.
- [6] J. L. Lin, W. K. Yao, S. P. Yang, "Analysis and design for a novel single-stage high power factor correction diagonal half-bridge forward ac-dc converter", IEEE Trans. Power Electron., Vol. 53, No. 10, pp. 2274-2286, 2006.
- [7] M. Prudente, L. L. Pfitscher, G. Emmendoerfer, E. F. R. Romaneli, R. Gules, "Voltage multiplier cells applied to nonisolated DC-DC converters", IEEE Trans. Power Electron., Vol. 23, No. 2, pp. 871-887, 2008.
- [8] Q. Zhao, F. C. Lee, "High-efficiency, high step-up DC-DC converters", IEEE Trans. Power Electron., Vol. 18, No. 1, pp. 65-73, 2003.
- [9] R.J.Wai, R.Y. Duan, "High step-up converter with coupled inductor", IEEE Trans. Power Electron., Vol. 20, No. 5, pp. 1025-1035, 2005.
- [10] R.J. Wai, R.Y. Duan, "High-efficiency power conversion for low power fuel cell generation system", IEEE Trans. Power Electron., Vol. 20, No. 4, pp. 847-856, 2005.
- [11] P. F. de Melo, R. Gules, R. Romaneli, R. C. Annunziato, "A Modified SEPIC Converter for High-Power-Factor Rectifier and Universal Input Voltage Applications", IEEE Trans. Power Electron., Vol. 25, No. 2, pp. 310-321, 2010.

Dual-Band Annular-Ring Microstrip Patch Antenna for Satellite Applications

Tvs Divakar¹ Dr. D.C.Panda²

¹ Department Of ECE JITM-CENTURION UNIVERSITY

² Department Of Electronic Science BERHEMPUR UNIVERSITY

ABSTRACT: A dual-band circularly polarized antenna fed by four apertures that covers the bands of GPS, Galileo, is introduced. The ARSAs designed using FR4 substrates in the L and S bands have 3-dB axial-ratio bandwidths (ARBWs) of as large as 37% and 52%, respectively, whereas the one using an RT5880 substrate in the L band, 61%. In these 3-dB axial-ratio bands, impedance matching with $VSWR \leq 1.8$ is also achieved. Three wideband planar baluns are used to achieve good axial ratio and VSWR. The results of the annular-ring microstrip antenna show good performance of a dual-band operation, which meets the requirement of Global Navigation Satellite System (GNSS) applications.

INDEX TERMS: Broadband feed network, circularly polarized (CP), Annular Ring Slot Antenna (ARSA), dual-band patch antenna, Global Navigation Satellite System (GNSS).

I. INTRODUCTION

In recent years, antennas have been very intensively used in the satellite communication and Global Navigation Satellite System (GNSS) [1], [2]. For the single-feed circularly polarized (CP) antennas, the measured impedance bandwidth for and 3-dB axial-ratio bandwidths (ARBWs) are less than 3% and 1% [3]. The majority of Global Positioning System (GPS) receivers are requested to cover both 1575 MHz (L1) and 1227 MHz (L2) bands. Though the design bandwidth may be enough to support GPS applications or other navigation system requests, machine tolerances in production are inevitable and could result in bandwidth reductions. CP bandwidth could be enhanced by using the coupled feeding method and the dual-feed or multiple-feeds network. The single-feed CP ring antennas using the coupled feeding method have been investigated in [4], but the 3-dB ARBW is less than 2%. For the dual-feed CP antenna in [5], the ARBW is larger than 2% at both bands. The CP annular-ring patch antenna with two proximity-coupled L-probe feeds [6] obtains a 3-dB ARBW of larger than 30%. The ring microstrip antenna has the advantage of a smaller dimension than that of a circular or rectangular patch when operating in the fundamental mode at a certain frequency [7]. The width of the rings has the most influence to the input impedance of the ring microstrip [8]. Thus, the narrow rings produce higher the input impedance, and good impedance match is therefore more difficult to obtain [9]. In this paper, a dual-band CP antenna based on a concentric annular-rings microstrip fed by four apertures is designed. The broadband feed network based on the broadband phase shifter presented in [10] and [11] is used to obtain the required phase shift, thus allowing improvement of the axial ratio in the direction of maximum radiation. This antenna could be installed on a car or a ship for navigation use.

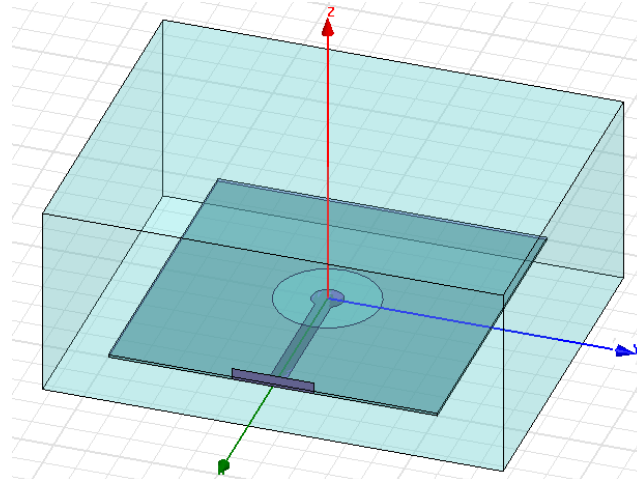


Fig. 1 Proposed annular ring antenna

II. ANTENNA CONFIGURATION

Fig. 1 shows the geometry of the proposed CP ARSA, in which the deformed bent feeding line and the perturbation structure consisting of a pair of grounded hat-shaped patches are redrawn separately for more clarity. The antenna is to be fabricated on a square microwave substrate with side length *G*, thickness *h*, dielectric constant ϵ_r , and loss tangent $\tan\delta$. The radiating annular-ring slot of outer radius *R1*(80mm) and inner radius *R2*(24mm) is fed from the direction *y*-by a -wide 50Ω microstrip line printed on the side of the substrate opposite to the slot. On the top of ground plane the substrate is placed and here the substrate is FR4(*h*=0.8mm) and RTduroid 5880(*h*=1mm). An SMA connector is used to give input to the antenna through the microstrip feed. If , a bent (or inverted-L) feeding microstrip line is formed, which can broaden the CP band of the CP ARSA fed by a straight feeding line and loaded with grounded rectangular patches. With the feeding structure is referred to as a deformed bent feeding line, which can improve the impedance matching of the designed antenna in the broadened CP band.

III. CONCEPTS AND PROCEDURE OF ANTENNA DESIGN

The antenna design begins with determining and of a microstrip-line-fed linearly polarized (LP) ARSA, which will be subsequently developed into a CP ARSA. During simulation a wave port is created along the YZ plane to receive the radiation. For good results the entire design is enclosed in a box which must be given perfect E during execution of the antenna. At the center frequency of the fundamental mode of a conventional microstrip line- fed LP ARSA where the width of the ring slot is only 22.2% the average radius of the slot [4], one guided wavelength is estimated to be the average perimeter of the ring slot. However, for a similar LP ARSA in [6] with the ring-slot width being 28.6% the average radius and with a ground-plane size of smaller than that of the antenna in [4], one guided wavelength is modified to be the outer perimeter of the ring slot. In fact, the ground-plane size and slot width complicatedly affect the resonant frequency of the fundamental mode of an LP ARSA. Nevertheless, to more accurately estimate the fundamental-mode resonant frequency of an LP ARSA, extensive simulations using Ansoft HFSS and experimental verifications for the substrates of small dielectric constant and low substrate thickness were performed again in this study. Results show that the fundamental-mode resonant magnetic current of the LP ARSA for one guided wavelength is mainly distributed between the average and outer perimeter of the ring slot at the fundamental resonant-band center frequency. An empirical formula can be found for certain ranges of structural parameters to be described below. The expression of the fundamental-mode resonant frequency of an LP ARSA can be slightly modified from those in [4] and [6] to

$$f_r = \frac{c_0}{2.2\pi R_m \sqrt{\epsilon_{reff}}} \text{----- (1)}$$

$$\epsilon_{reff} = \frac{2\epsilon_r}{1+\epsilon_r} \text{----- (2)}$$

In this empirical formula, f_r is the resonant frequency of the fundamental mode, C_0 the speed of light in free space, and ϵ_{reff} the effective dielectric constant.

IV. RESULTS AND DISCUSSION

Fig 2 shows the total gain of the proposed antenna which is approximately 7.9 dB in both the bands L1 and L2. Fig 3 and 4 shows the return loss and active VSWR of the proposed antenna. Return loss is approximately -19dB and VSWR is 1. Ansoft High Frequency Structure Simulator (HFSS) is utilized to validate the proposed structure. First, for obtaining the good coupling between the radiation patch and feed line and also making a resonance with the patch by the feed and thus increasing the matching bandwidth, we optimize the mentioned parameters of the feed line. On the other hand, the height of the substrate between slot and patch is also an important parameter because it changes the matching bandwidth and gain. The best values of the mentioned parameters for the matching bandwidth and gain enhancement are given above. The proposed antenna can support many existing wireless services, broadband applications over the frequency range of 3, 4, and 5 GHz, and multi standard mobile communication systems.

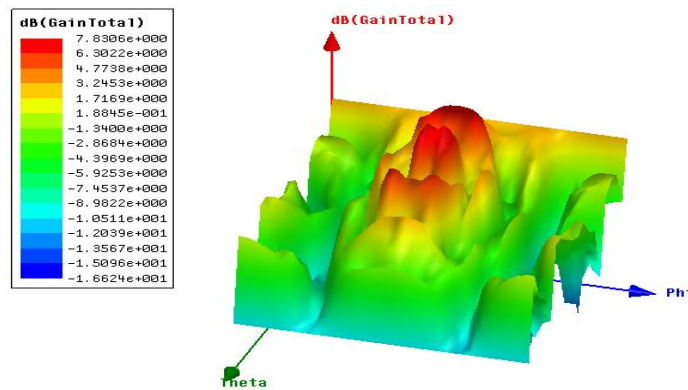


Fig-2. Simulated total gain of the antenna

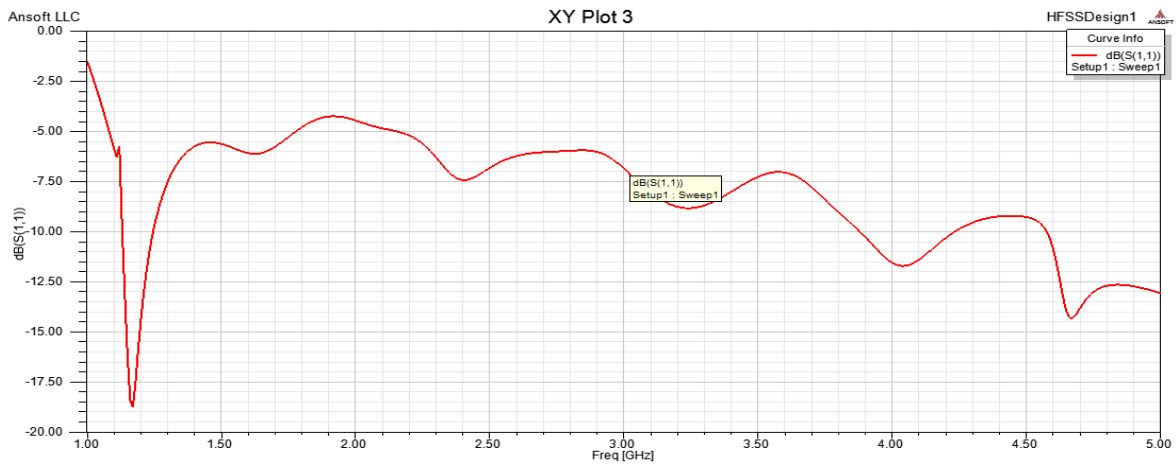


Fig-3. Return loss of the proposed antenna

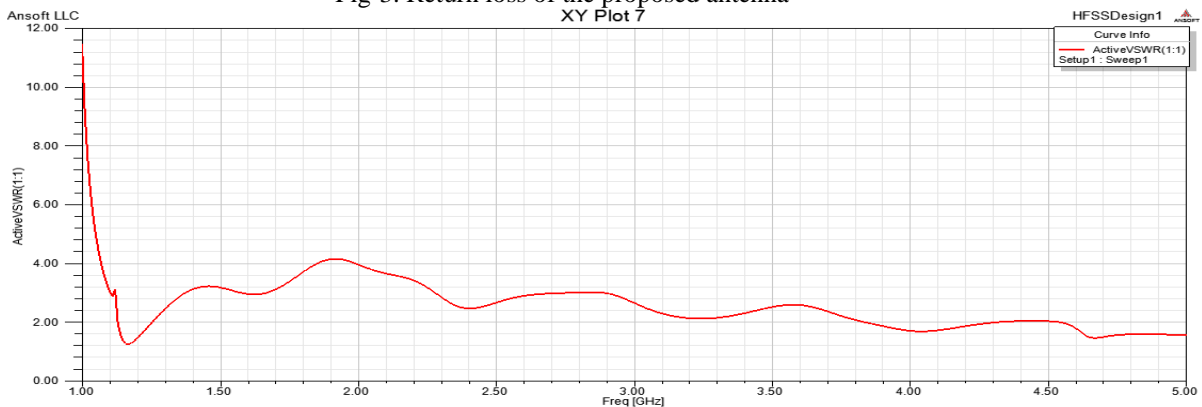


Fig-4. Active VSWR of the proposed antenna

V. CONCLUSION

In this paper we propose an annular ring antenna in which the broadband operation is a result of suitable design of the transmission line, slot, and patch. The shape and size of the patch are main parameters that affect the matching bandwidth and the gain of the antenna, thus we designed them carefully. An annular ring patch satisfied expectations. The measurement results showed a broad matching bandwidth of 61% for VSWR < 1.8. Maximum gain is 7.9dB, and 1-dB gain ripple bandwidth is nearly 37%. Also, the radiation pattern, radiation efficiency, and cross polarization is adequate on the matching bandwidth.

REFERENCES

- [1] Y.-Q. Zhang, X. Li, L. Yang, and S.-X. Gong "Dual-Band Circularly Polarized Annular-Ring Microstrip Antenna for GNSS Applications" *IEEE Antennas Wireless Propag. Lett.*, vol. 12, pp. 615–618, 2013.
- [2] F. Ferrero, C. Luxey, G. Jacquemod, and R. Staraj, "Dual-band circularly polarized microstrip antenna for satellite applications," *IEEE Antennas Wireless Propag. Lett.*, vol. 4, pp. 13–15, 2005.
- [3] L. I. Basilio, R. L. Chen, J. T. Williams, and D. R. Jackson, "A new planar dual-band GPS antenna designed for reduced susceptibility to low-angle multipath," *IEEE Trans. Antennas Propag.*, vol. 55, no. 8, pp. 2358–2366, Aug. 2007.
- [4] W.-T. Hsieh, T.-H. Chang, and J.-F. Kiang, "Dual-band circularly polarized cavity-backed annular slot antenna for GPS receiver," *IEEE Trans. Antennas Propag.*, vol. 60, no. 4, pp. 2076–2080, Apr. 2012.
- [5] K.-F. Tong and J.-J. Huang, "New proximity coupled feeding method for reconfigurable circularly polarized microstrip ring antennas," *IEEE Trans. Antennas Prop.*, vol. 56, no. 7, pp. 1860–1866, Jul. 2008.
- [6] X.-Y. Sun, Z.-J. Zhang, and Z.-H. Feng, "Dual-band circularly polarized stacked annular-ring patch antenna for GPS application," *IEEE Antennas Wireless Propag. Lett.*, vol. 10, pp. 49–52, 2011.
- [7] Y.-X. Guo, L. Bian, and X. Q. Shi, "Broadband circularly polarized annular-ring microstrip antenna," *IEEE Trans. Antennas Propag.*, vol. 57, no. 8, pp. 2474–2477, Aug. 2009.
- [8] J.W.Mink, "Circular ringmicrostrip antenna elements," in *Proc. IEEE Antennas Propag. Soc. Int. Symp.*, Jun. 1980, vol. 18, pp. 605–608
- [9] M. Ramírez, J. Parrón, J.M.González-Arbesú, and J. Gemio, "Concentric annular-ring microstrip antenna with circular polarization," *IEEE Antennas Wireless Propag. Lett.*, vol. 10, pp. 517–519, 2011.
- [10] S. I. Latif and L. Shafai, "Microstrip square-ring antenna with capacitive feeding for multi-frequency operation," in *Proc. IEEE Antennas Propag. Soc. Int. Symp.*, Jul. 2008, pp. 1–4.
- [11] Z.-Y. Zhang, Y.-X. Guo, L. C. Ong, and M. Y. W. Chia, "A new wide-band planar balun on a single-layer PCB," *IEEE Microw. Wireless Compon. Lett.*, vol. 15, no. 6, pp. 416–418, Jun. 2005.

An Appraisal of the Population Total of Nigeria Using One Unit per Stratum (Based On 2006 Census Result)

T.J. Akingbade¹O.S. Balogun² O.S. Babatunde³

¹Department of Mathematical Sciences, Kogi State University, P.M.B. 1008, Anyigba, Kogi State, Nigeria.

²Department of Statistics and Operations Research, Modibbo Adama University of Technology, P.M.B 2076, Yola, Adamawa State, Nigeria.

³Department of Mathematics/Statistics/Computer Science P.M.B. 1019, Wukari, Taraba State. Nigeria.

ABSTRACT: This research has been done to show the efficiency level of variance estimation with one unit per stratum in collapsing of strata and to estimate the population total of Nigeria based on 2006 census result, to study the precision of variance estimation in collapsing of strata and to examine the effect of the use of auxiliary information in estimating variance in collapsing of strata with one unit per stratum in various level of collapsing. Two stage sampling method was used for the sample selection, which involves two phases of selection. In the first stage, 12 states and 24states were selected out of 36 states using random number table. The Local Government Areas (774) were taken to be the second stage and purposive sampling method was used. Based on the research work, considering one unit per stratum, then one LGA was selected from each of the selected state. Based on the result obtained, estimation with sample size 12 using stratified random sampling with variable of interest only and with addition of auxiliary variable, the least standard error of \hat{Y}_{str} was 3,501,901.105 under the collapsing of 12 strata in six into two groups with an estimated population total of 139,295,482 which was very close to the actual population total of Nigeria based on 2006 census result (140,003,542). It also shows that, the higher the extent of collapsing of strata, the lower the standard error of \hat{Y}_{str} . Estimation with sample size 24 : using stratified random sampling with variable of interest only, and with addition of auxiliary variable, shows that the higher the extent of collapsing of strata, the standard error of \hat{Y}_{str} was inconsistent (i.e. decreasing). The least standard errors falls under collapsing of strata in twelve for estimation with sample size 24. Therefore, lower strategy of collapsing of strata should be employed for large number of strata (24), so that the variation within the collapsed strata will not be much. Estimation using stratified random sampling with addition of an auxiliary variable gave a better result than estimation with variable of interest only.

KEYWORDS: Population, Collapse strata, Stratified Sampling, Stratum

I. INTRODUCTION

The general knowledge of our day to day activities is all based to a very large extent on sample. Hence, sample survey has been very useful in almost every area of lives. Sample survey is an investigation that involves collection of data or measurement taken on sample of element for making inferences about the population. Sample survey theory deals with the method and processes of sampling, data collection and estimation of the population parameters.

Collapsing of strata: A feature of many surveys Sample design is the selection of a single primary sampling unit (PSU) per stratum. The selection of a single PSU per stratum gives efficiency in design since stratification is carried out to fullest possible extent, but it does not generally permit an unbiased variance estimator to be obtained. A widely used method of variance estimation for this situation is known as collapsed strata technique (Rust and Kalton, 1987). With this techniques, strata and their corresponding sample PSU's are collapsed

together in groups and then the variability among the unit within these groups is used to derive a variance estimator.

If the strata can be ordered approximately in ascending order of the stratum means, the method of successive difference (Kish, 1965) is attractive. This method is an extension of collapsing of strata in pairs. Frequently, these methods have similar biases but the method of successive differences has some-what greater precision.

(Isaki, 1983) used auxiliary information to reduce the bias of the collapse strata variance estimator. The results suggest that when auxiliary variable is highly correlated with the survey variables, there is a substantial improvement in the accuracy of variance estimation. The collapsed strata estimator (Cochran, 1977, section 5A.12) is a well-known estimator of variance estimation in one-per-stratum problem. The procedure collapses strata with one unit per stratum into groups and treats the strata in a group as independent samples from the combined stratum. In this research, collapsing can be accomplished separately among the strata containing small and medium sized districts with one district in the sample. First arrange the strata in a non-increasing sequence based on total enrolment size. Then collapse strata into pairs or groups sequentially. The variance estimator of a group is given by (5A.56) in Cochran's (1977).

Estimation of Variance with One Unit Per Stratum ($n_h = 1$)

Let the sample observation in a typical pair be y_{j1}, y_{j2} , where j goes from 1 to $L/2$. Let $\hat{y}_{j1} = N_{g1}y_{g1}$, $\hat{y}_{j2} = N_{g2}y_{g2}$ be the estimated stratum totals.

$$V_{CS}(\hat{Y}_{str}) = \sum_{g=1}^{L/2} \frac{L_g}{L_{g-1}} \sum_{k=1}^{L_g} \left(\hat{Y}_{gh} - \frac{\hat{Y}_g}{L_g} \right)^2 \quad \text{(Cochran, 1977)}$$

Where \hat{Y}_g is the estimated total for group g for $L_g = 2$ when $\hat{Y}_g = \hat{Y}_{g1} + \hat{Y}_{g2}$. This method of estimation is called "collapsed strata".

When an auxiliary variate X_h is known for each stratum that predicts the total Y_h , (Hansen, Hurwitz, and Madow, 1953) suggested the alternative variance estimator.

$$V_{CSx}(\hat{Y}_{str}) = \sum_{g=1}^{L/2} \frac{L_g}{L_g - 1} \sum_{k=1}^{L_g} \left(\hat{Y}_{gh} - \frac{x_{gh} \hat{Y}_g}{x_g} \right)^2 \quad \text{(Hansen, Hurwitz & Madow, 1953)}$$

Strata pairs are formed so that the strata in each pair are as similar as possible in respect to the characteristics of interest. In addition, strata that do not vary much in size as measured by an auxiliary variate are often collapsed. Pairs are not formed on the basis of selected sample units.

When to Collapse Strata

- (a) When the sample contains only one unit per stratum in such a way that variance estimation within stratum (S_{yh}) is not possible to estimate.
- (b) When the first stage of sampling consist of primary sampling unit such as cities or counties and the ultimate sampling unit are households.

II. METHODOLOGY AND DATA PRESENTATION

The data were collected based on female population, male population and total population for each of the 36 states and 774 local government areas (LGA) in Nigeria based on 2006 census result. The number of states was taken to be the first stage and there were 36 states in Nigeria. The second selection is known as second stage unit. The number of the Local Government Areas in the selected states was taken as the second stage. The method of selection used here was a non-probability sampling schemes using purposive sampling. Based on this research work, considering one unit per stratum, the 36 states are called 36 strata and each of the state is called a stratum and each state constitute a number of LGA's. Therefore, one LG was

selected from each of the selected states. The LGA that has a close value to the average value of the state was chosen as a representative for the selected state.

Collapsed strata method used

Deterministic mixing method was employed.

Procedure: The probability $P_g=x_g/X$ were determined and were rearrange in ascending order with respect to P_i for each of the tables. That is:

Estimation based on sample size 12, were rearrange in ascending order and were also collapsed in pair, three, four and six w.r.t. P_i in order to form homogeneous collapsed strata. The same procedure also applies to estimation with sample size 24 and sample size 30

Collapsing of strata in pair means, dividing the number of strata by two to form number of groups.

For example, if $L=12$, $L/2=6$ groups, taking the first two strata as a group and the next two strata as another group until the sixth group is obtained.

Collapsing of strata in five means, dividing the number of strata by five to form number of groups. For example, if $L=30$, $L/5=6$ groups, taking the first five strata as a group and the next five strata as another group until the sixth group is obtained. See table 1

III. DATA ANALYSIS AND RESULT

In this section, the analysis of this research was carried out. Estimation of population total (\hat{Y}), Bias percentage (\hat{Y}) and variance of the population total ($V(\hat{Y})$) with one unit per stratum were estimated with $n= 12$ using stratified random sampling

Estimation of population total \hat{Y}_{str} with variable of interest only

$$\bar{Y}_{str} = \sum_{h=1}^n W_h \bar{y}_h \quad \hat{Y}_{str} = \frac{N}{n} M \sum_{h=1}^n W_h \bar{y}_h$$

$$n=12, \quad N=36, \quad M=774, \quad \sum W_h \bar{y}_h = 54428.8825$$

$$\hat{Y}_{str} = \frac{36}{12} \times 774 \times 54428.8825 = 126,383,865$$

$$\begin{aligned} \text{Bias Percentage} &= \frac{\text{Actual Population} - \text{Estimation Population Total}}{\text{Actual Population Total}} \times 100 \\ &= \frac{(140003542 - 126383865)}{140003542} \times 100 \\ &= 9.728\% \end{aligned}$$

Estimation of population total \hat{Y}_{str} with addition of auxiliary variable using combine Ratio Stratified Random Sampling

$$X=68,293,683$$

$$\hat{Y}_{restr} = \frac{\bar{y}_{str}}{\bar{x}_{str}} X$$

$$\hat{Y}_{restr} = \frac{\sum_{h=1}^{12} W_h \bar{y}_h}{\sum_{h=1}^{12} W_h \bar{x}_h} X = \frac{54428.88}{26685.35} \times 68293683 = 139,295,482$$

$$\begin{aligned} \text{Bias Percentage} &= \frac{(140003542 - 139295482)}{140003542} \\ &= 0.506\% \end{aligned}$$

See table 2

Estimation of $V(\hat{Y}_{str})$ in collapsing of strata in pair into six groups

a)

E

estimation of $V(\hat{Y}_{str})$ with variable of interest only

$$V_{cs}(\hat{Y}_{str}) = \sum_{g=1}^G \frac{L_g}{L_g - 1} \sum_{h=1}^{L_g} \left(\hat{Y}_{gh} - \frac{\hat{Y}_g}{L_g} \right)^2$$

$$L_g = 2, g = 1, 2, \dots, 6$$

$$\sum_{g=1}^6 \sum_{h=1}^2 \left(\hat{Y}_{gh} - \frac{\hat{Y}_g}{L_g} \right)^2 = 1.040765998 \times 10^{13}$$

$$V_{CS(2)}(\hat{Y}_{str}) = 2 \times (1.040765998 \times 10^{13}) = 2.081531996 \times 10^{13}$$

Standard error of \hat{Y}_{str}

$$SE_{cs(2)}(\hat{Y}_{str}) = \sqrt{V_{cs(2)}(\hat{Y}_{str})} = 4562380.953$$

b)

Estimation of $V(\hat{Y}_{str})$ with addition of Auxiliary

Variable

$$V_{c,xx}(\hat{Y}_{str}) = \sum_{g=1}^G \frac{L_g}{L_g - 1} \sum_{h=1}^{L_g} \left(\hat{Y}_{gh} - \frac{x_{gh}}{x_g} \hat{Y}_g \right)^2$$

$$\sum_{g=1}^6 \sum_{h=1}^2 \left(\hat{Y}_{gh} - \frac{x_{gh}}{x_g} \hat{Y}_g \right)^2 = 7.095878997 \times 10^{12}$$

$$V_{c,xx(2)}(\hat{Y}_{str}) = 2 \times (7.095878997 \times 10^{12}) = 1.419175799 \times 10^{13}$$

Standard error of \hat{Y}_{str}

$$SE_{c.sx(2)}(\hat{Y}_{str}) = \sqrt{V_{c.sx(2)}(\hat{Y}_{str})} = 3767194.977$$

Summary for the Estimated \hat{Y} and $S.E(\hat{Y})$ Based on Sample Size 12 (See table 3)

IV. DATA ANALYSIS AND RESULT

Analysis using estimation of population total (\hat{Y}), Bias percentage (\hat{Y}) and variance of the population total ($V(\hat{Y})$) with one unit per stratum were estimated with $n= 24$ using stratified random sampling. (See table 4)

Estimation of population total \hat{Y}_{str} with variable of interest only

$$\bar{Y}_{str} = \sum_{h=1}^n W_h \bar{y}_h \quad \hat{Y}_{str} = \frac{N}{n} M \sum_{h=1}^n W_h \bar{y}_h$$

$$n=24, N=36, M=774, \quad \sum_{h=1}^{24} W_h \bar{y}_h = 112723.6$$

$$\hat{Y}_{str} = \frac{36}{24} \times 774 \times 112723.6 = 130,872,095$$

$$\begin{aligned} \text{Bias Percentage} &= \frac{(140003542 - 130872095)}{140003542} \times 100 \\ &= 6.522\% \end{aligned}$$

Estimation of population total \hat{Y}_{str} with addition of auxiliary variable using combine Ratio Stratified Random Sampling

$$\begin{aligned} \hat{Y}_{rcstr} &= \frac{\bar{y}_{str}}{\bar{x}_{str}} X \\ \hat{Y}_{rcstr} &= \frac{\sum_{h=1}^{24} W_h \bar{y}_h}{\sum_{h=1}^{24} W_h \bar{x}_h} X = \frac{112723.6}{55294.39} \times 68293683 \\ &= 139,224,066 \end{aligned}$$

$$\begin{aligned} \text{Bias Percentage} &= \frac{(140003542 - 139224066)}{140003542} \times 100 \\ &= 0.557\% \end{aligned}$$

See table 5

Estimation of $V(\hat{Y}_{str})$ in collapsing of strata in pair into six groups

a)

Estimation of $V(\hat{Y}_{str})$ with variable of interest only

$$V_{cs}(\hat{Y}_{str}) = \sum_{g=1}^G \frac{L_g}{L_g - 1} \sum_{h=1}^{L_g} \left(\hat{Y}_{gh} - \frac{\hat{Y}_g}{L_g} \right)^2$$

$$L_g = 2, g = 1, \dots, 12$$

$$\sum_{g=1}^{12} \sum_{h=1}^2 \left(\hat{Y}_{gh} - \frac{\hat{Y}_g}{L_g} \right)^2 = 1.8812 \times 10^{13}$$

$$V_{CS(2)}(\hat{Y}_{str}) = 2 \times (1.8812 \times 10^{13}) = 3.7624 \times 10^{13}$$

STANDARD ERROR OF \hat{Y}_{str}

$$SE_{cs(2)}(\hat{Y}_{str}) = \sqrt{V_{cs(2)}(\hat{Y}_{str})} = 6,133,840.559$$

b) Estimation of $V(\hat{Y}_{str})$ with addition of Auxiliary Variable

$$V_{csx}(\hat{Y}_{str}) = \sum_{g=1}^G \frac{L_g}{L_g - 1} \sum_{h=1}^{L_g} \left(\hat{Y}_{gh} - \frac{x_{gh}}{x_g} \hat{Y}_g \right)^2$$

$$\sum_{g=1}^{12} \sum_{h=1}^2 \left(\hat{Y}_{gh} - \frac{x_{gh}}{x_g} \hat{Y}_g \right)^2 = 1.86269 \times 10^{13}$$

$$V_{csx(2)}(\hat{Y}_{str}) = 2 \times (1.86269 \times 10^{13}) = 3.72538 \times 10^{13}$$

STANDARD ERROR OF \hat{Y}_{str}

$$SE_{csx(2)}(\hat{Y}_{str}) = \sqrt{V_{csx(2)}(\hat{Y}_{str})} = 6,103,589.108$$

See table 6

V. TABLES

Table 1: Random digits of the selected 12 states with the Population Total, Female Population of the selected LGA and the number of LGA in the selected states

Random No Digits	selected States-L.G.A.	Pop Total of LGA	Female Pop of LGA	No of LGA
03	Akwa-Ibom-Itu	127033	59467	31
29	Osun -Obokun	116511	60965	30

13	Ekiti -Aiyekire	148193	70980	16
02	Adamawa-Mubi North	151072	72850	21
16	Imo-Ikeredu	149316	73084	27
25	Nasarawa-Obi	148874	74462	13
21	Kebbi-KokoBesse	154605	76201	21
26	Niger-Paikoro	158086	77280	25
33	Sokoto-Wurno	162307	78964	23
12	Edo-Orhionmwon	182717	90051	18
11	Ebonyi-Ohaukwu	196337	103489	13
18	Kaduna-Je,a'a	278735	133068	23

TABLE 2: Estimation of variance in collapsing of 12 strata pair into 6 groups

No of groups	Pop. Total (y_{gh})	Female Pop (x_{gh}).	$P_{gh} = \frac{x_{gh}}{X}$	N_{gh}	$N_{gh}y_{gh} = \hat{Y}_{gh}$	$\left(\hat{Y}_{gh} - \frac{\hat{Y}_g}{2}\right)^2$	$\left(\hat{Y}_{gh} - \frac{x_{gh}}{x_g} \hat{Y}_g\right)^2$	
1	Akwa-Ibom	127033	59467	0.000871	31	3938023	48994273062	71597227953
	Osun	116511	60965	0.000893	30	3495330	48994273062	71597227953
	Subtotal	243544	120432			7433353	97988546125	1.43194E+11
2	Ekiti	148193	70980	0.00104	16	2371088	1.6057E+11	1.32988E+11
	Adamawa	151072	72850	0.00107	21	3172512	1.6057E+11	1.32988E+11
	Subtotal	299265	143830			5543600	3.2114E+11	2.65975E+11
3	Imo	149316	73084	0.00107	27	4031532	1.09848E+12	1.15767E+12
	Nassarawa	148874	74462	0.00109	13	1935362	1.09848E+12	1.15767E+12
	Subtotal	298190	147546			5966894	2.19696E+12	2.31533E+12
4	Kebbi	154605	76201	0.00112	21	3246705	1.24413E+11	1.07202E+11
	Niger	158086	77280	0.00113	25	3952150	1.24413E+11	1.07202E+11
	Subtotal	312691	153481			7198855	2.48826E+11	2.14405E+11
5	Sokoto	162307	78964	0.00116	23	3733061	49318416006	2.04657E+11
	Edo	182717	90051	0.00132	18	3288906	49318416006	2.04657E+11
	Subtotal	345024	169015			7021967	98636832013	4.09313E+11
6	Ebonyi	196337	103489	0.00152	13	2552381	3.72205E+12	1.87383E+12
	Kaduna	278735	133068	0.00194	23	6410905	3.72205E+12	1.87383E+12
	Subtotal	475072	236557			8963286	7.4441E+12	3.74766E+12
	Overall Total						1.04077E+13	7.09588E+12

Table 3: Summary Table for the Estimated \hat{Y} and $S.E(\hat{Y})$ Using Stratified Random Sampling with Sample Size 12

Methods	$\hat{Y}_{str} = 126,383,865$ $Bias(\hat{Y}_{str}) = 9.728\%$ $S.E_{cs}(\hat{Y}_{str})$	$\hat{Y}_{str} = 139,295,482$ $Bias(\hat{Y}_{str}) = 0.506\%$ $S.E_{csx}(Y_{str})$
Collapsing in pair	4,562,380.953	3,767,194.927
Collapsing in three	4,274,185.051	3,652,067.891
Collapsing in four	4,102,367.353	3,580,511.818
Collapsing in six	3,879,691.526	3,501,901.105

Table 4: Random digits of the selected 24 states with the Population Total, Female Population of the selected LGA and the number of LGA in the selected states

Random No Digits	Selected States-L.G.A.	Popn Total of LGA	Female Pop of LGA	No of LGA
03	Akwa-Ibom-Itu	127033	59467	31
29	Osun -Obokun	116511	60965	30
13	Ekiti -Aiyekire	148193	70980	16
02	Adamawa-Mubi North	151072	72850	21
16	Imo-Ikeredu	149316	73084	27
25	Nasarawa-Obi	148874	74462	13
21	Kebbi-KokoBesse	154605	76201	21
08	Borno-Konduga	156564	77356	27
26	Niger-Paikoro	158086	77280	25
22	kogi -Olambolo	160152	78667	21
17	Mallammadori-Jigawa	161413	77819	27
09	Cross-river-Ikom	162383	79374	18
33	Sokoto-Wurno	162307	78964	23
10	Delta-IkaSouth	162594	82966	25
20	KatsinaMusawa	171714	83513	34
12	Edo-Orhionmwon	182717	90051	18
31	Plateau-Bassa	186859	94210	17
04	Anambra-Idemilisouth	207683	98693	21
14	Enugu-Agwu	198134	102713	17
11	Ebonyi-Ohaukwu	196337	103489	13
15	Gombe	236087	112303	11
05	Bauchi -Shira	234014	114351	20
06	Bayelsa -Ekeremor	270257	127050	8
18	Kaduna-Je,a'a	278735	133068	23

TABLE 5: Estimation of variance in collapsing of 24 strata pair into 12 groups

No of Groups	Pop. Total (y_{gh})	Female Pop (x_{gh}).	$P_{gh} = \frac{x_{gh}}{X}$	N_{gh}	$N_{gh}y_{gh} = \hat{Y}_{gh}$	$\left(\hat{Y}_{gh} - \frac{\hat{Y}_g}{2}\right)^2$	$\left(\hat{Y}_{gh} - \frac{x_{gh}}{x_g}\hat{Y}_g\right)^2$	
1	Akwa-Ibom	127033	59467	0.000871	31	3938023	48994273062	71597227953
	Osun	116511	60965	0.000893	30	3495330	48994273062	71597227953
	Subtotal	243544	120432			7433353	97988546125	1.43194E+11
2	Ekiti	148193	70980	0.00104	16	2371088	1.6057E+11	1.32988E+11
	Adamawa	151072	72850	0.00107	21	3172512	1.6057E+11	1.32988E+11
	Subtotal	299265	143830			5543600	3.2114E+11	2.65975E+11
3	Imo	149316	73084	0.00107	27	4031532	1.09848E+12	1.15767E+12
	Nassarawa	148874	74462	0.00109	13	1935362	1.09848E+12	1.15767E+12
	Subtotal	298190	147546			5966894	2.19696E+12	2.31533E+12
4	Kebbi	154605	76201	0.00112	21	3246705	2.40356E+11	2.13586E+11
	Borno	156564	77356	0.00113	27	4227228	2.40356E+11	2.13586E+11
	Subtotal	311169	153557			7473933	4.80713E+11	4.27172E+11
5	Niger	158086	77280	0.00113	25	3952150	41209203000	35555070526
	Jigawa	161413	77819	0.00114	27	4358151	41209203000	35555070526
	Subtotal	319499	155099			8310301	82418406001	71110141052
6	kogi	160152	78667	0.00115	21	3363192	48465582201	54854077799
	Cross-river	162383	79374	0.00116	18	2922894	48465582201	54854077799
	Subtotal	322535	158041			6286086	96931164402	1.09708E+11
7	Sokoto	162307	78964	0.00116	23	3733061	27520985130	4835007948
	Delta	162594	82966	0.00121	25	4064850	27520985130	4835007948
	Subtotal	324901	161930			7797911	55041970261	9670015896
8	Katsina	171714	83513	0.00122	34	5838276	1.62482E+12	2.09263E+12
	Edo	182717	90051	0.00132	18	3288906	1.62482E+12	2.09263E+12
	Subtotal	354431	173564			9127182	3.24964E+12	4.18525E+12
9	Plateau	186859	94210	0.00138	17	3176603	3.50902E+11	2.54803E+11
	Anambra	207683	98693	0.00145	21	4361343	3.50902E+11	2.54803E+11
	Subtotal	394542	192903			7537946	7.01804E+11	5.09606E+11
10	Enugu	198134	102713	0.0015	17	3368278	1.66422E+11	1.75636E+11
	Ebonyi	196337	103489	0.00152	13	2552381	1.66422E+11	1.75636E+11
	Subtotal	394471	206202			5920659	3.32844E+11	3.51271E+11
11	Gombe	236087	112303	0.00164	11	2596957	1.08506E+12	1.01764E+12
	Bauchi	234014	114351	0.00167	20	4680280	1.08506E+12	1.01764E+12
	Subtotal	470101	226654			7277237	2.17012E+12	2.03529E+12
12	Bayelsa	270257	127050	0.00186	8	2162056	4.51318E+12	4.10165E+12
	Kaduna	278735	133068	0.00194	23	6410905	4.51318E+12	4.10165E+12
	Subtotal	548992	260118			8572961	9.02636E+12	8.20331E+12
	overall Total						1.8812E+13	1.86269E+13

Table 6: Summary Table for the Estimated \hat{Y} and $S.E(\hat{Y})$ Using Stratified Random Sampling with Sample Size 24

Methods	$\hat{Y}_{str} = 130,872,095$ $Bias(\hat{Y}_{str}) = 6.522\%$ $S.E_{cs}(\hat{Y}_{str})$	$\hat{Y}_{rcstrx} = 139,224,066$ $Bias(\hat{Y}_{str}) = 0.557\%$ $S.E_{csx}(Y_{str})$
Collapsing in pair	6,133,840.559	6,103,589.108
Collapsing in three	5,208,694.654	5,449,171.191
Collapsing in four	5,515,106.527	5,449,171.191
Collapsing in six	5,289,514.155	5,250749.168
Collapsing in twelve	5,223,300.942	5,194,504.089

V. CONCLUSIONS

According to the results obtained from the analysis, **estimation with sample size 12** using stratified random sampling with variable of interest only and with addition of auxiliary variable, shows that the higher the extent of collapsing of strata, the lower the standard error of \hat{Y}_{str} .

This implies that, the higher the extent of collapsing of 12 strata, the more precise the variance estimator but it was not so using Simple random sampling. Comparing the two estimators, stratified random sampling with addition of auxiliary variable seems to be the best estimator, because it gives the least standard error of \hat{Y}_{str} to be **3,501,901.105** under the collapsing of 12 strata in six into two groups and least bias of **0.506** percentage and estimated population total of **139,295,482** which was very close to the actual population total of Nigeria based on 2006 census result (**140,003,542**). Therefore, higher group of collapsing of strata should be employed for smaller number of strata 12. Estimation with sample size 24 using stratified random sampling with variable of interest only, and with addition of auxiliary variable show that the higher the extent of collapsing of strata, the standard error of \hat{Y}_{str} was inconsistent (i.e. decreasing). The least standard error falls under collapsing of strata in twelve for estimation with sample size 24. Therefore, lower group of collapsing of strata should be employed for large number of strata (24), so that the variation within the collapsed strata will be minimized.

Estimation using stratified random sampling with addition auxiliary variable gave a better result than estimation with variable of interest only.

REFERENCES

- [1] Cochran, William G., description of method of "collapsed strata" in Sampling Techniques, 1977, pp 139-140.
- [2] Hansen, M.H., Hurwitz, W.N., and Madow, W.G. (1953): Sample Survey Methods and Theory. Vol.II. Methods and Applications.
- [3] Kish, L. (1965): Survey sampling. John Wiley and Sons, New York.
- [4] Parsons, V.L. and Eltinge, J.L. (1999). Stratum partition, collapse and mixing in construction of Balanced repeated replication variance estimators. Paper presented at the 1999 Joint Statistical Meetings, Baltimore, Maryland.
- [5] Rust, K. and Kalton, G. (1987). Strategies for collapsing strata for variance estimation. *Journal of Official Statistics* 3, pp69-81.

Performance and Emission Characteristics of Direct Injection Diesel Engine Running On Canola Oil / Diesel Fuel Blend

Anbarasu.A^{*1}, Karthikeyan.A.²

¹Research Scholar, Sathyabama University, Chennai, India ; Eami: senthilram199@yahoo.co.in.

²Sathyabama University, Chennai, India

ABSTRACT : The increase of petroleum price and environmental problems has triggered the finding of alternative and renewable energy. In this study, biodiesel produced by transesterification of triglycerides with alcohol. Canola oil was used as raw oil to produce biodiesel by transesterification reaction. The prepared biodiesel was then subjected to performance and emission tests in order to evaluate its actual performance, when used as a diesel engine fuel. A single cylinder direct injection diesel engine was used for this work to investigate the engine performance and emission characteristics of the biodiesel, The brake specific fuel consumption (BSFC) and brake thermal efficiency (BTE) were calculated from the recorded data. From the emission tests, it is observed Hydrocarbon and NO_x pollutants are decreased along with the percentage of biodiesel.

KEYWORD : Canola biodiesel, Diesel Engine, Emission, Engine performance, Esterification

I. INTRODUCTION

The exponential growth of world population would ultimately lead to increase the energy Demand in the world. Petroleum is a non-renewable energy source, which means that the resources of this kind of fossil fuel are finite and would be run out upon continuous use. Both of the shortage of resources and increase of petrol price have led to the findings of new alternative and renewable energy sources. Apart from these situations, environmental issues are also the driving forces for the development of alternative energy sources, since the burning of fossil fuels would cause various environmental problems including global warming, air pollution, acid precipitation, ozone depletion, forest destruction, and emission of radioactive substances [1]. The alternative energy sources of fossil fuels including hydro, wind, solar, geothermal, hydrogen, nuclear, and biomass [2]. Among these alternative energy sources, biofuels derived from biomass are considered as the most promising alternative fuel sources because they are renewable and environmental friendly. Like canola oil, it can be directly used in diesel engines as they have a high cetane number and calorific value very close to diesel [3]. Canola oil is environment friendly and does not produce Volatile organic Compounds as atmospheric pollutants. The aim of the study was to check the performance and the emission of fuel properties of canola oil (biodiesel), diesel and its blends of direct injection diesel engine.

II. MATERIALS AND METHODS

Preparation of biodiesel

Biodiesel was prepared in the laboratory using the seed oil of the Canola. 1.5g of NaOH per litre of oil was mixed with 200 ml of methyl alcohol to produce methoxide [4]. Oil was heated to 60°C and the prepared methoxide was poured into the oil. The reaction was allowed for one hour and the final products were allowed to settle in the separating funnel overnight to produce two distinct liquid phases: crude ester phase at the top and glycerol phase at the bottom. The crude ester phase separated from the bottom glycerol phase was transferred to a clean conical flask. The biodiesel produced contains some residues including excess alcohol, excess catalyst, soap and glycerin. It was purified by washing with distilled water to remove all the residual by-products. The volume of water added was approximately 30% (volume) of the biodiesel. The flask was shaken gently for 1 minute and placed on table to allow separation of biodiesel and water layers. After separation, the biodiesel was

transferred to a clean conical flask. The washing process was repeated for several times until the washed water became clear. The clean biodiesel was dried in incubator for 48 hours, followed by using sodium sulphate. The final products were analyzed to determine related properties including viscosity, total acid numbers (TAN). The properties of biodiesel are listed in Table 1. The experiments were conducted in different loads like 25%, 50% and 75% of full load and full load. Similar experiments were done with diesel and biodiesel so as to make a comparison.

Experimental setup and procedure :The performance tests for the stable Diesel-biodiesel are carried out on a computerized single cylinder four stroke direct injection variable compression ratio engine. The Table 2 shows the specification of the engine. No modification or alteration has been made in the engine. The experimental setup consists of a variable compression ratio engine is coupled to an eddy current dynamometer. A computerized data acquisition system is used to collect, store and analyze the data during the engine testing. A Kistler piezoelectric pressure transducer and a crank angle encoder is used to measure the in-cylinder gas pressure and the corresponding crank angle. The load applied on the engine is measured by the load cell connected to the eddy current dynamometer. A burette with two infra red optical sensors measures the fuel flow rate, an air flow sensor measure the inlet air flow rate, K type thermocouples measure the inlet air and exhaust gas temperatures. AVL DIGAS analyzer is used to measure the exhaust gas constituents such as CO, HC, NO and the smoke is measured using the AVL smoke meter. All the experiments are conducted at the compression ratio of 17.5 and the results are recorded under steady state conditions.

The fuels which have been used in this study are: Commercial diesel (D) and a blend of 20% biodiesel (B20), 40% biodiesel (B40), 60% biodiesel (B60) and 100% biodiesel (B100). The main properties of the test fuels are given in Table 3. The test engine were fueled with diesel, B20, B40, B60 and B100 to conduct the experiments on an electrical dynamometer earlier, experiment were performed by using different blends of biodiesel and diesel. In this study, speed characteristics tests have been carried out for wide open throttle (WOT), while load characteristics tests have been conducted at 1500 rev/min speed at 220bar injection pressure. Following major parameters were measured: Fuel flow rate, Crank angle, Instantaneous pressure in cylinders, Combustion characteristics.

III. RESULTS AND DISCUSSIONS

Performance characteristics

Brake Thermal Efficiency (BTE)

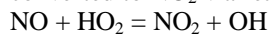
The Brake thermal efficiency is the true indication of the efficiency with which the chemical energy input in the form of fuel is converted into useful work [5]. In the present study BTE of the diesel engine is measured using different blends of biodiesel and diesel. The variations of brake thermal efficiencies at different loads for various combinations have been shown in figure 1. Brake thermal efficiency increases with the increasing load. However, the load reaches 75% and above, it almost constant. The brake thermal efficiency of biodiesel (B100) is 98.2% same compared with diesel(D100), which is clearly shown in the figure 1. BTE for D100 is maximum compared with blends and biodiesel, this may be due to lower heat value of the fuel. It is well known that the lower heat value of the fuel affects the engine power. The effective power decreases with the increase of blends and biodiesel. Thus, the engine needs more fuel consumption to maintain the same amount output power[6].

Brake Specific Fuel Consumption : Brake specific fuel consumption is the ratio between mass fuel consumption and brake power. Figure 2 shows the variations of brake specific fuel consumption with load for different fuels. For all fuels tested, brake specific fuel consumption is found to decrease with increase in the load also it is lower than the blends of biodiesel(B20, B40, B60 and B100) compared with diesel(D100). The BSFC of pure biodiesel (B100) is 113% higher than that of diesel (D100). The BSFC will appear when the rate of increase of fuel consumption is larger than that of engine power output with the increase of engine speed.

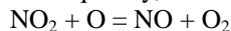
Exhaust Gas Temperature :The exhaust gas temperature (EGT) increases while the load is increased. The EGT of biodiesel is lower than that of diesel. It is shown in the figure 3.

Emissions characteristics :The emissions of HC and NO_x are illustrated in figures 4 and 5. Figure 4 demonstrates HC emissions at different loads for various fuels. HC gradually decreases with biodiesel-diesel blends although, there is no significant change is observed for B40. which is due to almost even mixer of biodiesel and diesel. The higher load, the lower the HC emissions expect diesel(D100) is observed. This phenomenon can be attributed to better mixing of air and fuel at higher load.

The higher the biodiesel percentage in biodiesel-diesel blends, the lower the HC emissions are observed. This is due to the fact that the higher O₂ concentration in the air-fuel mixture can help enhance oxidation of unburned hydrocarbons. Figure 5 illustrates NO_x emissions at different loads for various fuels. NO_x emissions of biodiesel blends and neat biodiesel are higher than diesel at all loads. This is the opposite tendency with the results reported by Geo et al., 2008 [7]. Smoke emissions decreased with increase in biodiesel concentration in the biodiesel blends with diesel. In general, NO_x emissions is increases if load is increases with all fuels. In light loads emission is slightly lower for biodiesel and blends compared with diesel. At light load operations, the engine runs at a very lean state and with a small biodiesel or canola oil blends. Extra O₂ in biodiesel and canola oil blends in this case does not help produce higher NO_x, because the mixture is already very lean. This might be a reason why no NO_x increase with 2–5% blends is observed. Higher NO_x emissions are obtained with higher percentage of biodiesel and canola oil in the blends. This is common trend in NO_x emissions with biodiesel blends. This is mainly attributed to O₂ content in biodiesel and higher combustion temperature. Higher canola oil–diesel blend produces much higher NO_x probably because of lower cetane number and its consequence of longer ignition delay; NO₂ production at high idling operations is very significant and even higher than NO production and its share in total NO_x is more than 50%. This is ignored most of the times as in describing the state that in most high temperature combustion processes, the majority (95%) of NO_x produced is in the form of NO. Even some gas analyzer has used the same principle to calculate the NO_x emissions from NO measurements and considering that NO is 95% of total NO_x. This might be true for gasoline engine, however, diesel engine emits much higher NO₂. NO formed in the flame zone can be rapidly converted to NO₂ via reactions such as



Subsequently, conversion of this NO₂ to NO occurs via



unless the NO₂ formed in the flame is quenched by mixing with cooler fluid. Under light load operating conditions, there are many cooler regions and NO₂ formed in the flame is quenched and could not be converted back to NO. Hence, higher amount of NO₂ is produced at light load operations. This suggests that a proper care be needed to report NO_x emissions from biodiesel combustion, especially at high idling operation. This also suggests that NO_x abatement technology must include a system to address both NO₂ and NO reduction.

Smoke opacity : The variation of fuel smoke opacity of the engine with various fuels is demonstrated in figure 6. The smoke opacity of biodiesel is lower than the smoke opacity of diesel. Agarwal et al., 2008[8] reported that 20% biodiesel blend showed maximum lowest smoke opacity compared to all other biodiesel blends (10, 30, 50 and 100%, v/v). In the present study the same trend was observed. B20 blend having lower smoke opacity compared with other blends and diesel. An important observation is that all biodiesel blends have higher thermal efficiency than diesel fuel.

IV. CONCLUSIONS

Biodiesels have been produced and their fuel characteristics have been investigated. An experimental investigation has been conducted to explore the performance and emissions of biodiesel and its blends at high idling operations on a small DI diesel engine. The results obtained suggest the following conclusions:

- [1] The fuel properties of canola oil are slightly different from those of diesel. The BSFC and exhaust gas temperature for canola oil are higher than that for diesel fuel while BTE for canola oil is generally lower than that for diesel fuel. This is probably resulting of lower heat value of canola oil, which is distinctly lower than that of the diesel fuel.
- [2] HC emissions for all blends and biodiesel fuels are lower at different loads, and the higher the biodiesel percentage in biodiesel– diesel blends, the lower the HC emissions. Higher blends of canola oil and higher loads deteriorate HC emissions.
- [3] Up to 5% biodiesel and canola oil in the blends, there is no increase in NO_x emissions, in fact canola oil up to 5% in the blends shows a little reduction of NO_x emissions than diesel. However, B20 has 12–26% NO_x increase at different engine loads. Canola oil and diesel fuels exhibit different combustion and emission characteristics with the variation of engine load due to their different properties. Based on the exhaustive engine tests, it can be concluded that biodiesel can be adopted as an alternative fuel for the existing conventional diesel engines without any major modifications required in the system hardware. The use of canola-based biodiesel solves the problem of the toxic organic pollutant emissions from the diesel engines. Indian government should increase the rate of canola oil production to produce more biodiesel. Furthermore, not only for India, the conclusion of this study also applies to many other countries in the world.

REFERENCES

[1] A Demirbaş, Biodiesel production from vegetable oils via catalytic and non-catalytic supercritical methanol transesterification methods. Progress in Energy and Combustion Science, 31, 2005, 466-487.

[2] Dincer Ibrahim, Renewable energy and sustainable development : a crucial review. Renewable & Sustainable Energy Reviews, 4 2000, 157-175.

[3] Hossain, A.B.M.S., Mekhled, M. A.. Biodiesel fuel production from waste canola cooking oil as sustainable energy and environmental recycling process, Australian journal of crop science, (2010), 4(7):543-549.

[4] Kannan,T.K., R.Marappan , Study of Performance and Emission Diethy Characteristics of a Diesel Engine using Thevetia Peruviana Biodiesel with Ether Blends. European Journal of Scientific Research,2010, 43 (40) 563-570.

[5] Jaichandar, S. and Annamalai, K. Effects of open combustion chamber geometries on the performance of pongamia biodiesel in a DI diesel engine. Fuel. 98 (2012) 272-279.

[6] Sayin cenk, Metin Gumus and Mustafa canakci. Effect of fuel injection pressure on the injection, combustion and performance characteristics of a DI diesel engine fueled with canola oil methyl esters-diesel fuel blends. Biomass and bioenergy . 46 (2012) 435-446.

[7] Geo VE, Nagarajan G, Nagalingam B. A comparative combustion analysis of rubber seed oil and its methyl ester in a DI diesel engine. SAE (2008) 01, 1386.

[8] Agarwal D, Kumar L, Agarwal AK. Performance evaluation of a vegetable oil fuelled compression ignition engine. Renewable Energy,(2008), 33, 1147–56.

Table 1. Properties of biodiesel (canola oil)

Viscosity	5.38(cst)
Density	886.5(Kg/m ³)
Flash point	172°c
Fire point	186°c
Calorific Value	38758 KJ/Kg

Table 2. Specification of the single cylinder four stroke direct injection engine

Brake Power	3.7 kW
Speed	1500 rpm
Compression ratio	17.5 (Variable)
Bore	80 mm
Stroke	110 mm
Ignition	Compression ignition
Cooling	Water cooled
Loading System	Eddy current dynamometer

Table 3 Properties of test fuels

Acidity as mg of KOH/gm	0.01
Density (kg/m ³)	886.5
Viscosity at 40 °C	5.38
Gross calorific value (KJ/kg)	38758
Cetane number	48
Sulfur content (mg/L)	< 50ppm
Flash point	172°c
Fire point	186°c

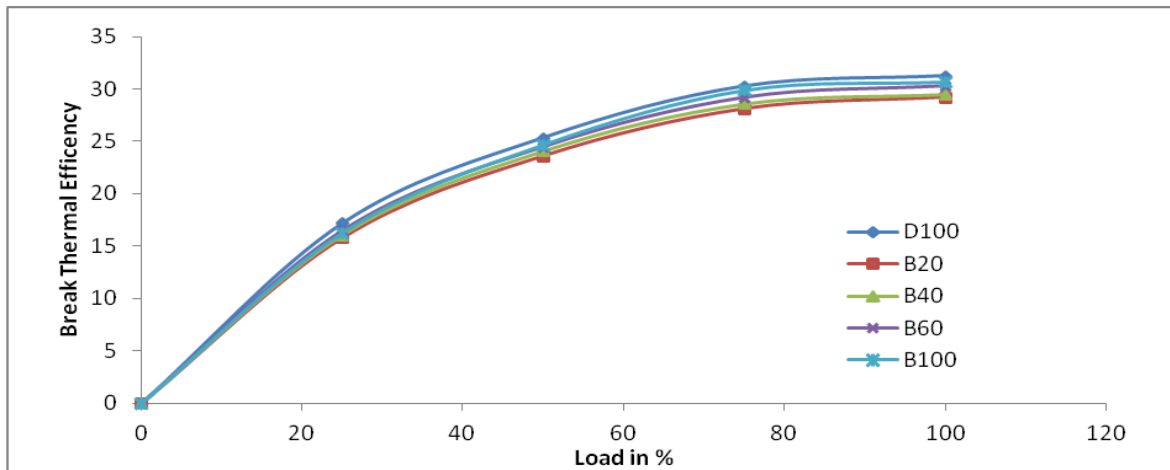


Figure 1. Load Vs Break Thermal Efficiency for different blends of biodiesel and diesel

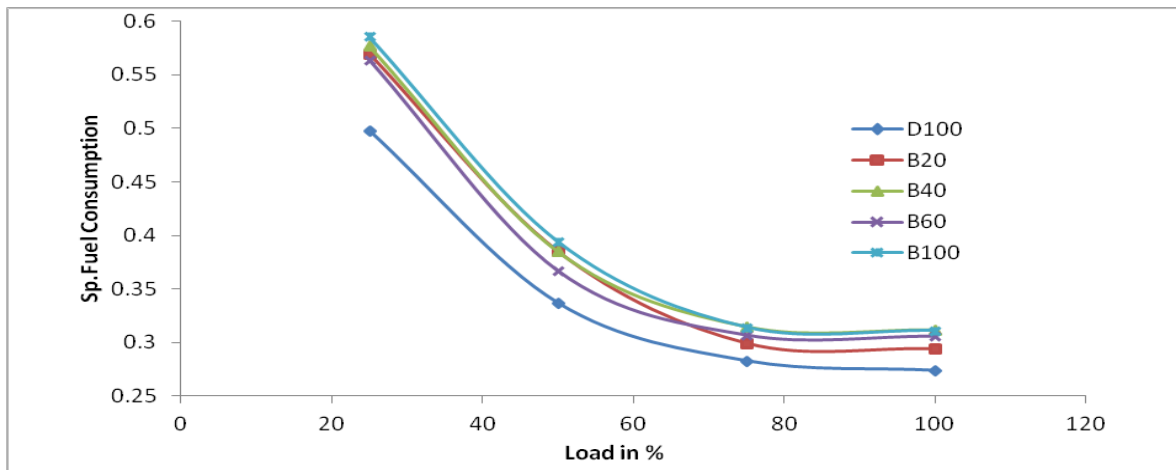


Figure 2. Load Vs Brake specific fuel consumption for different blends of biodiesel and diesel

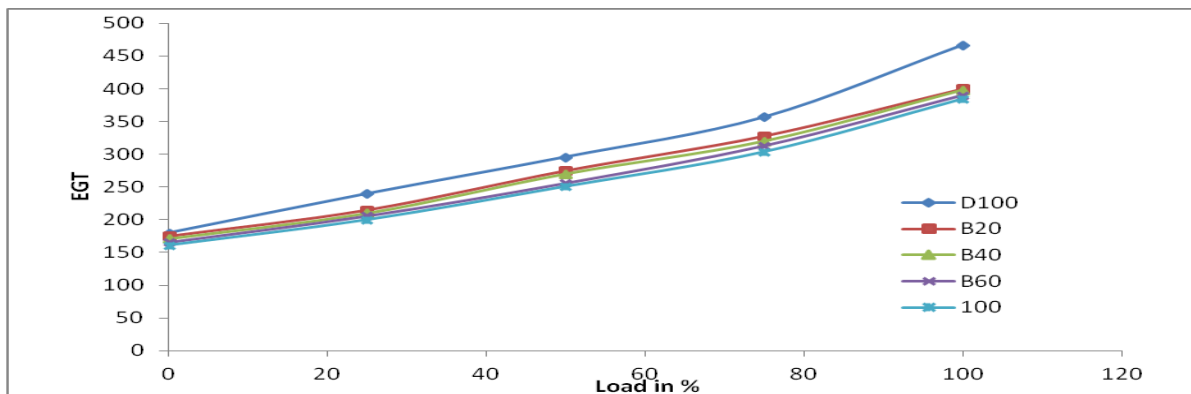


Figure 3. Load Vs Exhaust Gas Temperature for different blends of biodiesel and diesel

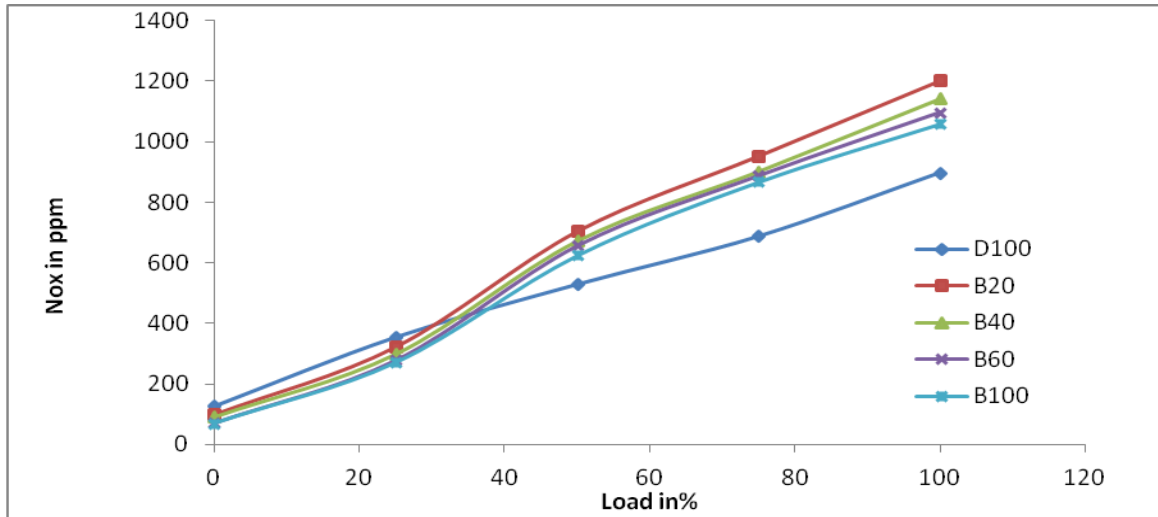


Figure 4. Load Vs Hydro carbon emission for different blends of biodiesel and diesel

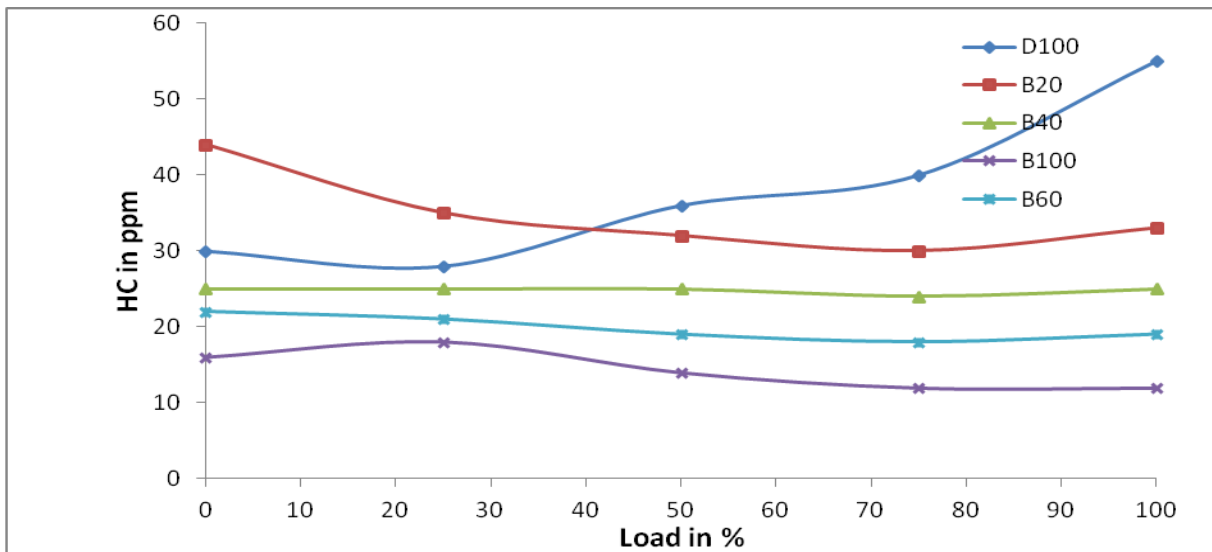


Figure 5. Load Vs NOx emission for different blends of biodiesel and diesel

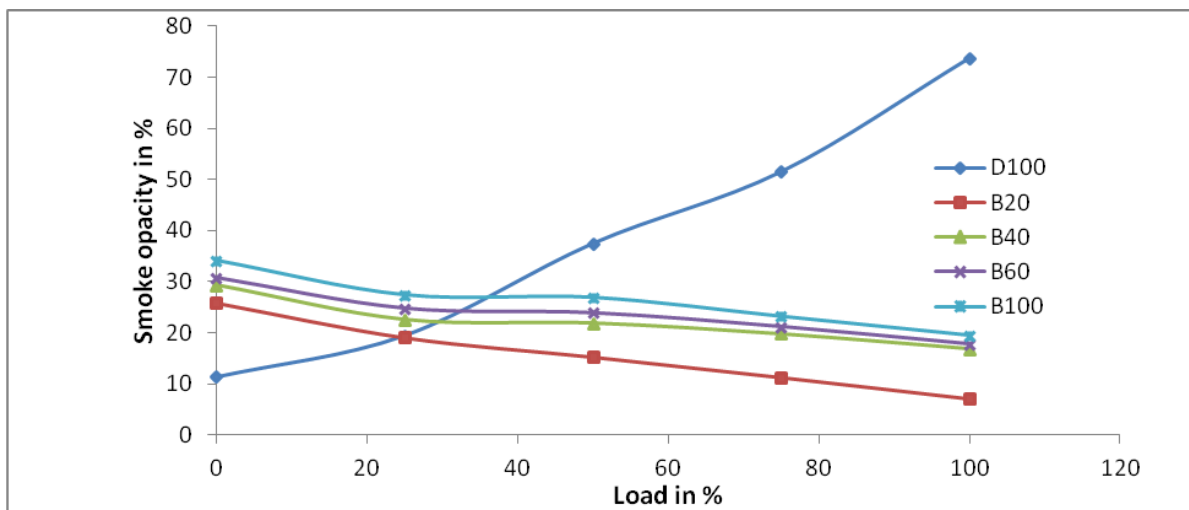


Figure 6. Load Vs smoke opacity for different blends of biodiesel and diesel

Investigation of the Potential of Jatropha Seed Oil as Austempering Quenchant for Medium Carbon Steel

Akor, T.¹ Ashwe, A.²

¹ Department of Mechanical Engineering, Nigerian Defence Academy Kaduna

² Department of Mechanical Engineering, University of Agriculture, Makurdi.

ABSTRACT: This study investigates the suitability of jatropha seed oil as quenching medium for austempering medium carbon steel. Test samples were austenitized at 950°C; soaked for 1hr; austempered for varying periods of 1, 2, 3, 4 and 5hrs. The result showed significant increase in tensile strength and impact energy apart from achieving an appreciable increase in hardness. It also tally with recommended values of medium carbon steel austempered in salt bath, implying that jatropha oil can be used as hot bath for the austempering of medium carbon steel.

KEY WORDS: austempering, austenitized, bainite, soaked, matrix.

I. INTRODUCTION

Heat treatment can be defined as a process in which steels or alloys are acted upon thermally so as to change their structures and properties in the desired direction. Austempering heat treatment is a high performance isothermal heat treatment alternative to conventional quenching and tempering, that imparts superior performance to ferrous metals. It is a multi-step process that includes austenitizing, followed by cooling rapidly enough to avoid the formation of pearlite to a temperature above the martensite start (Ms) and then holding until the desired microstructure is formed, [1]. The metallurgical phase obtained is called bainite. In conventional heat treatment, parts are quenched to room temperature, and martensite reaction begins immediately which is actually a “non-uniform phase transformation” due to inside and outside temperature differences in the quenched part, [2]. This non-uniformity causes distortion and tiny micro-cracks to appear which reduce the strength of the part. However, during the austempering cycle, occurrence of bainite takes place over a longer period of time (many minutes or hours). This results in uniform growth, and a much stronger (less disturbed) microstructure.

Austempering is usually a preferred heat treatment especially to conventional quenching and tempering. This is mainly because this type of heat treatment offers:

- improved mechanical properties (particularly higher ductility or notch toughness at a given high hardness);
- a reduction in the likelihood of distortion and cracking which can occur in martensitic transformations;
- lower cost than that of conventional quenching and tempering. ;
- conventional quenching and tempering comprise a three step operation – that is, austenitizing, quenching and tempering, whereas austempering requires only two processing steps, [3].

Salt bath has been the conventional quenching medium for austempering heat treatment of steels. However, oils are among the quenching media of industrial significance. Oils of mineral and vegetable origins have been used as quenchant. The use of oils of mineral origin is however compromised by the film or nucleate boiling heat transfer they exhibit, resulting to lower-temperature cooling rates. This characteristic is absent in vegetable oils, where heat transfer is dominated by convective cooling, [4]. The cooling rate for vegetable oils is faster than that of comparable quenchant, making them suitable for austempering heat treatment. The cooling time-temperature and cooling-rate curves obtained show that the cooling properties of series of vegetable oils appear to be comparable to each other. The development of a quenchant from locally available vegetable oils as feed stock, especially the non consumable oils is expected to be a significant contribution to the foundry industry. Jatropha seed oil is non consumable vegetable oil which has little or no application in human nutrition.

In this study the potential of jatropha seed oil as austempering quenchant for medium carbon steel has been investigated .

II. METHODOLOGY

The raw materials used in this study include jatropha seed oil and medium carbon steel. The medium carbon steel was procured from Total Steel Kaduna. It was analyzed at the National Geosciences Research Laboratory Kaduna for the experimental work. The chemical composition of the steel is shown in Table 1. Jatropha seeds were harvested from Rafin Sewa Gora; Zango LGA of Kaduna State and processed for oil at National Research Institute for Chemical Technology, (NARICT), Zaria, Kaduna State.

Table 1: Chemical Composition of the Material

C	Mn	Si	S	P	Mg	Cu	Al	Balance
0.62	0.7	0.31	0.004	0.046	0.001	0.119	0.002	Fe

Due to the fact that the chemical composition of AISI 1080 steel is similar to that of medium carbon steel; TTT diagram of 1080 steel was used as a reference during this study. Samples for tensile tests and charpy impact tests were machined from the medium carbon steel procured from Total Steel. Prior to testing, the samples were austenitised at 950^oC for 1hr and then austempered in hot jatropha oil bath at 250^oC for varying periods of 1hr, 2hrs, 3hrs, 4hrs and 5hrs. After austempering samples were air cooled, after which they were washed with kerosene. Samples were tested in the as recieved and austempered condition. A minimum of three samples were tested for each heat-treatment condition. Screw-type samples (ASTM.A370-68) with 5mm diameter and 75mm gauge length were used for tensile tests. All tensile tests were performed at room temperature. Each sample was subjected to tension till fracture, at a strain rate 1.3x10⁻³s⁻¹. The dimensions of the notched charpy samples were 5x5x50mm. Standard ASTM procedure defined with designation number E 23-93a (Standard test methods for notched bar impact testing of metallic materials) was employed in this study. The test consists of measuring the energy absorbed in breaking, by one blow from a pendulum. At least three samples were tested for each austempering period and an average value taken. Hardness test was done according to standard ASTM procedure defined with designation number E18–1989.

III. RESULT AND DISCUSSION

Fig. 1 displays the effect of austempering time on the tensile strength of medium carbon steel specimens austenitised at 950^oC and austempered in hot jatropha oil bath maintained at 250^oC. It can be observed from the figure that the tensile strength of the medium carbon steel increased with increase in austempering time up to the optimum values at 5hrs. This increase in tensile strength is attributed to the formation of bainite in the matrix of the medium carbon steel, [5]. The figure indicates that the reaction is within stage one (Stage I reaction $\gamma_H \rightarrow \alpha + \gamma_{HC}$ -toughening); since there is no downward movement of the plot to indicate embrittlement as a result of the formation of cementite. Fig. 2 shows percentage elongation of the austempered medium carbon steel decreasing with austempering time. This is also in agreement with the stage I austempering reaction shown above. Fig. 3 shows the effect of austempering time on the hardness of medium carbon steel specimens austempered in hot jatropha oil bath. It is evident that as the austempering time increased the hardness values of the austempered specimens decreased to minimum value of 239BHN. Fig. 3 shows the effect of austempering time on the impact energy and hardness of medium carbon steel specimens austempered at 250^oC in hot jatropha oil baths. The impact energy values increase progressively with austempering time, whereas the hardness is observed to decrease with austempering time. This indicates a progression in the stage 1 reaction, increasing the amount of bainite in the matrix of the medium carbon steel. This is in agreement with [6].

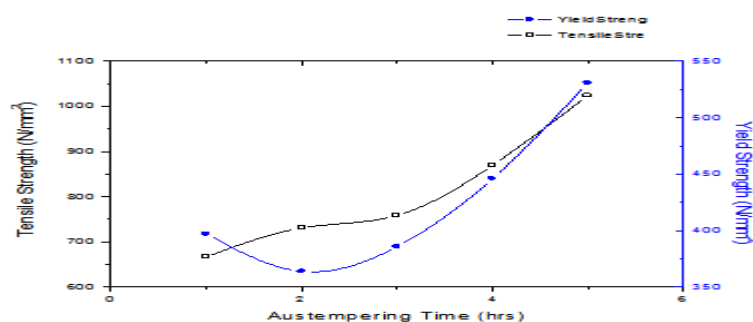


Figure 1: Effect of austempering time on the tensile strength and yield strength of medium carbon steel austenitized at 950^oC and austempered in hot jatropha oil at 250^oC for varying periods.

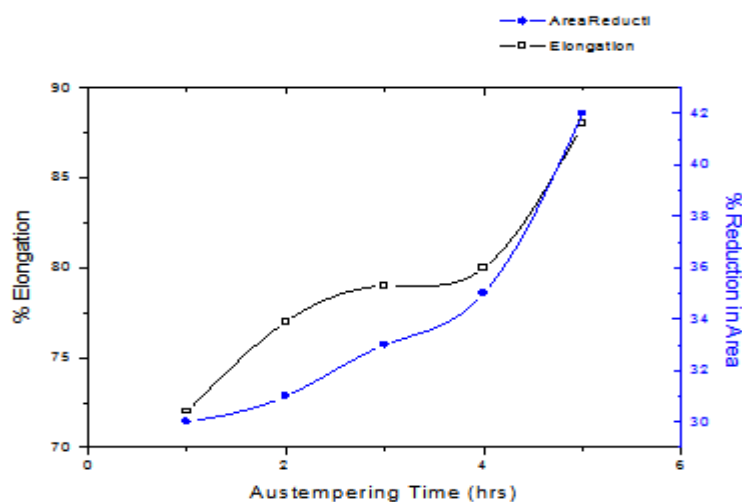


Figure 2: Effect of austempering time on percentage elongation and reduction in area of medium carbon steel austenitized at 950°C and austempered in hot jatropa oil at 250°C for varying periods

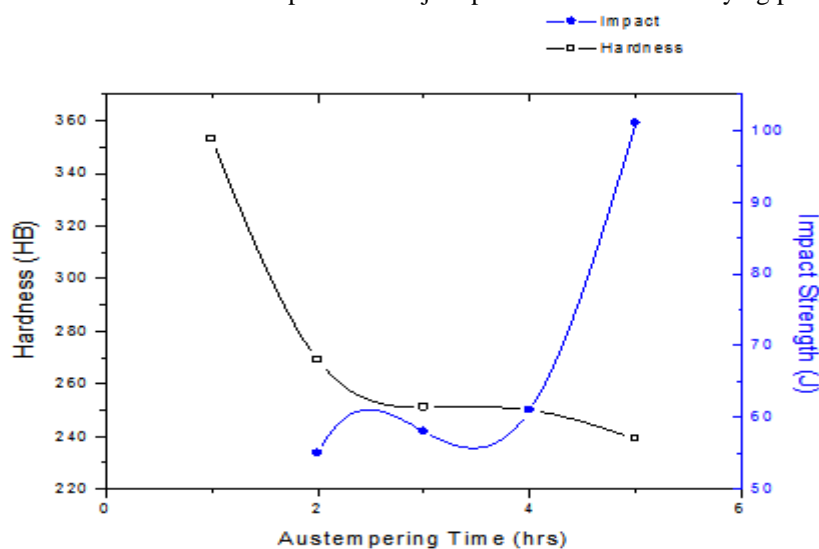


Figure 3: Effect of austempering time on Hardness superimposed on Impact strength values of medium carbon steel austenitized at 950°C and austempered in hot jatropa oil at 250°C for varying periods

IV. CONCLUSION

This research work investigated the potential of Jatropa, seed oils as austempering quenchants for medium carbon steel. From the observations and analysis of the results obtained, it can be deduced that; Jatropa was able to cause the formation of 'bainite' structure at 250 °C in the medium carbon steel. There is appreciable improvement in mechanical properties of the medium carbon steel when austempered in jatropa seed oil. The as-cast tensile, hardness and impact energy values of 570 N/mm²; 196 BHN and 31J increased to 962 N/mm²; 349 BHN and 47 J. The results indicate improvement in the mechanical properties of the ductile cast iron.

REFERENCES

- [1] Z. Li and D.Wu, Effects of Holding Temperature for Austempering on Mechanical Properties of Si- Mn TRIP Steel, *Journal of Iron and Steel Research International*, 11(6), 2004, 40-44.
- [2] R.A. Higgins, *Engineering Metallurgy* 1st Edition. (Edward Arnold Ltd London, UK). 34-49, 218-234, 239-257, 259-278
- [3] Metals Handbook, *Heat Treating of Ductile Irons*, (American Society for Metals), 9(4), 1981.
- [4] G.E Totten, H.M Tensi and K. Lanier. Performance of vegetable oils as cooling medium in comparison to a standard mineral oil, *Journal of Materials Engineering.*, 8(4), 1999. 409-416.
- [5] Z. Lawrynowicz, Transition from upper to lower bainite in Fe-C-Cr steel, *Materials Science and Technology Journal*, 20, 2004, 1447-1454
- [6] Putatunda S.K., Influence of Austempering Temperature on Microstructure and Fracture Toughness of a High- Carbon, High-Silicon and High-Manganese Cast Steel", *Materials & Design*, 24(6), 2003, 435-443.

Denoising Of TDM Signal Using Novel Time Domain and Transform Domain Multirate Adaptive Algorithms

C Mohan Rao¹, Dr. B Stephen Charles², Dr. M N Giri Prasad³

¹Asso. Prof., Department of ECE, NBKRIST, Vidhyanagar, India

²Principal, SSCET, Kurnool, India

³Prof. & Head, Department of ECE, JNTUACE, Anantapuram, India

ABSTRACT : The Gaussian noise is obvious in most of the communication channels. The impulsive noise tends to Gaussian form as the time slot extends over a significant period. In this paper a channel with Gaussian noise is considered. A TDM signal passed through this kind of channel was applied to denoising. The denoising was implemented in time as well as transform domain. The adaptive algorithms like LMS, NLMS, RLS, LSL and transform domain LMS implementations using wavelet packets are designed. Two new algorithms are proposed and verified with the above application; one a variation of LMS and second binary step size LMS. From the simulation results it was found that the multirate adaptive algorithms proposed give better performance than the existing techniques.

KEYWORDS : Denoising, TDM, LMS, Wavelet Packet

I. LMS ALGORITHM

The simplified block diagram of a transversal adaptive FIR filter is depicted in figure 1, where the block denoted by adaptive filter comprises as adaptive filter $\hat{h}(n) = [\hat{h}_1(n), \hat{h}_2(n), \dots, \hat{h}_N(n)]$ and algorithm, $x(n)$ is the input sequence from which the input vector $X(n) = [x(n), x(n-1), \dots, x(n-N+1)]^T$ is obtained, $e(n)$ is the output error, $\hat{y}(n)$ is the output of the adaptive filter and $d(n)$ is the desired signal. All the theoretical derivations are referred to figure 1.

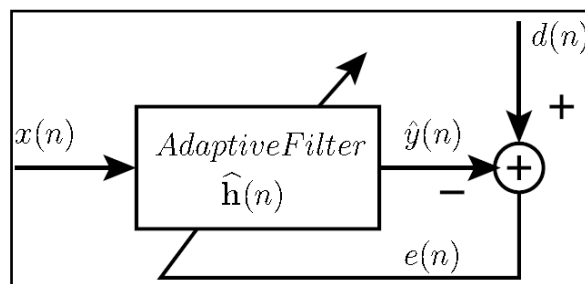


Fig. 1 Simplified block diagram of an adaptive FIR filter

In connection with figure 1, the output of the adaptive filter can be written as follows:

$$\hat{y}(n) = \hat{h}^T(n) X(n) = X^T(n) \hat{h}(n) = \sum_{i=1}^N \hat{h}_i(n) x(n-i+1) \quad (1)$$

where T is the transposition operator. The output error is expressed by the following equation [1][2]:

$$\hat{h}(n+1) = \hat{h}(n) - \frac{1}{2} \mu \nabla J(n) \quad (10)$$

$$\text{where } \nabla J(n) = \left[\frac{\delta J(n)}{\delta \hat{h}_1(n)}, \frac{\delta J(n)}{\delta \hat{h}_2(n)}, \dots, \frac{\delta J(n)}{\delta \hat{h}_N(n)} \right]^T \text{ and}$$

$$\frac{\delta J(n)}{\delta \hat{h}_i(n)} = -2 E[x(n-i+1)e(n)] \quad (11)$$

In order to compute the elements of the gradient in equation (11), the expectation operator must be used. A simpler alternative is to use the instantaneous gradient instead of the true gradient and the obtained algorithm is called the Least Mean Square (LMS). As a consequence, the LMS algorithm uses the following coefficient update formula:

$$\hat{h}(n+1) = \hat{h}(n) + \mu e(n) X(n) \quad (12)$$

where the step-size μ was introduced to control the stability of the algorithm. Finally, the LMS algorithm can be described by the following four steps:

1. From the input vector $X(n) = [x(n), x(n-1), \dots, x(n-N+1)]^T$ from the input sequence $x(n)$.
2. Compute the output of the adaptive filter: $\hat{y}(n) = X^T(n) \hat{h}(n) = \hat{h}^T(n) X(n)$.
3. Compute the output error: $e(n) = d(n) - \hat{y}(n)$.
4. Update the coefficients of the adaptive filter: $\hat{h}(n+1) = \hat{h}(n) + \mu e(n) X(n)$.

II. VARIATION OF LMS

If it were possible to make exact measurements of the gradient vector in all iterations and if the step-size parameter μ is suitably chosen, then the tap-weight vector computed by using the method of steepest-descent would indeed converge to the optimum Wiener solution. In reality, however, exact measurements of the gradient vector are not possible, and it must be estimated from the available data. In other words, the tap-weight vector is updated in accordance with an algorithm that adapts to the incoming data. One such algorithm is the least mean square algorithm. A significant feature of LMS is its simplicity; it does not require measurements of the pertinent correlation functions, nor does it require matrix inversion. The LMS algorithm is a search algorithm in which a simplification of the gradient vector computation is made possible by appropriately modifying the objective function. The LMS algorithm, as well as others related to it, is widely used in various applications of adaptive filtering due to its computational simplicity. The convergence speed of the LMS is shown to be dependent on the eigenvalue spread of the input signal correlation matrix. The LMS algorithm is by far the most widely used algorithm in adaptive filtering for several reasons. The main features that attracted the use of the LMS algorithm are low computational complexity, proof of convergence in stationary environment, unbiased convergence in the mean to the Wiener solution, and stable behavior when implemented with finite-precision arithmetic. Let $x(n)$ and $d(n)$ represent the reference input and the desired output signal, respectively, to the adaptive filter. Let L denote the total number of filter coefficients. Define the $L \times 1$ coefficient vector $H(n)$ and the input vector $X(n)$ as

$$H(n) = [h_0(n), h_1(n), \dots, h_{L-1}(n)]^T \quad (13)$$

$$X(n) = [x(n), x(n-1), \dots, x(n-L+1)]^T \quad (14)$$

The LMS is described as

$$e(n) = d(n) - H^T(n)X(n) \quad (15)$$

$$H(n+1) = H(n) + \mu_s X(n)e(n) \quad (16)$$

In practice, (16) may be replaced with

$$H(n+1) = H(n) + \frac{\mu}{X^T(n)X(n) + \sigma} X(n)e(n) \quad (17)$$

or

$$H(n+1) = H(n) + \frac{\mu}{Lr(0)} X(n)e(n) \quad (18)$$

where the positive step-size μ is bounded by 2, σ is a small positive number and $r(0)$ is the estimated

autocorrelation function value of $x(n)$ for lag 0.

Digital filter is the basic building block of Digital Signal Processing systems. Finite Impulse Response is preferred when compared to Infinite Impulse Response, because of its properties like guaranteed stability, linear phase and low response, but with expense of large number of arithmetic operations are involved. In communication systems channel noise and Inter Symbol Interference degrades the performance of communication system. To reduce this problem adaptive equalizers are used to shape the signals at the receivers. Least Mean Square technique is the one of the adaptive techniques. It is easy to realize, the computational complexity causes a long output delay, which is not tolerable. This computational complexity can be reduced using frequency domain adaptive filtering, but nonlinear systems performance degrades drastically. To overcome this, problem of derivative base and derivative free learning algorithm, we use natural selection or derivative free algorithms. A new evolutionary computation algorithm based on natural learning to update the weights of adaptive filter was used. In this method Genetic Algorithm (GA) is used to update weights of filter coefficients.

III. BINARY STEP-SIZE LMS

In practical applications adaptive algorithms which possess high convergence speed while maintaining small convergence error rate are of great interest. For instance, in channel equalization during the transient period, the frequency characteristic of the adaptive equalizer is far from the inverse of the frequency response of the channel therefore the data transmitted during this time will be corrupted. In echo cancellation application, if the coefficients of the adaptive canceler are not close to the coefficients of the FIR filter which models the echo path the resulting echo signal is not attenuated. Actually, it is possible in this application, that during the transient period, the echo will be actually amplified. As a consequence, the transient period of the adaptive filter must be as small as possible for most of the practical applications in order to improve the overall quality of the system. The LMS algorithm has a small computational complexity therefore; it is very simple to be implemented in practice. Although it is simplicity, one of its main drawbacks is the fact that the speed of convergence and steady state error depends on the same parameter, the step-size μ .

In conclusion, when a constant step-size is used in LMS, there is a tradeoff between the steady-state error and the convergence speed, which prevent a fast convergence when the step-size is chosen to be small for small output error. In order to deal with this problem, a simple idea is to use a step-size which is time-varying during the adaption. At early stages of the adaption, when the adaptive filter is far from the optimum, a larger value of the step-size should be used. This will shorten the transient period and increase the convergence speed of the adaptive filter. As the adaptive filter goes close to the optimum Wiener solution, the step-size should be decreased and so the misadjustment. The adaptive algorithms derived from the LMS, which uses time-varying step-size modified as described above, belong to the class of variable step-size LMS algorithms. The variable step-size LMS algorithm first introduced by Kwong and Johnston in [4] uses the following update formula for the adaptive filter coefficients:

$$\hat{h}(n+1) = \hat{h}(n) + \mu(n)e(n)x(n) \quad (19)$$

where $\hat{h}(n)$ is the $N \times 1$ vector of the adaptive filter coefficients, $x(n)$ is the vector of the past N samples from the input sequence, $\mu(n)$ is a time-varying step-size and $e(n)$ is the output error. The time-varying step-size is also adapted as in the following equation:

$$\mu'(n+1) = \alpha\mu'(n) + \gamma e^2(n),$$

$$\mu(n+1) = \begin{cases} \mu_{\max} & \text{if } \mu'(n+1) > \mu_{\max} \\ \mu_{\min} & \text{if } \mu'(n+1) < \mu_{\min} \\ \mu'(n+1) & \text{otherwise} \end{cases} \quad (20)$$

with $0 < \alpha < 1$ and $\gamma > 0$ being some constant parameters and μ_{\max} and μ_{\min} being the upper and lower bounds of the time-varying step-size. The constant parameter μ_{\max} which is normally selected close to the instability point of the conventional LMS algorithm is used to increase the convergence speed, while the parameter μ_{\min} is chosen provide a good compromise between the steady-state misadjustment and the tracking capacity of the algorithm. The parameter γ is used to control the convergence time and also the steady-state level of the

misadjustment. The behavior of the step-size as described in (20) is the following: at early stages of the adaption the step-size is increased due to the large value of the output error. As the algorithm goes closer to the steady-state the value of $e(n)$ decreases which decrease the step-size μ_n . The following approximate analytical expression for the steady-state misadjustment of the variable step-size LMS algorithm was derived in [4]:

$$M = \frac{J_{ex}}{J_{min}} = \frac{1 - \sqrt{1 - 2 \frac{(3 - \alpha) \gamma J_{min} tr[\mathbf{R}]}{1 - \alpha^2}}}{1 + \sqrt{1 - 2 \frac{(3 - \alpha) \gamma J_{min} tr[\mathbf{R}]}{1 - \alpha^2}}} \quad (21)$$

Clearly, the steady-state misadjustment depends on the parameter γ and on the minimum value of the MSE J_{min} . Since the speed of convergence of the algorithm depends also on the parameter γ , one can conclude that there is still dependence between the misadjustment and the convergence time [5]. Another drawback of this algorithm is the fact that the steady-state misadjustment depends also on J_{min} . For instance in system identification applications, the minimum MSE equals the output noise variance, therefore the steady-state misadjustment depends on the system noise. In this section, a new variable step-size algorithm is presented in which the step-size varies in two ways thereby naming binary step-size variation algorithm. Supervised channel equalization is considered [6]. Depending on the error the step-size gets updated. The updation process is shown in the figure 2.

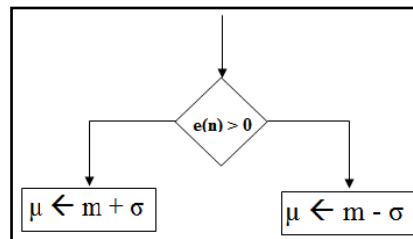


Fig. 2 Updation process

In another observation it has been identified that if with the NLMS the maximum change of step-size is limited to 0.01, the convergence speed is very high [7].

IV. TRANSFORM DOMAIN LMS

The transform-domain LMS algorithm is another technique to increase the convergence speed of the LMS algorithm when the input signal is highly correlated. The basic idea behind this methodology is to modify the input signal to be applied to the adaptive filter such that the conditioning number of the corresponding correlation matrix is improved. In the transform-domain LMS algorithm, the input signal vector $\mathbf{x}(k)$ is transformed in a more convenient vector $\mathbf{s}(k)$, by applying an orthonormal (or unitary) transform [4], i.e.,

$$\mathbf{s}(k) = \mathbf{T}\mathbf{x}(k) \quad (22)$$

where $\mathbf{T}\mathbf{T}^T = \mathbf{I}$. The MSE surface related to the direct-form implementation of the FIR adaptive filter can be described by $\xi(k) = \xi_{min} + \Delta\mathbf{w}^T(k)\mathbf{R}\Delta\mathbf{w}(k)$ (23)

where $\Delta\mathbf{w}(k) = \mathbf{w}(k) - \mathbf{w}_o$. In the transform-domain case, the MSE surface becomes

$$\begin{aligned} \xi(k) &= \xi_{min} + \Delta\hat{\mathbf{w}}^T(k) E[s(k)s^T(k)] \Delta\hat{\mathbf{w}}(k) \\ &= \xi_{min} + \Delta\hat{\mathbf{w}}^T(k) \mathbf{TRT}^T \Delta\hat{\mathbf{w}}(k) \end{aligned} \quad (24)$$

where $\hat{\mathbf{w}}(k)$ represents the adaptive coefficients of the transform-domain filter. Figure 3 depicts the transform-domain adaptive filter. It can be noticed that the eccentricity of the MSE surface remains unchanged by the application of the transformation, and, therefore, the eigenvalue spread is unaffected by the transformation [8]. As a consequence, no improvement in the convergence rate is expected to occur. The Transform-Domain LMS Algorithm is as follows:

Initialization

$$\mathbf{x}(0) = \hat{\mathbf{w}}(0) = [0 \ 0 \ \dots \ 0]^T$$

$\gamma =$ small constant

$$0 < \alpha \leq 0.1$$

Do for each $\mathbf{x}(k)$ and $d(k)$ given for $k \geq 0$

$$\mathbf{s}(k) = \mathbf{T}\mathbf{x}(k)$$

$$e(k) = d(k) - s^T(k)\hat{w}(k)$$

$$\hat{w}(k+1) = \hat{w}(k) + 2\mu e(k)\Sigma^{-2}(k)s(k)$$

In the literature, Karhunen-Loève Transform (KLT) is used as unitary transform for the transform-domain adaptive filter. However, since the KLT is a function of the input signal, it cannot be efficiently computed in real time. An alternative is to choose a unitary transform that is close to the KLT of the particular input signal [9]. By close is meant that both transforms perform nearly the same rotation of the MSE surface. In any situation, the choice of an appropriate transform is not an easy task. Some guidelines can be given, such as (however these are just conventions not rules):

1. Since the KLT of a real signal is real, the chosen transform should be real for real input signals;
2. For speech signals the discrete-time cosine transform (DCT) is a good approximation for the KLT;
3. Transforms with fast algorithms should be given special attention. A number of real transforms such as DCT, discrete-time Hartley transform, and others, are available.

Most of them have fast algorithms or can be implemented in recursive frequency-domain format [10]. In particular, the outputs of the DCT are given by

$$s_o(k) = \frac{1}{\sqrt{N+1}} \sum_{l=0}^N x(k-l) \quad (25)$$

$$s_i(k) = \sqrt{\frac{2}{N+1}} \sum_{l=0}^N x(k-l) \cos \left[\pi i \frac{(2l+1)}{2(N+1)} \right] \quad (26)$$

For complex input signals, the discrete-time Fourier transform (DFT) is a natural choice due to its efficient implementations [11]-[14].

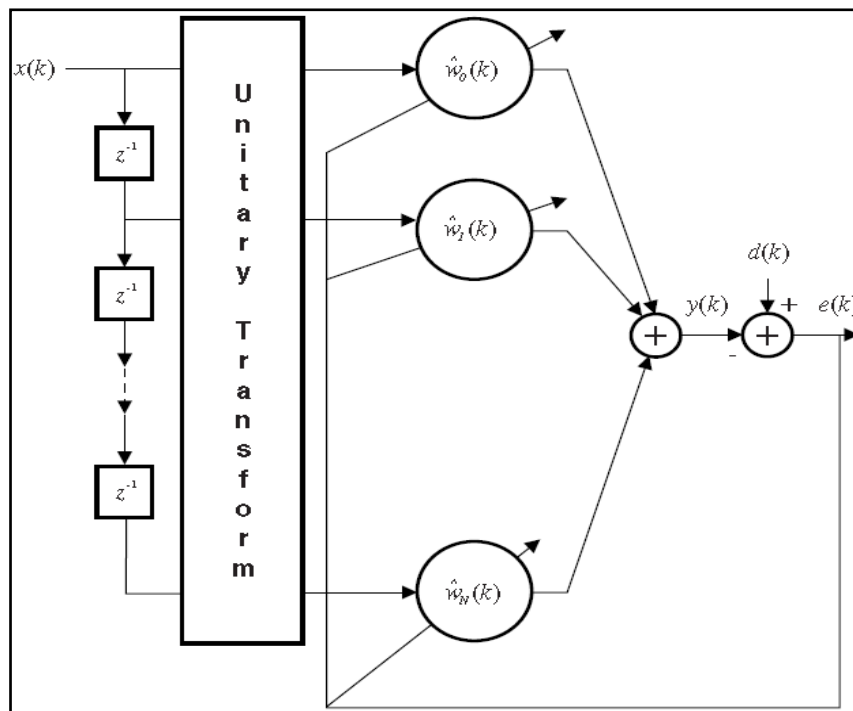


Fig. 3 Transform-domain adaptive filter

V. WAVELET PACKET TRANSFORM

In this paper, the unitary transform used is wavelet packet transform. For almost all signals, the low-frequency component is the most important part. It is what gives the signal its significance and identity. The high-frequency content, on the other hand, adds flavor. Consider an audio signal.

If the high frequency components are removed, the audio sounds different, but one can still tell what's being said in the audio. However, if enough of the low-frequency components are removed, one hears gibberish. Wavelet analysis often speaks about approximations and details. The approximations are the low-frequency, high-scale components of the signal. The details are the high-frequency, low-scale components. The filtering process in wavelet analysis, at its basic level, looks something like figure 4. The original sequence, S , applied to two complementary filters and emerges as two signals as shown in figure 4. If a digital sequence of say 512 samples is applied to the filter bank consisting of one low and one high pass filter as mentioned above, the length of A will be 512 and that of D will also be 512. Hence the data to handle was doubled. But note that in A as well as in D only 256 samples are irredundant. To remove the redundant samples, the downsamplers are employed as shown in figure 5. The outputs are denoted by cA and cD .

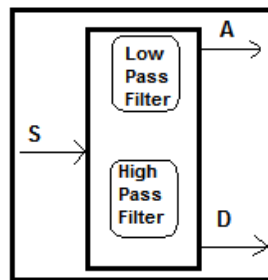


Fig. 4 Filtering Process in Wavelet Analysis

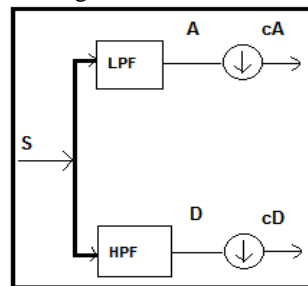


Fig. 5 Wavelet processing with downsamplers

This process, i.e., the conversion of S into cA and cD is called decomposition; the filters at this stage are referred as decomposition low pass and decomposition high pass filters. These filters have direct relation to the basis function used in a specific wavelet. The vectors cA and cD constitutes the DWT coefficients.

a. Multiple Stages of Decomposition

The decomposition process can be repeated means iterated, with successive approximations being decomposed in turn, so that one signal is broken down into many lower resolution components. This is called the wavelet decomposition tree shown in figure 6.

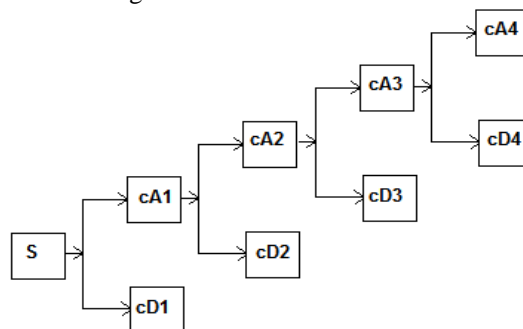


Fig. 6 Multistage Decomposition

The maximum number of decomposition stages should be taken so that the length of the sequence in the last stage is not less than 1. From the wavelet coefficients the original signal need to be recovered. The process of obtaining the original signal by using the wavelet coefficients is called reconstruction or synthesis

shown in figure 7. The downsampling performed at decomposition stage introduces an aliasing effect. The reconstruction filters need to be selected so that the aliasing effect introduced at the decomposition stage should be cancelled. The overall process of wavelet is depicted in the figure 8. The wavelet packet analysis is an extension of wavelet analysis with an inclusion of analysis of both approximation (cA) and detail (cD) components. The wavelet packet analysis looks like a complete tree structure. The multistage wavelet packet analysis looks like as shown in figure 9.

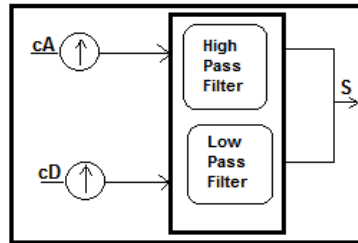


Fig. 7 Reconstruction Stage

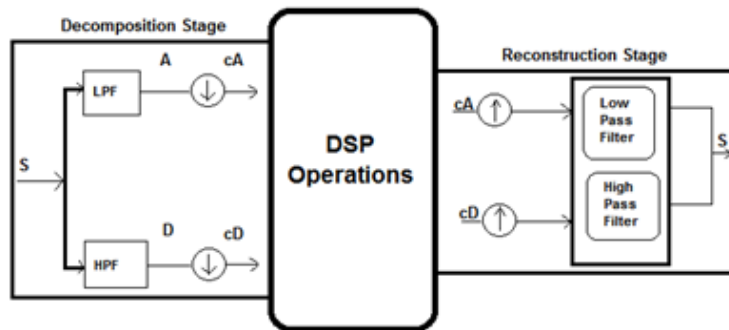


Fig. 8 Wavelet Transform as a multirate filter

The wavelet packet analysis is an extension of wavelet analysis with an inclusion of analysis of both approximation (cA) and detail (cD) components. The wavelet packet analysis looks like a complete tree structure. The multistage wavelet packet analysis looks like as shown in figure 9.

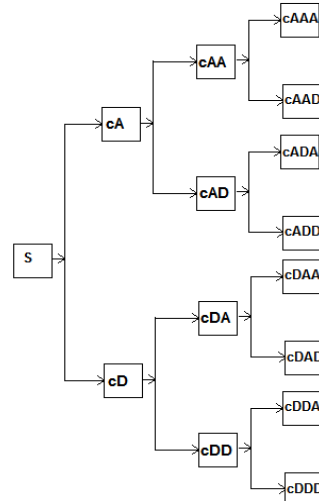


Fig. 9 Wavelet Packet Analysis

The wavelet packets use the wavelet filters to decompose and reconstruct the signals. The wavelet filters corresponds to the perfect reconstruction condition as well as to represent the data to suite different applications.

VI. SIMULATION RESULTS

In this section the simulation results of adaptive filters, Wavelets Packet based transform domain LMS, the variation of LMS (Var LMS), Binary step size LMS (BSS LMS), and multirateVar LMS and multirate BSS LMS in wavelet packet domain on de-noising of TDM signal are presented. The flow graph in figure 10 represents the total process that was considered in this paper.

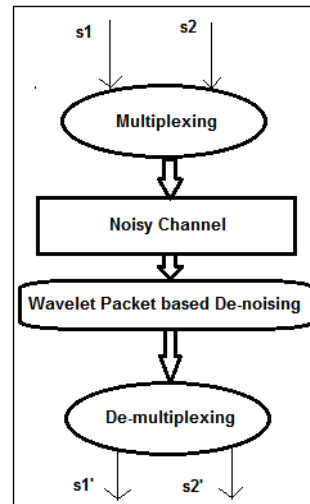


Fig. 10 De-noising of TDM signals based on Wavelet Packet based denoising
The two signals that are multiplexed in TDM, multiplexed signal and noisy signals are shown in the figure 11.

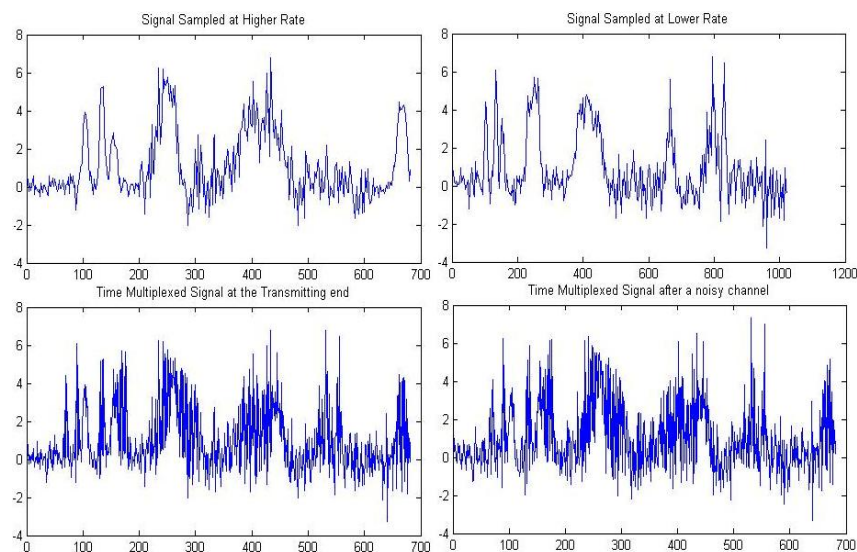


Fig. 11 Input, TDM and Noisy signals

The Peak Signal to Noise Ratio (PSNR), Mean Square Error (MSE), Maximum Squared Error (MAX ERR), Ratio of Squared Norms (L2RAT) are calculated and tabulated for different types of techniques. The simulation results of adaptive filters on denoising are presented in table I. LMS, Normalized LMS, RLS and LSL based denoising are implemented. It is observed that the maximum value of maximum error is 5.03 with LMS in the second signal case. The standard LMS has produced highest MSE and LSL a lowest MSE.

Table I: Denoising with Adaptive Filters

Denoising with Adaptive Filters								
	PSNR		MSE		MAX ERR		L2RAT	
	FS	SS	FS	SS	FS	SS	FS	SS
LMS	49.19	48.02	0.78	1.02	4.21	5.03	0.93	0.98
NLMS	52.30	52.32	0.38	0.38	2.04	3.17	0.95	0.93
RLS	53.37	52.39	0.30	0.38	1.93	2.74	0.98	1.03
LSL	54.02	53.87	0.26	0.27	1.56	2.13	0.91	0.96
Average	52.22	51.65	0.43	0.51	2.44	3.27	0.95	0.97

Table II presents the simulation results of denoising using LMS based on DCT and DFT. The performance of these techniques is almost similar to that of the previous adaptive filters except LMS. The standard LMS has shown fragile performance.

Table II: Denoising with Transform domain LMS based on DCT & DFT

Denoising with Transform domain LMS based on DCT & DFT								
	PSNR		MSE		MAX ERR		L2RAT	
	FS	SS	FS	SS	FS	SS	FS	SS
DFT	53.30	53.04	0.30	0.32	1.81	2.14	1.02	0.93
DCT	53.88	51.62	0.27	0.45	2.08	4.15	0.92	0.88
Average	53.59	52.33	0.28	0.39	1.94	3.15	0.97	0.91

Table III shows the performance of LMS in wavelet packet domain with different wavelets. Haar, Daubechies, Symlets, Coiflets, Biorthogonal, demeyer and reverse biorthogonal wavelets are considered. The performance with different wavelet combinations is almost similar. The PSNR is in the range of 54dB with almost all wavelets. The maximum error is around 1.6.

Table III: Denoising with LMS in Wavelet Packet Domain

Denoising with LMS in Wavelet Packet Domain								
	PSNR		MSE		MAX ERR		L2RAT	
	FS	SS	FS	SS	FS	SS	FS	SS
Haar	54.02	54.12	0.26	0.25	1.78	1.87	1.08	1.13
db10	54.51	53.76	0.23	0.27	1.33	1.86	1.06	1.06
db45	54.64	54.15	0.22	0.25	1.39	1.54	1.04	1.06
sym6	54.41	54.09	0.24	0.25	1.25	1.55	1.04	1.02
coif4	54.89	53.56	0.21	0.29	1.56	1.67	1.09	1.06
bior2.4	54.29	54.06	0.24	0.26	1.52	1.79	1.02	1.08
dmey	54.01	54.11	0.26	0.25	1.62	1.76	1.02	1.10
rbio1.3	54.39	54.05	0.24	0.26	1.70	1.78	1.04	1.06
Average	54.40	53.99	0.24	0.26	1.52	1.73	1.05	1.07

Table IV gives the simulation results of variation of LMS on denoising in five runs. The performance is almost similar to that of the previous techniques. The maximum value of PSNR is 54.08dB while the maximum error is 4.37.

Table IV: Denoising with Var LMS

Denoising with Var LMS								
	PSNR		MSE		MAX ERR		L2RAT	
	FS	SS	FS	SS	FS	SS	FS	SS
Var LMS-1	53.34	51.14	0.30	0.50	3.53	3.67	0.91	0.88
Var LMS-2	54.08	52.82	0.25	0.34	2.93	4.09	0.92	0.89
Var LMS-3	53.15	51.79	0.31	0.43	2.87	4.37	0.94	0.83
Var LMS-4	53.07	51.54	0.32	0.46	3.30	4.11	0.96	0.82
Var LMS-5	53.84	51.95	0.27	0.42	2.77	3.91	0.86	0.94
Average	53.50	51.85	0.29	0.43	3.08	4.03	0.92	0.87

Table V presents the performance of BSS LMS on denoising. The table gives the values of parameters in five runs. The average value of PSNR with first signal is 53.07dB, with second signal 53.99dB, while the maximum error is 1.52 and 2.73 with two signals respectively. The performance of BSS LMS is found to be slightly better than the traditional LMS and transform domain LMS based on DCT and DFT and the variation of LMS, but the improvement is not significant.

Table V: Denoising with BSS LMS

Denoising with BSS LMS								
	PSNR		MSE		MAX ERR		L2RAT	
	FS	SS	FS	SS	FS	SS	FS	SS
BSS LMS-1	51.83	51.93	0.43	0.42	4.56	4.81	0.87	0.97
BSS LMS-2	54.22	52.11	0.25	0.40	2.52	3.70	0.89	0.89
BSS LMS-3	52.83	51.38	0.34	0.47	2.58	4.02	0.95	0.84
BSS LMS-4	53.33	52.11	0.30	0.40	2.99	3.92	0.91	0.86
BSS LMS-5	53.18	52.37	0.31	0.38	2.76	3.16	0.94	0.85
Average	53.07	51.98	0.33	0.41	3.08	3.92	0.91	0.88

Table VI presents the performance of the multirate variation of LMS by using wavelet packet domain on denoising. The simulation results show that the performance is improved by a great extent. The PSNR values at times 66.37dB and 64.46dB. The minimum value of PSNR is 58.86 with demeyer wavelet. The maximum error is in the range of 1.5. The results are obvious because of the correlated data coming out of wavelet packet representation.

Table VI: Denoising with MultirateVar LMS using Wavelet Packet Domain

Denoising with MultirateVar LMS using Wavelet Packet Domain								
	PSNR		MSE		MAX ERR		L2RAT	
	FS	SS	FS	SS	FS	SS	FS	SS
Haar	60.10	66.37	0.06	0.02	1.50	1.31	1.04	1.04
db10	59.11	61.16	0.08	0.05	1.60	1.57	1.06	1.06
db45	61.26	64.46	0.05	0.02	1.34	1.35	1.07	1.07
sym6	60.56	61.74	0.06	0.04	1.54	1.75	1.07	1.06
coif4	61.25	61.61	0.05	0.04	1.63	1.45	1.12	1.01
bior2.4	61.17	63.65	0.05	0.03	2.15	1.56	1.04	1.07
dmey	58.86	61.53	0.08	0.05	1.55	1.63	1.07	1.08
rbio1.3	62.28	61.21	0.04	0.05	1.33	1.52	1.04	1.05
Average	60.58	62.72	0.06	0.04	1.58	1.52	1.06	1.06

Table VII describes the performance of multirate BSS LMS by using wavelet packet domain on denoising. The table shows that the performance of BSS LMS in wavelet packet domain is even better than that of Var LMS. The average values of PSNR of Var LMS in wavelet packet domain is 60.58dB and 62.72dB with the two signals while that of BSS LMS is 63.55dB and 62.31dB. The maximum error and ratio of squared norms are similar with Var LMS and BSS LMS in wavelet packet domain.

Table VII: Denoising with Multirate BSS LMS using Wavelet Packet Domain

Denoising with Multirate BSS LMS using Wavelet Packet Domain								
	PSNR		MSE		MAX ERR		L2RAT	
	FS	SS	FS	SS	FS	SS	FS	SS
Haar	64.35	59.81	0.02	0.07	2.29	1.82	1.07	1.09
db10	66.74	63.15	0.01	0.03	1.19	1.41	1.08	1.06
db45	61.04	62.29	0.05	0.04	1.40	1.64	1.04	1.09
sym6	62.55	64.95	0.04	0.02	1.34	1.56	1.06	1.03
coif4	59.06	60.45	0.08	0.06	1.94	1.94	1.12	1.07
bior2.4	67.23	62.25	0.01	0.04	1.25	1.36	1.01	1.10
dmey	61.02	62.11	0.05	0.04	1.36	1.53	1.05	1.03
rbio1.3	66.42	63.47	0.01	0.03	1.54	1.32	1.05	1.09
Average	63.55	62.31	0.04	0.04	1.54	1.57	1.06	1.07

The comparison of all these techniques is presented in the table VIII and figures 12 to 15.

Table VIII: Denoising by different techniques

Denoising by different techniques								
	PSNR		MSE		MAX ERR		L2RAT	
	FS	SS	FS	FS	SS	FS	FS	SS
Adaptive Filter	52.68	51.88	0.38	0.47	2.27	3.23	0.95	0.95
DCT &DFT based LMS	53.59	52.33	0.28	0.39	1.94	3.15	0.97	0.91
BSS LMS	53.07	51.98	0.33	0.41	3.08	3.92	0.91	0.88
Var LMS	53.50	51.85	0.29	0.43	3.08	4.03	0.92	0.87
AdFl in WP	54.40	53.99	0.24	0.26	1.52	1.73	1.05	1.07
MultirateVar LMS WP	60.58	62.72	0.06	0.04	1.58	1.52	1.06	1.06
Multirate BSS LMS WP	63.55	62.31	0.04	0.04	1.54	1.57	1.06	1.07

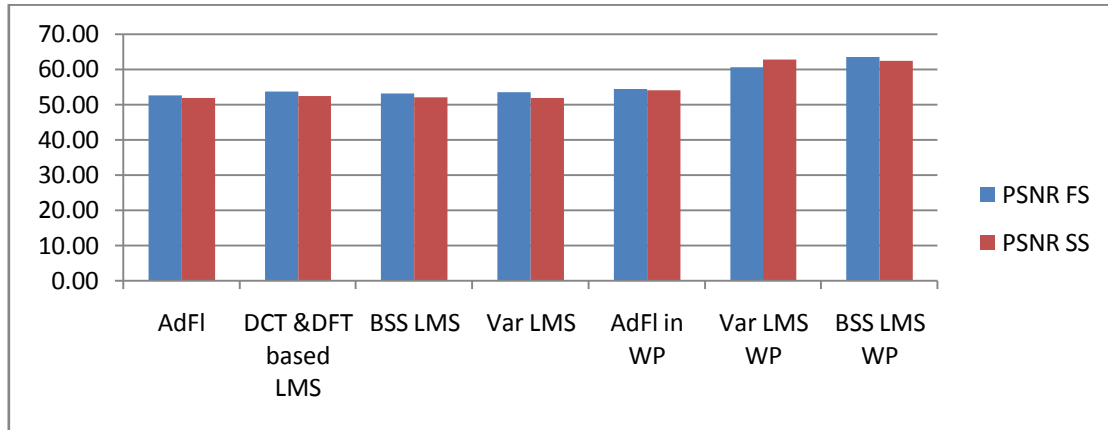


Fig. 12 PSNR values with different techniques

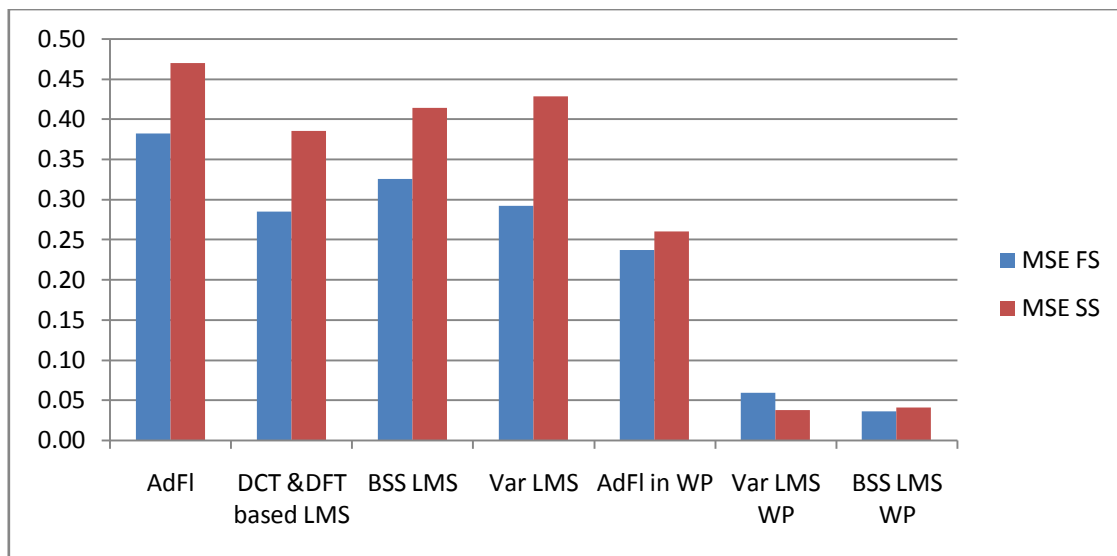


Fig. 13 MSE values with different techniques

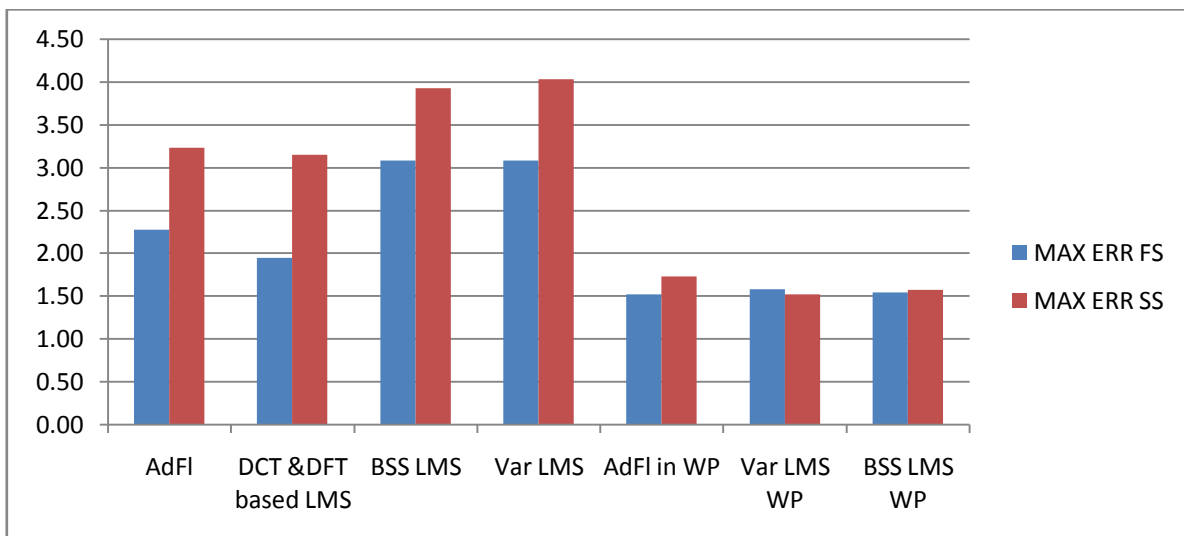


Fig. 14 Maximum error values with different techniques

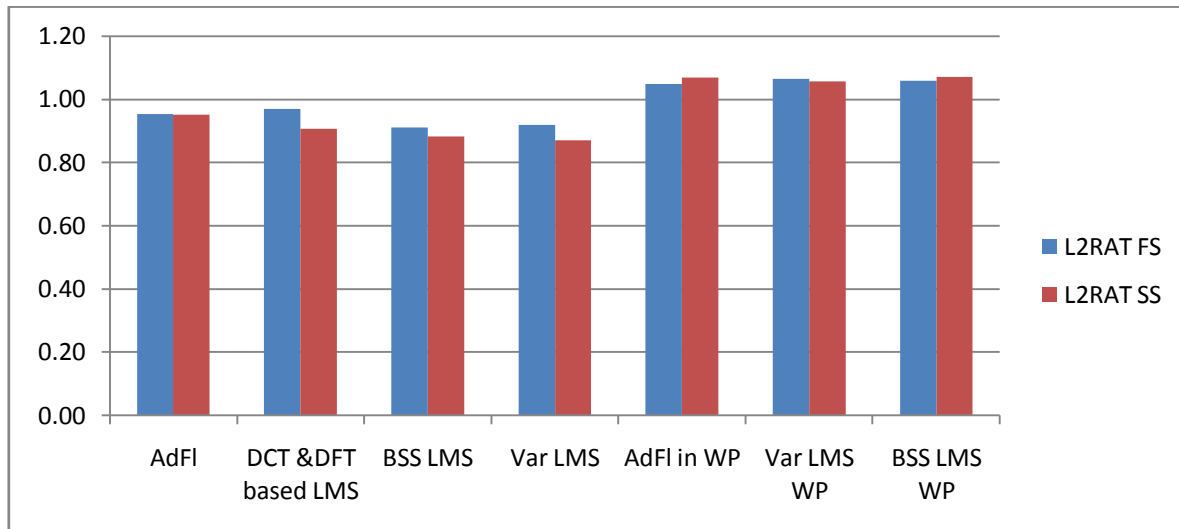


Fig. 15 L2RAT values with different techniques

VII. CONCLUSIONS

In this paper the denoising of time division multiplexed version of two signals sampled at different rate is considered. Traditional adaptive algorithms including DCT and DFT based transform domain LMS, transform domain LMS based on wavelet packets with different wavelets, a new variation of LMS, binary step size LMS and transform domain version of these two algorithms using wavelet packets with different wavelets are implemented for the specified denoising. The average PSNR with the traditional adaptive algorithms excluding DCT and DFT based transform domain LMS is calculated to be 52.28dB, with DCT and DFT based transform domain LMS 52.96dB, with BSS LMS 52.53dB, with Var LMS 52.67dB, with LMS in wavelet packet domain 54.19dB, Var LMS in wavelet packet domain 61.65dB and with BSS LMS in wavelet packet domain 62.93dB. From these results one can conclude that the new algorithms devised outperforms the existing techniques.

REFERENCES

- [1] S.S. Hykin, "Adaptive Filter Theory", NJ: Prentice – Hall, Englewood Cliffs, 1991.
- [2] Dixit S., Nagaria D., "Neural network implementation of Least-Mean-Square adaptive noise cancellation", IEEE International Conference on Issues and Challenges in Intelligent Computing Techniques (ICICT), pp. 134 – 139, Feb. 2014
- [3] R.H. Kwong and E. W. Johnston, "A variable step size LMS algorithm", IEEE transactions on signal processing, vol. 40, pp. 1633-1642, July 1992.
- [4] J. C. M. Bermudez and N. J. Bershad, "A nonlinear analytical model for the quantized LMS algorithm: The arbitrary step size case," IEEE Transactions on Signal Processing, vol. 44, pp. 1175-1183, May 1996.
- [5] Borisagar.K.R, Kulkarni.G.R., "Simulation and Performance Analysis of Adaptive Filter in Real Time Noise over Conventional Fixed Filter", IEEE International Conference on Communication Systems and Network Technologies (CSNT), pp. 621 – 624, May 2012.
- [6] Haichen Zhao, Shaolu Hu, Linhua Li, Xiaobo Wan, "NLMS adaptive FIR filter design method", TENCON 2013 - 2013 IEEE Region 10 Conference, pp. 1 – 5, Oct. 2013.
- [7] Koike S, "Performance analysis of adaptive step-size least mean modulus-Newton algorithm for identification of non-stationary systems", IEEE 8th International Colloquium on Signal Processing and its Applications (CSPA), pp. 184 – 187, March 2012
- [8] Singh A, Bansal B.N., "Analysis of Adaptive LMS Filtering in Contrast to Multirate Filtering", 4th International Conference on Emerging Trends in Engineering and Technology (ICETET), pp. 22 – 26, Nov. 2011.
- [9] Yuan Feng, ZhihaiZhuo, Shengheng Liu, Xiaokang Cheng, Letao Zhang, Zhipeng Zhang, "A novel adaptive filter based on FDLMS and modified MFLMS", IEEE International Conference on Information Science and Technology (ICIST), pp. 1326 – 1329, March 2013.
- [10] Kusljevic M.D., Poljak P.D., "Simultaneous Reactive-Power and Frequency Estimations Using Simple Recursive WLS Algorithm and Adaptive Filtering", IEEE Transactions on Instrumentation and Measurement, Vol. 60, Issue 12, pp. 3860 – 3867, Dec. 2011.
- [11] Vityazev V.V., Linovich A.Y., "A subband equalizer with the flexible structure of the analysis/synthesis subsystem", IEEE Region 8 International Conference on Computational Technologies in Electrical and Electronics Engineering (SIBIRCON), pp. 174 – 178, July 2010
- [12] Ramya J.V.S.L, "Alias free sub-band adaptive filtering", IEEE Conference on Recent Advances in Space Technology Services and Climate Change (RSTSCC), pp. 119 – 124, Nov. 2010.
- [13] Yan Liu, MucongZheng, "Adaptive receiver for multirate CDMA systems on Kalman criterion", IEEE International Conference on Computer Science and Service System (CSSS), pp. 2963 – 2965, June 2011
- [14] P. S. R. Diniz, E. A. B. da Silva, and S. L. Netto, "Digital Signal Processing: System Analysis and Design", Cambridge University Press, Cambridge, UK, 2002.



C. Mohan Rao (India) born on 21st April 1975, is pursuing Ph.D in Jawaharlal Nehru Technological University Anantapur. He received Master of Technology from Pondicherry Central University in the Year 1999, Bachelor of Technology form S.V University, Tirupati in the year 1997. He started his carrier as hardware Engineer in Hi-com technologies, during 1999 to 2001, after he worked as Assistant Professor in G. P. R. E. C during 2001 to 2007 and as Associate Professor in N. B. K. R. I. S. T. from 2007 to till date. He is a member of IETE and ISTE.



Dr. B. Stephen Charles (India) born on the 9th of August 1965. He received Ph.d degree in Electronics & Communication Engineering from Jawaharlal Nehru Technological University, Hyderabad in 2001. His area of interest is Digital signal Processing. He received his B.Tech degree in Electronics and Communication Engineering from Nagarjuna University, India in 1986. He started his carrier as Assistant professor in Karunya institute of technology during 1989 to 1993, later joined as Associate Professor in K. S. R. M. College of Engg. During 1993 to 2001 after that he worked as Principal of St. John's College of Engineering & Technology during 2001 to 2007 and now he is the Secretary, Correspondent and Principal in Stanley Stephen College of Engineering & Technology, Kurnool. He has 24 years of teaching and research experience. He published more than 40 research papers in national and international journals and more than 30 research papers in national and international conferences. He is a member of Institute of Engineers and ISTE.



Dr. M.N. Giri Prasad received his B.Tech degree from J.N.T University College of Engineering, Anantapur, Andhrapradesh, India in 1982. M.Tech degree from Sri Venkateshwara University, Tirupati, Andhra Pradesh, India in 1994 and Ph.D degree from J.N.T. University, Hyderabad, Andhra Pradesh, Indian in 2003. Presently he is working as a Professor in the Department of Electronics and Communication at J.N.T University College of Engineering Anantapur, Andhrapradesh, India. He has more than 25 years of teaching and research experience. He has published more than 50 papers in national and international journals and more than 30 research papers in national and international conferences. His research areas are Wireless Communications and Biomedical instrumentation, digital signal processing, VHDL coding and evolutionary computing. He is a member of ISTE, IE & NAFEN.

Social safety's women in urban public space (Case study: Mashhad metropolitan)

¹, Yasha Taheri Khameneh, ²Maryam Ebrahimpour

¹. Department of social science, M.Sc. in women studies, Islamic Azad University, Rudehen, Iran

². PhD student, Department of Art and Architecture, Science and Research branch, Islamic Azad University, Tehran, Iran (corresponding outer)

ABSTRACT : *Urban spaces are places in order happening crime. Considering of them both of quality and quantity aspects is necessary. On the other hand, gender urban design is important due to some urban spaces are unsafely for attendance of women. Planning and designing safe public spaces for women and girls means creating public spaces with features that enhance women's safety and feelings of safety, and detract from features that cause women's insecurity and feelings of insecurity. While planning and designing safe public spaces for women, planners, designers and architects place special focus on lighting, landscaping, visibility, motorized traffic, pedestrian traffic, urban furniture, potential hiding spots, signage, security personnel, proximity to other public spaces, proximity to emergency services, and access to public transportation. Each of these areas is given particular consideration from the perspective of the women and girls who use public spaces. In order to, this research is applied and the research method is "descriptive – analytical". The method of data collected is field and questionnaire. Therefore were used 180 questionnaires. Also, was used "SPSS" method for analyzing data. The finding shows that urban space safeties in studied area have decreased. on the other hand if the time of attendance women increase , urban security will increase .*

KEY WORD: *Urban public space, women security, safe space, Mashhad metropolitan*

I. INTRODUCTION

Safety planning and design also involves more than just the concrete, physical features of a space, although interventions at this level may occur first in safe cities for women programmed (Zarabi, 2013, 47). It is a necessarily participatory process whereby community members (especially women) work together to create spaces that accommodates strong social relations. In order to be successful, planners and designers must pay attention to how people express themselves in, and interact with, public space. In any given day, public spaces are the setting for a myriad of gendered social interactions. As a result of these interactions, public spaces themselves become gendered. For example, in a school yard, young girls may gather together under a certain tree and watch young boys play soccer in a field. As this process continues, the space under the tree will become understood as a "girl's space" and the soccer field will become understood as a "boy's space". This can be problematic because public space should belong to everyone and everyone should have a right to use it – girls should feel free to use the soccer field and boys should feel free to sit under the tree. Thus, planning and designing safe public spaces for women and girls also means analyzing the various uses of public spaces, who uses them, when, and for how long. This kind of planning and design also focuses on who *doesn't* use a particular public space, when, and why. This is because when certain groups, like women or girls, do not use a space, it is usually an indication that the space feels insecure to members of that group. Planning and designing safe public spaces for women and girls requires constant attention to physical and social characteristics of space. It also requires constant evaluation of the social and physical implications of the planning and design process.

The planning and design of a space has the potential to either reinforce gender inequality or to advance gender equality. For this reason, the planning and design process is a crucial facet of creating safe cities for women and girls. Gender is a particularly important consideration when planning and designing essential services in communities. Often, when essential services are badly planned or missing, women and girls bear the brunt of the insecurity that accompanies such situations. For example, “Sexual harassment is rampant when girls go out in the open for defecation. Men disguise themselves as women and hide themselves in the fields...There have been instances when girls were abducted from the fields and men were caught for sexually harassing them. After 11pm, girls are usually forbidden from going to the fields unless they are accompanied by an elder” (Asdaq, 2012, 56). Planning and designing safe public spaces for women and girls is the process whereby urban planners, designers, architects, women, grassroots and other community actors collaborate to make the physical features of public spaces safe and welcoming for women and girls. If public spaces are dark, abandoned, unclean, overgrown, or lacking certain elements like benches or emergency phones, they are potentially unsafe for everybody, but for women and girls in particular. Therefore, there is an increased chance that women and girls will not use spaces where they feel fear and/or experience violence. In safe cities for women and girls initiative, it is necessary that the safety needs of women and girls are taken into account in planning and design. Experience shows that when a space is occupied by women and girls, it is also occupied by more people in general. Streets, parks, bus stops, sports fields, squares, parking lots, etc. that have been planned and designed according to the specific safety needs of women and girls exhibit the following

characteristics (Sistani, 2012 : 89):

- Easy access to and from the location
 - Easy movement within the location
 - Good lighting so that users can see and be seen
 - Easy-to-read signs to help users find their way
 - Clear, well-kept paths where users can easily see each other
 - General visibility of the entire space, free from hiding places where a person could wait unseen
 - Includes mixed uses – many places to hangout, walk, play, eat, exercise, etc. for diverse user groups at different times of day
 - Provisions for different seasons (shade in hot weather and protection in cold weather)
 - Provisions for young children and the elderly (because women are often caretakers), e.g. in urban areas this could mean low, wide sidewalks for strollers, wheelchairs, and walkers, and areas with slow-moving traffic
 - Access to clean, secure, easily accessible toilet facilities with space for changing children’s diapers
- Safety planning and design for women and girls is important because it creates public spaces where women and all users have equal opportunity to be healthy, secure and happy. This kind of planning is based on the fact that the physical design of urban spaces affects women’s use and enjoyment of the public realm. Designing and planning safe public spaces for women and girls is important because:
- It raises awareness of the fact that space is not neutral; the design of spaces can either facilitate or impede their use, appropriation and safety for women and girls.
 - It recognizes that gender and gender relations between women and men are key factors in how urban spaces are organized and developed.
 - It recognizes that the city spatially reflects specific social, economic and historical characteristics that are unique to local women’s situations.
 - It recognizes that spaces in the city reflect the relations of power that determine the behaviors and differences in the lives of women and men.
 - It recognizes that the public spaces in a city are usually designed based on a traditional conception of the family and a traditional division of labor among women and men (men as workers in the public space and women as caretakers and home keepers in the home and private spaces). Furthermore, it promotes initiatives to change this spatial organization in order to reflect changing gender roles in society.
 - It recognizes that women’s fears are based on reality (the relationship between feelings of fear and experiences of violence) and that women know when and where they feel unsafe in the cities and why.
 - It is a useful tool to improve the quality of urban and community life and to reduce women’s fear and victimization.
 - It recognizes that if women and girls avoid using certain public spaces because they do not feel safe, these spaces will become more insecure for women, girls, and other users. Therefore, it is a useful tool to

improve the quality of urban and community life for everyone, and to reduce women's fear and victimization.

- It promotes the right to the city and to citizenship for women and girls as a condition for equitable and sustainable cities and communities.

The best way to ensure that spaces are welcoming to women and girls is to consult with women and girls who are the intended users of a space. However, women and girls may find it difficult to participate in public planning and design discussions for a variety of reasons. The following list should be considered by any person or organization wishing to involve women and girls in the planning and design of public spaces (Esfahani, 2009:75).

Women may not attend public planning discussions on safer communities because:

- They have difficulty getting to or from the discussion
- They are unaware of women's safety issues because there is little public or media discussion of them
- They may have internalized/accepted gender-based forms of violence (e.g. sexual harassment) as normal and not see them as a problem.
- They have difficulty reading materials for the discussion
- They cannot afford childcare for the time it takes to participate in discussions
- They do not have time to participate in discussions because of work/family/ volunteer commitments
- They cannot attend discussion meetings which are being held at an inconvenient time
- Their culture may not be supportive of such activities
- They do not have the support of their spouse or friends
- They are afraid of speaking in public
- They are poor and feel as though they do not belong
- They are disabled and cannot access the space where discussions are being held
- They are unaware that resources exist to plan communities to support women's safety
- They have no computer to access information about discussions
- They do not speak the language in which the discussion is being held
- They have more pressing personal concerns such as poverty or poor health
- They cannot find the place where the discussion is being held
- They do not feel safe in the place where the discussion is being held
- They have to look after elderly members of their family and have no time
- They do not believe that they are smart enough to participate in the discussion
- They have participated in public meetings in the past and had bad experiences
- They feel intimidated by large groups and/or public officials
- They do not feel confident speaking in front of men
- They feel like their age makes their concerns irrelevant (whether they are old or young)
- They feel apathetic about public issues (Biyabangard, 2010:34).

Women consistently express greater fears for their personal safety in urban environments than do men. Statistics demonstrate that, conversely, young men are the most vulnerable to actual attack in towns and cities, while women are more likely to be attacked in their own homes by someone they know well. However, these figures are possibly skewed by the fact that if women are afraid to go out on the streets alone they are less likely to become victims of crime in the urban environment. Research by Women's Design Service reveals that it is fear of sexual assault which underlies women's anxiety. Women have been at risk from male sexual assault through history and across cultures, a situation often legitimated by a concept of women's inherent inferiority to men. Furthermore, they are rarely treated as innocent victims of assault. Where rape cases are brought to law, the woman often ends up 'more accused than the accused' (Javadi , 2009 :90) In the UK today only 7.5% of reported rapes result in a conviction, and it is widely thought that 90% of rapes go unreported. During the 1970s, when the second wave of the Women's Liberation Movement was at its height, a number of "Reclaim the Night" marches were organized. The aim was to give women the confidence to go out into urban public spaces after dark. One of the popular chants was 'However we dress, wherever we go, Yes means Yes and No means No!' These demonstrations helped to push the agenda of women's safety forward, but recently the marches have been revived by the London Feminist Network because the pace of change has been too slow (Syed Hussain, 1998:23).

Women's fear of going out alone after dark means that, in northern Europe, they confine themselves indoors from 4.0pm onwards during the winter months. This has a huge impact on women's ability to engage in employment, adult education, civic and community participation and social and leisure activities (Ozer,

2003:12). Our Making Safer Places projects, initiated in the late '90s, set out to identify how changes to the physical environment might help women to reclaim the right to use public space as and when they wish (Slusky, 2004 :56). Whereas previously many women may not have questioned the social factors that have contributed to their fears, the process of engaging with these issues through discussion with other women has led many of our participants to join groups and organizations working to change the relations between the genders and the social frameworks that perpetuate them (Williams, 2000: 84).

II. STUDIED AREA

Mashhad has been located between Hezar Masjed & Binaloud Mountains. The city is located at 36.20° North latitude and 59.35° East longitude, in the valley of the Kashaf River near Turkmenistan, between the two mountain ranges of Binalood and Hezar-masjed. Mashhad divided 7 parts in planning based on environmental, physical, economical, social indicators (Farnahad consultant, 2008). This area consists of natural and physical opportunities. Thus, middle area is one of the main economical and physical areas in Mashhad. This area has some factors. Such as:

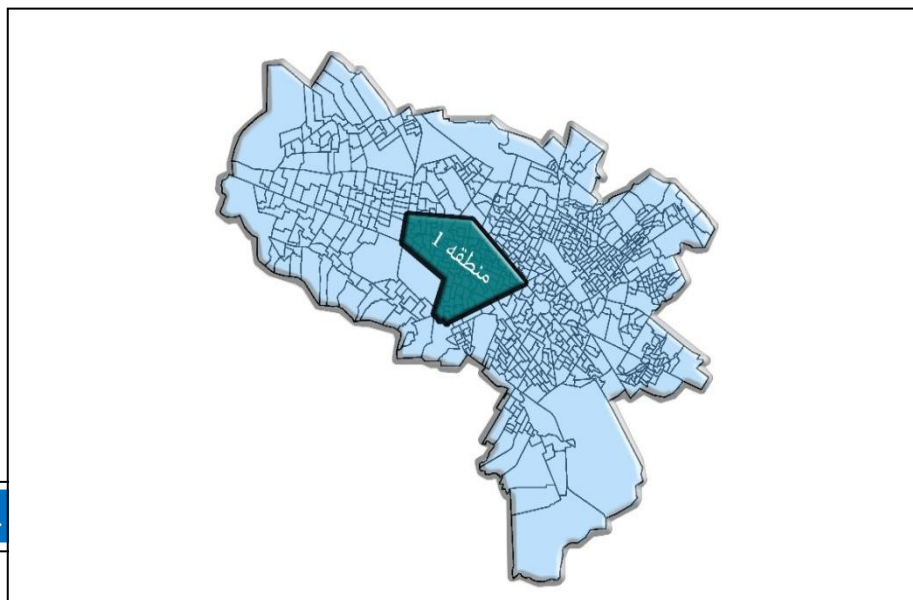
- appropriate place in urban spatial space
- appropriate relation between with natural area such as Binalood mountain
- consisting of structure and various physical fabrics
- centralization of activities in urban scale
- there is value environmental such as : gardens , canals
- there is the most network in this area due to holly shrine
- there is problems about urban spaces and physical structure , so it is necessary urban planning

Mashhad divide 12 municipally regions. Studied are have located in 1 region that has been mentioned in figure one. Social characters of studied area have been shown in table (1).

		Gender			
		Frequency	Percent	Valid Percent	Cumulative Percent
Valid	Male	23	38.3	38.3	38.3
	Female	37	61.7	61.7	100.0
	Total	60	100.0	100.0	

Table (1) .mentioned community

Figure area



1: studied

III. Finding

In this part has been considered mentioned questionnaire.

3.1. Correlation test

There is Coefficient correlation (-0.01) between gender and urban space quality as two main variable. It means if increase urban space quality, secure will decrease between women. On the other hand, there is Coefficient correlation (+0.022) between gender and social attendance as other variables. It means while increasing time of social attendance, so increasing security in urban open space especially for women.

Table (2): Coefficient correlation between variables

Correlations				
		Gender	Destroyed security	Usable time
Gender	Pearson Correlation	1	-.001	.022
	Sig. (2-tailed)		.996	.869
	N	60	60	60
Destroyed security	Pearson Correlation	-.001	1	.240
	Sig. (2-tailed)	.996		.065
	N	60	60	60
Usable time	Pearson Correlation	.022	.240	1
	Sig. (2-tailed)	.869	.065	
	N	60	60	60

Hypothesis test

It seems that attendance of women in studied are has been decreased.

According analyzing of questionnaire, finding show 78.4 percentages of women were attended between Am to Pm. also, only 1.7 percentages of women at night.

Table (3): attendance time to studied area

Time					
		Frequency	Percent	Valid Percent	Cumulative Percent
Valid	Morning	43	71.7	71.7	71.7
	Afternoon	12	20.0	20.0	91.7
	Night	4	6.7	6.7	98.3
	Late night	1	1.7	1.7	100.0
	Total	60	100.0	100.0	

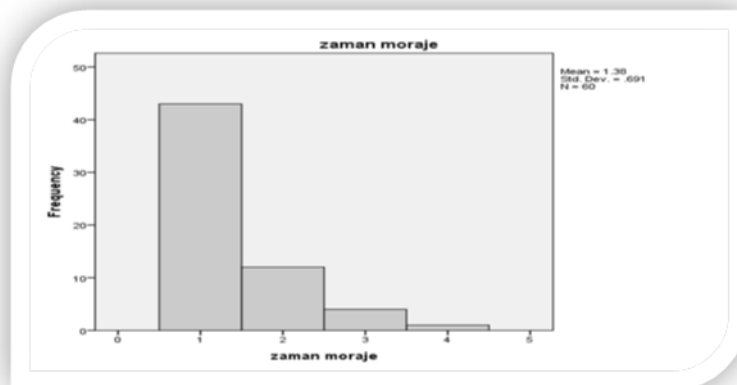


Figure (2): histogram graph of attendance women

So, the hypothesis is true according to above information. Attendance of women during day has been decreased.

1- It seems, that has decreased urban space safety in order to women attendance.

Studied community expose to discussion that there are some factors in order to decreasing safety in studied area. 61.7% believed one of the reasons that have been led to unsafe in studied area was vacant lands. 13.3 believed there isn't adequate light in studied area. And 10% believed addict persons have been led to unsafe place.

Table (4): considering of unsafe factors

Distribution of safety					
		Frequency	Percent	Valid Percent	Cumulative Percent
Valid	Addict person	8	13.3	13.3	13.3
	Vacant lands	37	61.7	61.7	75.0
	The lake of light	8	13.3	13.3	88.3
	Robbery	6	10.0	10.0	98.3
	Other	1	1.7	1.7	100.0
	Total	60	100.0	100.0	

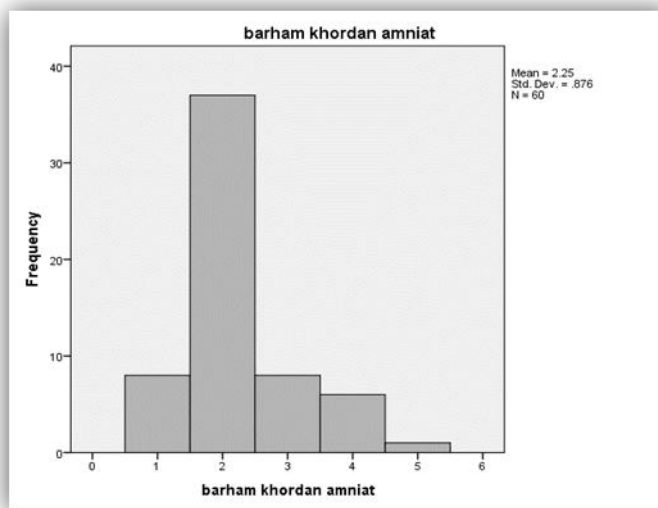


Figure (3): histogram graph of unsafe factors

So the second hypothesis is true and the qualities of urban space in studied area are reduction.

IV. CONCLUSION

Both societal norms for behavior and the built environment affect a woman's safety in public spaces. Knowledge of women's issues might begin to make a shift in the way women are treated and respected in the society. While retaliation and rejecting the notion that it is okay to be inappropriately treated in public is perhaps a beginning, the journey is much longer. A crucial step is to generate more awareness about women's safety issues in public spaces. The behavior and attitudes of the society cannot be transformed overnight, but the built environment can be controlled and can be used as a medium for change. Further research needs to be done while engaging various community organizations, municipal authorities, police departments and other important stakeholders. Workshops need to be organized and future women's safety audits need to be designed and led by community members. This would help form crucial links between the

REFERENCES

- [1] Asdqy, E., 2013, to review and assess subjective factors affecting residential satisfaction housewives, BS, University of Ferdowsi
- [2] Sistani, Eram, 2012, the impact of environmental perception in the design of urban spaces, BA, Ferdowsi University
- [3] Zarrabi, A. - Sharafi, Zakia - Zangene, M., 1391, citizen safety assessment factors Brahsas Mshhdbatakyd city police on mass media
- [4] Esfahani, MM (2009), health law, Qom University of Medical Sciences and Health Services
- [5] Biyabangard, E. and F. Javadi (2010) Psychological health of adolescents and youth in Tehran, Journal of Social Welfare
- [6] Javadi, F., 2009: Evaluation of the psychological health of people in Tehran 81 years, the Center of Research and Evaluation Program
- [7] Syed Hussaini, A. (1998), Principles of Mental Health, Mashhad University of Medical Sciences, Vol 1
- [8] Ozer, Em. Park, Mg. Paul, T. Brindis, CD. Irwine, CE (2003), America's
- [9] Adolescents: Are they healthy? San Francisco, CA, University of California, National Adolescent health information center.
- [10] Slusky, RI. (2004). Decreasing high risk behavior in teens. A theater program Empower students to research out to their peers, Health Care Exec,
- [11] Lindberg, LF. Biggest, S. Williams, S. (2000), multiple threat: the Concurrence Of teen health risk behaviors, The Urban Institute

Using A Battery Storage Wind / PV Hybrid Power Supply System Based Stand-Alone PSO To Determine The Most Appropriate.

Amam Hossain Bagdadee

¹Energy Field of Study, AIT

ABSTRACT : Wind / PV hybrid power systems, completed in time and geography, both economical and reliable than PV or wind turbine, but the hybrid system wind / PV to increase capacity. Installation of experience with traditional power design and optimization of design and operation cannot be seen with. To solve the problem in a comprehensive objective function to present the objective function of the solar wind. And reliability of the storage cells can be calculated with an investment of erosion format system resources, including the number of solar cells and batteries, but the type and amount of solar wind to change. As well as to improve not only to make the results more accurate investment costs and reliability cost of conversion optimization problems several optimization problems today. Improved optimization algorithms, PSO are used to solve nonlinear hybrid analysis is any integer optimization problem on the basis of PSO algorithm standard techniques then there is the first step convergence factor is applied to improve the detection performance of both migration are used to improve the ability of the algorithm to find the best in the whole world.

I. INTRODUCTION

In recent years, many new renewable energy technologies are into commercial applications, the maximum possible and the fastest growing wind and solar power. Low efficiency and poor reliability of wind and solar power, however, although the study of solar and wind energy, time and geography found in. Complete two very small wind most of the day in the sun when the wind began to strengthen. Because there are significant changes in the surface temperature of the light is very weak cold summer, sunshine, windy and weak winter sunlight is reduced and windy, so the best match for energy assets. Solar energy storage system and a full wind, wind / solar wind is provided by renewable solar electricity / assembly and storage. Material security, both in terms of the cost of solar or wind power to generate more profitable. Wind / diesel power system components and how the various components of the system to match the key advantages to the full game systems, hybrid power, and the optimization of the composition of the linearity of the power plant itself. Itself and the complexity of the linear system; Creating Nonlinear optimization problem some wind / current power systems research alone hybrid solar to supplement their education with some valuable advice on optimization problems that will be sent, but it is unclear as well the failure of some of the problems that continue in spite of the tendency of the PV cell system reliability and find out how best to deal with the hassles and inefficiencies. To solve this problem based on Optimization of this project is to improve the PSO algorithm proposed in this calculation model was established on a project to simulate the actual operation of the system can work not only with modern facilities , including the advantages of PSO and genetic algorithms . Fix the PSO algorithm, the global convergence properties of both higher capacity and efficiency. Quick search is in this article, the validity of the proposed method is tested with classical test cases.

II. PROBLEM FORMULATION

Typically, wind / solar renewable energy systems, wind turbines, solar panels, solar panels listed in the battery drain voltage control devices and other components of the cost of the first studies that follow this system.

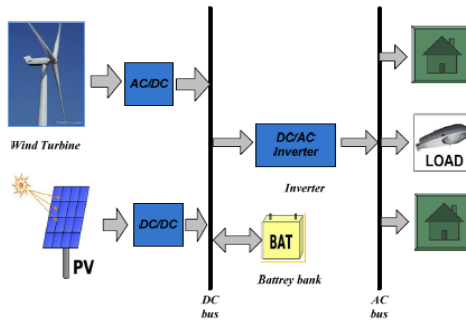


Fig. 1. Block diagram of a hybrid system.

Wind turbine output model : Wind turbine output characteristic curve shown in Figure 2. So the wind turbine output characteristic equation that can be exported by using the curve fit.

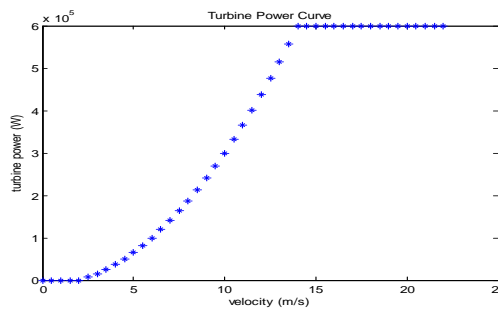


Fig.2 The output of wind turbines

The output characteristics equation of wind turbine is given as below:

$$P_{wt} = \begin{cases} 0, & V_w \leq V_c, V_w \geq V_f \\ P_R \times \frac{V_w^2 - V_c^2}{V_R^2 - V_c^2}, & V_c \leq V_w \leq V_R \\ P_R, & V_c \leq V_w \leq V_R \end{cases}$$

Where,

P_{WG} : The wind turbine output power (Watt)

P_R : The wind turbine rated power (Watt)

V_w : The wind speed (m/s)

V_c, V_f, V_R : Cut-in, cut-out and rated or nominal speed of the wind turbine (m/s)

PV cells output model : Turn on solar photovoltaic installed capacity is an important factor. The decision to change the PV array, which will be the highest yield, but this can cause one of the solar power system, in fact, solar power generation system. By turning the power output of the turbine, and other issues related to the design changes were put into operation as a decision variable in PV cells (PPV (T)) and replacement (Θ) a. the relationship between the output powers as a function of the model can be written as a singer.

$$PPV(t) f(VM(\theta) I(\theta)) = (2).$$

I and V_m respectively, the voltage and current is from the solar cell.

The battery output model : Because, the output is the random behavior of solar cells and wind turbines, the capacity of the battery is a hybrid of the changes to the system. Turbines and solar cells are larger than the total amount of electrical load and battery charge state of the battery on the T (3) can be expressed as:

$$Pb(t) = Pb(t - 1). (1 - \sigma) + \left[Pz(t) - \frac{P1(t)}{\eta_{inv}} \right]. \eta_{bc} \quad (3)$$

Where,

$Pb(t)$: Battery charged quantity at time (t);

$P_b(t-1)$: Battery charged quantity at time ($t-1$);
 σ : Battery self-discharge rate per hour;
 $P_z(t)$: The total output power of the turbine and PV cells in the time interval ($t-1$)-(t);
 $Pl(t)$: The total load power in the time interval ($t-1$)-(t);
 η_{inv} : Inverter efficiency;
 η_{bc} : Battery charging efficiency;
 η_{bf} : Battery discharging efficiency;

The reliability model : The reliability is an important indicator in evaluating a power generation system, which measures in terms of loss of power supply probability (LPSP). The LPSP for a considered period T is defined by:

$$LPSP = \sum_{t=1}^T LSP(t) / \sum_{t=1}^T Pl(t) \quad (5)$$

The LPSP for the time t is obtained through (6):

$$LPS(t) = [Pl(t) - (P_z(t) + P_b(t - t) - P_{bmin}) \cdot \eta_{inv}] \cdot u(t) \quad (6)$$

Where, T is the running time considered, here T =8760 hours; $Pl(t)$ The total load power in the time interval ($t-1$)-(t); $P_z(t)$ The total output power of turbines and PV cells in the time interval ($t-1$)-(t); $P_b(t-1)$ Battery charged quantity at time ($t-1$); P_{bmin} the minimum charged quantity of battery ; η_{inv} is Inverter efficiency; $u(t)$ is a step function^[5];

III. RESEARCH

A. The objective function

The objective function is the total annual cost of system, which consists of the cost of various components in the system and the annual cost of power loss. It can be obtained in (7):

$$\min C_z = \min(C_w + C_{pv} + C_b + C_r) \quad (7)$$

Where,

C_z The total annual cost of components in the system;
 C_w The total cost of wind turbines;
 C_{pv} The total cost of PV panel;
 C_b The total cost of the batteries;
 C_r The total annual cost of power loss of system.

1) The total cost of wind turbines

$$C_w = \sum_{i=1}^{W_n} (a_i N_i \cdot \frac{r_0(1+r_0)^m}{(1+r_0)^m - 1} + u(N_i)) \quad (8)$$

$$u(P_i) = \frac{r_0(1+r_0)^m}{(1+r_0)^m - 1} [\sum_{t=t}^n a_i N_i (1+r_0)^{n-t} + \sum_{t=n+1}^m a_i N_i \cdot \frac{1}{(1+r_0)^{t-n}}] \quad (9)$$

2) The total cost of PV cells

$$C_{pv} = \sum_{j=1}^{S_n} (b_j N_j \cdot \frac{r_0(1+r_0)^m}{(1+r_0)^m - 1} + u(N_j)) \quad (10)$$

$$u(P_j) = \frac{r_0(1+r_0)^m}{(1+r_0)^m - 1} [\sum_{t=t}^n b_j N_j (1+r_0)^{n-t} + \sum_{t=n+1}^m b_j N_j \cdot \frac{1}{(1+r_0)^{t-n}}] \quad (11)$$

3) The total cost of batteries

$$C_b = \sum_{k=1}^{B_n} (c_k N_k \cdot \frac{r_0(1+r_0)^m}{(1+r_0)^m - 1} + u(N_k)) \quad (12)$$

$$u(P_k) = \frac{r_0(1+r_0)^m}{(1+r_0)^m - 1} \left[\sum_{t=t'}^n c_k N_k (1+r_0)^{n-t} + \sum_{t=n+1}^m c_k N_k \cdot \frac{1}{(1+r_0)^{t-n}} \right] \quad (13)$$

Where, W_n, S_n, B_n are respectively the style of the turbines, PV cells and batteries; a_i, b_j, c_k are respectively the unit cost of the turbine, PV cells, and battery for the type of i, j, k ; P_i, P_j, P_k are capacity of the turbine, PV cells, and battery for the type of i, j, k respectively; $u(P_i), u(P_j), u(P_k)$ are the annual maintenance and operation costs of the turbine, PV cells, and battery with capacity of P_i, P_j, P_k for the type of i, j, k respectively; n is the period of the installation and construction of equipments; t' is the starting age of equipments put into operation; m is depreciable lifetime of equipment; r_0 is discount rate; and t is the year.

4) The total cost of power loss of system considering supply reliability

$$Cr = coe \times \sum_{t=1}^T LPS(t) \quad (14)$$

Where, coe means compensation coefficient, from (14) it can be seen that if coe is improved, the cost of power loss of system will be increasing. In order to avoid the cost of power loss is too large, hybrid generating system has to reconfigure the various components and to lower loss of power supply probability (LPSP), thereby the reliability can be controlled by controlling coe .

B. Decision variables

From the above analysis, operational decision variables include the following variables:

$$X = \{S_n, N_{pv,p}, \theta, W_n, N_{WT}, B_n, N_{BAT,P}\} \quad (15)$$

Where, W_n, S_n, B_n are respectively the style of the turbines, PV cells and batteries; $N_{pv,p}, N_{WT}, N_{BAT,P}$ are respectively the number of turbines, PV cells and batteries; θ is the inclination of PV cells.

C. Constraints

1) The constraints of the inclination of PV cells:

$$0 < \theta < 90^\circ \quad (16)$$

2) The constraints of the number of turbines, PV cells and batteries;

$$\begin{aligned} 0 &\leq N_{pv,p} \leq N_{pv,pmax} \\ 0 &\leq N_{WT} \leq N_{WTmax} \\ 0 &\leq N_{BAT,P} \leq N_{BAT,Pmax} \end{aligned} \quad (17)$$

Where $N_{pv,Pmax}, N_{WTmax}, N_{BAT,Pmax}$ are respectively the maximum allowable number of the installation of turbines, PV cells and batteries.

3) The constraints of the capacity of batteries;

$$P_{bmin} \leq P_{b(t)} \leq P_{bmax} \quad (18)$$

Where, P_{bmax} means the maximum allowable capacity of batteries, which is generally set to rated battery capacity P_{bc} ; P_{bmin} means the minimum allowable battery capacity, which is determined by the maximum depth of discharging DOD, that is $P_{bmin} = (1-DOD) \cdot P_{bc}$, and DOD is generally set to 30%~50%.

IV. IMPROVED PSO ALGORITHM

A. PSO algorithm

Particle Swarm Optimization (PSO) was first proposed by J. Kennedy and R.C. Eberhart in 1995. The algorithm began as a simulation of the predatory behavior of birds flocking, in which each agent, according to its own flying experience and that of its neighbors, constantly modifies its flight direction and velocity, and ultimately approaches to the global best position through the whole searching space. In PSO algorithm the particle of i can be expressed by a D-dimensional vector and the position vector $x_i = (x_{i1}, x_{i2}, \dots, x_{iD})^T$, the velocity vector $v_i = (v_{i1}, v_{i2}, \dots, v_{iD})^T$

The particle swarm optimizer adjusts velocities and positions by the following formula:

$$v_{id}^{k+1} = v_{id}^k + c_1 r_1 (P_{best,id}^k - x_{id}^k) + c_2 r_2 (g_{best,d}^k - x_{id}^k) \quad (19)$$

$$x_{id}^{k+1} = x_{id}^k + v_{id}^{k+1} \quad (20)$$

Where,

v_{id}^k current d-dimensional velocity of agent i at iteration k ,

c_1, c_2 acceleration factor (known as study operator), respectively adjusts the largest step length of flying direction to the g_{best} and the p_{best} , generally $c_1 = c_2 = 2.0$;

x_{id}^k current d-dimensional position of agent $t i$ at iteration k ;

$P_{best,id}^k$ D-dimensional p_{best} of agent $t i$ at iteration k ;

$g_{best,id}^k$ D-dimensional g_{best} of the group;

B. The improved form of PSO algorithm

1) The introduction of a confluence of factors.

The movement of the particles (21) can be updated accordingly, in order to accelerate the rate of convergence, the convergence factor of the PSO algorithm is introduced [4], which has been developed in the literature.

$$v_{id}^{k+1} = K[v_{id}^k + c_1 r_1 (P_{best,id}^k - x_{id}^k) + c_2 r_2 (g_{best,id}^k - x_{id}^k)] \quad (21)$$

Where, K is a function of c_1, c_2 as reflected in equation (22)

$$K = 2 / |2 - \varphi - \sqrt{\varphi^2 - 4\varphi}|, \varphi = c_1 + c_2, \varphi > 4 \quad (22)$$

Generally, $\varphi = 4.1, c_1 = c_2 = 2.05$. Different types of functions are tested and the result showed that the PSO algorithm which has been introduced the convergence factor is superior to the standard PSO algorithm in improving the convergence speed.

2) Migration and mutation.

Standard PSO algorithm, it is easy to read because the competition is one of the best local, more particles to improve the global search. Transition Genetic algorithms have been introduced in the paper this idea, mutations to expand the optimization of overlapping particles and fitness monitoring the parent mass used overlap.

Definition: Let the particle's number n, f_i is the fitness of the i th particle, f_{av} is the average fitness at present, f_{best} is the best fitness of particles, σ^2 is the fitness variance of particles, then σ^2 can be defined as below:

$$\sigma^2 = \sum_{i=1}^n [(f_i - f_{av}) / f_{best}]^2 \quad (23)$$

This definition shows that the fitness variance of particles σ^2 reflects the extent of "converge" of particles, the smaller σ^2 is, the higher the degree of aggregation of particles is; conversely, the more dispersed the distribution of individual of particles is. In the process of the mutation of particle swarms, the mutation probability should be dynamic, and the selection of the mutation probability should be related to overlapping condition of the swarms. It can be seen from (23) that the fitness variance is in the range between 0 and n . Therefore, the mutation probability is obtained by (24):

$$P_m^k = P_{min} + (P_{max} - P_{min})(1 - \sigma_k^2 / n) \quad (24)$$

Where, P_m^k mutation probability of the swarms at iteration k ; σ^2 is the fitness variance of the swarms at iteration k ; P_{max}, P_{min} is respectively, the maximum and minimum values of mutation probability, P_{min} is generally set to 0.

V. CAPACITY OPTIMIZATION OF STANDALONE HYBRID WIND/PV POWER SYSTEM

Independent process to configure the power supply system for hybrid wind / PV, wind turbines lowest electricity costs of PV cells and the battery power supply configuration can be completed in accordance with reliability action:

(1) The default parameters

The population of particles, each sample was tested up to sixty Run = 40 and $C1 = C2 = 2.05$ the accelerating factor mutation particle swarm limited in potential between 0 and 0.4.

- (2) Particles with random position and initial velocity are set to start at 0.
- (3) calculate the fitness of each agent and Xpbest and Xgbest;
- (4) Exercise Reed (23) for admission;
- (5) The possibility. Mutation (24) is calculated by using;
- (6) To find a new point (21) is calculated using (20), mutations in which agents are required.

If you are unable to reach an advanced PSO algorithm to reproduce (7) and $k = k + 1$, and (3) to set the stage.

- (8) Output for the best solution.

VI. SIMULATION RESULTS

In this paper, the calculation was done based on a certain region selected as an example with geographic latitude of $36^{\circ}48'$. The wind speed data (8760 hours), solar radiation data (a typical 24- hour of the month of 1,4,7,10), the load data (8760 hours) as follows:

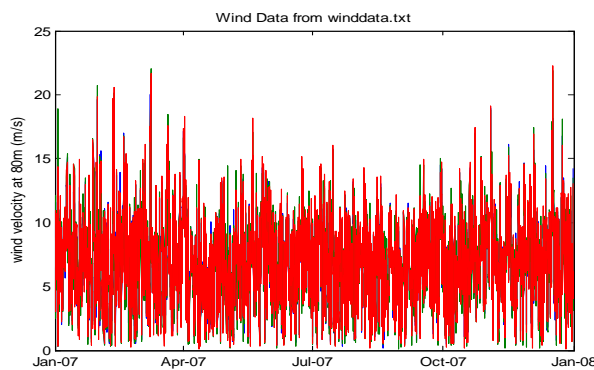


Fig.3 Wind speed

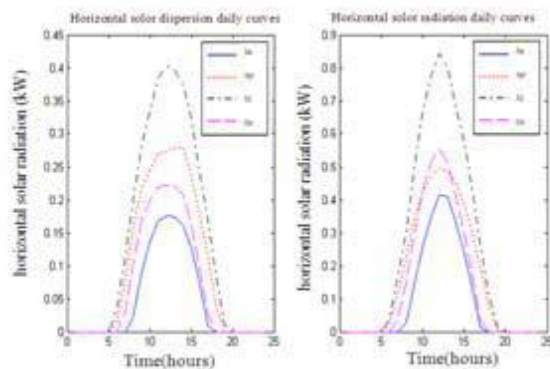


Fig.4 Solar irradiation

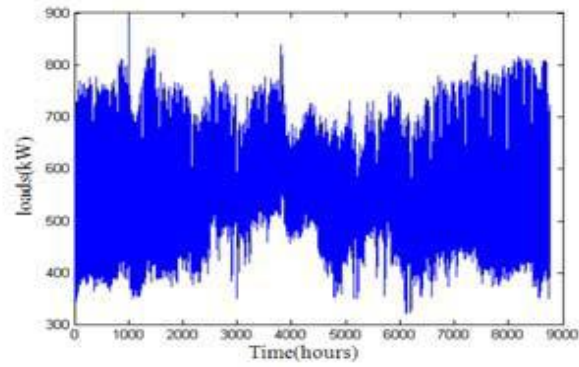


Fig.5 Load

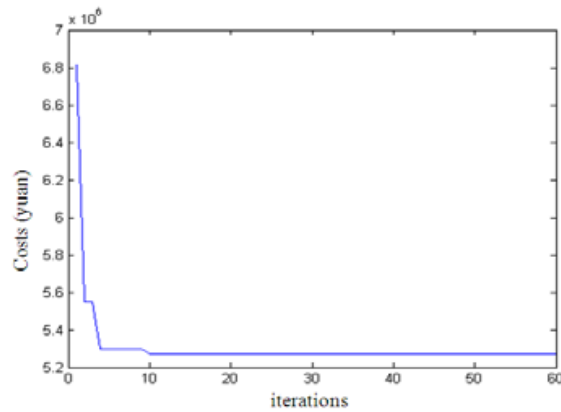


Fig.6 Process of evolution

The specific parameters used for computing are shown in table 1, where a mix of different types of turbines will not be taken into consideration, but only a single type of turbine as an example for demonstration.

Tab.1 System parameters

System parameters	Parameter values
Rated power of the wind turbine	600kW
Cut-in wind speed of the wind turbine	3m/s
Rated wind speed of the wind turbine	12m/s
Cut-off wind speed of the wind turbine	25m/s
Life expectancy of the wind turbine	20 years
Cost of the wind turbine	3,900,000 RMB
Cost of PV cells	4000 RMB
Open-circuit voltage of PV cells	29.2V
Short-circuit current of PV cells	8.09A
maximum power current of PV cells	7.42A
maximum power voltage of PV cells	23.6V
Life expectancy of PV cells	22 years
Rated power of the battery	12kW
Rated voltage of the battery	12V
Depth of discharge	50%
Life expectancy of the battery	10 years
Cost of the battery	7000 RMB
Discount rate	0.06

The final scheme of the capacity configuration obtained by using the improved PSO algorithm has been shown in table 2:

Tab.2 Optimal solution

Parameters	Parameter values
Best inclination of PV cells	17°45'
Number of the wind turbine	5
Number of PV cells	203×10
Number of the battery	65×20
Minimum cost	5.2705×10 ⁶
LPSP	0.0287

It turns out that solar power in the summer than compensate for the lack of geographic latitude air assets installation location is smaller than can be seen from Table 2 turbines, PV cells and the battery will be paid accordingly. Table 2 and change the number of solar cells and solar cells will turn into the relationship between changes in total costs can be drawn.

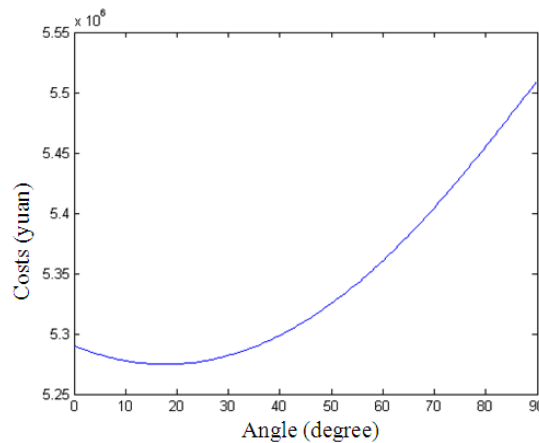


Fig.7 The relationship between Photovoltaic angle and total costs

From the figure it can be seen that the best inclination is 17° or so and the property of the best configuration provided by improved PSO algorithm has been verified. The power curves of turbines, PV cells, batteries and the load demand (from 3800 hours to 4000 hours in a whole year) are shown in Fig. 8:

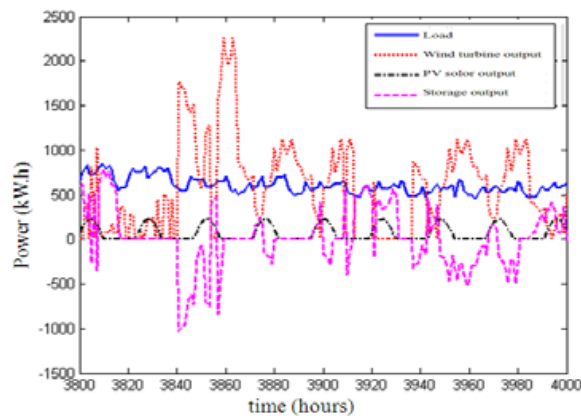


Fig.8 Change of storage capacity \Photovoltaic power \Wind power

From the Fig. 8 it can be seen that wind power is very unstable and varies considerably, however, PV cells and batteries can supply very good so that it guarantees reliable power supply for residents.

VII. CONCLUSIONS

Optimization of advanced algorithms based on PSO. Reliability electric hybrid wind / PV stand-alone project that will be added to the function of the target, which reduces the energy consumption of the system is fixed, and in this article is proposed to adjust. Compensation factor is reliable, easy management and control of the facilities to be provided by variable in determining the optimization algorithms traditional solar cells and batteries only, but kind and the number of turbines and solar panels for the project will change. More accurate results

REFERENCES

- [1] Mohammad Reza Javadi, Abolfazl Jalilvand, Reza Noroozian, Majid Valizadeh, (2011), "Optimal design and economic assessment of battery based stand-alone wind/PV generating system using ABC" Proceedings of the 3rd Conference on Thermal Power Plants (CTPP), Tehran, 18-19 October.
- [2] Y. S. Zhao, J. Zhan, Y. Zhang, D. P. Wang and B. G. Zou, (2009), "The Optimal Capacity Configuration of an Independent Wind/Pv Hybrid Power Supply System Based on Improved PSO Algorithm" 8th International Conference on Advances in Power System Control, Operation and Management (APSCOM 2009), Hong Kong, China, 8-11 November.
- [3] Ishita Biswas, Vaishalee Dash, Prabodh Bajpai, (2012), "Sizing optimization of PV-FC-Battery system with hybrid PSO-EO algorithm" Annual IEEE India Conference (INDICON), 2012, Kochi, India, 7-9 December, pp. 869 – 874.
- [4] R. C. Eberhart, Y. Shi. Comparing Inertia Weights and Constriction Factors in Particle Swarm Optimization. *IE*.2000:84~88.
- [5] Borowy Bogdan S, Salameh Ziyad M. Methodology for optimally sizing the combination of a battery bank and PV array in a wind PV hybrid system. *IEEE Transaction on Energy Conversion*, 1996, 11(2): 367 —375.
- [6] Celik, A.N.: ' Optimization and techno-economic analysis of autonomous photovoltaic-wind-hybrid energy systems in comparison to single photovoltaic and wind systems'. *Energy Conversion and Management*. 2002, 43 (18), pp.2453-2468.
- [7] S.M. Shaahid , I. El-Amin. : 'Techno-economic evaluation of off-grid hybrid photovoltaic-diesel-battery power systems for rural electrification in Saudi Arabia-A way forward for sustainable development' . *Renewable and Sustainable Energy Reviews*, 2009, 13,(3),pp. 625-633.
- [8] Orhan Ekren, Banu Y. Ekren.: 'Size optimization of a PV/wind hybrid energy conversion system with battery storage using simulated annealing' . *Applied Energy*. 2010, 87, (2), pp. 592-598.
- [9] Ajai Gupta, R.P. Saini, M.P. Sharma.: ' Modeling of hybrid energy system-Part I: Problem formulation and model development'. *Renewable Energy*. 2010, 35, (2), pp. 520-535.
- [10] Belfkira, R., Barakat, G., Nichita, C.: ' Sizing optimization of a stand-alone hybrid power supply unit: wind/PV system with battery storage'. *International Review of Electrical Engineering (IREE)*, 2008, 3 (5).

Numerical Solution of Higher Order Linear Fredholm – Integro – Differential Equations.

¹,Gegele. O.A , ²,Evans. O.P , ³,Akoh,D

^{1,2,3}Department of Mathematics and Statistics, Federal Polytechnics, Bida. Niger State

ABSTRACT : Power series and Chebyshev series approximation methods were used to solve higher order linear Fredholm integro – differential equations via two collocation points: Standard collocation point and Chebyshev – Gauss – Lobatto collocation point. Numerical examples were given to demonstrate the effectiveness of the methods.

KEY WORDS: Fredholm integro differential equation, Power series, Chebyshev series, Standard collocation point, Chebyshev – Gauss – Lobatto collocation point.

I. INTRODUCTION:

In recent years considerable work has been done both in the development of the technique, its theoretical analysis and numerical application in the treatment of Integro – Differential equations, because of its wide range of applications in scientific field such as fluid dynamics, solid state physics, plasma physics and mathematical biology [2]. Integro – differential equations are classified into various types among which Fredholm – integro – differential equation, the focus of this paper.

Generally, Fredholm – integro – differential equation is of the form

$$u^{(j)}(x) = F(x) + \int_a^b k(x, t) u(t) dt \quad (1)$$

$$u^{(k)}(0) = b_k, \quad 0 \leq k \leq n - 1 \quad (2)$$

Where $u^{(j)}(x)$ are the n^{th} derivatives, $F(x)$, $k(x, t)$ are given continuous smooth functions, $u(x)$ is the unknown function to be determined and a, b, b_k are constants. Because the result of (1) combine the differential and integral operators, then it is necessary to define initial conditions as in (2). The Fredholm – integro – differential equation of the second kind appear in a variety of scientific application such as the theory of signal processing and neural networks [1]. Because of the importance of Fredholm – integro – differential equation in scientific research, several numerical methods were used to solve both linear and non – linear Fredholm – integro – differential equation such as Tau operational method [8], Haar wavelets method [5], Lagrange interpolation method [11] and Differential transformation method [3], just to mention but a few.[11] focused on the use of Chebyshev interpolation to solve mixed linear integro – differential equation with piecewise interval. Also in [12], Lagrange and Chebyshev interpolation was applied on functional integral equation. The use of inverse Fuzzy transforms based on fuzzy partition with combination in collocation techniques has been investigated (see [4]). Research has been conducted on the use of Legendre multi-wavelets to solve weakly singular Fredholm – integro – differential equations [7]. Power series method was use by [9] to solve system of linear and non-linear integro – differential equations and obtain a close form solution if the exact solutions are polynomial otherwise produces their Taylor series solution. Chebyshev series has been used to solve Fredholm integral equations at three different collocation points [6].In this paper we consider the use of power series and Chebyshev series approximation methods to solve higher order Fredholm – integro – differential equations using two collocation points.

II. POWER SERIES APPROXIMATION METHOD

In this section we consider the use of power series approximation solution of the form

$$u(x) = \sum_{i=0}^N a_i x^i, \quad a_i (i \geq 0) \tag{3}$$

Where the coefficients a_i are unknown to be determined.

Putting (3) in (1) gives,

$$\left(\sum_{i=0}^N a_i x^i \right)^{(j)} = F(x) + \int_a^b k(x, t) \left(\sum_{i=0}^N a_i x^i \right) dt \tag{4}$$

(4) can be written in a simpler form as

$$\left(a_0 + a_1 x + a_2 x^2 + \dots \right)^{(j)} = F(x) + \int_a^b k(x, t) (a_0 + a_1 t + a_2 t^2 + \dots) dt \tag{5}$$

We integrate the right hand side of (5) and after simplification, the resulting equation is then collocated using the following collocation points

(1) Standard collocation point defined as

$$x_p = a + \frac{(b-a)}{N} * p, \quad p = 1, 2, \dots, N-1. \tag{6}$$

(2) Chebyshev – Gauss – Lobatto collocation point defined as

$$x_q = \cos \left(\frac{\pi}{N} \right) * q, \quad q = 1, 2, \dots, N-1. \tag{7}$$

Each of the two collocation points describe above together with the initial condition given in (2) resulted in (N + 1) linear algebraic equations in (N + 1) unknown constants which are then solved to obtain the unknown constants that are substituted in (3) to get the numerical solution of (1).

III. CHEBYSHEV SERIES APPROXIMATION SOLUTION:

In this section we consider the use of Chebyshev series approximation solution of the form

$$u(x) = \sum_{j=0}^N a_n T_n(x), \quad a_n (n \geq 0) \tag{8}$$

Where $T_n(x)$ is Chebyshev polynomial defined as

$$T_n(x) = \cos(n \cos^{-1} x), \quad x \in [-1, 1] \tag{9}$$

and it satisfied the recurrence relation

$$T_{n+1}(x) = 2xT_n(x) - T_{n-1}(x), \quad n \geq 1 \tag{10}$$

Putting (10) in (1), we obtain

$$\left(\sum_{j=0}^N a_n T_n(x) \right)^{(j)} = F(x) + \int_a^b k(x, t) \sum_{j=0}^N a_n T_n(t) dt \tag{11}$$

(11) can be written in a simpler form as

$$\left(a_0 + a_1 T_1(x) + a_2 T_2(x) + \dots \right)^{(j)} = F(x) + \int_a^b k(x, t) (a_0 + a_1 T_1(t) + a_2 T_2(t) + \dots) dt \tag{12}$$

Using the same procedure as in 2.0 above and using shift Chebyshev polynomial where applicable, (12) together with (2) gives (N + 1) linear algebraic equations in (N + 1) unknown constants. These equations are solved using maple 13 to obtain the unknown constants a_n 's which are then substituted into (8) to get the numerical solution of (1).

IV. NUMERICAL EXAMPLES AND RESULTS:

In this section we consider the following examples on linear Fredholm - integro – differential equations. These examples have been chosen from [1].

Example 1:

$$u''(x) = 32x + \int_{-1}^1 (1 - xt) u(t) dt$$

Subject to the conditions

$$u(0) = 1, \quad u'(0) = 1$$

The analytical solution is given as

$$u(x) = 1 + \frac{3}{2} * x^2 + 5 * x^3$$

Table 1: Numerical solution of example 1 for N = 10

x	Exact solution	Power series solution		Chebyshev series solution	
		Standard Collocation	C.G.L Collocation	Standard Collocation	C.G.L Collocation
0	1.000000000	1.000000000	1.000000000	1.000000000	1.000000000
0.1	1.020000000	1.019987500	1.019987508	1.019855160	1.019853296
0.2	1.100000000	1.099500000	1.099500027	1.097441281	1.097438523
0.3	1.270000000	1.269562500	1.269562557	1.267989324	1.267963120
0.4	1.560000000	1.559963000	1.550000098	1.558530249	1.558512781
0.5	2.000000000	1.999737500	1.995937649	1.944095018	1.984063738
0.6	2.620000000	2.619800000	2.617600207	2.595914590	2.606907820
0.7	3.450000000	3.449812500	3.447812774	3.437419929	3.347742003
0.8	4.520000000	4.518700000	4.509700350	4.509241993	4.418242167
0.9	5.860000000	5.858787500	5.849787937	5.678611744	5.759611462
1.0	7.500000000	7.497500000	7.489800353	7.395160143	7.399962085

Example 2:

$$u'''(x) = 1 - e + e^x + \int_0^1 u(t) dt$$

Subject to the conditions

$$u(0) = u'(0) = u''(0) = 1$$

The analytical solution is give as

$$u(x) = e^x$$

Table 2: Numerical solution of example 2 for N = 10

x	Exact solution	Power series solution		Chebyshev series solution	
		Standard Collocation	C.G.L Collocation	Standard Collocation	C.G.L Collocation
0	1.000000000	1.000000000	1.000000000	0.999999998	0.999999973
0.1	1.105170918	1.105170918	1.105170317	1.105170906	1.105170586
0.2	1.221402758	1.221402759	1.221393616	1.221402664	1.221402328
0.3	1.349858808	1.349858808	1.349796664	1.349858494	1.349853557
0.4	1.491824698	1.491824698	1.491779456	1.491824493	1.491822318
0.5	1.648721271	1.648721270	1.648687634	1.648720056	1.648681450
0.6	1.822118800	1.822118800	1.822091428	1.822117485	1.822097068
0.7	2.013752707	2.013752706	2.013736257	2.013751484	2.013735387
0.8	2.225540928	2.225540929	2.225110041	2.225542106	2.225528215
0.9	2.459603111	2.459603109	2.459401851	2.459602032	2.459591944
1.0	2.718281828	2.718281828	2.718165764	2.718304575	2.717964004

Example 3:

$$u^{(iv)}(x) = \frac{1}{4} + (1 - 2 \ln(2)) * x - \frac{6}{(1+x)^4} + \int_0^1 (x-t) u(t) dt$$

Subject to the conditions

$$u(0) = 0, u'(0) = 1, u''(0) = -1, u'''(0) = 2$$

The analytical solution is given as

$$u(x) = \ln(1+x).$$

Table 3: Numerical solution of example 3 for N = 10

x	Exact solution	Power series solution		Chebyshev series solution	
		Standard Collocation	C.G.L Collocation	Standard Collocation	C.G.L Collocation
0	0	0	0	2.538281×10^{-11}	2.538237×10^{-11}
0.1	0.095310180	0.095309970	0.095308282	0.094929653	0.094900490
0.2	0.182321557	0.182320192	0.182285697	0.181952718	0.181969997
0.3	0.262364265	0.262341612	0.262329925	0.262019395	0.262013595
0.4	0.336472237	0.336448896	0.336437637	0.336129984	0.336131787
0.5	0.405465108	0.405437993	0.405430058	0.401196354	0.401908328
0.6	0.470003629	0.469975523	0.469967299	0.467508962	0.466601689
0.7	0.530628251	0.530595414	0.530091041	0.528493721	0.528138621
0.8	0.587786665	0.587608614	0.587374025	0.586233239	0.585401225
0.9	0.641853886	0.641684342	0.641502316	0.640367171	0.639716176
1.0	0.693147181	0.692912617	0.692874871	0.691938947	0.691122621

Tables of Errors:

Table 4: Errors for example 1

X	Power series		Chebyshev series	
	Standard Collocation	C.G.L Collocation	Standard Collocation	C.G.L Collocation
0	0	0	0	0
0.1	1.250×10^{-5}	1.2492×10^{-5}	1.4484×10^{-4}	1.46704×10^{-4}
0.2	5.000×10^{-4}	4.99973×10^{-4}	2.558719×10^{-3}	2.561477×10^{-3}
0.3	4.375×10^{-4}	4.37443×10^{-4}	2.010676×10^{-3}	2.036880×10^{-3}
0.4	3.700×10^{-4}	9.999902×10^{-3}	1.469751×10^{-3}	1.487219×10^{-3}
0.5	2.625×10^{-4}	4.062351×10^{-3}	5.5904982×10^{-2}	1.5936262×10^{-2}
0.6	2.000×10^{-4}	2.399793×10^{-3}	2.4085410×10^{-2}	1.3092180×10^{-2}
0.7	1.875×10^{-4}	2.187226×10^{-3}	1.2580071×10^{-2}	$1.02257997 \times 10^{-1}$
0.8	1.300×10^{-3}	1.0299650×10^{-2}	1.0758007×10^{-2}	$1.01757833 \times 10^{-1}$
0.9	1.2125×10^{-3}	1.0212063×10^{-2}	$1.81388256 \times 10^{-1}$	$1.00388538 \times 10^{-1}$
1.0	2.5000×10^{-3}	$1.01996468 \times 10^{-2}$	$1.04839857 \times 10^{-1}$	$1.00037915 \times 10^{-1}$

Table 5: Errors for example 2

X	Power series		Chebyshev series	
	Standard Collocation	C.G.L Collocation	Standard Collocation	C.G.L Collocation
0	0	0	2.0×10^{-9}	2.7×10^{-8}
0.1	0	6.01×10^{-7}	1.2×10^{-8}	3.32×10^{-7}
0.2	1.0×10^{-9}	9.142×10^{-6}	9.4×10^{-8}	4.23×10^{-7}
0.3	0	6.2144×10^{-5}	3.14×10^{-7}	5.251×10^{-6}
0.4	0	4.5242×10^{-5}	2.05×10^{-7}	2.378×10^{-6}
0.5	1.0×10^{-9}	3.3637×10^{-5}	1.315×10^{-6}	3.9821×10^{-5}
0.6	0	2.7372×10^{-5}	1.297×10^{-6}	2.1732×10^{-5}
0.7	1.0×10^{-9}	1.6450×10^{-5}	1.223×10^{-6}	1.7320×10^{-5}
0.8	1.0×10^{-9}	4.30887×10^{-4}	1.178×10^{-6}	1.2713×10^{-5}
0.9	2.0×10^{-9}	2.01267×10^{-4}	1.079×10^{-6}	1.1167×10^{-5}
1.0	0	1.16064×10^{-4}	2.2747×10^{-5}	3.1782×10^{-4}

Table 6: Errors for example 3

X	Power series		Chebyshev series	
	Standard Collocation	C.G.L Collocation	Standard Collocation	C.G.L Collocation
0	0	0	2.58281×10^{-11}	2.538237×10^{-11}
0.1	2.1×10^{-7}	1.898×10^{-6}	3.80527×10^{-4}	4.0969×10^{-4}
0.2	1.365×10^{-6}	3.586×10^{-5}	3.68839×10^{-4}	3.5156×10^{-4}
0.3	2.2653×10^{-5}	3.434×10^{-5}	3.44870×10^{-4}	3.5067×10^{-4}
0.4	2.3341×10^{-5}	3.460×10^{-5}	3.42253×10^{-4}	3.4045×10^{-4}
0.5	2.7115×10^{-5}	3.505×10^{-5}	4.268754×10^{-3}	3.55678×10^{-3}
0.6	2.8371×10^{-5}	3.633×10^{-5}	2.494667×10^{-3}	3.40194×10^{-3}
0.7	3.2837×10^{-5}	5.3721×10^{-4}	2.134530×10^{-3}	2.48963×10^{-3}
0.8	1.78051×10^{-4}	4.1264×10^{-4}	1.553426×10^{-3}	2.38544×10^{-3}
0.9	1.69544×10^{-4}	3.5157×10^{-4}	1.486715×10^{-3}	2.13771×10^{-3}
1.0	2.34564×10^{-4}	2.7231×10^{-4}	1.208234×10^{-3}	2.02456×10^{-3}

V. CONCLUSION:

Most integro – differential equations are difficult to solve analytically, in many cases it require to obtain the approximate solutions, for this purpose we present the solution of higher order linear Fredholm integro – differential equations. Our methods are based on Power series and Chebyshev series which reduces a linear Fredholm integro – differential equation to a set of linear algebraic equations that can be easily solved by computer. The result obtained show that the two methods used can handle those problems effectively as can be seen in the tables of errors.

REFERENCES

- [1] Abdul – Majid.W (2011): Linear and Non – linear integral equations, Methods and Applications. Springer Heidelberg Dordrecht London New York.
- [2] Belbas. S.A (2007): A new method for optimal control of Volterra integral equations. Journal of Mathematics and Computation 189 Pp 1902 – 1915.
- [3] Darania. P and Ebadian. A (2007): A method for the Numerical Solution of integro – differential equations. Journal of Applied Mathematics and Computation 188. Pp 657 – 668.
- [4] Ezzati. R and Mokhtari. F (2012): Numerical Solution of Fredholm Integral Equations of the Second kind by using Fuzzy Transforms. International Journal of Physical sciences 7(10). Pp 1578 – 1583.
- [5] Fayyaz. M and Azram. M (2013): New Algorithms for Numerical Solution of Non – linear Integro – Differential Equations of Third Order Using Haar Wavelets. Journal of Sciences International (Lahore). 25(1). Pp 1 – 6.
- [6] Ishola. C.Y and Abolarin. O.E (2009): Solutions of Linear Fredholm Integral Equations Using Chebyshev Series Method. Nigeria Journal of Art, Sciences and Technology (NIJASAT). 5(1). Pp 55 – 60.
- [7] Mehrdad. L, Behzad. N.S and Mehdi. D (2011): Numerical Solution for Weakly Singular Fredholm – Integro – differential Equations Using Legendre Multi – Wavelets. Journal of computational and Mathematics 235. Pp 3291 – 3303.
- [8] Mohammad. S.H and Shahmorad. S (2005): Numerical Piecewise Approximate solution of Fredholm – Integro – Differential Equations by the tau Method. Journal of Applied Mathematical Modeling 29. Pp 1005 – 1021.
- [9] Mortaza. G (2009): Numerical Scheme to Solve Integro – Differential Equations System. Journal of Advanced Research in Scientific Computing 1(1). Pp 11 – 21.
- [10] Mustafa. G and Yalcin. O (2012): On the Numerical Solution of Linear Fredholm – Volterra – Integro – Differential Equations with Piecewise Interval. International Journal of Application and Applied Mathematics 7(2). Pp 556 – 570.
- [11] Rashed. M.T (2004): Lagrange Interpolation to Compute the Numerical Solution of Difference, Integral and Integro – Differential Equations. Journal of Applied Mathematics and Computation 151. Pp 869 – 878.
- [12] Rashed. M.T (2004): Numerical Solution of Functional Difference, Integral and Integro – Differential Equations. Journal of Applied Mathematics and Computation 156. Pp 485 – 492.

Insight on the Projective Module

Udoye Adaobi Mmachukwu¹ Akoh David²

¹ Department of Mathematics, Federal University Oye-Ekiti, Ekiti State, Nigeria.

² Department of Mathematics, Federal Polytechnic, Bida, Niger State, Nigeria.

Abstract : In this work, we focus on some important results on modules and projective modules. We discuss some aspects of modules laying emphasis on its axioms, exactness and free module.

Keywords: submodules, exactness, split exactness, homomorphism

1. Introduction

The theory of module is an important branch in Algebra. There are many applications of projective module as studied by some researchers. Yengui (2011) observed that for any finite-dimensional ring, all finitely generated stably free modules over $R[X]$ of rank $> \dim R$ are free; the result was only known for Noetherian rings. According to Tütüncü et al. (2012) if M is a semi-projective w -coretractable module with finite hollow dimension and $S = \text{End}R(M)$, there exist $h_1, \dots, h_n \in S$ such that $J(S) = A_{h_1}, \dots, A_{h_n}$, where $\text{Im } h_i$ is a nonzero hollow submodule of M_R and $A_{h_i} = \{s \in S | \text{Im } s + \text{Ker } h_i \neq M\}$ for each $1 \leq i \leq n$. The paper discusses concept of module, exactness of sequence. There are two classes of R -modules: left and right R -modules. The result on left R -modules yields a corresponding result on right R -modules. Since R is commutative, both left R -module and right R -module will be regarded as R -module.

Definition 1.1. Let R be a ring with identity. A left R -module is a set together with a binary operation “+” on M under which M is an abelian group, and an action on M , that is, a map $R \times M \rightarrow M: (r, x) \mapsto rx, \forall m \in M$, which satisfies the following axioms:

$$(a.) (r + s)m = rm + sm$$

$$(b.) (rs)m = r(sm)$$

$$(c.) r(m + n) = rm + rn \forall r, s \in R \text{ and } m, n \in M$$

$$(d.) 1 \cdot m = m \forall m \in M.$$

Similarly, a right R -module M is an abelian group together with a map $M \times R \rightarrow M: (m, r) \mapsto mr, \forall m \in M$, satisfying the following axioms: For $r, s \in R, m, n \in M$

$$(a.) m(r + s) = mr + ms$$

$$(b.) m(rs) = (mr)s$$

$$(c.) (m + n)r = mr + nr$$

$$(d.) m \cdot 1 = m \forall m \in M.$$

Every abelian group is a \mathbb{Z} - module.

1.2. Submodule. Let M be an R -module. A non-empty subset N of M is called a Submodule of M if N is an additive subgroup of M closed under the “same” multiplication by elements of R , as for M . This implies that the axioms of an R -modules must be satisfied by N .

2. R -Homomorphisms between two modules

Let M and N be two R -modules, then a function $f: M \rightarrow N$ is a homomorphism in case $\forall a, b \in R$ and all $x, y \in M; f(ax + by) = af(x) + bf(y)$. The function ' f ' must preserve the defining structure in order to be a module homomorphism. Precisely, if R is a ring and M, N are R -modules. A mapping $f: M \rightarrow N$ is called an R -module homomorphism if

$$(i) f(x + y) = f(x) + f(y) \forall x, y \in M.$$

$$(ii) f(ax) = af(x) + bf(y).$$

2.1. Epimorphisms and Monomorphisms

A homomorphism $f: M \rightarrow N$ is called an epimorphism in case it is surjective. That is, if f maps the elements of module M onto N . An injective R -homomorphism $f: M \rightarrow N$ is called an R -monomorphism (that is, one-to-one). An R -homomorphism $f: M \rightarrow N$ is an R -isomorphism in case it is a bijection. Thus, two modules M and N are said to be isomorphic, denoted by $M \cong N$, if there is an R -isomorphism $f: M \rightarrow N$. An R -homomorphism $f: M \rightarrow M$ is called an R -endomorphism. If $f: M \rightarrow M$ is bijective, then, it is called an R -automorphism.

2.1.1 Kernel and Image of R-homomorphism. Let R be a ring. Let M and N be R -modules and $f: M \rightarrow N$ be an R -homomorphism. The Kernel of f denoted by $\text{Ker } f$ is given by $\text{Ker}(f) := \{x \in M \mid f(x) = 0_N\}$.

The image of f denoted by $\text{Im}(f)$ or $f(M)$ is defined as

$$\text{Im}(f) := \{y \in N \mid y = f(x) \text{ for some } x \in M\}.$$

Proposition 2.1.2.

Let M and N be R -modules and $f: M \rightarrow N$ be an R -module homomorphism.

- (i) $\text{Ker } f$ is a submodule of M .
- (ii) $\text{Im } f$ is a submodule of N .
- (iii) The R -homomorphism $f: M \rightarrow N$ is a monomorphism if and only if $\text{Ker } f = 0_M$.

Proof: (i) Let $\alpha, \beta \in \text{Ker } f$. We claim that $\alpha - \beta \in \text{Ker } f$. Let 0_N be a zero of N . Then $f(\alpha) = 0_N$ and $f(\beta) = 0_N$ by the definition of $\text{Ker } N$. $\Rightarrow f(\alpha) = f(\beta)$ since 0_N is arbitrary. This implies that $f(\alpha) - f(\beta) = f(\alpha - \beta)$ since f is a homomorphism. $\Rightarrow \alpha - \beta \in \text{Ker } f$.

Again, let $r \in R$ and $k \in \text{Ker } f$. $f(k) = 0_N$. $\Rightarrow r0_N = rf(k) = f(rk)$ since f is a homomorphism. Since M is a module, $rk \in \text{Ker } f$. Hence, $\text{Ker } f$ is a submodule of M .

(ii) Let $n_1, n_2 \in \text{Im } f$. Then, there exists $m_1, m_2 \in M$ such that $f(m_1) = n_1, f(m_2) = n_2$; $n_1 - n_2 = f(m_1) - f(m_2) = f(m_1 - m_2)$ since f is a homomorphism. But $m_1 - m_2 \in M$ (since M is a module). Therefore, $(n_1 - n_2) \in \text{Im } f$. Also, let $r \in R$ and $n \in \text{Im } f$. There exists $m \in M$ such that $f(m) = n$. $rn = rf(m) = f(rm)$, since f is a homomorphism. But $rm \in M$ since M is a module. Therefore, $rn = f(rm) \in \text{Im } f$.

Thus, $\text{Im } f$ is a submodule of N .

(iii) If: Let $\text{Ker } f = 0_M$ and $f(b) = f(c)$ for $b, c \in M$.

$$f(b - c) = f(b) - f(c) = 0_N - 0_N = 0_N \Rightarrow b - c \in \text{Ker } f \Rightarrow b - c = 0 \Rightarrow b = c \Rightarrow$$

f is a monomorphism.

Only if: Let f be a monomorphism and $x \in \text{Ker } f$. Then, $f(x) = 0_N = f(0_M)$ since f is a monomorphism and $x \in \text{Ker } f, x = 0_M$. \square

2.2. Factor Module

Theorem and definition: Let M be an R -module. Let N be a submodule of M and $M/N = \{x + N | x \in M\}$. Then M/N is an R -module, where addition in M/N is defined by $(x + N) + (y + N) = (x + y) + N$ for any $x, y \in M$ and closure under multiplication by scalars in R is defined as follows: for $r \in R; x + N \in M/N, r(x + N) = rx + N$.

Proof: M/N is an additive abelian group. Also, closure by scalars in R follows from definition. Now, to verify module axioms. Generally, for $x \in M, \bar{x} = x + N$. Let $a, b \in R$.

$$(i) \quad (a + b)\bar{x} = (a + b)x + M = (ax + bx) + M = (ax + M) + (bx + M) \\ = a(x + M) + b(x + M) = a\bar{x} + b\bar{x}.$$

$$(ii) \quad a(\bar{x} + \bar{y}) = a((x + N) + (y + N)) = a((x + y) + N) = (a(x + y)) + N \\ = (ax + ay) + N = (ax + N) + (ay + N) = a\bar{x} + a\bar{y}.$$

$$(iii) \quad (ab)\bar{x} = ab(x + N) = ((ab)x) + N \text{ (by associativity in } R) \\ = a(bx + N) = a(b\bar{x}).$$

If R has identity '1', then, $1\bar{x} = 1(x + N) = (1x) + N = \bar{x}$. \square

2.3 Exactness

2.3.1 Exact Sequence. Let $f: M' \rightarrow M$ and $g: M \rightarrow M''$. The pair of homomorphisms $M' \xrightarrow{f} M \xrightarrow{g} M''$ is said to be exact at M in case $\text{Im } f = \text{Ker } g$. That is, let $y \in M$, then $g(y) = 0$ if and only if there exists $x \in M'$ such that $f(x) = y$. In general, a finite or infinite sequence of homomorphism $\dots \xrightarrow{f_{n-1}} M_{n-1} \xrightarrow{f_n} M_n \xrightarrow{f_{n+1}} M_{n+1} \rightarrow \dots$ is exact in case it is exact for each successive pair f_n and f_{n+1} . $\Rightarrow \text{Im } f_n = \text{Ker } f_{n+1}$. \Rightarrow for any three consecutive terms, the subsequence $M_{n-1} \rightarrow M_n \rightarrow M_{n+1}$ is exact.

2.3.2 Short exact Sequence

An exact sequence of the form $0 \rightarrow M' \xrightarrow{f} M \xrightarrow{g} M'' \rightarrow 0$ is called a short exact sequence.

Proposition 2.3.3. If the sequence $0 \rightarrow M' \xrightarrow{f} M \xrightarrow{g} M'' \rightarrow 0$ is a short exact sequence. Then, f is a monomorphism and g is an epimorphism. $\text{Ker } g = \text{Im } f$.

Proof. The exactness of $0 \rightarrow M' \xrightarrow{f} M$ means that $\text{Ker } f = 0$. This implies that f is injective. Similarly, f is surjective is equivalent to $M \xrightarrow{f} M'' \rightarrow 0$ is exact.

Thus, in the given short exact sequence $0 \rightarrow M' \xrightarrow{f} M \xrightarrow{g} M'' \rightarrow 0$, ' f ' is injective, ' g ' is surjective and $\text{Ker } g = \text{Im } f$. $\Rightarrow f$ is a monomorphism and g is an epimorphism.

Remark. Let M and N be any two R -modules. Every R -homomorphism from M to N is an element of the set of functions from M to N . These homomorphisms form a set with standard notation; $\text{HOM}_R(M, N)$.

Theorem 2.3.4. $\text{HOM}_R(M, N)$ is an R -module, where R is a commutative ring and M, N are R -modules.

Proof: Suppose R is commutative. For $\alpha \in \text{HOM}_R(M, N)$, $r \in R$, define $(r\alpha)$ by $(r\alpha)(x) = r(\alpha x)$. Since $r, s \in R$, $\alpha \in \text{HOM}_R(M, N)$ and $x \in M$,

$$(r\alpha)(sx) = r(\alpha(sx)) = r(s(\alpha(x))) = rs(\alpha(x)) = r((s\alpha)(x)).$$

We have that $r\alpha \in \text{HOM}_R(M, N)$. Also, let $f, g \in \text{HOM}_R(M, N)$ and $f + g$ preserves the scalar multiplication. Let $\alpha \in R$ and $x \in M$ be arbitrarily given. Then, we have;

$$(f + g)(\alpha x) = f(\alpha x) + g(\alpha x) = \alpha f(x) + \alpha g(x) = \alpha[f(x) + g(x)] = [\alpha(f + g)(x)].$$

Hence, $f + g$ preserves scalar multiplication. Since R is commutative, for arbitrary given $\alpha \in R$ and $f \in \text{HOM}_R(M, N)$, we define a function $\alpha f: M \rightarrow N$ by taking $(\alpha f)(x) = \alpha[f(x)]$ for every $x \in M$. Thus, $\text{HOM}_R(M, N)$ is an R -module. \square

Remark. From the above theorem, if R is a commutative ring and M is an R -module, then, $\text{HOM}_R(M, N)$ is also an R -module, where $N = R$ is considered an R -module over itself. $\text{HOM}_R(M, N)$ is a module called the dual of M and it is denoted by M^* .

2.4 Direct Summands, Split Homomorphism

Suppose M_1 and M_2 are submodules of a module M . M_1 and M_2 span M in case $M = M_1 + M_2$. M_1 and M_2 are linearly independent in case $M_1 \cap M_2 = 0$. Let $i: (x_1, x_2) \mapsto x_1 + x_2, ((x_1, x_2) \in M_1 \times M_2)$ be a canonical R -homomorphism ' i ' from the cartesian product $M_1 \times M_2$ module with $\text{Im } i = M_1 + M_2, \text{ Ker } i = \{(x, -x) | x \in M_1 \cap M_2\}$. Then, i is *epic* if and only if M_1 and M_2 span M , and *monic* if and only if M_1 and M_2 are independent. If ' i ' the canonical homomorphism is an isomorphism, then M is the (internal) direct sum of its submodules M_1 and M_2 , and it is denoted by $M = M_1 \oplus M_2$. Thus, for each $m \in M$, there exists unique $m_1 \in M_1$ and $m_2 \in M_2$ such that $m = m_1 + m_2 \in M$ if and only if $M = M_1 \oplus M_2$.

A submodule M_1 of M is a direct summand of M in case there is a submodule M_2 of M such that $M = M_1 \oplus M_2$. M_2 is also a direct summand. M_1 and M_2 are called *Complementary direct summands*. More generally, Let M_1, \dots, M_n be submodules of an R -module M . Suppose

$$M = \sum_{i=1}^n M_i \text{ and each } x \in M \text{ has a unique representation } x = \sum_{i=1}^n x_i, \quad x_i \in M_i. \text{ Then, } M \text{ is}$$

called the *internal direct sum* of M_i 's and it is written as $M = \bigoplus_{i=1}^n M_i$.

2.4.1 Split exact Sequence

Let $f: M \rightarrow N$ and $g: N \rightarrow M$ be homomorphisms with $fg = 1_N$, then f is a split epi and we write $M \xrightarrow{f} N \rightarrow 0$ and we say g is a split mono, and write $0 \rightarrow N \xrightarrow{g} M$. Thus, a short exact sequence $0 \rightarrow M_1 \xrightarrow{f} M \xrightarrow{g} M_2 \rightarrow 0$ is split or is split exact in case f is a split mono and g is a split epi.

Lemma 2.4.2. Let $f: M \rightarrow N$ and $f': N \rightarrow M$ be homomorphisms such that $ff' = 1_N$. Then, f is an epimorphism, f' is a monomorphism, and $M = Ker f \oplus Im f'$.

Proof: Clearly, f is epi, f' is monic. If $f'(y) = x \in Ker f \cap Im f'$ then $0 = f(x) = ff'(y) = y$, and $x = f'(y) = 0$. If $x \in M$, then $f(x - f'f(x)) = f(x) - f(x) = 0$ and

$$x = x - f'f(x) + f'f(x) \in Ker f + Im f. \Rightarrow M = Ker f \oplus Im f'. \quad \square$$

Proposition 2.4.3. The following statements about a short exact sequence

$$0 \rightarrow M_1 \xrightarrow{f} M \xrightarrow{g} M_2 \rightarrow 0$$

are equivalent in R^M .

- (a.) The sequence is split;
- (b.) The monomorphism $f: M_1 \rightarrow M$ is split;
- (c.) The epimorphism $g: M \rightarrow M_2$ is split;
- (d.) $Im f = Ker g$ is a direct summand of M ;
- (e.) Every homo $h: M_1 \rightarrow N$ factors through f ;
- (f.) Every homo $\bar{h}: N \rightarrow M_2$ factors through g .

3.1 Free Module

Definition 3.1.1.

Let S be a non-empty subset of an R -module M . S is called a set of free generators or basis or base for M if every element $x \in M$ can be uniquely expressed as a linear combination of elements of S . That is, $x = \sum a_y y$ uniquely where y ranges through the elements of S and only a finite number of a_y 's are non-zero in R . A subset S of a module M over R is said to be linearly independent if and only if for every finite number of distinct elements $x_1, \dots, x_n \in S$, $\sum_{i=1}^n \alpha_i x_i = 0, \alpha_i \in R, \Rightarrow \alpha_i = 0 \forall i = 1, \dots, n$. An R -module M is free if it has a basis. A non-zero cyclic module R_x is said to be free if given $a \in R, ax = 0 \Rightarrow a = 0$. Precisely, S is a basis for M if $M = \bigoplus_{x \in S} R_x$ where each R_x is a free cyclic module. Thus, S is a basis for M if and only if S is linearly independent and generates M .

Theorem 3.1.2. Given any R -module M , there exists an exact sequence

$$0 \longrightarrow K \longrightarrow F \longrightarrow M \longrightarrow 0$$

such that F is a free R -module.

Proof: Let F be a free R -module with basis $S = M$. Define a mapping $f: S \rightarrow M$ by $f(x) = x$. Then, f extends to a unique homomorphism $g: F \rightarrow M$, g is surjective since $F = \langle M \rangle$. Let $K = \text{Ker } g$. Then, $0 \longrightarrow K \xrightarrow{\alpha} F \xrightarrow{g} M \longrightarrow 0$ is exact. \square

Definition 3.1.3. An R -module M is said to be finitely generated (FG) if M can be generated by some finite set of elements. Thus, a module M is finitely generated if there is a finite subset N of M with $RN = M$. If M and M_1 are finitely generated, so is $M \oplus M_1$.

Theorem 3.1.4. Let S be a basis for a free R -module, F and N any R -module. Let $\alpha: S \rightarrow N$ be any mapping. Then, there exists a unique R -homomorphism, $\beta: F \rightarrow N$ such that $\beta|_S = \alpha$.

Proof: Let $z \in F$, then, z can be expressed in the form $z = \sum_{x \in S} a_x x$ where only a finite number of the a_x 's are non-zero. Define a map $\beta: F \rightarrow N$ by $\beta(z) = \sum_{x \in S} a_x \alpha(x)$. Thus, $\beta|_S = \alpha$. \square

Remark. A homomorphism $f: M \rightarrow N$ that is composite of homomorphisms $f = gh$ is said to factor through g and h . A homomorphism f factors uniquely through every epimorphism whose kernel is contained in that of f and through every monomorphism whose image contains the image of f .

3.2 Projective modules

Projection. Let M be an R -module. Let K be a direct summand of M with complementary direct summand K' , that is, $M = K \oplus K'$. Then, $P_K: K \oplus K' \rightarrow K$, where $k \in K, k' \in K'$ defines an epimorphism $P_K: M \rightarrow K$ called the *projection of M on K along K'* .

Proposition 3.2.1. Let $M = K \oplus K'$ as given above, then, the projection of M on K along K' is the unique epimorphism $M \xrightarrow{P_K} K \longrightarrow 0$ which satisfies $P_K|_K = 1_K$ and $\text{Ker } P_K = K'$.

Proof: P_K satisfies the given conditions. Let $f: M \rightarrow K$ be such that $f|_K = 1_K$ and $\text{Ker } f = K'$, then, for all $k \in K, k' \in K', f(K + K') = f(K) + f(K') = K + 0 = K = P_K(K + K')$. Again, if K is the direct summand of M with complementary direct summand $K', M = K \oplus K'$. Then, K' is a direct summand of M with K as its complementary direct summand. If P_K is the projection of M on K along K' , then the projection P'_K of M on K' along K can be characterized by; $P'_K: m \mapsto m - P_K(m), m \in M$.

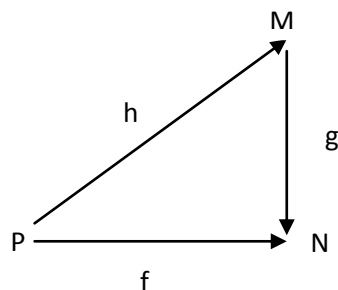
Theorem 3.2.2. Suppose that $i_K: K \rightarrow M$ and $i_{K'}: K' \rightarrow M$ represent inclusion mapping where $M = K \oplus K'$, then

$$\begin{aligned} 0 &\longrightarrow K' \xrightarrow{i_{K'}} M \xrightarrow{P_K} K \longrightarrow 0 \\ 0 &\longrightarrow K \xrightarrow{i_K} M \xrightarrow{P_K} K \longrightarrow 0 \end{aligned}$$

are split exact.

Proposition 3.2.3 Let $M = K \oplus K'$. Let P_K be the projection of M on K along K' , and let L be a submodule of M . Then, $M = L \oplus K'$ if and only if $P_K|_L: L \rightarrow K$ is an isomorphism.

Projective modules: A module P is called a *Projective module* if given any diagram



where $g: M \rightarrow N$ is surjective and $f: P \rightarrow N$ is an R -module homomorphism, there exists a homomorphism $h: P \rightarrow M$ such that the diagram is commutative. ' h ' is a lifting of f . In other

words, given an epimorphism $g: M \rightarrow N$, then, any homomorphism $f: P \rightarrow N$ can be factored as $f = gh$ (f is lifted to h).

Theorem 3.2.4. A free module is projective.

Proof: Suppose that the R -module F is free. Let $\alpha: K \rightarrow M$ be an R -epimorphism and $\beta: F \rightarrow M$ be any R -homomorphism. Since F is free, it has a basis. Let S be a basis for F . $\alpha(K) = M$ and for each $s \in S$, there exists $y_s \in K$ such that $\alpha(y_s) = \beta(s)$. Define $\beta': F \rightarrow K$ by $\beta'(s) = y_s$. Then, $\alpha\beta' = \beta$. $\Rightarrow F$ is projective. \square

Theorem 3.2.5. Every direct summand of a projective module over R is projective.

Proof: Let $M \oplus N$ be a projective module with M , a direct summand of $M \oplus N$. Let $\pi: M \oplus N \rightarrow M$ be a projection map, $\beta: A \rightarrow B$ be an epimorphism, $\delta: M \rightarrow B$ be any R -homomorphism; where $i: M \rightarrow M \oplus N$ is an inclusion map. $\delta \circ \pi: M \oplus N \rightarrow B$, $\delta \circ \pi \circ i = (\delta \circ \pi) \circ i = \delta \circ (\pi \circ i) = \delta$. Then, $\delta \circ \pi = \beta \circ \gamma \Rightarrow \delta \circ \pi \circ i = \beta \circ \gamma \circ i = \delta \Rightarrow \delta$ is a lifting to $\gamma \circ i \Rightarrow M$ is projective. \square

Theorem 3.2.6. Let M be an R -module. Then, M is projective if and only if M is a direct summand of a free R -module.

Proof: Assume M is projective and F is a free module, there exists an exact sequence

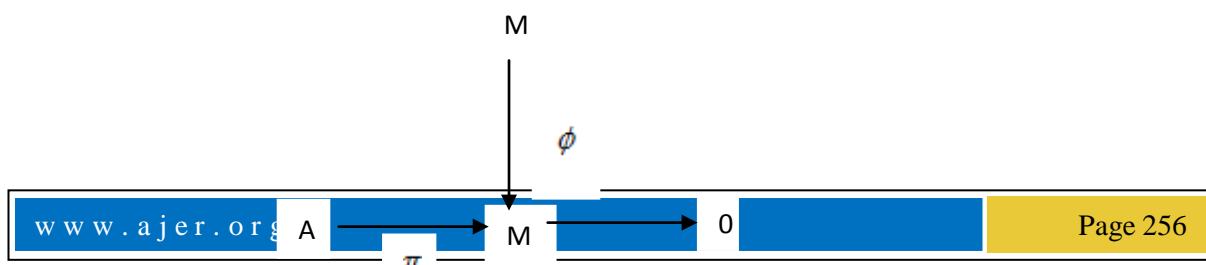
$$0 \longrightarrow K \xrightarrow{\alpha} F \xrightarrow{\beta} M \longrightarrow 0$$

Let $1_M: M \rightarrow M$ be identity map. Then, there exists $\gamma: M \rightarrow F$ such that $\beta\gamma = 1_M$. $\Rightarrow 0 \longrightarrow K \longrightarrow F \longrightarrow M \longrightarrow 0$ is a split short exact sequence. $\Rightarrow F \cong K \oplus M$.

Conversely, let $\pi: M \oplus N \rightarrow M$ be the projection map, $\beta: A \rightarrow B$ an R -epimorphism and $\delta: M \rightarrow B$ any R -homomorphism, then, $\delta\pi: M \oplus N \rightarrow B$ lifts to $\gamma: M \oplus N \rightarrow A$ since $M \oplus N$ is free and is projective. $\delta\pi = \beta\gamma$. Let $i: M \rightarrow M \oplus N$ be the inclusion map. Then, $\beta(\gamma i) = \delta(\pi i) = \delta \Rightarrow \delta$ lifts to γi . $\Rightarrow M$ is projective. \square

Theorem 3.2.7. A direct sum of projective modules is projective if and only if each summand is projective.

Proof: Let M be the direct sum of R -module $M_i, i = 1, 2, \dots, n$. Suppose each M_i is projective and consider the diagram



where the row is exact. Let $\phi|_{M_i} = \phi_i$ be the restriction of ϕ to M_i . By projectivity of M_i , there exists $\varphi_i \in \text{HOM}_R(M_i, A)$ with $\varphi_i \pi = \phi_i$. Let $\varphi = \sum_i \varphi_i \in \text{HOM}_R(M, A)$. Then, $\varphi \pi = \phi \Rightarrow M$ is projective.

Conversely, assume M is projective and we have the diagram with exact row,

$$\begin{array}{ccccc}
 & & M_\lambda & & \\
 & & \downarrow & \phi_\lambda & \\
 A & \xrightarrow{\pi} & B & \longrightarrow & 0
 \end{array}$$

extend ϕ_λ to $\phi \in \text{HOM}_R(M, B)$ by defining $\phi = \delta_{i\lambda} \phi_\lambda$. Let $\varphi \pi = \phi$ for some $\varphi \in \text{HOM}_R(M, A)$. Then the restriction $\varphi_\lambda = \varphi|_{M_\lambda} \in \text{HOM}_R(M_\lambda, A)$ make the diagram to be commutative. Thus, $\pi \varphi_\lambda = \phi_\lambda \Rightarrow$ each summand of M is projective. \square

Theorem 3.2.8. An R -module P is projective if and only if every short exact sequence $0 \longrightarrow M \longrightarrow N \longrightarrow P \longrightarrow 0$ splits.

Proof: Assume P is projective. Let

$$0 \longrightarrow M \xrightarrow{f} N \xrightarrow{g} P \longrightarrow 0$$

be exact. Given the diagram below

$$\begin{array}{ccc}
 & P & \\
 & \downarrow & 1_P \\
 N & \xrightarrow{g} & P
 \end{array}$$

By hypothesis, we can fill in the diagram with $g': P \rightarrow N$ to obtain a commutative diagram. Thus, $gg' = 1_P$ and the short exact sequence $0 \longrightarrow M \xrightarrow{f} N \xrightarrow{g} P \longrightarrow 0$ splits.

Conversely, suppose the short exact sequence $0 \longrightarrow M \xrightarrow{f} N \xrightarrow{g} P \longrightarrow 0$ splits, then, P is a direct summand of N and hence, P is projective. \square

Theorem 3.2.9. Let R be a commutative ring with identity; M and N , R -modules. Suppose $\alpha: N \rightarrow N'$, then

- (a.) $\alpha_*: \text{HOM}_R(M, N) \rightarrow \text{HOM}_R(M, N')$ given by $\alpha_*(y) = \alpha y$ is an R -homomorphism.
- (ii) $(y'y)_* = y'_*y_*$ if $y'y$ is defined.

(b.) Let $0 \longrightarrow M' \longrightarrow M \longrightarrow M'' \longrightarrow 0$ be an exact sequence. Then,

$0 \longrightarrow \text{HOM}_R(N, M') \longrightarrow \text{HOM}_R(N, M) \longrightarrow \text{HOM}_R(N, M'') \longrightarrow 0$ is exact.

Proof: (a.) Let $\alpha_*: N \rightarrow N'$ be a homomorphism. To show that $\alpha_*: \text{HOM}_R(M, N) \rightarrow \text{HOM}_R(M, N')$ given by $\alpha_*(y) = \alpha y$ is an R -homomorphism. Let $y \in \text{HOM}_R(M, N)$, then for each y , there exists $\alpha y \in \text{HOM}_R(M, N')$. We claim that α_* is an R -homomorphism. $\alpha_*: \text{HOM}_R(M, N) \rightarrow \text{HOM}_R(M, N')$. For $y_1, y_2 \in \text{HOM}_R(M, N)$ and $r_1, r_2 \in R$ and for all $m \in M$,

$$f(r_1 y_1 + r_2 y_2)m = f[y_1(mr_1) + y_2(mr_2)] = f[y_1(mr_1)] + f[y_2(mr_2)] = r_1 f(y_1)(m) + r_2 f(y_2)(m)$$

$\Rightarrow \alpha_*: \text{HOM}_R(M, N) \rightarrow \text{HOM}_R(M, N')$ is an R -homomorphism.

(ii.) α_* is epic if and only if for each $\bar{y} \in \text{HOM}_R(M, N')$, there exists $y \in \text{HOM}_R(M, N)$ such that $\alpha(y) = \bar{y}$. Let $\bar{y}\bar{y}' \in N$. Since α_* is an R -homomorphism, $\alpha_*(\bar{y}, \bar{y}') = \alpha_*(\bar{y})\alpha_*(\bar{y}') \Rightarrow (yy')_* = y_*y'_*$ where $yy' \in N'$.

(b.) Given that $0 \longrightarrow M' \xrightarrow{i} M \xrightarrow{p} M'' \longrightarrow 0$ is exact. To show that

$$0 \longrightarrow \text{HOM}_R(N, M') \xrightarrow{\text{HOM}_R(N, i)} \text{HOM}_R(N, M) \xrightarrow{\text{HOM}_R(N, p)} \text{HOM}_R(N, M'') \longrightarrow 0$$

is exact. Let $f \in \text{HOM}_R(N, M'')$. There exists $g \in \text{HOM}_R(N, M)$ such that $\text{HOM}_R(N, M'') = pg = f \Rightarrow \text{HOM}_R(N, M'')$ is surjective. Thus, the exactness of

$0 \longrightarrow \text{HOM}_R(N, M') \longrightarrow \text{HOM}_R(N, M) \longrightarrow \text{HOM}_R(N, M'') \longrightarrow 0$ is established. \square

Theorem 3.2.10. An R -module P is projective if and only if for any exact sequence $0 \longrightarrow M' \longrightarrow M \longrightarrow M'' \longrightarrow 0$ of R -modules, the sequence

$0 \longrightarrow \text{HOM}_R(P, M') \longrightarrow \text{HOM}_R(P, M) \longrightarrow \text{HOM}_R(P, M'') \longrightarrow 0$ is exact.

Proof: Let $0 \longrightarrow M' \xrightarrow{i} M \xrightarrow{p} M'' \longrightarrow 0$ be exact. Suppose P is projective, then given $f \in \text{HOM}_R(P, M'')$, there exists $g \in \text{HOM}_R(P, M)$ such that $\text{HOM}_R(P, p)(g) = pg = f$. In this case, $\text{HOM}_R(P, p)$ is surjective and we have the exactness of

$$0 \longrightarrow \text{HOM}_R(P, M') \xrightarrow{\text{HOM}_R(P, i)} \text{HOM}_R(P, M) \xrightarrow{\text{HOM}_R(P, p)} \text{HOM}_R(P, M'') \longrightarrow 0.$$

The converse holds. Suppose $\text{HOM}_R(P, -)$ is exact and $p: N \rightarrow M$ (with $N \xrightarrow{p} M$). Let $\text{Ker } p = K$. Then, we have the exact sequence $0 \longrightarrow K \xrightarrow{i} N \xrightarrow{p} M \longrightarrow 0$ where i is the injection map. Applying the exactness of $\text{HOM}_R(P, -)$ we have that P is projective. \square

Conclusion.

A module P is finitely generated and projective if and only if P is a direct summand of a free module with a finite base since if P is a direct summand of a free module F with a finite base, then P is projective and is also a homomorphic image of a free module F . Thus, P has a finite set of generator. Also, P being a finitely generated and projective module implies that we have an exact sequence $0 \longrightarrow P' \longrightarrow F \longrightarrow P \longrightarrow 0$ where F is free and has a finite base. P is projective implies that F is isomorphic to $P \oplus P'$, thus, P is a direct summand of a free module with finite base.

Bibliography

- [1] Anderson, W.F., *Graduate text in Mathematics: Rings, and Categories of Modules*, Springer-Verlag, New york, 1992.
- [2] Dummit, S. and Foote, M., *Abstract Algebra*, University of Vermont, 1991.
- [3] Eckmann, B., Moser J.K. and Stenstrom, B., *“Rings of Quotients: An introduction to Methods of Rings”*, Springer-Verlag, New york, 1975.
- [4] Hartley, B. and Hawkes ,T.O., *Rings, Modules and Linear Algebra*, Chapman And Hall Ltd., London, 1970.
- [5] Ilori, S.A , *Lecture Note on MAT 710*, University of Ibadan, 2008.
- [6] Jacobson ,N., *Basic Algebra II*, Revised Edition, Vol.2, W.H Freeman and Company, 1989.
- [7] Kaplansky , I., *Chicago Lectures in Mathematics: Field and Rings*, Second Edition, University of Chicago, 1972.
- [8] Kuku, A. O., *Abstract Algebra*, Ibadan University Press, Ibadan, 1992.
- [9] Maclane S.and Birkhoff, G., *Algebra*, Third Edition, New York, 1965.
- [10] Reis, C., *Ring Theory*, Academic Press, New York, 1972.
- [11] Silvester, J.R., *Introduction to Algebra K-theory*, Chapman and Hall, Great Britain, 1981.
- [12] Sze-Tsen, H., *Elements of Modern Algebra*, University of Carlifornia, Los Angeles, 1965.

- [13] **Tütüncü**, D.K., Toksoy, S.E. and Tribak,R., *A Note on Endomorphism Rings of Semi-Projective Modules*, Mathematical Proceedings of the Royal Irish Academy, Vol. 112A, No. 2, (pp. 93-99), 2012.
- [14] Yengui, I., *Stably Free Modules over $R[X]$ of Rank $> \dim R$ are free*, Mathematics of Computation. Vol. 80, No. 274, (pp. 1093-1098), 2011.

Durability of Laterite/Sand Hollow Blocks in Magnesium Sulphate Environment

ATA Olugbenga

Department of Building, Obafemi Awolowo University, Nigeria

ABSTRACT: *The effects of exposure of laterite/sand block to magnesium sulphate environment were studied. Change in compressive strength of machine compacted hollow block specimens of mix 1:6 and 10% laterite content were measured after 56 days of continuous immersion in 1%, 3% and 5% of magnesium sulphate solutions. Test results showed that the compressive strength significantly reduced with increase in magnesium sulphate concentration and immersion period. Laterite/sand block made with ordinary Portland cement cannot be recommended for use in sulphate-laden environment since it produced a compressive strength of less than 2.07N/mm², as required by the Nigerian Standards, after 28 days of immersion in magnesium sulphate solution.*

KEYWORDS - *compressive strength, laterite, magnesium sulphate, sand*

I. INTRODUCTION

Sulphate attack is one of the most aggressive environmental deteriorations that affect the long-term durability of cement-based structures and can cause huge economic loss. The production of cement-based structures consumes a large amount of natural resources. As a step in ensuring the availability of resources for future generations, it is necessary to adopt engineering practices which focus on the conservation of non-renewable resources and energy. Researchers have been formulating new technologies, which provide a sustainable approach in the construction industry. One of such is the use of laterite as partial or whole replacement for sand as fine aggregate in cement-based structures production. Laterite is a cheap, environmentally friendly and abundantly available building material in the tropical region [1, 2, 3]. Laterite has other advantages which make it potentially a very good and appropriate material for construction, especially for the construction of rural structures in the less developed countries [4]. These advantages include: no specialized skilled labour is required for the production of lateritized concrete and for its use in the construction of structures and also, lateritized concrete structures have potentially sufficient strength compared with that of normal concrete. Despite these advantages, laterite is sometimes considered to be a construction material for the poor and hence undesirable. Loss of traditional knowledge resulting in deterioration in the quality of recent lateritic constructions has, in many cases, compounded these beliefs. This fact might not be unconnected with the non-availability of accepted standards and codes as regards its performance.

Although studies on the compressive strength of stabilized lateritized block have shown encouraging results, the lack of sufficient technical data, especially about its long-term performance, has limited its wider application in construction work. This dearth of research data informed the need for this further work to evaluate the durability of cement stabilized lateritized block to enhance a safe application of the material.

II. MATERIALS AND METHODS

The major materials used in this study are sharp sand, laterite and ordinary Portland cement conforming to British standard, BS 197-1, [5]. All the materials were sourced from within Ile-Ife in Ife Central Local Government Area of Osun State, Nigeria. Aggregates gradation conformed to BS 932 [6] and the maximum particle size of the fine aggregates (sand and laterite) used was 2.36 mm. Having been previously adjudged [7] to be suitable for building construction; machine compacted sandcrete hollow blocks made from mix (1:6) and 10% laterite content was adopted for this study. Batching was by volume. The mix was such that

mix (1:6) at 10% laterite content means one volume of cement and six volumes of aggregate with 10% of the aggregate being laterite, while the remaining 90% was sand. Water was added until reasonable workable mix was obtained to simulate field conditions. This means that the amount of water added was not measured but was just added till the mix was workable. Practical experiences from the rule of thumb have revealed that different batches of the same mix will experience little or no significant variation in compressive strength [4]. As a matter of fact, this is the practice in the production of commercial blocks in Nigeria. Water sprinkling curing method was used. The size of the block samples was 450x150x225mm.

Some selected samples of sand and laterite used as fine aggregate in this research work were subjected to various tests and analyses in order to ensure their compliance with various established standards. Sample grading, moisture content determination, specific gravity test and Atterberg limit determination are some of the tests carried out on the samples.



Figure 3: A diesel powered engine machine-compacted mould

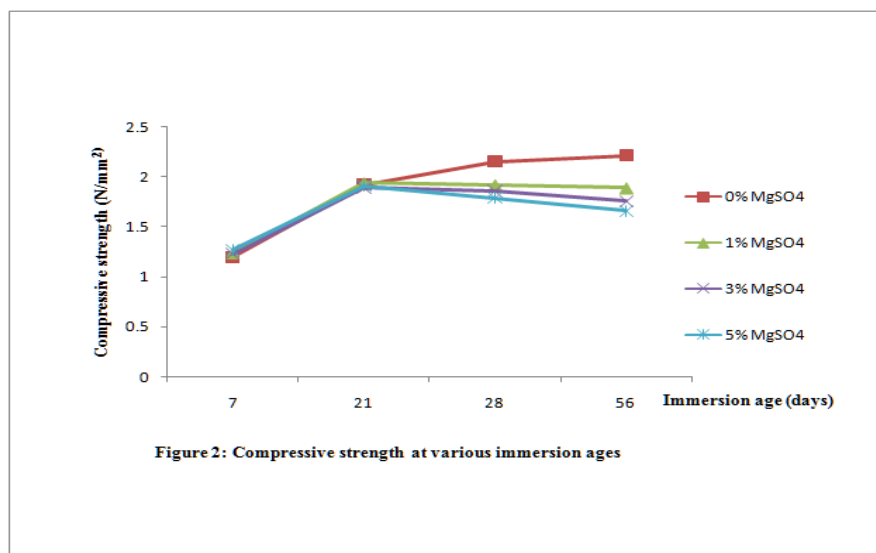
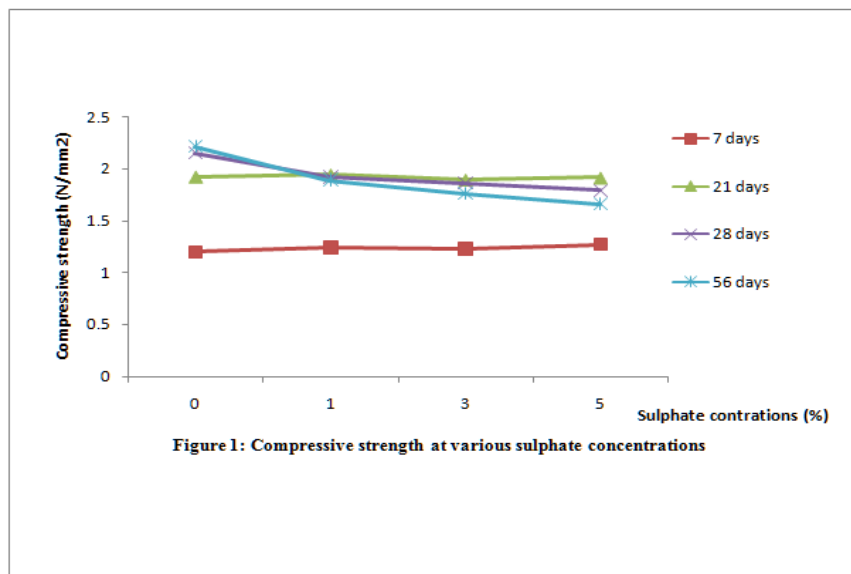
The machine compacted equipment (Fig. 3) is built for easy use and can be operated by unskilled labour. It requires little maintenance and hence the design is very suitable for remote areas [8]. Both electric motors and diesel engines can support it. Its design principle includes the use of solid frames for safe handling and stability. Three levers operate it and produce a hydraulic pressure, which is constant. The framework is about 1.85m high. It operates on a motor placed underneath the wooden pallet upon which the mould rests. The diesel types incorporate the use of a fan belt fixed over the motor and a roller, which actually turns the roller. Actual vibration occurs when the fixture on the motor, a metallic mass, hits underside of the wooden pallet. The moulded unit is removed by the operation of the longest lever, which is normally on the right side of the machine. Actual compaction is achieved by bringing the “presser” down to bear on the cement/aggregate mixture in the mould below. This is done by the operation of the highest lever. A second lever turns off the vibration. The operation of the last lever, the longest on the right hand side slowly lifts the mould for a quick removal of the compact unit. Pressure applied is fairly constant.

The sulphate-water proportion required for 0%, 3% and 5% sulphate concentrations were volumetrically determined. The blocks were immersed in the various magnesium sulphate concentrations. At the end of the immersion periods of 7days, 14days, 28days and 56days three blocks were removed from each of the different concentrations of the sulphate medium, wiped dried and tested for their compressive strengths. The compressive strength test was carried out at 7, 14, 28 and 56 days immersion age using ELE 2000kN compressive testing machine. Three specimens were crushed. All crushings were done on the edge face with a 3mm thick flat steel plate placed at top and bottom of sample for even distribution of load. The compressive strength was then calculated for each block sample.

III. RESULTS AND DISCUSSION

Visual inspection of the specimens did not show any distinctive visual features of damage such as cracking and spalling. Previous studies of external sulphate attack on ordinary Portland cement (OPC) based structures show that the reactions involve calcium silicate hydrate (C-S-H) and the aluminate component of hardened cement paste [9, 10, 11,12]. As a result of these reactions, expansion and cracking are caused directly or indirectly, by ettringite formation, while softening and disintegration are caused by destruction of C-S-H. Therefore, the presence of ettringite was very remote [13]. This is in conformity with identified

behavioural pattern of magnesium sulphate by [10] that unlike the attack of other alkali sulphates, attack by magnesium sulphate is characterized mainly by a loss of strength and disintegration of the concrete under attack, rather than by an expansion and scaling. This type of sulphate attack falls into first form of sulphate attack according to [14] which is akin to eating away of the hydrated cement paste and progressively reducing it to cohesionless granular mass leaving the aggregates exposed. He concluded by saying that this type of deterioration may lead to reduction in the cross-sectional area of the structural component (i.e. loss in weight of concrete) and decrease in strength. This mode of failure which is attributed mainly to the formation of gypsum and it is known as the acidic type of sulphate attack.



Figs. 1 and 2 show the compressive strengths of lateritic blocks immersed in different concentrations of magnesium sulphate over a period of 56 days. Generally, specimens immersed in magnesium sulphate solution exhibited relatively slightly high compressive strengths at early age. Though in all cases, specimens continuously stored in water exhibited higher compressive strength. This initial increase in compressive strength of specimens exposed to sulphate solution might be due to continuing hydration of cement in magnesium sulphate solution at the early part of the exposure period. This increase in strength stopped as soon as complete hydration of cement was achieved and should not be interpreted as increased resistance to magnesium sulphate

attack. Another likely reason for the initial increase in compressive strength according to [15] and [16] occurs as result of the action of alkali sulphates on concrete made with Portland cement which is brought about by development of early hydrated microstructure as well as filling of the existing pores with secondary ettringite and gypsum. However, as the formation of this phase continues and the available pore space loses its capacity to accommodate additional amounts of ettringite, potential damaging expansion forces start to be generated within the material. This explains the reason for subsequent relative reduction in strength.

Figs. 1 and 2 show that increasing the solution concentration increases its rate of attack. At the early period of exposure, there was no pronounced difference in the rate of attack due to increase in concentration. However, after 28 days, the specimen immersed in 5% magnesium sulphate concentration had the least compressive strength whereas the one immersed in 1% magnesium sulphate concentration had the highest compressive strength after the control specimen. It can thus be said that the rate of deterioration increased with increasing solution concentration. The higher the magnesium sulphate solution concentration, the lower the specimen compressive strength. This is also in line with [17] assertion that the rate of sulphate attack increases with an increase in the strength of the solution.

IV. CONCLUSION

The study was conducted to evaluate the durability of laterite/sand hollow block in magnesium sulphate environment. Based on the extensive experimental test results it can be concluded that the compressive strength of laterite/sand block decreased with increasing magnesium sulphate concentration and the exposure period. Laterite/sand block made with ordinary Portland cement cannot be recommended for use in sulphate-laden environment since it produced a compressive strength of less than 2.07N/mm^2 , as required by the Nigerian Standards, after 28 days of immersion in magnesium sulphate solution.

REFERENCES

- [1] O. Ata, *Effect of applied stress on moduli of elasticity and deformability of terracrete*, M.Sc Thesis Submitted to the Department of Building, Obafemi Awolowo University, Ile-Ife.2003.
- [2] H. Biniçi, O.,Aksogan. and T. Shan.. Investigation of fibre reinforced mud brick as a building material. *Construction and Building Materials*, 19(2), 2004, 313-318.
- [3] K.O. Olusola., *Some factors affecting compressive strength and elastic properties of laterized concrete*. Doctoral Thesis Submitted to the Department of Building, Obafemi Awolowo University, Ile-Ife, 2005.
- [4] J.A. Osunade, Effect of replacement of laterite soils with granite fines on the compressive and tensile strengths of laterized concrete. *Building and Environment*, 37(5), 2002, 491-496.
- [5] British Standard Institution, composition, specification and conformity criteria for common cements, BS EN 197: Part 1, BSI, London, 2001.
- [6] British Standard Institution, Tests for general properties of aggregates, BS EN 932, BSI, London, 1999.
- [7] O. Ata, K. Olusola, O. Omojola, and E. Olanipekun.. A study of compressive strength characteristics of laterite/sand hollow blocks. *Civil Engineering Dimensions*, 9(1), 2007, 15-18.
- [8] Baiden,B.K and Asante,C.K.O.(2004) Effects of orientation and compaction methods of manufacture on strength properties of sandcrete blocks. *Construction and Building Materials*, 18(7): 717-725.
- [9] B. Tian, and M.D. Cohen. Does gypsum formation during sulfate attack on concrete lead to expansion? *Cement and Concrete Research*, 30(1), 2000, 117-123.
- [10] J.P. Skalny, I. Odler. and J. Marchand. (2002). *Sulfate Attack on Concrete*, Spon Press, New York, 2002.
- [11] M.J. Shannag and H.A. Shaia. Sulfate resistance of high-performance concrete. *Cement and Concrete Composites*, 25(3), 2003. 363 - 369.
- [12] M. Santhanam, M.D. Cohen and J. Olek Mechanism of sulfate attack: a fresh look Part 2: Proposed mechanisms. *Cement and Concrete Research*, Vol.33, 2003, 341-346.
- [13] T. Aye and C.T. Oguchi. Resistance of plain and blended cement mortars exposed to severe sulfate attacks. *Construction and Building Materials*, 25(6), 2011, 2988-2996.
- [14] O.S.B. Al-Amoud, Attack on plain and blended cements exposed to aggressive sulfate environments. *Cement and Concrete Composites*, 24(3), 2002, 305-316.
- [15] P.W. Brown and H.F.W. Taylor, The role of ettringite in external sulfate attack, In: J. Marchand and J. Skalny (eds) *Materials Science of Concrete Special Volume: Sulfate Attack Mechanism*, *The American Ceramic Society*, Westerville, OH, 1999, 73-98.
- [16] M.D.A. Thomas, R.F. Bleszynsk and C.E. Scott., Sulphate attack in marine environment; In: J. Marchand and J. Skalny (eds) *Materials Science of Concrete Special Volume: Sulfate Attack Mechanism*, *The American Ceramic Society*, Westerville, OH, 1999, 301-313.
- [17] A.M. Neville (1995). *Properties of Concrete*. Addison Wesley Longman Limited, England, 1995.

Design and Analysis of Compact UWB Bandpass Filter with Wide Passband Using Defected Ground Structure

Yashika Saini¹, Mithilesh Kumar²

^{1,2}Electronics Department, University College of Engineering, Rajasthan Technical University, Kota, India

ABSTRACT : A compact ultra-wideband (UWB) bandpass filter (BPF) with wide passband using defected ground structure (DGS) is proposed. The proposed UWB filter is constructed by cascading a high pass filter (HPF) and a lowpass filter (LPF). HPF with short-circuited stubs is used to realize the lower stopband and a LPF is used to attenuate the upper stopband. In order to make the filter size compact, DGS technology is incorporated in the filter design, with this technique the size of filter becomes extremely compact compared with the other UWB bandpass filters in different published papers. In designing the filter integrated with DGS, four rectangular shaped DGS were etched on the ground plane. Furthermore, the bandwidth is enhanced from the original UWB filter, by varying the widths of the rectangular shaped DGS in the ground plane. The BPF is designed with the desired frequency band of 3.1GHz-10.6GHz and a flat group delay across the pass-band. The occupied area of the proposed filter is 22.4mm × 12mm, both simulated and experimental results are provided with good agreement.

Keywords - Band pass filter (BPF); Defected ground structure (DGS); High pass filter (HPF); Low pass filter (LPF); Ultra Wide band (UWB).

I. INTRODUCTION

In 2002, the Federal Communication Commission (FCC) has authorized the unlicensed band 3.1 GHz to 10.6 GHz for commercial communication purposes [1]. UWB BPFs, as one of the essential components of the UWB systems, have gained much attention in recent years. In concerning to the development of UWB filter especially bandpass filter, some problem which often arises is that parameters of filter are unsatisfied for some UWB application. Hence, the physical dimension is becoming crucial issues particularly for communication devices which have small size. Defected ground structure (DGS) is one of the new design techniques used to improve the quality of the system [2, 3]. DGS adds an extra degree of freedom in microwave circuit design and opens the door to a wide range of applications. A large number of reports on UWB BPF's have been published [4]-[10] to achieve UWB characteristics. In [4,5] UWB BPF's are designed using DGS, whereas, in [6]-[9] the cascaded low-pass/high-pass Filters are proposed. In [10] a compact microstrip UWB bandpass filter with triple-notched bands and wide upper stopband is proposed.

DGS is now widely used to enhance the performance of the filter. The various technologies of size reductions are used by the researchers such as photonic band gap structure (PBG), frequency selective surface (FSS) etc. Furthermore, DGS has extensively applied to the design of microwave circuits such as filters, couplers, circulators, amplifiers, power dividers, and so on [11]-[16]. The defected ground structures demonstrate advantages that include compactness, wide-band operation and competent and flexible usage of the ground plane structure for changing characteristics of microwave devices [17].

In this paper, we present a new compact UWB bandpass filter. The initial UWB BPF without DGS with overall size of 26.4mm × 16mm is stated. To make the size of the filter more compact, an attempt is carried out by applying DGS on the ground plane of the initial filter. The BPF is designed to have working bandwidth of 3.1GHz-10.6 GHz. In the design process, the performances of filter and its physical dimension are investigated to obtain the optimum design for realization. Hence, the filter parameters such as insertion loss, return loss, and working bandwidth will be used as indicators for the performance evaluation, after hardware realization and experimental characterization, the measured results are then compared to the design results for

verification and analysis. The organization of this paper is as follows. In section II, the design is briefly described. While fabricated and measured results are discussed in section III. Finally the work is concluded in section IV.

II. DESIGN DESCRIPTION OF UWB BPF

2.1. UWB bandpass filter without DGS

The structure of initial UWB bandpass filter is depicted in Figure 1. In this the optimum distributed HPF is embedded in the step impedance LPF with 9 reactive elements as reported in [8,9]. Here, the length of the filter is 13.8mm. This filter has overall size of 26.4mm × 16mm with thickness of 0.8mm and relative dielectric constant 2.2. The simulated insertion loss and return loss are depicted in Figure 2.

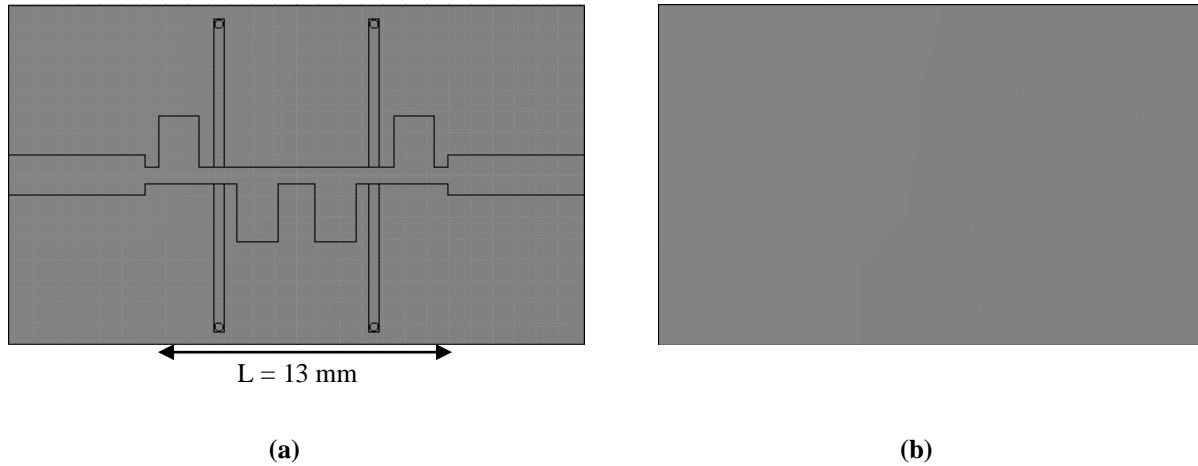


Figure 1. Schematic of initial UWB BPF (a) Top view, (b) Bottom view.

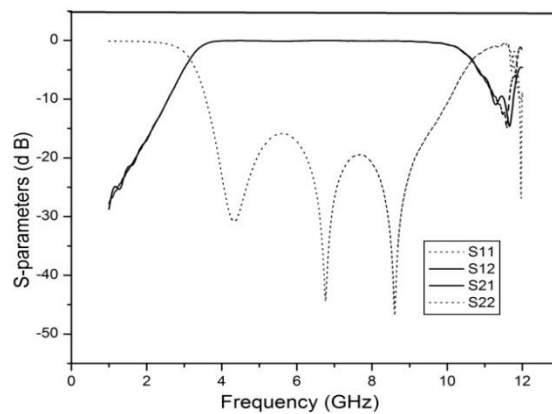


Figure 2. Simulated S-parameters of initial UWB BPF.

In the further section we will be designing UWB BPF using DGS technique. We will be observing that the size of the structure will become more compact.

2.2 DGS based UWB bandpass filter

Using the similar technique as applied for initial UWB microstrip BPF, a new compact UWB BPF is proposed, to make the size of the filter more compact DGS is incorporated in the filter design. Figure 3 shows the layout of the proposed UWB BPF with DGS. The length of the filter here is 8mm, which is extremely small than the initial filter and the overall size of the filter is 22.4mm × 12mm. Figure 3(a) shows the top view of the proposed UWB filter. The designed structure consists of two short circuited stubs of equal length acting as optimum distributed HPF embedded in step impedance LPF. Here for HPF the cutoff frequency is 3.1GHz and

for LPF the cutoff frequency is 10.6 GHz. The dimensions of the filter elements are as given in Table 1. The width of lines section for series inductor is 0.75mm and for shunt capacitor elements are 3.306mm and 2.6mm respectively. These widths correspond with the high impedance value (Z_{high}) of 82Ω for series inductor elements and with the low impedance value (Z_{low}) of 36Ω and 42Ω for shunt capacitor elements. The end of each stub is short-circuited to the ground plane through a wire. It is a vertical symmetry structure and the two stubs have the same length 5.15mm and width of 0.7mm. Figure 3(b) shows the bottom view of the proposed UWB filter. It shows that the proposed DGS is constructed of 4 rectangular slots etched on the ground plane symmetrically. The slots are cut beneath the step impedance LPF in the ground plane. The rectangular slots dimensions are $h_1 = 3.306\text{mm}$ and $h_2 = 2.6\text{mm}$. These 2 slots are symmetrical to the other 2 slots. Figure 4(a) depicts the simulated return loss and insertion loss of the filter. In the passband area, the minimum insertion loss is 0.104dB which occurs at 6.8GHz. The simulated group delay is depicted in Figure 4(b). The variation of group delay is below 0.3ns within the band. CST microwave studio software is used for the simulation of the designed structures.

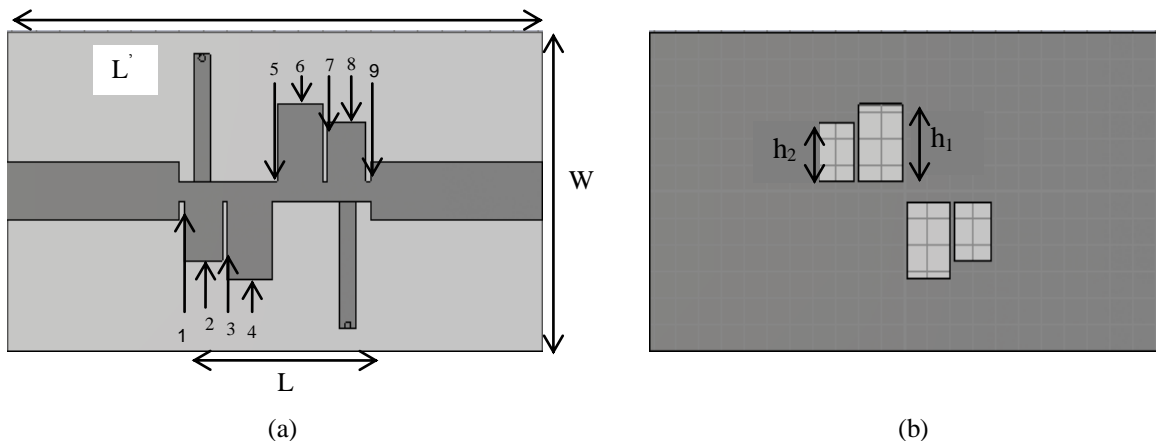


Figure 3. (a) Layout of Compact UWB filter (Top view), (b) Ground plane with DGS (Bottom view).

Table 1 Key dimensions of filter design

Elements	1	2	3	4	5	6	7	8	9	L	L'	W
Length of element Values(mm)	0.2	1.6	0.2	1.9	0.2	1.9	0.2	1.6	0.2	8	22.4	12

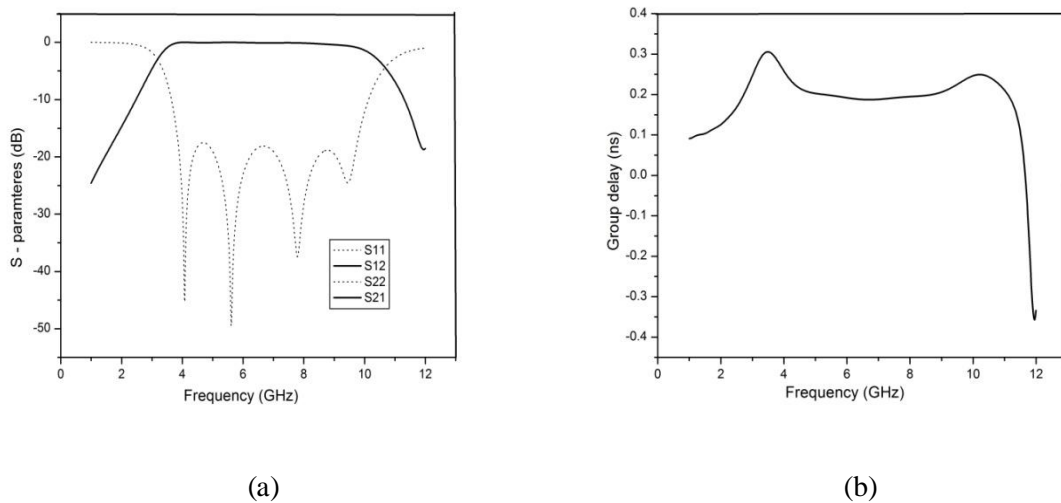


Figure 4. Simulated responses of the UWB filter (a) S-parameters, (b) Group delay.

2.3 Bandwidth enhancement by varying the height of the rectangular slots in ground plane

To demonstrate the bandwidth enhancement of the DGS-based UWB BPF is designed by locating 4 rectangular slots etched on the ground plane symmetrically. Figure 5 illustrates the utilization of DGS over the ground plane. The top view dimensions are same as stated in section 2.2 of this paper. The variations of the rectangular slots in the ground plane are as shown in Table 2.

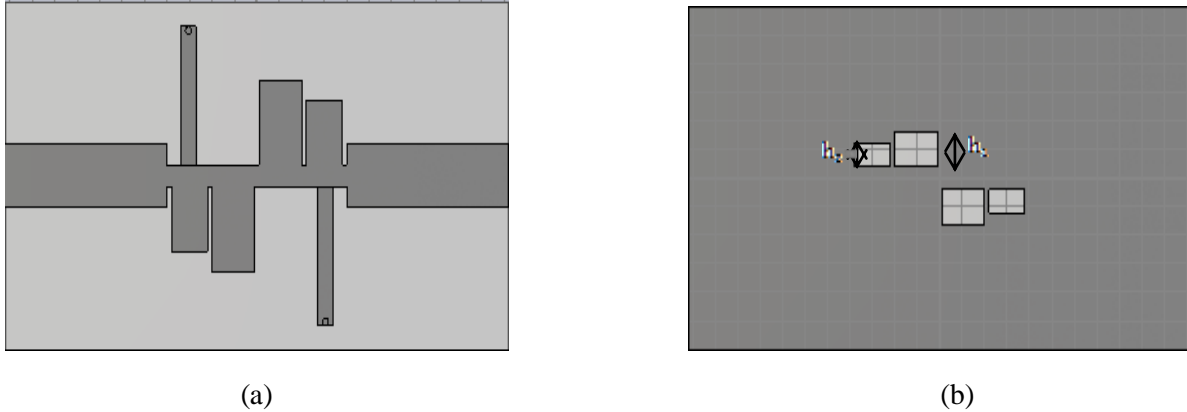


Figure 5. (a) Layout of Compact UWB filter (Top view), (b) Ground plane with DGS (Bottom view).

Table 2. Variation of bandwidth with height variation

S.No	Height variation h_1	Height variation h_2	Frequency range (GHz)	Bandwidth (GHz)
a	1.62mm	1.22mm	3.1~10.6	7.5
b	2.2mm	1.8mm	3.17~10.71	7.54
c	2.5mm	2.09mm	3.19~10.91	7.72
d	3.09mm	2.6mm	3.23~11.18	7.95

From Table 2, it should be noted that as the height of the rectangular DGS increases, the frequency shifts. Hence, the bandwidth is enhanced. The comparative S-parameters graphs at different height variation are depicted in Figure 6.

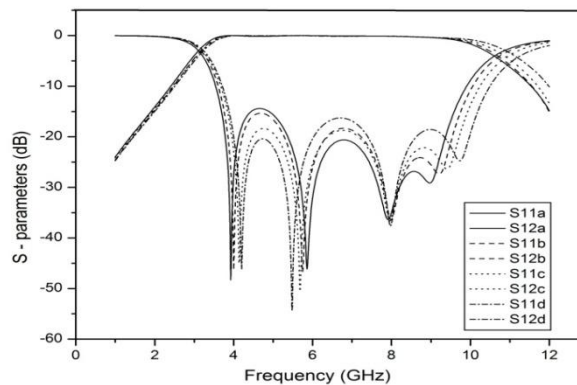
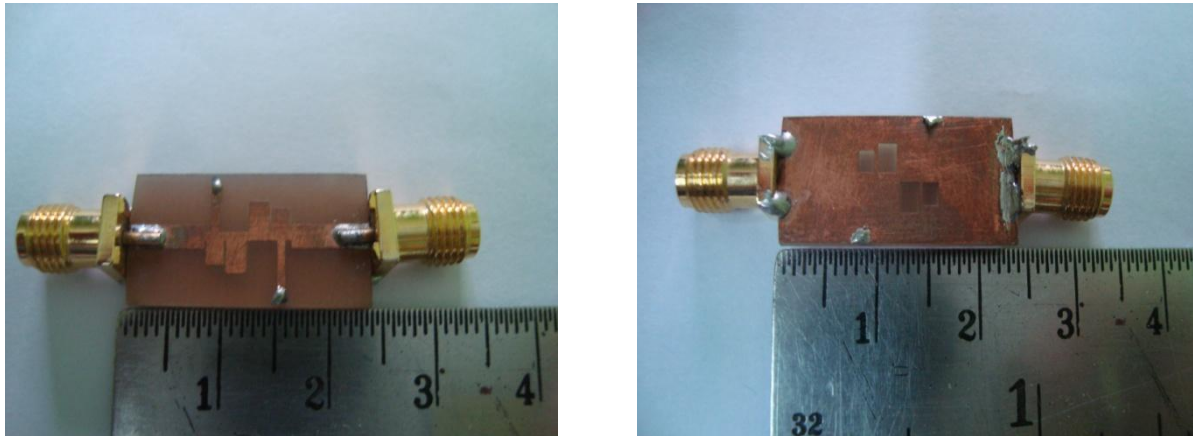


Figure 6. Comparative S-parameters graph at different height variation of h_1 and h_2 .

III. FABRICATION AND MEASURED RESULTS

Figure 7 shows the picture of fabricated filter. A compact ultra-wideband BPF using DGS is fabricated on FR-4 substrate with a relative dielectric constant of 4.05 with thickness of 1mm and loss tangent of the filter is 0.02. The overall size of the filter is 22.4mm × 12mm. The filter use microstrip line feed impedance of 50Ω with the width of each port 2.18mm. The results of the filter are measured on the vector network analyzer Rohde & Schwartz ZVB20 calibrated using SOLT method.

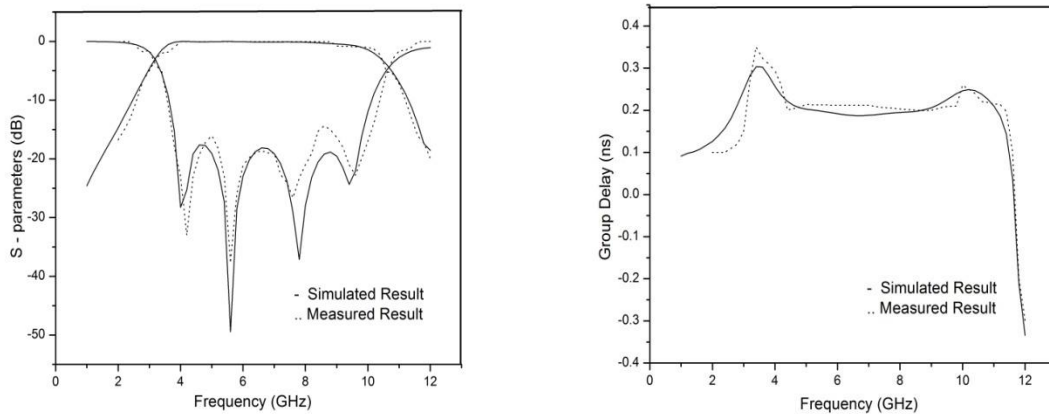
Figure 8 depicts the measured result of proposed UWB BPF with the simulated result is plotted together for comparison. Although there is slight difference in the return loss along passband area, in general the measured results have agreed very well with the simulated ones. The compact UWB bandpass filter has a bandwidth of 7.5 GHz with the desired frequency band of 3.1GHz-10.6GHz.



(a)

(b)

Figure 7. Fabricated picture of the compact UWB filter (a) Top view, (b) Bottom view.



(a)

(b)

Figure 8. Simulated and Measured responses of the compact UWB filter (a) S-parameters, (b) Group delay.

It is evident from figure 8(a) that 3dB start and stop frequencies of the filter are 3.1GHz and 10.6GHz, which implies that 3dB fractional bandwidth as given by following

$$B.W\% = \frac{F_H - F_L}{F_{centre}} = \frac{(10.6 - 3.1)}{6.85}$$

is 109%.

The measured group delay response is below 0.35 ns over the whole passband. This work is compared with the already reported UWB BPF [4][8][9] in Table 3. The size of the filter is extremely small in the current work than the reported filter.

Table 3. Comparison with other proposed UWB BPF's.

Parameters	[4]	[8]	[9]	This work
Passband (GHz)	3.1~10.6	3.1~10.6	2~12	3.1~10.6
Bandwidth (GHz)	7.5	7.5	10	7.5
length of filter (mm)	-	13.8	13.9	8
Return Loss (dB)	<11	<16	<9	<18
Insertion Loss (dB)	-	0.15	-	0.104
Group delay (ns)	-	Below 0.5	-	Below 0.35
Overall size	30mm×15mm	26.4mm×16mm	25mm×25mm	22.4mm×12mm

IV. CONCLUSION

A compact UWB BPF with wide passband using defected ground structure has been designed. A filter without DGS is first designed acting as reference, by comparing reference filter with DGS filter, it shows that DGS do gives beneficial results and the size becomes compact. Furthermore, the bandwidth enhancement of UWB BPF has been investigated by varying the defected rectangular slots on the ground plane surface. Good agreement between simulation and measurement results validates the introduced design method. With the advantages of excellent performance and compact size, the proposed filter is useful in UWB systems.

REFERENCES

- [1] "Revision of part 15 of the Commission's rules regarding ultra-wideband transmission systems," FCC, Washington, DC, Tech. Rep, ET-Docket 98-153, FCC02-48, adopted in Feb. 2002.
- [2] Oraizi, H. and M. S. Esfahlan, "Miniaturization of Wilkinson power dividers by using defected ground structures," *Progress In Electromagnetics Research Letters*, Vol. 4, 113- 120, 2008.
- [3] Wu, B., B. Li, T. Su, and C. H. Liang, "Study on transmission characteristic of split ring resonator defected ground structure," *Progress In Electromagnetics Research*, Vol. 50, 710-714, 2006.
- [4] Shobeyri, M. and M.-H. Vadjed-Samiei, "Compact ultra-wideband bandpass Filter with defected ground structure," *Progress In Electromagnetics Research Letters*, Vol. 4, 25-31, 2008.
- [5] Naghshvarian-Jahromi, M. and M. Tayarani, "Miniature planar UWB bandpass Filters with circular slots in ground," *Progress In Electromagnetics Research Letters*, Vol. 3, 87-93, 2008.
- [6] Comez-Garcia, R. and J.-I. Alonso, "Systematic method for the exact synthesis of ultrawideband Filtering responses using high-pass and low-pass sections," *IEEE Trans. On Microw. Theory and Tech.*, Vol. 54, No. 10, 3751-3764, 2006.
- [7] Hao, Z.-C. and J.-S. Hong, "UWB bandpass Filter using cascaded miniature high-pass and low-pass Filters with multilayer liquid crystal polymer technology," *IEEE Trans. on Microw. Theory and Tech.*, Vol. 58, No. 4, 941-948, 2010.
- [8] Yashika Saini, Mithilesh Kumar, "Ultra-wideband Bandpass filter using short circuited stubs," *International Journal of Engineering Research and Technology*, Vol. 3 (01), ISSN 2278 -0181, January 2014.
- [9] Achmad Munir, Ivan Pradibta, Mohammad Ridwan Effendi, "Microstrip based ultrawideband composite BPF with short circuited stubs," in *IEEE Electrical Engineering/Electronics Computer, Telecommunications And Information Technology (ECTI-CON)*, 2013.
- [10] Huaxia Peng, Junding Zhao and Bing Wang, "Compact Microstrip UWB Bandpass Filter with Triple-Notched Bands and Wide Upper Stopband," *Progress In Electromagnetics Research Letters*, Vol. 144, 185-191, 2014.
- [11] D. Ahn, J. S. Park, C. S. Kim, Y. Kim, Y. Qian, and T. Itoh, "A design of the low-pass filter using the novel microstrip defected ground structure," *IEEE Trans. Microw. Theory Tech.*, vol. 49, no. 1, pp. 86-93, Jan. 2001.
- [12] J. S. Lim, S.W. Lee, C. S. Kim, J. S. Park, D. Ahn, and S. Nam, "A 4:1 unequal Wilkinson power divider," *IEEE Microw. Wireless Compon. Lett.*, vol. 11, no. 3, pp. 124-126, Mar. 2001.
- [13] J. S. Lim, J. S. Park, Y. T. Lee, D. Ahn, and S. Nam, "Application of defected ground structure in reducing the size of amplifiers," *IEEE Microw. Wireless Compon. Lett.*, vol. 12, no. 7, pp. 261-263, Jul. 2002.
- [14] J. S. Lim, C. S. Kim, Y. T. Lee, D. Ahn, and S. Nam, "A spiral-shaped defected ground structure for coplanar waveguide," *IEEE Microw. Guided Wave Lett.*, vol. 12, no. 9, pp. 330-332, Sep. 2002.
- [15] Y. T. Lee, J. S. Lim, S. Kim, J. Lee, S. Nam, K. S. Seo, and D. Ahn, "Application of CPW based spiral-shaped defected ground structure to the reduction of phase noise in V - band MMIC oscillator," *IEEE MTTs Int. Microwave Symp. Dig.*, vol. 3, pp. 2253-2256, Jun. 2003.
- [16] Han-Jan, C., H. Tsung-Hui, C. Chin-Sheng, "A novel cross-shape DGS applied to design ultra-wide stopband low-pass filters", *IEEE Microwave and Wireless Components Letters*, vol. 16, no. 5, pp. 252-254, 2006.
- [17] X.-H. W. a. B.-Z. Wang, "Compact Broadband Dual-Band Bandpass Filters using Slotted Ground Structures," *Progress In Electromagnetics Research*, vol. 82, pp. 151-166, 2008.

Laboratory and Field Performance of stabilized soft subgrade

SATISH SAJJA¹, V K CHAKRAVARTHI²

¹ Corresponding Author, PG Student, Department of Civil Engineering, GMR Institute of Technology, Rajam, A.P, India

² Sr Associate Professor, Department of Civil Engineering, GMR Institute of Technology, Rajam, A.P, India

Abstract: Usually the service life of pavement on weaker clayey subgrade is affected due to their high plasticity and compressibility behaviour. These soils possess low strength, CBR value and have high affinity to moisture. Hence seasonal changes affect properties of these soils adversely. Stabilization techniques using waste materials are listed in literature for improving properties of these types of soft subgrades. This paper discusses the performance of stabilized soft clayey soil for suitability as subgrade using two types of admixtures Robo sand and fly ash. Dynamic cone penetration test and CBR tests are carried out in lab and field on composite soil with varying admixture content and the results are presented. It is observed that there is a considerable improvement with admixture in both index & engineering properties. A reduction in plasticity and improvement in soaked CBR with admixture is observed. Results indicated a relatively high performance of robo sand admixture over fly ash.

Keywords: Clayey soil, CBR, stabilization, fly ash, robo sand.

I. INTRODUCTION

1.0 General

Transportation engineers often face problems in pavement due to soft subgrades. These soft subgrades have low density and high affinity towards moisture. Due to this the life of pavement will be affected. In general soft subgrades are identified by their insitu density and CBR value. One of the remedy as suggested previously is improving engineering properties using various techniques. Among all techniques stabilization technique is best suited for soft soils. Various researchers carried out studies using admixtures namely lime, cement and flyash etc. Laboratory experiments confirmed that strength and stability of clayey soils can be improved by adding various admixtures like lime, cement, flyash, kiln dust etc., the lime clayey soil mixture exhibits higher strength compare to clayey soil fly ash mixture [1]. The influence of fly ash on organic and inorganic clayey soils is different; strength improvement with varying percentage of fly ash for inorganic soils is high compared to organic soils [2]. Influence of waste sand on engineering properties on clayey soils varies with varying percentages and CBR value increased by 20% with the addition of 20% of waste sand [3]. The influence of sand on cohesive soil is significant and with addition of 15% of fine sand strength of soil is doubled [5]. The field performance of stabilized expansive soil with fly ash and density is maximum at 25% fly ash and workable in field [6]. Few complex situations with soft subgrade can be solved by providing stiffer aggregate layer over soft subgrade and the problem of mixing of subgrade with aggregate can be avoided with separator geotextile [7]. The lab performance may be different to that of field due to heterogeneous conditions. Inorder to understand the actual behaviour of subgrade, field tests are recommended. The field performance of marine clayey soil treated with lime, GBFS and geotextile - clay foundation soil bed has exhibited the justified load carrying capacity in wet season [4]. In few cases owing due to the difficulty in field set up the field CBR performance can be predicted indirectly from DCPT (Dynamic cone penetration test) data conducted in field and later can be correlated using equations [8].

1.1 Scope and objective of present study

The scope of present study is to suggest suitable stabilizing materials and evaluate the quantum of improvement. The main objective of the present study is to perform i) laboratory studies on stabilized soil, ii) field CBR test on the stabilized soft subgrade bed, iii) DCPT in field on stabilized bed, iv) comparison of results. The admixtures utilized for study are waste industrial materials. The details of tests and results obtained are presented in the subsequent sections.

II. EXPERIMENTAL STUDY

2.1 Materials used

During the experimental study tests are conducted using the following three types of materials. The material includes i) local soil predominantly clayey in nature, ii) Artificial sand (robo sand) a product obtained from stone crushers, iii) flyash a product obtained from Thermal power plant NTPC. The robo sand is a well graded soil containing predominantly sand size particles. The fly ash is class C type containing predominantly silt sized particles with no plasticity. Mechanical stabilization is followed by mixing proportions of robo sand and fly ash to soil. The details of proportions adopted are described in the subsequent headings.

2.2 Preparation of soil admixture mix, details of tests and parameters studied

The soil admixture mix is prepared by mixing the soil with admixture of desirable proportion by weight of soil. For a given admixture content, admixture is mixed with soil and required weight of soil mix is taken from the mixture prepared. For all the mix proportions dry weight of soil is taken as basis. Using the prepared mix, laboratory and field tests are conducted. Laboratory tests include index properties, gradation, proctor compaction Tests and CBR. Field tests include, field CBR and dynamic cone penetration test. The tests were carried out in accordance of Indian Standard code of practice. The following parameters are determined in experimental study on stabilized soil;

- Atterberg limits
- Grain size distribution
- Optimum moisture content and maximum dry density
- CBR(soaked) in lab and field
- Dynamic cone penetration index.

CBR test is conducted on sample after soaking for 96 hours. The sample is prepared in mould maintaining density and moisture content as obtained during compaction test. The moisture content and density after soaking is noted for preparation of sample in field later. The additives are varied from 0 to 50% by weight of soil. Since the testing program involves different admixtures in varying proportions, for indicating purpose, symbols are adopted for admixtures and for different combination of admixture and soil. Table-1 describes the ranges of admixture and nomenclature adopted for describing various samples with admixture.

2.3 Subgrade preparation for field CBR test

Field CBR is conducted on few prepared subgrade samples with additives. The tests are conducted on subgrade prepared by filling with admixture soils in pits. Initially pits of size 0.5m x 0.5m x 0.5m are excavated. The pits are filled and compacted with prepared soil-additive mixture. For uniformity density and moisture content of lab CBR (soaked) test samples is maintained for filling. Field density tests are carried out for ensuring required conditions. For application of load, reaction loading method is adopted. Observations are recorded for load and corresponding deformation of plunger. The field CBR is calculated from the load-penetration data. The tests are conducted on different stabilized subgrade fills in different test pits. The layout of test pits, schematic diagram of testing and field test set up are shown in fig I, II and III.

2.4 Dynamic Cone Penetrometer Test

DCPT test is carried on the same subgrade prepared for Field CBR test (section 2.3 above). The test is conducted by driving a cone of 60° apex angle and 20mm diameter by dropping weight of 8kg from a height of 640mm. The penetration with blows is recorded. A graph is drawn between penetration and blows. The slope of graph is indicated as DCPI (mm/ blow). The test trails are conducted at few locations over the prepared subgrade and average of DCPI is reported. Test set up for DCPT and testing is shown in the fig IV.

III. PRESENTATION OF LABORATORY RESULTS AND DISCUSSIONS

3.0 Tests are carried out on soil with varying admixtures namely, index and engineering properties. The results of lab tests are presented from section 3.1 to 3.4 in tables II to IV and from fig. V to VIII.

3.1 Presentation of Index properties of parent soil

The index properties of samples are presented in table-II. It is implied from the CBR value that the soil is very soft and needs improvement. From the index properties the soil is grouped as CI. The results on admixture robo sand indicate the soil is well graded sand and the fly ash is non-plastic.

3.2 Variation of index properties of stabilized soil

The variation of index properties with admixture is presented in table-III. It is noted that with the addition of admixtures the plasticity index has decreased. This is an indication of improvement in soil properties. The result trend indicates effect of fly ash is more than that of robo sand. The net decrease in PI is due to reduction of liquid limit in the case of Robo sand whereas the same due to increase of plastic limit in the case of flies ash. This explains that the soil is becoming stiffer due to admixtures. The consistency indices showed a decrease of liquid limit and Plasticity index from 48.32 to 41.45, 23.3 to 18.59 and 48.32 to 37.6, 23.3 to 6.49 respectively using robo sand and fly ash. With the increase in robo sand affinity to water decreased due to which liquid limit is decreased. The same trend is observed with fly ash also. However as expected the amount of decrease is more with fly ash than robo sand. The reduction is negligible from 40 to 50% for both the admixtures.

3.3 Presentation of results of compaction test

The compaction characteristics of soil with admixture soil are presented as detailed below. The compaction curve for various samples is presented in fig. V. The effect of robo sand and fly ash in on maximum dry density (MDD) and optimum moisture content (OMC) is plotted in the figure VI.

From Fig V it is observed that the density affected due to decrease of robosand content. As expected low density of fly ash than robo sand has affected the density of mixture. The reason of decrease in density can be substantiated with the trend shown for OMC i.e, increase with fly ash. The addition of fly ash adds more fines resulting increase in OMC. The density trend showed a peak of 18.31 kN/ cu.m for the sample SRSFS41 containing 40% sand and 10% fly ash. The performance of stabilized mixture is due to the reduction of void ratio with increasing robo sand for SRFS41. This is evident from table IV.

3.4 Presentation of laboratory CBR results for stabilized soil

The laboratory results of CBR test (soaked) are presented and fig. VII. The variation of CBR is similar to that of density. From table VI it is observed that peak CBR is obtained for SRSFS41 followed by SRS4. SRSFS41 which contains 40% sand and 10% flyash and SRS4, which, contains 40% sand alone. The improvement in CBR with robo sand and fly ash is presented in Fig. VIII. It is evident that the influence of sand is higher than fly ash at high contents. The trend in CBR increase shows that the variation is gradual for robo sand. However with fly ash the variation is gradual till 40% but sudden increase from 40% to 50%. It may be due to filling of voids in coarser robo sand and cementations properties in fly ash.

IV. PRESENTATION OF IN-SITU RESULTS AND DISCUSSIONS

4.0 In situ tests namely field CBR and Dynamic cone penetration tests are conducted on stabilized subgrade fill. The tests are conducted on selected fills for comparison. Field CBR are conducted on four types of samples S, SRS4, SFS3 and SRFS41 The results of field tests are presented in section 4.1 to 4.2 and in fig. IX & X and tables V , VI & VII.

4.1 Presentation of field moisture and density

As discussed in 2.3 above, the field testing is carried out maintaining moisture and density corresponding to four days soaking. The field density tests are conducted after filling and are presented in table V. The data shows that the difference in moisture content is less than 2%. The same difference is obtained for density also. This shows that the fill prepared is identical to lab and can be compared for performance. Field CBR test results and lab CBR results are presented in table VI.

It is observed that field CBR is higher than lab for all samples. The heterogeneous surrounding soil has influence on the result. From Table-VI it is seen that for SRS4 strength in laboratory was improved by 1.9 times and for SFS3 increment was 1.36 times. This is due to when robo sand is added the voids in coarser particles of robo sand were occupied by clayey particles and maximum dry density increased contributing to higher strength. When fly ash is added to clayey soil, water reacts with pozzolans SiO_2 , Al_2O_3 present in fly ash and attains cementaceous properties contributing to strength. When robo sand and fly ash are added in combination the maximum CBR is obtained for SRSFS41 combination and the increment is 2.34 times the natural soil CBR.

3.2 Dynamic Cone Penetrometer Test Results

DCP tests were conducted on the same subgrade indicated with S, SRS4, SFS3 and SRFS41. The DCPT graphs were shown in fig. IX, it is observed that the trend is almost same for all the subgrade types. The obtained DCP index is reported in table VII Higher DCPI indicates poor subgrade and vice versa. The DCPI results obtained are consistent with maximum density and CBR.

4.2.1 Variation of DCPI with Field CBR

The variation of the DCPI with field CBR is presented in fig. X, DCPI decreased with increasing CBR values for different compacted subgrade samples. CBR and DCPI both represent the penetration resistance. Higher CBR values represents the higher resistance to penetration and the higher value of DCPI characterizes the poor sub grade and vice versa. From the fig. X it can be seen that DCPI results are consistent with soaked CBR. With CBR increase from 2.06% to 4.54% the DCPI is found to be decreasing from 25.02 to 18.55 mm/blow respectively.

The variation of DCPI is related to CBR as

$$\log(\text{DCPI}) = -2.5945\log(\text{CBR}) + \log(30.144) \dots (1)$$

Simplifying

$$\log(\text{CBR}) = 0.5701 - 0.385\log(\text{DCPI}) \dots (2)$$

V. CONCLUSIONS

The following conclusions are drawn based on the field studies carried out comparing with the laboratory Investigations:

- i. The addition of the admixtures shall contribute in reducing plasticity and improve gradation.
- ii. In general both the admixtures have influence on compaction characteristics. However the influence of Robo sand is more that of fly ash. The max density is obtained at 40%RS+10%FS.
- iii. From the results on few of the field CBR tests conducted on natural soil and treated soil, it is concluded that, in-situ conditions have influence when compared with intact specimens. The field results obtained is higher than that of lab. However the stress-strain response is similar in both the type of tests.
- iv. From Laboratory and field CBR results it can be concluded that S+40%RS+10%FS can be considered as optimum mix.
- v. DCPI test results are in consistence with field CBR. The DCPI can be used to determine approximate CBR and based on the few tests a relation can be drawn as $\log(\text{CBR}) = 0.5701 - 0.385\log(\text{DCPI})$.

REFERENCES

- [1] Athanasopoulou A, *Addition of Lime and Fly Ash to Improve Highway Subgrade Soils*, *Journal of Materials in Civil Engineering*, Vol. 26, No. 4, April 1, 2014. ASCE, ISSN 0899-1561/2014/4-773-775.
- [2] Tuncer B. Edil, Hector A. Acosta and Craig H. Benson, *Stabilizing Soft Fine-Grained Soils with Fly Ash* *Journal of Materials in Civil Engineering*, Vol. 18, No. 2, April 1, 2006. ASCE, ISSN 0899-1561/2006/2-283-294.
- [3] Babu Shemy S., Nair SM., Rohit P B., Soman N., Kumar M. Mohan., Hari Gadha, (2010), *Improvement of Clayey Sub Grade Using Waste Sand from English Indian Clay Limited*, *Indian Geotechnical Conference – 2010, GEOTrendz, December 16–18, 2010 IGS Mumbai Chapter & IIT Bombay*.
- [4] Koteswara Rao.D., Prasada Raju.G.V.R., Jyothi Babu.K.,(2011), *Field Studies on the Marine Clay Foundation Soil Beds Treated with Lime, GBFS and Reinforcement Technique*, *International Journal of Engineering Science and Technology (IJEST)*, ISSN : 0975-5462 Vol. 3 No. 4 Apr 2011, PP-3105-3112.
- [5] Tapas Kumar.R.,(2013), *Influence of sand on strength characteristics of cohesive Soil for using as Subgrade of road*, *2nd Conference of Transportation Research Group of India (2nd CTRG)*, *Procedia - Social and Behavioral Sciences* 104 (2013) 218 – 224.
- [6] Bhuvaneshwari.S., Robinson.R.G., Gandhi.S.R., *Stabilization of Expansive Soils using Flyash*, *Fly Ash Utilization Programme (FAUP)*, *TIFAC, DST, New Delhi – 110016*. PP VIII 5.1 – VIII 5.10.
- [7] Chakravarthi,V.K, Jyotsna.B, 2013, *Efficacy of overlying coarse aggregate and Geosynthetic separator on CBR value for soft subgrade of varying plasticity - a lab study” IJRET: International Journal of Research in Engineering and Technology*, Vol.2 , Issue 12, December 2013, pp: 749-755, eISSN: 2319-1163 | pISSN: 2321-7308.
- [8] Deepika Ch, Chakravarthi V K, 2012 *Evaluation of Properties of Soil Subgrade Using Dynamic Cone Penetration Index – A Case Study*, *International Journal of Engineering Research and Development e-ISSN: 2278-067X, p-ISSN: 2278-800X, Volume 4, Issue 4 (October 2012), PP. 07-15.*

BIOGRAPHIES



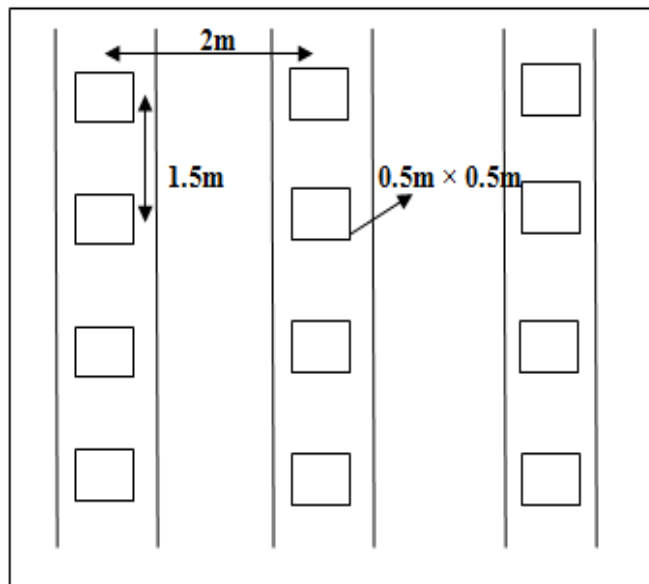
Satish Sajja, presently pursuing M.Tech in Transportation engineering in Department of Civil Engineering, GMR Institute of Technology, Rajam, AP, India. He had one year academic experience and two and half years of industry experience.



Mr. V.K. Chakravarthi is currently associated as Senoir Associate Professor in Department of Civil Engineering at GMR Institute of Technology, Rajam, A.P, India. He has a total 19 years of experience in Industrial projects and academics.



(a)



(b)

Figure I a) Marking of Test pits b) Layout of Testing area

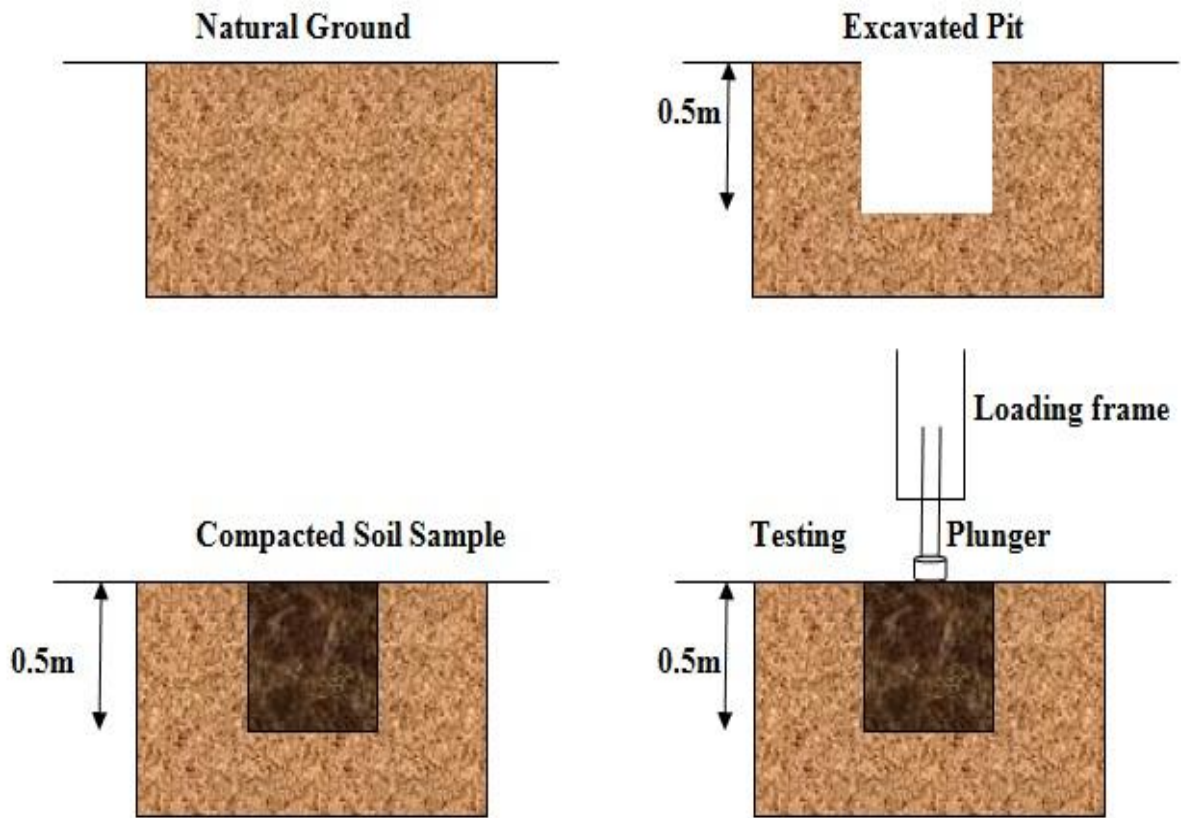


Figure II Schematic line diagram of Field CBR test



Figure III Author's performing Field CBR Test

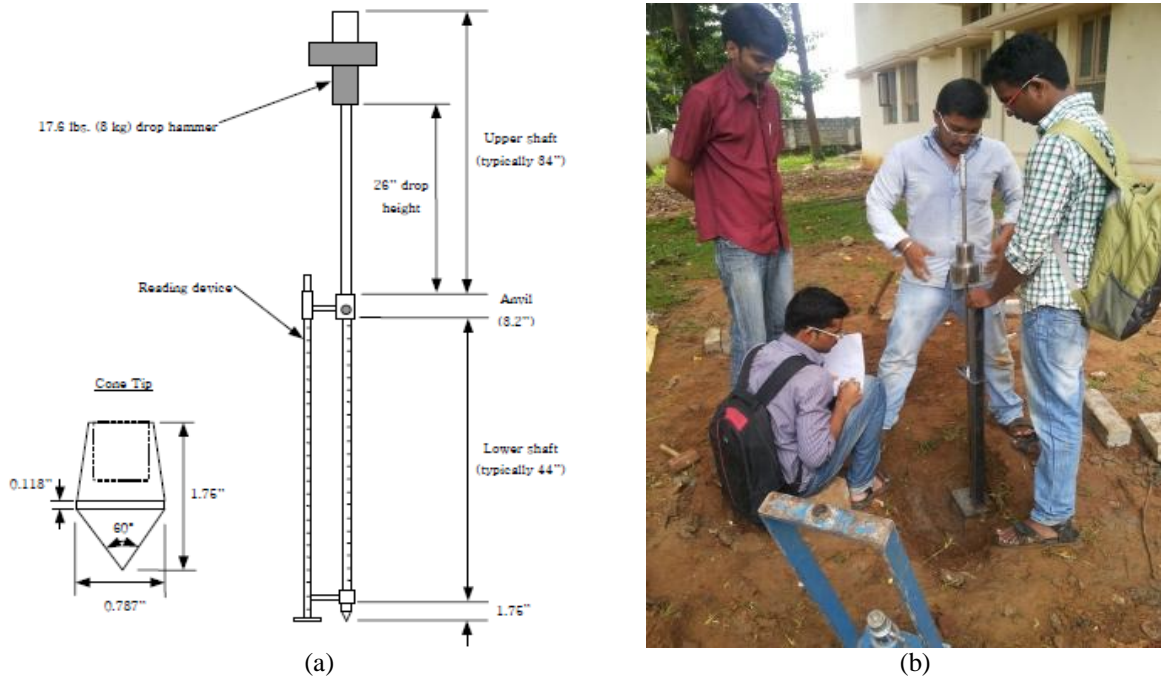


Figure IV a) DCPT test arrangement b) Author performing DCPT

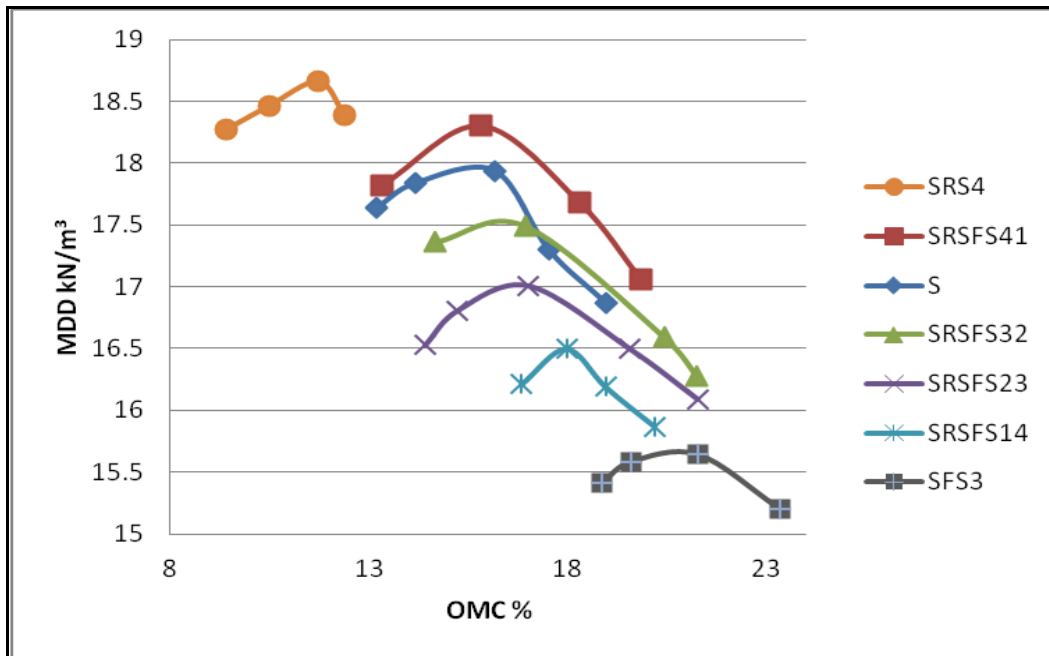


Figure V Compaction characteristics of soil –sand- fly ash mixtures

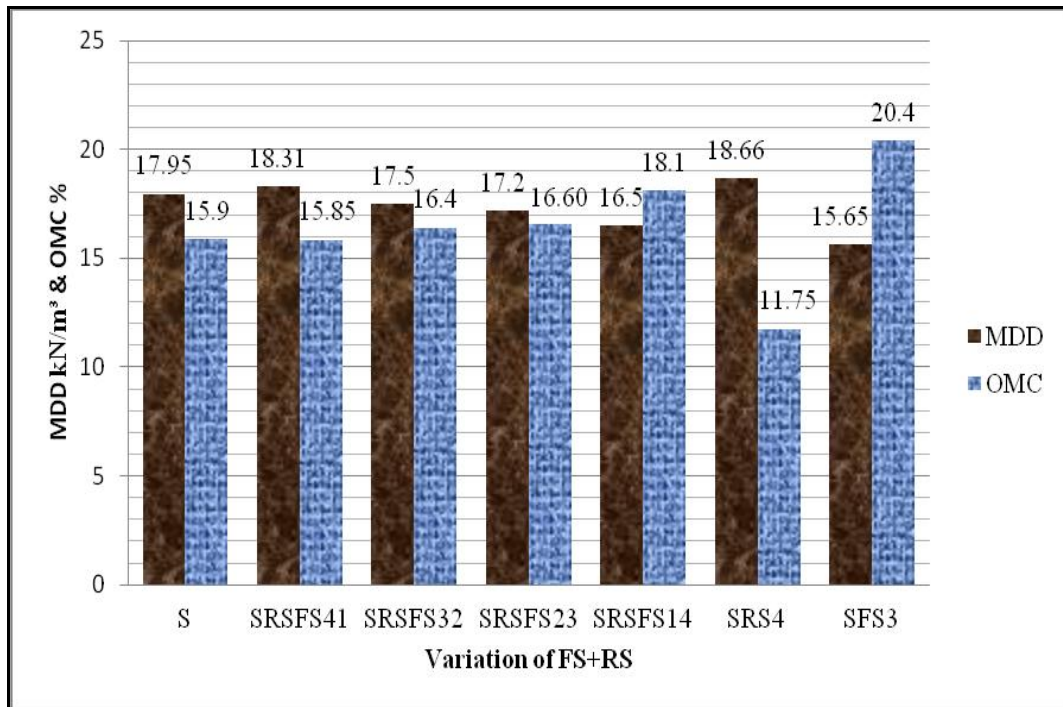


Figure VI Variation of MDD and OMC of soil-robot sand -fly ash mixtures

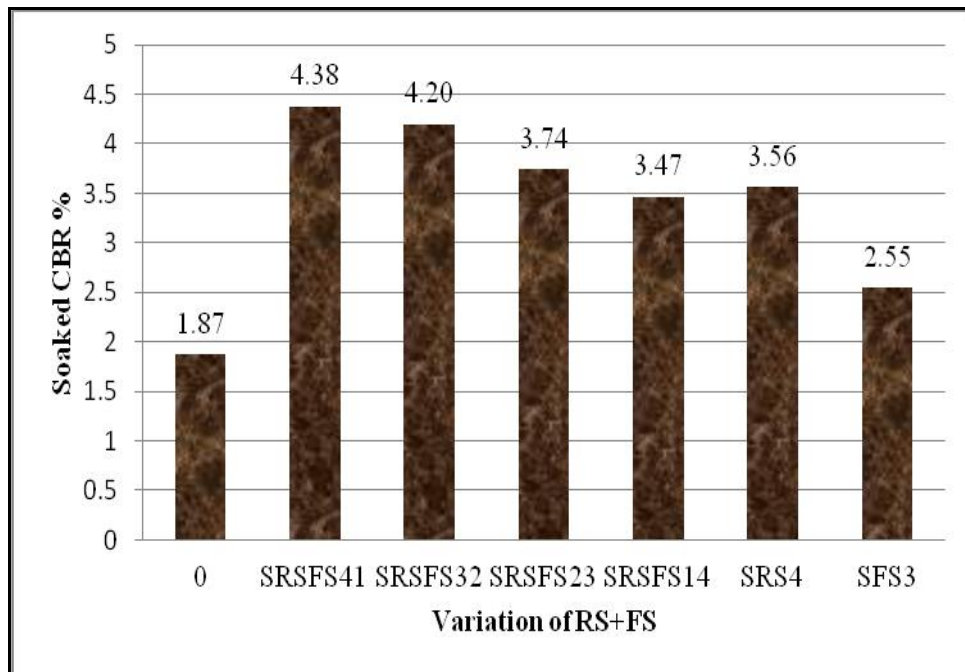


Figure VII Variation of CBR of soil mixed with varying percentages of robo sand & fly ash

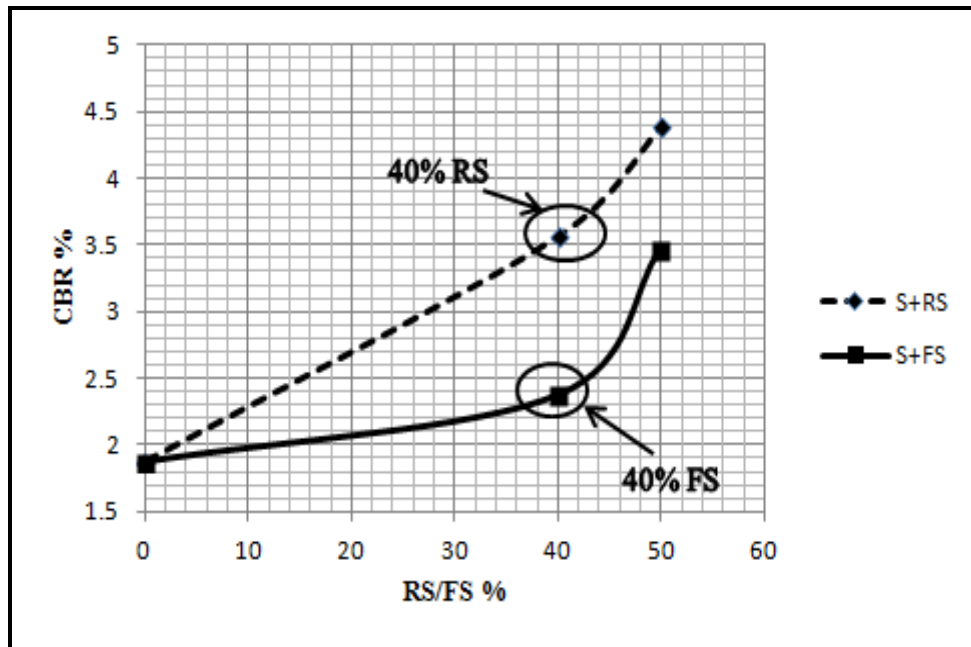


Figure VIII Comparison of CBR of soil mixed with varying percentages of robo sand & fly ash

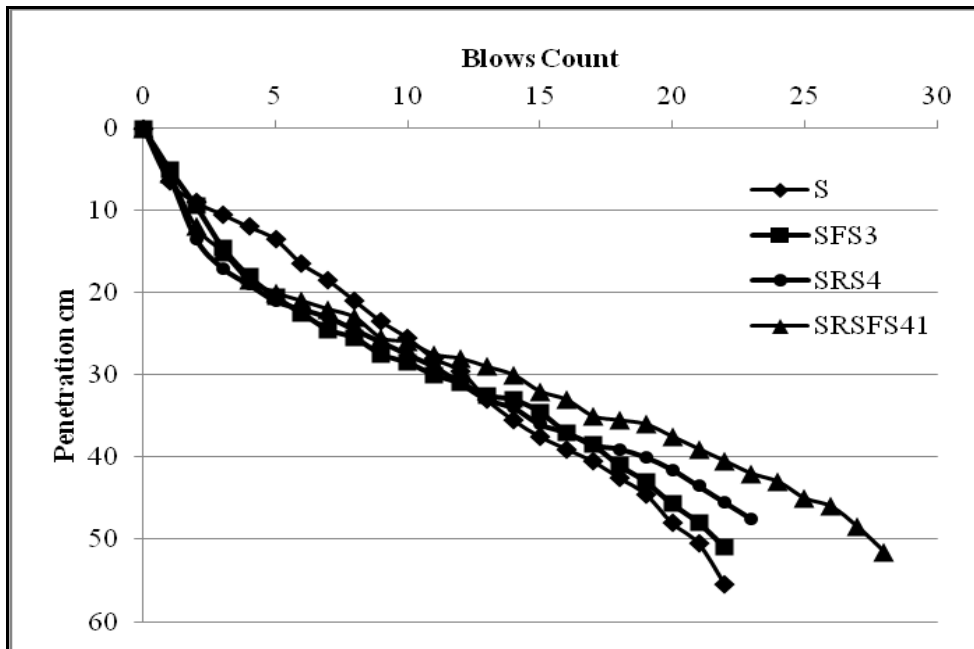


Fig IX Graph of DCP Test on various subgrades

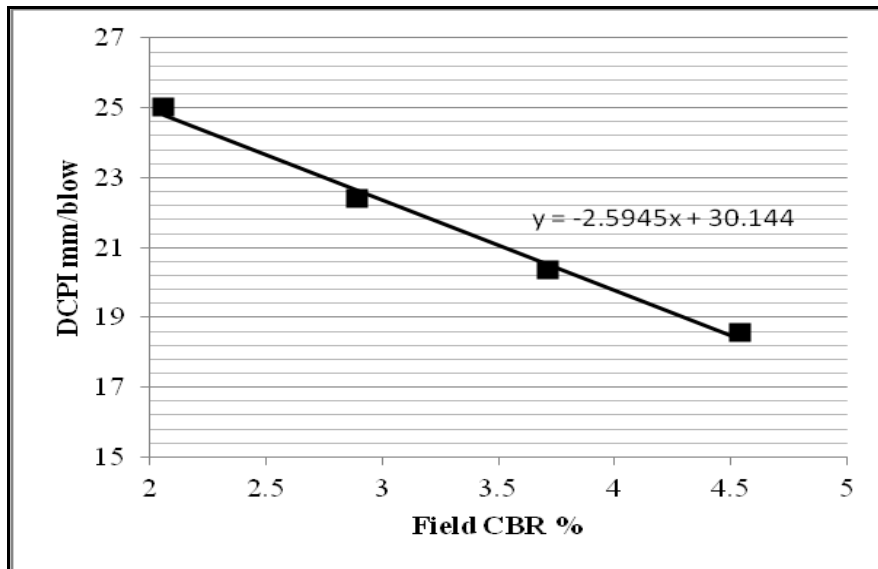


Figure X Variation of DCPI with CBR

Table I Ranges of admixtures and nomenclature adopted

Proportions of sample, admixture	Symbol
Soil	S
Robo Sand	RS
Fly ash	FS
Soil+40%Robo Sand+10%Fly ash	SRSFS41
Soil+30%Robo Sand+20%Fly ash	SRSFS32
Soil+20%Robo Sand+30%Fly ash	SRSFS23
Soil+10%Robo Sand+40%Fly ash	SRSFS14
Soil+40%Robo Sand	SRS4
Soil+30%Fly ash	SFS3

Table II Geotechnical properties of materials used

Property	Soil type	S	RS	FS
Specific Gravity		2.64	2.66	2.04
Liquid Limit, %		48.32	-	-
Plastic Limit, %		25.02	-	-
Plasticity Index, %		23.3	-	-
Fines(%)		65.24	0.00	71.94
Uniformity Coefficient, C_u		-	6.00	-
Coefficient of Curvature, C_c		-	1.127	-
USCS Classification		CI	SW	NP silt
MDD, kN/m^3		17.95	16.09	10.4
OMC, %		15.9	7.8	22.1
CBR (Soaked) (%)		1.87	-	-

Table III Consistency limits with varying percentages of robo sand and fly ash

RS %	LL %	PL %	PI %	FS%	LL%	PL %	PI %
0	48.32	25.02	23.3	0	48.32	25.02	23.3
10	46.00	24.54	21.46	10	46.20	26.71	19.49
20	44.30	24.05	20.25	20	44.40	28.28	16.12
30	43.40	23.71	19.69	30	40.60	30.11	10.49
40	42.10	23.07	19.03	40	39.00	31.18	7.82
50	41.45	22.86	18.59	50	37.60	31.11	6.49

Table IV Void Ratio for different soil- robosand -fly ash mixtures.

Soil	Density kN/m ³	void ratio
S	17.95	0.4708
SRSFS41	18.31	0.4134
SRSFS32	17.5	0.4434
SRSFS23	17.2	0.4326
SRSFS14	16.5	0.4558

Table V Presentation of Laboratory, Field Bulk Density and moisture content

Soil	Lab CBR bulk Density kN/m ³	Field CBR Bulk Density kN/m ³	Moisture content after 4days soaking in Lab %	Moisture content in field %
S	20.66	20.69	21.54	21.16
SRS4	20.77	20.83	17.93	17.29
SFS3	18.84	18.55	20.46	19.17
SRSFS41	21.05	20.91	18.67	17.73

Table VI Presentation Laboratory and Field CBR results

Test Pit No.	Soil	Lab CBR(%)	Field CBR (%)
1	S	1.87	2.06
2	SRS4	3.56	3.71
3	SFS3	2.55	2.89
4	SRSFS41	4.38	4.54

Table VII Presentation of DCPI vs. Field CBR

Soil type	DCPI (mm / blow)	Field CBR (%)
S	25.02	2.06
SRS4	20.37	3.71
SFS3	22.39	2.89
SRSFS41	18.55	4.54

Fast and Secure Initial Access Authentication Protocol for Wireless LANs

Sandhya K¹, Nagaraju Rayapati²

¹(CSE, Sree Vidynakethan Engineering College, India)

²(CSE, Sree Vidynakethan Engineering College, India)

ABSTRACT: Nowadays there is widespread use of WLAN enabled devices, so it is equally important to have efficient initial link setup mechanism. In this paper a fast access authentication process is implemented which is faster than current 802.11i. Through experiments, it is observed that the inefficiency of 802.11i is due to its design from the framework perspective which introduces too many messages. Due to more number of round-trip messages in 802.11i authentication delay is intolerable under some scenarios. To overcome this, an efficient initial access authentication protocol FLAP is proposed which introduces two round-trip messages with authentications and key distribution. Proposed FLAP protocol scheme is more secure than 4-way handshake protocol. Simulations are conducted using different scenarios like Authentication delay, Throughput, Packet Delivery Ratio (PDR), Packet Drops are measured for different scenarios and compared between the 802.11i and FLAP protocol. The results show that the FLAP is more advantageous when WLAN gets crowded.

Keywords - WLAN, Authentication delay, 802.11i, Throughput, PDR, Packet drops

I. INTRODUCTION

Wireless local area networks (WLAN) technology [1], [2] gaining its popularity continuously for its good mobility, high bandwidth, and important flexibility. The portable equipments that support WLAN increase greatly, such as smart phones, laptops, tablet computers, and so on. Users can easily access a variety of network applications through WLAN, for example, face book, twitter, e-mail, and online music and videos. However, security is a serious concern because the wireless medium is open for public access within a certain range.

The 802.11 Task Group proposed the Wired Equivalent Privacy (WEP) to provide secure data communications over wireless links. WEP used to encrypt the data stream and authenticate the wireless devices. However, significant deficiencies have been identified in both the encryption and the authentication mechanisms [3], [4]. To repair the problems in WEP, the Wi-Fi Alliance proposed an authentication mechanism based on EAP/802.1X/RADIUS[5], [6], [7] to replace the poor open system authentication and shared key authentication in WEP. The latest IEEE standard 802.11i [8] was ratified on June 24, 2004 as a solution to securing wireless links. The authentication process combines 802.1X authentication with key management procedures to generate a fresh pairwise key and/or group key, followed by data transmission sessions. Most of the security issues in the WLAN are solved by 802.11i.

However, with the rapid increase of the WLAN and its enabled mobile devices, new scenarios emerge that challenge the current WLAN standards, especially 802.11i. In a WLAN, every time the mobile device enters an Extended Service Set (ESS), it has to do an initial set-up to establish WLAN connectivity which generally includes the discovery and association of an Access Point (AP), along with 802.11i authentication and acquisition of an IP address. This works well when the number of new stations (STAs) in a given time period is small. However, when a large number of users simultaneously enter an ESS, an efficient mechanism that scales well is required to minimize the time STAs spend in the initial link setup, while maintaining a secure authentication. While the setup of the initial connectivity consumes a lot of time, consequently, mobile devices

cannot make fullest use of the WLAN and a lot of services are difficult to carry out, such as:

1. In rush hours, a large amount of passengers enter into a metro station or get off the train simultaneously, their WLAN-enabled terminals try to establish links with the WLAN to get network services.
2. Real-time services are offloaded from 3G to WLAN seamlessly. If the 3G and WLAN are not conducted by a same operator, the pre-authentication cannot be performed, and a fast initial authentication is required to establish a link with the WLAN efficiently.
3. Without a stop, a car or truck in the expressway can complete the payment or exchange the goods information through the WLAN when it passes by a toll station or a weighbridge station.
4. The express train provides network service to passengers through on-board APs, and in the backend the APs keeps the connection with the infrastructure networks along the trail through the beamed antenna using the 802.11.
5. When a user passes by a shop, his WLAN-enabled device can connect the WLAN of the shop and gets an electrical coupon without a stop; and the shop can identify the user and push the appropriate advertisements and electrical coupons.
6. An ambulance can upload vital patient information to the hospital, they are going to (or to any other specialists that need to be consulted) through the APs along the roadway while enroute.
7. All fleets attempt to keep track of all of their vehicles at all times. Widespread Wi-Fi hotspots along roads and throughout urban areas can be used by trucking fleets to quickly link to their home office to not only indicate where they are located, but at the same time to download necessary updates to the driver.

The IEEE 802.11ai is established to reduce the initial link setup establishment time. The IEEE 802.11i specified authentication process is a bulky time consuming for initial link setup. To explore the 802.11i authentication efficiency, numerous experiments are conducted and observed that 802.11i will become inefficient when WLAN is crowded. Time taken to perform DHCP and channel scan process will also make the initial link setup time even longer. Therefore, 802.11i cannot meet the requirements and it became an obstacle by preventing users from making use of WLAN.

The main reason leading to 802.11i inefficiency is due to its framework perspective which introduces too many messages between the terminals and network. Eleven round-trip messages are designed for EAP-TLS and practically it needs 13 round-trips due to fragmentation in the MAC layer.

To improve the efficiency, an efficient authentication method is implemented which introduces only two round-trip messages to make the authentications and key distributions between mobile Station (STA), Access Point (AP) and Authentication Server (AS). The contributions are as follows:

1. A fast WLAN initial access authentication method FLAP is proposed, and we formally prove that it is more secure than the four-way handshake protocol.
2. We implement FLAP and the measured authentication delay is just 5.3 percent of EAP-TLS. Based on the implementation, we ran thorough simulations with different background traffic and STA numbers. The results indicate that the advantage of our scheme is more salient than EAP-TLS in the crowded network environment. Furthermore, based on the experimental result, we get an authentication delay estimation method for EAP-TLS and FLAP. To the best of our knowledge, we are the first to investigate the authentication delay under different background traffic and STA numbers.
3. From the real-world implementation perspective, we give a simple and practical method which makes the proposal compatible with 802.11i.

Some performance metrics are calculated to measure the performance of a network. Network throughput shows the number of packets delivered per unit time in communication channel. Throughput is measured in bits/sec or bps. Authentication Delay specifies how long time it took to complete the authentication process. It gives ratio of sum of time taken to deliver packets for destination by number of packets received by destination. Packet delivery ratio is defined as the ratio of data packets received by the destinations to those packets sent by the sources. The greater value of packet delivery ratio means the better performance of the

protocol. Packet drops specify the number of packets dropped during the communication. It is measured as the difference of number of packets sent with number of packets received.

Section 2 presents 802.11i and its drawback analysis. Our scheme FLAP is given in Section 3. Section 4 presents some implementation considerations. Section 5 shows the performance measures. Security provided by FLAP is given in Section 6 and the paper is concluded in Section 7.

II. 802.11i BACKGROUND

802.11i robust security network association (RSNA) [9] establishment procedure consists of 802.1X authentication and key management (AKM) protocols. Three entities are involved, called the Supplicant (the STA), the authenticator (the AP), and the AS (de facto a RADIUS [7] server).

Generally, a successful authentication means that the supplicant and the authenticator verify each other's identity and generate secret keys for subsequent key derivations. Based on this secret key, the key management protocols compute and distribute usable keys for data communication sessions. Assuming the link between the AS and the authenticator is physically secure, the AS can be implemented either through a separate server or as a single device with Authenticator. The complete handshakes of establishing an RSNA are shown in Fig. 1.

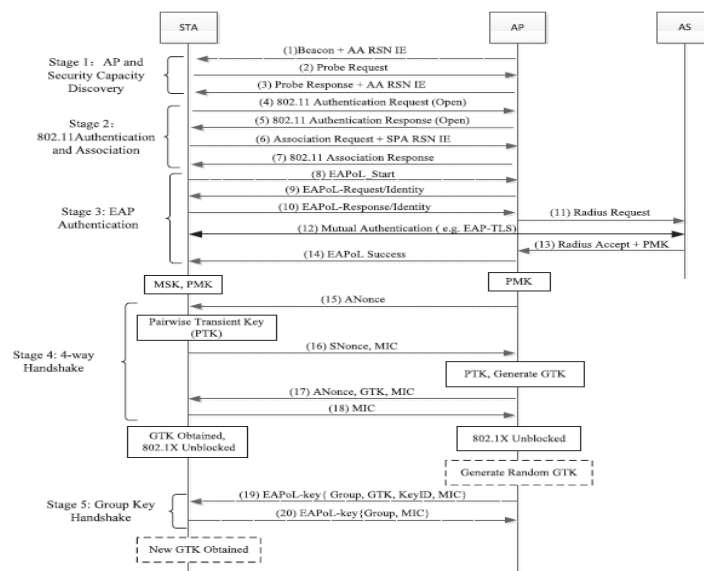


Figure 1: 802.11i 4-Way Handshake

2.1 Drawbacks of 802.11i

A test bed is established to explore the efficiency of 802.11i and EAP-TLS authentication delay is practically measured i.e., 50s, on average if there are 10 STA. Furthermore, we conducted thorough experiments with STA numbers and traffic. The results are shown from which it can be seen that with the average authentication delay of 30 new incoming STAs is 450s. We believe that if the network discovery and DHCP process are taken into account, the initial link setup time will get even longer; such inefficiency is intolerable for some applications.

Why is 802.11i so inefficient? From Fig. 1, it can be seen that 802.11i takes multiple round-trip messages to achieve the authentications and key distribution. The number of the message interactions varies for different authentication protocols used, for example, in the design, EAP-TLS has 11 round-trips (not including the scan process) and its implementation takes 13 round-trip messages because in MAC layer one of its messages is fragmented into three. While for each station of a WLAN, it has to compete each other for the wireless channel using the distributed coordinated function (DCF). If the WLAN is crowded, an STA will wait for a long time before it gets the channel to transmit a message. Large numbers of message interactions mean that a lot of time has to be spent to get the channel. As a result, AP cannot efficiently establish links with multiple users at the same time or the dwelling time is not enough to establish the initial link before an STA moves out the coverage of the AP.

The main reason leading to its inefficiency is that 802.11i is designed from the framework perspective which introduces too many extra messages. Rather than being a specific protocol, 802.11i is designed as a uniform framework where different authentication protocols can be incorporated. Compared with the design of a specific authentication protocol, devising a uniform framework will take more factors into consideration to make the framework more general and suitable for most scenarios. First, to achieve backward compatibility, the open system authentication is preserved. Yet, the two messages are useless for the initial link establishment. Second, the EAP authentication is employed; the advantage of which is that it is open and any two-party authentication protocol can be integrated and run within it. Furthermore, to keep the uniformity of the framework, EAP authentication and four-way handshake protocol have to be sequentially executed. That is, only after the EAP phase, can the four-way handshake protocol be performed to realize the mutual authentication between the STA and the AP. But in practice, to some degree the authentication between AP and STA can be performed in parallel with the one between the STA and the AS.

III. PROPOSED SCHEME

From the analysis, we get the goal and guideline for our scheme as follows:

Performance: The new scheme should greatly improve the performance of 802.11i.

Functionality: The least two round-trip messages are used to realize the authentication and key distribution between Station (STA), Access Point (AP), and Authentication Server (AS).

Orientation: The new scheme is just a complement instead of replacement of 802.11i and should be compatible with it.

Scope: Just a new initial access authentication is introduced which should not affect the subsequent procedure of the 802.11i.

Security: The security level of the new scheme is more than the current standard.

According to the drawback analyzed in 802.11i and the design goal outlined above, we get the design idea of new scheme as follows: A specific authentication protocol is designed with the least messages (two messages) which are used to realize the authentication between the STA and the AS, and the four-way handshake protocol messages are integrated rationally to realize the authentication between the STA and the AP.

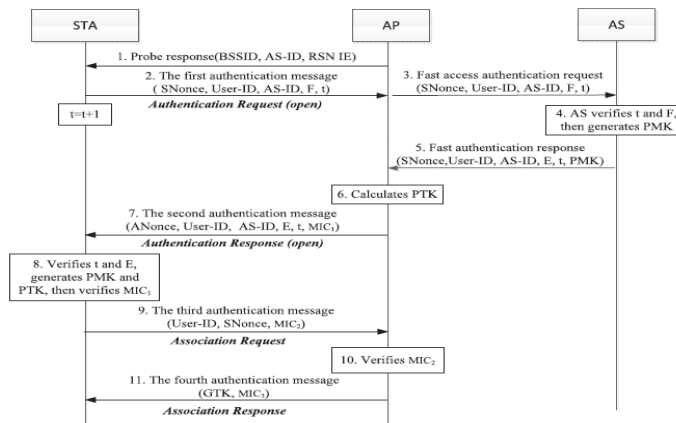


Figure 2: FLAP Scheme

3.1 Protocol Procedure

In the proposed scheme, each STA shares a key k with the AS, and it is also assumed that the link between the AS and the AP is secure. Our scheme is shown in Figure. 2 and its interaction procedure are as follows:

1. Through the proactive scan, the STA gets the WLAN information which includes the BSS identity, the security capacity of the networks and Authentication Server (AS) identity.

2. The first authentication message {SNonce, User-ID, AS-ID, F, t} is sent to the AP from the STA. Where SNonce is the random value generated by STA. User-ID is the user's identity, while AS-ID is the AS identity. And t is a counter; the STA increases its value by 1 once sending a message. Initial t value is 1. $F=f(k, t||SNonce||User-ID||AS-ID)$, where f() is a hash function and || denotes the concatenation.

3. AP sends the fast access authentication request message {SNonce, User-ID, AS-ID, F, t} to the AS.

4. A counter is also set in the AS for each user and its initial value is also set as 1. Upon receiving the fast access authentication request message, the AS gets its current t value according to the User-ID and compares it with the received one. If the received t value is less than the current t value in the AS, the authentication of the STA fails and the current t value of the AS will keep unchanged. Otherwise, the AS will further verify F according to the received t and the key k. If correct, the authentication of the STA by the AS succeeds, and the AS increases the received t value by one and sets it as its current t value. Thereafter, AS computes Pair wise Master Key (PMK).

$$PMK = h(k, \text{"FLAP PMK"} || t || \text{User-ID} || \text{AS-ID})$$

Where h is a hash function and "FLAP PMK" is a constant string.

5. The AS sends the authentication response message {SNonce, User-ID, AS-ID, E, t, PMK} to AP. Where $E = f(k, t||SNonce||AS-ID||User-ID)$.

6. After receiving the message 5, the AP generates its own random value ANonce and computes the PTK.

$$PTK = PRF-X (PMK, \text{"Pairwise key expansion"} || \text{Min} (AA, SPA) || \text{Max} (AA, SPA) || \text{Min} (ANonce, SNonce) || \text{Max} (ANonce, SNonce))$$

Where PRF-X is Pseudo random function. AA is MAC address of AP; SPA is MAC address of STA. "Pair wise key expansion" is a constant string. Min() means getting the minimum value; Max() means getting the maximum value; the derivation of the PTK here is exactly same as that of 802.11i. If the AS coexists with the AP, there is no need of message interactions between the AS and the AP, and the related operations are performed by the AP.

7. The AP sends to STA the second authentication message {ANonce, User-ID, AS-ID, E, t, MIC1}, where MIC1 is the message authentication code computed on this message by the AP using the PTK, and t is the current value of the AS.

8. After receiving the message, the STA will compare the received t value with its current t value, and if equal the STA will validate E. If correct, the authentication of the AS will pass. Thereafter, the STA will compute the PMK and PTK, using the same method as that of the AS and AP. At the same time, the STA will verify the MIC1 taking use of the PTK. If valid, the STA authenticates the AP successfully.

9. The STA sends the third authentication message {User-ID, SNonce, MIC2}, where MIC2 is the message authentication code computed on this message by the STA using the PTK. Meanwhile, the STA also indicates that whether the group temporal key GTK is required or not. Furthermore, this message carries the necessary RSN IE parameters to complete the association.

10. After receiving the message, the AP verifies the MIC2. If correct, it means that the STA generates the same PTK and the AP authenticates the STA successfully. So far, the networks side completes the authentication of the STA, and the AP installs the derived PTK. In addition, the AP registers the STA in the distributed system to complete the association operation. If the MIC2 is verified invalid or in a given time the third authentication message is not received, the AP will delete the STA's authentication information and deauthenticate it. Meanwhile, the authentication failure message will be sent to the AS which will in turn delete the authentication information of the STA and rollback its t value.

11. The AP sends the STA the fourth authentication message {GTK, MIC3}, where the GTK is encrypted using the PTK. Upon receiving this message, the STA verifies the MIC3. If correct, the STA decrypts and gets the GTK and other related information. At the same time, the STA installs the PTK and GTK.

IV. IMPLEMENTATION

The proposed scheme does not intend to replace 802.11i; instead, it is oriented as a complement of the current standard for some special applications. Thus, a method has to be provided to enable the new scheme to be compatible and coexist with 802.11i. Before the standard 802.11i, when a user makes the initial authentication, he can choose the open system authentication or WEP. Referring to this method, we also provide the user two options, including 802.11i and the proposed scheme.

Specially, a new AKM Suite Selector [9] is added to the 802.11i AKM Suite List in the 802.11i RSN IE. The authentication request is extended and new authentication algorithm identification is added that is to add dot11AuthenticationAlgorithm [9] value denoted by "FLAP." In such a way, totally there are three optional values, including the existing "Open System" and "Shared Key". Meanwhile, a new IE is added which encapsulates the message field of the proposed scheme.

When the networks support the FLAP and the STA prefers to the new scheme, the STA will set the dot11AuthenticationAlgorithm as "FLAP" in the first authentication message, and add its corresponding information element into the frame body. After the AP receives the message, it will first check the dot11AuthenticationAlgorithm and if it is "Open System," it will reply with authentication response (Open). In such a way, WLAN will run 802.11i as usual. If "FLAP," then the AP will forward the message to the AS. To enable the radius server to understand the message, we can still use the EAP over-radius format to transmit the message. Consequently, the AP needs to perform the EAP encapsulation of the first authentication message received, specifically, to extract the information element and encapsulate it into EAP message. And then send the EAP message to the AS through the radius message. To enable the AS to recognize the protocol, the new scheme has to be implemented in the AS and a new value "FLAP-method" is added into the type field of the EAP message to identify the scheme, and the rest fields are put into the following type-data field correspondingly. After the AS receives the fast access authentication request, it will first check the type field in the EAP message, and if it is "FLAP-method" the AS will execute the new scheme.

To proceed as above, the STA has to first get to know whether the networks support the fast access authentication or not. In the scan phase, AP will broadcast whether the new scheme is applicable or not in the RSN IE. Only when both the AS and the AP support FLAP, can the AP claim the WLAN supports this method. To implement the proposed scheme, the AP has to be updated. From the implementation perspective, the reasons to adopt the four message interactions are as follows:

- 1) The message framework of authentication (open) and association are reused. Consequently, the new scheme just needs to modify the contents of the four messages instead of its framework.
- 2) The message contents of the four-way handshake are reused. The four messages between the STA and the AP in the proposed scheme are similar to the four-way handshake. Therefore, the implementation of the new scheme can be achieved through the appropriate modification of the contents of the four-way handshake. Thus, the new scheme is easy to implement.
- 3) The state machine of the STA in 802.11i can be maintained unchanged.

Its initial state is "State 1: Unauthenticated, Unassociated." After the successful mutual authentication with the AS, the STA enters into the "State 2: Authenticated, Unassociated." When the protocol completes successfully, the STA enters into "State 3: Authenticated, Associated." This accords with the specification of 802.11i.

V. PERFORMANCE ANALYSIS

5.1 Compatibility Analysis

From above section, it can be seen that the proposed scheme can be compatible with 802.11i. And the new scheme provides users another choice in addition to 802.11i. FLAP scheme will be executed only when both the STA and the network support the fast initial access authentication. If the new scheme is not supported on both sides, 802.11i can be used instead. In addition, our scheme is involved only in the initial access authentication and the resulting outputs are the PMK and PTK which are same as those of 802.11i, therefore, the subsequent procedure (e.g., the update of the PTK) of 802.11i will not be affected. In such a way, FLAP can achieve nearly full compatibility with the current standard.

5.2 Security Analysis

If the hash function $f()$ and $h()$ is secure, our scheme FLAP can achieve mutual authentications among the STA, AP and AS, and generates a secure key PTK. Furthermore, the FLAP is more secure than the four-way handshake protocol.

5.3 Performance Analysis

According to the implementation consideration, we implement the proposed scheme. A test bed is established whose topology is shown in Figure. 3.

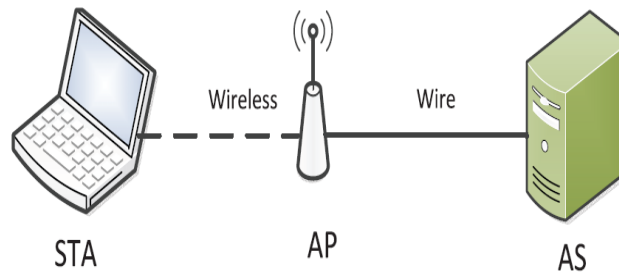


Figure 3: Test bed Topology

In this paper, simulation is done for the concept as the number of stations increases authentication delay increases, it consume lot of time in authentication process. And here along with the authentication delay some other parameters are also considered like throughput, packet delivery ratio and packet drops. These parameters are also equally important to say the protocol is efficient.

The authentication delay is made up of two components and they are process delay and communication delay. The former mainly consists of computation time, packet encapsulation and decapsulation time. The communication delay is the time spent to transmit messages over the wireless and the wire. In a WLAN, all the STAs have to compete with each other using CSMA/CA [1] to get the wireless channel, which costs considerable time. Comparing with the time spent in the wireless, the time in the wire is negligible because the bandwidth is very high and APs do not need to compete for the wire channel.

When a new STA is added (the original STA number is assumed to be n , and then now there are $n + 1$ STAs in total), for each of the original n STAs, its process time basically will not increase (we assume that the AS's computation capacity is enormous and it can handle authentications in parallel), while the communication delay gets longer because one more STA comes to compete for the channel with it. Consequently, for each of the original n STAs, the addition of one STA results in the increase of its communication delay. It is assumed that the average authentication delay is D when the STA number is n and the extra average communication delay resulting from one additional STA is δ , then for each of the original n STAs, the new average authentication delay is $D + \delta$. For the new incoming STA, its authentication delay also approximates to that of the rest n STAs. Therefore, the average authentication delay of the $n + 1$ STAs will also be $D + \delta$.

We vary the number of new incoming STAs that concurrently authenticate with the WLAN from 1 to 40. We simulated 10, 20, 30 and 40 nodes. The authentication delay simulation result for 802.11i EAP-TLS and proposed protocol are as show below:

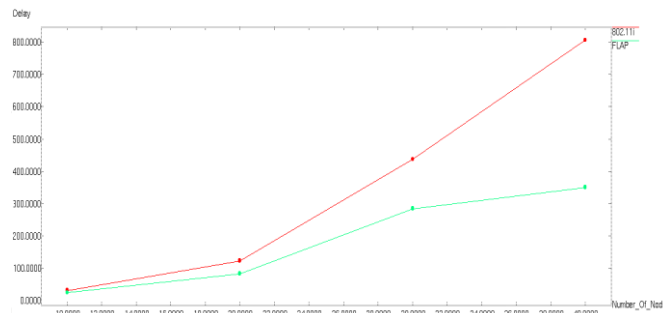


Figure 4: Authentication Delay simulation of 802.11i and FLAP

Furthermore, we notice that in Fig. 4, when the STA number is less than 10 the delay increases slowly, while the delay increases quickly (nearly linearly) when there are more than 10 STAs. This is because an additional STA does not affect the communication delay too much when the node number is small, but when the number gets large, the affect becomes considerable. This result accords with that of [11] which uses a Markov chain to analyze the WLAN performance. We found that when the STA number was greater than 10, the model was much closer to the practical situation. Based on the analysis model proposed in [11], [10] reaches the conclusion that WLAN access delay increases nearly linearly with the number of STAs.

Throughput is the number of packets/bytes received by source per unit time. It is an important metric for analysing network protocols. The throughput comparison between EAP-TLS and FLAP schemes are shown in below figure:

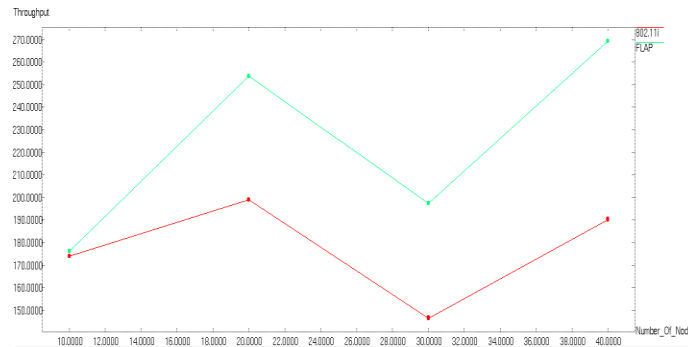


Figure 5: Throughput comparison between 802.11i and FLAP

From the above graph it is clear that throughput is efficient in FLAP than EAP-TLS 802.11i. When the number of STA is 10 the throughput values of both the protocols are approximately similar. As the number of STA increases to 30 then the values are 256 for FLAP and 198 for EAP-TLS. Throughput is measured in kbps.

Packet delivery ratio is defined as the ratio of data packets received by the destinations to those packets sent by the sources. The PDR for 10, 20, 30 and 40 number of STA for both 802.11i and FLAP are shown as below:

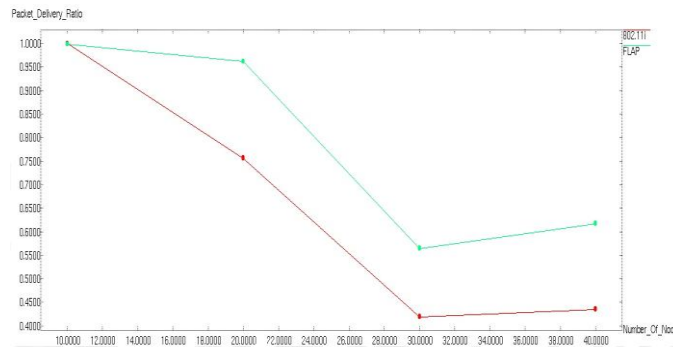


Figure 6: PDR comparison between 802.11i and FLAP

Above graph shows that the PDR for both EAP-TLS and FLAP schemes is same when there is 10 number of STA i.e., 1. When the number of STA increases to 40 then PDR of FLAP is 0.68 where as for EAP-TLS is 0.43. The greater value of packet delivery ratio means the better performance of the protocol.

And finally Packet Drops are considered and compared between both the existing and proposed schemes. Packet Drops show the total numbers of packets those drops during the transmission from source to destination. The below figure shows, the simulation results of packet drops for both protocols.

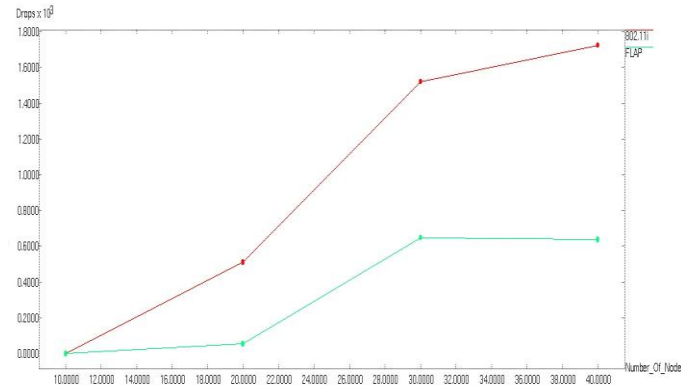


Figure 7: Packet drops comparison of 802.11i and FLAP

By considering the results of all these parameters we can say that FLAP is more efficient in many scenarios than 802.11i EAP-TLS.

- EAP-TLS is inefficient; especially when the incoming STAs number increases dramatically or the WLAN is crowded. For example, when there are 40 number of STA the average authentication is 820s.

Taking into account the scan and DHCP process, the initial link setup time will get even longer. With this performance, the offloading of real applications from 3G to WLAN cannot be realized for certain. In addition, let us image such a scenario where the radius of a WLAN is assumed to be 100 m and a car with the speed of 45 km/h passes through the WLAN. It will take the car up to 16 s, which is not quite enough for the onboard STA to establish the initial link if there is background traffic or the WLAN is crowded.

- Our scheme has salient advantage over the EAP-TLS, especially when the WLAN is crowded. With the new incoming STAs number increases, the authentication delay difference between EAP-TLS and our scheme gets bigger and bigger.

The below table shows the performance analysis results of our two protocols based on some performance metric such as number of nodes, authentication delay, throughput, PDR and packet drop:

Table 1: Performance Results of 802.11i and FLAP

Number of Nodes	Existing 802.11i values				Proposed FLAP values			
	Delay	Throughput	PDR	Drops	Delay	Throughput	PDR	Drops
10	29.49	173.89	1	0	23.12	176.08	0.99	0
20	122.4	198.90	0.75	512	82.73	253.59	0.96	53
30	436.8	146.56	0.41	1521	283.8	197.43	0.56	648
40	807.1	190.18	0.43	1724	350.0	269.10	0.61	638

Simulation result analysis: There are three factors that contribute to the salient advantage of our protocol over EAP-TLS.

1) Rather than being an authentication framework, our proposal is a specific authentication protocol. Therefore, some messages in the 802.11i can be eliminated, such as the open authentication request/response messages. Meanwhile, some messages in the 802.11i are integrated, for example, the identity information in our protocol is sent with other authentication information, while 802.11i employs two independent messages to carry this information.

Furthermore, the authentication between the STA and the AS is incorporated skilfully with the four-way handshake, without introducing extra messages. To realize the integration, the AS has to authenticate the STA successfully after receiving the first message (the fast access authentication request). Otherwise, the AP cannot get PMK or generate PTK before it generates the second message, and it cannot proceed to the four-way handshake. While, in the design of the two-message authentication protocol between the AS and the STA, how to ensure the freshness of the fast authentication request is a crucial problem. In our scheme, a loose counter t is utilized which is unnecessarily strictly synchronous. In such a method, the authentication between the STA and the AS can be integrated with the four-way handshake without introducing extra messages. Through the efforts mentioned above, our proposal just needs two roundtrip message interactions while 802.11i has 13 roundtrip messages. By means of reducing message exchanges, the time to spend in competing for the wireless channel is greatly cut down, especially when the WLAN is crowded.

2) The symmetric cryptographic algorithm is utilized in our scheme while EAP-TLS employs the asymmetric algorithm; therefore, the computation delay of EAP-TLS is much longer than ours.

3) The data amount of EAP-TLS is 14,341 bytes (from the EAPoL-Response/ identity to the end of four-way handshake) wherein the transmission of public key certificates is a major contributor, and ours is just 1,129 bytes.

VI. SECURITY IN FLAP

In our scheme, there is no strict synchronization requirement for the t values in the STA and the AS. We just require that the t value in the STA is no less than the one maintained by the AS. Therefore, it does not have a high demand for the system.

In addition, when the environment (e.g., the system failure) results in an asynchronization of the t values, an 802.11i authentication is executed and after the successful authentication both parties send the other the t value that it finally used and the bigger one is chosen as the new synchronized t value. It should be noticed that even the new synchronized t value is smaller than the last t value used before (this situation will happen when both the STA and the AS lose their t values), it will not do harm to the security of the scheme. Because under this circumstance the attacker can just replay the used fast authentication request but cannot get the PMK, which disables it to launch the third authentication message. Furthermore, it can not disturb the synchronization of the t values between the STA and the AS, because if the attacker cannot proceed the scheme, the AS's t value will be rolled back upon receiving the failure message from the AP (refer to the Step (10)). That is, the AS will not update its t value if FLAP cannot be completed fully. In such a way, the t values get synchronized again. From this procedure, it can be seen that AS's rollback of its t value is necessary in the Step (10) if the AP does not authenticate the STA successfully, otherwise, in the resynchronization process if an attacker replays a fast authentication request, the AS's t value will get bigger than the STA's, resulting that the legal STA cannot proceed the authentication.

In 802.11i, only after the successful authentication can the STA' IP address acquisition is executed. But in our scheme, the IP address acquisition can be performed in parallel with the FLAP. If the legacy DHCP [12] is employed to get the IP address, then each of its four messages can be carried by the corresponding message in our protocol as a new field. If the address is allocated with DHCP Rapid Commit Option [13], then its two messages can be carried through the first two messages of our scheme. But in either case, only when the AP authenticates the STA successfully (that is, after the message 9), can the allocated IP address is delivered to the STA.

VII. CONCLUSION

With the rapid increase of the WLAN-enabled devices, the current WLAN security standard IEEE 802.11i is challenged for its low efficiency. In this paper, we first demonstrate its inefficiency through experiments, and then point out that the essential reason leading to such inefficiency is the fact that 802.11i is designed from the framework perspective which introduces too many message interactions. To overcome this drawback and meet the requirement of new applications, an efficient initial access authentication protocol FLAP is proposed, which takes just two roundtrip messages between the client and the networks to complete the authentications and key distribution between the STA, AP, and AS. Analysis indicates that our scheme is more secure than the four-way handshake protocol. Furthermore, simulations are done in different scenarios using different number of nodes like 10, 20, 30 and 40. Delay, Throughput, PDR and Packet drops are compared between 802.11i and FLAP. Results indicate that with the STA number increases, our scheme has more salient advantage over EAP-TLS.

REFERENCES

- [1] IEEE 802.11, "Information Technology-Telecommunications and Information Exchange between Systems-Local and Metropolitan Area Networks-Specific Requirements-Part 11: Wireless LAN Medium Access Control and Physical Layer Specifications," IEEE Standard, 2007.
- [2] IEEE 802.11b, "Higher-Speed Physical Layer Extension in the 2.4 GHz Band, Supplement to IEEE Standard for Information Technology-Telecommunications and Information Exchange between Systems-Local and Metropolitan Area Networks- Specific Requirements-Part 11: Wireless LAN Medium Access Control (MAC) and Physical Layer (PHY) Specifications," IEEE Standard, Sept. 1999.
- [3] W.A. Arbaugh, N. Shankar, and J. Wang, "Your 802.11 Network Has No Clothes," Proc. IEEE First Int'l Conf. Wireless LANs and Home Networks (ICWLHN '01), pp. 131-144, 2001.
- [4] N. Borisov, I. Goldberg, and D. Wagner, "Intercepting Mobile Communications: The Insecurity of 802.11," Proc. ACM MOBiCOM, pp. 180-189, 2001.
- [5] B. Aboba, L. Blunk, J. Vollbrecht, and J. Carlson, "Extensible Authentication Protocol (EAP)," RFC 3748, June 2004.
- [6] IEEE 802.1X, "IEEE Standard for Local and Metropolitan Area Networks-Port-Based Network Access Control," IEEE Standard, June 2001.
- [7] C. Rigney, S. Willens, A. Rubens, and W. Simpson, "Remote Authentication Dial in User Service (RADIUS)," RFC 2865, June 2000.
- [8] X. Li, J. Ma, and Y. Shen, "An efficient WLAN Initial Authentication Protocol," Proc. IEEE Global Comm. Conf. (Globecom '12), 2012.
- [9] IEEE P802.11i, "Medium Access Control (MAC) Security Enhancements, Amendment 6 to IEEE Standard for Information Technology-Telecommunications and Information Exchange between Systems-Local and Metropolitan Area Networks- Specific Requirements -Part 11: Wireless Medium Access Control (MAC) and Physical Layer (PHY) Specifications," IEEE Standard, Apr. 2004.
- [10] P. Chatzimisios, A. Boucouvalas, and V. Vitsas, "Packet Delay Analysis of IEEE 802.11 MAC Protocol," Electronics Letters, vol. 39, no. 18, pp. 1358-1359, 2003.
- [11] G. Bianchi, "Performance Analysis of the IEEE802.11 Distributed Coordination Function," IEEE J. Selected Areas in Comm., vol. 18, no. 3, pp. 535-547, Mar. 2000.
- [12] R. Droms, "Dynamic Host Configuration Protocol," RFC 2131, 1997.
- [13] S. Park, P. Kim, and B. Volz, "Rapid Commit Option for the Dynamic Host Configuration Protocol Version 4 (DHCPv4)," IETF RFC 4039, 2005.
- [14] C. He and J.C. Mitchell, "Analysis of the 802.11 i 4-WayHandshake," Proc. Third ACM Workshop Wireless Security (Wisec'04), pp. 43-50, 2004.

THIRI KURAL?...

(jph Fuy;)



*M. Arulmani, B.E.
(Engineer)*

m.arulmani58@gmail.com



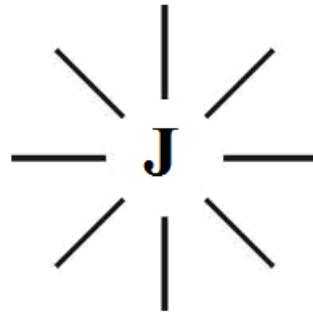
*V.R. Hema Latha, M.A., M.Sc., M.Phil.
(Biologist)*

vrhemalatha58@gmail.com

ABSTRACT: This scientific research article focus that “J-RADIATION” shall be considered as “SOUL” of Universal elements and matters also called as “VIRGIN LIGHT”. In proto Indo Europe language “THIRI KURAL” shall mean “WHITE ELEMENT” or “WHITE CLOUD”. White cloud consider contains billions of THREE-IN-ONE minute particles.

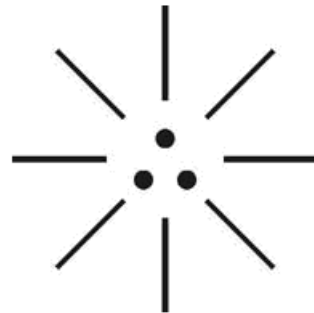
- i. “THIRI” shall mean “VIRGIN LIGHT”
- ii. “KURAL” shall mean “IONS”
- iii. “THIRI KURAL” shall mean “WHITE CLOUD”

(i)



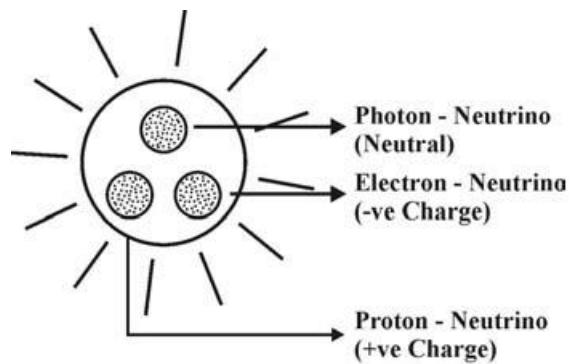
THIRI (திரி)

(ii)



KURAL (கூரல்)

(iii)



(THIRI KURAL)

“WHITE CLOUD (White plasma Element) shall be considered as the “SOUL” of Universal matters formed of three-in-one fundamental ions Photon, Electron, Proton and free from hydrogen, carbon, nitrogen, ozone.

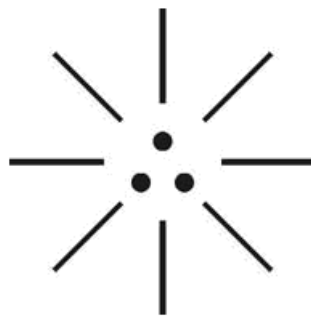
Key Words:

- a) “AKKINI” (Lightning)
- b) “EDI” (Thunder)
- c) “MAZHAI” (Rain)
- d) “ANNIAN” (Alien)

I. INTRODUCTION:

The Author of this article when doing 9th standard (Rural school) was beaten one day by school “TAMIL TEACHER” for pronouncing Thirukural (jpUf;Fws;) as “jphp Fuy;” (Thirikural). After taking practice as advised by the teacher the tongue was managed and could pronounce correctly as jpUf;Fws; at later date.

In this article the author tries to emphasize that “Thirikural” (jphpFuy;) shall be considered as fundamental “white matter” composed of billions of ions under THREE-IN-ONE domain called “e-logic”. In Proto Indo Europe language e-logic shall be called as “ESAI” (Music).



**e-LOGIC
(MUSIC)**

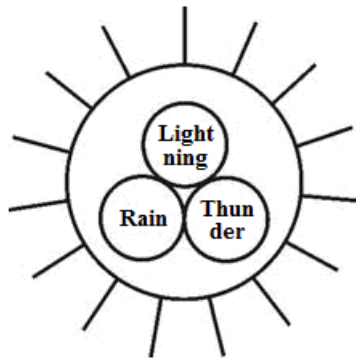
“MUSIC” (ESAI) shall be considered as predefined “e-logic” rather than mere sound or “language” responsible for evolution of all universal matters in systematic pre defined sequence”. In other words language shall be considered as expressive state of logic.

- Author

Hypothesis

a) Philosophy of white cloud?...

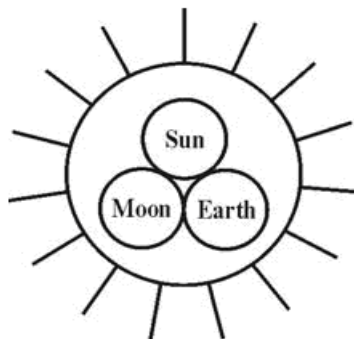
It is hypothesized that white clouds shall be considered as the most fundamental "PLASMA ELEMENT" (MULAM) derived from "J-RADIATION". It is further focused that the white clouds shall be considered as the source of three-in-one most fundamental elements "Akkinī" (Lightning), "Edi" (Thunder), "Mazhai" (Rain). In proto Indo Europe language the white clouds shall be called as "MUKIL". Billions of various other elements such as fire, water, air, landmark, snow, fog, honey, blood etc., shall be considered as "sub elements" to the fundamental elements.



White Cloud (മുകിൽ)

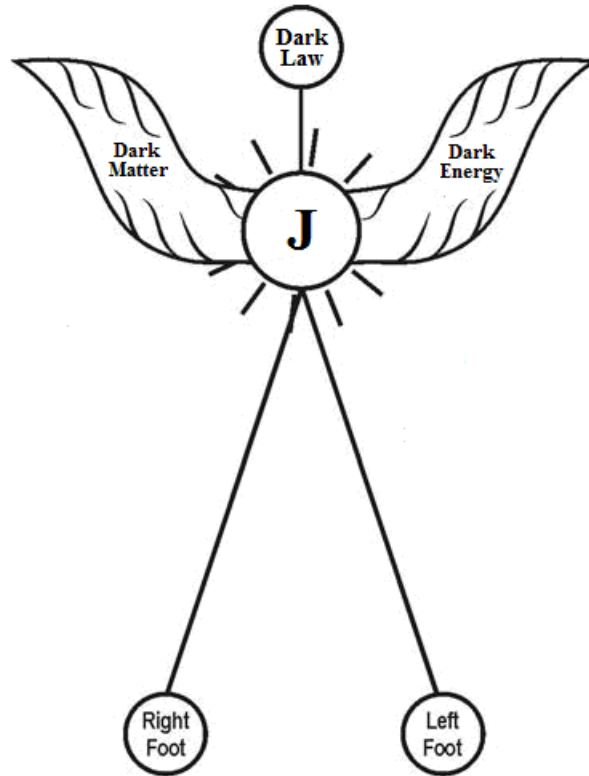
- i) "Akkinī" is like "Photon" (Rhythm)
- ii) "Edi" is like "Electron" (Melody)
- iii) "Mazhai" is like Proton (Pitch)
- iv) "Thiri" is like "J-Radiation" (Tala)

Further in Astrophysics "Kural" (White clouds) shall be referred as three-in-one fundamental ions and source of energy responsible for evolution of all matters of universe. The source of Kural shall be considered as dark flame which is called in proto Indo Europe language as AKKI-e.



Dark Flame (AKKI-e)

b) Philosophy of “ALIEN”?...



(AKKILEN)

(திரி வல்லுவர்)

Case study shows that ‘ALIEN’ is considered as prehistoric human lived in other planet. It is hypothesized that Alien shall be considered as genetically distinguished human population lived in “MARS PLANET” in early universe. In proto Indo Europe language Alien shall also be called as “**me;epad;**”. Further “Alien” shall be considered expert in Astrophysics, Astronomy in effect management of planetary systems. Alien shall also be called as “**THIRI VALLUVAR**”.

It is further focused that the various words pertain to Astrophysics, Astronomy might be derived from proto Indo Europe language origin as detailed below:

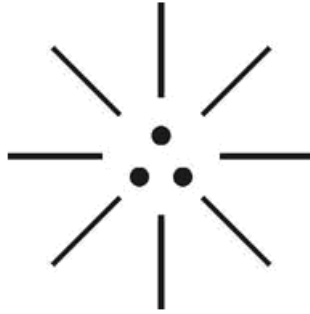
Sl.No.	Proto Indo Europe (PIE)	English Words
1	jphp	Virgin light (Milky)
2	Fuy;	Ion (Particle)
3	Kfpy;	White clouds
4	mf;fpdp	Lightning
5	,b	Thunder

6	kio	Rain
7	me;epad;	Alien
8	jphpld;	Tribe
9	%yk;	Trinity
10	jphpjy;	Diversity
11	mb	Threshold (Base)
12	,ir	Energy
13	jhap	Mother

c) Case study on Thirukkural Poem?...

Case study shows that “THIRUVALLUVAR” is considered as “Divine Poet” who made “THIRUKKURAL” which is accepted as “Global veda” or “Ethics”.

It is hypothesized that the philosophy of Thirukkural (jpUf;Fws;) under three-in-one domain might be derived from the philosophy of “Thirikural” (jphpFuy;)

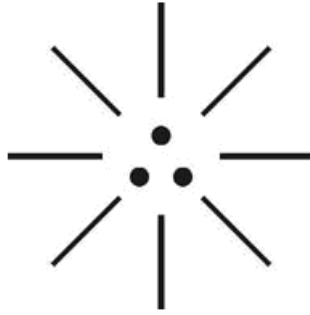


Thirikural (திரிகுரல்)

- i) Right dot is like “Pitch” (Rain)
- ii) Left dot is like “Melody” (Thunder)
- iii) Centre dot is like “Rhythm” (Lightning)

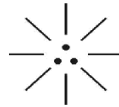
The philosophy of “Thirikural” (jphpFuy;) shall be defined within the following scope.

- 1) Thirikural shall mean “e-logic” rather than language
- 2) Thirikural shall mean “Law of music”
- 3) Thirikural shall mean “Source” (Soul) of all matters.
- 4) Thirikural shall mean “Mother of Alphabets”
- 5) Thirikural shall mean “Three domain life”



Triphthong (திரி)

- i) Right dot is "Vowel" (Proton)
- ii) Left dot is "Consonant" (Electron)
- iii) Centre dot is "Vibration" (Photon)



THAI-e
(திரிகுரல்)

III. CONCLUSION:

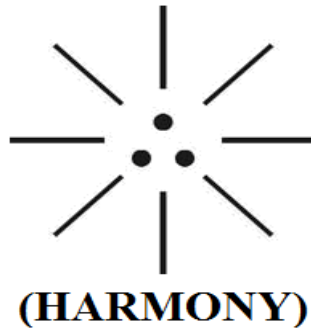
It is focused that "Thirikural" shall be considered as "MUSIC" and fundamental Harmony derived from "SPIRIT". All other man made languages shall be considered as "Harmonics" (Matters) to the fundamental "Harmony" (Soul).

(i)

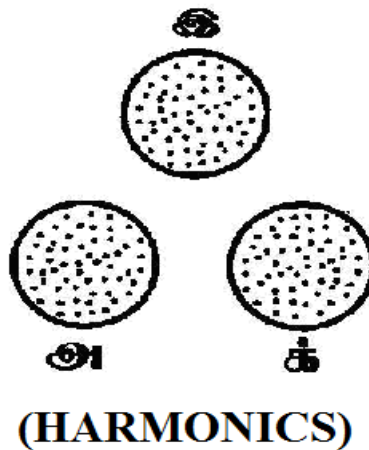


(SPIRIT)

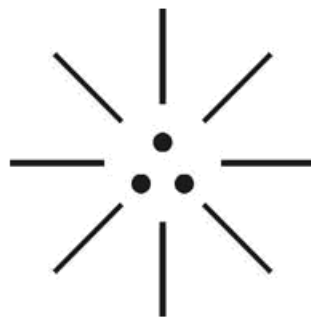
(ii)



(iii)



It is focused that the Tamil word “THIRI” shall be considered belong to the period of proto Indo-Europe language root. The three dot alphabet (13th alphabet) cited in **Thirukural** might belong to **prehistoric triphthong logic** indicating relative position of **SUN, EARTH, MOON**. The divine poet Thiruvalluvar might have lived during 2nd Generation (say Dravidian race) and hence the Tamil word “**THIRI**” might not be in much usage in Thirukural. **SANSKRIT** shall be considered as the classical language pertains to 3rd Generation population (say Aryan race).



Previous Publication: The philosophy of origin of first life and human, the philosophy of model Cosmo Universe, the philosophy of fundamental neutrino particles have already been published in various international journals mentioned below. Hence this article shall be considered as **extended version** of the previous articles already published by the same author.

- [1] Cosmo Super Star – IJSRP, April issue, 2013
- [2] Super Scientist of Climate control – IJSER, May issue, 2013
- [3] AKKIE MARS CODE – IJSER, June issue, 2013
- [4] KARITHIRI (Dark flame) The Centromere of Cosmo Universe – IJIRD, May issue, 2013
- [5] MA-AYYAN of MARS – IJIRD, June issue, 2013
- [6] MARS TRIBE – IJSER, June issue, 2013
- [7] MARS MATHEMATICS – IJERD, June issue, 2013
- [8] MARS (EZHEM) The mother of All Planets – IJSER, June issue, 2013
- [9] The Mystery of Crop Circle – IJOART, May issue, 2013
- [10] Origin of First Language – IJIRD, June issue, 2013
- [11] MARS TRISOMY HUMAN – IJOART, June issue, 2013
- [12] MARS ANGEL – IJSTR, June issue, 2013
- [13] Three principles of Akkie Management (AJIBM, August issue, 2013)
- [14] Prehistoric Triphthong Alphabet (IJIRD, July issue, 2013)
- [15] Prehistoric Akkie Music (IJST, July issue, 2013)
- [16] Barack Obama is Tamil Based Indian? (IJSER, August issue, 2013)
- [17] Philosophy of MARS Radiation (IJSER, August 2013)
- [18] Etymology of word “J” (IJSER, September 2013)
- [19] NOAH is Dravidian? (IJOART, August 2013)
- [20] Philosophy of Dark Cell (Soul)? (IJSER, September 2013)
- [21] Darwin Sir is Wrong?! (IJSER, October issue, 2013)
- [22] Prehistoric Pyramids are RF Antenna?!... (IJSER, October issue, 2013)
- [23] HUMAN IS A ROAM FREE CELL PHONE?!... (IJIRD, September issue, 2013)
- [24] NEUTRINOS EXIST IN EARTH ATMOSPHERE?!... (IJERD, October issue, 2013)
- [25] EARLY UNIVERSE WAS HIGHLY FROZEN?!... (IJOART, October issue, 2013)
- [26] UNIVERSE IS LIKE SPACE SHIP?!... (AJER, October issue, 2013)
- [27] ANCIENT EGYPT IS DRAVIDA NAD?!... (IJSER, November issue, 2013)
- [28] ROSETTA STONE IS PREHISTORIC “THAMEE STONE” ?!... (IJSER, November issue, 2013)
- [29] The Supernatural “CNO” HUMAN?... (IJOART, December issue, 2013)
- [30] 3G HUMAN ANCESTOR?... (AJER, December issue, 2013)
- [31] 3G Evolution?... (IJIRD, December issue, 2013)
- [32] God Created Human?... (IJERD, December issue, 2013)
- [33] Prehistoric “J” – Element?... (IJSER, January issue, 2014)
- [34] 3G Mobile phone Induces Cancer?... (IJERD, December issue, 2013)
- [35] “J” Shall Mean “JOULE”?... (IRJES, December issue, 2013)
- [36] “J”- HOUSE IS A HEAVEN?... (IJIRD, January issue, 2014)
- [37] The Supersonic JET FLIGHT-2014?... (IJSER, January issue, 2014)
- [38] “J”-RADIATION IS MOTHER OF HYDROGEN?... (AJER, January issue, 2014)
- [39] PEACE BEGINS WITH “J”?... (IJERD, January issue, 2014)
- [40] THE VIRGIN LIGHT?... (IJCRAR, January issue 2014)
- [41] THE VEILED MOTHER?... (IJERD, January issue 2014)
- [42] GOD HAS NO LUNGS?... (IJERD, February issue 2014)
- [43] Matters are made of Light or Atom?!... (IJERD, February issue 2014)
- [44] THE NUCLEAR “MUKKULAM”?... (IJSER, February issue 2014)
- [45] WHITE REVOLUTION 2014-15?... (IJERD, February issue 2014)
- [46] STAR TWINKLES!?... (IJERD, March issue 2014)
- [47] “E-LANKA” THE TAMIL CONTINENT?... (IJERD, March issue 2014)

- [48] HELLO NAMESTE?... (IJSER, March issue 2014)
- [49] MOTHERHOOD MEANS DELIVERING CHILD?... (AJER, March issue 2014)
- [50] E-ACHI, IAS?... (AJER, March issue 2014)
- [51] THE ALTERNATIVE MEDICINE?... (AJER, April issue 2014)
- [52] GANJA IS ILLEGAL PLANT?... (IJERD, April issue 2014)
- [53] THE ENDOS?... (IJERD, April issue 2014)
- [54] THE "TRI-TRONIC" UNIVERSE?... (AJER, May issue 2014)
- [55] Varied Plasma Level have impact on "GENETIC VALUE"?... (AJER, May issue 2014)
- [56] JALLIKATTU IS DRAVIDIAN VETERAN SPORT?... (AJER, May issue 2014)
- [57] Human Equivalent of Cosmo?... (IJSER, May issue 2014)
- [58] THAI-e ETHIA!... (AJER, May issue 2014)
- [59] THE PHILOSOPHY OF "DALIT"?... (AJER, June issue 2014)
- [60] THE IMPACT OF HIGHER QUALIFICATION?... (AJER, June issue 2014)
- [61] THE CRYSTAL UNIVERSE?... (AJER July 2014 issue)
- [62] THE GLOBAL POLITICS?... (AJER July 2014 issue)
- [63] THE KACHCHA THEEVU?... (AJER July 2014 issue)
- [64] THE RADIANT MANAGER?... (AJER July 2014 issue)
- [65] THE UNIVERSAL LAMP?... (AJER July 2014 issue)
- [66] THE MUSIC RAIN?... (IJERD July 2014 issue)

REFERENCE

- [1]. Intensive Internet "e-book" study through, Google search and wikipedia
- [2]. M.Arulmani, "3G Akkanna Man", Annai Publications, Cholapuram, 2011
- [3]. M. Arulmani; V.R. Hemalatha, "Tamil the Law of Universe", Annai Publications, Cholapuram, 2012
- [4]. Harold Koontz, Heinz Weihriah, "Essentials of management", Tata McGraw-Hill publications, 2005
- [5]. M. Arulmani; V.R. Hemalatha, "First Music and First Music Alphabet", Annai Publications, Cholapuram, 2012
- [6]. King James Version, "Holy Bible"
- [7]. S.A. Perumal, "Human Evolution History"
- [8]. "English Dictionary", Oxford Publications
- [9]. Sho. Devaneyapavanar, "Tamil first mother language", Chennai, 2009
- [10]. Tamilannal, "Tholkoppiar", Chennai, 2007
- [11]. "Tamil to English Dictionary", Suravin Publication, 2009
- [12]. "Text Material for E5 to E6 upgradaton", BSNL Publication, 2012
- [13]. A. Nakkiran, "Dravidian mother", Chennai, 2007
- [14]. Dr. M. Karunanidhi, "Thirukkural Translation", 2010
- [15]. "Manorama Tell me why periodicals", M.M. Publication Ltd., Kottayam, 2009
- [16]. V.R. Hemalatha, "A Global level peace tourism to Veilankanni", Annai Publications, Cholapuram, 2007
- [17]. Prof. Ganapathi Pillai, "Sri Lankan Tamil History", 2004
- [18]. Dr. K.K. Pillai, "South Indian History", 2006
- [19]. M. Varadharajan, "Language History", Chennai, 2009
- [20]. Fr. Y.S. Yagoo, "Western Sun", 2008
- [21]. Gopal Chettiar, "Adi Dravidian Origin History", 2004
- [22]. M. Arulmani; V.R. Hemalatha, "Ezhem Nadu My Dream" - (2 Parts), Annai Publications, Cholapuram, 2010
- [23]. M. Arulmani; V.R. Hemalatha, "The Super Scientist of Climate Control", Annai Publications, Cholapuram, 2013, pp 1-3

THE WHITE BLOOD ANCESTOR?...

(A New theory on "**Angel Blood**")



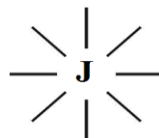
M.Arulmani, B.E.
(Engineer)



V.R.Hema Latha, M.A., M.Sc., M.Phil.
(Biologist)

Abstract: This scientific research article focus that "**Red colour blood**" of human shall be considered as the **3rd generation Blood** and the **Human on origin** shall be considered having **white colour Blood**. The white colour blood of human Ancestor shall be considered composed of only ions of **Photon, Electron, Proton** and free from Hydrogen, Carbon, Nitrogen, Ozone. The white blood shall be called as "**Pure Blood**" (or) "**white Fluid**". In proto Indo Europe language the white blood shall be called as "**AMMUTHAM**" (mKjk;)

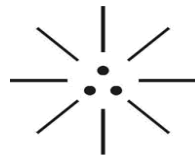
(i)



WHITE BLOOD LOGO

(அமுதம்)

(ii)



**LAW OF LIFE
(Three Domain)**

The source of **AMMUTHAM** (mKjk;) shall be considered as the “**WHITE SOUL**” (or) “**J-RADIATION**”. During the course of “**Expanding Universe**” the colour of human Ancestor might be consistently changed due to birth of various radiations like alpha, beta, gamma under different pressure, Temperature, Density environment conditions in **three Nuclear ages**. **AB** type blood is universal acceptor?... **NO... NO... NO...**

The “White Blood” (White fluid) free from atomic matters shall be considered as Universal blood (or) Universal acceptor and compatible not only to Human blood but to billions of all organisms of the Universe. The white blood shall also be called as “J-BLOOD”.

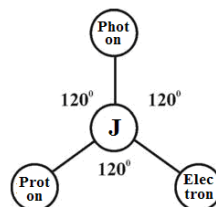
-Author

1. Key Words:

- a) Philosophy of “**J-Blood**” of human?
- b) Philosophy of “**Black Blood**” human?...
- c) Philosophy of “**Blue Blood**” human?...
- d) Philosophy of “**Green Blood**” human?...
- e) Philosophy of “**Red Blood**” human?...

I. INTRODUCTION:

It is focused that “**BLOOD**” is considered essential for sustainability of Life of all organisms including human. Blood is a bodily fluid in animals that delivers necessary substances such as Nutrients, Oxygen to the cells and transports metabolic waste product away from those same cells. Case study shows that “**AB**” blood type of human is considered as “**Universal Acceptor**”. It is the questions of the author can “**AB**” type blood of human accept the blood type of all organisms?... If the answer is “**NO**” means then how the **AB** type shall be called as **Universal acceptor**?...



**WHITE BLOOD
(Universal Acceptor)**

In this research article the author tries to emphasize that the “**White blood**” (**white fluid**) shall be considered as Universal Acceptor of blood of all organisms including blood types of “**Apes family**”.

It is further focused that the **four types** of blood of human (AB, A, B, O) shall be considered derived from most fundamental **White Blood** in different geological periods under different environmental conditions.

“DARWIN SIR” probably due to jealousy wrongly focused beautiful and genius Human Ancestor blood derived from Apes family.

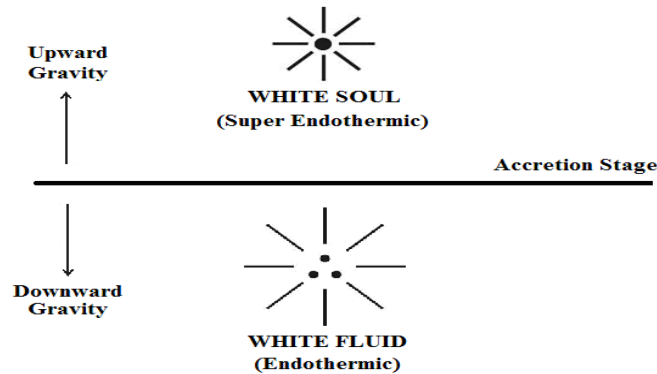
- Author

2. Hypothesis

a) “What “White blood” is made up of?...

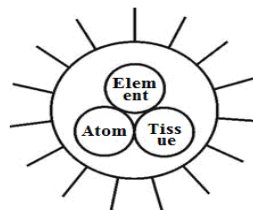
It is hypothesized that the white blood (White Fluid) shall be considered composed of only fundamental ions of photon, Electron, proton, exist under. **“ZERO GRAVITY”** (or) **“LOW GRAVITY”** endothermic environment. The white blood shall be considered as evolved due to Impact of **“J-RADIATION”**. The conventional blood matter consider composed of Trillions of various atoms, molecules with blood constituents, **Plasma Platelets, Red blood cell, white blood cell** shall be considered derived subsequently under various **“higher gravity”** environmental conditions. The philosophy of evolution of **“White Blood”** shall be described below.

b)



It is further hypothesized that the **“Universal blood matter”** shall be considered having **“three-in-one”** Domain say,

- a) **White element matter**
- b) **White Tissue matter**
- c) **White atomic matter.** The philosophy of 3rd Generation Blood with three-in-one Domain shall be described as below.



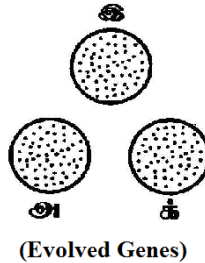
(Three Blood Domain)

The philosophy of **“3RD GENERATION BLOOD”** (red blood) shall be defined within the following scope.

- i. **“RED BLOOD”** shall mean three-in-one fundamental Domain matter (i.e) Elementary matter, Tissue matter, Atomic matter

- ii. "RED BLOOD" shall be considered as the state of "Liquid phase matter" rather than the state of "FLUID" exist under "higher gravity" environment compared to "White Blood".
- iii. "RED BLOOD" shall be considered having "higher viscosity" and varied most fundamental characteristics compared to "White Blood"

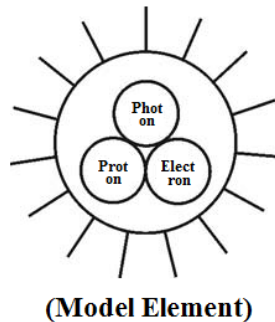
The 3rd Generation blood considered acquired thousands of characteristics in **three geological period** shall be described as below.



c) **Philosophy of three Domain structure of Blood?...**

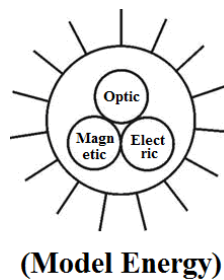
It is hypothesized that the three-in-one blood system shall be considered as the most fundamental domain matter. Billions of various phases of Blood matters shall be considered as **species** to the three fundamental domain matter.

i) **Model Elementary matter:**



The smaller unit of "Elementary matter" shall be considered as composed of ions of **Photon, Electron, Proton** having definite charge property also called as "White Cell". Varied **cell mass** might lead to varied characteristics of Blood.

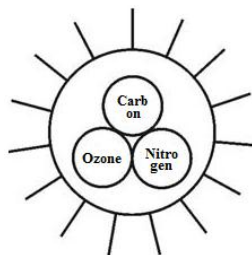
ii) **Model Tissue matter**



The smaller unit of "Tissue matter" shall be considered as composed of energy of **Optic, Electric, Magnetic** parameter also called as "white energy". Varied level of **energy intensity** might lead to varied

characteristics of blood.

iii) **Model Atomic matter**



(Model Atom)

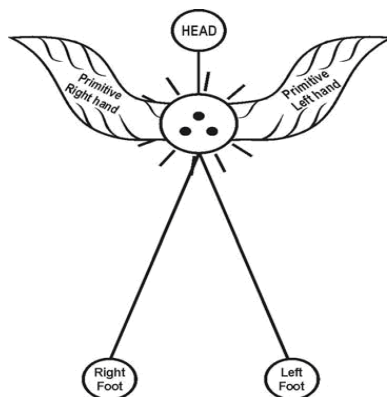
The smaller unit of “**Atomic matter**” shall be considered as composed of Carbon, Nitrogen, Ozone also called as “**White Atom**”. Varied atomic weight to the fundamental nuclei might lead to varied atomic matter

*“The **Standard Blood system** shall be considered composed of most fundamental parameter of “**White cell**”, “**White Energy**” and “**White Atom**” exist under **three-in-one** domain. Further the standard blood cell shall be considered as composed of **THREE-IN-ONE** nuclei”.*

- Author

d) **Philosophy of “Angel” blood?...**

It is hypothesized that the prehistoric human population lived in “**MARS PLANET**” shall be considered belong to “**Angel family**” having highest level of “**Wisdom**”. The Angel population shall be considered breath “**WIND**” rather than ozone, oxygen and having “**White fluid blood**”. The wind shall be considered as absolutely pre air composed of ions of **Photon, Electron, Proton** are free from **Hydrogen, Carbon, Nitrogen, Oxygen**.



ANGEL FAMILY
(Universal White Blood)

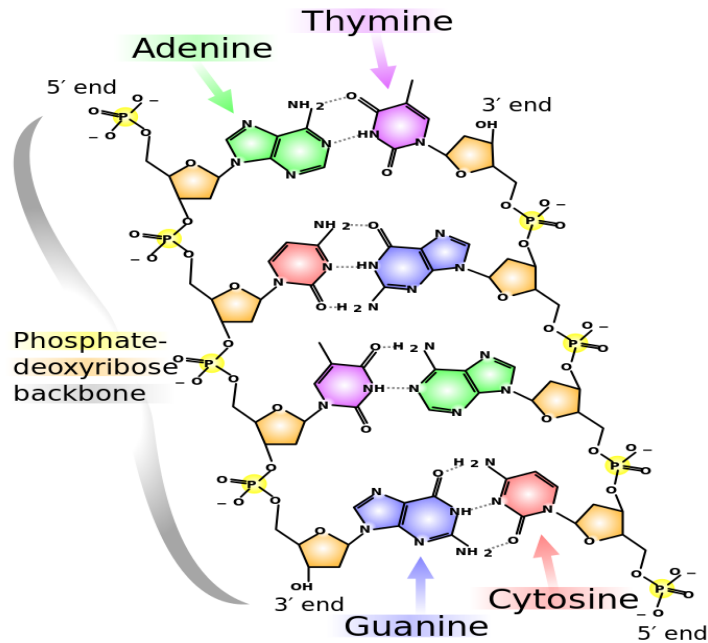
e) **Philosophy of “Black Blood” human?...**

It is hypothesized that “**Black Blood**” shall be considered as the Transformed stage of White blood. During the expanding Universe Angel family lived in **MARS PLANET** shall be considered transformed to “**EARTH PLANET**”. The **BLACK BLOOD** population of the Earth planet shall also be called as “**TRIBE POPULATIONS**”.

It is further focused that **Blue blood, Green Blood, Red Blood** populations shall be considered as the three distinguished family of population with varied “**genetic structure**” in three Nuclear Ages say 1st generation, 2nd generation, 3rd generation populations.

f) **Case study on congenital Blood?...**

Case study shows that in the congenital Blood the blood cell considered composed of “**Trillion**” of atomic particles responsible for various function of blood cells.



The DNA molecule is an example of matter under the "atoms and molecules" definition.

It is hypothesized that the conventional blood types **AB, A, B, O** shall be considered as containing **various atoms** and evolved in three different geological period derived from the fundamental **"White Blood"**.

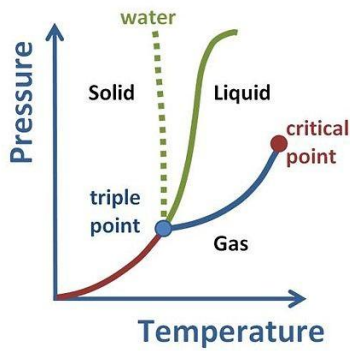
g) Case study on Blood types?...

Various blood types shall be considered having evolved in different geological period from the most fundamental **universal white blood** and acquiring distinguished **magnetic, electric, optic** properties due to impact of **UV, RF, IR** environment. It is hypothesized that the white blood shall be considered as containing only **"ANTIBODIES"** and free from **"ANTIGEN"**. During the course of time the **white blood** could have acquired various level of antigens which results to become evolution of different type of blood group.

	Group A	Group B	Group AB	Group O
Red blood cell type				
Antibodies in Plasma	Anti-B	Anti-A	None	Anti-A and Anti-B
Antigens in Red Blood Cell	A antigen	B antigen	A and B antigens	None

h) Case study on phases of matter?...

Scientific study shows that all matter exists in fundamental four states i.e. Plasma state, Solid state, Liquid state, Gas state and other exotic stages of super fluid, super solid.



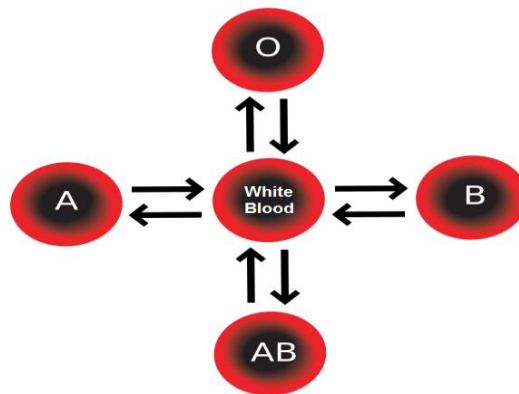
Phase diagram for a typical substance at a fixed volume. Vertical axis is Pressure, horizontal axis is Temperature. The green line marks the freezing point (above the green line is solid, below it is liquid) and the blue line the boiling point (above it is liquid and below it is gas). So, for example, at higher T, a higher P is necessary to maintain the substance in liquid phase. At the triple point the three phases; liquid, gas and solid; can coexist. Above the critical point there is no detectable difference between the phases. The dotted line shows the anomalous behavior of water:

It is hypothesized that the **WHITE BLOOD** shall be considered as existing in the state of “**SUPER FLUID**” under high endothermic environment and of highest **humidity level** and lowest PH level compared to 3rd Generation blood.

i) Philosophy of Universal Donor Blood?...

Case study shows that “**O**” type blood is considered as Universal donor to other blood groups AB, A, B and called as Universal donor. Can O type blood be donated to all other animals and organisms?... If the answer is no, then how the **O type blood** can be called as Universal donor?...

It is hypothesized that white blood (white fluid) shall be considered as not only Universal acceptor blood but shall also be considered as Universals donor. The Philosophy of Universal acceptor and Universal donor shall be descended as below.



j) Case study on Blood Serum?...

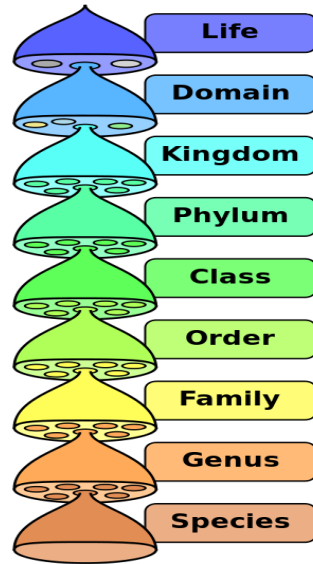
Case study shows that blood serum is the component (does not contain WBC, RBC) consider neither a blood cell nor a clotting factor. Further serum includes all “**PROTEINS**” and essential factor for self renewal of embryonic stem cells. It is hypothesized that **blood serum** shall be considered as the species matter to the fundamental “**WHITE BLOOD CELL**”.



- i) Right dot (Proton) – Responsible for functional (**DNA**)
- ii) Left dot (Electron) - Responsible for Structural (**HORMONE**)
- iii) Center dot (Photon) - Responsible for Sequence (**RNA**)

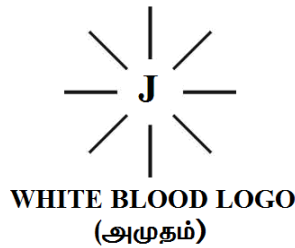
k) Case study on Phylum?...

Case study shows that in biology a principal taxonomic category that ranks above class and below kingdom.



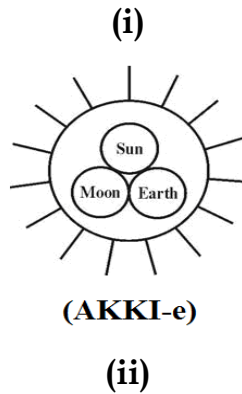
The hierarchy of biological classification's eight major taxonomic ranks. A kingdom contains one or more phyla. Intermediate minor rankings are not shown.

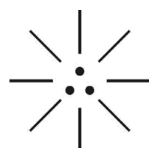
It is hypothesized that “**J-Blood**” (Universal white blood) shall be considered as the **LIFE** from which all the life of universal organism considered descended from.



1) **Case study on Dark Energy?...**

Case study shows that the Universe contains 70% dark energy, 26% dark matter and balance other matters. It is hypothesized that “**AKKI-e**” shall be considered as the source of dark energy and “**white soul**” responsible for existence of all matters in the Universe.





(WHITE SOUL)

3. Conclusion:

The white blood (With fluid) shall be considered as the “Fluid state” of matter rather than Plasma state of matter. Fluid state shall mean free from atomic matter Hydrogen, Carbon, Nitrogen, and Ozone.

Further in **Human Anthropological system** the various genetically varied populations shall be considered having different type of blood system since origin of “**Human Ancestor**” as described below.

Sl.No.	Human race	Period	Blood type
1.	Angel family	Prehistoric Time (Wind breath)	“White blood”
2.	Plasma Human (Tribe)	Ancient time (Transformation to Ozone breath)	“Black blood”
3.	Proto Dravidian	Post Ancient (1 st generation) (Ozone breath)	“Blue blood” (AB)
4.	Dravidian	Pre modern (2 nd generation) (Oxygen breath)	“Green blood” (AB, A, B)
5.	Aryan	Moderations(3 rd generation) (Oxygen allotrope)	Red blood (AB,A,B,O)

4. Previous Publication:

The philosophy of origin of first life and human, the philosophy of model Cosmo Universe, the philosophy of fundamental neutrino particles have already been published in various international journals mentioned below. Hence this article shall be considered as **extended version** of the previous articles already published by the same author.

- [1] Cosmo Super Star – IJSRP, April issue, 2013
- [2] Super Scientist of Climate control – IJSER, May issue, 2013
- [3] AKKIE MARS CODE – IJSER, June issue, 2013
- [4] KARITHIRI (Dark flame) The Centromere of Cosmo Universe – IJIRD, May issue, 2013
- [5] MA-AYYAN of MARS – IJIRD, June issue, 2013
- [6] MARS TRIBE – IJSER, June issue, 2013
- [7] MARS MATHEMATICS – IJERD, June issue, 2013
- [8] MARS (EZHEM) The mother of All Planets – IJSER, June issue, 2013
- [9] The Mystery of Crop Circle – IJOART, May issue, 2013
- [10] Origin of First Language – IJIRD, June issue, 2013
- [11] MARS TRISOMY HUMAN – IJOART, June issue, 2013
- [12] MARS ANGEL – IJSTR, June issue, 2013
- [13] Three principles of Akkie Management (AJIBM, August issue, 2013)
- [14] Prehistoric Triphthong Alphabet (IJIRD, July issue, 2013)
- [15] Prehistoric Akkie Music (IJST, July issue, 2013)
- [16] Barack Obama is Tamil Based Indian? (IJSER, August issue, 2013)
- [17] Philosophy of MARS Radiation (IJSER, August 2013)
- [18] Etymology of word “J” (IJSER, September 2013)
- [19] NOAH is Dravidian? (IJOART, August 2013)
- [20] Philosophy of Dark Cell (Soul)? (IJSER, September 2013)
- [21] Darwin Sir is Wrong?! (IJSER, October issue, 2013)
- [22] Prehistoric Pyramids are RF Antenna?!... (IJSER, October issue, 2013)
- [23] HUMAN IS A ROAM FREE CELL PHONE?!... (IJIRD, September issue, 2013)
- [24] NEUTRINOS EXIST IN EARTH ATMOSPHERE?!... (IJERD, October issue, 2013)

- [25] EARLY UNIVERSE WAS HIGHLY FROZEN?!... (IJOART, October issue, 2013)
- [26] UNIVERSE IS LIKE SPACE SHIP?!... (AJER, October issue, 2013)
- [27] ANCIENT EGYPT IS DRAVIDA NAD?!... (IJSER, November issue, 2013)
- [28] ROSETTA STONE IS PREHISTORIC “THAMEE STONE”?!... (IJSER, November issue, 2013)
- [29] The Supernatural “CNO” HUMAN?... (IJOART, December issue, 2013)
- [30] 3G HUMAN ANCESTOR?... (AJER, December issue, 2013)
- [31] 3G Evolution?... (IJIRD, December issue, 2013)
- [32] God Created Human?... (IJERD, December issue, 2013)
- [33] Prehistoric “J” – Element?... (IJSER, January issue, 2014)
- [34] 3G Mobile phone Induces Cancer?... (IJERD, December issue, 2013)
- [35] “J” Shall Mean “Joule”?... (IRJES, December issue, 2013)
- [36] “J”- HOUSE IS A HEAVEN?... (IJIRD, January issue, 2014)
- [37] The Supersonic JET FLIGHT-2014?... (IJSER, January issue, 2014)
- [38] “J”-RADIATION IS MOTHER OF HYDROGEN?... (AJER, January issue, 2014)
- [39] PEACE BEGINS WITH “J”?... (IJERD, January issue, 2014)
- [40] THE VIRGIN LIGHT?... (IJCRAR, January issue 2014)
- [41] THE VEILED MOTHER?... (IJERD, January issue 2014)
- [42] GOD HAS NO LUNGS?... (IJERD, February issue 2014)
- [43] Matters are made of Light or Atom?!... (IJERD, February issue 2014)
- [44] THE NUCLEAR “MUKKULAM”?... (IJSER, February issue 2014)
- [45] WHITE REVOLUTION 2014-15?... (IJERD, February issue 2014)
- [46] STAR TWINKLES!?!... (IJERD, March issue 2014)
- [47] “E-LANKA” THE TAMIL CONTINENT?... (IJERD, March issue 2014)
- [48] HELLO NAMESTE?... (IJSER, March issue 2014)
- [49] MOTHERHOOD MEANS DELIVERING CHILD?... (AJER, March issue 2014)
- [50] E-ACHI, IAS?... (AJER, March issue 2014)
- [51] THE ALTERNATIVE MEDICINE?... (AJER, April issue 2014)
- [52] GANJA IS ILLEGAL PLANT?... (IJERD, April issue 2014)
- [53] THE ENDOS?... (IJERD, April issue 2014)
- [54] THE “TRI-TRONIC” UNIVERSE?... (AJER, May issue 2014)
- [55] Varied Plasma Level have impact on “GENETIC VALUE”?... (AJER, May issue 2014)
- [56] JALLIKATTU IS DRAVIDIAN VETERAN SPORT?... (AJER, May issue 2014)
- [57] Human Equivalent of Cosmo?... (IJSER, May issue 2014)
- [58] THAI-e ETHIA!... (AJER, May issue 2014)
- [59] THE PHILOSOPHY OF “DALIT”?... (AJER, June issue 2014)
- [60] THE IMPACT OF HIGHER QUALIFICATION?... (AJER, June issue 2014)
- [61] THE CRYSTAL UNIVERSE?... (AJER July 2014 issue)
- [62] THE GLOBAL POLITICS?... (AJER July 2014 issue)
- [63] THE KACHCHA THEEVU?... (AJER July 2014 issue)
- [64] THE RADIANT MANAGER?... (AJER July 2014 issue)
- [65] THE UNIVERSAL LAMP?... (IJOART July 2014 issue)
- [66] THE MUSIC RAIN?... (IJERD July 2014 issue)
- [67] THIRI KURAL?... (AJER August 2014 issue)
- [68] THE SIXTH SENSE OF HUMAN?... (AJER August 2014 issue)
- [69] THEE... DARK BOMB?... (IJSER August 2014 issue)
- [70] RAKSHA BANDHAN CULTURE?... (IJERD August 2014 issue)

REFERENCE

- [1]. Intensive Internet “e-book” study through, Google search and wikipedia
- [2]. M.Arulmani, “3G Akkanna Man”, Annai Publications, Cholapuram, 2011
- [3]. M. Arulmani; V.R. Hemalatha, “Tamil the Law of Universe”, Annai Publications, Cholapuram, 2012
- [4]. Harold Koontz, Heinz Wehriah, “Essentials of management”, Tata McGraw-Hill publications, 2005
- [5]. M. Arulmani; V.R. Hemalatha, “First Music and First Music Alphabet”, Annai Publications, Cholapuram, 2012
- [6]. King James Version, “Holy Bible”
- [7]. S.A. Perumal, “Human Evolution History”
- [8]. “English Dictionary”, Oxford Publications
- [9]. Sho. Devaneyapavanar, “Tamil first mother language”, Chennai, 2009
- [10]. Tamilannal, “Tholkoppiar”, Chennai, 2007
- [11]. “Tamil to English Dictionary”, Suravin Publication, 2009
- [12]. “Text Material for E5 to E6 upgradaton”, BSNL Publication, 2012
- [13]. A. Nakkiran, “Dravidian mother”, Chennai, 2007
- [14]. Dr. M. Karunanidhi, “Thirukkural Translation”, 2010
- [15]. “Manorama Tell me why periodicals”, M.M. Publication Ltd., Kottayam, 2009
- [16]. V.R. Hemalatha, “A Global level peace tourism to Veilankanni”, Annai Publications, Cholapuram, 2007
- [17]. Prof. Ganapathi Pillai, “Sri Lankan Tamil History”, 2004
- [18]. Dr. K.K. Pillai, “South Indian History”, 2006

- [19]. M. Varadharajan, "Language History", Chennai, 2009
- [20]. Fr. Y.S. Yagoo, "Western Sun", 2008
- [21]. Gopal Chettiar, "Adi Dravidian Origin History", 2004
- [22]. M. Arulmani; V.R. Hemalatha, "Ezhem Nadu My Dream" - (2 Parts), Annai Publications, Cholapuram, 2010
- [23]. M. Arulmani; V.R. Hemalatha, "The Super Scientist of Climate Control", Annai Publications, Cholapuram, 2013, pp 1-3

Evaluation of life quality indicators in cities & improving urban environmental (Case Study: Boroujerd city)

¹Fatemeh Olfaty, ² Mahdi Garavand

¹Department of Art and Architecture, Science and Research branch, Islamic Azad University, Boroujerd, Iran

²Department of Art and Architecture, Science and Research branch, Islamic Azad University, Boroujerd, Iran

ABSTRACT : One of the main urban issues is healthy life of residents. Today cities have created mental disaster due to some problems such as crowded, pollutions, high density population and etc. on the other hand , cities especially small cities have natural and appropriate conditions in order to improving urban life quality . So should be planned for using from them. This research is applied. Research method is "descriptive – analytical". Data collected is field. At first, was determined by using kukran method. The sample size is 384 people. In order to using from (GHQ-28) questionnaire (Human, 2005: 131). In this research was evaluated urban quality of Boroujerd city. In order to analyzing of data was used some technique such as: SPSS, Pierson correlation, T test, T Kendall, regression and keroskal. Also, was used questioner for determining sample size. The results shows, there is oriented relation between location and health of residents. Indeed, there is appropriate condition of life quality in welfare location. On the other hand, the most disorder between residents was stress that decreased urban life quality.

KEY WORDS : life quality, GHQ, indicator

I. INTRODUCTION

The term quality of life (QOL) references the general well-being of individuals and societies. The term is used in a wide range of contexts, including the fields of international development, healthcare, and politics. Quality of life should not be confused with the concept of standard of living, which is based primarily on income. Instead, standard indicators of the quality of life include not only wealth and employment, but also the built environment, physical and mental health, education, recreation and leisure time, and social belonging (Husseini, 1999: 45). According to ecological economist Robert Costanza: While Quality of Life (QOL) has long been an explicit or implicit policy goal, adequate definition and measurement have been elusive. Diverse "objective" and "subjective" indicators across a range of disciplines and scales, and recent work on subjective well-being (SWB) surveys and the psychology of happiness have spurred renewed interest. Also frequently related are concepts such as freedom, human rights, and happiness. However, since happiness is subjective and difficult to measure, other measures are generally given priority. It has also been shown that happiness, as much as it can be measured, does not necessarily increase correspondingly with the comfort that results from increasing income. As a result, standard of living should not be taken to be a measure of happiness. Also sometimes considered related is the concept of human security, though the latter may be considered at a more basic level, and for all people.

Unlike per capita GDP or standard of living, both of which can be measured in financial terms, it is harder to make objective or long-term measurements of the quality of life experienced by nations or other groups of people. Researchers have begun in recent times to distinguish two aspects of personal well-being: Emotional well-being, in which respondents are asked about the quality of their everyday emotional experiences the frequency and intensity of their experiences of, for example, joy, stress, sadness, anger, and affection and life evaluation, in which respondents are asked to think about their life in general and evaluate it against a scale. Such and other systems and scales of measurement have been in use for some time.

Research has attempted to examine the relationship between quality of life and productivity (nur bala, 2002: 5). In recent decade evaluating of life condition is important due to creating urban issues. today the modern method is led to created some problems such as : density , crowded , pollution (Zahedi , 2002 : 20) . Improving human urban quality is necessary for governments (Ganji, 2002: 67). In this research was evaluated urban quality of Boroujerd city. In order to analyzing of data was used some technique such as: SPSS, Pierson correlation, T test, T Kendall, regression and keroskal. Also, was used questioner for determining sample size .

II. STANDARD OF LIVING

Refers to the level of wealth, comfort, material goods and necessities available to a certain socioeconomic class in a certain geographic area. The standard of living includes factors such as income, quality and availability of employment, class disparity, poverty rate, quality and affordability of housing, hours of work required to purchase necessities, gross domestic product, inflation rate, number of vacation days per year, affordable (or free) access to quality healthcare, quality and availability of education, life expectancy, incidence of disease, cost of goods and services, infrastructure, national economic growth, economic and political stability, political and religious freedom, environmental quality, climate and safety. The standard of living is closely related to quality of life (Saliski, 2004: 48). Standard of living is generally measured by standards such as real (i.e. inflation adjusted) income per person and poverty rate (Ozur, 2003: 18). Other measures such as access and quality of health care, income growth inequality, Disposable Energy (people's disposable income's ability to buy energy) and educational standards are also used. Examples are access to certain goods (such as number of refrigerators per 1000 people), or measures of health such as life expectancy (Shahidi, 2003:35). It is the ease by which people living in a time or place are able to satisfy their needs and/or wants (Biyabangard, 2005:23). The idea of a 'standard' may be contrasted with the quality of life, which takes into account not only the material standard of living, but also other more intangible aspects that make up human life, such as leisure, safety, cultural resources, social life, physical health, environmental quality issues, etc (Isfahani , 2006 :34) . More complex means of measuring well-being must be employed to make such judgments, and these are very often political, thus controversial. Even between two nations or societies that have similar material standards of living, quality of life factors may in fact make one of these places more attractive to a given individual or group (Javadi , 2004 : 30).

However, there can be problems even with just using numerical averages to compare material standards of living, as opposed to, for instance, a Pareto index (a measure of the breadth of income or wealth distribution). Standards of living are perhaps inherently subjective (Palahang, 1994: 21). As an example, countries with a very small, very rich upper class and a very large, very poor lower class may have a high mean level of income, even though the majority of people have a low "standard of living". This mirrors the problem of poverty measurement, which also tends towards the relative. This illustrates how distribution of income can disguise the actual standard of living (Yaqubi, 1993:52).

III. RESEARCH HISTORY

Perhaps the most commonly used international measure of development is the Human Development Index(HDI), which combines measures of life expectancy, education, and standard of living, in an attempt to quantify the options available to individuals within a given society. The HDI is used by the United Nations Development Programmer in their Human Development Report. The Physical Quality of Life Index (PQLI) is a measure developed by sociologist Morris David Morris in the 1970s, based on basic literacy, infant mortality, and life expectancy. Although not as complex as other measures, and now essentially replaced by the Human Development Index, the PQLI is notable for Morris's attempt to show a "less fatalistic pessimistic picture" by focusing on three areas where global quality of life was generally improving at the time, and ignoring Gross National Product and other possible indicators that were not improving. The Happy Planet Index, introduced in 2006, is unique among quality of life measures in that, in addition to standard determinants of well-being, it uses each country's ecological footprint as an indicator. As a result, European and North American nations do not dominate this measure. The 2012 list is instead topped by Costa Rica, Vietnam and Colombia. Gallup researchers trying to find the world's happiest countries found Denmark to be at the top of the list. Switch publishes an annual quality of life index for European countries. France has topped the list for the last three years. A 2010 study by two Princeton University professors looked at 1,000 randomly selected U.S. residents over an extended period. It concludes that their life evaluations- that is, their considered evaluations of their life against a stated scale of one to ten - rise steadily with income.

On the other hand, their reported quality of emotional daily experiences(their reported experiences of joy, affection, stress, sadness, or anger) levels off after a certain income level (approximately \$75,000 per year);

income above \$75,000 does not lead to more experiences of happiness nor to further relief of unhappiness or stress. Below this income level, respondents reported decreasing happiness and increasing sadness and stress, implying the pain of life's misfortunes, including disease, divorce, and being alone, is exacerbated by poverty.^[11] The term quality of life is also used by politicians and economists to measure the livability of a given city or nation. Two widely known measures of livability are the Economist Intelligence Unit's quality-of-life index and Mercer's Quality of Living Reports. These two measures calculate the livability of countries and cities around the world, respectively, through a combination of subjective life-satisfaction surveys and objective determinants of quality of life such as divorce rates, safety, and infrastructure. Such measures relate more broadly to the population of a city, state, or country, not to individual quality of life. Some crimes against property (e.g., graffiti and vandalism) and some "victimless crimes" have been referred to as "quality-of-life crimes." American sociologist James Q. Wilson encapsulated this argument as the Broken Window Theory, which asserts that relatively minor problems left unattended (such as litter, graffiti, or public urination by homeless individuals) send a subliminal message that disorder in general is being tolerated, and as a result, more serious crimes will end up being committed (the analogy being that a broken window left broken shows an image of general dilapidation). Wilson's theories have been used to justify the implementation of zero tolerance policies by many prominent American mayors, most notably Oscar Goodman in Las Vegas, Richard Riordan in Los Angeles, Rudolph Giuliani in New York City and Gavin Newsom in San Francisco. Such policies refuse to tolerate even minor crimes; proponents argue that this will improve the quality of life of local residents. However, critics of zero tolerance policies believe that such policies neglect investigation on a case-by-case basis and may lead to unreasonably harsh penalties for crimes.

IV. RESEARCH PURPOSE

The main purpose of research is, improving life quality in studied area. So has been codified 5 theories. They are:

- [1] There are difference physical disorders in Boroujerd districts.
- [2] There are difference anxiety disorders in Boroujerd districts.
- [3] There are difference social functional disorders in Boroujerd districts.
- [4] There are, depress disorders in Boroujerd districts.
- [5] There is difference mental health in Boroujerd districts.

Research method : This research is applied. Research method is "descriptive – analytical". Data collected is field. At first, was determined by using kukran method. The sample size is 384 people. In order to using from (GHQ-28) questionnaire (Human, 2005: 131). In this research was evaluated urban quality of Boroujerd city. In order to analyzing of data was used some technique such as: SPSS, Pierson correlation, T test, T Kendall, regression and keroskal. Also, was used questioner for determining sample size . The results shows, there is oriented relation between location and health of residents. Indeed, there is appropriate condition of life quality in welfare location. On the other hand, the most disorder between residents was stress that decreased urban life quality.

Studied area : The studied area is 17 of Broujerd district. Borujerd is a city in and capital of Borujerd County, Lorestan Province in western Iran. At the 2006 census, its population was 227,547 in 59,388 families. Among the existing modern cities in Iran, Borujerd is one of the oldest reported at least since the 9th century. In Sassanid Empire, Borujerd was a small town and region neighboring Nahavand. Gaining more attention during Great Seljuk Empire in the 9th and 10th centuries, Borujerd stood as an industrial, commercial and strategic city in Zagros Mountains until the 20th century. In its golden ages, Borujerd was selected as the state capital of Lorestan and Khuzestan region during Qajar dynasty in the 18th and 19th centuries. Today, Borujerd is the second largest city of Lorestan; hence, the major industrial, tourist and cultural center of the region. The city has kept its old architecture and lifestyle mostly through mosques, bazaars and houses built in the Qajar era. Borujerd city is located approximately 1670 meters above sea level and has a moderate climate with cold winters. The highest point is Garrin Mountain 3623 m above sea level and the lowest area is Gel Rood River in South with 1400 m elevation. Borujerd Township has 2600 km² area with approximately 400,000 inhabitants distributed in the city of Oshtorinan and more than 180 villages. Borujerd is located on Silakhor Plain which is the largest agricultural land of Lorestan. The high-elevated Zagros Mountains surround it from South East to North West and the peaks are covered with snow most of the times. Rural people work in farms or keep their domestic animals. Other people work in governmental offices, armed forces, factories or small local businesses. The feet of Zagros Mountains is a great destination for nomads and many Lurs and Bakhtiari nomads move there in summer. The area is paved with highways and is a crossroad between Tehran and Khuzestan Province

as well as Isfahan Province and Kermanshah Province.



Figure 1: Lorestan province

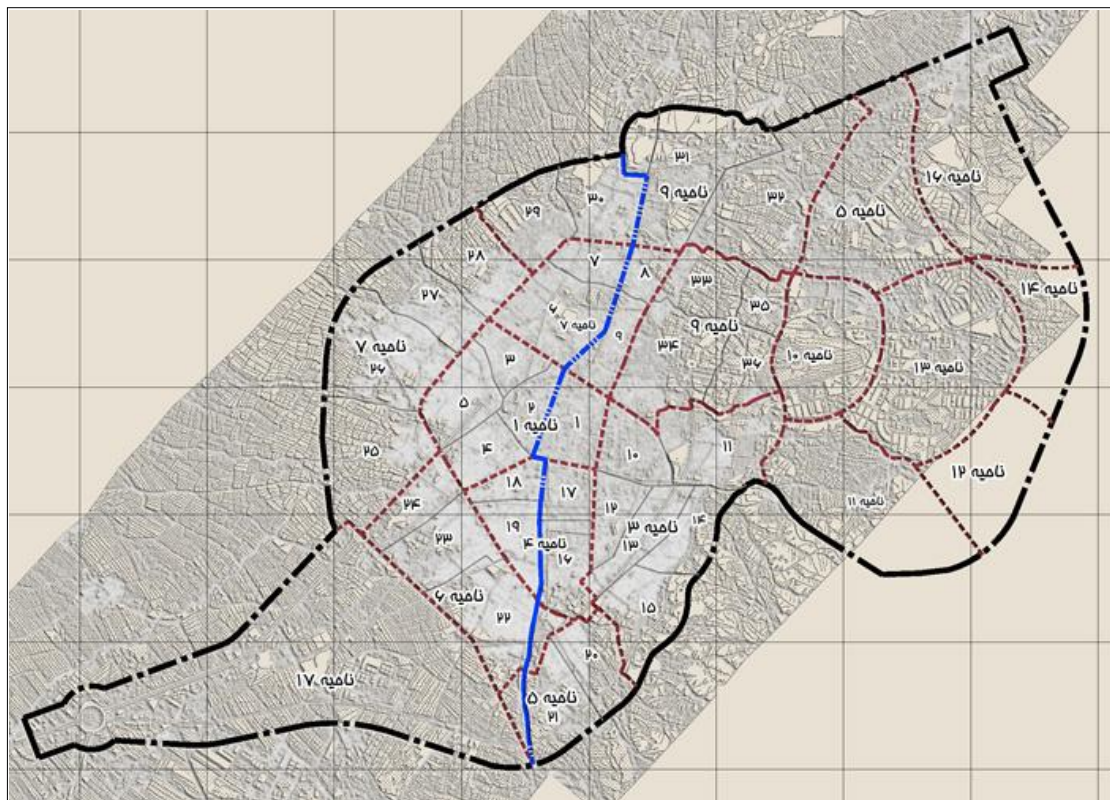


Figure 2: Borujerd city

V. FINDINGS RESEARCH

According to mentioned explanation was considered theories. They are:

H0- There isn't difference physical disorders in Boroujerd districts.

H1- There is difference physical disorders in Boroujerd districts.

Average	Districts	Average	Districts
162.10	10	173.1	1
143.25	11	178.8	2
297.30	12	176.56	3
63.00	13	151.9	4
358.50	14	269.4	5
132.73	15	256.03	6
66.75	16	250.04	7
290.33	17	113.59	8
		100.89	9
101.57	χ		
16	Freedom degree		
000	p		

Table 1: keroskal test for comparing physical disorders in various districts

Based on table 1, amount of "p" has been less than 0.01 ($p < 0.01$). So, the H0 theory was false and H1 theory was true. According to above table the most of physical disorders was in 14 of district.

H0: There aren't difference anxiety disorders in Boroujerd districts.

H1: There are difference anxiety disorders in Boroujerd districts.

Average	Districts	Average	Districts
74.5	10	168.8	1
82.75	11	161.4	2
258.6	12	195	3
100	13	137.90	4
321	14	283.80	5
114.05	15	256.5	6
96.6	16	249.2	7
298.5	17	124.1	8
		93.3	9
110.4	χ		
16	Freedom degree		
000	p		

Table 2: keroskal test for comparing stress disorders in various districts

Based on table 2, amount of "p" has been less than 0.01 ($p < 0.01$). So, the H0 theory was false and H1 theory was true. According to above table the most of stress disorders was in 14 of district.

H0: There aren't difference social functional disorders in Boroujerd districts.

H1: There are difference social functional disorders in Boroujerd districts.

Average	Districts	Average	Districts
52.60	10	188	1
147.2	11	180.2	2
208.4	12	185.14	3
83.83	13	172.5	4
219	14	286.1	5
124.3	15	249	6
33.38	16	246.3	7
261.5	17	108.3	8
		82.1	9
105.7	χ		
16	Freedom degree		
0	p		

Table 3: keroskal test for comparing social functional disorders in various districts

According to table 3, amount of "p" has been less than 0.01 ($p < 0.01$). So, the H0 theory was false and H1 theory was true. According to above table the most of social functional disorders was in 5 of district.

H0: There aren't, depress disorders in Boroujerd districts.

H1: There are, depress disorders in Boroujerd districts.

Average	Districts	Average	Districts
102.3	10	171.8	1
98.7	11	152.9	2
239.1	12	176.3	3
82.5	13	132.7	4
273.5	14	308.9	5
154.7	15	268.5	6
150.5	16	268.9	7
331	17	82	8
		84.3	9
157.7	χ		
16	Freedom degree		
0	p		

Table 4: keroskal test for comparing depress disorders in various districts

According to table 4, amount of "p" has been less than 0.01 ($p < 0.01$). So, the H0 theory was false and H1 theory was true. According to above table the most of depress disorders was in 17 of district.

H0: There isn't difference mental health in Boroujerd districts.

H1: There is difference mental health in Boroujerd districts.

Average	Districts	Average	Districts
86.4	10	174.1	1
101.7	11	163.3	2
260.4	12	182	3
72.8	13	140	4
324	14	303	5
118	15	267.7	6
80.3	16	251.2	7
304	17	94.5	8
		78.7	9
147	χ		
16	Freedom degree		
0	p		

Table 5: keroskal test for comparing mental health in various districts

According to table 5, amount of "p" has been less than 0.01 ($p < 0.01$). So, the H_0 theory was false and H_1 theory was true. According to above table the most of mental health was in 14 of district.

VI. DISCUSSION

Last years in Iran, don't achieve sustainable cities especially in small & middle cities such as borujerd due to development of cities with out regard improving urban life quality. In different section of cities exist problems such as air pollution, terrific, shortage of green spaces. Appropriate planning & effective management for improving urban life quality are necessary for eliminating these problems. Effective management is led to promotion of humane life quality in cities. As the major function of cities is to provide places for people to trade, produce, communicate and live, the urban environment needs to be assessed from a very specific human perspective: to provide an agreeable place to live while minimizing or balancing negative side effects. Quality of life in cities relies on a range of components such as social equity, income and welfare, housing, a healthy environment, social relations and education. The environmental elements of good quality of life include good air quality, low noise levels, clean and sufficient water, good urban design with sufficient and high-quality public and green spaces, an agreeable local climate or opportunities to adapt, and social equity. However, urban-specific data are patchy in Europe and, due to different timescales and reporting methods, are seldom directly comparable. This volume synthesizes past and current, international research on the quality of urban life. It emphasizes the contributions of the urban environment to the overall well-being of residents living in urban areas ranging in scale from small cities and their hinterlands to metropolitan regions. The term urban environment refers to the socio-physical aspects of urban living ranging from individual dwellings and neighborhoods to public services (i.e. transportation, rubbish collection, etc.) to neighbors and community organizations. The work emphasizes not only perceptions of and behaviors within urban environments but the actual conditions to which individuals are responding. The research covers both the subjective and behavioral aspects of urban living as well as the objective conditions which drive them. Drawing on collaborative research with a broad group of researchers in a variety of settings around the world, the book incorporates theoretical and methodological approaches to the conceptualizing and measuring of quality of life. It covers research designs that are based on both the analysis and modeling of aggregate secondary data and on the collection, analysis and modeling of primary survey data on subjective urban quality of life.

REFERENCES

- [1] 1-Esfahani, MM (1384), health law, Qom University of Medical Sciences and Health Services
- [2] 2-Biyabangard, E. and F. Javadi (1383) Psychological health of adolescents and youth in Tehran, Journal of Social Welfare - Pages 127-144
- [3] 3- Javadi, F., 1382: Evaluation of the psychological health of people in Tehran 81 years, the Center of Research and Evaluation Program
- [4] Syed Hussaini, A. (1377), Principles of Mental Health, Mashhad University of Medical Sciences, Vol 1, p 45
- [5] 4 - Ozer, Em. Park, Mg. Paul, T. Brindis, CD. Irwine, CE (2003), America's
- [6] Adolescents: Are they healthy? San Francisco, CA, University of California, National Adolescent health information center.
- [7] 5- Slusky, RI. (2004). Decreasing high risk behavior in teens. A theater program
- [8] Empower students to research out to their peers, Health Care Exec, 19 (1):48-9
- [9] 6- Lindberg, LF. Biggest, S. Williams, S. (2000), multiple threat: the Concurrence
- [10] Of teen health risk behaviors, The Urban Institute.

Design and Performance Analysis of MIMO-DSSS System for 2.4 GHz ISM Band Wi-Fi Applications Using Microstrip Antennas

Harshal Nigam¹, Mithilesh Kumar²

^{1,2} Electronics Engineering Department, UCE, RTU, Kota, India

ABSTRACT: In this paper, compact antenna has been designed and implemented in a 2X2 Multiple-Input Multiple-Output (MIMO) system. The antennas are compact double-sided printed microstrip patch antennas and fed by a microstrip line designed for a frequency of 2.4 GHz used for industrial, scientific and medical (ISM) band applications. Polarization diversity of the two antennas is used to construct independent and uncorrelated signals on each antenna. The antennas are designed on CST Microwave studio simulation software with return loss less than -10dB, and the two antennas are combined as a single system forming a MIMO array of two antennas. Further, using the results from CST, MIMO-DSSS system has been implemented and a performance analysis of this system is done on MATLAB software. The performance of this system is studied using BPSK modulation and finally bit error rate is obtained. The paper details the implementation of the digital communication system along with the simulated and measured results. The system is designed for 802.11n Wi-Fi family of standards that has an operation frequency of 2.4 GHz but with MIMO system that offers an increased data rate.

KEYWORDS : Direct sequence spread spectrum (DSSS), Multiple-Input Multiple-Output (MIMO) system, industrial scientific and medical (ISM)

I. INTRODUCTION

Wireless Communications are evolving from pure telephony systems to multimedia platforms offering a variety of services. Future wireless systems should be flexible to match different constraints concerning data rate, delay, reliability and quality-of-service. Multiple input multiple output (MIMO) system multiplies the data rate throughput achievable in wireless communication [1], it optimizes the use of the transmission spectrum and power [2,3] by using MIMO, additional paths can be used to increase the capacity of a link [4]. The 2.4 GHz industrial, scientific and medical (ISM) band is largely license exempt band also the regulation is minimum and there is free access. It is used for many applications like cordless phones, wireless medical telemetry equipments and for Wi-Fi family of standards (802.11 a,b,g,n) which are the most widely known network bearer standards. The 802.11n standard was defined in October 2009, is becoming widely adopted. It uses 2.4 GHz or 5.8 GHz ISM band frequency, it is interoperable with 802.11b and uses 802.11g-like modulation, but with MIMO. There have been many reported work on antenna design at 2.4 GHz ISM band frequency as in[5][6].The MIMO array design of antennas has been reported for a frequency of 2.4 GHz, apart from this polarization diversity [7] antennas have also been designed, all these designs were implemented with a goal to achieve independent antenna arrays where the signals on the two antennas are uncorrelated and independent of each other, efforts [8–10] have been contributed to the reduction of mutual coupling between antennas. In this paper, a simple and compact planar antenna is designed that shows acceptable return loss for 2.4 GHz ISM band frequency. This antenna is further used in the design of a 2X2 MIMO system.

The basic aim of MIMO antenna design is to minimize the correlation between the multiple signals as in [11], to achieve compactness in MIMO systems, the use of pattern diversity as in [12,13], multimode diversity as in [14], and polarization diversity techniques as in [15] in conjunction with space diversity are discussed in the literature. In the present design, the orthogonal polarization concept is applied to the proposed multi slot patch antenna yielding better results in terms of return loss and mutual coupling. This MIMO system is further used to design a communication system using DSSS technique where encoding is done using BPSK modulation. The system is further analyzed for its performance analysis. The paper is organized as follows, Section II details the single antenna design analysis, and this antenna is further used in Section III to form a MIMO array. In Section IV the two antenna array is fed equally by a directional coupler. Section V details the design a compact 2X2 MIMO system. Section VI details the coding implementation of MIMO-DSSS system using the results from above sections and finally Section VII concludes the analysis of paper.

II. SINGLE ANTENNA DESIGN ANALYSIS

The antenna is designed on a substrate which is printed on both sides, on one side is the patch and other side is a ground plane. The patch is fed by a micro strip feed line. The geometry of the given antenna is illustrated in Figure 1. It is fabricated on a $76.8 \times 59.6 \text{ mm}^2$ substrate with a dielectric constant of 4.1 and a substrate thickness of 1.5 mm. The top patch of the substrate has dimension of $43.4 \times 29.8 \text{ mm}^2$ which is fed by a strip line having a width of 3 mm. The bottom patch of substrate is just a ground plane. The proposed antenna has been simulated by CST Microwave studio.

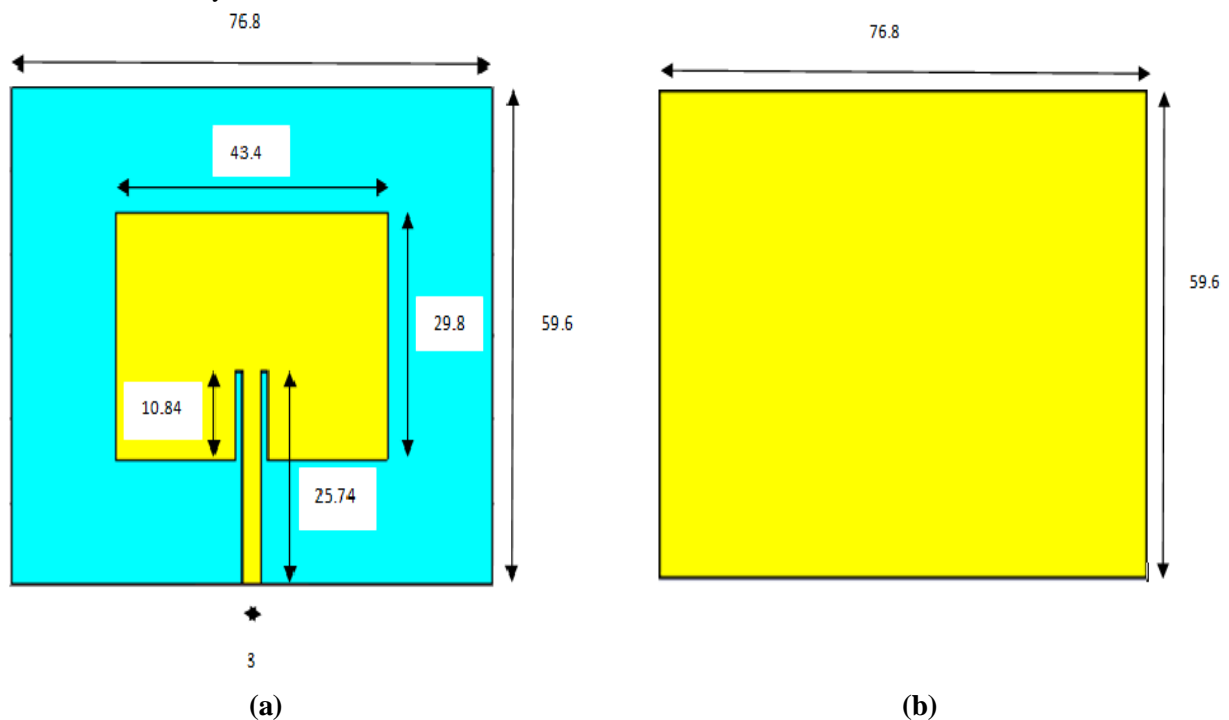


Figure 1. Geometry of the antenna with dimensions in mm (a) Top view (b) Bottom view

The simulation results of the antenna are shown in Figure 2, from the simulated graph it is observed that for frequency of 2.4 GHz, $S_{11} < -10\text{dB}$ showing a significant return loss.

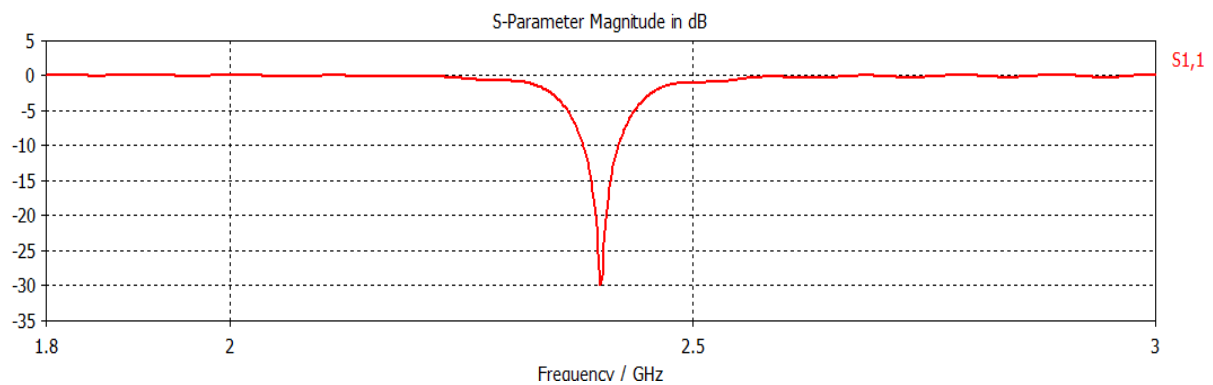


Figure 2. Simulated result of the single antenna

III. MIMO ARRAY DESIGN

The main criteria for MIMO system design is mutual coupling, which can be reduced by increasing the distance between the elements of the antennas. We can achieve less mutual coupling by diversity concept since miniaturization is the main task in the upcoming wireless devices, the mutual coupling can be mitigated more with the use of polarization diversity. In the design of our system to achieve orthogonal polarization, one antenna is rotated to 90° with respect to its adjacent element as shown in the Figure 3. The separation between the antennas is 7.12 mm which is 0.057λ . The antennas in the array have the same dimensions as mentioned in Section II. The antennas are mounted on a substrate symmetrically with $\epsilon_r = 4.1$, which in turn is mounted on a ground plane.

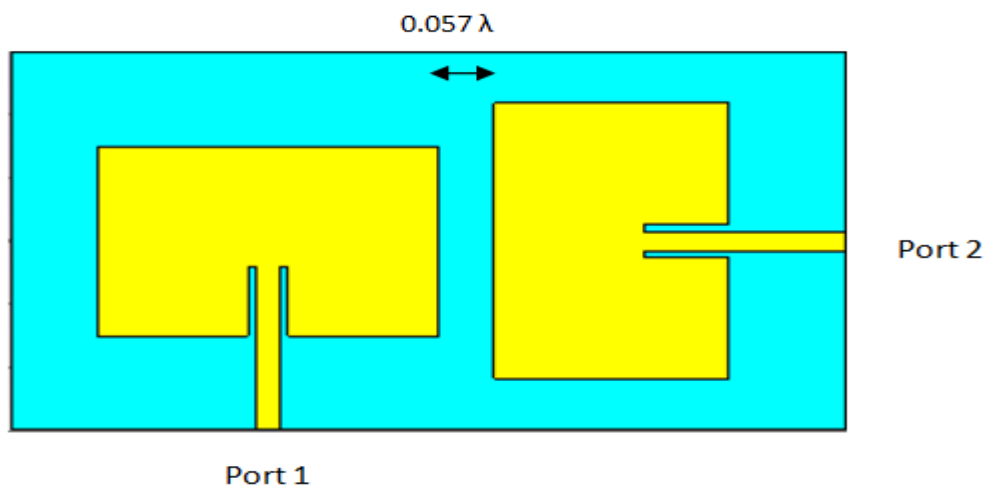


Figure 3. MIMO antenna array having two ports

The above two port system is simulated on CST Microwave Studio simulation software. We can see from the simulated results of Figure 4 that the two antennas are working independently of each other as seen from the S_{11} and S_{22} plots for the two antennas that both are working on the 2.4 GHz ISM band with a significant return loss, also the mutual coupling S_{12} and S_{21} between the two antennas is very low at this frequency.

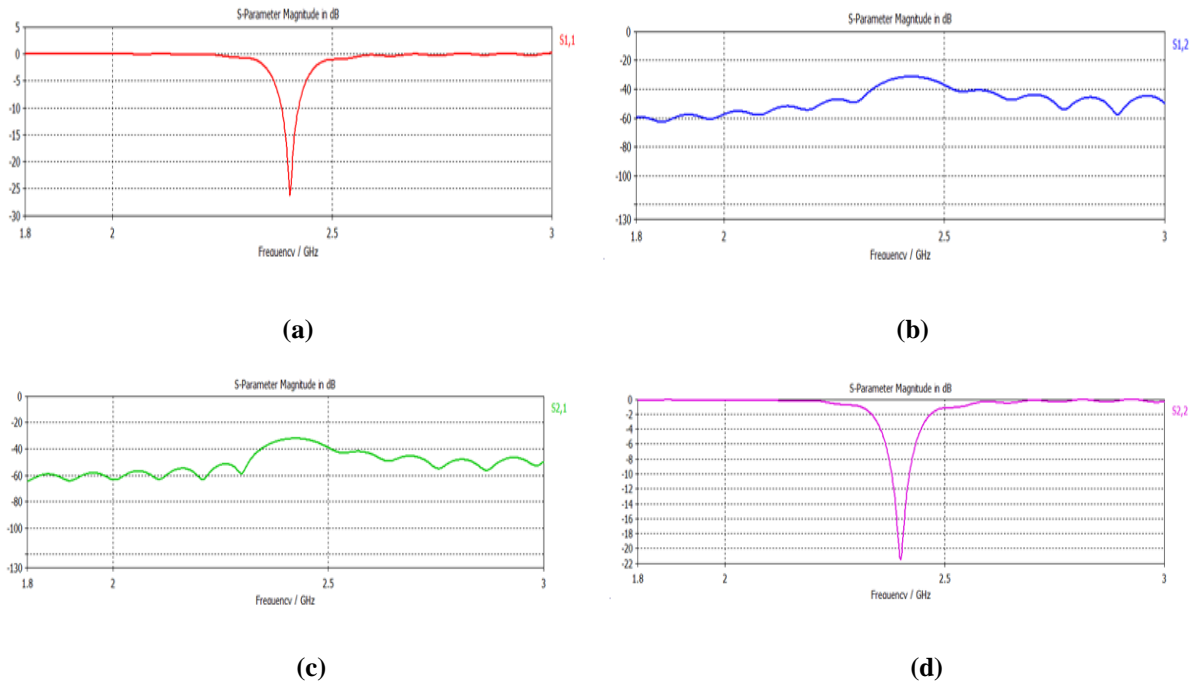


Figure 4. Plots for simulation of MIMO antenna array (a) S_{11} (b) S_{12} (c) S_{21} (d) S_{22}

We have also calculated the correlation coefficient and diversity gain for this two antenna array. The correlation coefficient is given by the formula as in (1)

$$\rho = \frac{|S_{11} \cdot S_{12} + S_{21} \cdot S_{22}|^2}{(1 - |S_{11}|^2 - |S_{21}|^2)(1 - |S_{22}|^2 - |S_{12}|^2)} \tag{1}$$

Using the values of S- parameters from the plots of Figure 4 at the 2.4 GHz frequency, the correlation coefficient comes out to be 0.001. The diversity gain is also calculated which is given by the formula as in (2)

$$DG = 10 * \sqrt{1 - (0.99 * \rho)^2} \tag{2}$$

Diversity gain comes out to be 9.9 dB. The values of correlation coefficient and diversity are in accordance that the antennas are working independently of each other and increase in signal to noise ratio due to diversity scheme is also significant respectively.

IV. FEEDING THE MIMO ARRAY

The MIMO array designed above has two antennas showing polarization diversity and are independent of each other, for a practical MIMO system there are two antennas on the transmitter side and two on the receiver side respectively separated by the same distance, also the two antennas should be fed equally with same phase Thus, in our case we will be using a directional coupler to feed the above two antennas respectively. A 3 dB directional coupler with four ports having design frequency of 2.4 GHz is designed, input is given from one port of the coupler, which is evenly divided between other two ports with a 90° phase shift between the outputs, also very little output is received at the isolated port. The isolated port is terminated by a matched load of 50 ohms. The coupler is as shown in Figure 5 along with the simulated results. The ratio of voltages between the output voltages at port 2 and port 3 with respect to the input port (port 1) is given by S_{21} and S_{31} respectively. This ratio will be utilized further in the channel matrix calculations.

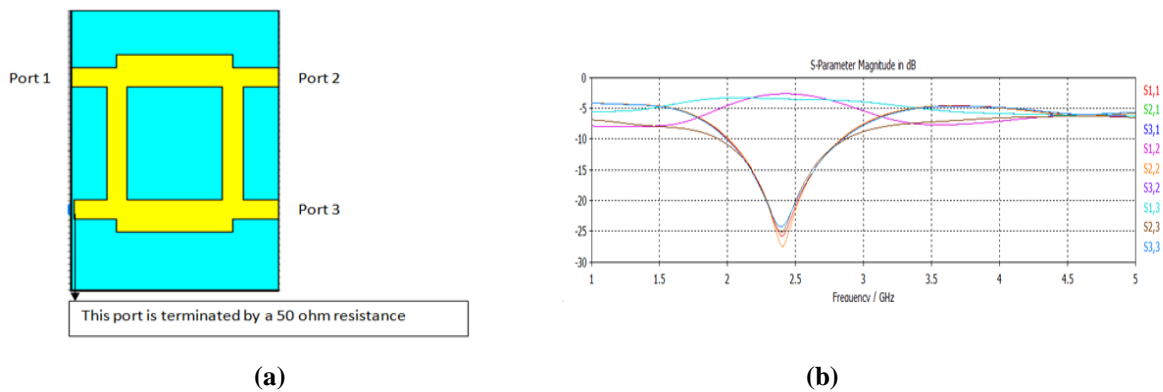


Figure 5. 3-dB directional coupler (a) Coupler design (b) Simulated result

To feed the two antennas with this coupler the feed lines from the output ports of coupler to the antennas are of different lengths such that the final input to the antennas is in phase. The antenna is as shown in Figure 6 along with the simulated result, we can see that $S_{11} < -10\text{dB}$ showing a significant return loss.

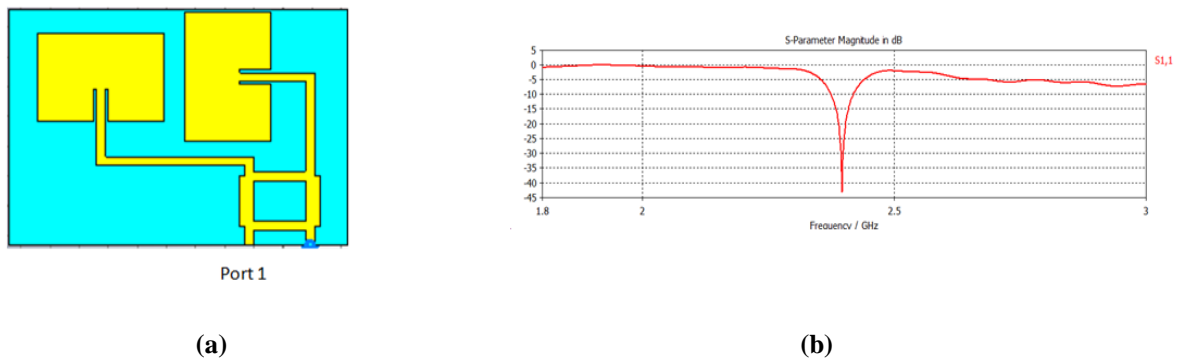


Figure 6. Compact MIMO antenna (a) antenna design (b) simulated result

The fabrication of the antenna was carried using the antenna substrate with dielectric constant of 4.1 and height 1.5 mm with microstrip line feed impedance of 50 ohms and ports of width 2.18mm. The testing of the fabricated design was done on vector network analyzer Rohde & Schwartz ZVB20 and calibrated using SOLT method. The photograph of the fabricated antenna is shown in Figure 7 along with the compared measured and simulated results in Figure 8 with the VNA screen output of measured results. We can see that there is a small difference in the two result which may be due to some measurement error or defects in hardware implementation.

V. 2X2 MIMO SYSTEM DESIGN

The two antenna system is fabricated as one system with a single port as discussed above, now the same antenna is fabricated again and the two antennas are kept separated with each other by a distance greater than the field distance taken to be 100 mm here and for this two port system S_{21} is measured. The design of the system having two ports is as shown in Figure 9 showing software design and practical design arrangement. The two antennas were first separated in the CST software environment and then in an actual scenario. Thus, we get two S parameters result for the software simulation and actual measurements respectively.



Figure 7. Photograph of fabricated antenna

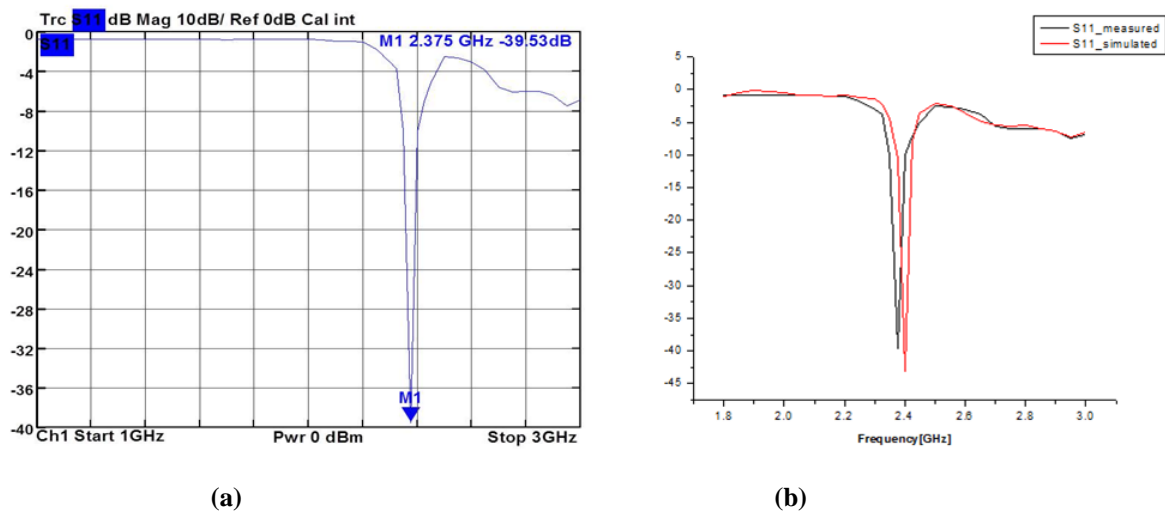
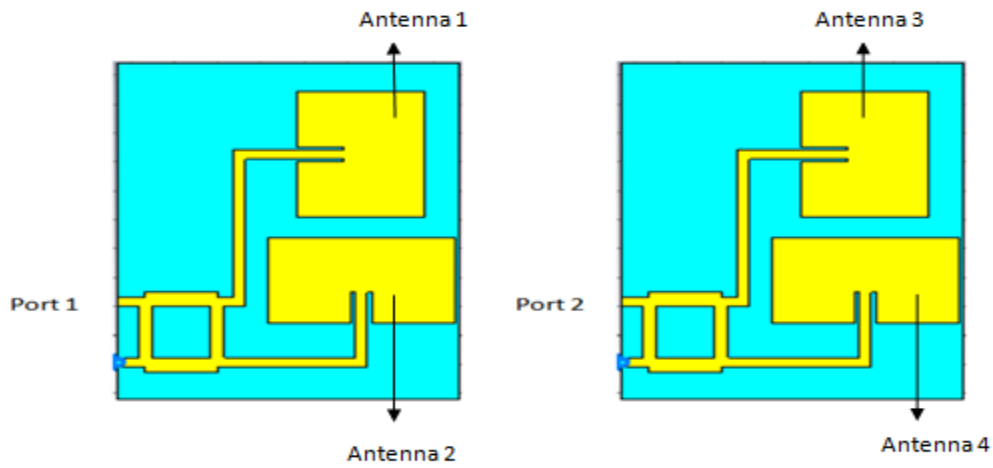


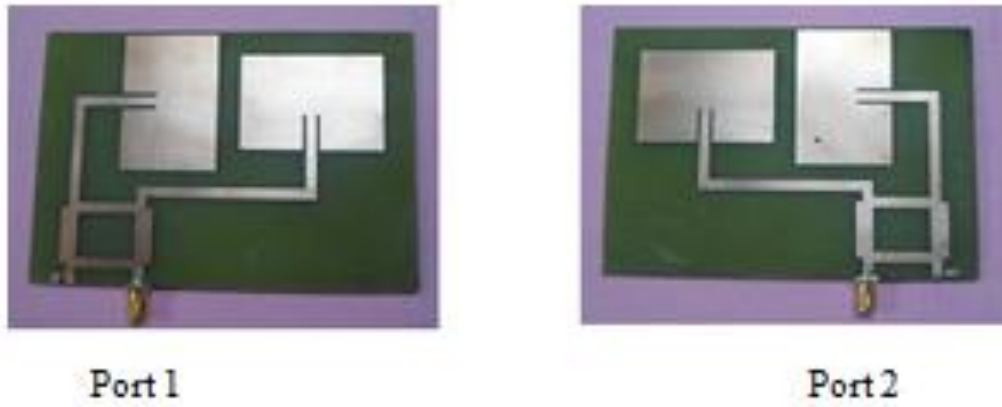
Figure 8. (a) VNA Screen Output (b) Compared measured and simulated results

which are shown compared in Figure 10. In the MIMO system of Figure 9 having four antennas number from 1-4. The channel matrix for the system will be given by (3) where V_{31} , V_{32} , V_{41} and V_{42} denote the ratio of voltages between antennas 3 and 1, 3 and 2, 4 and 1 and 4 and 2 respectively. Now, from the simulated S-parameter results of the coupler we know the ratio of voltages between different ports of the coupler, and from the simulated result of the 2 port MIMO system as in Figure 10 we know the ratio of voltages at port 1 and port 2 of the MIMO system of Figure 9. Using, these two ratios we can calculate V_{31} , V_{32} , V_{41} and V_{42} respectively thus we can obtain the channel matrix of the 2x2 system from (3).

$$H = \begin{bmatrix} V_{31} & V_{32} \\ V_{41} & V_{42} \end{bmatrix} \quad (3)$$



(a)



(b)

Figure 9. 2 port MIMO system (a) Software design (b) Practical Design

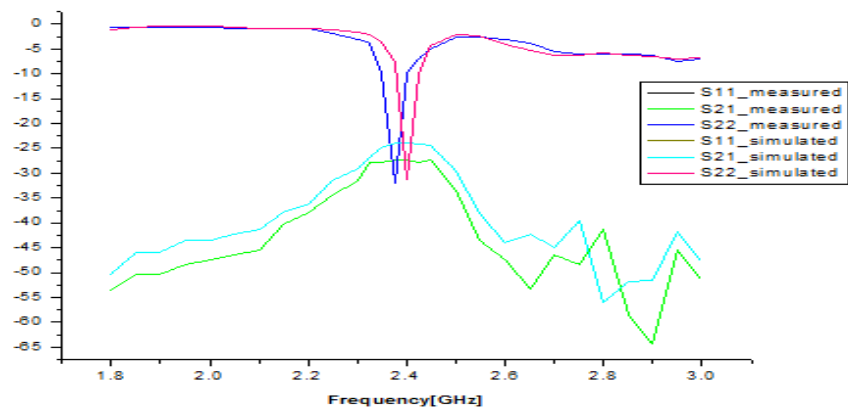


Figure 10. Comparison results for simulated and measured for 2X2 MIMO System

VI. MIMO-DSSS SYSTEM

DSSS is a technique where a signal is spread in a wider bandwidth using a spreading code. Here, the digital signal stream is combined with the spreading sequence bit stream using exclusive-OR. We incorporate coherent binary phase shift keying into the transmitter and receiver sections. The block diagram is as shown in Figure 11. We first generate random bits which are input to the system, then the incoming data stream is converted to a polar NRZ waveform $b(t)$ as shown in Figure 12 as the original bit sequence. The bit interval T_b for the bit sequence is taken to be 18 ns. Now, this data sequence is followed by two stages of modulation. The first one is where this data sequence is multiplied with a spreading code that is the pseudorandom bit sequence $c(t)$ as shown in Figure 12. The chip rate for this sequence T_c is taken to be 1 ns. The multiplied output sequence $b(t)*c(t)$ is as shown in Figure 12. This output sequence is then subjected to binary PSK modulator. The frequency of carrier used for BPSK modulation is 2.4 GHz. The transmitted signal is direct sequence spread binary phase shift keyed (DS-BPSK) signal as shown in Figure 12. The signal is then de-multiplexed into two separate streams and each stream is transmitted from an independent antenna. The channel matrix obtained from CST for a 2X2 system as obtained in previous section is used in coding the output from the 2X2 system with random noise added. This output is then followed by a BPSK demodulator using the same carrier as in the transmitting side and after this the sequence is multiplied by the pseudorandom code which is also the same as used at the transmitting side. The integration is carried out for the bit interval $0 \leq t \leq T_b$ providing a sample value and finally a decision is made at the receiver by doing a threshold detection. The output bits are compared to the input bits to evaluate the bit error rate (BER) at different signal to noise ratio. The channel matrix of the 2X2 system is taken both for software simulation and practical measurement and we get two plots for BER versus signal to noise ratio as shown in Figure 13. We can see that as the signal to noise ratio increase BER decreases and also for the measured system the BER is more as compared to the simulated one.

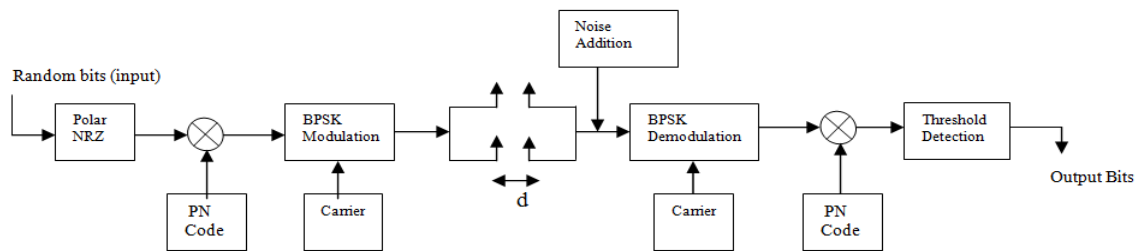


Figure 11. Block diagram for MIMO-DSSS system

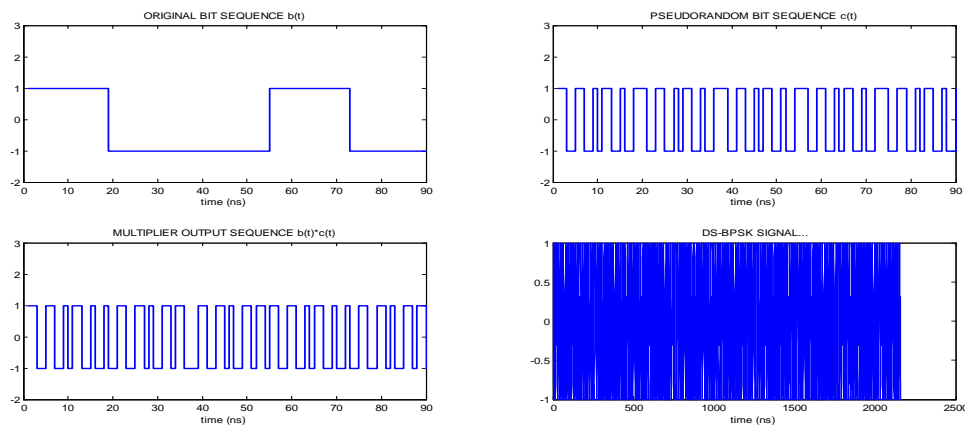


Figure 12. Waveforms for the digital communication system

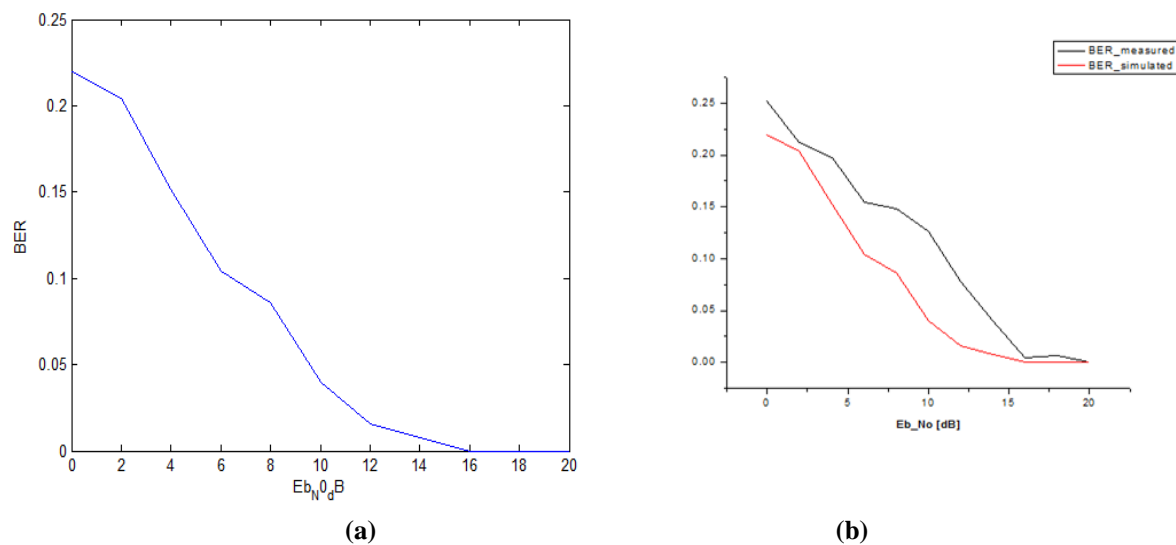


Figure 13. BER vs SNR (dB) (a) Simulated result (b) Compared result

VII. CONCLUSION

A new methodology has been defined to estimate the performance analysis of a 2X2 MIMO-DSSS system operating on 2.4 GHz ISM band frequency using practical antennas designed on CST Microwave studio, the two antennas in the array are working independently of each other and are fed with equally with same phase signals. The channel matrix from CST has been used for further coding DSSS-MIMO system instead of using a random channel matrix. The BER versus SNR curves are shown for the system, as expected the bit error rate decrease by increasing signal to noise ratio and also it can be seen that the measured BER values are coming higher than the simulated one. The system can be used for IEEE 802.11n Wi-Fi family of standards that uses 2.4 GHz ISM band frequency along with MIMO system using DSSS modulation technique.

REFERENCES

- [1] David Tse and Pramod Viswanath, Fundamentals of Wireless Communication, Cambridge University Press, 2005
- [2] Winters, J., On the capacity of radio communication systems with diversity in a Rayleigh fading environment, IEEE Journal on Selected Areas in Communications, Vol. 5, No. 5, 871-878, Jun. 1987.
- [3] Foschini, G. J. and M. J. Gans, On limits of wireless communications in a fading environment when using multiple antennas, Wireless Personal Commun., Vol. 6, No. 3, 311-335, Mar. 1998.
- [4] Concepcion Garcia-Pardo, Jose-Maria Molina-Garcia-Pardo, Jose-Victor Rodriguez, and Leandro Juan Llacer, MIMO capacity in UWB channels in an office environment for different polarizations, Progress In Electromagnetics Research C, Vol. 44, 109-122, 2013.
- [5] Sudip Kumar Murmu and Iti Saha Misra, Design of V-shaped microstrip patch antenna at 2.4 GHz ,Microwave and Optical Technology Letters Volume 53, Issue 4, pages 806–811, April 2011
- [6] Mahdi Moosazadeh and Zahra Esmati, Small Planar Dual-Band Microstrip-Fed Monopole Antenna for Wireless Local Area Network Applications Using Slotted Conductor-Backed Plane, Microwave and Optical Technology Letter Volume 55, Issue 10, pages 2380–2383, October 2013.
- [7] Zied Charaabi and Marc Testard ,Optimized WiMAX MIMO antenna for base station applications with polarization and spatial diversity, Bell Labs Technical Journal Volume 16, Issue 1, pages 217–234, June 2011.
- [8] Dau-Chyrh Chang, Yi-Jhen Li, and Chao-Hsiang Liao, Antenna array for IEEE 802.11/a/b MIMO application, PIERS Proceedings, 100-102 Moscow, Russia, August 19-23, 2012.
- [9] N.S. Awang Da, M. R. Dzulkifli, and M. R. Kamarudin, Polarization diversity monopole antenna , PIERS Proceedings, 466-469 Cambridge, USA, July 5-8, 2010.
- [10] Khaleghi,A., Diversity techniques with parallel dipole antennas: radiation pattern analysis, Progress In Electromagnetics Research, PIER 64,23–42,2006.
- [11] Emami-Forooshani, S. Noghianian, Semi-deterministic channel model for MIMO systems Part-II: results, IET microwaves, antennas & propagation, Vol.4 pp 26-34 2010.
- [12] Matilde Sanchez-Fernandez, Eva Rajo-Iglesias, Oscar Quevedo-Teruel, M. Luz Pablo-Gonzalez. Spectral Efficiency in MIMO Systems Using Space and Pattern Diversities Under Compactness Constraints, IEEE T 1637-1645, May 2008.
- [13] Mukherjee and Hyuck M. Kwon. Compact Multi-user Wideband MIMO System Using Multiple-Mode Microstrip Antennas, Proceedings of Vehicular Technology Conference Spring 2007, pp 584-588, Apr 2007.

- [14] Waldschmidt, C. Kuhnert, S. Schulteis, and W. Wiesbeck, Compact MIMO-Arrays Based on Polarization-Diversity, Proceedings of IEEE Antennas and Propagation. Symp., Vol.2 , pp. 499-502, June 2003.
- [15] M. A. Jensen, J. W. Wallace, A review of antennas and propagation for MIMO wireless communications, IEEE Trans. Antennas Propagation., Vol. 52, pp. 2810-2824, Nov. 2004.
- [16] Chien-Ching Chiu, Min-Hui Ho and Shu-Han Liao, MIMO-UWB smart antenna communication characteristics for different antenna arrays of transmitters, International Journal of RF and Microwave Computer-aided-Engineering, Volume 23, Issue 3, May 2013, Pages: 378–392,
- [17] A. R. Mallahzadeh, S. Eshaghi and H. R. Hassani, Compact U-array MIMO antenna designs using IWO algorithm, International Journal of RF and Microwave Computer-aided-Engineering, Volume 19, Issue 5, September 2009, Pages: 568–576

Analyzing of spatial-physical structure of urban spaces by using SWOT & GIS techniques (Case study: Borujerd historic bazaar)

¹Fatemeh Olfaty, ² Mahdi Garavand

¹Department of Art and Architecture, Science and Research branch, Islamic Azad University, Boroujerd, Iran

²Department of Art and Architecture, Science and Research branch, Islamic Azad University, Boroujerd, Iran

ABSTRACT : In recent decade, have been changed urban physical and social conditions. Today, historic Bazaar has lost previous function in our cities. Considering numerous problems related to the old textures, sustainable development can be mentioned as the most efficient approach to avoid consequent shortcomings. This research is applied. Also, method of research is "descriptive – analytical", and data collection method is "document –field". The data are generally gathered from academic centre libraries like universities, organizations, institutes and research centers such as management and planning organization and internet, official statistics and censuses, urban development plans by consulting engineers, and so on. Statistic society is citizens and city of Borujerd. At first by presentation of theoretical framework and by using models such as SWOT technique. After that was used from GIS software.

KEY WORD: bazaar, spatial spaces, SWOT technique, borujerd city

I. INTRODUCTION

Bazaar is a permanent merchandizing area, marketplace, or street of shops where goods and services are exchanged or sold. Originating from ancient Islamic civilizations, the bazaar is the precursor for the modern day supermarket, flea-market, and shopping mall, and has had a great influence on the economic development and centralization in modern cities around the world. The bazaar first appeared along the important trade routes. The constant flow of foreign and exotic goods, along with travelers, gave rise to systems of haggling and trade within the cities themselves. Special areas of cities were eventually designated as areas of trade, and the first bazaars were established. Bazaars rapidly became areas not just for the trading of goods, but were often the social, religious, and financial centers of cities. With their continuing connection to the religious aspects of life through the presence of mosques in the close vicinity, and their attraction to tourists, bazaars have retained more of a historical and local identity than the Western mall. The bazaar has a long history and has served all segments of society well; it continues to develop and modernize externally, retaining its internal character and purpose, it maintains its place in modern society (Moshaver zadeh, 2009:9). The word bazaar derives from the Persian word *bāzār*, the etymology of which goes back to the Pahlavi word *baha-char* meaning "the place of prices". During the time of the Crusades, when Europe and the Middle East had their first major encounters and cultural dissemination took place, the word was assimilated into Italian as *bazzara*, before being transferred to English in its current form, *bazaar*. While currently the word is most often used to denote outdoor shopping areas, particularly those of Islamic origins, the word is sometimes used loosely to refer to such places and events as flea markets or swap-meets (Azizi, 2009:89).

II. THEORETICAL PRINCIPLE

The bazaar first appeared in the Middle East, around the fourth century. At the time, the area was often at the axis of many important trade routes, which helped establish cities and ports. A constant flow of foreign and exotic goods, along with travelers, gave rise to systems of haggling and trade within the cities themselves. Special areas of cities were eventually designated as areas of trade, and the first bazaars were established. A strong economy has always been an Islamic ideal, so the bazaars were incorporated and actively fostered when the Islamic conquest swept over the region (Ziari, 2008:90).

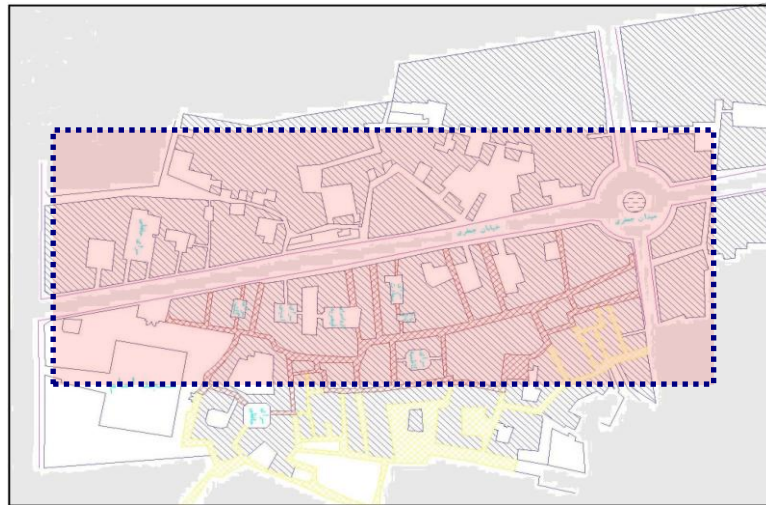
A bazaar, meaning "market"; from Middle Persian (*bahā-chār*), meaning "place of prices") is a permanent enclosed merchandising area, marketplace, or street of shops where goods and services are exchanged or sold. (A *souq*, by contrast, is an open-air marketplace or commercial quarter.) The term is sometimes also used to refer to the "network of merchants, bankers, and craftsmen" who works that area (Baqerian, 2009:34). Although the current meaning of the word is believed to have originated in Persia, its use has spread and now has been accepted into the vernacular in countries around the world. The rise of large bazaars and stock trading centers in the Muslim World allowed the creation of new capitals and eventually new empires. New and wealthy cities such as Isfahan, Golconda, Samarkand, Cairo, Baghdad, and Timbuktu were founded along trade routes and bazaars (Nouri ,2008 :82).

Bazaars became areas not just for the trading of goods, but were often the social, religious, and financial centers of cities. Mosques and coffee shops were often incorporated into established bazaars, as were forms of street entertainment. The idea of a bazaar was carried along trade routes, to east in areas of modern day Afghanistan, Pakistan, India and certain areas in South-East Asia, North to modern day Turkey, Hungary and sporadically into areas of Central Asia. However, the major world bazaars continued to be found in Middle Eastern states, as they still are today (Bernroider,2002 :12) .Many languages have names for this concept, including Arabic and Urdu: Albanian, Bosnian and Turkish: *pazar*, Bengali: Bulgarian and Macedonian: *пазар*, Cypriot Greek: *pantopoula*, Greek: Hindi: Hungarian: *vásár* (term originates from Persian influence around the 7th-8th century and means a regular market, but special occasion markets also exist, such as *Karácsonyi Vásár* or "Christmas Market", and *bazár* or Oriental-style market or shop, the term stemming from Turkish influence around the 16th-17th century), Indonesian and Malay: *pasar*, Polish: *bazar*, Russian: *базар* and Uzbek: *bozor* (Navabakhsh ,2008 :51) .In North America and the United Kingdom, the term can be used as a synonym for a "rummage sale", to describe charity fundraising events held by churches or other community organizations in which either donated used goods (such as books, clothes, and household items) or new and handcrafted (or home-baked) goods are sold for low prices, as at a church or other organization's Christmas bazaar, for example (Mahdizadeh ,2003 :32) .

III. RESEARCH METHOD

This research is applied. Also, method of research is "descriptive – analytical", and data collection method is "document –field". The data are generally gathered from academic centre libraries like universities, organizations, institutes and research centers such as management and planning organization and internet, official statistics and censuses, urban development plans by consulting engineers, and so on. Statistic society is citizens and city of Borujerd. At first by presentation of theoretical framework and by using models such as SWOT technique. After that was used from GIS software.

Studied area :The studied area is 17 of Borujerd district. Borujerd is a city in and capital of Borujerd County, Lorestan Province in western Iran. At the 2006 census, its population was 227,547 in 59,388 families. Among the existing modern cities in Iran, Borujerd is one of the oldest reported at least since the 9th century. In Sassanid Empire, Borujerd was a small town and region neighboring Nahavand. Gaining more attention during Great Seljuk Empire in the 9th and 10th centuries, Borujerd stood as an industrial, commercial and strategic city in Zagros Mountains until the 20th century. In its golden ages, Borujerd was selected as the state capital of Lorestan and Khuzestan region during Qajar dynasty in the 18th and 19th centuries. Today, Borujerd is the second largest city of Lorestan; hence, the major industrial, tourist and cultural center of the region. The city has kept its old architecture and lifestyle mostly through mosques, bazaars and houses built in the Qajar era. Borujerd city is located approximately 1670 meters above sea level and has a moderate climate with cold winters. The highest point is Garrin Mountain 3623 m above sea level and the lowest area is Gel Rood River in South with 1400 m elevation. Borujerd Township has 2600 km² area with approximately 400,000 inhabitants distributed in the city of Oshtorinan and more than 180 villages. Borujerd is located on Silakhor Plain which is the largest agricultural land of Lorestan. The high-elevated Zagros Mountains surround it from South East to North West and the peaks are covered with snow most of the times. Rural people work in farms or keep their domestic animals. Other people work in governmental offices, armed forces, factories or small local businesses. The feet of Zagros Mountains is a great destination for nomads and many Lurs and Bakhtiari nomads move there in summer. The area is paved with highways and is a crossroad between Tehran and Khuzestan Province as well as Isfahan Province and Kermanshah Province.



IV. FINDINGS RESEARCH

According to mentioned explanation, for analyzing data was used GIS. So has been explained in continue.

5.1. Physical analyzed in Bazaar

5.1.1. Land-uses area : Based on results, the residential land –use has been the most land –use in studied area (27%). On the other hand the religious and cultural land-uses have been the least area (1.3%, 1.2%). One of weakness of historic fabric was the lake of cultural land-use due to one of the main indicators of Bazaar in Islamic country such as Iran. Mosque was important building in Bazaar. On the other hand cultural land-use is importance because historic fabric attract tourism industry .

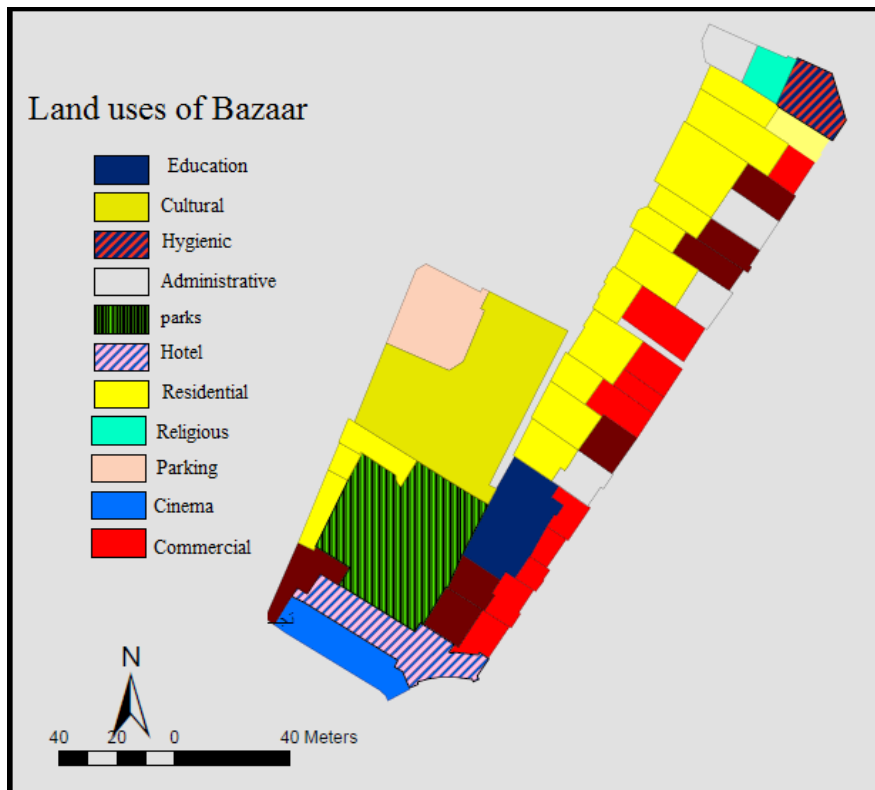


Figure2: exited land-uses plan

Land use	Area (m ²)	Percentage
residential	3786	27
Commercial	3237	23
parking	806	5.7
education	800	5.7
Administrative	905	6.4
hygienic	405	2.7
cultural	241	1.3
Tourism	1436	11
Religious	215	1.2
Parks	2140	16

Table 1: the area of land-uses (m²)

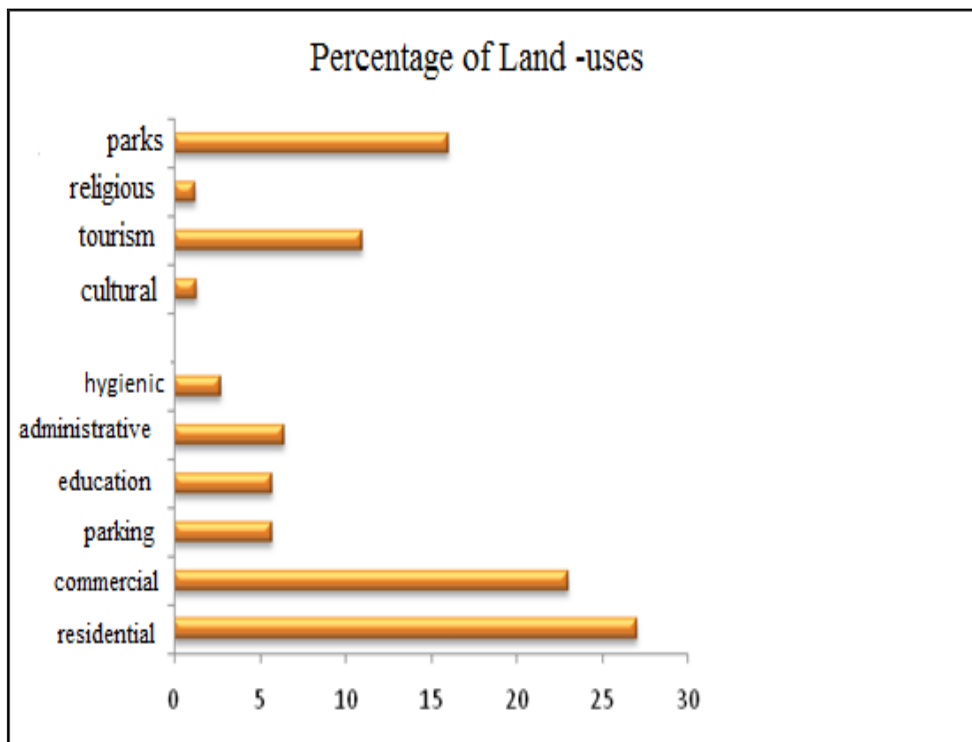


Figure 3: the percentage of land-uses

5.1.2. Antiquity of building

According to analyzed studied, 61% of building were 10-25 years. Also 30% of buildings were more than 30 years. So, 91% of buildings were outdated. Also, 9% of buildings were 6-10 years.

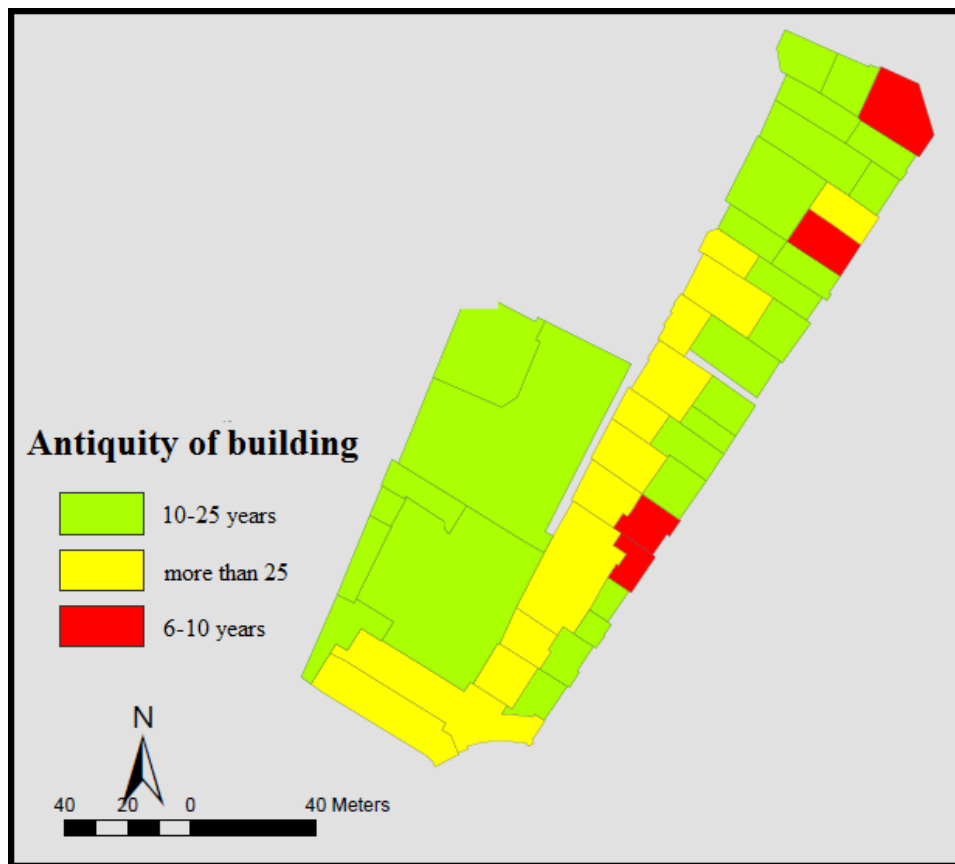


Figure 4: building antiquity of Bazaar plan

building antiquity	Area (m ²)	Percentage
6-10 years	1005	9
10-25 years	10886	61
More than 25 years	4675	30

Table2: percentage of building antiquity

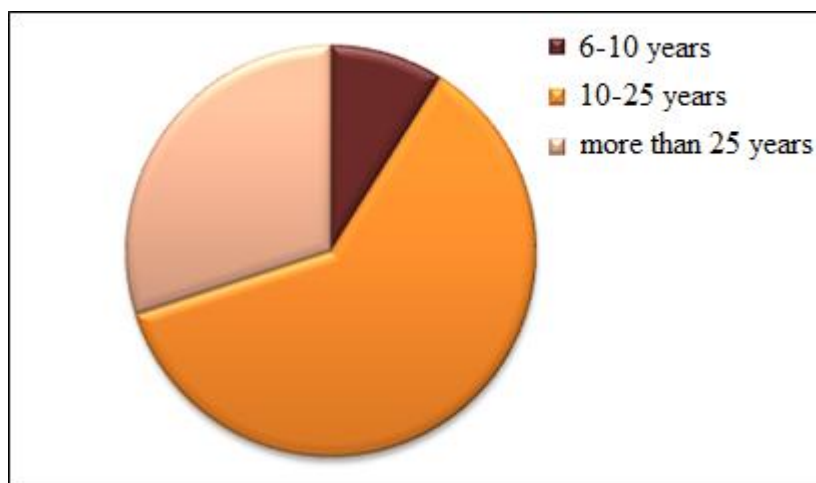


Figure 5: Antiquity of building

5.1.3. Material of building

Nearly 48% of buildings have been consisted break & iron. Also, 6.4% of building have been consisted Concrete. On the other hand, 13% buildings have been consisted of from unstable materials such as: wood. Thus, should be regarded to material in old fabric.

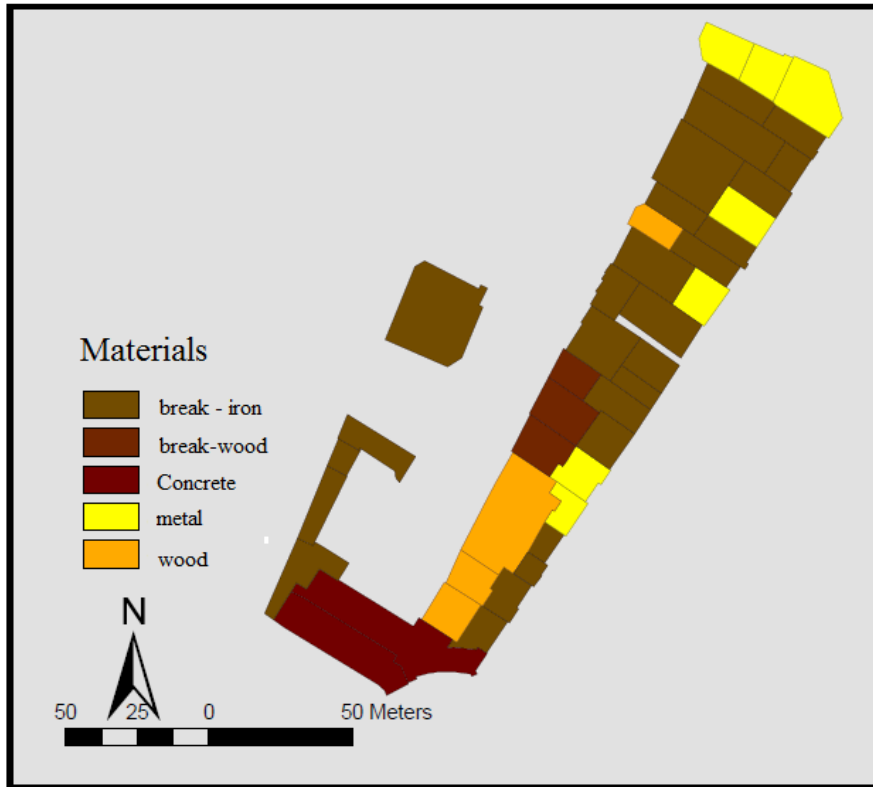


Figure 6: building materials plan

Materials	Area (m ²)	Percentage
Break-iron	6575	48
Break-wood	728	9.6
Concrete	1437	6.4
Metal	1668	22.5
Wood	1375	12.9

Table3: building materials (percentage %)

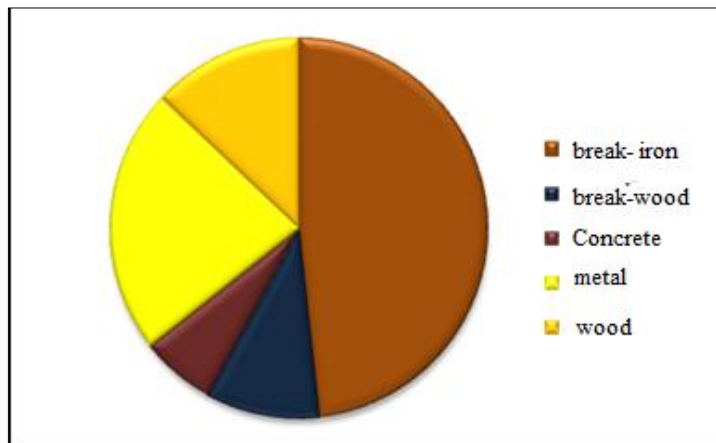


Figure 7: building materials

5.1.4. Building quality

In studied area, 9% of buildings is making now (newly building). 61 % of building had been tenability. But 6% of them were old and destruction. Although, 61% of them were tenability, but new and modern buildings were low. This issue didn't appropriate for important fabric in city .

Building quality	Area (m ²)	Percentage
Old	1648	6.8
Tenability	10886	61.3
destruction	1217	6.8
New	1005	9

Table3 Building quality (percentage %)

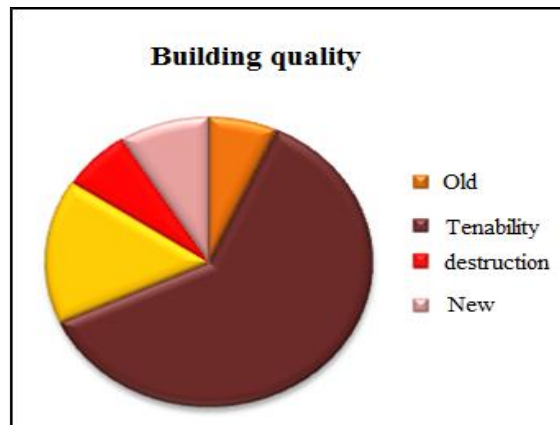


Figure 8: building materials

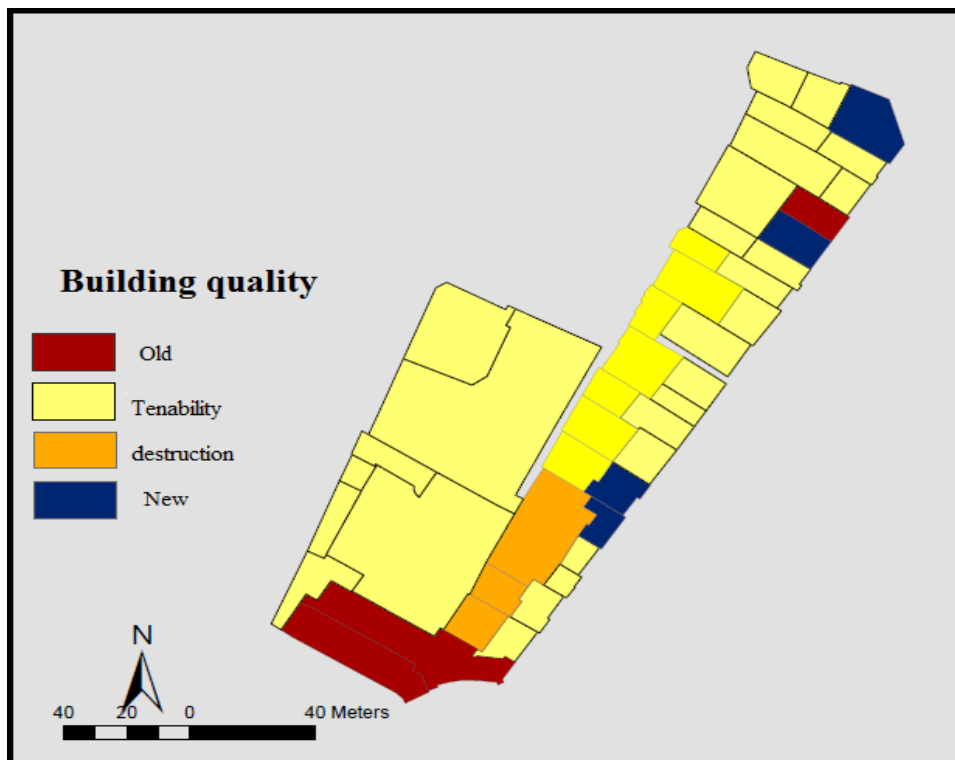


Figure 9: Buildings quality plan

V. Codification of goals, strategies policies implementation

After analyzing data that was used from GIS software, was planned in order to improving physical quality of borujerd bazaar. So, were codified strategies and goals in order to improving bazaar condition.

Micro problems	Problems
<ul style="list-style-type: none"> - there is informal construction in studied area - there isn't harmonic development in studied area - there is traffic problem in center of city due to bazaar location - there isn't parking in appropriate location - there is administrative centers in studied area - there isn't urban services and necessary per capita - there is narrow walkway and parking problems - there isn't appropriate cover walkway - there isn't appropriate urban landscape - there is social , environmental , viewpoint in neighborhood - there is inappropriate jobs around bazaar - inappropriate landscape in urban fabric in nearly land-uses 	<p>Physical & social problems in old fabric</p>

Table 4 : urban problems in bazaar

6.1. Codification of goals from problems

One of the main steps in urban planning, determining of problems. Also, after that determine goals based on problems. Table 5 shows classification of macro & micro goals according to problems.

Micro goals	Macro goals	Total
<ul style="list-style-type: none"> - improving urban viewpoint quality - preserving of liveability in public urban space - strengthening of urban spaces - creating of security in neighborhood - creating new construction - creating appropriate complex between new and old land-uses - improving new development according to old indicators - design based on natural disasters 	Updating old fabric	
<ul style="list-style-type: none"> - increasing resident participant and local organization - decreasing crime in old fabric - renovation social , historic , cultural in old fabric - preserving of population structure & improving life quality 	Preservation of old fabric as social & cultural welfare by emphasis on historic role	
<ul style="list-style-type: none"> - Preserving indicators and value of old fabric - updating old building - renovation of valuable spaces 	Renovation of historic identity	
<ul style="list-style-type: none"> - improving transport network - preventing from crowded area 	Improving transport system in old fabric	
<ul style="list-style-type: none"> - creating safe environmental - using from modern services - improving water surface 	Improving urban facilities and equipment	

Table 5: determining of goals from problems

SWOT technique :After analyzing of Tehran green spaces development was evaluated strategies by using SWOT technique. SWOT analysis (alternately SWOT Matrix) is a structured planning method used to evaluate the Strengths, Weaknesses, Opportunities, and Threats involved in a project or in a business venture. A SWOT analysis can be carried out for a product, place or person. It involves specifying the objective of the business venture or project and identifying the internal and external factors that are favorable and unfavorable to achieve that objective. The technique is credited to Albert Humphrey, who led a convention at the Stanford Research Institute (now SRI International) in the 1960s and 1970s using data from Fortune 500 companies.

Setting the objective should be done after the SWOT analysis has been performed. This would allow achievable goals or objectives to be set for the organization.

- Strengths: characteristics of the business, or project team that give it an advantage over others
- Weaknesses: are characteristics that place the team at a disadvantage relative to others
- Opportunities: *external* chances to improve performance (e.g. make greater profits) in the environment
- Threats: *external* elements in the environment that could cause trouble for the business or project

Identification of SWOT is essential because subsequent steps in the process of planning for achievement of the selected objective may be derived from the SWOT. First, the decision makers have to determine whether the objective is attainable, given the SWOT. If the objective is NOT attainable a different objective must be selected and the process repeated. Users of SWOT analysis need to ask and answer questions that generate meaningful information for each category (strengths, weaknesses, opportunities, and threats) in order to maximize the benefits of this evaluation and find their competitive advantage (Golkar, 2006 :89).

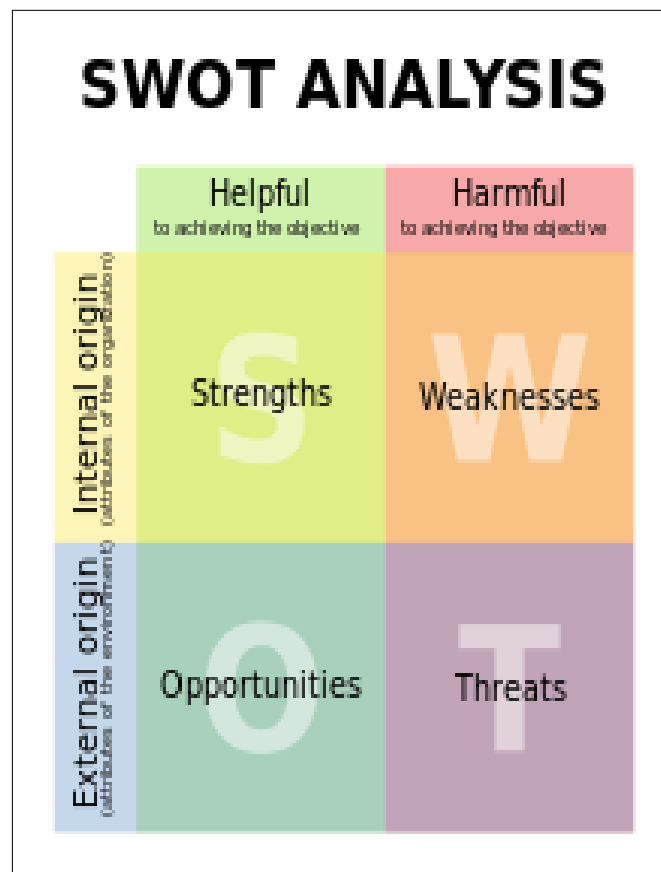


Figure (11): SWOT graph

Opportunities	Threats	Weaknesses	Strengths	Physical & social indicators
<ul style="list-style-type: none"> - there is native resident in old neighborhood - there is functional points in order to presenting to urban services - utilization of city according to natural condition , such as : other old cities 	<ul style="list-style-type: none"> - Unruly construction in old fabric - there is destroy fabric in studied area - there isn't harmonic development in studied area - there is traffic problem in center of city due to bazaar location - there is administrative centers in studied area - there is lack of urban services 	<ul style="list-style-type: none"> -there isn't parking in appropriate location - there isn't edge of valuable & proportion spatial - there is unstable building - there isn't appropriate access To houses 	<ul style="list-style-type: none"> - there is residential land-uses as the most area land-uses - appropriate composition of functional in studied area - there is participant residents in urban issues - there is important spaces in order to liveability in neighborhood - there is indicators of eligibility in studied fabric 	

Table 6: SWOT table of Bazaar

VI. STRATEGIES

In this research, was presented some strategies in order to improving urban life quality. On the other hand, old fabric in historic cities has special condition. Thus, could be improved urban life condition in current cities. The strategies are:

- [1] Respect to fabric identity
- [2] Regards, to local condition of studied area
- [3] Reformation transfer spaces
- [4] Improving parks and urban green spaces
- [5] Making eligibility of old fabric and urban spaces
- [6] Controlling terrific
- [7] Creating various land-uses in old fabric
- [8] Creating focal points in order to improving urban landscape
- [9] Connection indicators element trough view corridors

VII. RESULTS

Considering numerous problems related to the old textures, sustainable development can be mentioned as the most efficient approach to avoid consequent shortcomings. Fabric in borujerd, a city in the western part of Iran. By observing the social, economic, and environmental characteristics in the studied region, and by interviewing the residents in borujerd 's old textures, the SWOT analysis, the analysis of strengths, weaknesses, opportunities and threats using qualitative method, was adopted in order to detect the old textures. In this paper, efforts have been made to analyze the renovation of old urban textures as having in mind the sustainable development. To organize the old textures in borujerd, the SWOT type strategy was adopted from diverse strategies in this paper. The mentioned strategy mainly focuses on the internal strengths in order to eliminate the external threats. So, at finally some implementation policies are proposed.

They are:

- Renovation old bazaar in order to improving fabric quality
- Strengthening access axis in order to improving urban life quality
- Creating complex functional land-uses in studied area
- Gradation of environmental quantity & quality values in order to improving physical quality
- Improving transfer axis in old fabric in order to preserving crowded area

REFERENCES

- [1] Azizi ,M,Arasteh ,M. (2009) **The assessment of effective projects in the historical texture in Yazd city**, case study , Naft and Khatam residential areas , the urban and regional studies , No 28.
- [2] Baqerian, M. (2009) **The capabilities of renovation in worn textures based on the social and environmental characteristics , case study , the journal of the human geography researches** , No 73.
- [3] Bernroider ,Edward. (2002) **Factors in SWOT analysis applied to micro, Small to medium and large software enterprise**, an Austrian study, European management journal, Volume 20, Number 4.
- [4] Moshaver zadeh, Z, Sabri, s. (2009) **the comparative study of theories about the administrative parks and the urban sustainable development**, The journal of City's origin, No 8.
- [5] Mahdizadeh, Mahdi, Javad et al. (2003) **the strategic planning in urban development and the global experiences in Iran**, Tehran, the leadership and architecture domain in urbanization and dwelling.
- [6] Navabakhsh, Mehrdad. (2008) **the sociology of the information technology and urban communications**, Islamic Azad university publication.
- [7] Navabakhsh, Mehrdad. (2008) **an overview of urban sociology**, Islamic Azad university publication. - Navabakhsh, Mehrdad. (2008) **the application of social theories in methodology of research**, Jahan e Ketab publication.
- [8] Nouri, J.; Karbassi, A. R.; Mirkia, S., (2008). **Environmental management of coastal regions in the Caspian Sea**. Int. J. Environ. Sci. Tech., **5(1)**, 43-52.
- [9] Piers John, Richard Robinson. (2008) **Strategic management and planning**, translated by Sohrab Khalili Shorini, Yadvareh Ketab publication, Tehran.
- [10] Ziari, K, Mahdnejad, H, Parhiz. (2008), **the basis and techniques for urban planning**, International publication of Chabahar University, first edition.

Validation of Predicted California Bearing Ratio Values from Different Correlations

K Shiva Prashanth Kumar¹, P M B Raj Kiran Nanduri², Prof.N Darga Kumar³

^{1,2}(Lecturer, Department of Civil Engineering, Adama Science and Technology University, Adama, Ethiopia)

³(Professor, Department of Building and Civil Engineering, Fiji National University, Suva, Fiji)

ABSTRACT : In the present study different correlations were used to validate the experimental California Bearing Ratio (CBR) values with predicted values proposed by different investigators. For the present study, 17 samples were collected at different intervals of sub grade soil samples from Modjo to Hawassa, in Ethiopia. From the collected samples, the basic index properties like Liquid Limit (LL), Plastic Limit (PL), Shrinkage Limit (SL), Sieve Analysis, Optimum Moisture Content (OMC) and Maximum Dry Density (MDD) have been evaluated in the laboratory. Finally, the experimental results are validated with the predicted results of CBR. All most all the correlations are slightly validating with the experimental results except Agarwal & Ghanekar [1], Vinod & Cletus [2] and NCHRP [3].

Keywords - CBR value, correlation, pavement design, index properties

I. INTRODUCTION

Soil characterization plays a vital role in early stages of planning and design of an infrastructure projects such as highways, airports, seaports and railways etc., due to the fact that faulty information about the ground characterization can result in high cost and damage to the structures. Most of the pavement design guidelines are based on the assumption that aggregates are important ingredients of pavement structures. However, the availability of good quality aggregates may be a constraint in many instances in the construction. Collection and transport of good quality aggregates from long distances to the construction site may not be economically feasible. Due to the excessive investment and maintenance cost, researchers are striving to introduce appropriate design methods and building materials for cost effective infrastructure development. Sometimes soil characteristics can be improved by the locally available admixtures such as lime, cement, fly ash, stone dust, bitumen, recycled aggregate, glass powder and chemical admixtures so as to meet the design requirements of the intended project. In the recent past, the developed and developing countries are giving priority for development of transport facility so as to have effective connectivity for transporting passengers, goods and other important items for livelihood. Development of road network is regarded as an index of economic, social and commercial progress of a particular country. No region or country can flourish/progress, if it lacks adequate transport facilities and mainly in road network. Highways are the major infrastructures used for transport purpose. Sustainable and cost effective highway construction can be achieved with the help of exact soil sub grade information. In the design of highway pavement, the California Bearing Ratio (CBR) value can be treated as important parameter in the strength assessment of the pavement sub grade. CBR value can be measured directly from the laboratory CBR test. Decision making of proper CBR value to be chosen in the design is always a problem for highway design engineers. CBR value can be affected by the type of soil and different soil index properties. In the present paper, an attempt is made to bring up the correlations of CBR with

soil index properties. These types of correlations can help the designer to choose appropriate CBR value and cross verify the CBR value obtained from the laboratory testing. Along with the soil test data, some of the existing correlations are made use for further improvement of the correlations. Existing correlations for CBR are made use to validate the laboratory CBR values. The existing correlations for CBR were developed based on the soil parameters such as liquid limit, plasticity index and OMC by **Venkatraman et al. [4]**, **Karunaprema and Edirisinghe [5]**.

Agarwal and Ghanekar [1] developed a correlation between CBR values with the basic index properties such as Liquid Limit (LL) and Plasticity Index (PI). However, it is felt that exact information about soil LL and PI are essential to make use of the correlations for prediction of CBR. Further for prediction of CBR of a soil, they made a correlation between CBR, OMC and LL also was proposed. Instead, finally they found an improved correlation when they included the optimum moisture content and liquid limit. The correlation is defined as below.

$$\text{CBR} = 2 - 16 \log (\text{OMC}) + 0.07 (\text{LL}) \quad \dots\dots\dots (1)$$

Where OMC = Optimum Moisture Content and LL = Liquid Limit.

Vinod and Cletus [2] had proposed a correlation based on liquid limit and gradation characteristics of soils. Based on the result obtained from experimental study on lateritic soils, they suggested a correlation as defined below.

$$\text{CBR} = -0.889 (W_{\text{LM}}) + 45.616 \quad \dots\dots\dots (2)$$

Where W_{LM} is modified Liquid Limit and is given by

$$W_{\text{LM}} = \text{LL} \left(1 - \frac{C}{100} \right) \quad \dots\dots\dots (3)$$

Where LL is liquid limit on soil passing through 425 μm sieve (in percentage) and C is the fraction of soil coarser than 425 μm (percent).

Patel and Desai [6] had proposed a correlation between plasticity index, maximum dry density and optimum moisture content.

$$\text{CBR} = 43.907 - 0.093 (\text{PI}) - 18.78 (\text{MDD}) - 0.3081 (\text{OMC}) \quad \dots\dots\dots (4)$$

Where, MDD is Maximum Dry Density in gm/cc, PI is Plasticity Index in percentage and OMC is Optimum Moisture Content in percentage.

Roy et al [7] proposed a method for predicting the value of CBR in terms of the optimum moisture content and maximum dry density of a soil. The following relationship as mentioned below

$$\log(\text{CBR}) = \log \left(\frac{Y_{\text{dmax}}}{Y_w} \right) - \log(\text{OMC}) \quad \dots\dots\dots (5)$$

Where, γ_{dmax} or MDD = Maximum Dry Density and γ_w is unit weight of water. Both are in same units (i.e., gm/cc).

Patel and Desai [6] had proposed few correlations for alluvial soils to obtain the CBR value from liquid and plastic limit. The equation for CBR as a function of different soil properties by method of regression analysis has been established. The correlations are experienced using basic soil properties for no if samples at 100 m interval and it was checked by few test results obtained CBR values. The correlations are defined below.

$$\text{CBR} = 4.745 - 0.044(\text{LL}) + 0.1508 \quad \dots\dots\dots (6)$$

$$\text{CBR} = 5.176 - 0.028(\text{LL}) - 0.047 (\text{PL}) \quad \dots\dots\dots (7)$$

Where, CBR is California bearing ratio, LL is liquid limit and PL is plastic limit.

The **National Co-operative Highway Research Program (NCHRP) [3]** of United States of America (USA) through the “Guide for Mechanical - Empirical Design of New and Rehabilitated Pavement Structures” had been developed some correlations that clearly describes the relationship between soil index properties and CBR values. An equation was established for soils which contain 12% fines and exhibit some plasticity. For plastic, fine-grained soils, the soil index properties chosen to correlate CBR are the percentage passing No. 200 US standard sieve or 0.075mm size sieve and plasticity index. The suggested equation by NCHRP is shown below.

$$\text{CBR} = \frac{75}{1 + 0.728 (\text{wPI})} \quad \dots\dots\dots (8)$$

Where w is percentage passing No. 200 US sieve (in decimal) and PI is Plasticity Index.

II. EXPERIMENTAL PROGRAM

The soil samples were collected from 17 different points at each interval of 5m over a longitudinal stretch of 100m of existing sub grade soils between Modzo to Hawassa road, in Ethiopia. These samples were collected and preserved in air tight containers in the laboratory. The selected soil samples were tested for CBR value, optimum moisture content, maximum dry density, particle size distribution (or) grain size distribution, liquid limit, plastic limit, plasticity index and shrinkage limit. These tests were performed according to American Association of State Highway and Transportation Officials (AASHTO) soil code specifications. Almost all the soils are light brown to brown sandy clayey with little gravel. The index properties of soil samples are tabulated in Table 1. The comparison of CBR values predicted from different investigators with experimental values has done.

Table 1. Laboratory index properties of materials

S.No	LL	PL	PI	OMC (%)	MDD (gm/cc)	CBR (%)
1	55	26	29	20.0	1.633	2
2	44	25	19	15.0	1.764	5
3	29	20	9	10.0	1.958	21
4	45	29	16	21.0	1.556	4
5	46	31	15	22.5	1.512	3

6	41	24	17	19.0	1.690	4
7	26	18	8	14.0	1.779	10
8	25	22	3	17.5	1.595	18
9	35	27	8	17.0	1.560	9
10	36	30	6	25.0	1.537	8
11	35	32	3	17.0	1.322	18
12	23	21	2	12.0	1.847	7
13	38	30	8	17.0	1.389	4
14	40	30	10	19.0	1.674	9
15	38	35	3	10.0	1.650	18
16	56	43	13	19.5	1.066	17
17	31	25	6	15.0	1.635	8

III. RESULTS AND DISCUSSIONS

Various investigators have been made to develop suitable correlation between CBR values of compacted soils at optimum moisture content and results of some simple field tests. The CBR values are then evaluated from available correlations given by Agarwal and Ghanekar [1] (Eqn. 1), Vinod and Cletus [2] (Eqn. 2), Patel and Desai [6] (Eqn. 4), Roy et al [7] (Eqn. 5), Patel and Desai [6] (Eqn. 6 and 7) and NCHRP [3] (Eqn. 8). From different investigators, the predicted CBR values were then compared with experimental values reported in Table 1. The predicted values of various equations with experimental values are tabulated in Table 2. The values are further plotted in Fig. 1.

Table 2. Experimental and Predicted Values of CBR

S.No	Predicted CBR values (Vinod and Cletus)	Predicted CBR values (Patel and Desai) -1	Predicted CBR values (Roy et al)	Predicted CBR values (Patel and Desai) - 2	Predicted CBR values (Patel and Desai) - 3	Predicted CBR values (NCHRP)	Experimental Values of CBR
1	7.477	4.380	3.329	6.245	2.414	5.244	2
2	10.411	4.390	2.697	6.579	2.769	8.441	5
3	39.170	3.217	1.995	6.485	3.424	39.117	21
4	14.812	6.727	3.3308	7.138	2.553	9.122	4
5	9.629	7.184	3.467	7.395	2.431	7.790	3
6	13.540	4.732	3.273	6.560	2.900	7.474	4
7	28.742	5.439	2.538	6.315	3.602	20.713	10
8	27.836	8.282	2.845	6.962	3.442	44.146	18
9	23.213	8.628	2.703	7.276	2.927	18.352	9
10	16.812	6.781	3.916	7.685	2.758	18.286	8
11	33.792	13.563	2.290	8.030	2.692	48.512	18
12	36.005	5.337	2.259	6.899	3.545	53.835	7
13	22.306	11.839	2.407	7.597	2.702	19.461	4
14	15.034	5.685	3.242	7.509	2.646	14.564	9
15	35.143	9.56	1.681	8.351	2.467	54.693	18
16	28.191	16.670	2.118	8.765	1.587	21.095	17
17	31.285	8.022	2.5	7.151	3.133	31.279	8

From the previous investigators, it has been concluded that few relationships made by basic index properties of soil samples are matching with the laboratory test values. But the reliability of the predicted CBR values basically depends on the input parameters which we used in substituting already developed correlations by different investigators. The parameters such as Liquid Limit, Plasticity Index, Optimum Moisture Content, Maximum Dry Density and particle size or grain size values are playing vital role in predicted CBR value proposed by different investigators.

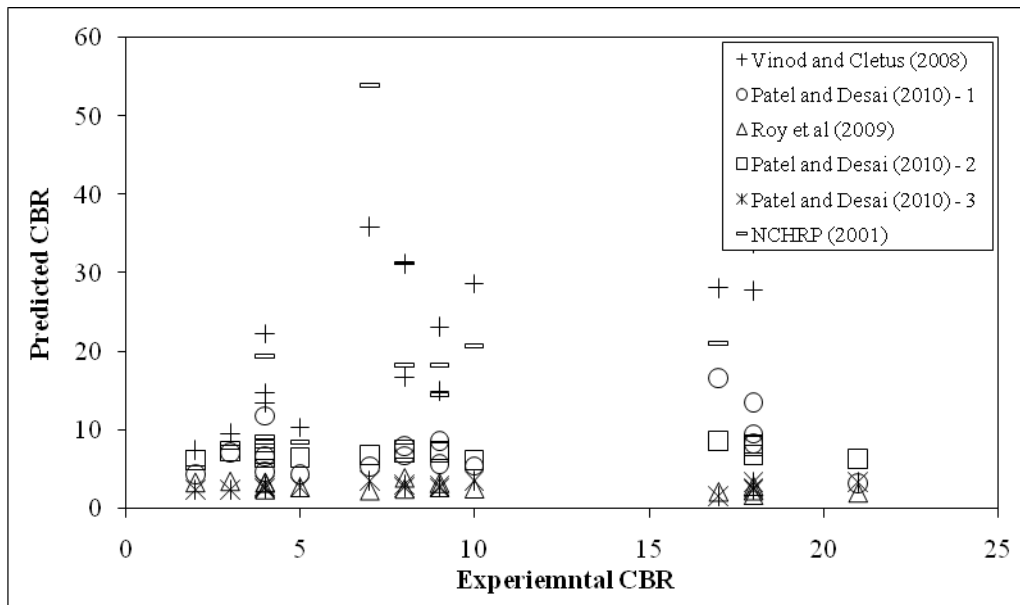


Fig. 1. Comparison of Experimental and Predicted CBR values by different investigators

Fig. 1 shows the comparison of predicted and experimental CBR values suggested by different investigators. From the above figure it is clearly observed that the predicted value of CBR from Vinod and Cletus [2] shows wide range of divergence from all other equations of the soils reported in Table 1. Almost all the equations are validating the predicted values with obtained experimental values. The predicted value of CBR from Vinod and Cletus [2] showing very high values of CBR compared with obtained experimental CBR. The remaining all investigators proposed equations are in moderate range of predicted CBR values as compared to experimental CBR. From the above figure it is clearly seen that the points of predicted and experimental CBR values are merging together (i.e., the values of experimental and predicted values are almost similar) except CBR values from Vinod and Cletus and NCHRP [3].

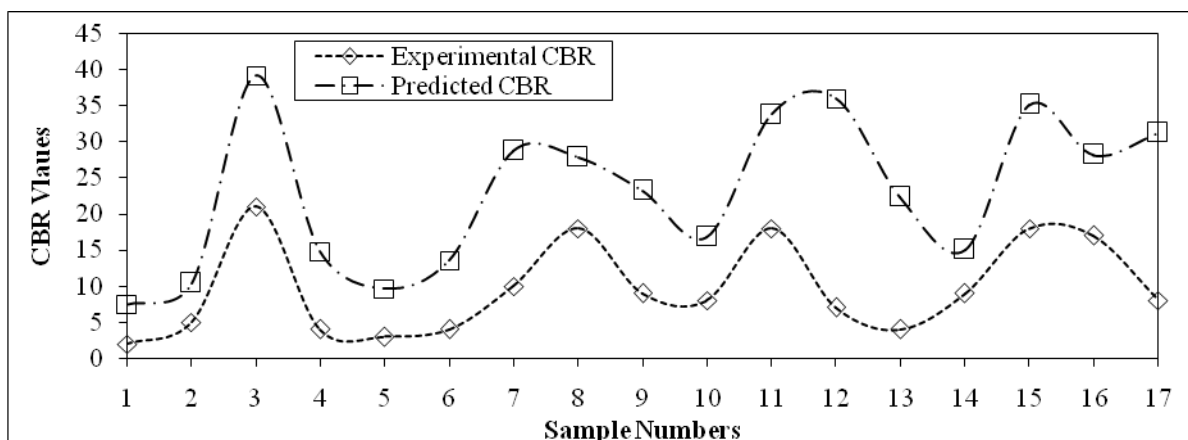


Fig. 2. Comparison of Experimental and Predicted values of CBR from Vinod and Cletus.

Fig. 2 shows the validation of CBR values between experimental and predicted from Vinod and Cletus. The values are not at all showing the similarity between experimental and predicted CBR. This may be due to the variation of basic index properties for different soils such as liquid limit and percentage fractions coarser than 425 μm . The values compared to the experimental CBR and predicted CBR values from Vinod and Cletus [2] are very higher.

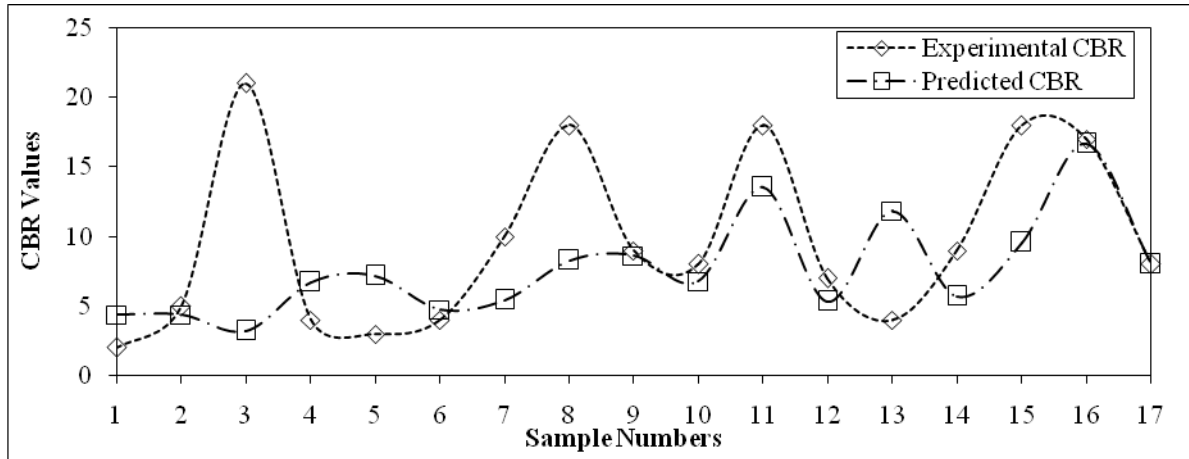


Fig. 3. Comparison of Experimental and Predicted values of CBR from Patel and Desai -1.

Fig. 3 shows the validation of experimental and predicted values of CBR from Patel and Desai [6] - 1. From the figure it is observed that the predicted CBR values are initially stated high and finally it is almost matching and moving together. The ranges of index properties such as plasticity index, optimum moisture content and maximum dry densities for the soils which we considered for laboratory testing is almost similar with investigated correlation ranges.

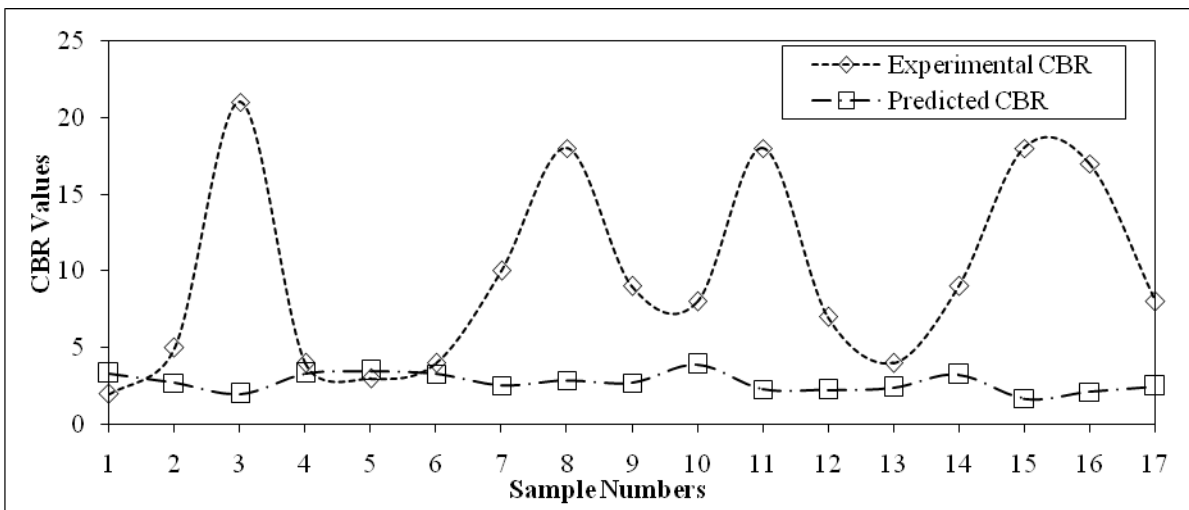


Fig. 4. Comparison of Experimental and Predicted values of CBR from Roy et al.

Fig. 4 shows the validation of experimental and predicted values of CBR from Roy et al [7] From the figure it is seen that the predicted value of CBR is initially more than experimental values. This may be due to the variation in parameters such as maximum dry density, unit weight and optimum moisture content. At sample number 4, 5 and 6 are matching the experimental and predicted CBR values. But there is no proper trend between the experimental and predicted CBR values.

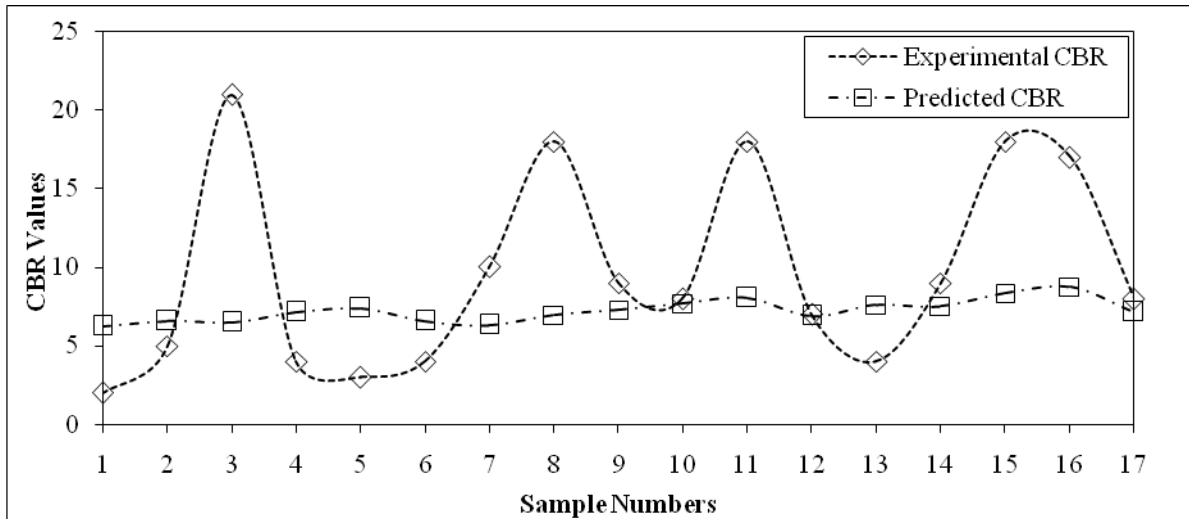


Fig. 5. Comparison of Experimental and Predicted values of CBR from Patel and Desai -2.

Fig. 5 shows the validation of experimental and predicted values of CBR from Patel and Desai [6] - 2. From the figure the values of predicted CBR is initially more than experimental CBR value. The values are matching with at sample number 10, 12 and 17. But it is not at all showing the similarity or proper trend along with the experimental data. This may be due to the variation of properties such as liquid and plastic limits of various soil samples.

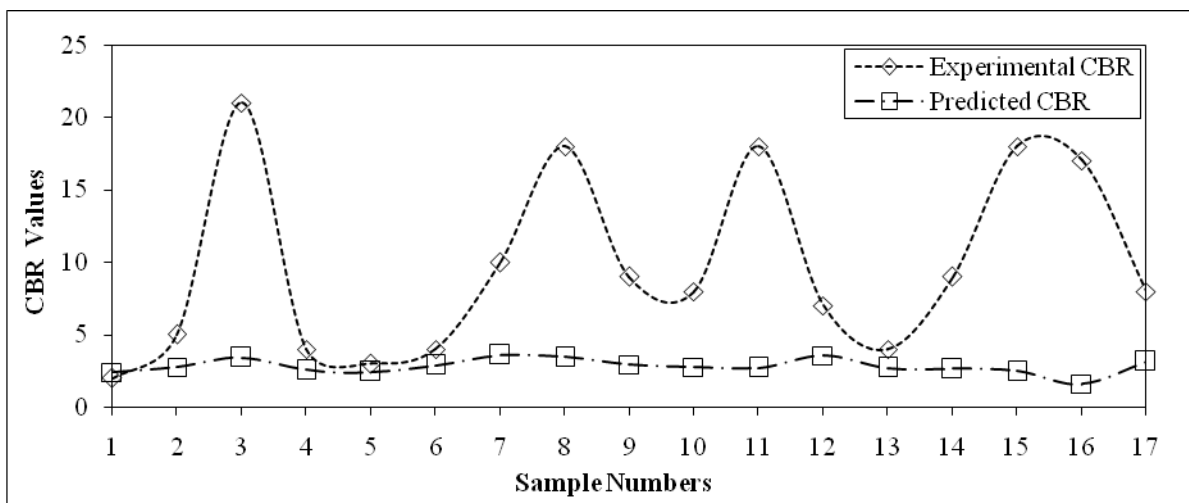


Fig. 6. Comparison of Experimental and Predicted values of CBR from Patel and Desai -3.

Fig. 6 shows the validation of experimental and predicted values of CBR from Patel and Desai [6] -3. From the figure, it is observed that the predicted values are not matching with the experimental values. At initial sample the experimental value of CBR coincide with the predicted value from Patel and Desai [6] - 3. The experimental values are higher than predicted values. This may be the variation in liquid and plastic limits of various soil samples. But finally, it is not following the trend as with the experimental value.

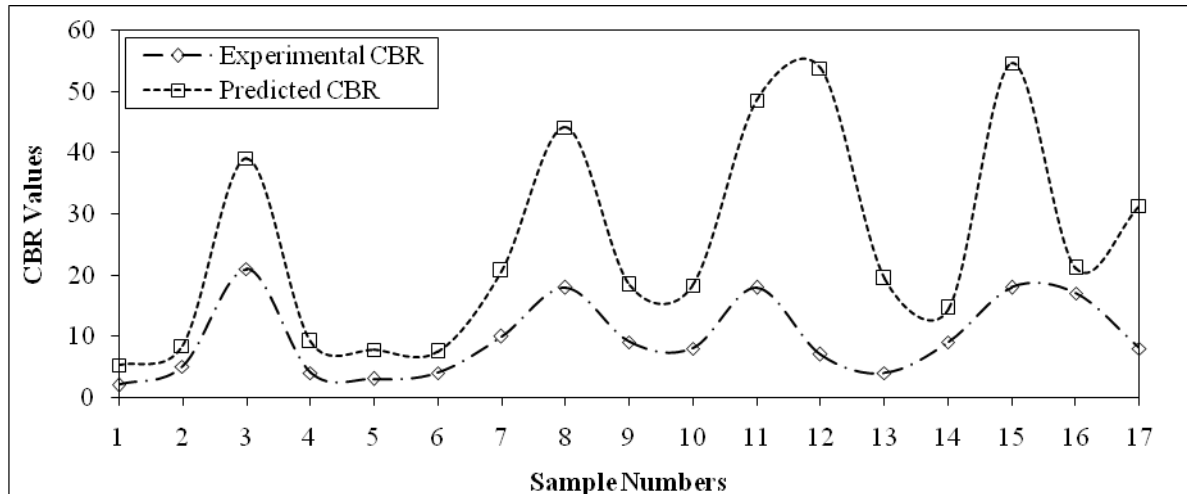


Fig. 7. Comparison of Experimental and Predicted values of CBR from NCHRP.

Fig. 7 shows the variation of experimental and predicted values of CBR from NCHRP [3]. From the figure it is clearly observed that almost both the values are following the trend but those values are not exactly matching together. The predicted values are little higher than the experimental values. Finally proper trend of the curve is following with slight deviation in predicted values.

IV. CONCLUSION

Experimental values of 17 samples of various index properties are given as input to validate the equations with predicted CBR values. Several tests have been conducted to measure the CBR and index properties of soils were performed. Finally few conclusions were brought out.

- 1) The results obtained from Agarwal and Ghanekar [1] has no way matching with the experimental as well predicted CBR values.
- 2) All most all the equations are moderately validating with different samples with the experimental values with predicted values of CBR except Vinod and Cletus [2].
- 3) From NCHRP [3], the experimental and predicted values are following the trend but the values are not matching exactly.

V. Acknowledgements

First of all, I would also thank to my colleagues Mr. Shumi and Mr. Esaias from Adama Science and Technology University (ASTU), Adama, Ethiopia, for their assistance in the laboratory.

REFERENCES

- [1] Agarwal, K.B.; and Ghanekar, K.D. (1970). Prediction of CBR from Plasticity Characteristics of Soil. Proceeding of 2nd South-east Asian Conference on Soil Engineering, Singapore. June 11-15, Bangkok: Asian Institute of Technology, 571-576.
- [2] Vinod, P.; and Cletus Reena. (2008). Prediction of CBR value of Lateritic Soils using Liquid Limit and Gradation Characteristics Data, Highway Research Journal, Vol. I, No. 1, 89-98.
- [3] NCHRP. (2003). Guide for mechanistic-empirical design of new and rehabilitated pavement structures. National Co-operative Highway Research Program Transportation Research Board National Research Council, Illinois 61820.
- [4] Venkataraman, T.S.; Samson, M.; and Ambili, T.S. (1995). Correlation between CBR and Clegg Impact Value, Proc. Nat. Sem. On emerging trends in Highway Engineering, Centre for Transportation Engineering, Bangalore, Vol. I, 25.1-25.5.
- [5] Karunaprema, K.A.K. and Edirisinghe, A.G.H.J. (2002). A Laboratory study to establish some useful relationship for the case of Dynamic Cone Penetration, Electronic journal of Geotechnical Engineering. Vol.7.
- [6] Patel, R. S.; and Desai, M.D. (2010). CBR Predicted by Index Properties of Soil for Alluvial Soils of South Gujarat, Indian Geotechnical Conference, Proc. IGC, Vol. I, 79-82.
- [7] Roy, T.K.; Chattopadhyay, B.C.; and Roy, S.K. (2009). Prediction of CBR from Compaction Characteristics of Cohesive Soil,

- Highway Research Journal, July-Dec., 77-88.
- [8] Chandrasekhar, B.P.; Vinayak Rao, V.R.; and Prasada Raju, G.V.R. (2003). A comprehensive study of soil CBR assessment through Clegg's Impact test, Field and Laboratory CBR test, *Indian Highways*, Vol.31, No 7, 39-45.
- [9] Venkatasubramanian, C.; and Dhinakaran, G. (2011). ANN model for predicting CBR from index properties of soils, *International Journal of Civil and Structural Engineering*, Volume 2, No.2.
- [10] American Standard Test Method. (1992). Standard Test Method for CBR (California Bearing Ratio) of Laboratory- Compacted Soils. United States of America, ASTM Designation D1883-92.
- [11] Sister, N.W.; and Powell, W.D. (1976). Design Practice for Bitumen Pavements in the United Kingdom, *Proceedings of 6th International Conference on Structural Design of Asphalt Pavements*, Volume 1.

Web based authentication scheme using images

Viswa Subramanian Sekar¹

Department of Computer Science and Engineering, PSG College of Technology, Coimbatore - 641004, India.

ABSTRACT: The most common computer authentication method is to use alphanumeric usernames and passwords. This method has been shown to have significant drawbacks. For example, users tend to pick passwords that can be easily guessed. On the other hand, if a password is hard to guess, then it is often hard to remember. In the developing world of technologies, Security breaching has become more popular. The more and more amount of data being stored in the networks, the more security is needed. On the other side of world, there arises a community called "Hackers"- a person who involves most of his time in breaking the security. They find the vulnerabilities, break your password, and try to steal the information in your database. The main idea of this "Image Password" is an authentication technique based on pictures as a possible solution to the most important problems concerning traditional passwords. The concept is having unique sequence of pictures for a user, by this way the attacker will not be aware of what the password is. This work brings together the technical (crypto logical) and non-technical (psychological) awareness into the research on passwords. Security issues of any authentication mechanism (relying on knowledge) should not be considered without analysis of the human factor – since the users' human nature was identified as a source of major weaknesses of conventional authentication. The "Image Passwords" brings out statistically significant superiority of picture passwords over alphanumeric. There is a resistance to 'key logging' and 'mouse tracking'. This method guarantees that users choose dissimilar, personalized and cryptographically strong graphical passwords.

KEYWORDS: Security, Image, Password, Picture passwords, graphical password, web authentication, browser password.

I. INTRODUCTION

According to recent reports, many researches and statistics from real systems, there are many vulnerabilities and threats typical of alphanumeric passwords. As usual, the users are 'the weakest link in the security chain'. One of the major problems is the difficulty of remembering passwords, the other, ignoring security requirements. Users tend to create either too short passwords or passwords that though long enough are easy to guess. There is an informal rule stating that passwords easy to remember, are mostly also easy to break. According to Schneier [1], passwords' length distribution based on 34,000 users shows that 65% of passwords have only up to 8 characters and almost 95% up to 10 characters. Other research [2] shows that only 17% of the inquired IT professionals use complex passwords (including letters, numbers and symbols) and 72% stated that they almost never or never change their access codes. 52% of professional users tend to share their passwords and 65% of them have only one or two passwords to access the majority of services. A study of information contained within the passwords [3] shows that 66% of users' passwords are designed making use of personal characteristics thereof, where 32% contained names of people, places or things. The common constructions involve full information in the passwords – 75%, partial – 13.5%, or combined – 7.5%. Almost all respondents reuse passwords – on average 4.45 passwords are used in 8.18 systems. On the other hand, strong passwords imposed on users bring no solution as well – people cannot and/or would not remember strong passwords and write them down instead. According to [4] we can say: there will be either about 80% remembered but weak passwords (created by users) or 80% strong passwords (generated by the system) but written down. Many alternative authentication solutions have been invented and developed to ensure the proper security level – in order to avoid weaknesses of traditional methods. One group of techniques (involving a physical factor in the authentication process – 'something you have') focuses on utilizing all kinds of tokens, one-time passwords, magnetic stripes and proximity cards, iButtons, cryptographic cards, etc. The other kind of research makes use of methods

(called ‘something you are’) based on biometric information like fingerprints, voiceprints, the patterns of blood vessels on the eye retina, the topography of the eye iris, the geometry of the hand, facial patterns, DNA codes or even thoughts (cerebral waves).

However, all of the aforementioned solutions have two significant disadvantages. First, they may become unacceptably expensive when a large number of users are involved. Second, access to the system is strongly dependent on the suitable interfaces – which makes such methods comparatively less universal (in the context of mobility) and in some cases, impossible to use. Additionally, biometrics is extremely vulnerable to a replay attack – the personal information is hard to hide (face, fingerprints) and cannot be changed. In the past few years we have been observing a growing interest in graphical authentication techniques – those of knowledge-based methods, which include graphical aspect(s) in the authentication process. There are a few distinct grounds, which aroused the interest in graphical techniques. There are methods particularly useful for mobile devices and/or systems that have no keyboards, methods resistant to shoulder-surfing attacks (enabling to log in ‘in the crowd’), there are also advantages coming from resistance to malicious software (malware). Notwithstanding, the leading inclination is still to construct a system, which will prevent from choosing trivial passwords and which will allow to remember passwords with the cryptographically proper length.

II. BACKGROUND

Alpha-numeric passwords were first introduced in the 1960s as a solution to security issues that became evident as the first multi-user operating systems were being developed. As the name indicates, an alpha-numeric password is simply a string of letters and digits. Although almost any string can serve as a password, these passwords only offer good security as long as they are complicated enough so that they cannot be deduced or guessed. Commonly used guidelines for alpha-numeric passwords are:

- 1) The password should be at least 8 characters long.
- 2) The password should not be easy to relate to the user (e.g., last name, birth date).
- 3) The password should not be a word that can be found in a dictionary or public directory.
- 4) Ideally, the user should combine upper and lower case letters and digits.

Since the best password would be a completely random one, people have devised ways to create pseudo-random passwords. One such method is to take a common word and perform certain actions on it. Using the word Dinosaur as an example, users often create passwords such as DiNoSaUr (by alternating upper and lower case), rUaSoNiD (by reversing the string), oSNaiUDr (by shuffling the string), D9n6s7u3 (combining numbers and letters). However, the better the password is, the harder it is to remember.

Another drawback of alpha-numeric password is the dictionary attack. Because of the difficulty in remembering random strings of characters, most users tend to choose a common word, or a name. Unfortunately, there are several tools that allow an individual to crack passwords by automatically testing all the words that occur in dictionaries or public directories. This attack will usually not uncover the password of a predetermined user; but studies have shown that this attack is usually successful in finding valid passwords of some users of a given system.

Because human beings live and interact in an environment where the sense of sight is predominant for most activities, our brains are capable of processing and storing large amounts of graphical information with ease. While we may find it very hard to remember a string of fifty characters, we are able easily to remember faces of people, places we visited, and things we have seen. These graphical data represent millions of bytes of information and thus provide large password spaces. Thus, graphical password schemes provide a way of making more human-friendly passwords while increasing the level of security.

Dictionary attacks are infeasible, partly because of the large password space, but mainly because there are no pre-existing searchable dictionaries for graphical information. It is also difficult to devise automated attacks. Whereas we can recognize a person’s face in less than a second, computers spend a considerable amount of time processing millions of bytes of information regardless of whether the image is a face, a landscape, or a meaningless shape.

III. PROPOSED IDEA

The idea is implemented for web service. Each user will have unique set of pictures, where user will select a unique sequence in selecting the order of the password.

Modules:

1. Creation of User account
2. Uploading pictures/setting sequence
3. Deploying in Web page

Creation of User Account

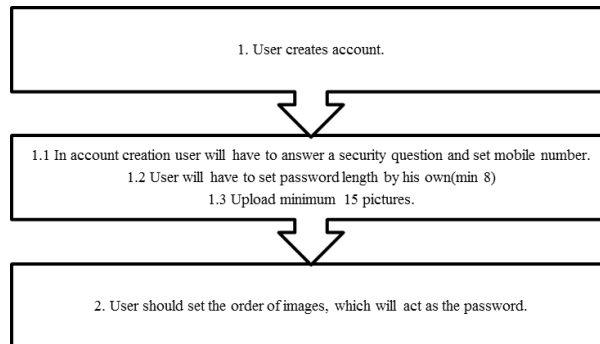


Fig 1: Flow of User account creation

Process

This module is the webpage where user will have the options to create a new user account. All mandatory questions will be included such as DOB, Age, Primary email address. Here the user will be specially asked to set a security question which will be the first phase of authentication. Next the user will be asked to upload images for the authentication. Once uploaded, the images will be scaled down to reduce the size. This will save the space required to store the images in the database. After setting up of picture sequence the password is now set. Now, when user logs in, firstly the user will be interfaced to type in their mail id. Once typed, the page will fetch their secret question and display it. Once displayed, user will have to answer to that question, if answered rightly, the page will fetch respective user's pictures and display them. Here user will have to drag the mouse and click the sequence. In order to escape from mouse tracing, or shoulder sniffing, each time the images are shuffled. The order is highlighted as a thin line around the picture box, which will not be visible to the person standing beside.

Features

Say the password is given wrongly for 3 times, a counter will be working behind to know the number of wrong attempts. If it exceeds, the page will send an SMS to the prescribed number and email id stating that there was exceeded number of try's. Instead of security question, user can set mobile verification, where user will have to type the code that he receives in his mobile. The sequence and pictures can be changed. This method will not take much space of database, because, once the picture is uploaded, it is scaled down and reduced to lower size for storage efficiency.

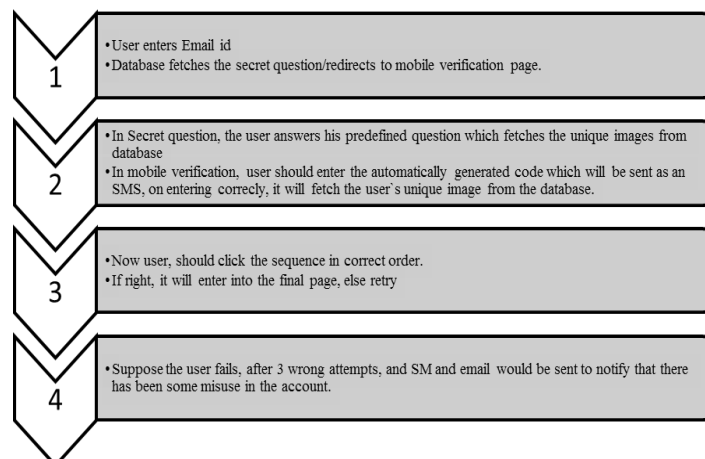


Fig 2: Flow of Login Process

This type of password is superior and safe, because the set of images is unique for each user. There are 2 Gateways to enter into final page. The hacker to find the password, must first find a way to break the first gateway.

Here brute force technique is difficult because, each user will have different set of images. So it is really hard to create a dictionary. No keylogging, because of images.

Mouse tracking is impossible because the hacker should know what is there in the screen to get the mouse traces.

Scope

1. This type of authentication can be used in military purposes, where high amount of security is needed.
2. To protect medical database.
3. To protect confidential information.

Advantages

1. There are possibilities of significant enlargement of the picture passwords space. In the traditional passwords, the base does not exceed one hundred ($b \times n$ – password space, b – base, n – password length). Picture passwords offer the password base up to ten times larger – technically, the only limitation is the resolution of the screen.
2. There is technical possibility to prevent users from choosing trivial passwords. Through the permutation of the set (only once – after the password creation) the users are forced to remember their passwords regarding only the meaning of elements and not the topological placement of elements (like row or column).
3. It's possible to personalize the passwords, which can prevent from (common) dictionary attacks. After removing irregular elements and pairs from the set, chosen passwords will depend only on individual thoughts, associations with one's past and personal feelings – in contrast to the common language dictionaries and attacks based on universal strings.
4. There is a possibility to make the authentication process resistant to 'key logging' and 'mouse tracking'. The first resistance is obvious (due to not using the keyboard). The second one is achieved (again) due to the permutation of the set. But in this case, the permutation table should be individual for each login name (and/or workstation). As a matter of fact the sequence of the screen coordinates (users' clicks) will be meaningless without the view of the screen.
5. Sharing passwords with other users as well as noting them down or giving them away as a result of a social engineering attack are much more difficult. While traditional passwords can be easily written down or spelled out, giving a picture password out is very troublesome. The effect can be especially intensive when the keypad consists of ambiguous symbols or symbols having similar names.
6. Passwords incrementation effect (i.e. recurrent and obvious changes made to the passwords – e.g. change from "2nd*SIS#07" to "3rd*SIS#08") can be neutralized. It is because there are no sequences or numbers when the keypad pictures were properly chosen (e.g. avoiding signs). Even when user changes only one element of the password - it is still hard to guess which one and which is the new one. Moreover, there is always a way of forcing users to change their passwords significantly by modifying (entirely or partially) the set of pictures.
7. There is a possibility for undemanding and inexpensive implementation (in comparison to biometrics and cryptographic hardware).
8. To prevent shoulder sniffing, each time the set of pictures displayed are shuffled.
9. There are many prospective possibilities (manipulation of the pictures colours, meanings of the elements, personalizing passwords sets) of achieving even better memory abilities and/or constructing much stronger mnemonics.

Disadvantages

1. Graphical interface is required - which means that the graphical authentication methods will be less universal (in terms of mobility) and troublesome in implementation (in comparison to traditional passwords).
2. We should not forget about visually impaired and blind people (who are using common internet services as well), for whom something like graphical authentication interface will be impassable or hard to get through.

IV. IMPLEMENTATION

The system is implemented using html with java and php, mysql as database. The snapshots shown below explain the idea.

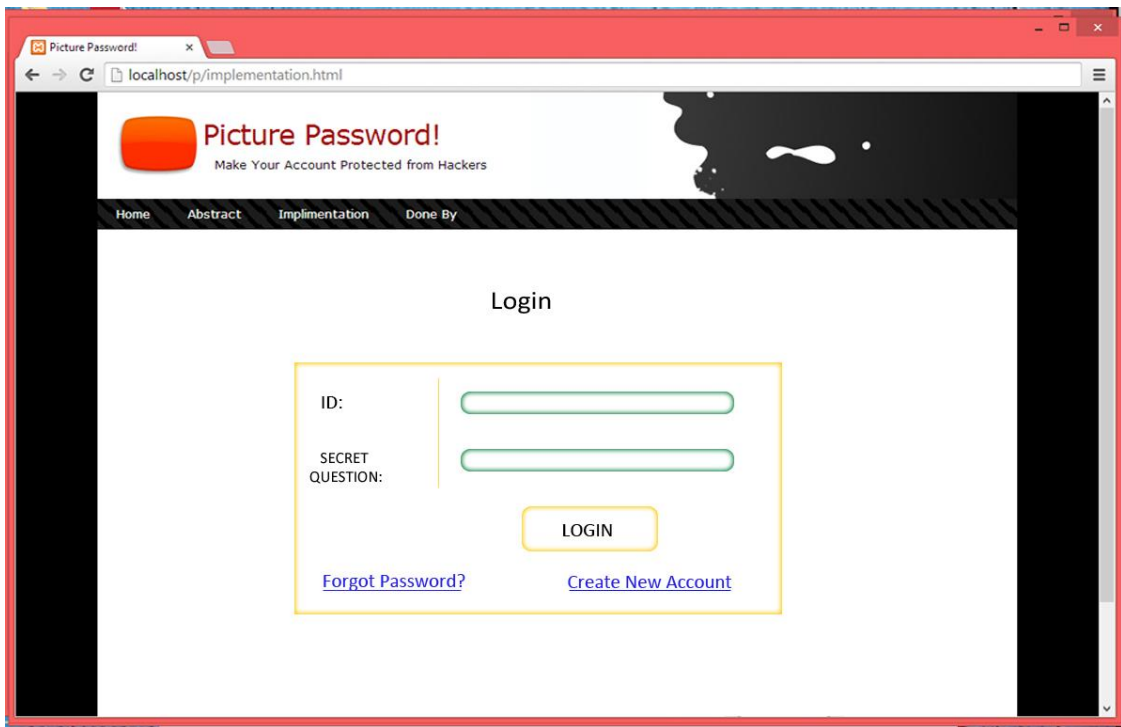


Fig 3: Login page – 1st step

This is the 1st page where user sees. When the user enters the mail id, the database fetches the secret question. When the user enters the correct answer for the secret question it fetches the user defined set of images

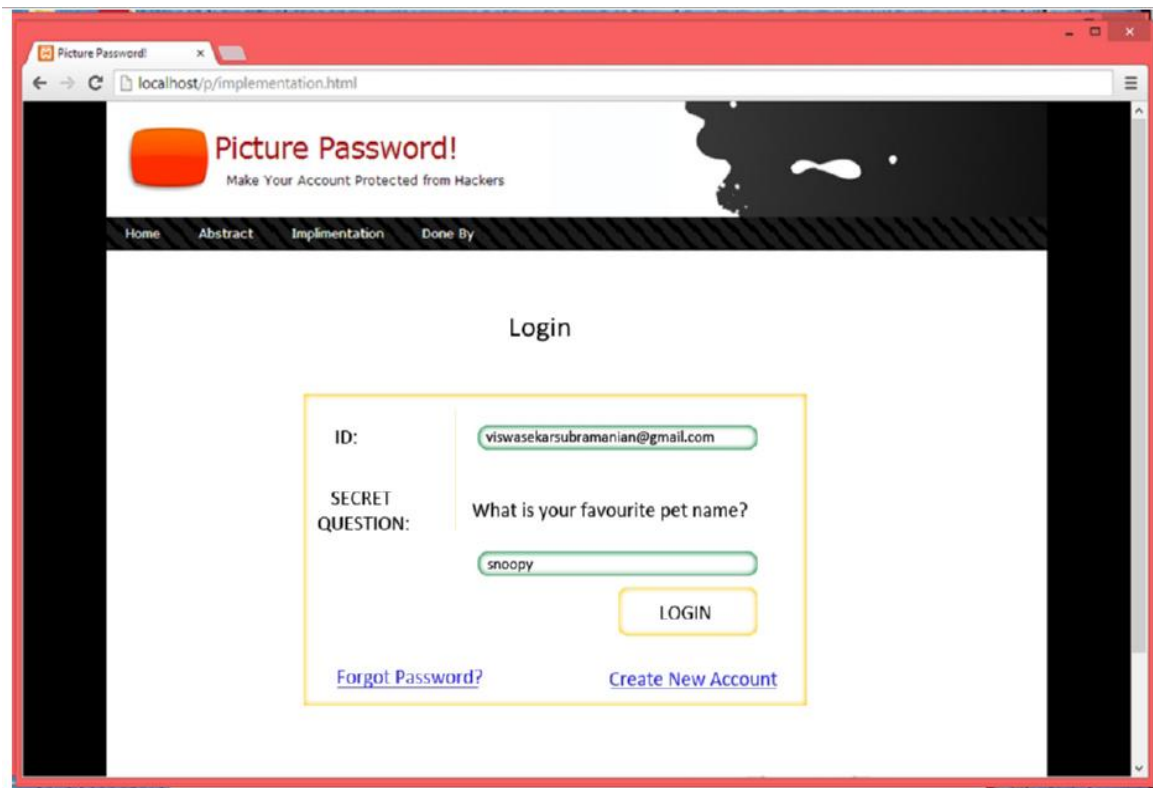


Fig 4

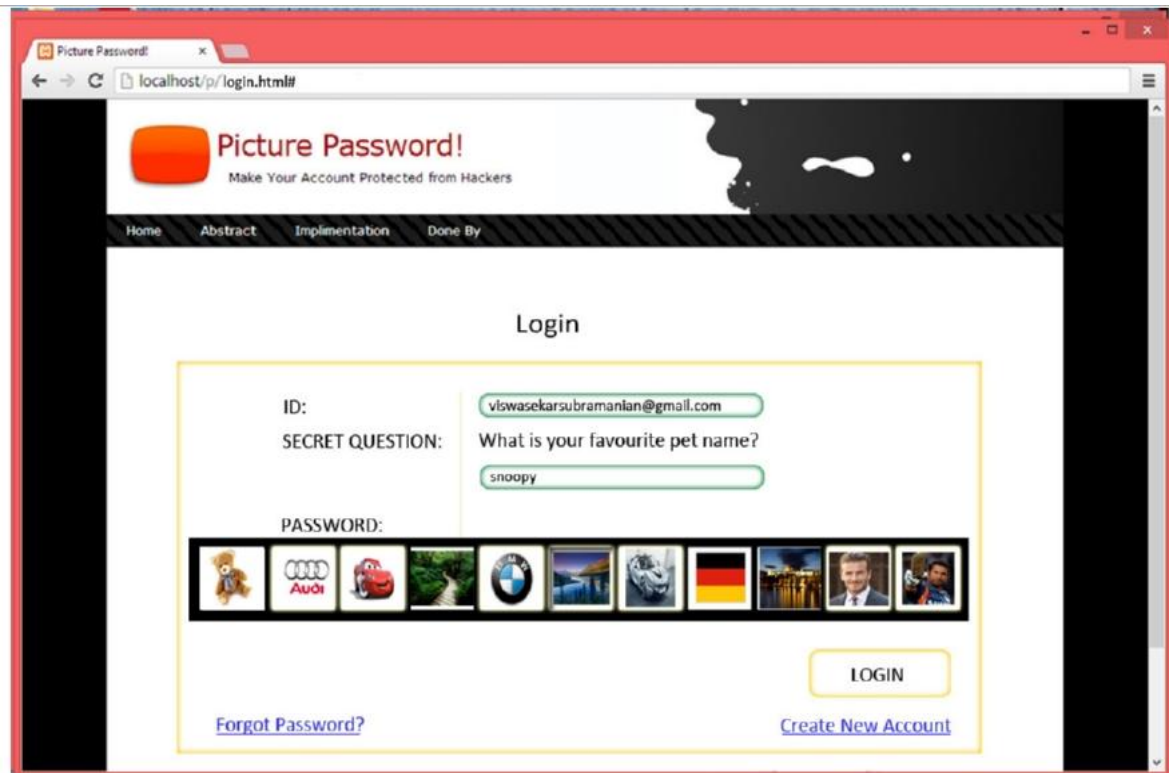


Fig 5: Correct answer for Secret question

In the above image, we can notice that user has entered the correct answer for the secret question, so the page fetches the user defined images stored already and displays it. Now the user should select the sequence of the images for the correct password.

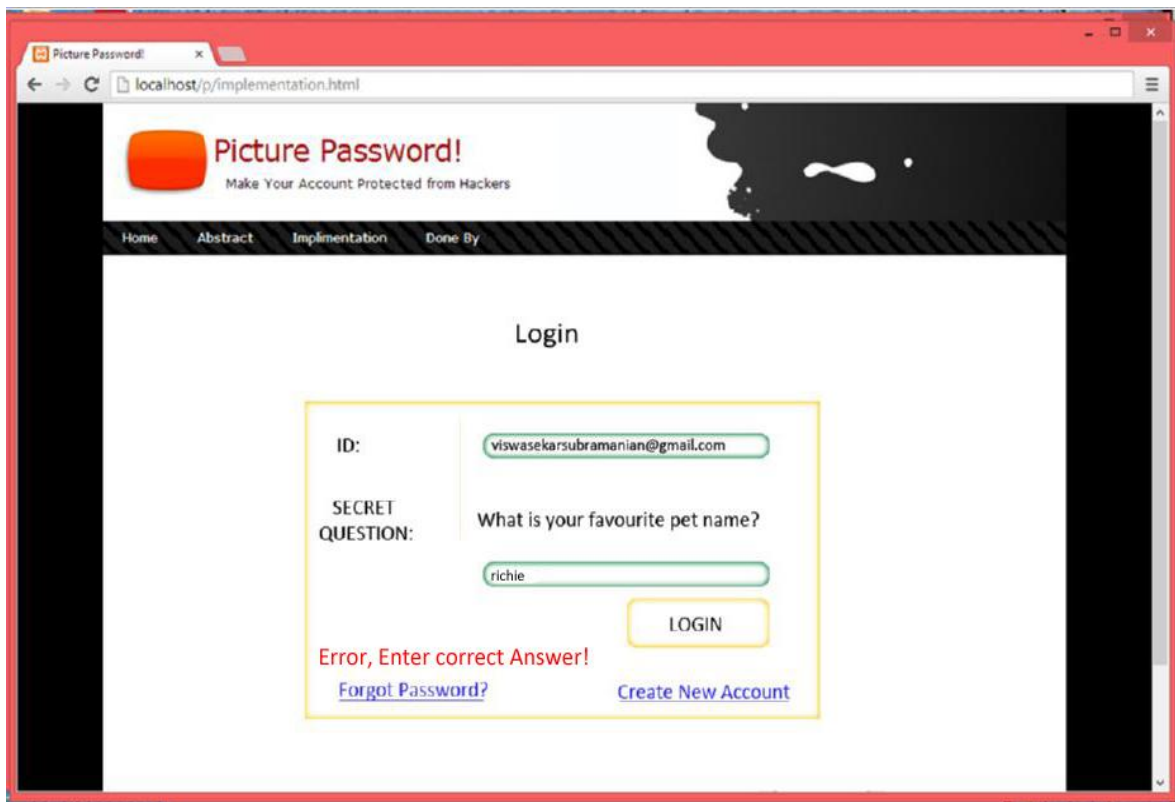


Fig 6

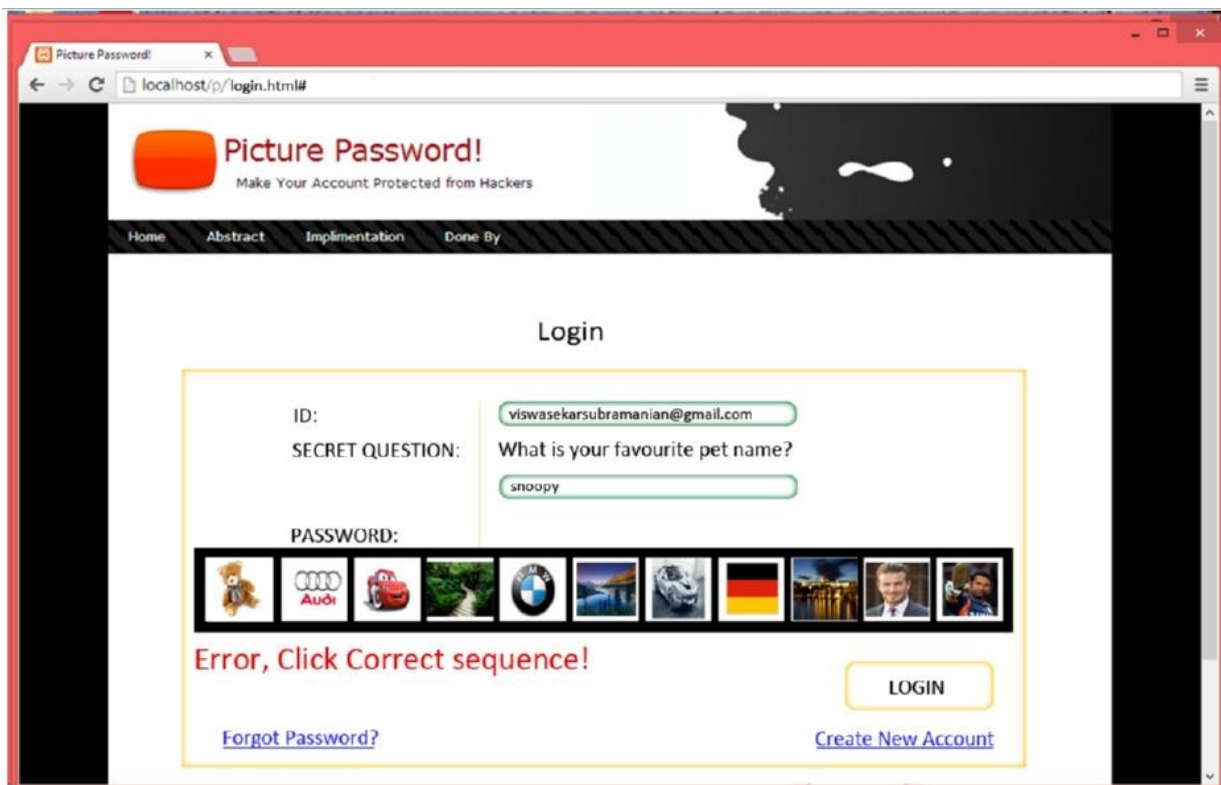


Fig 7: Incorrect sequence of images

In the above image we can notice that the user does not click the correct sequence of images, so it shows an error and the login is not successful.

V. RESULTS AND DISCUSSIONS

Is a graphical password as secure as textbased password?

Very little research has been done to study the difficulty of cracking graphical passwords. Because graphical passwords are not widely used in practice, there is no report on real cases of breaking graphical passwords. Here we briefly exam some of the possible techniques for breaking graphical passwords and try to do a comparison with text-based passwords.

Brute force search

The main defense against brute force search is to have a sufficiently large password space. Text-based passwords have a password space of 94^N , where N is the length of the password, 94 is the number of printable characters excluding SPACE. Some graphical password techniques have been shown to provide a password space similar to or larger than that of text-based passwords. Recognition based graphical passwords tend to have smaller password spaces than the recall based methods. It is more difficult to carry out a brute force attack against graphical passwords than text-based passwords. The attack programs need to automatically generate accurate mouse motion to imitate human input, which is particularly difficult for recall based graphical passwords. Overall, we believe a graphical password is less vulnerable to brute force attacks than a text-based password.

Dictionary attacks

Since recognition based graphical passwords involve mouse input instead of keyboard input, it will be impractical to carry out dictionary attacks against this type of graphical passwords. For some recall based graphical passwords, it is possible to use a dictionary attack but an automated dictionary attack will be much more complex than a text based dictionary attack. Overall, we believe graphical passwords are less vulnerable to dictionary attacks than text-based passwords.

Spyware

Key logging or key listening spyware cannot be used to break graphical passwords. It is not clear whether "mouse tracking" spyware will be an effective tool against graphical passwords. However, mouse mo-

tion alone is not enough to break graphical passwords. Such information has to be correlated with application information, such as window position and size, as well as timing information.

Shoulder surfing

Like text based passwords, most of the graphical passwords are vulnerable to shoulder surfing. But since that the order in which the image is selected is shuffled, it is difficult for attacker to remember the sequence of the images in that short period of time.

Social engineering

Comparing to text based password, it is less convenient for a user to give away graphical passwords to another person. For example, it is very difficult to give away graphical passwords over the phone. Setting up a phishing web site to obtain graphical passwords would be more time consuming. Overall, we believe it is more difficult to break graphical passwords using the traditional attack methods like brute force search, dictionary attack, and spyware. There is a need for more in-depth research that investigates possible attack methods against graphical passwords.

What are the major design and implementation issues of graphical passwords?

Security

In the above section, we have briefly examined the security issues with graphical passwords.

Usability

One of the main arguments for graphical passwords is that pictures are easier to remember than text strings. Preliminary user studies presented in some research papers seem to support this. However, current user studies are still very limited, involving only a small number of users. We still do not have convincing evidence demonstrating that graphical passwords are easier to remember than text based passwords. A major complaint among the users of graphical passwords is that the password registration and log-in process take too long, especially in the recognition-based approaches. For example, during the registration stage, a user has to pick images from a large set of selections. During authentication stage, a user has to scan many images to identify a few pass-images. Users may find this process long and tedious. Because of this and also because most users are not familiar with the graphical passwords, they often find graphical passwords less convenient than text based passwords.

Reliability

The major design issue for recall-based methods is the reliability and accuracy of user input recognition. In this type of method, the error tolerances have to be set carefully – overly high tolerances may lead to many false positives while overly low tolerances may lead to many false negatives. In addition, the more error tolerant the program, the more vulnerable it is to attacks.

Storage and communication

Graphical passwords require much more storage space than text based passwords. Tens of thousands of pictures may have to be maintained in a centralized database. Network transfer delay is also a concern for graphical passwords, especially for recognition-based techniques in which a large number of pictures may need to be displayed for each round of verification.

VI. CONCLUSION

The past decade has seen a growing interest in using graphical passwords as an alternative to the traditional text-based passwords. In this paper, we have conducted a comprehensive survey of existing graphical password techniques. The current graphical password techniques can be classified into two categories: recognition-based and recall-based techniques. Although the main argument for graphical passwords is that people are better at memorizing graphical passwords than text-based passwords, the existing user studies are very limited and there is not yet convincing evidence to support this argument. Our preliminary analysis suggests that it is more difficult to break graphical passwords using the traditional attack methods such as brute force search, dictionary attack or spyware. However, since there is not yet wide deployment of graphical password systems, the vulnerabilities of graphical passwords are still not fully understood. Overall, the current graphical password techniques are still immature. Much more research and user studies are needed for graphical password techniques to achieve higher levels of maturity and usefulness.

REFERENCES

- [1] Schneier B. Real-World Passwords. *Crypto-Gram* Newsletter, December 15, 2006.
- [2] Magalhaes S. T., Revett, K., Santos, H.D. Generation of Authentication Strings From Graphic Keys. *IJCSNS*, Vol. 6 No. 3 pp. 240-246, 2006.
- [3] Brown A. S., Bracken E., Zoccoli S. and Douglas K. Generating and remembering passwords. *Applied Cognitive Psychology* 18, 641-651, (2004).
- [4] Zviran, M., Haga, W. J., User authentication by cognitive passwords: an empirical assessment, 5 *JCIT*, 137-144, 1990.
- [5] Jansen W., Gavrilas S., Korolev V., Ayers R., Swanstrom R. Picture Password: A Visual Login Technique for Mobile Devices. NIST, NISTIR 7030.
- [6] Zhi L., Qibin S., Yong L., Giusto D. D. An Association-Based Graphical Password Design Resistant To Shoulder-Surfing Attack. *IEEE, ICME*, 2005.

Soil Improvement By Using Bamboo Reinforcement

Md Asaduzzaman¹ ; Muhammad Iftiarul islam²

¹ Department of civil engineering, RUET, Rajshahi-6204, Bangladesh

² Department of civil engineering, RUET, Rajshahi-6204, Bangladesh

ABSTRACT: The existing at a construction site may not always be totally suitable for supporting structures such as buildings, bridges, highways, and dams. In granular soil deposits, the in situ soil may be very loose and indicate a large elastic settlement. In such case, the soil needs to be improved to increase its unit weight and thus the shear strength and load bearing capacity. Sometimes the top layers of soil are undesirable and must be removed and replaced with better soil on which the structural foundation can be built. For this reason the improvement of load bearing capacity is much more important for making a structural foundation. This paper described a new soil improvement method with a minimum cost solution by using bamboo reinforcement having a length of 12 inch and 0.5 inch in diameter distributed in uniform medium dense soil at different depths (0.75 inch, 1.5 inch and 2.25 inch) below the footings. Three square footings have been used (3x3 inch, 3.5x3.5 inch, 4x4 inch) to carry the above investigation for such purposes. It was found that the initial vertical settlement of footing was highly affected in the early stage of loading in unreinforced soil with compared to bamboo reinforced soil. The failure load value for proposed model in any case of loading increased compared with the un-reinforced soil by increasing the depth of improving below the footing. The load carrying capacity of single layer reinforced soil is increased up to 1.77 times and 2.02 times for multiple reinforced soil system than the load carrying capacity of unreinforced condition of soil. Improvement in load carrying capacity was observed considerable in reinforced soil over the unreinforced soil. For single layer system, load carrying capacity is maximum and settlement is minimum when the reinforcement layer placed at 0.30B. For multilayer system, BCR increases with increasing number of reinforcing layer. One of which is highlighted in the paper, facilitates the improvement of load bearing capacity of soil and spreading the techniques on soft ground.

Keywords - Bearing capacity of soil, Square footing, Settlement, Bamboo Reinforcement, Bearing capacity ratio, Depth/breadth ratio or d/B ratio.

I. INTRODUCTION

The decision of ground improvement is taken for a site area when it needs such treatment methods and also based on the project design performance requirements that will dictate some of design parameters, including the required stability and the allowable deformation (settlements) of related soil under static or dynamic loading. Different types of structures will have different settlement requirement. The well-designed foundations induce stress-strain states in the soil that are neither in the linear elastic range nor in the range usually associated with perfect plasticity. Thus, in order to predict the settlement accurately underneath the foundation rest on soil, analysis that are more realistic than simple elastic analysis are required and a comparison can be made between the settlement for reinforced and unreinforced soil conditions .

Osman (2005) presents the results of a preliminary laboratory investigation on soft clay strengthened by fibers. The system consists of fiber-reinforced sand (the sand mixed with randomly oriented fiber and compacted in layers) between two geo-textiles sheets over fiber-reinforced sand columns inside the soft clay. The results have indicated that the settlement decreases and the bearing capacity increases by using the new system. It shows an effective solution to solve the problem of large settlement of footings over problematic soils such as soft clay.

Al Mosawe et al., (2010) investigated the effect of geo-grid reinforcement installed below square footing rest on sandy soil and subjected to eccentric loading. The results show improvement in the bearing capacity ratio by (22% to 48%) for one and two number of layers respectively without control on the initial settlement that is required for mobilizing reinforcement strength during loading.

Al Mosawe et al., (2011) present the results of improving soft clay soil (i.e. Kaolin) by compacted fly ash. The results show that there is a noticeable improving in the behavior of square footing settlement and bearing capacity ratio (BCR) of (1.3) in average but also without controlling the initial settlement.

It can be concluded from the above studies that reinforcement can increase the bearing capacity and reduce the corresponding settlement of the foundations compared with unreinforced soil. However, it was also found that an initial vertical movement of the reinforcement is still needed to mobilize the reinforcement strength which reflects such matter of the foundation settlements. In the previous studies the initial settlement at small loads still could not be avoided; such requirements is a very important design step that is usually controlled by limiting the expected settlement of footing rest on soil. The study shows new step method to improve soil strength and behavior not only by increasing the bearing capacity and reduce the settlement but also control the initial settlement at initial loads due to the complex interaction of such fibre materials with the soil through the investigated depths.

II. ABBREVIATIONS

2.1 Load bearing capacity:

In Geotechnical Engineering, bearing capacity is the capacity of soil to support the loads applied to the ground. The bearing capacity of soil is the maximum average contact pressure between the foundation and the soil which should not produce shear failure in the soil. Ultimate bearing capacity is the theoretical maximum pressure which can be supported without failure; allowable bearing capacity is the ultimate bearing capacity divided by a factor of safety. Sometimes, on soft soil sites, large settlements may occur under loaded foundations without actual shear failure occurring; in such cases, the allowable bearing capacity is based on the maximum allowable settlement

2.2 Settlement:

The downward movement of a structure with respect to its original position is referred to as settlement. The use of reinforcement materials to improve the bearing capacity of soil and to reduce settlement has been proven to be cost-effective solution for foundation design. The reinforcement materials are usually placed horizontally. However, there are cases in which vertical or sloped reinforcement may be used below the footing. The calculation of immediate settlement of footings for different soil types is estimated on the basis of elasticity, provided that the elastic properties of the soil (modulus of elasticity E , and Poisson's ratio ν) are known. These two parameters can be evaluated in the laboratory from soil samples obtained during site investigation processes for cohesive soils. However, for granular soils, it is much more difficult, if not impossible in most cases. The in-situ testing for granular soils may not accurately give these soil properties which are needed for the calculation of settlement.

III. EXPERIMENTAL PROGRAM

The soil sample was collected from Godagari, Rajshahi, Bangladesh. After collecting the soil sample, sieving was done by different sieve. Grain size curve was plotted by Hydrometer analysis, soil constituents also determined from this. The soil is classified into Sandy loam from textural classification. Then Atterberg limits were determined from Casagrande apparatus. The Atterberg limits are- Liquid Limit (LL)- 41.3, Plastic Limit (PL)- 23.7, Plasticity Index (PI)- 17.6;

Oven dried weight was used for determining dry density, moisture content, Specific Gravity. The soil properties are- Dry density- 104.7 pound per cubic feet, Moist density- 121 pound per cubic feet, Specific Gravity- 2.63, Moisture content of the soil sample- 16%, Void ratio- 0.59, Porosity- 0.37

After determining the soil properties, the soil sample was placed for CBR test. Bamboo reinforcement having 0.5 inch diameter and 12 inch long was placed into the soil at different depth. The bamboos were horizontally spaced at 1.75 inch interval to each. Density/degree of compaction was ensured by Standard Proctor Test. Every specimen was compacted in 3 layers by a hammer that delivers 25 blow to each. The hammer weights 5.5 lb and has a drop of 12 inch. Then the model type footing was placed over it and was taken into the CBR machine. The sample model was accustomed to load in the CBR machine and corresponding settlement data was recorded instantly. Using this procedure, the experiment was executed on different layer systems of bamboo reinforcement in different depth (i.e. 0.75 inch, 1.5 inch, 2.25 inch) and also changed of the footing dimension (i.e. 3x3inch, 3.5x3.5 inch, 4x4inch). The orientation of the multi-layer system was parallel-perpendicular-parallel. The bearing capacity and settlement of the footing resting on soil depend on the properties of soil such as the relative density, size, shape and embedment depth of footing (Lambe and Whitman,1979).The results obtained from such model tests are usually hindered by limitations associated with size and boundary effects. Consequently, it is important to keep such limitations in mind while designing such small model tests.



Fig. 1 Top view of placement of reinforcement and sample preparation



Fig. 2 General arrangement and loading the sample

IV. RESULT AND DISCUSSION

This experiment was performed for different dimensions of footing with different layer system of bamboo reinforcement. The layer systems were- single layer system, two layer system, three layer system of bamboo reinforcement. And the footing sizes were- 3 inch x 3 inch, 3.5 inch x 3.5 inch, 4 inch x 4 inch.

Table 1 Table for showing the data were tested in the experiment.

Footing Size (inch x inch)	No. Of reinforcing layers, N	Depth of top reinforcing layer below footing, d (inch)	Depth of layers below the footing, d (inch)
3x3	1	0.75, 1.5, 2.25	-
3.5x3.5	2	0.75	0.75, 2.0
4x4	3	0.75	0.75, 2.0, 3.0

The following parameters were considered in this study:

- a. Improvement for the bearing capacity of soil related to footing size.
- b. Experimental and calculated settlement comparison.
- c. Experimental and calculated comparison in bearing capacity ratio (BCR) with d/B ratio.

For the footing 3 x 3 inch, the settlement versus stress (load/area) graph are given below-

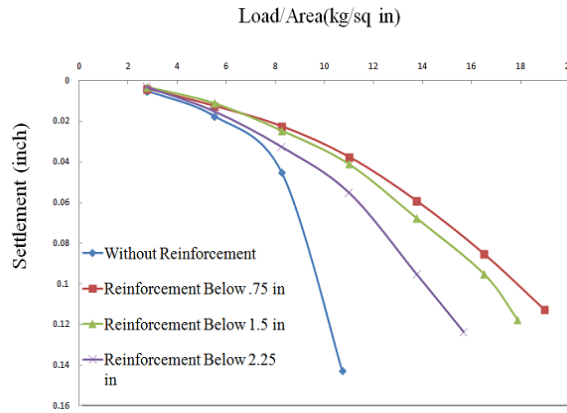


Fig. 3 Settlement versus stress (load/area) graph for 3inch x3inch footing

For the footing 3.5 x 3.5 inch, the settlement versus stress (load/area) graph are given below-

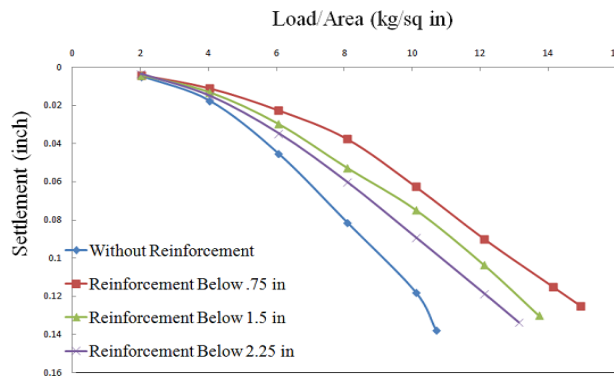


Fig. 4 Settlement versus stress (load/area) graph for 3.5 inch x 3.5 inch footing

For the footing 4 x 4 inch, the settlement versus stress (load/area) graph are given below-

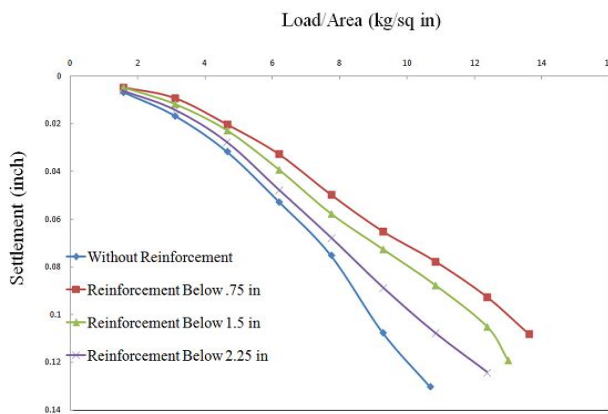


Fig. 5 Settlement versus stress (load/area) graph for 4 inch x 4 inch footing

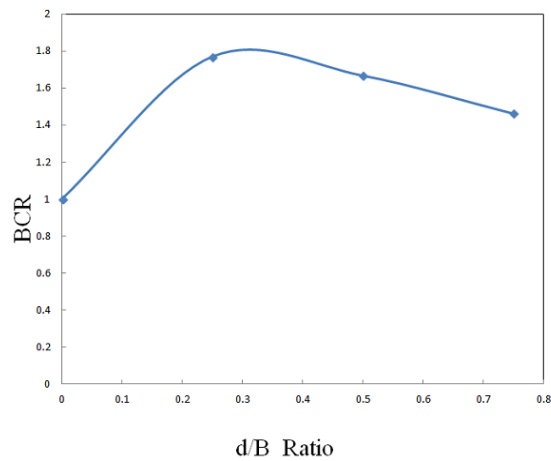


Fig. 6 Variation of Bearing Capacity Ratio (BCR) with respect to d/B Ratio for single layer.

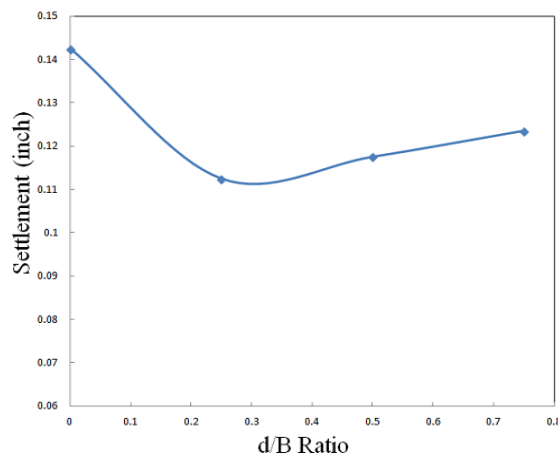


Fig. 7 Variation of Settlement (inch) with respect to d/B Ratio For single layer.

Multiple Layer Reinforcement System:

For the footing 3 x 3 inch

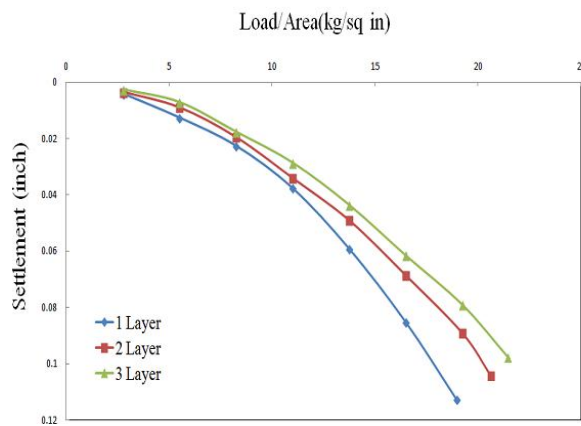


Fig. 8 Settlement versus stress (load/area) graph for 3 inch x 3 inch footing

For the footing 3.5 x 3.5 inch:

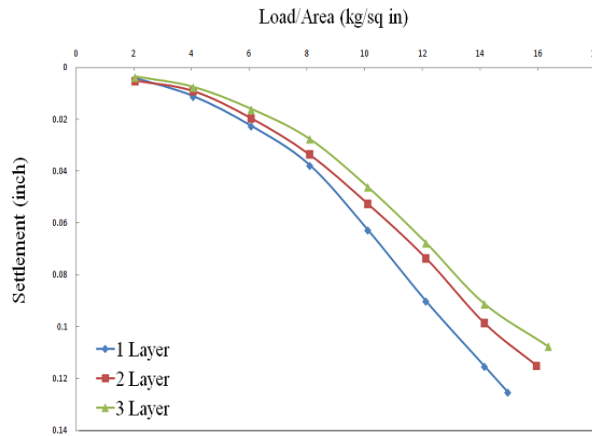


Fig. 9 Settlement versus stress (load/area) graph for 3.5 inch x 3.5 inch footing

For the footing 4 x 4 inch:

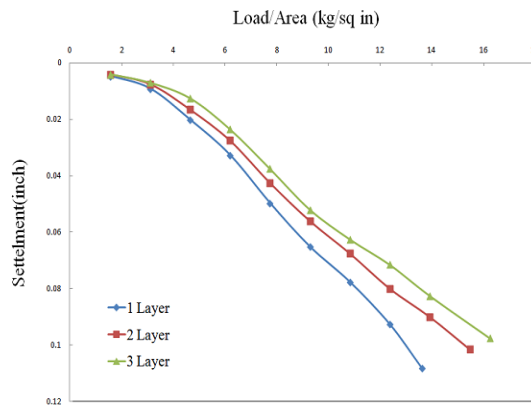


Fig. 10 Settlement versus stress (load/area) graph for 4 inch x 4 inch footing

Bearing Capacity Ratio (BCR) increases with the increase of number of reinforcing layers.

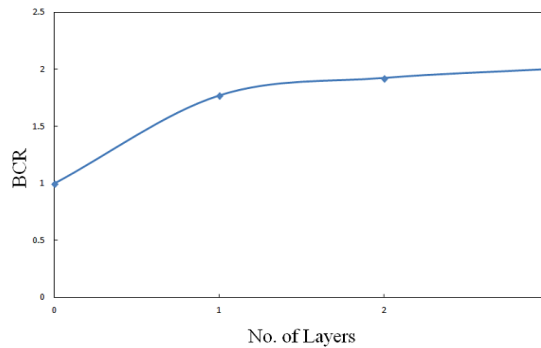


Fig.11 Variation of Bearing Capacity Ratio (BCR) with respect to number of reinforcing layer.

Settlement decreases with the increment of number of layers

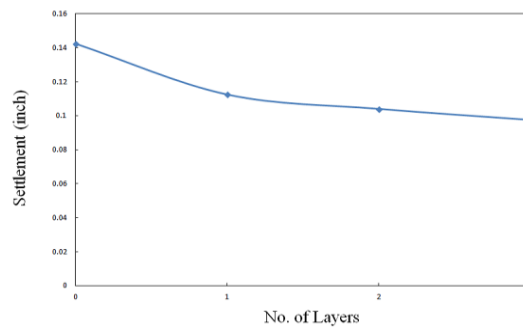


Fig. 12 Variation of Settlement (inch) with respect to number of layers

The bearing capacity of soil was improved by using bamboo reinforcement of single or multiple layers in 3 x 3 inch, 3.5 x 3.5 inch, 4 x 4 inch footings. The load/area-settlement relationships are shown in Figures (3) to (5) for single layer of bamboo reinforcement in different depth (i.e. 0.75 inch, 1.5 inch, 2.25 inch). For single layer reinforcement, settlement was more in using no reinforcement & it was decreased with decrease of depth of reinforcement layer. It was found that with the increase of depth/breadth (d/B) ratio, the Bearing Capacity Ratio (BCR) increased but after certain value of d/B ratio, the BCR value decreased. Again, settlement decreased with the increment of d/B ratio but after certain value of d/B ratio it increased. The high bearing capacity ratio (BCR) & low settlement was found in 0.30B depth as shown in the figures (6) & (7) for footing 3 x 3 inch.

For getting more bearing capacity, the layer of bamboo reinforcement was increased. Reinforcement was placed in 1, 2, 3 layers in square footing respectively. The variation of load/area-settlement for multiple layers reinforcement is shown in figures (8) to (10). In this diagram, it is found that the increasing of no. of layers decreases the settlement & thus it increases the soil bearing capacity. Figure (11) & (12) shows that the increase of number of bamboo reinforcement layers, increases the load bearing capacity and decreases settlement of soil.

V. Conclusion

1. The load bearing capacity of soil increases when the bamboo reinforcement placed within the depth of failure envelope.
2. The load bearing capacity is increased up to 1.77 times for single layer reinforced soil and 2.02 times for multiple layer reinforced soil system than the load bearing capacity of unreinforced condition of soil.
3. Improvement in load bearing capacity is observed considerable in reinforced soil over the unreinforced soil. For single layer system, load bearing capacity is maximum and settlement is minimum when the reinforcement layer placed at 0.30B.
4. For multilayer system, BCR increases with increasing number of reinforcing layer (N). The BCR is maximum for N=3 but the percentage increase in BCR for N=3 over N=2 is very small (4%).
5. In multi-layer reinforcing system, settlement is considerably decreases with the increasing number of reinforcing layer.

REFERENCES

- [1] Al Mosawe M. J., Al Albusoda B. S., and Yaseen A. S. (2011). "Bearing Capacity of Shallow Footing on Soft Clay Improved by Compacted Fly Ash" *Journal of Engineering*, No.6, Vol. 17, pp (1473-1482).
- [2] Al Mosawe M. J., Al Saidi A. A., and Jawad F. W. (2010). "Bearing Capacity of Square Footing on Geogrid Reinforced Loose Sand to Resist Eccentric Load", *Journal of Engineering*, No.2, Vol. 16, pp (4990-4999).
- [3] Bassat, R. H. and Last, N. C. (1978). "Reinforced Earth below Footing and Embankments", *Symposium Proc. conf. on Earth Reinforcement*, ASCE, Pittsburgh, pp(202-231).
- [4] Bieganousky, W. A. and Marcuson, W. F., (1976). "Uniform Placement of Sand" *J. of Geot. Eng.Div., ASCE*, Vol. (102), GT3. pp(229-235).
- [5] Binquet and Lee, K. L., (1975a). "Bearing Capacity Tests on Reinforced Earth Slabs". *J. of Geot. Eng.Div., ASCE*, Vol. (101), GT12. pp(1241-1255).
- [6] Das, B. M. (1988) "Shallow Foundation on Sand Underlain by Soft Clay with Geotextile Interface" *Geosynthetics for Soil Improvement conf.* pp(112-126).
- [7] Fragaszy, R. J. and Lawton, E., (1984). "Bearing Capacity of Reinforced Sand Subgrade". *J. of Geot. Eng.Div., ASCE*, Vol. (110), GT10. pp(1500-1507).
- [8] Jones, C. J. F. P. (1985). "Earth Reinforcement and Soil Structures". *Butter worth advance series in Geot Eng.*
- [9] Khan, S. A. (2005), "Stabilization of Soil Using Bamboo Industry Waste", 32:18-19 July, Coimbra, Portugal, pp (357-362).
- [10] Lambe, T. W., and Whitman, R. U. (1979). "Soil Mechanics"; Published by John Wiley and Sons. Inc.
- [11] Mekkiyah, H. M., and Alansari, O. M. (2004). "Settlement Reduction Underneath Surface Circular Footings Rest on Reinforced Sand". *Int. Conference on Geot. Eng., Oct., 3-6, Sharjah-UAE*, pp(327-333).
- [12] Milligan, G. W. E., and J. P. Love (1984) "Model testing of geogrids under and aggregate layer in soft ground" *Proceedings, Symposium on polymer Grid Reinforcement in Civil Engineering*, ICI, London, England, 4.2.1-4.2.11
- [13] Milovic, D. (1977) "Bearing Capacity Tests on Reinforced Sand", *Proc. of the 9th International conf. on Soil Mechanics and Foundation Engineering*, Tokyo, Japan, 1, pp(651-654).
- [14] Osman, E. A. M. (2005), "Reinforced Earth Mat Foundation over Fiber-Reinforced Sand Columns inside soft Clay", *J. of Nepal Geological Society*, Vol. 32, pp(16-24).

Effects of Particle Size on the Thermal Properties of Sawdust, Corncobs and *Prosopis Africana* Charcoal Briquettes.

Tokan, A., Sambo, A.S., Jatau, J.S. and Kyauta, E.E.

Department of Mechanical Engineering
Abubakar Tafawa Balewa University, Bauchi, Nigeria

ABSTRACT: The thermal properties of Sawdust, Corncobs and *Prosopis Africana* Charcoal briquettes were studied as a function of particle size. The particle sizes were 300, 425, 600, 1180 and 2000 μ m. The sieved materials were compressed into briquettes and pellets. The pellets were 12.5mm diameter and 13mm in length. The properties determined were moisture content, ash content and calorific value. The calorific value for Sawdust particle were 300 μ m = 16.04MJ/kg and 2000 μ m = 17.82MJ/kg which indicates an increased with increase in particle size. For Corncobs the calorific value also rises from 16.63MJ/kg to 17.51MJ/kg for 300 μ m and 2000 μ m respectively. In the same vain *Prosopis Africana* charcoal gives 24.94MJ/kg for 300 μ m size and 29.67MJ/kg for 2000 μ m. It was observed that for all the materials investigated, an increase in particle size was accompanied by higher energy output.

Keywords: Briquette, Moisture, Ash, Calorific value

I. INTRODUCTION

The Nigerian energy industry is probably one of the most inefficient in meeting the needs of its customers. The use of kerosene and gas for cooking and domestic heating on the other hand is very expensive and the common man in Nigeria cannot afford. Even though Nigeria is said to be endowed with many natural resources, (Sambo, 1992 and Adenikinju, 2005), there is problem of energy scarcity. More than 70% of the populace has no access to national grid and those who have are facing the problem of low and epileptic supply coupled with high cost as reported by Jekayinfa and Scholz, (2009) and Oladeji (2013a).

Renewable source of energy is the fastest growing source of world energy, with consumption increasing by 3% per year. This is due to its environmental friendliness as against the rising concern about the environmental impact of fossil fuel use and also strong government incentives for increasing renewable penetration in most countries around the world EIA, (2009). Globally, biomass currently provides around 46 EJ of bioenergy in the form of combustible biomass and wastes, liquid biofuels, solid biomass/charcoal and gaseous fuels. According to FAO, (1990) this share is estimated to be over 10% of global primary energy, with over two-thirds consumed in developing countries as traditional biomass for household use.

Currently there is a tremendous interest in using biomass materials in many countries for the production of liquid transportation fuels, combine heat and power, chemical and bio- products Abdullahi *et al*, (2011). The use of wood is increasing on daily basis especially in the less technologically developed countries of the world as stated by Aremu and Agarry (2013). But complete reliance on wood for domestic cooking would not solve the present energy crisis; rather it would lead to deforestation or desertification resulting in further scarcity of this resource (Salunkhe, *et al*, 2012).

To address the various energy challenges associated with non-renewable fuels, many countries have indicated commitment to Biofuels production that are renewable, sustainable, cheap and safe and geographically diversified. Fabian (2003). For example, Agricultural biomass residues have the potential for the sustainable production of bio-fuels and to offset greenhouse gas emissions Campbell *et al* (2002). According to Liu, (2005), straw from crop production and agricultural residues existing in the waste streams from commercial crop processing plants have little inherent value and have traditionally constituted a disposal problem. Oladeji, (2011) further stated that these residues represent an abundant, inexpensive and readily available source of renewable

lignocelluloses biomass. Agriculture offers much potential for renewable energy sources in the form of biomass. With advances in biotechnology and bioengineering, some resources, which could have been classified as waste, now form the basis for energy production Oladeji, (2010). The large quantities of agricultural residues produced in Nigeria can play a significant role in meeting her energy demand. Unfortunately, the abundant quantities of agricultural wastes and forest residues are neither managed effectively, nor utilized efficiently in all developing countries. The common practice is to burn these residues or they are left to decompose. This burning itself contributes to atmospheric pollution, but more than that; the burning or decomposition is a waste of available energy Wanukanya (1995). However, these problems can be handled through densification of biomass materials into pellets, briquettes and cubes.

A briquette is a block of combustible matter which is used to start and maintain a fire. Henry ford have been credited with the invention of charcoal briquettes from the wood scraps and saw dust from his car factory. Worthless fine coals were compressed into briquettes in the late 1800s allowing for stable transportable products to be made. www.virtualbilled.com. Charcoal briquetting have been used in emerging economies as cooking fuel in rural areas. The process of manufacture usually employs a devitalizing step whereby gas or volatile matter is driven prior to briquetting to produce a smokeless domestic fuel. Biomass briquettes produced through densification of Sawdust and other agro residues has been practiced for many years in several countries. The binding mechanisms of densification encompass the suitability of biomass based on its physical and chemical properties. Physical properties are most important in the description of the binding mechanism of biomass densification. Densification of biomass at high pressure brings about mechanical interlocking and increased adhesion between particles, forming interlocking bonds in contact areas Grover, (1996).

The densification of biomass into briquettes, logs, bales, chips, pellets, etc has become an important source of energy even in the rural communities. The main advantage of the Biofuel briquettes are its domestic origin, potential for reducing total dependence on oil and gas economy, jobs creation to the rural dwellers and help in the waste management by changing waste to wealth. Biofuels briquettes for utilization as energy source for domestic and industrial heating processes can significantly reduce emissions of air pollutants Fabian, (2003).

This work investigated the effects of particle size on the calorific values, moisture and ash content of Sawdust, Corncobs and *Prosopis Africana* charcoal briquettes.

II. MATERIALS AND METHODS

2.1. Raw Material Procurement

The raw materials used include Sawdust, Corncobs and *Prosopis Africana* charcoal. The Sawdust and Corncobs was obtained from a saw mill in Muda Lawan timber market. The Corncobs were obtained at the University farm while the charcoal was bought from local charcoal producers at the Galambi cattle ranch. The Sawdust and Corncobs samples were sundried. All the samples were hand crushed and grounded using a hammer mill at the Center for Industrial Studies, Abubakar Tafawa Balewa University, Bauchi. The grounded samples were sieved into five different particle sizes using (300, 425, 600, 1189 and 2000 μ m) sieves for all samples. The briquettes were then air dried then sieved

2.2. Briquettes Production

A wood/Agric waste briquetting machine shown in plate I is a device used to produce solid briquettes from wood and agricultural waste. It is manually operated based on the principle of piston cylinder arrangement. Basically, the briquettes were produced in cylinders when a mixture of raw materials and suitable binders were compacted by the piston. The machine consist of the following components: the compaction and ejection lever, Pillar caps, cylinder cover assembly, table, cylinder, connecting rods and piston assembly, pillars, lever for operating the cover, the base and the auto feed unit.

2.3. Briquetting Process

Binding agents were made into paste using hot water and the sieved waste material was added in the ratio of 1:5, 1:7, 1:10 (binder : waste) following the method of Akpabio and Illalu (1997). The paste and the waste were thoroughly mixed and loaded into the cylinders of the Briquetting machine shown in Plate I which is manually operated to achieve compaction.



Plate I: Manually operated Briquetting Machine



Plate II: Briquettes produced using the Briquetting Machine

The briquettes (Plate II) were extruded from the mould with the aid of the extruding ram. The procedure was repeated for all samples. The briquettes were then air-dried for two weeks.

2.4. Determination of Moisture Content

The procedure suggested by Dara (1999) was adopted. The weighed briquettes were put into an oven whose temperature has been adjusted to between 105°C to 110°C and left for 24 hours. They were then removed from the oven, allowed to cool and weighed. The procedure was repeated two times and the average taken. The moisture content of each sample was expressed as a percentage of its dry mass and was computed using equation (2):

$$\text{Moisture content } M_c = \frac{\text{loss of moisture}}{\text{dry mass}} \times 100, \% \tag{1}$$

- Let m_1 = mass of empty container
- m_2 = mass of container and wet sample.
- m_3 = mass of container and dry sample (after heating).

$$\text{Then } M_c = \frac{m_2 - m_3}{m_3 - m_1} \times 100 \tag{2}$$

2.5. Determination of Ash Content

The procedure suggested by Dara (1999) was adopted. Each sample was placed in a crucible weighed and burnt in a furnace at 350°C and left to cooled overnight in the furnace. Thereafter, the ash was later weighed. The ash content was then determined on dry basis using equation (3):

$$\text{Ash Content } A_c = \frac{m_a - m_1}{m_2 - m_1} \times 100 \tag{3}$$

- where m_2 = weight of sample and container
- m_a = weight of container and ash.
- m_1 = weight of container

2.6. Determination of Calorific Value

The bomb calorimeter was used to determine the calorific value of the briquettes and results obtained. The result of the calorific value was calculated using equation (4) as suggested by Dara, (1999) and the result tabulated in Table 7.

$$\text{Calorific value} = \frac{(W + w) \times \Delta T}{X}, \text{ kcal / kg} \tag{4}$$

where: W = weight of water in calorimeter, (kg)
 w = water equivalent of apparatus (kg)
 ΔT = temperature rise $^{\circ}C$
 X = weight of fuel sample taken (kg)

III. RESULTS AND DISCUSSION.

3.1. Results.

The results of the experiments carried out on the moisture, ash and calorific values on saw test, corncobs and Prosopis Africana charcoal are presented on tables 1 to 7.

Table 1: Results of Moisture Content of Sawdust

Sample size		300µm	425 µm	600 µm	1180 µm	2000 µm
Container label		A	B	C	D	E
Container and wet sample (g)	m_2	8,00	8.00	8.10	8.00	8.00
Container and dry sample (g)	m_3	7.90	7.90	8.00	7.90	7.90
Empty Container(g)	m_1	7.00	7.00	7.00	7.00	7.00
Dry Sample(g)	m_3-m_1	0.90	0.90	1.00	0.90	0.90
Moisture Loss (g)	m_2-m_3	0.10	0.10	0.10	0.10	0.10
Moisture Content (%)	w	11.11	11.11	10.00	11.11	11.11

Table 2: Results of Moisture Content of Corncobs

Sample size		300µm	425 µm	600 µm	1180 µm	2000 µm
Container label		A	B	C	D	E
Container and wet sample (g)	m_2	9.00	9.00	9.10	9.00	9.10
Container and dry sample (g)	m_3	8.80	8.70	8.90	8.70	8.90
Empty Container(g)	m_1	7.00	7.00	7.00	7.00	7.00
Dry Sample(g)	m_3-m_1	1.8	1.70	1.90	1.70	1.90
Moisture Loss (g)	m_2-m_3	0.20	0.30	0.20	0.30	0.20
Moisture Content (%)	w	11.11	17.65	10.52	17.65	10.53

Table 3: Results of Moisture Content of Prosopis Africana Charcoal

Sample size		300 µm	425 µm	1180 µm	2000 µm
Container label		A	B	C	D
Container and wet sample (g)	m_3	8.00	8.10	8.00	8.00
Container and dry sample (g)	m_3	7.90	8.00	7.90	7.90
Empty Container(g)	m_1	7.00	7.00	7.00	7.00
Dry Sample(g)	m_3-m_1	0.90	1.00	0.90	0.90
Moisture Loss (g)	m_2-m_3	0.10	0.10	0.10	0.10
Moisture Content (%)	w	11.11	10.00	11.11	11.11

Table 4: Results of Ash Content of Sawdust.

Sample Size	300µm	425 µm	600 µm	1180 µm	2000 µm
m _a (g)	7.50	7.30	7.20	7.20	7.10
m ₁ (g)	7.00	7.00	7.00	7.00	7.00
m ₂ (g)	8.10	8.20	7.90	8.00	8.30
m _a - m ₁	0.50	0.30	0.20	0.20	0.10
m ₂ -m ₁	1.10	1,20	0.90	1.00	1.30
A _c (%)	45.45	25.00	22.22	20.00	7.69

Table 5: Results of Ash Content of Corncobs.

Sample size	300µm	425 µm	600 µm	1180 µm	2000 µm
m _a (g)	7.40	7.30	7.30	7.20	7.10
m ₁ (g)	7.00	7.00	7.00	7.00	7.00
m ₂ (g)	8.10	8.10	8.10	8.10	8.10S
m _a - m ₁	0.40	0.30	0.30	0.20	0.10
m ₂ -m ₁	1.10	1.10	1.10	1.10	1.10
A _c (%)	36.36	27.27	27.27	18.18	9.09

Table 6: Results of The Ash Content of Prosopis Africana Charcoal

Sample size	300 µm	425 µm	1180 µm	2000 µm
m _a (g)	7.30	7.20	7.20	7.10
m ₁ (g)	7.00	7.00	7.00	7.00
m ₂ (g)	8.10	8.10	8.00	8.00
m _a - m ₁	0.30	0.20	0.20	0.10
m ₂ -m ₁	1.10	1.10	1.00	1.00
A _c (%)	27.27	18.18	18.18	10.00

Table 7: Results of Calorific value of the three materials

Sample size	300µm	425 µm	600 µm	1180 µm	2000 µm
Sawdust	16.04MJ/kg	17.50MJ/kg	17.20MJ/kg	17.72MJ/kg	17.82MJ/kg
Corncobs	16.63MJ/kg	16.94MJ/kg	17.20MJ/kg	17.35MJ/kg	17.51MJ/kg
Prosopis Africana Charcoal	24.71MJ/kg	29.15MJ/kg	29.24MJ/kg	29.38MJ/kg	29.67MJ/kg

3.2. DISCUSSIONS

3.2.1. Moisture content

From the tests conducted, results are presented in Tables 1, 2 and 3. For all the material samples, the moisture content was kept as low as possible. Compared with wood, biomass briquettes are unique in that they provide opportunity to control during the process of manufacture the fuel density, moisture content, size and geometry as reported in the works of Kaliyan and Morey (2007) and Chaney (2010). Generally for best performance, the range should be between 10 - 15 percent of moisture as discovered in this work. However, the corncob samples have higher amounts of moisture content because it was the most difficult to compact, thus more water and binder was needed to ensure adequate compaction.

3.2.2. Ash content

Tables 4 to 6 shows the results of the test conducted generally for all samples the smaller particle size (300 µm) contained more ash due to the fact that the smaller particle sizes are less coarse, compact easily leading to incomplete combustion due to small numbers of pore spaces. Coarse particle sizes (from 1180 µm to 2000 µm) have greater number of pore spaces allowing oxygen to flow easily within the sample. However, for the medium sizes (425 µm to 600 µm) the compaction was moderate thus there was available space for the oxygen to flow and combustion was near complete. Lastly, the larger particle which were the most difficult to compact were more loosely bond. Hence, allowing adequate flow of oxygen and so combustion was complete resulting in less ash content.

3.2.3. Calorific value

The result (Table 7) shows the difference in energy content of each sample. The amounts of energy released in the samples were in ascending order such that the smaller particle sizes release less energy as compared to the larger ones except for the Sawdust samples where there was a sharp contrast in values between particle size (425 μm and 600 μm) as a result of high moisture content.

Results from the analysis showed that for increasing particle sizes there was corresponding increase in thermal efficiency. The most thermal efficient particle size was the 2000 μm particle size of the samples. The fine grinding resulted in a loss of some heat and made the sample vulnerable to oxidation as reported by Kumar and Pratt (1996). Abdullahi et al. (2011) also obtained the same results when selected biomass was investigated. It can also be seen that the measured calorific value for all the particle sizes falls in the range of 16- 30 MJ/kg for the materials considered.

IV. CONCLUSION

The effects of particle size on the thermal properties of Sawdust, Corncobs and *Prosopis Africana* charcoal briquettes were carried out. The investigation involved, the collection crushing and milling of the samples. The characterization of samples based on particle size using British standard Sieves (aperture sizes 150, 300, 425, 600, 1180 and 2000 μm) and the production of briquettes and pellets of each sample was done. The ash content, moisture content and calorific value of each pellet were also determined using standard methods. The results of the research showed that the finely ground particles (300 μm) had low calorific value when compared to (2000 μm) grain size.

REFERENCES

- [1]. Adenikinju, A (2005) Analysis of the cost of infrastructure failures in a developing economy the case of electricity sector in Nigeria. African Economic Research Consortium AERC Research Paper 148, February 2005 Nairobi.
- [2]. Jekayinfa, S O., Scholz, V. (2009) Potential Availability of Energetically Usable Crop Residues in Nigeria” Energy Sources, Part A; 2009 (31): 687-697.
- [3]. Oladeji, J T. A Study of Effects of Different Particle Sizes on some Densification Characteristics of Corncobs Briquettes, Epistemics in Science, Engineering and Technology; 2013a (3), No. 1, pp 267- 271.
- [4]. EIA: Annual energy outlook with projections to 2030. Energy Information Administration. <http://www.eia.gov/oiaf/aeo> (2009). Accessed
- [5]. FAO: The briquetting of agricultural wastes for fuel: environment and Energy paper, vol. 11. FAO, Rome (1990)
- [6]. Abdullahi I, Ismail B, Musa A.O. and Galadima A.(2011) Effects of Kinetic parameters on Biogas Productions from Local Substrate Production using a batch feeding digester. Vol. 57. No. 4 pp 626-634.
- [7]. Aremu, MO, Agarry, SE. (2013) Enhanced Biogas Production from Poultry Droppings using Corn Cob and Waste Paper as Co-Substrates, International Journal of Engineering Science and Technology; 2013 Vol. 5 No. 2 pp 247-253.
- [8]. Salunkhe, DB, Rai, RK., Borkar, RB.(2012) Biogas Technology, International Journal of Engineering Science and Technology; (4) No.12 pp 4934-4940
- [9]. Fabian M. (2003) An introduction to anaerobic digestion of organic wastes. Scotland Remade.
- [10]. Campbell, CA, Zentner, RP, Gameda, S. Blomert,B, Wall, DD. Production of annual crops on the Canadian prairies: trends during 1976 – 1998. Canadian Journal of Soil Science; 2002 (82), pp. 45-57.
- [11]. Osadolor, O O. (2006) Performance Evaluation of Different Briquettes produced from Wood and Agricultural Wastes, Journal of Engineering Science and Applications; 2006 (4) No.2, pp. 90-95
- [12]. Liu, R, Yu, H, Huang, Y. Structure and morphology of cellulose in wheat straw. Cellulose; 2005 (12), pp. 25-34.
- [13]. Oladeji, JT. (2011) Investigations into the Effects of Different Binding Ratios on some Densification Characteristics of Corncobs Briquettes, New York Science Journal; 2011 (4) 11:55-58 (ISSN: 1554-0200) <http://www.sciencepub.net/newwork>.
- [14]. Oladeji, JT, Ogunsola, AD. (2010). Pyrolysis of Sawdust into Medium-Grade Fuels and Chemical Preservatives,. Proceedings of 2nd Engineering Conference of the School of Engineering; Federal Polytechnic, Offa, July 13-15, pp.64-67
- [15]. L Wanukanya, B. Jerkins (1995). Durability relaxation of Sawdust and wheat briquettes as posile fuels for Kenya. Biomass and Bioenergy 8. 175-179.
- [16]. Grover P.D. and Mishara S.K (1996). Biomass briquette Technology and Practice. Bangkok. Food and Agricultural Organisation of the United nations. pp 4-14, 41-45.
- [17]. All about charcoal. Retrieved from www.virtualbilled.com .0pm 7th Nov 2008.
- [18]. Akpabio, I.O. and Illalu, A. (1997). The conversion of Sugar cane Waste into Solid Fuels. Nigerian Journal of Renewable Energy, Vol.4 pp1-2
- [19]. Dara, S.S. (1999) A textbook on Experiments and Calculations in Engineering Chemistry, S. Chand publication, New Delhi, 70 – 72.
- [20]. Kaliyan N; Morey R V (2007). Roll press briquetting of corn Stover and switch grass: a pilot scale continuous briquetting study. ASABE Annual International Meeting, American Society of Agricultural and Biological Engineers, Minneapolis, Minnesota, June 17–20, Paper Number 076044, 2950 Niles Road, St. Joseph, MI 49085-9659, USA.
- [21]. Chaney, J.O., Clifford, M.J. and Wilson, R. (2010). An Experimental Study of the Combustion Characteristics of Low -Density Biomass Briquettes. Faculty of Engineering, University of Nottingham, University Park, Nottingham, NG7 2RD, UK, Email: joel.chaney@gmail.com. Biomass magazine, 2010 - appropriatetech.net. Assessed 13 April, 2014